SOVIET PHYSICS

JETP

A translation of the Journal of Experimental and Theoretical Physics of the USSR.

SOVIET PHYSICS JETP VOL. 37(10), NO. 5, pp. 837-1061 MAY, 1960

RESONANCE SCATTERING OF GAMMA RAYS BY Cd^{114}

N. N. DELYAGIN

Institute of Nuclear Physics, Moscow State University

Submitted to JETP editor May 19, 1959

J. Exptl. Theoret. Phys. (U.S.S.R.) **37**, 1177-1182 (November, 1959)

The lifetime of the first excited state of the Cd^{114} nucleus (556 kev) was measured by means of gamma-ray resonance scattering using a gaseous In^{114} source in the compound $InCl_3$. The value $\tau = (1.42 \pm 0.21) \times 10^{-11}$ sec for the lifetime of the level agrees satisfactorily with the data from Coulomb excitation investigations. The relation between excitation energy and reduced transition probabilities for even-even cadmium isotopes is discussed.

1. INTRODUCTION

RESONANCE scattering of gamma rays has been used in recent years to measure short lifetimes of excited nuclear states ($\tau \lesssim 10^{-10}$ sec). The cross section for the process is proportional to the width of the excited level, so that when all other conditions are unchanged the resonance scattering intensity increases inversely with the measured lifetime.

The widths of the lowest excited nuclear levels usually do not exceed 10^{-3} ev. The bombarding gamma rays must therefore correspond very precisely to the resonance energy of an excited state. As a source of these photons one naturally uses a radioactive isotope which decays to an excited state of the nucleus whose resonance excitation is under investigation. However, this is not a sufficient condition for obtaining photons of the required energy. The energy of a gamma ray emitted by a nucleus at rest is always somewhat smaller than the energy of the corresponding excited state, because a part of the transition energy is transformed into kinetic energy of the recoiling atom or molecule. A portion of the energy of an absorbed gamma ray also is converted into recoil energy of the absorbing nucleus. While such reductions of the gamma-ray energy are relatively small, they are always much greater than the excited level width. For the observation of resonance scattering the gamma energy must be increased to compensate the losses incurred through the recoils of both the emitting and absorbing nuclei. Various compensation methods based on the Doppler effect have been discussed in reviews by Dzhelepov[1] and by Metzger.[2]

The present investigation is concerned with the resonance scattering of 556-kev gamma rays emitted in $In^{114} \rightarrow Cd^{114}$ decay, by Cd^{114} nuclei. The method of cascade transitions[3] was used to compensate recoil losses. In In^{114} decay the 556-kev gamma ray is preceded by the emission of a 334-kev neutrino and a 772-kev gamma ray. After emission of the neutrino and first photon a recoiling Cd^{114*} nucleus remains, so that the 556-kev gamma ray is emitted by a nucleus which is already in motion. The 556-kev gamma energy is changed somewhat by the Doppler effect. Sufficiently great recoil velocities will result in the gamma energy required to produce resonance excitation of Cd^{114} nuclei. The mean free time of the recoiling atoms or molecules must considerably exceed the 556-kev level lifetime. Otherwise gamma rays may be emitted after collisions with neighboring molecules of the source material. The velocity of a molecule after a collision will generally be insufficient to supply the required energy to a 556-kev gamma ray. It is therefore necessary to use gaseous sources in which the mean free time of recoiling molecules is sufficiently long. The In^{114} source used in the

present experiment was contained in the compound $InCl_3$ volatilized at a relatively low temperature.

2. CALCULATION OF THE RESONANCE SCATTERING PROBABILITY

As a result of energy and momentum conservation the energy of a photon emitted or absorbed by a nucleus is less by the amount $E_0^2/2Mc^2$ than the transition energy E_0 (M is the mass of the recoiling molecule and c is the velocity of light). When the emitting and absorbing nuclei are included in molecules with masses M_1 and M_2, respectively, the total reduction of the photon energy is

$$\Delta E' = E_0^2 (M_1 + M_2) / 2M_1 M_2 c^2. \quad (1)$$

It is assumed here that no chemical bonds are disrupted during transitions. When a photon is emitted by a nucleus moving with the velocity v the photon energy is changed by the amount

$$\Delta E'' = E_0 (v/c) \cos \vartheta, \quad (2)$$

where ϑ is the angle between the direction of emission and the direction in which the recoiling nucleus is moving. For resonance scattering some photons must satisfy the condition

$$\Delta E' = \Delta E''. \quad (3)$$

In the present experiment metallic cadmium served as the scatterer, i.e., the mass M_2 was that of the cadmium atom. Equation (3) imposes a certain limitation on the mass M_1 which includes the emitting nucleus. If M_1 is too large the recoiling molecule may have insufficient velocity to satisfy (3). It is easily shown that the molecular weight of the source in the present instance must not exceed 300. This condition is satisfied by $InCl_3$. The energy transferred to the recoiling molecule in the emission of a neutrino and a 722-kev photon is 0.27 and 1.27 ev, respectively, which is insufficient to affect the molecular bonds.

The probability of resonance scattering was calculated using Eq. (5) of reference 4; the probability may be expressed as a function of the excited level width. This width can be determined by comparing the experimental with the calculated probability. Constants in the formula are determined from the characteristics of the In^{114} decay scheme and from the parameters of the scatterer. The total resonance scattering probability for the given experimental geometry is calculated by numerical integration over the volume of the scatterer. For a sufficiently thin scatterer Eq. (5) of reference 4 is equivalent to the formula used in reference 5 to calculate the resonance scattering cross section.

It follows from (2) that photons impinging on the scatterer are not strictly monoenergetic. Their energy depends on v and ϑ, not all values of which are consistent with the resonance energy E_r. To calculate the probability of resonance scattering we must determine $N(E_r)$, the density distribution of photon energies about E_r. It is easily shown in the present case of a neutrino $-\gamma-\gamma$ cascade that the energy distribution for 556-kev photons, without taking γ-γ angular correlation into account is represented by

$$N(E) = \begin{cases} M_1c^2 / 2E_0E_2, & 0 \leqslant |E| \leqslant E_0 (E_2 - E_1) / M_1c^2, \\ (M_1c^2 / 4E_0E_1E_2)(E_2 + E_1 - EM_1c^2 / E_0), & |E| \geqslant E_0 (E_2 - E_1) / M_1c^2, \end{cases} \quad (4)$$

where $E_2 = 722$, $E_1 = 334$, $E_0 = 556$ kev. The energy scale used in (4) is such that $E = 0$ represents a photon with the transition energy E_0. When the recoil energy loss (1) is taken into account the resonance energy E_r corresponds to the value $\Delta E'$ for E. For a source in $InCl_3$ and a metallic cadmium scatterer we have $N(E_r) = 0.092$ ev^{-1}. When the angular correlation of the 722- and 556-kev photons is taken into account we have $N(E_r) = 0.099$ ev^{-1}. The angular distribution of scattered photons was also taken into account in calculating the resonance scattering probability.[6]

3. EXPERIMENTAL TECHNIQUE

The $In^{114}Cl_3$ source was prepared from metallic indium, which was irradiated with thermal neutrons in a reactor and was then slightly heated while exposed to a stream of chlorine. The indium chloride was purified through distillation into a glass ampoule, which was then evacuated and sealed. The activity of the source was 15 microcuries, although only 3.5% of the In^{114} decays were accompanied by the emission of 556-kev photons. The $InCl_3$ source was volatilized in an electric oven at about 500° C. Complete volatilization resulted in a pressure of 0.2 atmos, thus excluding the possible influence of collisions of recoiling molecules. The technique used to produce $InCl_3$ permitted a possible admixture of $InCl_2$, the presence or absence of which could not be determined precisely. However $N(E_r)$, which determines the probability of resonance scattering, in the case of $InCl_2$ was very close to the result obtained above for $InCl_3$. The calculation of the overall error of the final results took into account the possible contribution from $InCl_2$. It was determined through control measurements that under the working conditions the entire active source was gaseous.

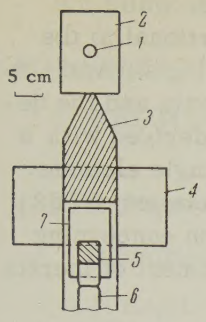

FIG. 1. Diagram of experimental setup. 1 – source, 2 – electric oven, 3 – lead cone, 4 – scatterer, 5 – NaI(Tl) crystal, 6 – photomultiplier tube, 7 – lead absorber.

Resonance scattering was measured using the circular geometry which is customary in such experiments[3,5] to permit the maximum solid angles and for convenience in calculating. The experimental setup is represented in Fig. 1. Scattered radiation was registered by a NaI(Tl) crystal measuring 4 cm in both height and diameter, and by a FEU-29 photomultiplier tube. A lead cone 22 cm high was used to shield the counter from direct radiation out of the source. The electric oven enclosing the source was located at the apex of the cone. The crystal was surrounded by a lead absorber 1 mm thick in order to reduce the pulse count produced by Compton-scattered photons. The scatterer was a hollow cadmium cylinder 30 cm in diameter, 15 cm long and 0.45 cm thick. Scatterers of the same dimensions, consisting of tin and lead instead of cadmium, were used for comparison. The scatterers were interchanged every two minutes in order to exclude any effect which drift of the electronic circuit would have on the results. The differential discriminator channel was set for a photopeak of 556 kev in the interval 530 — 590 kev. Measurements were obtained with the source in both the solid and vapor states. With the volatilized source the counting rate produced by the cadmium scatterer increased due to resonance scattering, whereas with a non-cadmium scatterer or with no scatterer the rate was independent of the state of aggregation of the source. The method described in reference 5 was used to determine the resonance scattering probability.

4. RESULTS AND DISCUSSION

The average counting rate produced by resonance scattering was 0.3 pulse/sec, which comprised 23% of the total rate, most of which was produced by the laboratory background. The effect was large enough to permit measurements of the resonance scattering spectrum shown in Fig. 2. The spectrum for the vaporized source exhibits a photopeak at 556 kev, which is the energy of resonance-scattered gamma rays. The lifetime of the first excited state

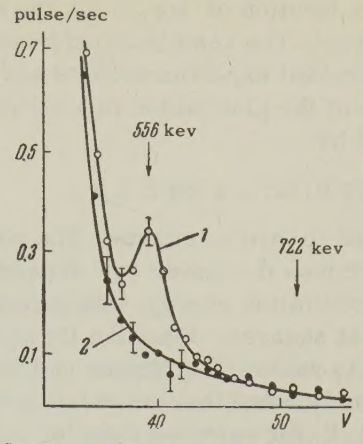

FIG. 2. Spectrum of resonance radiation from cadmium scatterer. 1 – gaseous source, 2 – solid source.

of Cd^{114} (556 kev) is found to be $\tau = (1.42 \pm 0.21) \times 10^{-11}$ sec. The reduced probability B(E2) of the 556-kev E2 gamma transition is calculated from the measured lifetime to be $0.108e^2 \times 10^{-48}$ cm^4. This is in excellent agreement with the results given in references 7 and 8 in connection with the Coulomb excitation of Cd^{114}, the numerical coefficients of B(E2) being 0.110 and 0.104, respectively. There is also agreement within experimental error with the value 0.117 given in reference 9. The hypothesis of reference 10 that the lifetime determined by resonance scattering will always be shorter than that obtained by Coulomb excitation is thus not confirmed. The results obtained in reference 11 for the Coulomb scattering of Cd^{114} disagree sharply with the results obtained in references 7 — 9 and in the present work and are probably incorrect.

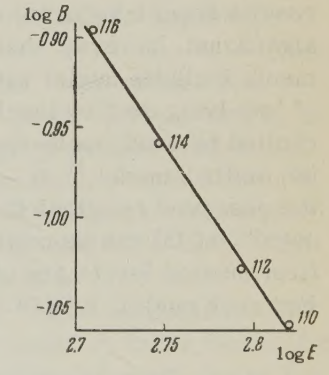

FIG. 3. Log B(E2) as a function of log E. The mass numbers of the cadmium isotopes are indicated.

In references 7 — 9 the reduced probabilities for E2 transitions were determined for even-even cadmium isotopes with mass numbers A = 110, 112, 114, and 116. These results are consistent among themselves, so that we may assume that reliable values of B(E2) have been established for these four cadmium isotopes. The data reveal the dependence of B(E2) on the excitation energy E of the corresponding levels. Figure 3 shows log

B(E2) as a function of log E for the four cadmium isotopes. The results of references 7 — 9 and of the present experiment were averaged for the purpose of the plot, which is a straight line represented by

$$\log B(E2) = a \log E + b, \qquad (5)$$

where a and b are constants. The constant a, which determines the power-law dependence of B(E2) on excitation energy, was calculated at -1.5 by least squares. Equation (5) agrees with experiment to within 1%. Stelson and McGowan[9] have previously noted that the relation between B(E2) and E for even-even nuclei with masses A = 90 — 130 can be represented satisfactorily by $B(E2) = bE^{-1}$. Van Patter[12] has suggested that the formula $B(E2)/Z^2 = bE^{-1.4}$ is accurate to within 25% over a broad range of mass numbers. The relation between B(E2) and E for the cadmium isotopes gives a different power in the functional dependence. It is also found that (5) is valid for isotopes of other elements but that the constant a, which is the power of E in the formula for B(E2), generally varies as a function of Z. For example, in the case of even-even gadolinium isotopes, for which the reduced probabilities for E2 transitions are given in reference 13, the experimental results agree to within 1% with (5) when $a = -1.1$. For Se and Dy isotopes the absolute value of a is greater than 3. For a large group of elements (Ru, Pd, Cd, Te, Sm, Gd, W, Pt) the values of a lie within a small range, from -1.1 to -1.5. It cannot be determined at the present time whether this spread of the values of a is significant or results from inaccurate experimental data. It is significant, however, that the given group of elements includes nuclei with a rotational spectrum of low-lying excited levels and nuclei which are excited by quadrupole-type vibrations according to the unified model.[14] It is difficult to interpret the observed relations theoretically, but it may be noted that (5) can be predicted for nuclei whose first excited levels are of rotational character. For such nuclei B(E2) is proportional to the square of the deformation parameter while the first excited-level energy is proportional to the nuclear moment of inertia. Assuming a power-law relation between the moment of inertia and the deformation parameter, (5) is easily derived with a and b constant for isotopes of a single element. The determination of the relation between B(E2) and E may thus furnish information concerning the relation between the nuclear moment of inertia and the deformation parameter.

The author is indebted to V. S. Shpinel' for directing this work and to V. I. Anikin for assistance.

[1] B. S. Dzhelepov, Usp. Fiz. Nauk **62**, 3 (1957).

[2] F. R. Metzger, Proc. Rehovoth Conference on Nuclear Structure, H. J. Lipkin, ed., Amsterdam, 1958.

[3] F. R. Metzger, Phys. Rev. **101**, 286 (1956).

[4] C. P. Swann and F. R. Metzger, Phys. Rev. **108**, 982 (1957).

[5] N. N. Delyagin and V. S. Shpinel', Izv. Akad. Nauk SSSR, Ser. Fiz. **22**, 861 (1958), Columbia Tech. Transl. p. 855.

[6] F. R. Metzger, Phys. Rev. **97**, 1258 (1955).

[7] G. M. Temmer and N. P. Heydenburg, Phys. Rev. **104**, 967 (1956).

[8] R. D. Sharp and W. W. Buechner, Phys. Rev. **109**, 1698 (1958).

[9] P. H. Stelson and F. K. McGowan. Phys. Rev **110**, 489 (1958).

[10] V. Knapp, Proc. Phys. Soc. (London) **71**, 194 (1958).

[11] Mark, McClelland, and Goodman, Phys. Rev. **98**, 1245 (1955).

[12] D. M. Van Patter, J. Franklin Inst. **266**, 411 (1958).

[13] Ramsak, Olesen, and Elbek, Nuclear Phys. **6**, 451 (1958).

[14] Alder, Bohr, Huus, Mottelson, and Winther, Revs. Modern Phys. **28**, 432 (1956). (Russ. transl. in Deformation of Atomic Nuclei, IIL, 1958, p. 9).

Translated by I. Emin
242

POLARIZATION OF NEUTRONS FROM THE T(p, n) He^3 REACTION AND OF PROTONS FROM THE He^3(n, p) T REACTION

K. P. ARTEMOV, N. A. VLASOV, and L. N. SAMOĬLOV

Submitted to JETP editor May 26, 1959

J. Exptl. Theoret. Phys. (U.S.S.R.) **37**, 1183-1186 (November, 1959)

Polarization of neutrons produced in the T (p, n) He^3 reaction by 8 — 10 Mev protons was determined by measuring the right-left asymmetry of protons produced in the inverse reaction He^3 (n, p) T. The dependence of the asymmetry on the angle of proton emission from the He^3 (n, p) T reaction has also been measured. Polarization of the T (p, n) He^3 neutrons and He^3 (n, p) T protons attains 30% for an angle of incidence of about 40° and primary proton energy of about 10 Mev. The polarization decreases as the proton energy is diminished but the angle of emission corresponding to peak polarization does not change appreciably.

THE energy dependence of the T (p, n) He^3 cross section[1,2] as well as that of the total neutron cross section[3] of He^3 exhibits resonance, from which it is inferred that alpha particles have a 22-Mev excited state with spin and parity 2^-.[2,4] This is confirmed by the shape of the neutron spectrum from the T (d, n) reaction[5] and by the spectrum of inelastically scattered electrons.[6] However the spectrum of protons scattered inelastically by He^4 contains broad groups[7,8] which are evidently associated with a large contribution by other states of the final He^4 nucleus. The great weight of the 1^- state at about 25 Mev is indicated by the energy dependence of the T (p, γ) He^4 and He^4 (γ, p) T reactions, which are electric dipole transitions.[9,10] Various experimental data and their interpretation are thus far not in agreement concerning the states of He^4, so that further investigation is of interest.

For this purpose it is important to study the polarization of neutrons from T (p, n) He^3 and of protons from He^3 (n, p) T, which is the subject of the present paper. In reference 11 it is shown that the polarization of T (p, n) He^3 neutrons for proton energy E_p = 1.46 Mev, which is somewhat above the reaction threshold (1.019 Mev) is close to zero at 50°. This does not exclude the possibility of appreciable polarization at proton energies greatly exceeding the threshold and the resonance value (~ 3 Mev).

The study of neutron polarization from T (p, n) He^3 is also of great methodological importance since this reaction is widely used as a convenient source of fast monoenergetic neutrons.

Barschall[12] has suggested the use of inverse reactions for the study of polarization. We have used this method to determine simultaneously the polarization of T (p, n) He^3 neutrons and of protons from the inverse reaction He^3 (n, p) T. When the products of both reactions are observed at certain definite (Barschall) angles the right-left asymmetry gives the square of the polarization directly. In our case the Barschall angles and the corresponding polarizations are quite small; our measurements were made principally at large angles. When polarization depends smoothly on the angle and on energy, Barshall's method can be extended to a broader angular range. We observed appreciable polarization at approximately twice the Barschall angle and determined the angular dependence and energy dependence of the polarization. Therefore the determination of the absolute value of the polarization is not confined to Barschall angles.

The reaction T (p, n) He^3 was excited in a tritium-zirconium target about 0.2 Mev thick by an external cyclotron beam of protons with initial energy 10 Mev. The protons were slowed down in platinum foils placed directly ahead of the target. A chamber 5 cm in diameter and 5 cm deep filled with He^3 at 10 atmos served as the radiator of the proportional telescope[13] and was positioned 50 cm from the target at the angle θ_1 to the beam. The grid of openings in the helium cell wall, facing the telescope counters, was covered with 10μ iron foil. The telescope rotated about an axis passing through the center of the radiator, so that protons from the reaction He^3 (n, p) T occurring in the radiator were registered at angles θ_2 to the right and to the left of the neutron beam emitted at angle θ_1. The symmetry of θ_2 was checked by replacing helium with hydrogen in the radiator and recording the intensity of recoil protons as a function of θ_2

to the right and left. The telescope was set for the steeply dropping final portion of the recoil-proton spectrum in order to accentuate the angular dependence. The position of the telescope corresponding to $\theta_2 = 0$ was determined within 0.1° from the steep slopes of the curve registered with the hydrogen radiator.

The proton intensity from the $He^3(n, p)T$ reaction at different angles θ_2 to the right and left was measured for different values of E_p and θ_1. The most pronounced effect was observed at $E_p = 9.9$ Mev and $\theta_1 = 40°$. Figure 1 shows the asymmetry coefficient $R = N_r/N_l$ as a function of θ_2.

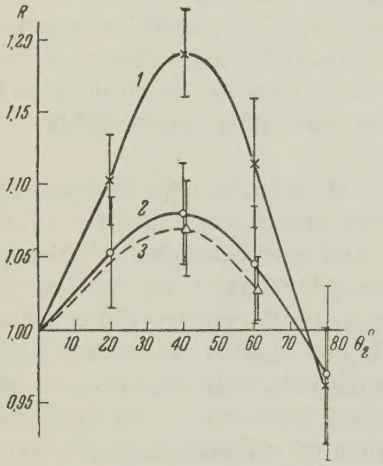

FIG. 1. Right-left asymmetry of protons from He^3 (n, p) T as a function of the angle of emmission. Curve 1 – $\theta_1 = 40°$, $E_p = 9.9$ Mev, $E_n = 7.7$ Mev; curve 2 – $\theta_1 = 16.5°$, $E_p = 9.9$ Mev, $E_n = 8.8$ Mev; curve 3 – $\theta_1 = 40°$, $E_p = 8.0$ Mev, $E_n = 6.1$ Mev.

Here N_r and N_l are the numbers of counts to the right and left relative to the same proton flux impinging on the target, as measured by an integrator. The indicated errors are entirely statistical. N_r and N_l are the differences between the counts obtained with the helium radiator and with an empty chamber. The background from the tritium target backing was also taken into account. In the general case we have

$$R = (1 + P_1P_2)/(1 - P_1P_2),$$

where P_1 is the polarization of neutrons from $T(p, n)He^3$ and P_2 is the polarization of protons from $He^3(n, p)T$. As θ_2 is varied only P_2 changes, while P_1 remains constant but of unknown magnitude. For $\theta_2 = \theta_1 = 40°$ $P_2 \neq P_1$ since θ_1 and θ_2 are greater than the Barschall angles and the second reaction takes place at a somewhat lower energy than the first reaction. At the Barschall angle $\theta_1 = 16.5°$ the energy of neutrons from the first reaction is $E_n(16.5°) = 8.85$ Mev, while at $\theta_1 = 40°$ we have $E_n(40°) = 7.72$ Mev. If only a slight change of polarization accompanies an energy difference of 1.1 Mev we may assume $P_1(40°) = P_2(40°)$ and use the $R(\theta_2)$ curve to calculate $P_{1,2}(\theta_{1,2})$. Figure 1 also gives the plot of $R(\theta_2)$ for the same energy $E_p = 9.9$ Mev at the Barschall angle $\theta_1 = 16.5°$ (curve 2). Because of the small polarization at $\theta_1 = 16.5°$ this curve is relatively less accurate but the angular distribution $R(\theta_2)$ is of the same character. Curve 3 was plotted for $E_p = 8.0$ Mev and $\theta_1 = 40°$. With decreasing proton energy the magnitude of the polarization is diminished but the angular distribution is of the same type. Therefore the polarization P calculated from R (40°, 40°) assuming $P_1 = P_2$ actually pertains to the intermediate energy $E_n \approx 8.3$ Mev and in the given experiment $P_1(40°) > P > P_2(40°)$. Having determined $P_1(40°)$ in this manner we may obtain $P_{1,2}(\theta)$ for all values of θ_2 for which $R(\theta_1 = 40°, \theta_2)$ was measured.

Figure 2 shows the polarization of neutrons from the reaction $T(p, n)He^3$ and of protons from $He^3(n, p)T$ as a function of the angle θ.

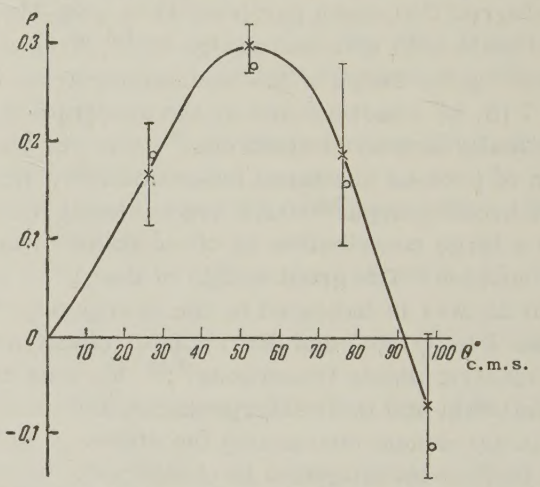

FIG. 2. Angular dependence of neutron polarization from $T(p, n)He^3$ at $E_p = 9.9$ Mev. × – $\theta_1 = 40°$, $E_n = 7.7$ Mev; o – $\theta_1 = 16.5°$, $E_n = 8.8$ Mev.

The plotted points were obtained by means of the curve $R(\theta_1 = 16.5°, \theta_2)$, which gives the polarization directly under the Barschall conditions. This result is relatively less accurate, although both results are in good agreement. Figure 3 shows the dependence of maximum polarization on primary particle energy for both reactions $T(p, n)He^3$ and $He^3(n, p)T$. It is evident from Figs. 2 and 3 that neutron polarization from $T(p, n)He^3$ at about 40° reaches 30% for $E_p = 9.9$ Mev and probably increases further with E_p. Thus the $T(p, n)He^3$ reaction is a good source of neutrons with a fairly high degree of polarization at $E_n = 8$ Mev and probably also at higher energies.

A different method would be required to deter-

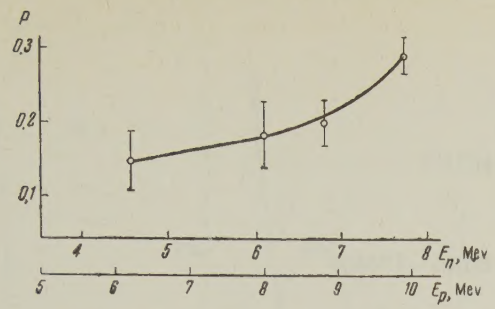

FIG. 3. Polarization of neutrons from T(p, n)He^3 and of protons from He^3 (n, p)T as a function of primary particle energy at 40° in the laboratory system.

mine also the direction of the polarization. The angular dependence of the polarization is apparently associated mainly with interference of the $P_{3/2}$ and $P_{1/2}$ states of emitted nucleons. The first of these states corresponds to resonance in T(p, n)He^3 at $E_p = 3$ Mev. The observed polarization and the energy dependence do not contradict the hypothesis of Baz' and Smorodinskiĭ[4] that a second state exists at an energy E_p greater than 3 Mev. Enhanced polarization is not surprising if the phases of the $P_{3/2}$ and $P_{1/2}$ states vary differently with energy. However, it follows from an analysis of neutron angular distributions that d phases become appreciable at $E_p = 10$ Mev and thus complicate the interpretation of the polarization.

[1] Willard, Bair, and Kington, Phys. Rev. **90**, 865 (1953).

[2] Bogdanov, Vlasov, Kalinin, Rybakov, Samoĭlov, and Sidorov, Ядерные реакции при малых и средних энергиях (Nuclear Reactions at High and Intermediate Energies), Acad. Sci. USSR Press, 1957, p. 7.

[3] D. J. Hughes and J. A. Harvey, Neutron Cross Sections, Brookhaven National Laboratory, Upton, New York, 1955.

[4] A. I. Baz' and Ya. A. Smorodinskiĭ, JETP **27**, 382 (1954).

[5] Bogdanov, Vlasov, Kalinin, Rybakov, and Sidorov, JETP **30**, 981 (1956), Soviet Phys. JETP **3**, 793 (1956).

[6] R. Hofstadter, Revs. Modern Phys. **28**, 214 (1956).

[7] Tyren, Tibell, and Maris, Nuclear Phys. **4**, 277 (1957).

[8] W. Selove and J. M. Teem, Phys. Rev. **112**, 1658 (1958).

[9] J. E. Perry and S. J. Bame, Phys. Rev. **99**, 1368 (1955).

[10] A. N. Gorbunov and V. M. Spiridonov, loc. cit. ref. 2, p. 427.

[11] Willard, Bair, and Kington, Phys. Rev. **95**, 1359 (1954).

[12] H. H. Barschall, Helv. Phys. Acta **29**, 145 (1956).

[13] Kondrashev, Kurashov, Linev, Sidorov, Sokolov, and Khaldin, Приборы и техника эксперимента (Instrum. and Meas. Engg.) No. 1, 17 (1958).

Translated by I. Emin
243

THE (d, t) REACTION IN C^{12}, F^{19}, *AND* Al^{27} *NUCLEI*

N. A. VLASOV, S. P. KALININ, A. A. OGLOBLIN, and V. I. CHUEV

Submitted to JETP editor May 27, 1959

J. Exptl. Theoret. Phys. (U.S.S.R.) **37**, 1187-1192 (November, 1959)

The spectra and angular distributions of tritons produced at 20 Mev deuteron energies in the reactions $C^{12}(d, t)C^{11}$, $F^{19}(d, t)F^{18}$, and $Al^{27}(d, t)Al^{26}$ were measured on the basis of the β radioactivity of tritium. The spins and parities of a number of states of F^{18} and Al^{26} were derived by comparing the obtained triton angular distributions with those obtained from Butler's theory. The probability of excitation of levels of the residual nucleus drops sharply with increasing level energy.

THE investigation of (d, t) reactions in Li^6, Li^7, and Be^9, which was begun in the preceding work,[1] has disclosed a characteristic feature of this reaction — a strong decrease in the excitation probability with increasing level energy of the final nucleus. This feature is apparently connected with the fact that in pickup reactions, particularly in the (d, t) reaction, only the hole levels corresponding to the stripping of a neutron from the external shell of a target nucleus in the ground state have a high excitation probability. In (d, p) and (d, n) stripping reactions, as is known, the levels with the greatest excitation probability are the single-particle levels of the nucleon captured by the nucleus, and the spectral distribution of the emitted nucleons has an entirely different character.

In the present paper we report on an investigation of the (d, t) reaction in F^{19} and Al^{27}. It is natural to expect the spectrum of the excited levels to be more complicated even when only hole levels are excited, since a neutron can be extracted not only from the 2s and 1d outer shells, but also from the filled 1p shell.

The triton spectra were obtained on the basis of the β activity of the resultant tritium. The tritons emitted from the thin target were trapped in stacks of aluminum foils, arranged 15 cm away from the target at various angles, starting with 7°. After irradiation, the tritium was extracted from the foils by heating and was introduced into the Geiger counter. Measurement of the activity of the tritium contained in each individual foil has made it possible to determine the distribution of the tritons by ranges at various angles. To study the $F^{19}(d, t)F^{18}$ reaction we used a 2.97 mg/cm^2 MgF_2 target sputtered on an aluminum foil 0.4 mg/cm^2 thick, and also a teflon (CF_2) target 8.2 mg/cm^2 thick. The deuteron energy was 20 Mev. The $Al^{27}(d, t)Al^{26}$ reaction was investigated at a deuteron energy of 19 Mev. The target was made of aluminum foil 2.15 mg/cm^2 thick.

Figure 1 shows the triton spectrum, measured at an angle of 11°, due to deuteron bombardment of a MgF_2 target. The contribution from the (d, t) reaction on magnesium isotopes at triton energies greater than 9 Mev was negligibly small. The dotted line shows the contribution from the (d, t) reaction on an aluminum base. Analogous spectra, but with worse resolution, were obtained in the bombardment of the teflon target. Furthermore, these spectra show clearly a group of tritons from the $C^{12}(d, t)C^{11}$ reaction (ground state).

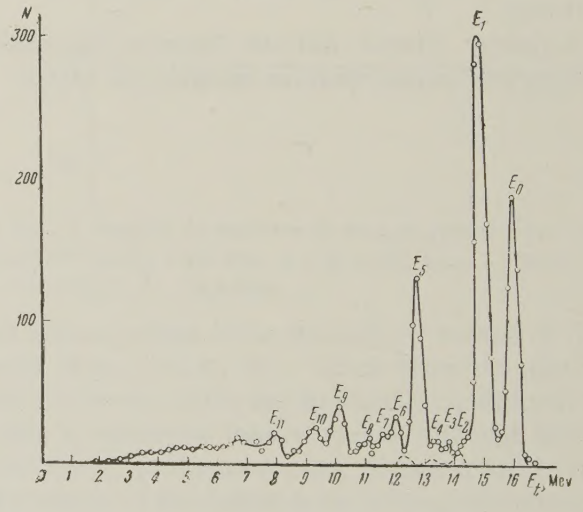

FIG. 1. Triton spectrum in the $F^{19}(d, t)F^{18}$ reaction at angle of 11°. The dotted line shows the contribution from the $Al^{27}(d, t)Al^{26}$ reaction.

The angular distributions of various groups of tritons formed in the $F^{19}(d, t)F^{18}$ reaction are shown in Fig. 2. The solid curves were calculated by the Butler theory[2] for the (d, t) reactions, and the triton form factor suggested by French[3] was

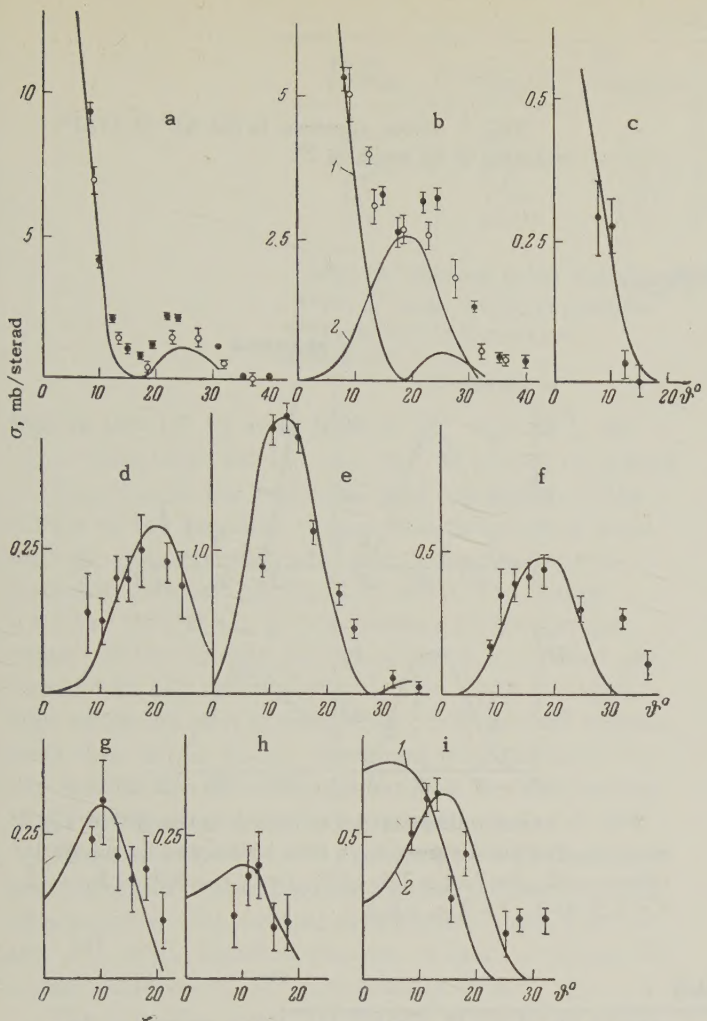

FIG. 2. Angular distributions of tritons in the $F^{19}(d, t)F^{18}$ reaction. The solid curves were calculated by Butler's theory, while the full and open circles denote the results of various types of irradiation (for groups E_0 and E_1). a) ground state, $l = 0$, $r_0 = 7.0$; b) 1.0 Mev, $l = 0$ (curve 1), $l = 2$ (curve 2), $r_0 = 7.0$; c) 1.8 Mev, $l = 0$, $r_0 = 7.0$; d) 2.6 Mev, $l = 2$, $r_0 = 7.0$; e) 3.3 Mev, $l = 1$, $r_0 = 7.0$; f) 3.9 Mev, $l = 2$, $r_0 = 8.0$; g) 4.4 Mev, $l = 1$, $r_0 = 8.0$; h) 5.0 Mev, $l = 1$, $r_0 = 8.0$; i) 5.9 Mev, $l = 1$, $r_0 = 8.0$ (curve 1), $l = 2$, $r_0 = 9.0$ (curve 2).

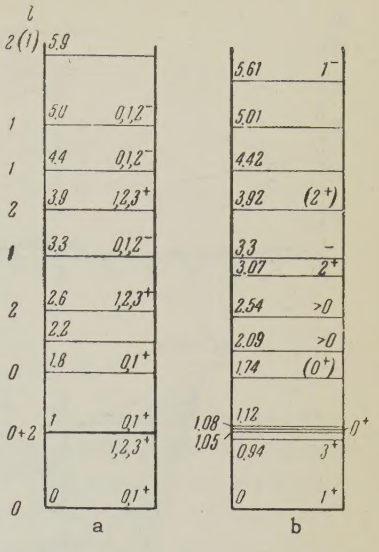

FIG. 3. Level scheme of F^{18}. a) from the (d, t) reaction, b) from the $O^{16}(He^3, p\gamma)F^{18}$, $Ne^{20}(d, \alpha)F^{18}$, $N^{14}(\alpha, \gamma)F^{18}$, and $F^{19}(p, d)F^{18}$ reactions.

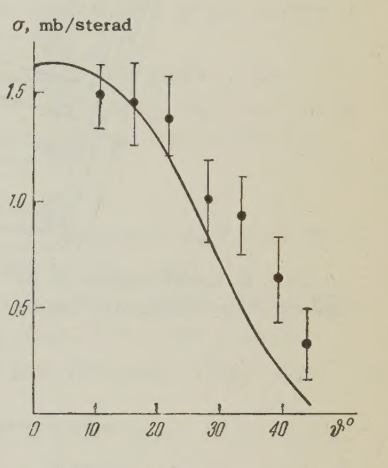

FIG. 4. Angular distribution of the tritons in the $C^{12}(d, t)C^{11}$ reaction with formation of C^{11} in the ground state ($l = 1$, $r_0 = 4.5$)

used. The parameters l and r_0 are indicated in the diagram. The angular distribution of group E_1 ($E^* = 1.0$ Mev) contains two components corresponding to $l = 0$ and $l = 2$. This is apparently connected with the fact that the E_1 group corresponds not to one but to several levels, known to be located near 1 Mev for F^{18} (reference 4). The presence of a component with $l = 1$ in the angular distribution of group E_1 is not completely excluded, but if it does exist, its intensity is several times smaller than the intensity of the components with $l = 0$ and $l = 2$.

The level scheme we obtained for F^{18} (Fig. 3) is in good agreement with the results of other experiments.[4-8] However, certain neighboring levels (for example, near 1 Mev) have not been resolved in our experiments. The values of the parities of levels 2.6, 4.4, and 5.0 Mev were determined here for the first time.

Figure 4 shows the angular distribution of the tritons from the $C^{12}(d, t)C^{11}$ reaction (ground state).

Figure 5 shows the triton spectrum of the $Al^{27}(d, t)Al^{26}$ reaction, measured at an angle of 7°. The level scheme of Al^{26}, which is known from other investigations,[9] is shown in Fig. 6 together with the transitions we observed. The angular distributions of the groups E_0, E_1, E_2, and E_8 are shown in Fig. 7. For groups E_4 and E_5 we were able to determine the values of l from the change in the form of the unresolved peak near 11 Mev.

The principal results of the work are listed in Table I. The reduced widths θ^2 are given in percentages of the single-particle width [$\theta^2 = 3\mu_n/2\hbar^2)\gamma^2 \times 100$, where μ_n is the reduced mass of the neutron, and γ^2 is the width in the usual units].

It is seen from the spectra and from Table I

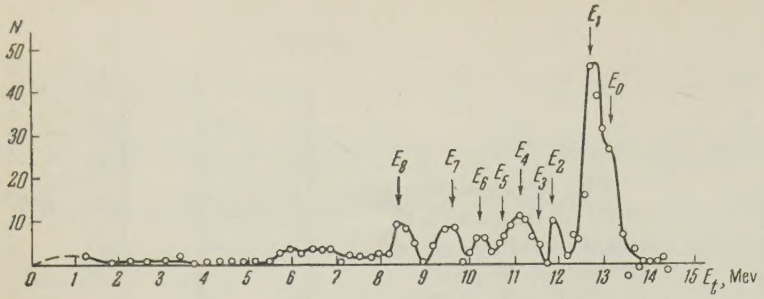

FIG. 5. Triton spectrum in the Al^{27} (d, t) Al^{26} reaction at an angle of 7°.

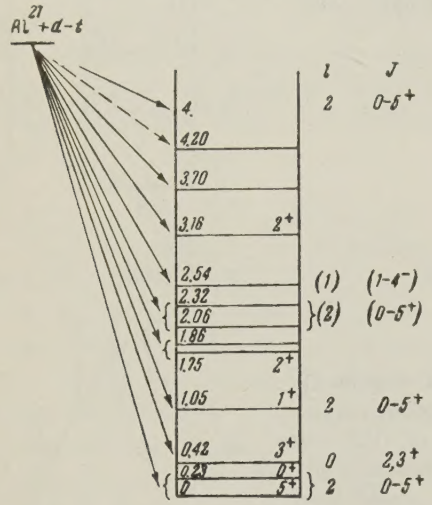

FIG. 6. Level scheme of Al^{26} (reference 9). The arrows indicate the transitions observed in the (d, t) reaction.

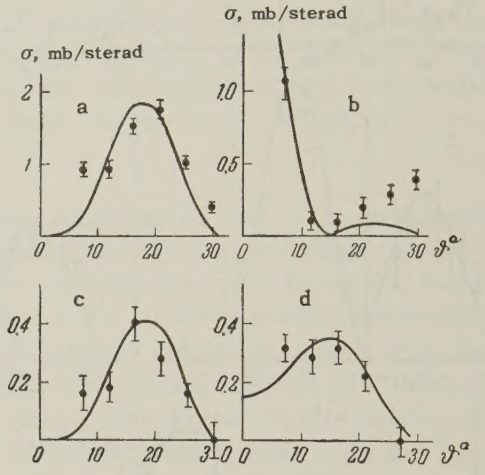

FIG. 7. Angular distributions of tritons in the Al^{27} (d, t) Al^{26} reaction. The solid curves have been calculated by the Butler theory. a) E_0, $l = 2$, $r_0 = 7.5$; b) E_1, $l = 0$, $r_0 = 8.0$; c) E_2, $l = 2$, $r_0 = 7.5$; d) E_8, $l = 2$, $r_0 = 8.0$.

TABLE I

Residual nucleus	Triton group	Excitation energy of the residual nucleus, Mev	l	$r_0 \cdot 10^{13}$, cm	$\sigma_{max}(\vartheta)$ in c.m.s., mb/sterad	θ^2, %	Error $\Delta(\theta^2)$, %
C^{12}	E_0	0	1	4.5	1.50 (11°)	1.3	±12
	E_1	1.85			<0.4 (11°)		
F^{18}	E_0	0	0	7.0	9.4 (8°)	1.5	± 4
	E_1	1.0	2	7.0	2.5 (20°)	1.6	±10
			0	7.0	5.0 (8°)	0.6	±10
	E_2	1.8	0	7.0	0.26 (10°)	0.05	±25
	E_3	2.2			0.15 (12°)		±50
	E_4	2.6	2	7.0	0.25 (17.5°)	0.2	±25
	E_5	3.3	1	7.0	1.95 (12.5°)	0.73	± 5
	E_6	3.9	2	8.0	0.44 (18°)	0.37	±10
	E_7	4.4	1	8.0	0.32 (10°)	0.1	±25
	E_8	5.0	1	8.0	0.20 (13°)	0.08	±30
	E_9	5.9	2(1)	9.0—8.0	0.65 (13°)	{0.4 (l=2) {0.3 (l=1)	±10
Remaining levels in the excitation energy interval 7–13 Mev					<0.1 (8—20°)		
Al^{26}	E_0	0÷0.23 *	2	—	1.7 (21°)	1.1	±10
	E_1	0.42 *	0	—	1.1 (7.5°)	0.11	±10
	E_2	1.1	2	—	0.40 (17°)	0.28	±15
	E_4	2.2	(2)	—	0.5 (15—23°)	0.35	±20
	E_5	2.6	(1)	—	0.5 (11°)	0.15	±20
	E_8	4.7	2	—	0.32 (16.5°)	0.23	±15
Remaining levels in the excitation energy interval 5–11 Mev					<0.05 (7—17°)		

*Indicated level energy from reference 9.

TABLE II

Final nucleus	$r_0 \cdot 10^{13}$, cm		Final nucleus	$r_0 \cdot 10^{13}$, cm	
	Reaction (p, d)	Reaction (d, t)		Reaction (p, d)	Reaction (d, t)
Li^5	4.5*	5.5	C^{13}	5.4****	5.0—5.9
Li^6	5.5	5.0—7.0	F^{18}	5.0	7.0—8.0
Be^8	3.0	4.0—5.0	Na^{22}		6.5—7.0
C^{11}	4.2**	4.5	Al^{26}	5.0	7.5—9.0
C^{12}	4.0***	6.5			

*For He^5 from the Li^6(n, d)He^5 reaction (reference 15).
**For B^{11} from the (d, p) reaction.
***From the (d, p) reaction.
****For N^{13}.

that in the (d, t) reactions in F^{19} and Al^{27}, as in the reactions on Li^7 and Be^9, a strong decrease is observed in the probability of excitation of the levels of the residual nuclei with increasing level energy. Levels with energies 3 — 4 Mev correspond to reduced widths that are 3 — 10 times smaller than those corresponding to the ground state. If levels with energies above 5 — 7 Mev are excited at all, their probability is $\frac{1}{20}$th or $\frac{1}{30}$th that of the ground state. This confirms the hypothesis that in the (d, t) reactions it is the hole levels that are predominantly excited, corresponding to the stripping of the outer nucleon.

The lower levels F^{18} are excited with approximately equal probability as a result of the stripping of a neutron with orbital momentum 0 and 2 from the F^{19}. This denotes that the s and d states of outer nucleons of F^{19} are greatly mixed.

The 3.3-Mev level, the parity of which is negative, is excited with a relatively greater probability. Apparently this level is excited by stripping of a neutron from the p shell. It is interesting to note that the neighboring nucleus, O^{17}, also has a first level with negative parity at an energy of approximately 3 Mev, the excitation probability of which is small in the O^{16}(d, p)O^{17} reaction,[10] as is to be expected for a hole level.

The investigation of the Al^{27}(d, t)Al^{26} reaction did not make it possible to refine greatly the level scheme of Al^{26}, owing to insufficient resolution. There is no doubt however that the stripping of the neutron with $l = 2$ is one order of magnitude more probable than that with $l = 0$. Consequently, the outer neutrons of Al^{27} are predominantly in the d state, and the admixture of s state is small.

In the investigation of the (d, t) reaction in Li^7 and Be^9 we noted[1] a systematic increase in the most suitable value of r_0 with a decreasing energy of the corresponding level, indicating an inaccuracy in the simplest expressions for the triton form factor. The tendency of increasing r_0 with increasing level energy is observed also for the reaction F^{19}(d, t)F^{18}. The absolute values of r_0, obtained from the reactions (d, t) in our investigations and in others,[11-13] are found to be as a rule greater than those from (p, d)[14] and (d, p) reactions (Table II). This discrepancy can also naturally be ascribed to the inaccuracy in the triton form factor employed.

The authors are grateful to the staff of the cyclotron laboratory for performing the irradiation and to D. P. Grechukhin and V. G. Neudachin for evaluating the results.

[1] N. A. Vlasov and A. A. Ogloblin, JETP **37**, 54 (1959), Soviet Phys. JETP **10**, 39 (1960).
[2] H. C. Newns, Proc. Phys. Soc. **A65**, 916 (1952).
[3] A. P. French, Phys. Rev. **107**, 1655 (1957).
[4] Kuchner, Almqvist, and Bromley, Phys. Rev. Lett. **1**, 260 (1958).
[5] R. Middleton and C. T. Tai. Proc. Phys. Soc. **A64**, 801 (1951).
[6] Kuchner, Almqvist, and Bromley. Bull. Am. Phys. Soc. II, No. 3, 27 (1958).
[7] Almqvist, Bromley, and Kuchner. Bull. Am. Phys. Soc. II, No. 3, 27 (1958).
[8] E. F. Bennet, Bull. Am. Phys. Soc. II, No. 3, 26, (1958).
[9] P. M. Enid and C. M. Braams. Revs. Modern Phys. **29**, 683 (1957).
[10] T. S. Green and R. Middleton. Proc. Phys. Soc. **A69**, 28 (1956).
[11] Holmgren, Blair, Simmons, Stratton, and Stuart. Phys. Rev. 95, 1544 (1954).
[12] Vogelsang, McGruer, and Hamburger. Phys. Rev. Lett **1**, 29 (1958).
[13] Moore, McGruer, and Hamburger. Phys. Rev. Lett **1**, 29 (1958).
[14] J. B. Reynolds and K. G. Standing. Phys. Rev. **101**, 158 (1956).
[15] G. M. Frye. Phys. Rev. **93**, 1086 (1954).

Translated by J. G. Adashko
244

ON THE FINE STRUCTURE OF THE CORE OF EXTENSIVE AIR SHOWERS

S. N. VERNOV, G. V. KULIKOV, Z. S. STRUGAL' SKIĬ, and G. B. KHRISTIANSEN

Nuclear Physics Institute, Moscow State University

Submitted to JETP editor May 28, 1959

J. Exptl. Theoret. Phys. (U.S.S.R.) **37**, 1193-1196 (November, 1959)

Experimental data are presented which indicate the presence of well-collimated particle beams in the cores of extensive air showers. Various possible explanations of the observed phenomenon are considered.

A detailed study of the core structure of extensive air showers (EAS) by means of cloud chambers has been attempted in recent years in a number of experiments.[1,2] However, the lack of a sufficiently sensitive method for identifying the passage of a shower core through the array, and also the short time of exposure of the arrays, have made it impossible to obtain conclusive data on the structure of the shower in the core region.

We have previously reported on the observation of events of the passage of EAS cores through a diffusion chamber with an area of 0.6 m^2. The chamber was operated for 1800 hours simultaneously with an array consisting of counters and ionization chambers connected to a hodoscope, which made it possible to determine the core position in EAS.[3]

In the present article we wish to point to an important feature of the distribution of shower particles in the core region. This feature is the appearance, in this region, of a narrow (4 cm diameter) particle beam consisting of a large number (from 4 to 15) of particles with collinear trajectories. If we construct the lateral distribution of the particle flux with this beam as the axis, and extrapolate the lateral distribution observed at distances larger than the dimensions of the beam towards this axis in accordance with a power law, we find that the number of particles expected on the basis of such an extrapolation is much smaller than the one actually observed in the beam. The experimental data are given in the table. On the average, the number of particles in the beam is 7, while the number indicated by the extrapolation is 0.7. As can be seen from the table, it is very improbable that the observed particle beams can be due to Poissonian fluctuations in the lateral distribution of the trajectories of shower particles. In reality, fluctuations in the core region can be substantially different from Poissonian. However, for any type of fluctuations, one would expect a frequent appearance of a group consisting of a small number of particles in the diffusion chamber, and also a simultaneous appearance of several such groups, while this is, in fact, not observed. We shall discuss different possible explanations of the observed effect.

It is well known from the electromagnetic cascade theory[4,5] that the photon-flux density in the shower increases faster than the electron-flux density with decreasing distance from the axis of the electron-photon shower. Accordingly, we can assume that the observed feature of the lateral distribution of shower particles near the axis is related to the transition effect in the materials placed above the sensitive layer of the chamber. We shall estimate the value of the transition effect. According to Guzhavin and Ivanenko,[5] the lateral distribution of the electron flux at the maximum of the electron-photon shower is, at distances in the range of interest, of the form $\rho_e = C_e/r$, while that of the photon flux is of the form $\rho_f = C_f|\ln r|/r$, where C_e and C_f are constants and r is the distance from the shower axis in Molière units. For distances of the order of 1 cm ($r \sim 10^{-4}$) from the axis, $\rho_f/\rho_e \approx 3$. The ratio of the number of photons to the number of electrons in a circle with radius r ($r \sim 1$ cm) with its center at the shower axis $n_f/n_e = 3\,(1+1/9.2) \approx 3$.

The sensitive layer of the diffusion chamber was shielded by the glass cover of the chamber 1.5 g/cm^2 in thickness and the plastic room roof 1.5 g/cm^2 in thickness. Assuming that the radiation length for these materials is equal to ~ 25 g/cm^2, we obtain the value of ~ 0.1 for the probability of photon conversion.

Assuming that each photon produces a pair of charged particles, we find that, owing to the transition effect, the number of charged particles in a

r, m	N	n	r, m	N	n
4	$3.1 \cdot 10^4$	8	<1	$1.4 \cdot 10^4$	6
<1	$2.5 \cdot 10^4$	5	<1	$5.5 \cdot 10^4$	6
5	$8.8 \cdot 10^4$	5			
3	$2.1 \cdot 10^4$	5	2	$3.0 \cdot 10^4$	5
			<1	$1.8 \cdot 10^4$	4
<1	$4.5 \cdot 10^4$	8	<1	$2.7 \cdot 10^4$	4
<1	$3.5 \cdot 10^4$	15	9	$5.0 \cdot 10^4$	6
~1	$2.5 \cdot 10^4$	14			
<1	$7.2 \cdot 10^4$	11	<1	$5.0 \cdot 10^4$	6
			6	$9.0 \cdot 10^4$	6
2,5	$1.5 \cdot 10^4$	7	<1	$1.4 \cdot 10^4$	8
~1	$4.5 \cdot 10^3$	6	7	$1.0 \cdot 10^5$	6
~1	$3.5 \cdot 10^4$	5			
<1	$2.9 \cdot 10^4$	12	<1	$7.0 \cdot 10^3$	8
			2	$1.0 \cdot 10^4$	8
~1	$1.5 \cdot 10^4$	6	<1	$1.0 \cdot 10^4$	10
8	$1.5 \cdot 10^5$	10	<1	$8.5 \cdot 10^3$	5

Note: N is the number of particles in the EAS; n is the observed number of particles in the beam 4 cm in diameter; r is the distance of the beam from the shower axis as determined from hodoscope data.

circle with a radius of the order of a few centimeters can increase by a factor of 1.5. However, because of the small variation of the ratio ρ_e/ρ_f with r, we practically take the transition effect already into account when determining the number of charged particles in the circle with radius r (see table) from the distribution function of charged particles at distances larger than r. Thus, the observed effect cannot be explained by the transition effect.*

Let us now consider one possible explanation of the observed particle beams, namely that they are due to the nuclear-active component of EAS. High-energy nuclear-active particles interacting near the observation level can produce secondary particles of different nature, among them π^0 mesons.

The secondary particles produced in the interaction can form a beam, provided their energy is sufficiently high. Thus, for a nuclear interaction at the distance of the order of one nuclear mean free path (500 m), the particles which arrive at the observation level spread over a distance of $\sim 2 \times 10^{-2}$ m should have an energy $E \geq (5 \times 10^2/2 \times 10^{-2}) p_\perp \approx 2 \times 10^{12}$ ev, where $p_\perp \geq 10^8$ ev/c is the transverse momentum carried away in nuclear interactions by a secondary particle. Taking the number of particles in the beam into account, we find that the energy of the nuclear-active particles belonging to the beam is $\sim 10^{13}$ ev. According to reference 6, the number of nuclear-active particles with energy $> E$ at sea level is given by the expression k/E (where E is given in ev, and $k = 2.5 \times 10^{11}$ ev for showers with a total number of particles $N \sim 10^4$). Hence it follows that the probability of a nuclear-active particle with energy $\geq 10^{13}$ ev near sea level appearing in a shower with a number of particles $N \sim 10^4$ is very small. At the same time, the expected number of showers with $N \geq 3 \times 10^4$ incident on the diffusion chamber during the observation time coincides with the number of beams accompanied by such showers, or is even smaller than it.[3]

It can easily be seen that, since the spectrum of the nuclear-active particles is of the form k/E, so that the number of nuclear-active particles does not increase greatly with decreasing energy, the probability of beams of low-energy nuclear-active particles appearing is also very small. It should also be noted that, if the beams were being produced by nuclear-active particles in the manner described above, we would obtain beams of different size.

It can be assumed that the observed particle beams represent the cores of electron-photon showers initiated by γ quanta originating in the decay of π^0 mesons produced in nuclear interactions. If the age of such an electron-photon shower is $s < 1$, then a sharp concentration near the axis is characteristic for the distribution of shower particles.

The electromagnetic cascade theory makes it possible to determine the energy of the π^0 mesons necessary for the production of the observed num-

*In reference 5, only electrons and photons with energy $E > \beta$ are considered. The number of electrons with energy $E < \beta$ in the distance range of interest amounts to only ~10% of the total number of electrons at these distances. The number of photons with energy $E < \beta$ can be considerably greater, since the high-energy electrons traveling near the shower axis can produce radiative photons of low energy. It is clear that the probability of radiating photons in the range from β to 0 decreases with increasing electron energy. Therefore, $\rho_f(>\beta,r)$ and $\rho_f(>0,r)$ should be identically equal for $r \to 0$. Hence it follows that, for $E > 0$, $\rho_f(r)$ will be still less dependent on the distance than for $E > \beta$, so that the ratio ρ_f/ρ_e will also be less dependent on the distance.

ber of beam particles in a circle with radius r. The number of particles in a circle with a given radius is determined by the degree of development of the electron-photon shower and by the lateral distribution of shower particles. Using the data of Ivanenko and Guzhavin on the lateral structure of an electron-photon shower produced by a particle with energy E_0, we find that, for an energy $E_0 = 10^{11} - 10^{12}$ ev, the maximum number of particles in a circle 2 cm in radius will be obtained for $s < 0.6$. If we set up the requirement that the number of particles in the circle be similar to that observed experimentally, then we find $E_0 \geq 10^{12}$ ev.

The point of origin of such a shower with $s < 0.6$ is located at an altitude of less than 150 g/cm^2 from the observation level. The flux of nuclear-active particles in an EAS is absorbed according to the law $e^{-x/\lambda}$, where $\lambda = 200$ g/cm^2, and, consequently, the number of nuclear-active particles of such a young shower is twice as large at the production level than at the observation level. Thus, not more than one particle with energy $\geq 10^{12}$ ev is contained in a shower with a number of particles $N = 3 \times 10^4$ at the observation level. Therefore, if the observed particle beams were the cores of young showers,* it would, at any rate, indicate a marked role of nuclear interactions in which the main part of the energy is concentrated in the π^0 meson.† It should be noted that Grigorov and Shestoperov[7] have indicated the possibility of an important role being played by such an energy concentration in the development of EAS.

Furthermore, it can be assumed that the observed beam of particles consists of high-energy μ mesons. The data on the energy of the nuclear-active component discussed above exclude the possibility of the production of such a beam in the lower layers of the atmosphere.

From the observed dimensions of the beam, and assuming an order of magnitude of the production height, we can estimate the energy of the μ mesons. We shall underestimate this energy, assuming that the transverse deviation of the μ mesons is due to Coulomb scattering only. The mean square deviation of particles with energy E is, neglecting the ionization loss in the atmosphere, given by the expression[8]

$$\overline{r^2} = \left(\frac{E_s}{E}\right)^2 t_0 \alpha \int_0^H h^2 e^{-\alpha h}\, dh.$$

The notation and numerical values are the same as in reference 7. Assuming H to be of the order of 7×10^3 m, we obtain $\sqrt{\overline{r^2}} = 1.5 \times 10^{11}/E$. Hence, the minimum energy of μ mesons traveling in such a concentrated beam should be of the order of 10^{13} ev.*

For the production of beams of such μ mesons, the requirement is clearly either a direct production of μ mesons in nuclear interactions at energies $\geq 10^{14}$ ev, or their production through particles with a lifetime by one or two orders of magnitude shorter than the lifetime of π and K mesons. In fact, even assuming the maximum acceptable multiple production of particles with energy $E \sim 10^{13}$ ev, we find† their number to be of the order of 10 for $E_0 \sim 10^{14}$ ev. The probability of the decay of a μ meson with energy of the order of $\sim 10^{13}$ ev at an altitude corresponding to the mean height of shower production is not greater than $1/30$. Thus, such an interpretation of the observed particle beams demands a basic revision of our ideas concerning the origin of the μ-meson component.

At present, it is impossible to make a final choice between the electron-photon and the μ-meson nature of the beam, and a further study of the effect is therefore necessary.

[1] W. E. Hazen, Phys. Rev. **85**, 455 (1952).

[2] K. E. Relf, Phys. Rev. **97**, 172 (1955).

[3] Vernov, Goryunov, Zatsepin, Strugal'skiĭ, Nechin, Kulikov, and Khristiansen, JETP **36**, 669 (1959), Soviet Phys. JETP **9**, 468 (1959).

[4] L. Eyges and S. Fernbach, Phys. Rev. **82**, 23 (1951).

[5] V. V. Guzhavin and I. P. Ivanenko, JETP **34**, 746 (1958), Soviet Phys. JETP **7**, 512 (1958).

[6] Abrosimov, Dmitriev, Massal'skiĭ, Kulikov, Solov'ev, and Khristiansen, JETP **36**, 751 (1959), Soviet Phys. JETP **9**, 528 (1959).

[7] N. L. Grigorov and V. Ya. Shestoperov, JETP **34**, 1539 (1958), Soviet Phys. JETP **7**, 528 (1958).

[8] G. B. Khristiansen, JETP **34**, 956 (1958), Soviet Phys. JETP **7**, 661 (1958).

Translated by H. Kasha
245

*We are indebted to I. P. Ivanenko for the discussion of this problem and his valuable remarks.

†This assumption is strengthened by the absence of the high-energy nuclear-active component in the region around the beam. From the data of the second row of ionization chambers of the core detectors,[3] nuclear-active particles with energy $\geq 10^{11}$ ev were observed in none of the 28 cases given in the table.

*As can be seen from the formula given above, the estimate is not very sensitive to the altitude H. It should furthermore be noted that the taking into account of the transverse momentum obtained by particles in the $\pi \to \mu$ decay does not greatly influence the estimate.

†This follows from the energy and momentum conservation laws.

SHIFT OF THE CURIE TEMPERATURE BY HYDROSTATIC COMPRESSION OF MANGANESE AND COBALT FLUORIDES

D. N. ASTROV, S. I. NOVIKOVA, and M. P. ORLOVA

All-Union Institute of Physico-technical and Electronic Measurements

Submitted to JETP editor May 30, 1959

J. Exptl. Theoret. Phys. (U.S.S.R.) **37**, 1197-1201 (November, 1959)

The shift of the Curie temperature in the antiferromagnetics MnF_2 and CoF_2, under the influence of hydrostatic compression, has been determined for polycrystalline specimens by measurement of the magnetic susceptibility and of the change of the coefficients of linear expansion at the transition temperatures. For MnF_2 the shift is $(1.5 \pm 0.2)°$ at pressure (1900 ± 100) atmos; for CoF_2 no shift was observed. The antiferromagnetic transition temperatures are respectively 68 and 39°K.

INTRODUCTION

THE change of the Curie temperature of ferromagnetics under the influence of hydrostatic compression has been investigated repeatedly (cf., for example, the bibliography in the work of Patrick[1]). The effect of hydrostatic compression on the antiferromagnetic manganese telluride (an intermetallic compound) was studied by Grazhdankina[2] at room temperature. The amount of the shift of Curie temperature for antiferromagnetic substances appeared to be much larger than for ferromagnetics. It seemed interesting to investigate the change of Curie temperature for typical antiferromagnetic substances, for example ionic crystals.

To this end, measurements of the shift of Curie temperature of MnF_2 and CoF_2, under the influence of hydrostatic compression, were undertaken by two methods: by a shift of the magnetic susceptibility curve, and by calculation by means of the relation, known from thermodynamics,[3]

$$dT/dp = 3VT\Delta\alpha/\Delta c_p, \qquad (1)$$

where $\Delta\alpha$ and Δc_p are respectively the jump in the coefficient of thermal expansion and the jump in the specific heat at constant pressure at the transition point.

The measurements were made on polycrystalline specimens of manganese fluoride and of cobalt fluoride. The antiferromagnetism of MnF_2 was discovered by Bizette and Tsai.[4] Its antiferromagnetic transition temperature is 68°K. The antiferromagnetism of CoF_2 was established by Erickson.[5] The antiferromagnetic transition temperature is 38°K.[6]

METHOD

The measurements of magnetic susceptibility were made by Faraday's method, with balance and cryostat like those described in the work of Borovik-Romanov and Kreĭnes.[7] There was a change in construction in that the pulling of the balance was accomplished with a tungsten filament of diameter 0.2 mm. Consequently the balance could stand a load of the order of 20 grams. Furthermore there was introduced a zero corrector, consisting of a tungsten filament of diameter 0.1 mm bent to U shape. One end of it was fastened to the beam of the balance, the other was brought out of the vacuum jar through a sylphon seal.

The apparatus permitted measurements from 300°K to 10°K. The temperature measurement was made by means of a copper-constantan thermocouple, which was calibrated by comparison with a platinum resistance thermometer over the whole temperature range from 20 to 300°K. To increase the accuracy of the temperature determination, the "cold" junctions of the thermocouple were placed in an ampoule held at the triple point of water. The precision of the temperature measurement was estimated as ± 0.2° at hydrogen temperatures and ± 0.1° at nitrogen. The pressure was produced by the method of Lazarev,[8] with ice in a bomb. The bomb was manufactured of beryllium bronze with subsequent heat treatment. The pressure created was of the order of 1900 ± 100 kg/cm^2.

The specimens were made from a powder of "chemically pure" grade. To remove sorbed water, the powder was dried in a vacuum by heating to 150°C. The dried powder was pressed under a pressure of about 15000 atm to cylindrical specimens of diameter about 2.5 mm and length 4 mm. To pro-

tect the specimen from the effect of water, its surface was coated with several layers of BF-4 gum, which was subsequently polymerized. It was established that the coating of the specimen with gum did not change the temperature dependence of the magnetic susceptibility $\chi(T)$.

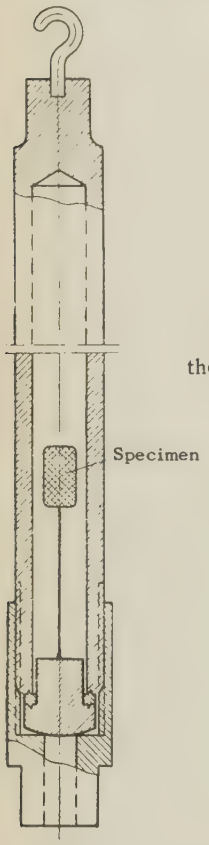

FIG. 1. Schematic sketch of the bomb with the specimen.

The specimen prepared by this method was placed in the bomb (Fig. 1). The bomb with the specimen was suspended on the balance. Three series of measurements were made on each fluoride. The magnetic susceptibility of the specimen was measured in the bomb without pressure, then with pressure, and again without pressure, to verify the absence of irreversible changes in the specimen. The repeated measurements without pressure gave values of the magnetic susceptibility in agreement with the initial values.

The measurements were made on two specimens of manganese fluoride and three of cobalt fluoride. The error of the relative measurements of susceptibility was less than ±1%. In the calculation of the value of the magnetic susceptibility of the specimens, a correction was introduced for the susceptibility of the bomb and the water. At the antiferromagnetic transition temperature it amounts to 2.5% of the susceptibility of the MnF_2 specimen and 10% of the susceptibility of the CoF_2 specimen.

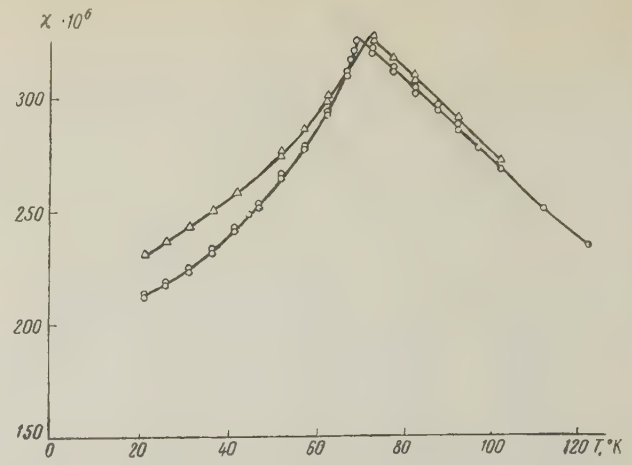

FIG. 2. Dependence of the magnetic susceptibility on temperature for MnF_2: Δ – with pressure; o – without pressure.

All the basic measurements were made in a field of about 3500 oe.

To determine the shift of the Curie temperature from the relation (1), it is necessary to know the values of the jumps in specific heat and in the coefficient of thermal expansion, Δc_p and $\Delta\alpha$. The value of Δc_p is known from specific heat measurements with manganous fluoride and cobaltous fluoride.[9] The coefficients of linear expansion of these substances had not been measured previously. We made a measurement of the coefficients of thermal expansion in the temperature range from 22 to 200° K for MnF_2 and from 22 to about 130° K for CoF_2, on a low-temperature dilatometer of Strelkov's design.[10] The specimen was made by the same method as for the magnetic susceptibility measurement, except that it was not coated with the layer of gum. It was a cylinder of diameter 5 mm and length 9 mm.

RESULTS

Measurements on MnF_2. The curves in Fig. 2 show the dependence of the magnetic susceptibility of manganese fluoride on temperature with and without pressure. The curves in the absence of pressure coincide with the $\chi(T)$ curves for unpressed powder (the values of χ corresponding to this curve were obtained on the same specimen before application of the pressure and after release of the pressure). The branches of the curve above the antiferromagnetic transition temperature are displaced parallel to one another. The left branches of the curve, corresponding to manganese fluoride in the antiferromagnetic state, are very different. The curve corresponding to the measurement under pressure is higher. We have not found a satisfactory explanation of this phenomenon.

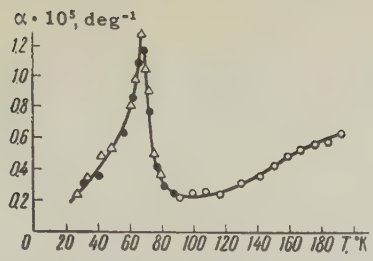

FIG. 3. Dependence of the coefficient of linear expansion on temperature for MnF_2: Δ – for specimen no. 1 in a hydrogen bath; ● – for specimen no. 2 in a hydrogen bath; ○ – for specimen no. 2 in a nitrogen bath.

It is evident from comparison of the curves that the shift of the Curie temperature under the influence of hydrostatic compression (at pressure of 1900 ± 100 kg/cm^2) amounts to (1.5 ± 0.2)°, or $dT/dp = (0.8 \pm 0.1) \times 10^{-3}$ deg/(kg/cm^2).

The antiferromagnetic transition temperature is 68°K. Figure 3 shows the dependence on temperature of the linear coefficient of expansion. The measurements were made on two specimens: on specimen No. 1 in a hydrogen bath, and on specimen No. 2 in hydrogen and nitrogen baths. The antiferromagnetic transition temperature from measurements of the coefficient of expansion can be taken as 67.5°. For the jump of the coefficient of thermal expansion, the value 1.2×10^{-5} deg^{-1} was obtained.

The value of the jump of specific heat, Δc_p, was determined from the measurements of Adams and Stout[9] and was equal to 2.4 cal/mole-deg.

For MnF_2, the calculated value of dT/dp according to formula (1) was equal to $+0.78 \times 10^{-3}$ deg/(kg/cm^2).

Measurements on CoF_2. Magnetic susceptibility measurements were made on three specimens of CoF_2. Within the limits of error, no shift of the $\chi(T)$ curves with pressure was observed. The antiferromagnetic transition temperature is 39.0°. The left branch of the $\chi(T)$ curve corresponding to the measurements under pressure is above the curve without pressure, as was the case also for MnF_2.

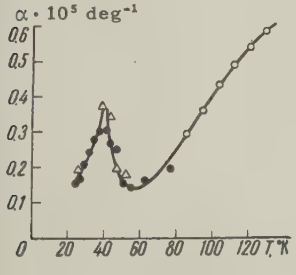

FIG. 4. Dependence of the coefficient of linear expansion on temperature for CoF_2. The symbols are the same as in Fig. 3.

Figure 4 shows the dependence of the linear coefficient of expansion on temperature, measured on two specimens. The antiferromagnetic transition temperature from measurements of the coefficient of expansion is 40.0°. The value obtained for the jump of the coefficient of thermal expansion for CoF_2 was 0.2×10^{-5} deg^{-1}.

The value of the jump of specific heat, Δc_p, was also determined from the measurements of Adams and Stout[9] and corresponds to 3 cal/mole-deg.

For CoF_2 the calculated value of dT/dp was equal to 0.09×10^{-3} deg/(kg/cm^2), at pressure (1900 ± 100) kg/cm^2. The shift should be +0.2, i.e., of the order of the error in the temperature measurement, and could scarcely be observed with our apparatus.

DISCUSSION OF RESULTS

It must be mentioned that the values of the antiferromagnetic transition temperatures of MnF_2 and CoF_2 determined by the two methods differ by 2°. This difference occurs for both salts. The discrepancy exceeds the error of the temperature measurements in either of the methods; it can be attributed to a difference in the thermocouple calibrations.

In the measurement of the coefficients of thermal expansion near the Curie point, larger anomalies were observed.

TABLE I

Substance	Curie temperature, °K	$10^6 \Delta\alpha$, deg^{-1}
MnO	122	50 [11]
CoO	293	12 [11]
FeO	193	25 [11]
MnF_2	68	12
MnTe	310	4 [12]
CoF_2	39	2

Table I gives approximate values of the jumps in the coefficient of thermal expansion, $\Delta\alpha$, at the antiferromagnetic transitions. The values of $\Delta\alpha$ for MnF_2 are of the same order as for other antiferromagnetics, such as MnO, CoO, and FeO. The value of $\Delta\alpha$ for CoF_2 is much smaller.

It should be mentioned that in the measurements of the magnetic susceptibility of the fluoride specimens at various fields under pressure, starting at 300 oe, we observed no deviation from linearity in the dependence of magnetic moment on field, such as would correspond to a piezomagnetic effect.[13,14] This may be attributed to the fact that we used polycrystalline specimens and a hydrostatic compressive strain. Under these conditions, piezomagnetism could be observed only in the case of large elastic anisotropy in MnF_2 and CoF_2.

For comparison of our results on the shift of the Curie temperature under hydrostatic compression, we present Table II.

TABLE II

Specimens	Curie temperature	
	°K	deg/1000 atmos
Co	1393	0±0.1 [1]
Fe	843	0±0.1 [1]
Ni	633	+0.35±0.02 [15]
MnTe	310	+2±0.4 [2]
MnF_2	68	+0.73±0.1
CoF_2	39	0±0.1

It is evident that for MnF_2 the shift is larger than in ferromagnetics, and that in CoF_2 it is of the same order as in ferromagnetics.

[1] L. Patrick, Phys. Rev. **93**, 384 (1954).

[2] N. P. Grazhdankina, JETP **33**, 1524 (1957), Soviet Phys. JETP **6**, 1178 (1958).

[3] L. D. Landau and E. M. Lifshitz, Статистическая физика, (Statistical Physics), Gostekhizdat, 1951.

[4] H. Bizette and B. Tsai, Compt. rend. **209**, 205 (1939).

[5] R. A. Erickson, Phys. Rev. **90**, 779 (1953).

[6] Astrov, Borovik-Romanov, and Orlova, JETP **33**, 812 (1957), Soviet Phys. JETP **6**, 626 (1958).

[7] A. S. Borovik-Romanov and H. M. Kreĭnes, JETP **29**, 790 (1955), Soviet Phys. JETP **2**, 657 (1956).

[8] B. G. Lazarev and L. S. Kan, JETP **14**, 470 (1944).

[9] J. W. Stout and H. F. Adams, J. Am. Chem. Soc. **64**, 1535 (1952).

[10] P. G. Strelkov and S. I. Novikova, Приборы и техника эксперимента (Instrum. and Meas. Engg.) **5**, 105 (1957).

[11] M. Foëx, Compt. rend. **227**, 193 (1948).

[12] N. P. Grazhdankina and D. I. Gurfel', JETP **35**, 907 (1958), Soviet Phys. JETP **8**, 631 (1959).

[13] A. S. Borovik-Romanov, JETP **36**, 1954 (1959), Soviet Phys. JETP **9**, 1390 (1959).

[14] I. E. Dzyaloshinskiĭ, JETP **33**, 807 (1957), Soviet Phys. JETP **6**, 621 (1958).

[15] A. Michels and S. R. de Groot, Physica **16**, 249 (1950).

Translated by W. F. Brown, Jr.
246

FORBIDDEN TRANSITIONS IN THE DEFORMED Tm^{169} *NUCLEUS*

É. E. BERLOVICH, V. N. KLEMENT'EV, V. G. FLEĬSHER, O. V. LARIONOV, F. Sh. MURTAZIN, and D. A. APOSTOLOV

Leningrad Physico-technical Institute, Academy of Sciences, U.S.S.R.

Submitted to JETP editor June 1, 1959

J. Exptl. Theoret. Phys. (U.S.S.R.) **37**, 1202-1206 (November, 1959)

Lifetimes of $(3.6 \pm 0.1) \times 10^{-8}$ sec and $(6.7 \pm 0.2) \times 10^{-7}$ sec were obtained by delayed-coincidence measurements for the 379 and 316 kev levels of Tm^{169} nucleus. The partial probabilities for eight transitions have been determined on the basis of these data and from data on the relative transition intensities from both levels and on the multipolarity ratios. For the 177-kev (E2), 177-kev (M1), 198-kev (E2), 198-kev (M1), 308-kev (E2), 240-kev (E1), and 260-kev (E1) transitions, which are forbidden with respect to the projection of the total angular momentum on the deformation axis, the delay factor comprises $10^3 - 10^4$ per unit forbiddenness, a value which differs significantly from the usual value $(10 - 100)$. The 63-kev (E1) transition, which is forbidden with respect to the projections of the orbital and spin momenta and also with respect to the quantum number that characterizes the oscillations along the deformation axis, is five orders of magnitude less probable than that predicted by Weisskopf's estimates. However, it is in good qualitative agreement with Nilsson's calculations of the probability for deformed nuclei.

1. INTRODUCTION

MIHELICH et al.[1] measured the lifetimes of three excited states of the Tm^{169} nucleus produced by electron capture in Yb^{169}. Furthermore, in addition to the known 316-kev isomer level, long lifetimes were obtained for the 379- and 473-kev levels (4.5×10^{-8} and 0.4×10^{-6} sec respectively). Hatch and Alburger showed in a later paper[2] that, in contradiction to the result of reference 1, the lifetime of the 473-kev level was less than 3×10^{-9} sec, and confirmed the presence of an isomer state for 379 kev.

Transitions from the 316-kev and 379-kev levels are transitions between levels with different states of internal motion and, as shown by analysis, are forbidden either with respect to the projection of the angular momentum on the deformation axis, or with respect to the asymptotic quantum numbers. At the present time the relative intensities of the partial transitions from each of these two levels have been sufficiently well determined,[3] together with the mixture ratios.[4] Therefore a knowledge of the exact values of the lifetimes of the levels is quite desirable for the purpose of comparing the values of the partial probabilities of the transitions with the theory. We have measured the lifetimes for the levels with energies of 316 and 379 kev with the aid of a double scintillation spectrometer with NaI(Tl) crystals and type FEU-33 photomultipliers.

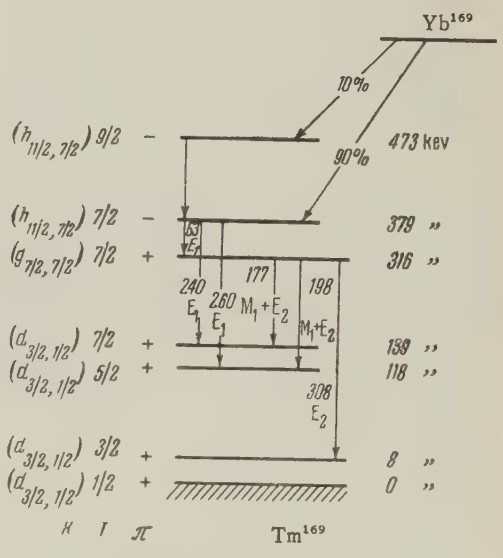

FIG. 1. $Yb^{169} - Tm^{169}$ conversion scheme.

2. THE 379-kev LEVEL

Figure 1 shows the Yb^{169} decay scheme taken from reference 3, in which only the transitions of interest to us are shown. In measuring the lifetimes of the 379-kev level, we used the characteristic 51-kev x-rays that accompany K-capture of Yb^{169}, and the 63-kev γ rays in a fast-slow coincidence circuit.[5] The delay was introduced in the x-ray registering channel. In addition to the x-rays of interest to us, which accompany the K capture at

the 379-kev level, the same channel registered also the x-rays that accompanied K-capture at the 473 kev level. The coincidences obtained thereby should correspond to the total lifetimes of the 379 and 473 kev levels. However, the error connected with the additional delay for capture at 473 kev is small, since the number of such captures is one-ninth of the number of captures at the measured level and furthermore, according to an estimate given in reference 2, the lifetime of the 473-kev level does not exceed 3×10^{-9} sec. This means that in measuring the lifetimes, of the order of several times 10^{-8} seconds, expected for the 379-kev level the error due to the 473-kev level does not exceed 1%.

Because of the close values of the x-ray and gamma energies (51 and 63 kev, respectively), pulses due to x-rays could be produced in the gamma channel. The number of "fast" coincidences is increased here by coincidences due to x-rays accompanying the internal conversion in 177 and 131 kev cascade transitions, as well as in those with energies of 198 and 110 kev. Actually, preliminary measurements with a double magnetic spectrometer have shown that the lifetimes of the corresponding levels of the lower rotational band (131 and 118 kev) are of the order of 10^{-9} sec and less. On the other hand, coincidences of these quanta with x-rays that accompany electron capture increase the number of delayed coincidences, owing to the long lifetime of the 316-kev level. When the lifetime of the 379-kev level is measured, these coincidences produce an additional background (on top of the random-coincidence background). This additional background is determined from the number of double coincidences in the "slow" part of the circuit by introducing long delays (0.6 to 1.1 microseconds).

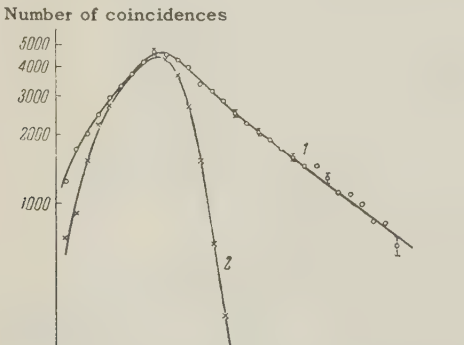

FIG. 2. Decay curve of the 379-kev state of Tm^{169}.

Figure 2 shows the coincidence curve for the 379-kev level of Tm^{169} (curve 1) and a "fast" coincidence curve obtained with a Lu^{173} source (curve 2). The half-life determined from the slope of curve 1 was found to be $T_{1/2} = (3.6 \pm 0.1) \times 10^{-8}$ sec and differs considerably from that given in reference 1 ($T_{1/2} = 4.5 \times 10^{-8}$ sec). This may be due to the inaccurate allowance for the background in that paper (the resolution time of the circuit used in reference 1 is greater than in our measurements). We indicate the magnitude of the statistical error.

3. THE 316-kev LEVEL

The lifetime of the 316-kev level was measured from the slope of the delayed-coincidence curve, with one channel registering 63-kev quanta and the other quanta with energies of 177 and 198 kev. A double-coincidence circuit was used with a resolution time of 1×10^{-7} sec. The delay was introduced in the first channel successively every 0.1 microsecond. The 2-microsecond twenty-section delay line was calibrated against an RK-2 cable. The measurement results are shown in Fig. 3. The half-life was found to be $(0.67 \pm 0.02) \times 10^{-6}$ sec, which coincided, within the limits of errors, with the result of reference 1, but which was closer to the results obtained in references 6 and 7.

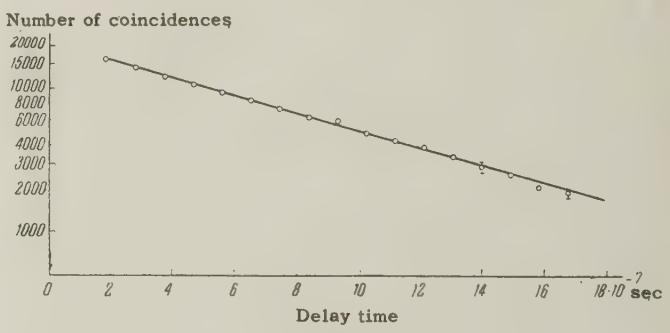

FIG. 3. Decay curve of the 316-kev state of Tm^{169}.

4. ANALYSIS OF THE EXPERIMENTAL RESULTS

From the data on the relative intensities of the 177, 198, and 308 kev γ lines, as well as on the 63, 240, and 260 kev lines, as given in the paper by Hatch, Boehm, et al.,[3] it is easy to obtain the partial times for these transitions, using the formula

$$\tau_{i\gamma} = (\tau_{\text{exp}} / I_{i\gamma}) \sum_{k=1}^{n} I_{k\gamma} (1 + \alpha_k),$$

where $\tau_{i\gamma}$ is the partial time of the γ transition, $I_{i\gamma}$ the relative intensity of the γ line, α_k is the internal conversion coefficient, τ_{exp} is the experimental lifetime of the level, and n is the number of discharge channels for the level.

The sixth column of Table I gives the partial lifetimes $(\tau_\gamma)_{\text{exp}}$ for the 316 and 379 kev levels.

TABLE I

Level energy, kev	Transition energy, kev	Type of transition	Relative intensity of γ line	α_{tot}	$(\tau_\gamma)_{exp}$, sec	$(\tau_\gamma)_W$, sec	$F=(\tau_\gamma)_W/(\tau_\gamma)_{exp}$
	177	$E2$	5.6	0.54	$2.9\cdot10^{-5}$	$8.3\cdot10^{-8}$	$2.9\cdot10^{-3}$
	177	$M1$	25	0.37	$6.4\cdot10^{-6}$	$5.8\cdot10^{-12}$	$0.9\cdot10^{-6}$
316	198	$E2$	4.6	0.45	$3.5\cdot10^{-5}$	$4.8\cdot10^{-8}$	$1.4\cdot10^{-3}$
	198	$M1$	46	0.83	$3.5\cdot10^{-6}$	$4.1\cdot10^{-12}$	$1.2\cdot19^{-6}$
	308	$E2$	18	0.05	$9.0\cdot10^{-6}$	$5.2\cdot10^{-9}$	$0.58\cdot10^{-3}$
	63	$E1$	65	0.9	$1.1\cdot10^{-7}$	$1.2\cdot10^{-12}$	$1.1\cdot10^{-5}$
379	240	$E1$	1	0.03	$6.4\cdot10^{-6}$	$2.2\cdot10^{-14}$	$0.34\cdot10^{-8}$
	260	$E1$	8	0.03	$7.8\cdot10^{-7}$	$1.8\cdot10^{-14}$	$2.3\cdot10^{-8}$

The multipolarity data for 177 and 198 kev transitions were graciously supplied by V. M. Kel'man and V. A. Romanov.[4] The 177 and 196 kev transitions are mixed transitions of type M1 + E2, with the E2 admixture amounting to 18% in the former and 9% in the latter.

The conversion coefficients for the K and L shells were taken from the tables of Sliv and Band.[8] For the M + N shells we assumed a value of $0.3\,\alpha_L$, where α_L is the conversion coefficient on the L shell. The theoretical value $(\tau_\gamma)_W$ was calculated by the Weisskopf formulas.[9] The last column of the table gives the F-factor that characterizes the slowing down of the transition, relative to that predicted by Weisskopf's formulas.

It is seen from the table that the electric quadrupole transitions are slowed down by approximately three orders, and the magnetic dipole transitions by approximately six orders of magnitude. The 240 and 260 kev electric dipole transitions are slowed down by ~ 8 orders, and the 63-kev transition by ~ 5 orders.

The long lifetime of the 316-kev level was attributed in reference 10 to forbiddenness with respect to the quantum number K, which represents the projection of the spin of the nucleus on its prolate axis. Actually, as can be seen from the decay scheme of Tm^{169} in Fig. 1, transitions with energies 177, 198, and 308 kev correspond to a change in K by three units (from $7/2$ to $1/2$). According to the classification introduced by Alaga et al.[11] the degree of forbiddenness is characterized by a number $\nu = \Delta K - L$, where L is the multipolarity. Thus, $\nu = 1$ for electric quadrupole transitions from the 316-kev level, and $\nu = 2$ for magnetic dipole transitions. From the data in Table I it is seen that the unit of forbiddenness corresponds, for this level, to a slowing down by approximately three orders.

Since $K = 7/2$ for the 379-kev level, 240 and 260 kev, γ transitions to the levels with $K = 1/2$ are also slowed down because of K-forbiddenness. For these transitions, one unit of forbiddenness causes a slowing down by ~ 4 orders. Usually one unit of forbiddenness with respect to the quantum number K reduces the transition probability by a factor of $10 - 100$.[11] In the case of Tm^{169}, however, this probability is decreased by a factor of 1000 — 10,000. This may be connected with the peculiarity of the Tm^{169} ground-state band, for which $K = 1/2$.

As to the 63-kev transition, as can be seen from the decay scheme, it is not forbidden with respect to the projection of the angular momentum. Nevertheless, the probability of this transition is reduced by 5 orders. The cause of this effect must be sought in possible forbiddenness with respect to other quantum numbers, which characterize the motion of the nucleons in strongly deformed nuclei, which include also the Tm^{169} nucleus with a deformation parameter of ~ 0.28.[12] These quantum numbers are as follows:[13] N — principal oscillator quantum number, n_z — quantum number of the nucleon oscillations along the prolate axis, and also Ω, Λ, and Σ — quantum numbers that represent the projections of the total, orbital, and spin angular momenta of the particle on the prolate axis of the nucleus.

As follows from Fig. 1 and Nilsson's paper,[13] the quantum numbers, Ω, Λ, Σ, N, and n_z should be assigned the values $7/2$, 4, $-1/2$, 4, and 0 respectively for the 316-kev level and $7/2$, 3, $1/2$, 5, and 2 respectively for the 379-kev level.

TABLE II

$\Delta\Omega = \Omega_f - \Omega_i$	$\Delta\Lambda = \Lambda_f - \Lambda_i$	$\Delta\Sigma = \Sigma_f - \Sigma_i$	$\Delta N = N_f - N_i$	$\Delta n_z = n_{zf} - n_{zi}$
0	1	—1	—1	—2
$\pm(L-1)$	$\pm(L-1)$	0	$L, (L-2), \ldots, -L$	±1
0	0	0	±1	—1

*The index f denotes the 316-kev level, while i denotes the 379-kev level.

The upper row of Table II gives the change in the quantum numbers due to a 63-kev γ transition, while the lower line gives the selection rules obtained by Voĭkhanskiĭ[14] for E1 transitions. It is seen from the table that the 63-kev transition

is forbidden with respect to the quantum numbers Λ, Σ, and n_z (one unit of forbiddenness with respect to each of these quantum numbers).

As shown in reference 14, a one-unit forbiddenness decreases the transition probability by a factor of 10 — 100, which indeed takes place in our case. On the other hand, for a 63-kev transition that is allowed with respect to the quantum number K, the probability can be calculated from the Nilsson formulas [see Eqs. (29) and (35) of reference 13]. The calculation yields $(\tau_\gamma)_N = 2.3 \times 10^{-8}$ sec, which agrees[14] with the experimental value to a degree that is usual for such cases, namely $(\tau_\gamma)_N/(\tau_\gamma)_{exp} = 0.21$.

Thus, the slowing down of the 63-kev transition is connected with forbiddenness with respect to the asymptotic quantum numbers, and the long lifetime of the 379-kev level is explained by simultaneous action of K-forbiddenness for the 240 and 260-kev transitions and forbiddenness with respect to the numbers Λ, Σ, and n_z for the 63-kev transition.

[1] Mihelich, Ward, and Jacob, Phys. Rev. **103**, 1285 (1956).

[2] E. N. Hatch and D. E. Alburger, Phys. Rev. **110**, 1116 (1958).

[3] Hatch, Bòehm, Marmier, and Du Mond, Phys. Rev. **104**, 745 (1956).

[4] Kel'man, Metskhvarishvili, Preobrazhenskiĭ, Romanov, and Tuchkevich, JETP **37**, 639 (1959), Soviet Phys. JETP **10**, 456 (1960).

[5] É. E. Berlovich, Izv. Akad. Nauk SSSR, Ser. Fiz. **20**, 1438 (1956), Columbia Tech. Transl. p. 1315.

[6] E. Fuller, Proc. Phys. Soc. **63A**, 1044 (1950).

[7] Martin, Jensen, Hughes, and Nicols, Phys. Rev. **82**, 579 (1951).

[8] L. A. Sliv and I. M. Band, Таблицы коэффициентов внутренней конверсии гамма-излучения (Tables of Coefficients of Internal Conversion of Gamma Radiation), U.S.S.R. Acad. Sci., 1956.

[9] J. Blatt and V. Weisskopf, Theoretical Nuclear Physics, Wiley, N.Y., 1952, ch. XII, (Russ. Transl. IIL, 1954).

[10] S. Koicki and A. Koicki, Bull. Inst. Nucl. Sci. Boris Kidrich **6**, 1 (1956).

[11] Alaga, Alder, Bohr, and Mottelson, Dan. Mat. Fys. Medd. **29**, 9 (1955).

[12] B. Mottelson and S. Nilsson, Проблемы современной физики (Problems of Modern Physics), No. 1, 186 (1956)(Russ. Transl.).

[13] S. Nilsson, Dan. Mat. Fys. Medd. **29**, 16 (1955).

[14] M. E. Voĭkhanskiĭ, JETP **33**, 1004 (1957), Soviet Phys. JETP **6**, 771 (1958).

Translated by J. G. Adashko
247

CROSS SECTION FOR THE PRODUCTION OF Fm^{250} *IN THE REACTIONS* $Pu^{241}(C^{13}, 4n)Fm^{250}$ *AND* $U^{238}(O^{16}, 4n)Fm^{250}$

V. V. VOLKOV, L. I. GUSEVA, B. F. MYASOEDOV, N. I. TARANTIN, and K. V. FILIPPOVA

Submitted to JETP editor June 1, 1959

J. Exptl. Theoret. Phys. (U.S.S.R.) **37**, 1207-1211 (November, 1959)

The cross section for production of Fm^{250} in the reaction $Pu^{241}(C^{13}, 4n)$ and $U^{238}(O^{16}, 4n)$ has been determined as a function of the energy of bombarding particles. The comparison of the cross section for production of Fm^{250} with the fission cross section in these reactions shows that in the overwhelming majority of cases the excited compound Fm^{254} nucleus undergoes fission, and only in a few cases does deexcitation take place as a result of neutron emission. The maximum cross section for the production of Fm^{250} by irradiation with oxygen or carbon ions is 1×10^{-30} and 5×10^{-30} cm^2 respectively. The difference between the cross sections is probably due to the effect of the Coulomb barrier.

THE present work is a part of research done on the synthesis of transuranic elements with the aid of multiply-charged ions (see references 1 — 4).

The compound nucleus formed as a result of collision between a multiply-charged ion and a heavy nucleus disintegrates essentially either by fission[5] or by neutron emission.[1-4,6] A study of the competition between these processes as a function of the energy and nuclear characteristics (Z and A) of the colliding particles is of great interest, particularly for the synthesis of new transuranic elements.

1. THE REACTION $Pu^{241}(C^{13}, 4n)Fm^{250}$

In the present investigation we studied the reaction $Pu^{241}(C^{13}, 4n)Fm^{250}$ with the aid of the same Pu^{241} targets as were used in the experiments on the production of the 102nd element.[2] The Pu^{241} was deposited on thin (1.5 — 2) niobium foils; the layer thickness amounted to 90 and 200 $\mu g/cm^2$. To prevent possible crumbling of the substance, the Pu^{241} was covered from above with a layer of copper approximately 70 $\mu g/cm^2$ thick, deposited by evaporation in vacuum. The targets were irradiated in the internal beam of the cyclotron. The reaction products were gathered by the same procedure as used by Flerov et al.[2] to obtain the 102nd element. This procedure is based on causing the heavy ions to impart to the compound nucleus so large a momentum that the reaction products are knocked out from a layer of target of noticeable thickness. The scheme of the experiment is shown in Fig. 1.

Such a procedure has made it possible to employ the same target many times and to avoid working with highly active matter. The reaction products were gathered on a 15 μ aluminum foil, placed several millimeters from the target. The irradiation was at different cyclotron radii. The energy of the $^{+4}C^{13}$ ions was determined from the absorption in aluminum filters. The intensity of the current of the $^{+4}C^{13}$ ions was 0.3 — 0.5 μa.

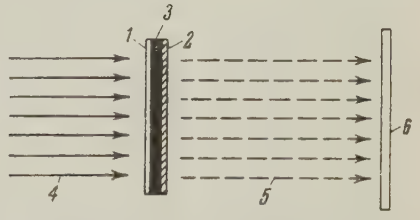

FIG. 1. Arrangement of the experiment. 1 — niobium foil 1.5 μ thick; 2 — protective copper layer (70 $\mu g/cm^2$); 3 — layer of Pu^{241} (90 or 200 $\mu g/cm^2$); 4 — $^{+4}C^{13}$ ions; 5 — Fm nuclei and other reaction products; 6 — aluminum collector 15 μ thick.

After irradiation, which lasted for 45 — 60 minutes, the collector with the reaction products was removed from the cyclotron and subjected to radiochemical analysis. The collector was dissolved in concentrated hydrochloric acid, to which 400 μg of lanthanum and known amounts of Am^{241} were introduced as a carrier to determine the fermium chemical yield; the lanthanum fluoride was then precipitated. The fluorides were decomposed with nitric acid. The nitrate solution was deposited on a platinum disc, which after drying and roasting was placed in an ionization chamber with spherical electrodes. The pulses from the ionization chamber were fed to a 50-channel amplitude analyzer. The Fm^{250} was identified by the energies of the α particles and by the half-life (E = 7.43 Mev, $T_{1/2}$ = 30 min[7]). In the calculation of the reaction cross section, we took into account the effectiveness with which the Fm^{250}

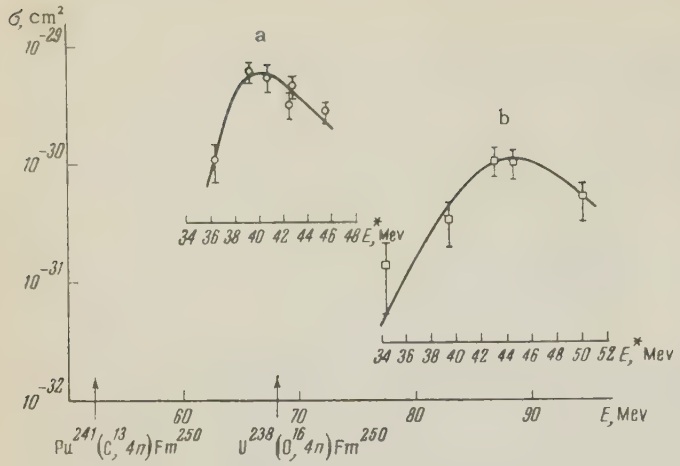

FIG. 2. Reaction cross sections for the production of Fm^{250} as a function of the energy E of the bombarding particles. a – The reaction $Pu^{241}(C^{13}, 4n)Fm^{250}$; b – the reaction $U^{228}(O^{16}, 4n)Fm^{250}$. The arrows mark the reaction thresholds.

nuclei were knocked out from the target matter. To estimate the fraction of the Fm^{250} nuclei knocked out from the target, we used experimental results on the determination of the range of the nuclei of the radon formed in the reaction $Au^{197}(N^{14}, xn)$, where $x = 4 - 6$, in aluminum and in copper. A recalculation of these data for the $Pu^{241}(C^{13}, 4n)Fm^{250}$ reaction was based on a relation derived by Firsov. The basic principles of this relation were verified in experiments on the ranges of the nuclei formed in the reactions under the influence of 14-Mev neutrons (see Appendix).

The values obtained for the cross section of the $Pu^{241}(C^{13}, 4n)Fm^{250}$ reaction as a function of the energy of bombarding particles are shown in Fig. 2.

2. THE REACTION $U^{238}(O^{16}, 4n)Fm^{250}$

In the investigation of this reaction we used targets comprising layers of uranium, deposited by evaporation in vacuum on thin (2μ) nickel foils. To avoid crumbling of the uranium, which is possible when operating with thick layers, we used "packets" of pairs of nickel foils with the uranium layers facing each other. The total thickness of the uranium layer reached ~ 1.3 mg/cm^2. The irradiation was with $^{+5}O^{16}$ ions. The irradiation procedure, the subsequent chemical processing, and the identification of the Fm^{250} were the same as in the investigation of the preceeding reaction. In individual cases, the resultant reaction products were separated chromatographically. A study of the Fm^{250} yield was also made by irradiating thick (15μ) uranium foils. The cross section for the production of Fm^{250} could be estimated in this case by differentiating the curve of the energy dependence of the yield. The data obtained were found to be in satisfactory agreement with the results of experiments on the irradiation of thin targets.

The cross section of the reaction $U^{238}(O^{16}, 4n)Fm^{250}$ is also shown in Fig. 2 as a function of the oxygen-ion energy. This figure shows, along with the energy of the bombarding particles, also the excitation energy (E*) of the compound Fm^{254} nuclei produced in the reactions $Pu^{241} + C^{13}$ and $U^{238} + O^{16}$. The errors indicated are statistical counting errors. Errors in the measurement of the ion current and of the chemical yields of the reaction products are insignificant. The total measurement error in the case of the $Pu^{241}(C^{13}, 4n)Fm^{250}$ may be 1.5 or 2 times greater, owing to inaccuracies in the determination of the fraction of the knocked-out Fm^{250} nuclei.

The results obtained in the present work for the cross sections of the reactions $Pu^{241}(C^{13}, 4n)Fm^{250}$ and $U^{238}(O^{16}, 4n)Fm^{250}$ are in agreement with those obtained by others.[8,9]

It must be noted that in the investigation of the products of the reaction $U^{238} + O^{16}$, the isotope Cf^{246} was identified in amounts considerably in excess of the Cf^{246} produced through α decay of Fm^{250}. It is obvious that in this case the Cf^{246} is produced directly via the reaction $U^{238}(O^{16}, \alpha 4n)Cf^{246}$, the cross section of which has tentatively been estimated to be ten times the cross section of the reaction $U^{238}(O^{16}, 4n)Fm^{250}$.

DISCUSSION OF RESULTS

A comparison of the cross section for production of Fm^{250}, through bombardment of Pu^{241} or U^{238} by C^{13} and O^{16}, with the fission cross sections for these reactions shows that in the overwhelming majority of cases the excited compound nucleus Fm^{254} experiences fission, and only in a negligible number of cases is the excitation removed by emission of neutrons. Comparison of the cross sections of the various reactions (see references 3 and 4) shows that the cross section of neutron-evaporation reaction diminishes with increasing Z of the compound nucleus. Thus, for example, in bombardment by carbon ions the maximum cross section of the reaction of evaporation of four neutrons amounts to 8×10^{-29} cm^2 in the case of production of the compound nucleus Cm^{244} (reference 4), 6×10^{-29} cm^2 in the case of Cf^{250} (reference 3), and 5×10^{-30} cm^2 in the case of Fm^{254}. A detailed precise evaluation of the competition between the neutron-evaporation and fission processes requires not only the comparison of the magnitudes of the neutron-evaporation cross sections, but also allowance for such factors as the dependence of the cross section for the production of the compound nucleus on the energy and the probability of evaporation of

a given number of neutrons at a given excitation energy.

In the case of the $Pu^{241}(C^{13}, 4n)Fm^{250}$ and $U^{238}(O^{16}, 4n)Fm^{250}$ reactions we deal with the production of the same compound nucleus Fm^{254} with subsequent evaporation of four neutrons. As can be seen from the diagram, the cross section for the production of Fm^{250} by irradiation with oxygen ions is found to be several times smaller than in irradiation by carbon ions. The reduction in the cross section of the reaction in irradiation with oxygen ions is due to the influence of the Coulomb barrier. The large Coulomb barrier in the case of the reaction $U^{238} + O^{16}$ causes a large shift in the maximum of the reaction of evaporation of four neutrons, towards the higher energies. At these excitation energies the evaporation of four neutrons becomes less probable and takes second place to the more probable reaction of evaporation of five neutrons.

It should be noted that in the present experiments we observed no formation of other fermium isotopes, besides Fm^{250}. Therefore, the fermium isotope which we obtained earlier[10] by bombarding uranium with oxygen ions is obviously Fm^{250}.

In conclusion, the authors express their deep gratitude to Prof. G. N. Flerov for continuous attention and interest in this work.

APPENDIX

We give below the results of experiments on the determination of the ranges of the nuclei produced in nuclear reactions. In one of these experiments thin layers of Au^{197}, coated on the side opposite to that of the beam, with thin layers of aluminum or copper, were irradiated with N^{14} ions of known energy. The nuclei of the radon produced by the $Au^{197}(N^{14}, xn)$ reaction were knocked out of the layer of gold and, partially passing through the layer of absorber (Al or Cu), entered the collector. The distribution of the ranges of the radon nuclei in aluminum and copper was determined from the ratios of the intensities of the radon decay-product α radiations in absorber layers of different thicknesses to that in the collector.

Analogous experiments were carried out by A. F. Georgobiani, N. I. Tarantin, and G. N. Flerov in 1954. They determined the ranges of nuclei produced upon irradiation of various substances (Al, Si, Cu, Ag, and Sb) by 14-Mev neutrons. The experimental setup was similar to that shown in Fig. 1. The average range of the reaction products in the target substance was determined by comparing the numbers of radioactive nuclei produced in (n, 2n) and (n, p) reactions in the target and on a Plexiglas collector.

The results obtained, both in the case of irradiation with N^{14} ions and in the case of irradiation with 14-Mev neutrons, were found to be in satisfactory agreement with the formula obtained in 1954 by O. B. Firsov for the ranges of atoms at initial velocities of $\sim 10^7 - 10^8$ cm/sec. In the derivation of this formula the author described the interaction of two colliding atoms by means of a potential approximated by a function inversely proportional to the square of the distance.[11] The value obtained is

$$R = 0.5A_2(A_1 + A_2)(Z_1 + Z_2)^{1/2}E / A_1Z_1Z_2.$$

where R is the range of the atom, expressed in $\mu g/cm^2$, Z_1A_1 and Z_2A_2 are the atomic number and the mass number of the moving atom and of the atoms of the retarding medium, and E is the kinetic energy of the moving atom, expressed in kev. The mean square spread of the ranges of the radon nuclei, formed in the reaction $Au^{197}(N^{14}, xn)$ was found to be 0.4 of the average range.

[1] Gerlit, Guseva, Myasoedov, Tarantin, Filippova, and Flerov, JETP **33**, 339 (1957), Soviet Phys. JETP **6**, 263 (1958).

[2] Flerov, Polikanov, et al. Dokl. Akad. Nauk SSSR **120**, 73 (1958), Soviet Phys.-Doklady **3**, 546 (1959).

[3] Volkov, Guseva, Pasyuk, Tarantin, Filippova, JETP **36**, 762 (1959), Soviet Phys, JETP **9**, 536 (1959).

[4] Guseva, Myasoedov, Tarantin, and Filippova, JETP **37**, 973 (1959), Soviet Phys. JETP **10**, 694 (1960).

[5] S. M. Polikanov and V. A. Druin, JETP **36**, 744 (1959), Soviet Phys. JETP **9**, 522 (1959).

[6] Baraboshkin, Karamyan, and Flerov, JETP **32**, 1298 (1957), Soviet Phys. JETP **5**, 1059 (1957).

[7] Amiel, Chetham-Strode, Choppin, Ghiorso, Harvey, Holm, and Thompson, Phys. Rev. **106**, 553 (1957).

[8] Sikkeland, Thompson, and Ghiorso, Phys. Rev. **112**, 543 (1958).

[9] Perelygin, Donets, and Flerov, JETP **37**, 1558 (1959), Soviet Phys. JETP **10**, in press.

[10] Guseva, Filippova, Gerlit, Druin, Myasoedov, and Tarantin, Атомная энергия (Atomic Energy) **2**, 50 (1956).

[11] O. B. Firsov, Dokl. Akad. Nauk SSSR **91**, 515 (1953).

Translated by J. G. Adashko
248

HALL EFFECT IN FERRITES NEAR THE CURIE POINT

K. P. BELOV and E. P. SVIRINA

Moscow State University

Submitted to JETP editor June 2, 1959

J. Exptl. Theoret. Phys. (U.S.S.R.) **37**, 1212-1216 (November, 1959)

The Hall emf was measured in nickel-zinc and manganese ferrites (both in polycrystalline and single-crystal specimens) in the vicinity of the Curie temperature. A new method for the determination of the ordinary Hall constant is proposed. The calculated values of the carrier density and mobility in the investigated ferrites conform in order of magnitude with the values obtained for nonferromagnetic semiconductors. The Hall emf is one order of magnitude greater in a single-crystal specimen of manganese ferrite than in a polycrystalline specimen.

1. INTRODUCTION

UNTIL now there have been very few works devoted to the study of the Hall effect in ferrites.[1,2] Yet, analysis of this effect is of great interest from the point of view of disclosing the nature of conductivity of ferrites and the interdependence of their magnetic and electric properties.

We have chosen to investigate the Hall effect near the Curie point because it is here that the spontaneous magnetization varies very abruptly, and consequently it is here that the influence of this change on the electric phenomena in ferrites should be most clearly pronounced. We have measured the temperature dependence of the Hall emf, of the electric resistance and of the spontaneous magnetization in nickel-zinc and manganese ferrites (in polycrystalline and single crystals specimens) within a temperature range close to the Curie point.

The electric resistance of the ferrites under study was not very high at these temperatures, and this allowed a dc measurement of the Hall emf by means of a PPTV-1 potentiometer. In order to obtain the exact value of the Hall current density, the sample was prepared by the Vol'kenshteĭn and Fedorov method:[3] a ferrite bar was cut in three (cf. Fig. 1). Thin mica wafers were placed between the parts and all three pieces were then glued together. Magnetization was measured using differential ballistic coils. The specimen was placed in a bifilar winding and inserted together with the winding inside the solenoid.

The primary Hall current was made to flow in the z direction through the whole shaded surface by means of contacts 1-1. The Hall emf was measured along the y axis (contacts 2-2). The contacts were in the form of silver layers deposited on the surface of the ferrite by firing-on a silver paste. The Hall current of 10 ma was within the range where Ohm's law was obeyed by the ferrites under study. Electromotive forces clearly dependent on the magnetic field were compensated by means of an additional difference of potentials. The measurements were taken with the specimen under vacuum. Under these conditions, the hysteresis of the specimen's electrical properties during the course of heating and cooling was negligible.

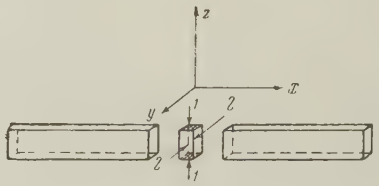

FIG. 1

2. NICKEL-ZINC FERRITE (37.5% NiO, 12.5% ZnO, 50% Fe_2O_3)

Figures 2 and 3 show the dependence of the Hall emf and of the magnetization on the magnetic field at different temperatures (Curie point ~ 40° C). The spontaneous magnetization I_S and the spontaneous Hall emf E_S in the vicinity of the Curie point were determined by the method of thermodynamic coefficients described previously.[4,5] The spontaneous (or ferromagnetic) Hall constant R_S, defined by the relation $E_S = R_S I_S$, decreased with increasing temperature and approached some constant value at the Curie temperature (cf. Fig. 4). Figure 5 shows the dependence of the constant R_S

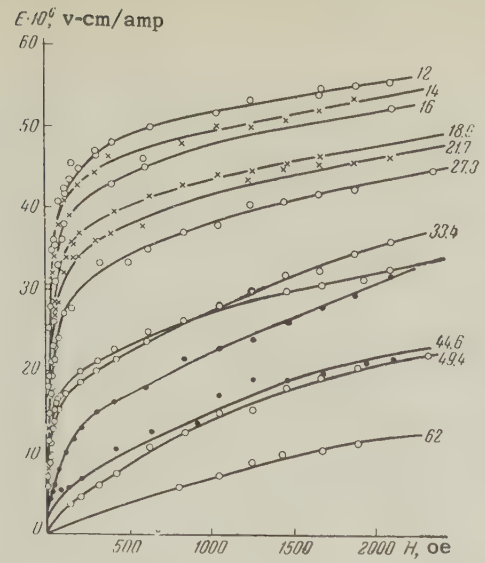

FIG. 2. Dependence of the Hall emf on the magnetic field in polycrystalline nickel-zinc ferrite at different temperatures (the numbers adjacent to the curves indicate °C).

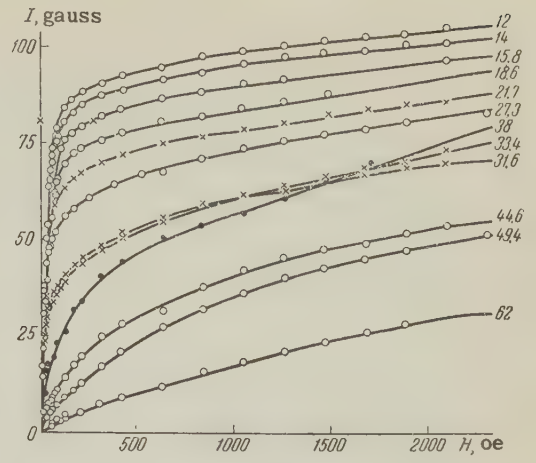

FIG. 3. Magnetization isotherms for nickel-zinc ferrite (the numbers adjacent to the curves indicate °C).

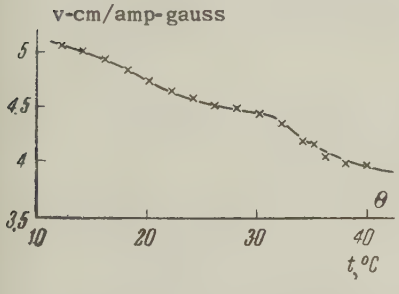

FIG. 4. Temperature dependence of the spontaneous Hall constant ($10^7 \cdot R_s$) for the nickel-zinc ferrite.

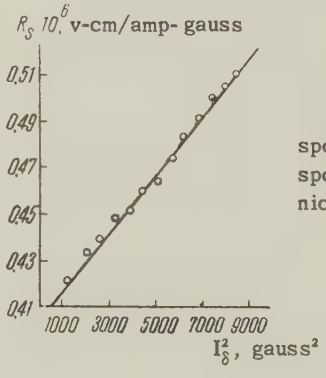

FIG. 5. Dependence of the spontaneous Hall constant on the spontaneous magnetization for nickel-zinc ferrite.

on the square of the spontaneous magnetization, I_S^2. At the Curie temperature both the spontaneous magnetization I_S and the spontaneous Hall emf are zero while the constant R_S is different from zero. The intercept of the line $R_S(I_S^2)$ and the ordinate axis possibly corresponds to the Hall constant due to the presence of paramagnetism above the Curie point.[6] The linear dependence of R_S on the square of the spontaneous magnetization is in agreement with existing theoretical concepts concerning the Hall effect in ferromagnetic materials.[7,8]

For magnetic fields H exceeding technical saturation, we propose to describe the Hall effect by the relation

$$E = R_0 H + R_s I_s + R_i I_i, \qquad (1)$$

where R_0 is the so-called ordinary or "classical" Hall constant, the value of which enables us to estimate the number and the sign of the carriers, R_i is the ferromagnetic Hall constant corresponding to the paramagnetic process, I_i is the magnetization of the paraprocess. Here the product $R_S I_S$ plays the role of a constant because it is independent of the magnetic field. Formula (1) is particularly suitable in the neighborhood of the Curie point, where the processes of technical magnetization are concluded in very weak fields and where the whole ferromagnetic behavior of a ferrite is almost fully determined by the paraprocess.

Volkov[9] was the first to point out the necessity of introducing two separate Hall constants, corresponding to the technical magnetization and to the paraprocess. By differentiating (1) with respect to H we obtain

$$\partial E / \partial H = R_0 + R_i \partial I_i / \partial H, \qquad (2)$$

where $\partial E/\partial H = \chi_E$ is the "susceptibility" of the Hall emf, and $\partial I_i / \partial H = \chi_i$ is the susceptibility of the paraprocess. Figure 6 shows the dependence of χ_E on χ_i for the nickel-zinc ferrite at 12° C. The intercept with the ordinate axis yields $R_0 = -0.9 \times 10^{-8}$ v-cm/amp-oe and the slope of the line determines the constant $R_i = +1 \times 10^{-6}$ v-cm/amp-gauss.

The conduction in the ferrite under study (at

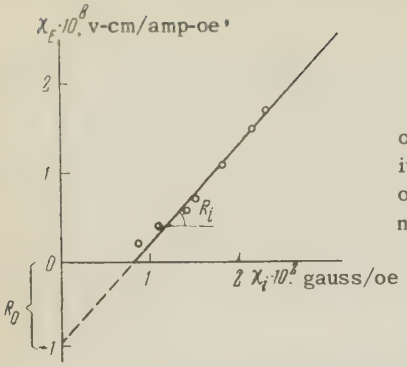

FIG. 6. Dependence of Hall emf susceptibility on the susceptibility of the paraprocess for nickel-zinc ferrite.

12°C) is electronic, as evidenced by the negative sign of the constant R_0. The number of the carriers can be estimated from the relation $R_0 = -3\pi/8en$, where n is the electron concentration and e the electron charge. It was found that $n \cong 1 \times 10^{19} cm^{-3}$. The concentration n and the electric conductivity at 12°C being known, we found the carrier mobility to be 0.08 cm^2/v-sec. This agrees with the values obtained for nonferromagnetic oxide semiconductors.

To conclude this section we wish to point out, that the method previously used of determining R_0 as the slope of the curve E(B) (where B is the magnetic induction) cannot always be used in strong magnetic fields (cf. references 1, 2, 10, 11, and others) for the study of the Hall effect in ferromagnetic materials, because this method does not take into account the influence of the paraprocess. The presence of the paraprocess demands evaluation of the product $R_i \partial I_i / \partial H$ for a correct estimate of R_0.

3. POLY- AND SINGLE CRYSTALS OF MANGANESE FERRITE ($MnO \cdot Fe_2O_3$)

Figure 7 shows the isotherms of the Hall emf for polycrystalline and single-crystal specimens of manganese ferrite of nearly stoichiometric composition. The Hall emf in a single crystal is one order of magnitude greater than in the polycrystalline specimen, while the magnetizations are almost the same. The smaller value of the Hall emf in the polycrystalline specimen may be due to the effect of the potential barriers between the grains on the movement of the electrons that produce the Hall potential difference. In a single crystal such barriers should not exist. However this problem requires additional study.

Figure 8 shows the temperature dependences of R_S for manganese-ferrite polycrystalline and single-crystal specimens, determined in the foregoing manner (the method of thermodynamic coefficients). In the polycrystalline specimen R_S

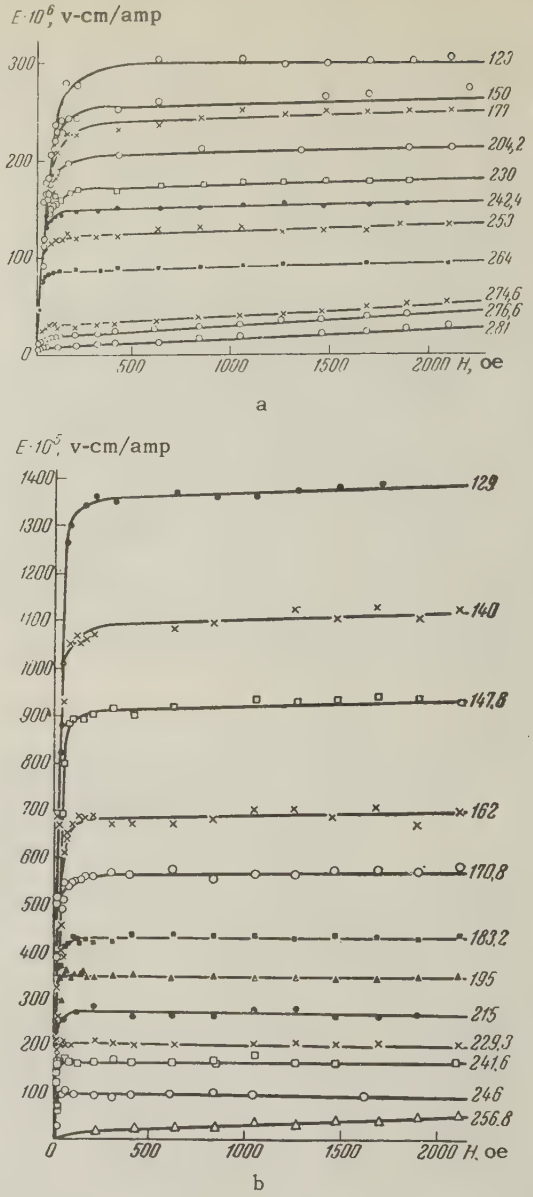

FIG. 7. Dependence of the Hall emf on the magnetic field at different temperatures. a – manganese polycrystalline ferrite, b – a single crystal of manganese ferrite. (The numbers adjacent to curves indicate °C).

increases with temperature up to a certain maximum and then falls rapidly as the Curie point is approached.

In the single crystal the constant R_S decays exponentially with rising temperature, analogous to the curve of electrical resistance vs. temperature. Using the above method, we obtained the following results at 120°C

polycrystalline manganese ferrite	single-crystal manganese ferrite
$R_0 = -1 \times 10^{-7}$ v-cm/amp-oe	$R_0 = -50 \times 10^{-7}$ v-cm/amp-oe
$R_i = +2 \times 10^{-6}$ v-cm/amp-gauss	$R_i = +20 \times 10^{-6}$ v-cm/amp-gauss
$n = 1 \times 10^{18}$ cm^{-3}	$n = 2 \times 10^{16}$ cm^{-3}
u = 0.08 cm^2/v-sec	u = 2.6 cm^2/v-sec

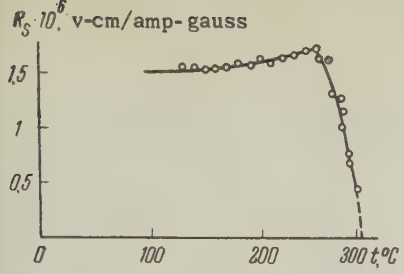

a

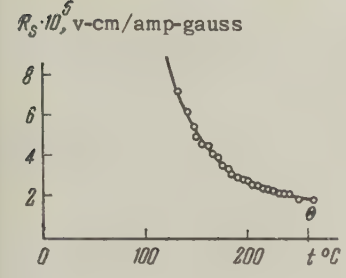

b

FIG. 8. Temperature dependence of the spontaneous Hall constant. a – polycrystalline manganese ferrite, b – single-crystal manganese ferrite.

The data obtained are in agreement with the electrical properties of nonferromagnetic oxide semiconductors.

[1] S. Foner, Phys. Rev. **88**, 955 (1952).

[2] A. A. Samokhvalov and I. G. Fakidov, Физика металлов и металловедение (Physics of Metals and Metallography) **4**, 249 (1957).

[3] N. V. Vol'kenshteĭn and G. N. Fedorov, ibid. **2**, 377, (1956).

[4] K. P. Belov and A. N. Goryaga, ibid. **2**, 3 (1956).

[5] Belov, Svirina and Belous, ibid. **6**, 621 (1958).

[6] Kikoin, Buryak, and Murashkin, Dokl. Akad. Nauk SSSR **125**, 1011 (1959), Soviet Phys.–Doklady **4**, 386 (1959).

[7] Vonsovskiĭ, Kobelev, and Rodionov, Izv. Akad. Nauk SSSR, Ser. Fiz. **16**, 569 (1952).

[8] N. P. Patrakhin, JETP **16**, 584 (1952).

[9] D. I. Volkov, Вестник МГУ (Bull. Moscow State Univ.) **3**, 567 (1954).

[10] E. M. Pugh and N. Rostoker, Revs. Modern Phys. **25**, 151 (1953).

[11] J. Smith, Physica **21**, 877 (1955).

Translated by Z. Scheidlinger
249

ISOTOPIC MASSES AND BINDING ENERGIES OF NUCLEI FOR MASSES BETWEEN 186 AND 196

R. A. DEMIRKHANOV, T. I. GUTKIN, and V. V. DOROKHOV

Submitted to JETP editor June 4, 1959

J. Exptl. Theoret. Phys. (U.S.S.R.) 37, 1217-1224 (November, 1959)

Values of the masses and binding energies are presented for the nuclei of isotopes of osmium, iridium, platinum, gold, and mercury. The masses were measured on a mass-spectrograph possessing a resolving power of 60,000 — 80,000. The isotope masses were derived from doublets by direct comparison with the masses of corresponding organic compounds. The masses of 18 stable isotopes were measured and the masses of 18 radioactive isotopes were computed. The data thus obtained were used to evaluate the binding energy of nuclei, the binding energy per nucleon (E/A), the binding energies of the last neutron and proton (B_n and B_p) and the pair energies of neutrons and protons (P_n and P_p). For N = 116, the binding energy of nuclei has been found to vary in a nonmonotonous manner for both odd and even values of Z.

INTRODUCTION

THE masses of isotopes and the coupling energies of nucleons in the nucleus have previously[1] been measured in the region of magic numbers up to 82 protons and 126 neutrons. In the present research, a second series of measurements has been carried out in the mass range $186 \leq M \leq 201$. Measurement of the masses of mercury, gold, platinum, iridium and osmium isotopes was carried out on a mass spectrograph described previously,[2] with a resolving power of 60,000 — 80,000. The measurements were made by means of doublets. A doublet pair was formed from a given isotope with a corresponding organic compound of type C_nH_m, $C_nH_mN_p$ or $C_nH_mO_k$. For high resolving power of the apparatus and dispersion calculations of high accuracy ($\sim 10^5$), this guaranteed a high accuracy of measurement.

Such a method of measurement makes it possible to determine the mass of the nucleus of a given isotope, avoiding intermediate measurements, making use only of the values of the masses of H^1, C^{12}, N^{14} and O^{16} which have been measured with sufficient accuracy previously.[2] Determination of the masses of the isotopes Os^{186}, Os^{187}, Os^{188}, Os^{189}, Ir^{191}, Ir^{193}, Pt^{192} and Au^{197} by the mass-spectrograph method has not been carried out up to the present time. The single research of Johnson and Bhanot, applying to the given mass range,[3] was carried out on a mass spectrometer with a low resolving power ($A_{max} \sim 14{,}000$). In this work mass differences per unit mass were measured for stable isotopes with even Z in the range $64 \leq Z \leq 82$. The value of the isotopic masses was not given in reference 3. Other mass-spectrographic measurements[4,5] were carried out for a small number of isotopes and have a very incomplete character. The values of masses computed in the work of Wapstra[6] from the energy balance of nuclear reactions were obtained with significant error ($\sim 2 - 3$ mMu). In the calculation of the isotopic masses of heavy nuclei the error becomes so large that, as a supporting value, the mass of the isotope Pb^{208} was used in place of O^{16}.[7] With such a large error of measurement, the calculated values of the binding energy of the last neutron or proton do not permit one to make an unambiguous estimate of the nuclear structure.

Ions of the elements thus measured were obtained by introducing vapors of the metal into the gas discharge region of a plasma ion source by means of an evaporator of special construction. The corresponding organic compounds were also introduced into the gas discharge region in the same manner.

As a check for the absence of errors of measurement,[8] determination of the isotopic masses in most cases was carried out with a check for internal consistency, including such cases in which the molecular weight of the organic compound was equal to the weight of the isotope under investigation. In some cases, in addition to this, control of the resultant measurements was obtained by measurement of masses of isotopes of a given element, using as a doublet the lines of isotopes with mass difference of unity.

In each case, the results of measurement were

obtained after analysis of 12 — 15 mass spectra with 4 — 6 photo plates.

MEASUREMENT OF ISOTOPIC MASSES

1. Osmium isotopes Os^{186}, Os^{187}, Os^{188}, Os^{189}, Os^{190} and Os^{192}. For all the osmium isotopes, the measurements were carried out with a check on internal consistency, while different doublet combinations were formed by use of different organic compounds and compounds of osmium. The osmium ions were obtained by introduction into the gas discharge region of a plasma ion source of vapors of OsO_4. The organic compounds perylene ($C_{20}H_{12}$, M = 252) and terphenyl ($C_{18}H_{14}$, M = 230) were used both in molecular form and in the form of fragments of these compounds as the organic compounds for the formation of doublet pairs with ions Os, OsO, OsO_2, OsO_3 and OsO_4. Internal consistency for the masses of the isotopes Os^{186}, Os^{187}, Os^{189} and Os^{192} were determined from three independent doublets for each isotope, Os^{188} from four and Os^{190} from five doublets. The value of the mass of each isotope was computed with account taken of the "weight" of the measurement. The values of the doublets and the masses of the isotopes are given in Table I.

2. Iridium isotopes Ir^{191} and Ir^{193}. Iridium ions were obtained by evaporation of metallic iridium. For the formation of a doublet pair with the isotope Ir^{191}, the splinter ($C_{15}H_{11}$, M = 191) of benzalacetophenone ($C_{15}H_{12}O$, M = 208) was used" and for the isotope Ir^{193}, the splinter ($C_{14}H_9O$, M = 193) of anthrone ($C_{14}H_{10}O$, M = 194). The values of the differences of masses of doublets and the values of the isotopic masses computed from these data are given in Table II.

3. Platinum isotopes Pt^{192}, Pt^{194}, Pt^{195}, Pt^{196} and Pt^{198}. The platinum ions were obtained by evaporation of metallic platinum with successive ionizations of the vapor in the discharge. Testing of internal consistency in the measurements of the isotopic masses of platinum was carried out by utilization of two different organic compounds for the formation of doublet pairs. As organic compounds, benzalphenylhydrazone ($C_{13}H_{12}N_2$, M = 196) was used in one case and a fragment of benzoin ($C_{14}H_{12}O_2$, M = 212) in the other. The values of the mass differences of the doublet and the values of the isotopes are given in Table III. For comparison, data obtained from mass-spectrographic measurements of Hogg and Duckworth[4] are also shown in the table.

4. Gold isotope Au^{197}. Measurement of the mass of the isotope Au^{197} was carried out by comparison of the mass of the gold ion with the mass of benzanilide ($C_{13}H_{11}ON$, M = 197). The value of the doublet $C_{13}H_{11}ON$–Au^{197} and of the mass of the gold isotope are given in Table II. Values of the masses of the isotope Au^{197}, computed in terms of Hg^{198} and $C_{13}H_{10}ON$ (mass differences ~1). The mean value for Au^{197} was computed with account of the "weight" of the measurements.

5. Mercury isotopes Hg^{196}, Hg^{199}, Hg^{200} and Hg^{201}. In the present work, measurements of the mass of the isotope Hg^{196} were carried out and a test for the internal consistency of the masses of the isotopes Hg^{199}, Hg^{200} and Hg^{201} was carried out; the measurements in the latter case were made in a previous research.[1] Use was made of

TABLE I

Mass, A	Doublet	Volume of ΔM, mMu	Value of the mass of the isotope, Mu	Mean value of the mass, Mu
186	$C_{15}H_6$—Os^{186}	92.157±0.150	186.013635±150	186.013246±300
	Os^{187}—Os^{186}	1002.797±0.150	186.012624±220	
	$C_{20}H_{12}$—$Os^{186}O_4$	144.659±0.141	186.013161±140	
187	$C_{15}H_7$—Os^{187}	98.892±0.080	187.015402± 80	187.015370±230
	Os^{188}—Os^{187}	1000.253±0.150	187.015858±220	
	$C_{19}C^{13}H_{10}$—$Os^{187}O_4$	146.481±0.170	187.015010±170	
188	$C_{15}H_8$—Os^{188}	106.549±0.110	188.015887±110	188.015759±200
	Os^{189}—Os^{188}	1002.420±0.150	188.015973±180	
	$C_{18}H_4$—$Os^{188}O_2$	84.948±0.320	188.016380±330	
	$C_{20}H_{12}$—$Os^{188}O_4$	158.472±0.070	188.015632± 70	
189	$C_{15}H_9$—Os^{189}	112.236±0.110	189.018342±110	189.018362± 80
	$C_{16}H_6$—$Os^{189}O_2$	90.949±0.150	189.018521±150	
	$C_{19}H_9$—$Os^{189}O_3$	127.541±0.090	189.018317± 90	
190	$C_{15}H_{10}$—Os^{190}	119.060±0.090	190.019660± 90	190.019176±150
	Os^{191}—Os^{189}	1000.944±0.150	190.019337±160	
	$C_{14}C^{13}H_9$—Os^{190}	115.092±0.080	190.019157± 80	
	$C_{16}H_8$—$Os^{190}O_2$	98.638±0.064	190.018974± 60	
	$C_{19}H_{10}$—$Os^{190}O_3$	135.210±0.240	190.018790±240	
192	$C_{13}N_2H_9$—Os^{192}	107.044±0.110	192.022806±110	192.022529±120
	$C_{16}H_8$—$Os^{192}O_2$	111.363±0.040	192.022533± 50	
	$C_{19}C^{13}H_{11}$—$Os^{192}O_3$	143.323±0.030	192.022490± 40	

TABLE II

Mass, A	Doublet	Value of ΔM, mMu	Value of the mass of the isotope, Mu	Mean value of the mass, Mu
191	$C_{15}H_{11}$—Ir^{191}	125.037±0.201	191.021825±202	191.021825±202
193	$C_{14}H_9O$—Ir^{193}	102.194±0.100	193.024564±104	193.024564±104
197	$C_{13}H_{11}ON$—Au^{197}	117.572±0.200	197.029177±205	197.029181±120
	Hg^{196}—Au^{197}	1000.709±0.240	197.029004±245	
	Au^{197}—$C_{13}H_{10}ON$	890.805±0.278	197.029412±280	

TABLE III

Mass, A	Doublet	Value of ΔM, mMu	Value of the mass, Mu	Value of the isotopic masses of platinum, Mu	
				According to data of the present research	According to mass-spectrographic measurements[4]
192	$C_{13}H_8N_2$—Pt^{192}	107.289±0.221	192.022561±225	192.022561±225	—
194	$C_{13}H_{10}N_2$—Pt^{194}	121.564±0.087	194.024570± 90	194.024604± 96	194.024100±600
	$C_{14}H_{10}O$—Pt^{194}	110.207±0.234	194.024693±236		
195	$C_{13}H_{11}N_2$—Pt^{195}	127.039±0.100	195.027237±102	195.027199± 95	195.026500±600
	$C_{14}H_{11}O$—Pt^{195}	115.924±0.210	195.027118±215		
196	$C_{13}H_{12}N_2$—Pt^{196}	134.529±0.111	196.027889±115	196.027889±115	196.026700±600
198	Pt^{198}(no Hg^{198})	—	198.029880±200	198.029880±200	198.032700±600

TABLE IV

Mass, A	Doublet	Value of ΔM, mMu	Value of the isotopic masses, Mu	Value of the isotopic masses of mercury, Mu	
				According to data of the present research	According to mass-spectrographic measurements[5] (1958)
196	$C_{14}H_{12}O$—Hg^{196}	122.638±0.176	196.028546±180	196.028362±185	196.027260±230
	$C_{13}H_{10}ON$—Hg^{196}	110.251±0.020	196.028356± 32		
199	$C_{16}H_7$—Hg^{199}	85.994±0.079	199.032120± 82	199.031684±460	199.030960±100
	$C_{13}H_{11}O_2$—Hg^{199}	107.674±0.038	199.031548± 45		
200	$C_{16}H_8$—Hg^{200}	94.354±0.043	200.031902± 47	200.031913± 68	200.031270± 80
	$C_{12}C^{13}H_{11}O_2$—Hg^{200}	110.913±0.111	200.031980±115		
201	Hg^{201}—Hg^{200}	1002.254±0.021	201.034167± 71	201.034603±220	201.033510±120
	Hg^{202}—Hg^{201}	1000.398±0.032	201.034564± 62		
	$C_{16}H_9$—Hg^{201}	99.128±0.069	201.035270± 83		

a splinter ($C_{14}H_{12}O$, M = 196) of benzoin ($C_{14}H_{12}O_2$, M = 212) and a splinter ($C_{13}H_{10}ON$, M = 196) of benzanilide ($C_{13}H_{11}ON$, M = 197) for the formation of doublet pairs with the isotope Hg^{196}. For a test of the internal consistency for the isotope Hg^{199}, the doublet $C_{13}H_{11}O_2$–Hg^{199} was measured in addition to the doublet $C_{16}H_7$—Hg^{199}.[1] Similarly, additional measurements were carried out of the doublet $C_{12}C^{13}H_{11}O_2$—Hg^{200}, Hg^{201}–Hg^{200} and Hg^{202}–Hg^{201} were also carried out for the isotopes Hg^{200} and Hg^{201}; in this case the organic compound benzoin ($C_{14}H_{12}O_2$, M = 212) and the mercury spectrum were employed. Masses of the isotopes Hg^{196}, Hg^{199}, Hg^{200} and Hg^{201} were determined from these doublets with account of the "weight" of measurement. The value of the mass differences of the doublets and the values of the isotopic masses of mercury computed from these doublets are given in Table IV. For comparison, data are also given in this table obtained from the mass-spectrographic measurements of Kerr and Duckworth.[5]

MEASUREMENT RESULTS

By comparing the values of the isotopic masses obtained in the present research with the corresponding data computed from nuclear reactions (see Table V), one can see that they are generally in agreement within the limits of error. However, this agreement is obtained at the cost of a very large error in the determination of the masses of the isotopes in terms of the values of Q obtained from nuclear reactions. In the final analysis, the mass of the isotope O^{16} was used as a supporting value for these isotopes, and consequently a large error of measurement is obtained as the result of the use of a large number of steps with corresponding values of Q. The most significant divergences in the

TABLE V

Isotope	Value of the isotopic mass M from the data of the present research, Mu	Values of the isotopic mass M′ according to data from nuclear reactions,[6] Mu	$\Delta = M - M'$, mMu
Os^{186}	186.013246±200	186.009550±2300	3.696
Os^{187}	187.015370±150	187.011045±2200	4.325
Os^{188}	188.016058±140	188.014100±2000	1.958
Os^{189}	189.018362± 50	189.018120±2000	0.242
Os^{190}	190.019127±110	190.017400±2000	1.727
Os^{192}	192.022470±160	192.022500±3000	−0.030
Ir^{191}	191.021825±202	191.021240±2100	0.585
Ir^{193}	193.024564±104	193.025200±2000	−0.636
Pt^{192}	192.022561±225	192.023100±2050	−0.539
Pt^{194}	194.024604± 96	194.024000±1500	0.604
Pt^{195}	195.027199± 95	195.026400±1500	0.799
Pt^{196}	196.027889±115	196.026880±1500	1.009
Pt^{198}	198.029880±200	198.029000±2000	0.880
Au^{197}	197.029181±120	197.028470±3000	0.717
Hg^{196}	196.028362±185	196.027350±3010	1.012
Hg^{199}	199.031684±460	199.030550±3050	1.134
Hg^{200}	200.031913± 68	200.031910±3010	0.003
Hg^{201}	201.034603±220	201.034000±3000	0.603

values of the mass take place in the isotopes of osmium. For two of them (Os^{186} and Os^{187}, see Table V), the difference in values exceeds twice the value of the very large error of nuclear measurements. According to existing evidence,[9] the values of the masses of these isotopes (Os^{186} and Os^{187}) given in the work of Wapstra,[6] are unreliable. In addition to these isotopes, significant divergences also take place in the value of the masses of the isotopes Os^{188}, Os^{189}, Pt^{192} and Hg^{199}. The most accurate measurements in the region under consideration were made in the work of Johnson and Bhanot.[3] Unfortunately, the work did not cover differences of masses with odd Z, and for elements with even Z several isotopes were not measured (Os^{192}, Pt^{192}, Hg^{198}, etc.). However, comparison of the mass differences obtained in this work with similar data of the present research and nuclear data computed directly from nuclear reactions shows that all comparable values are in excellent agreement within the limits of the errors of measurement. Quite a different picture is obtained for

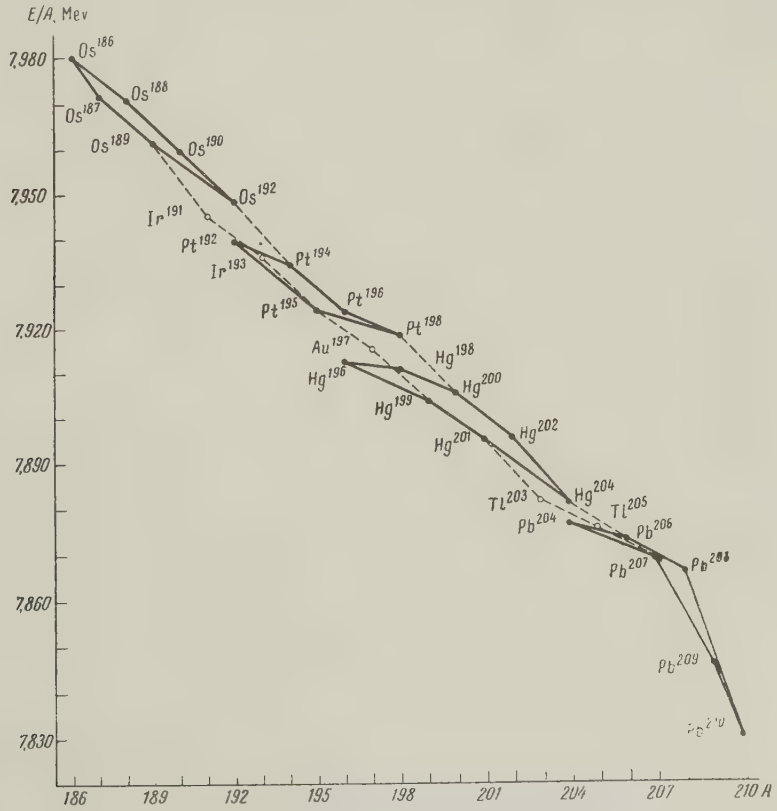

Binding energies per nucleon in the range $186 \leq M \leq 210$.

comparison of the same quantities computed from the values of the mass given by nuclear data.[6] The divergences in a number of cases exceed 2 — 2.5 mMu. Analysis of the data of the present research and of reference 3 shows the error of measurements of the masses of the isotopes Os^{186}, Os^{187}, Os^{188}, Os^{189}, and Pt^{192} advanced in reference 6.

Additional measurements of the masses of the isotopes Hg^{199}, Hg^{200}, and Hg^{201} with "internal consistency" for Hg^{200} made it possible to carry out a comparison of the values of Q obtained from nuclear reactions with the corresponding values computed according to the current measurements of isotopic masses. Thus, for example, the value for the mass of the isotope Hg^{200}, according to the data of the present work is equal to $M(Hg^{200})$ = 200.031913 ± 68 Mu. This quantity is in excellent agreement with data obtained from nuclear reac-

TABLE VI

Isotope	Z	N	Binding energy of the nucleus,* Mev	Binding energies of the nucleon, E/A, Mev	B_n, Mev*	B_p, Mev*	P_n, Mev*	P_p, Mev*
Os^{186}		110	1484.142	7.9792				
Os^{187}		111	1490.530	7.9708	6.388			
Os^{188}		112	1498.256	7.9694	7.726		1.338	
Os^{189}		113	1504.477	7.9602	6.221			
Os^{190}	76	114	1512.056	7.9582	7.579		1.358	
Os^{191}		115	1517.765	7.9464	5.709			
Os^{192}		116	1525.751	7.9466	7.986		2.277	
Os^{193}		117	1531.022	7.9328	5.271			
Ir^{190}		113	1510.015	7.9474		5.538		
Ir^{191}		114	1517.200	7.9435	7.185	5.144		
Ir^{192}		115	1523.438	7.9346	6.238	5.673		
Ir^{193}	77	116	1531.382	7.9346	7.944	5.631	1.706	
Ir^{194}		117	1537.521	7.9254	6.139	6.499	0.906	
Ir^{195}		118	1543.566	7.9157	6.045			
Pt^{192}		114	1524.096	7.9380		6.896		1.752
Pt^{193}		115	1530.549	7.9303	6.453	7.111		1.438
Pt^{194}		116	1538.926	7.9326	8.377	7.544	1.924	1.913
Pt^{195}		117	1544.876	7.9224	5.950	7.355		0.856
Pt^{196}	78	118	1552.600	7.9214	7.724	9.034	1.774	
Pt^{197}		119	1559.014	7.9138	6.414			
Pt^{198}		120	1567.479	7.9166	8.465		2.051	
Pt^{199}		121	1571.945	7.8992	4.466			
Au^{194}		115	1535.590	7.9154		6.142		
Au^{195}		116	1543.820	7.9170	8.230	4.894		
Au^{196}		117	1550.902	7.9128	7.082	6.026		
Au^{197}		118	1558.979	7.9136	8.077	6.379	0.995	
Au^{198}	79	119	1565.357	7.9058	6.378	6.243		
Au^{199}		120	1572.929	7.9042	7.572	5.450	1.194	
Au^{200}		121	1579.234	7.8962	6.305	7.289		
Au^{201}		122	1585.896	7.8900	6.662		0.357	
Hg^{195}		115	1541.861	7.9070		6.271		0.130
Hg^{196}		116	1550.590	7.9112	8.729	6.770		1.876
Hg^{197}		117	1558.000	7.9086	7.410	7.098		1.072
Hg^{198}**		118	1566.100	7.9096	8.100	7.121	0.690	0.742
Hg^{199}		119	1572.596	7.9025	6.496	7.239		0.896
Hg^{200}	80	120	1580.749	7.9037	8.153	7.820	1.657	2.370
Hg^{201}		121	1586.610	7.8936	5.861	7.376		0.087
Hg^{202}**		122	1594.685	7.8945	8.075	8.789	2.214	
Hg^{203}**		123	1600.048	7.8820	5.363			
Hg^{204}**		124	1607.614	7.8805	7.566		2.203	
Hg^{205}**		125	1613.388	7.8702	5.774			

*Errors in the values of the binding energy do not exceed 0.2 Mev and correspondingly in B_n and B_p — 0.3 Mev and P_n and P_p — 0.4 Mev

**Data taken from reference 1.

tions according to which (see Table V) $M(Hg^{200})$ = 200.031910 ± 3010 Mu. Moreover, the mass difference $Hg^{202} - Hg^{200}$, obtained in the data of reference 1 and in the present work, is ΔM = 2.003039 ± 180, which is in good agreement with the corresponding value obtained from mass-spectrometric measurements by Johnson and Bhanot[3] (ΔM = 2.002900 ± 150). Because of this we can consider that the value for the mass of Hg^{202}, obtained in reference 1, is sufficiently reliable. Moreover, there is good agreement between the values obtained from the cycle of mass-spectrographic measurements[1] and the data of nuclear reactions in the calculation of the mass of Tl^{203} by means of the reaction Hg^{204}–Tl^{203}. The agreement of the value for the mass of Tl^{203} obtained from the reaction $Tl^{203}(\gamma, n)Tl^{202}$ by means of the chain $Hg^{202} \rightarrow Tl^{202} \rightarrow Tl^{203}$ leads to a discrepancy for the mass of Tl^{203} ~ 1.7 mMu. Thus, joint consideration of nuclear and mass-spectrographic measurements leads to the conclusion that in all probability the assumed value of the quantity Q for the reaction $Tl^{203}(\gamma, n)Tl^{202}$ [10] is in error and it would be desirable to repeat the measurement of this quantity Q.

BINDING ENERGY OF NUCLEONS IN THE NUCLEUS

The mass values of the isotopes of osmium, iridium, platinum, gold and mercury obtained in the present research make possible a more accurate determination of the binding energy of nucleons in the nucleus over the mass range $186 \leq M \leq 200$. In addition to the results of the present research, the masses of 18 radioactive isotopes were computed by means of the values of Q obtained from nuclear reactions and beta decay energies. In this case the values of the masses of stable isotopes obtained in the present research were used as standardizing values.

Evidence on the general characteristics of nucleon binding can be obtained from a study of the binding energy per nucleon. The binding energy per nuclecon E/A is plotted in the drawing in Mev as a function of A. For completeness of the picture, the region of values of A is expanded over the range of values used in reference 1. In the drawing the solid lines connect the binding energies of stable (measured) isotopes with the same Z. The binding energies of nuclei with odd Z (Ir, Au, Tl) are denoted by circles and are connected with odd A of elements with even Z. As is seen from the figure, a certain periodicity in the binding energy of stable nuclei in this mass region is indicated. The peculiarity noted in reference 1 of the isobaric pair of nuclei Hg^{204} and Pb^{204} is preserved and even expanded to the isobars Pt^{198}–Hg^{198}; Pt^{196}–Hg^{196} and Os^{192}–Pt^{192}. In the isobaric pairs shown, the binding energies of the nucleus in which two protons are replaced by two neutrons is larger than in the opposite case. Values of the binding energy of nuclei, the binding energy of the last neutron B_n, of the last proton B_p, the pair energies of neutrons P_n and protons P_p are shown in Table VI. Analysis of the data of Table VI shows that nuclei having N = 116 for both even and odd Z possess an increased stability. This is evident from the values of B_n and P_n. In contrast to this, nuclei with N = 115 are distinguished by a lower value of coupling energy in comparison with other nuclei of odd N. For even-even nuclei, an increased value of the pair energies of protons P_p occurs for N = 116 ($^{116}_{78}Pt^{194}$ and $^{116}_{80}Hg^{196}$).

In conclusion the authors express their gratitude to E. E. Baroni and their co-workers K. A. Kovyrzina and V. M. Soĭfer for preparation of the organic compounds and also to M. I. Dzkuya and G. A. Dorokhova for help in the research.

[1] Demirkhanov, Gutkin, and Dorokhov, JETP **35**, 917 (1958), Soviet Phys. JETP **8**, 639 (1959).

[2] Demirkhanov, Gutkin, Dorokhov, and Rudenko, Атомная энергия (Atomic Energy) **2**, 21 (1956).

[3] W. H. Johnson, Jr., and V. B. Bhanot, Phys. Rev. **107**, 1669 (1957).

[4] B. G. Hogg and H. E. Duckworth, Canad. J. Phys. **32**, 65 (1954).

[5] I. T. Kerr and H. E. Duckworth, Canad. J. Phys. **36**, 986 (1958).

[6] A. H. Wapstra, Physica **21**, 385 (1955).

[7] I. R. Huizenga, Physica **21**, 410 (1955).

[8] T. I. Gutkin, Приборы и техника эксперимента (Instrum. and Meas. Engg.) No. 5, **46** (1957).

[9] H. E. Duckworth, Progress in Nuclear Physics (Pergamon, N. Y., 1957); p. 138.

[10] Sher, Halpern, and Mann, Phys. Rev. **84**, 387 (1951).

Translated by R. T. Beyer
250

*INTERACTION OF 9-Bev PROTONS WITH FREE AND QUASIFREE NUCLEONS IN PHOTOGRAPHIC EMULSIONS**

N. P. BOGACHEV, S. A. BUNYATOV, I. M. GRAMENITSKIĬ, V. B. LYUBIMOV, Yu. P. MEREKOV, M. I. PODGORETSKIĬ, V. M. SIDOROV, and D. TUVDÉNDORZH

Joint Institute for Nuclear Research

Submitted to JETP editor June 7, 1959

J. Exptl. Theoret. Phys. (U.S.S.R.) **37**, 1225-1232 (November, 1959)

The problem of the angular and energy characteristics of secondary particles produced in collisions between protons and nucleons is considered.

AN emulsion camera was used to study interactions of 9-Bev protons with nucleons. It consisted of layers of NIKFI type R emulsion and was irradiated with the internal proton beam of the proton synchrotron to the high-energy laboratory of the Joint Institute for Nuclear Research (see also references 2 and 3). Scanning was carried out along the tracks of the primary protons, with 600-fold magnification. All stars and scatterings through angles larger than 5° were detected. In track length of 978 m, 2623 cases of nuclear interaction were found. The mean free path was 37.3 ± 0.3 cm, in agreement with results obtained earlier.[2]

1. In order to segregate proton-proton (p-p) and proton-neutron (p-n) interactions, cases having no more than two slow protons (with ionization $I \geq 1.4\, I_{plateau}$) were chosen. Lack of a recoil nucleus and, in cases with an even number of prongs, lack of a β-electron were also required. The subsequent selection was carried out according to the criteria:

(1) The slow proton should have a track length $l \geq 4$ mm ($E_p \geq 31$ Mev). This makes it possible to exclude cases of proton-nucleus interaction with evaporation of a single proton.

(2) For a given energy of the proton, its angle of emission should not exceed the angle of elastic proton-proton scattering.

(3) For a given multiplicity n the angle of proton emission should not exceed some $\vartheta_{max}(n)$, corresponding to the kinematics of the proton-nucleon (p-N) collision.

(4) The following inequality[4] should be fulfilled:

$$\sum (E_i - p_i \cos \vartheta_i) \leqslant M + E_0 - p_0,$$

where E_i, p_i and ϑ_i are the energy, momentum and angle of emission of the i-th secondary charged particle in the laboratory system (l.s.), M is the proton mass, E_0 and p_0 are the energy and momentum of the incident proton in the l.s. Since no measurements were made of the momenta of the fast particles, in applying this criterion, particles having a blob density $b \leq 1.4\, b_{plateau}$ were considered to be π mesons. The values 196 Mev and 137 Mev/c were employed for these as lower limits of energy and momentum, respectively.

In this way, 170 cases with an even number and 110 with an odd number of prongs were chosen. Cases with an even number of prongs were considered to be interactions with free protons or with quasifree protons in the photoemulsion nuclei. Cases with an odd number of prongs were considered to be interactions with quasifree neutrons. In addition, 20 cases of elastic p-p scattering were found. Criteria of selection of these cases and the efficiency of detecting them were taken from the work of reference 2.

The total cross section for elastic p-p scattering turned out to be $\sigma_{pp}^{el} = (10 \pm 3)$ mb, consistent with values found in other works.[2,5]

2. In selecting cases of inelastic interactions of nucleons with nucleons in the photoemulsions, the question of the purity of selected events arose, since the criteria indicated above are necessary, but not sufficient.

First of all, it is necessary to make sure that the cases discarded by criterion (1) are practically free of p-N interactions. If p-N interactions were contained among cases with one slow proton ($l \leq 4$ mm), one would expect a forward-backward asymmetry for these protons. We present the data on the number of slow protons emitted into the forward and backward hemispheres in the l.s. for the

*Some results of this work were contained in the report of V. I. Veksler to the International Conference on Peaceful Uses of Atomic Energy, Geneva, August 1958.[1]

cases discarded because of criterion (1) only:

	Number of slow protons forwards	backwards
Cases with an even number of prongs:	26	27
Cases with an odd number of prongs:	28	26
Total:	54	53

From this it can be seen that the same number of slow protons were emitted into the forward and backward hemispheres. This is evidence that the overwhelming proportion of slow protons comes from the evaporation process.

In interactions with quasifree nucleons, it is possible for a neutron to be emitted by the residual nucleus. In order to estimate the importance of this, let us consider the p-n interaction. In the emission of a single neutron from a photoemulsion nucleus, one should see a β-electron in more than 75% of the cases. In the selected p-n cases, β-electrons were observed in 43% of the cases. This indicates the possibility of emission of two neutrons by the photoemulsion nucleus, with the residual nucleus being stable. Experimental data[6] on the cross sections for (p, pn) and (p, p2n) reactions do not contradict the above assumption. Apparently the emission of the second neutron is mainly connected with the evaporation process. This is confirmed by comparison of characteristics of the interactions with a β-electron and without a β-electron. The mean multiplicity of these two types of interaction (2.54 ± 0.15 and 2.67 ± 0.22, respectively) and their angular distributions, given in Fig. 1, do not differ.

The ratio of p-p to p-n collisions was 1.55 ± 0.12. The cross section for inelastic p-p interactions turned out to be approximately 21 mb, and the ratio $\sigma_{pp}^{el}/\sigma_{pp}^{inel} \sim 0.5$. In evaluating the cross section for inelastic p-p interactions, it was assumed that the interactions with quasifree protons and quasifree neutrons were equally probable. This is confirmed by the equality of numbers of cases with even and odd numbers of prongs, and having one evaporation proton. The value σ_{pp}^{inel} agrees with the experimental data obtained in references 2 and 7 and with the theoretical estimates.[8,9]

All of the facts mentioned testify to the purity of selected cases. However, it should be emphasized that in work with photoemulsions, some arbitrariness always remains in the choice of inelastic proton-nucleon interactions. In particular, on account of secondary interactions inside the nucleus, p-p collisions can sometimes be taken to be p-n ones, and vice versa.

3. The distributions with number of charged secondary particles are given in Tables I and II for p-p and p-n collisions. In the lower lines of the tables are given results of calculations carried out with the statistical theory, taking the iso-

TABLE I. Distribution of p-p interactions with number of charged particles

Number of interactions, %	2	4	6	8
Experiment	45.3±5.2	44.7±5.1	8.8±2.3	1.2±0.8
Theory	32.8	58.5	8.6	0.1

TABLE II. Distribution of p-n interactions with number of charged particles

Number of interactions, %	1	3	5	7
Experiment	33.6±5.5	52.7±7.9	12.7±3.4	0.9±0.9
Theory	14.5	59.4	25.0	1.1

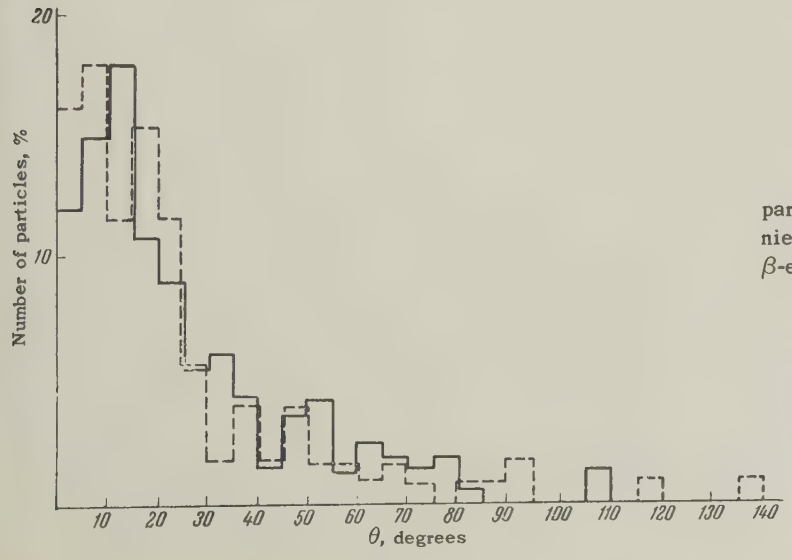

FIG. 1. Angular distributions of the secondary particles in the l.s. for p–n interactions accompanied by a β-electron (dashed line) and without a β-electron (solid line).

baric states into account.* The mean number of charged particles in p-p interactions was equal to 3.22 ± 0.12, and for p-n interactions, to 2.62 ± 0.13. The corresponding theoretical values are 3.53 and 3.25.

Some of the variance between experimental and theoretical data may be connected with a possible discrimination in selection of cases of interaction with quasifree nucleons for high multiplicities.

4. Identification of particles and measurement of their energy was carried out for only the slow particles ($b \geq 1.4\, b_{plateau}$). For particles coming to rest, the energies were determined from the range-energy curve. Ionization measurements were carried out on the tracks of particles not stopping in the camera. In this case the ionization was determined from the density of blobs[10] for particles with $b \leq 2b_{plateau}$, and according to the method outlined in reference 11 for particles with $b > 2b_{plateau}$. In this way the energies of 53 protons and 9 π mesons in p-p interactions and 22 protons and 5 π mesons in p-n interactions were determined.†

From these data it is possible to obtain some information about the angular distribution of secondary protons in the center-of-mass system (c.m.s.) and about the energy losses of the primary protons in production of π mesons. In the case of p-p interactions, 53 protons came off in the angular interval between 155 and 180° in the c.m.s. If the protons are assumed to have an isotropic angular distribution in the c.m.s., then we can expect

$$53 \Big/ \frac{1}{2} \int_{155^\circ}^{180^\circ} \sin\vartheta d\vartheta = 53 \Big/ 0.047 = 1230 \text{ protons}$$

in the 170 interactions.

This estimate shows that the angular distribution of protons is strongly anisotropic in the c.m.s. If one assumes that in each interaction, one or two secondary protons are produced, the half-angles for protons emitted into the backwards or forwards hemispheres are equal to ~20° or ~30°, respectively. The mean momentum in the c.m.s. of the selected protons in p-p and p-n interactions was equal to

$$(p_c)_{pp} = (1380 \pm 40) \text{ Mev/c} \quad \text{and} \quad (p_c)_{pn} = (1250 \pm 50) \text{ Mev/c}.$$

Knowing the energy of the protons emitted between 155 and 180° in the c.m.s. and assuming symmetrical emission of nucleons, it is possible to evaluate a lower limit for the energy loss. The energy transferred to π mesons is, in the l.s.,

$$E_{\pi l} = 2\gamma_c (E_{0c} - \bar{E}_{pc}),$$

where E_{0c} is the energy of the protons in the c.m.s. before the interaction, $\bar{E}_{pc}$ is the mean energy of the protons after interaction, $\gamma_c = (1 - \beta_c^2)^{-1/2}$, where β_c is the velocity in the c.m.s. The proportion of energy transferred to π mesons in p-p interactions was $E_{\pi l}/E_0 \approx 30\%$.

If it is assumed that, on the average, there is one secondary proton in each interaction,* then $\frac{2}{3}$ of all protons emitted into the backwards hemisphere were identified. Assuming that in the remaining cases the protons give up all of their kinetic energy in the c.m.s. into production of π mesons, it is possible to find an upper limit for the energy loss, which turned out to be 45%. However, this value is much too high for the actual loss. In fact, within the interval 155 — 180° in the c.m.s. the mean momentum does not change rapidly with changing angle (see Table III) and, consequently, it might be supposed that at angles less than 155° the momentum will not differ much from the values given above. Therefore the mean loss is apparently equal to 30%.

TABLE III

Angular interval, degrees	p_c, Mev/c
180—169	1380±60
169—155	1380±60

This corresponds to a mean energy for the π mesons (under the assumption that in each interaction there is one secondary proton) of $\bar{E}_{\pi l} \sim 800$ Mev in the l.s. and $\bar{E}_{\pi c} \sim 340$ Mev in the c.m.s.

5. In order to obtain the angular distributions of secondary particles in the c.m.s., it is necessary to know the momenta of all particles. The momenta of the fast particles were not measured, and it was assumed that their velocity in the c.m.s. β_{ic} was equal to the velocity of the c.m.s. β_c. For the particles whose momenta were measured, the transformation of emission angle was carried out

*The authors are grateful to V. S. Barashenkov and V. M. Maksimenko for acquainting them with the results of their calculations.

†In cases in which the particle did not stop in the camera and its momentum was not determined by multiple scattering, it was taken to be a proton with velocity calculated from the ionization. The possible admixture of π mesons and deuterons in these cases was probably small, since in the 22 particles identified (by scattering and ionization) only one turned out to be a π meson, and no deuterons were observed.

*This follows, for example, from the statistical theory. In any case, the mean number of protons in the interaction is less then 1.7 (see the later footnote † on page 875.

according to

$$\tan \vartheta_{ic} = \frac{1}{\gamma_c} \frac{\sin \vartheta_{il}}{\cos \vartheta_{il} - \beta_c / \beta_{il}}.$$

The angular distributions of secondary particles in p-p interactions are given in Fig. 2. The distributions obtained were roughly symmetrical. As a measure of asymmetry, one can employ $\Delta = \Sigma(n_f - n_b)/N$, where n_f and n_b are the number of particles going forwards and backwards, respectively, in the c.m.s. in a given interaction, and N is the total number of interactions. For all p-p interactions, $\Delta_{pp} = 0.16 \pm 0.13$, i.e., was practically zero. This indicates that the assumption $\beta_{ic} = \beta_c$ in our case is a sufficiently good approximation. In Fig. 2 it can be seen that for small multiplicities (n = 2) the angular distribution is sharply anisotropic. With increasing multiplicity the degree of anisotropy decreases, and for n = 6 — 8 the distribution is practically isotropic. It can be shown that the observed anisotropy cannot be produced by an erroneous transformation to the c.m.s. if the initial distribution in the true c.m.s. is isotropic.

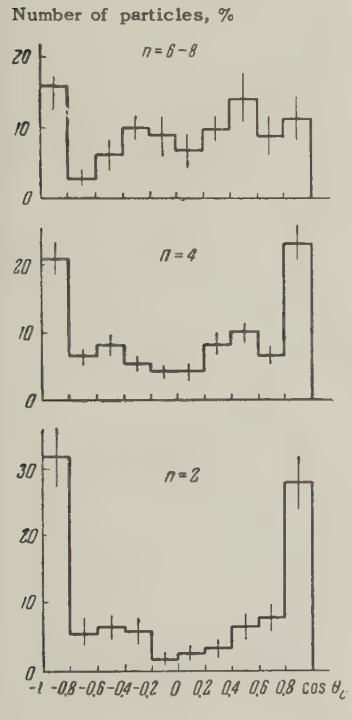

FIG. 2. Angular distributions of secondary particles in p—p collisions in the c.m.s. for various multiplicities n.

It has been shown earlier that the protons have a strongly anisotropic distribution. It seems natural to relate the anisotropy obtained for all secondary particles to them. Then the π mesons should have a substantially broader distribution than the protons. This is confirmed by the following considerations. Within the angular interval 155 — 180° in the c.m.s. there are 53 protons. In the asymmetrical interval 0 — 25° there should be, on the average, the same number of protons; in fact, 72 particles were observed. The remainder, equal to 72 — 53 = 19 ± 11, is an upper limit to the number of π mesons in the interval 0 — 25°.*

In addition, in those cases in a p-N collision with a slow proton, it is possible to evaluate a limiting angle in the l.s. by kinematical considerations[4] inside which a second nucleon can be emitted.† All particles emitted outside this angle are π mesons. Since the calculated limiting angles in the l.s. were roughly equal to 15 — 20°, it is possible to construct the angular distribution of π mesons emitted into the backwards hemisphere in the c.m.s. Angular distributions are given in Table IV for two assumptions about β_{ic}.

TABLE IV

$\cos \vartheta_c$	0—0.5	—0.5—1.0
	Number of particles	
$\beta_{ic}=\beta_c$	18	32
$\beta_{ic}=1$	24	20

Thus, it is possible to conclude that the distribution of π mesons in the c.m.s. is broader than that of the protons. The data obtained also are not in contradiction with an isotropic distribution of π mesons in the c.m.s.

6. The angular distributions of secondary particles in the c.m.s. for p-n collisions, constructed in the same way as for p-p interactions, are given in Fig. 3. In the case of p-n collisions, a noticeable forwards-backwards asymmetry was observed.‡ The value of Δ_{pn} for all p-n interactions was $\Delta_{pn} = 0.60 \pm 0.15$.

First of all, one must make sure that the observed asymmetry cannot arise from an erroneous transformation to the c.m.s. The distribution of charged π mesons in the c.m.s. should be symmetrical, because of the symmetry of the initial state with respect to isotopic spin (just as many

*As noted earlier, the transformation to the c.m.s. is carried out under the assumption $\beta_{ic} = \beta_c$ in the case of fast particles. However, for particles emitted at small angles in the c.m.s. the true value of β_{ic} hardly affects the transition from l.s. to c.m.s. The effects of throwing slow particles into the interval considered from the backwards cone by an incorrect transformation would be quite small.

†This makes it possible to evaluate an upper limit to the mean number of protons in p—p interactions. In 36 out of 53 interactions with a slow proton, at least one fast charged particle — which might be a proton — is emitted within this limit. Thus $\bar{n}_p \leqslant (53 + 36)/53 \sim 1.7$

‡For cases with n = 1 there was a substantial discrimination, since only scatterings through angles greater than 5° were considered. Therefore, the angular distribution in the c.m.s. was strongly distorted in the small-angle region.

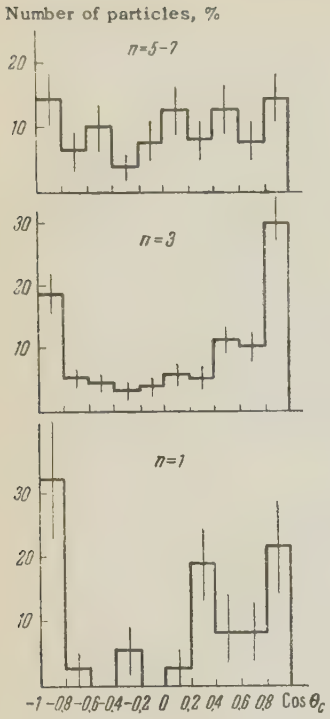

FIG. 3. Angular distributions of secondary particles in p–n collisions in the c.m.s. for various multiplicities n.

π^- mesons should go into the back hemisphere as π^+ mesons into the front and vice versa). The asymmetry of the π mesons may be due to the fact that their velocity $\beta_{\pi c}$ in the c.m.s. is much less than β_c, whereas in the transformation it has been assumed that $\beta_{\pi c} = \beta_c$. This would show up as a marked difference between the energy spectra of secondary particles for p-p and p-n interactions. It has been shown above that the mean value of the momentum in the c.m.s. (calculated from the slow protons in the l.s.) and, consequently, the lower limit of the energy loss, is approximately equal in the cases of p-p and p-n interactions. Therefore, it is difficult to assume that the energy spectra of secondary particles are different in these interactions. The most marked asymmetry shows up in p-n interactions with three secondary particles ($\Delta_3 = 0.83 \pm 0.23$). It is useful to compare the angular distribution of three-pronged events with the summed angular distributions of two- and four-pronged events ($\Delta_{2;4} = 0.12 \pm 0.14$), since the energetic characteristics of these groups do not appear to differ. The angular distributions for $n = 2 - 4$ for all particles and, consequently, for π mesons, is symmetrical. Therefore, the angular distribution of π mesons for $n = 3$ should be symmetrical. The observed asymmetry can come only from the protons. However, the mean energy of secondary nucleons in p-p and p-n interactions in the c.m.s. is the same. Therefore, it follows that the asymmetry in p-n interactions arises because protons go mainly forwards in the c.m.s. and neutrons, backwards.

7. Thus, the analysis of p-p and p-n interactions makes it possible to draw the following conclusions.

(a) The angular distribution of nucleons in p-p interactions is strongly anisotropic in the c.m.s. The angular distribution of all particles in p-p interactions is anisotropic for small multiplicities and becomes approximately isotropic with increasing multiplicity.

(b) The proportion of the energy of the initial proton which is transferred to π mesons is $\sim 30\%$ in the l.s.

(c) The observed asymmetry in the angular distribution of secondary particles in p-n interactions comes from the fact that in the c.m.s. the protons are emitted preferentially into the forward hemisphere, and the neutrons into the backward one.

Experimental data on p-p interactions at lower energies[12] also show the nucleons to be anisotropic in the c.m.s. Some proton asymmetry in n-p interactions was observed at 1.7 Bev.[13] In recent papers[14,15] on p-p interactions at 6.2 Bev, the authors came to conclusions, confirmed by our results.

The totality of data seems to indicate that periphery nucleon-nucleon collisions play an important role.* One of many possible theoretical models of such collisions is the scheme considered by Tamm,† in which it is assumed that the interaction goes by way of exchange of one π meson, with formation of two isobars. Such a model makes it possible to explain qualitatively both the anisotropy of the nucleons in p-p collisions and the asymmetry of protons in p-n collisions in the c.m.s. A more detailed analysis of experimental data and comparison with the theory would only be possible with a substantial increase in statistics.

The authors take pleasure in thanking Acad. V. I. Veksler and Prof. V. P. Dzhelepov for continued assistance in carrying out this work and fruitful discussions, N. G. Birger for essential help in carrying out the kinematical analysis of the material, Prof. M. Ya. Danysh, G. I. Kopylov and D. S. Chernavskiĭ for participation in discussions. The authors are grateful to all of the laboratory assistants who carried out the scanning and measurements.

[1] Proc. Second Internat. Conf. on Peaceful Uses of Atomic Energy, Reports of Soviet Scientists

*This was emphasized by V. I. Veksler in discussion of the results of the present work. Analogous considerations were presented in references 16 and 17.

†We are very grateful to I. E. Tamm for detailed information about calculations connected with various models of periphery collisions.

(In Russian). Vol. 1, M. 1959, p. 260.

[2] Bogachev, Bunyatov, Merekov, and Sidorov, Dokl. Akad. Nauk SSSR **121**, 617 (1958), Soviet Phys.-Doklady **3**, 785 (1959).

[3] Barashenkov, Belyakov, Bubelev, Wang Shou Feng, Mal'tsev, Ten Gyn, and Tolstov, Nuclear Phys. **9**, 74 (1959).

[4] N. G. Birger and Yu. A. Smorodin, JETP **36**, 1159 (1959), Soviet Phys. JETP **9**, 823 (1959).

[5] Lyubimov, Markov, Tsyganov, Cheng P'u-Ying, and Shafranova, JETP **37**, 910 (1959), Soviet Phys. JETP **10**, 651 (1960).

[6] Kuznetsova, Mekhedov, and Khalkin, JETP **34**, 1096 (1958), Soviet Phys. JETP **7**, 759 (1958).

[7] Wright, Saphir, Powell, Maenchen, and Fowler, Phys. Rev. **100**, 1802 (1955).

[8] V. G. Grishin and I. S. Saitov, JETP **33**, 1051 (1957), Soviet Phys. JETP **6**, 809 (1958).

[9] V. S. Barashenkov and Huang Nen-Ning, JETP **36**, 1319 (1959), Soviet Phys. JETP **9**, 935 (1959).

[10] N. M. Viryasov and L. P. Pisareva, Приборы и техника эксперимента (Instrum. and Meas. Engg.) No. 2, 17 (1958).

[11] P. H. Fowler and D. H. Perkins, Phil. Mag. **46**, 587 (1955).

[12] Fowler, Shutt, Thorndike, Whittemore, Cocconi, Hart, Block, Harth, Fowler, Garrison, and Morris, Phys. Rev. **103**, 1489 (1956).

[13] Fowler, Shutt, Thorndike, and Whittemore, Phys. Rev. **95**, 1026 (1954).

[14] Kalbach, Lord, and Tsao, Phys. Rev. **113**, 325 (1959).

[15] Kalbach, Lord, and Tsao, Phys. Rev. **113**, 330 (1959).

[16] D. I. Blokhintsev, CERN Symposium **2**, 155 (1956).

[17] Blokhintsev, Barashenkov, and Barbashov, Usp. Fiz. Nauk **68**, 417 (1959), Soviet Phys.-Uspekhi **2**, 505 (1960).

Translated by G. E. Brown
251

SPUTTERING OF COPPER BY HYDROGEN IONS WITH ENERGIES UP TO 50 kev

N. V. PLESHIVTSEV

Institute of Chemical Physics, Academy of Sciences, U.S.S.R.

Submitted to JETP editor June 10, 1959

J. Exptl. Theoret. Phys. (U.S.S.R.) **37**, 1233-1240 (November, 1959)

The dependence of the sputtering ratio S (atoms/ion) on energy, angle of incidence, and mean ion current density was investigated by means of an ion gun. The angular distribution of sputtered particles and the microrelief of the surface were also studied. $S \sim (\ln E)/E$ was found for ion energies $E = 15 - 55$ kev. The sputtering ratio grows with increase of the angle of incidence and within a certain range is independent of the mean beam current density. For both normal and oblique beam incidence the angular distribution of sputtered particles differs significantly from a cosine law. Grooves are formed along the direction of incidence when the beam strikes the surface at an oblique angle. The data indicate that at intermediate energies momentum transfer plays the most important part in the elementary sputtering act.

INTRODUCTION

IN several recent investigations[1-11] cathode sputtering has been studied by means of an ion beam instead of a gas discharge. Heavy ions were used for the most part to study the dependence of the sputtering ratio on ion energy and mass[1-5,8,11] and on target temperature,[7] as well as to study the mass and velocity spectra of the sputtered particles[10] and their angular distribution.[11] Most of the investigations were performed with low-energy heavy ions, but in a few instances[2,8,11] the energy was carried to 25 — 30 kev. However, in some electric vacuum devices, experimental apparatus and accelerators light ions are employed with energies measured in tens of kev or in Mev. In such cases sputtering is accompanied by many undesired effects which must be suppressed. Information concerning sputtering by light ions has been limited to energies up to 2 kev. The sputtering of copper by hydrogen ions of 10 — 50 kev and higher is therefore of decided interest.

1. EXPERIMENTAL TECHNIQUE

The experimental apparatus is shown schematically in Fig. 1. The hydrogen ion beam was produced by an ion gun containing a source with a doubly-confined plasma.[12,13] Commercially pure hydrogen passed through the walls of a heated nickel tube into the gas-discharge chamber of the source. After ionization in an arc from a hot cathode, in an inhomogeneous magnetic field, the hydrogen ions were drawn from the chamber, and were

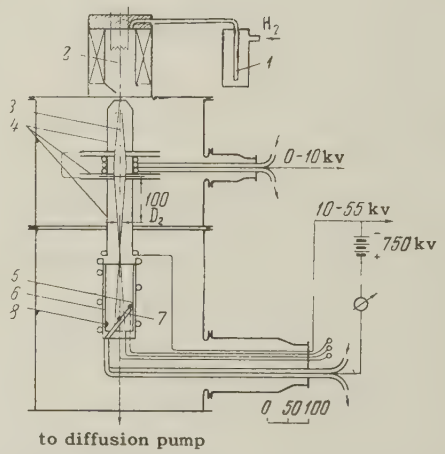

FIG. 1. Diagram of apparatus. 1 — nickel diffusion leak, 2 — ion source, 3 — ion beam, 4 — electrodes of univoltage electrostatic lens, 5 — target for angle of incidence $\alpha = 60°$, 6 — Faraday cup, 7 — copper-kopel thermocouples, 8 — collector of sputtered copper.

then focused and accelerated by a univoltage (symmetrical) electrostatic lens. The accelerating potential was measured by a class-1.5 electrostatic kilovoltmeter.

The ion gun produced hydrogen ion beams with currents up to 30 ma at U = 55 kv. However, smaller currents of 3 — 10 ma were used in order to keep the beam from striking and consequently sputtering the lens electrodes. The ion beam was observed distinctly and measured visually by means of the radiation from excited and recombining atoms, through openings in the electrodes. Difficulties of experimental design prevented a mass-spectrographic analysis of the beam, since a high voltage

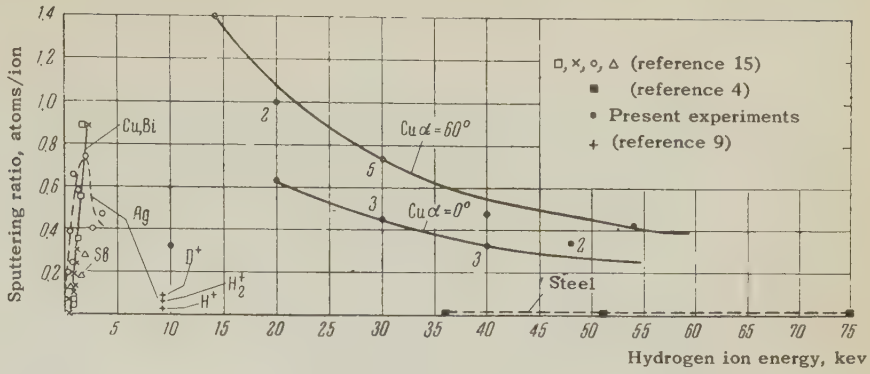

FIG. 2. Sputtering ratio as a function of hydrogen ion energy and angle of incidence. The numerals on the curves indicate the number of experimental runs.

was applied to the Faraday cup, which was followed directly by the vacuum apparatus. In order to maintain a beam of constant composition the source was operated under steady conditions. The arc voltage and current were 100 v and 0.5 amp; the pressure was 3×10^{-2} mm Hg; the current in the constraining magnetic coil was 2 amp.

The number of ions striking the target was measured calorimetrically since electric measurements by means of a cutoff potential give current values which are often too high by a factor of 3 or 4. Inlet and outlet temperatures of the target-cooling water were measured by thermocouples with 1° C scale divisions, with a consequent error of 10 — 25%.

The targets varied in design. At angle of incidence $\alpha = 0°$ the target was usually a copper disk 70 mm in diameter and 2 — 4 mm thick, to one side of which three thermocouples were attached. This surface was cooled by water. The target used at $\alpha = 60°$ was an ellipse 1 mm thick produced by a 60° intersection of a plane with a cylinder 70 mm in diameter. A cooling tube was soldered to the target perimeter and three thermocouples were also attached in this instance. The target surfaces were washed in alcohol before the first experiment and were subjected to no further treatment.

The collectors of sputtered copper were made of 260 × 200 × 0.1 mm nickel foil held by two snap rings against the inside surface of a water-cooled Faraday cup 80 mm in diameter.

The quantity of sputtered copper was determined from the changes of target and collector weights, using an ADV-200 analytical balance for double weighing to eliminate random errors. The weighing was accurate to within 0.1 or 0.2 mg. In some instances an assay balance accurate to within 0.02 mg was used. The sputtered material weighed from 3 to 35 mg.

The experimental error is estimated at 15 — 30% depending on the beam energy. The sputtering ratio was calculated by means of the formula

$$S = 1.5\, m/Q,$$

where m is the weight of sputtered copper in milligrams and Q is the quantity of ions striking the target measured in coulombs.

The vacuum for the ion gun was produced by a 1000-liter oil diffusion pump with a standard water trap. A vacuum of 6×10^{-6} mm Hg was attained, while the working pressure was $3 - 5 \times 10^{-5}$ mm Hg according to a LM-2 air gauge, or $1 - 2 \times 10^{-5}$ mm Hg when converted to hydrogen.

Measurements of the several experimental parameters (ion current, accelerating voltage, target temperature, pressure etc.) were obtained in 5 — 10 minutes, with a single measurement requiring 5 minutes.

2. DEPENDENCE OF SPUTTERING RATIO ON ION ENERGY; ANGLE OF INCIDENCE AND MEAN CURRENT DENSITY

The sputtering of metals by hydrogen and deuterium ions has not been investigated very thoroughly. The available data are shown in Fig. 2. Guntherschulze and Meyer obtained data on copper sputtering in a gas discharge for the energy range 0.3 — 2 kev.[15]

When an ion beam interacts with a metal surface residual gas molecules may form surface films of different colors and shades (black or blue). A similar effect, which is probably polymerization, is produced by electron bombardment of specimens in electron microscopes. Investigations of this phenomenon are reported in reference 16. Experiments on copper sputtering using an ion gun (10 — 55 kev) and in an accelerator tube (300 — 600 kev) provide a basis for a few remarks concerning the building up of such films. The formation of a film depends on the ion current density, sputtering ratio, and target temperature and on the presence of a diaphragm in the path of the beam. With 20 — 600 kev ion energies at normal incidence, when the copper surface temperature is 50 — 100° C a film is not formed if the density of H_2^+ or D_2^+ exceeds 0.5 — 1.5 ma/cm^2. At $\alpha = 60°$ with H_2^+ ions of 15 — 55 kev and the

Data from experiments to determine the sputtering ratio as a function of ion energy and angle of incidence

No. of experiment	Ion energy, kev	Ion current, ma	Mean ion current density, ma/cm²	Target temperature, °C	Quantity of ions, Q, coulombs	Weight of copper on collector, mg	Decrease of target weight, mg	Correction for ion weight, mg	Weight of sputtered copper, mg	Sputtering ratio, Cu atoms/ion
Angle of incidence $\alpha = 0°$										
23	10	1.5	0.2	25	12.5	3.0	2.1	0.2	2.3	0.28—0,36
5	20	5.0	0.2	550	55	—	36.6	0.8	37.4	1.04
6	20	5.2	0.2	650	27.5	—	11.5	0.4	11.9	0.65
1	30	8.6	0.45	250	100	—	23.0	1.5	24.5	0.37
7	29	10.0	0.6	80	50	—	18.3	0.75	19.1	0.57
8	29	9.3	1.1	80	93	—	23.4	1.4	24.8	0.40
2	39	7.7	0.4	250	67	—	13	1.0	14.0	0.31
4	40	6.2	0.9	400	15	—	3.7	0.25	4.0	0.40
9	40	10.5	0.8	80	125	—	15.8	1.9	17.7	0.21
20	48	4.5	1.6	100	16.7	3.5	4.2	0.25	4.5	0.40—0,31
21	49	9.3	1.3	100	75	9.4	16.4	1.1	17.5	0.35—0,19
Angle of incidence $\alpha = 60°$										
13	14	3.0	0.07	60	15.1	14	13.0	0.2	13.2	1.30—1.40
14	20	5.3	0.13	80	19.0	11.9	21.2	0.3	21.5	1.7—1.0
11	21	5.1	0.18	40	23.0	—	16.2	0.35	16.6	1.1
12	26	7.0	0.22	100	31.5	—	12.1	0.5	12.6	0.60
16	30	5.6	0.30	100	20.1	7.2	10.4	0.3	10.7	0.80—0.54
17	30	5.7	0.16	100	20.5	8.3	9.7	0.3	10.0	0.73—0.61
18	30	5.8	0.22	100	21.0	7.4	9.3	0.3	9.6	0.69—0,53
10	31	6.9	0.23	100	20.7	—	10.6	0.3	10.9	0.80
15	32	7.0	0.26	150	29.5	13.3	15.3	0.45	15.8	0.81—0.68
19	40	5.7	0.21	150	42.2	6.3	13.0	0.65	13.7	0.49—0.23
22	54	7.3	0.42	240	55.0	16.0	34.4	0.80	35.2	0.96—0.44

same temperature range a film is not formed with $0.2 - 0.4$ ma/cm². Diaphragm apertures in the beam path assist the production of films, which do not appear, however, when the target temperature exceeds $400 - 450°$ C. The longest experiment yielded ~ 0.5 mg as the weight of the film at the periphery of the spot burned by the beam.

The experimental conditions and results are given in the table. In most instances the weight of sputtered copper leaving the target was approximately equal to the weight of the copper deposited on the collector. Figure 2 shows the sputtering ratio as a function of energy and angle of incidence. S as a function of energy is quite well approximated by the relation $S \sim (\ln E)/E$, where E is the ion energy.

In experiments 1 and 2 it was established by means of a divided target consisting of nine copper foils that the radial distribution of beam current density can be represented by a Gaussian error curve. Therefore the column for "Mean ion current density" in the table gives the total current to the target divided by the area of the beam spot. Figure 3 shows the relation between S and the mean ion current density.

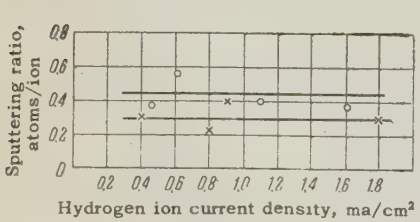

FIG. 3. Sputtering ratio as a function of ion current density ($\alpha = 0°$), o — E = 30 kev, T = 80–250°C; × — E = 40 kev, T = 80–400°C

3. ANGULAR DISTRIBUTION OF SPUTTERED PARTICLES

The angular distribution of sputtered particles was investigated by Seeliger and Sommermeyer,[17] who were the first to use ion beams to study cathode sputtering. When silver and gallium were bombarded at $\alpha \leq 45°$ by argon ions with $5 - 10$ kev a cosine-law angular distribution of the sputtered particles was observed. Guntherschulze[18] observed a departure from the cosine law in the sputtering of silver by hydrogen ions with $0.5 - 3$ kev. A departure from the cosine law was also reported in reference 11.

For the purpose of studying the angular distribution at $\alpha = 60°$, 14 nickel foils of dimensions $20 \times 20 \times 0.1$ mm³ were attached to the nickel collecting cylinder (Fig. 4). These were weighed to within 0.02 mg. The experimental results are represented in Figs 4a and 4b, where the numerals inside the squares denote the identifying numbers of the collecting foils and the quantity of sputtered

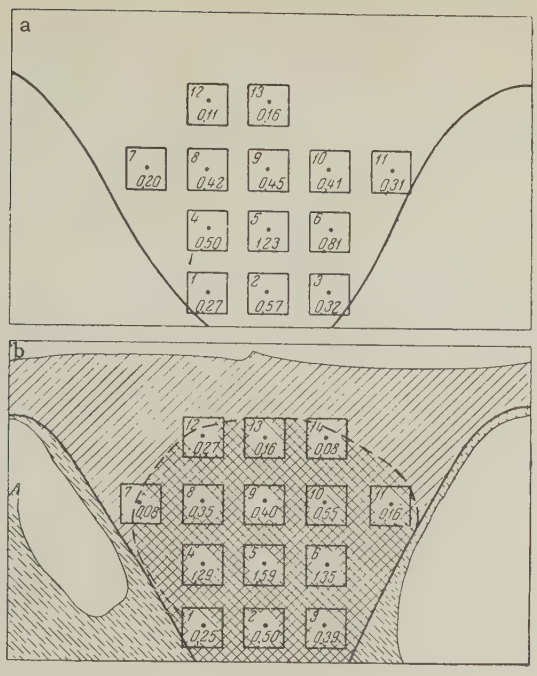

FIG. 4. Distribution of sputtered copper on square collecting foils ($\alpha = 60°$), a – E = 40 kev, T = 150°C; b – E = 54 kev, T = 240°C.

copper in milligrams. In Fig. 4b the bright spot of deposited copper is represented by crosshatching. The distribution of sputtered copper at $\alpha = 0°$ was studied by means of strips attached parallel to the Faraday cylinder axis. Figure 5a – d shows the angular distributions of copper for $\alpha = 60°$ and $\alpha = 0°$, which in all cases deviate considerably from a cosine law. This is especially marked in the case of 54-kev ions. In this case, at $\alpha = 60°$, the angular distribution peak is shifted from the normal to the target by approximately half the angle of incidence.

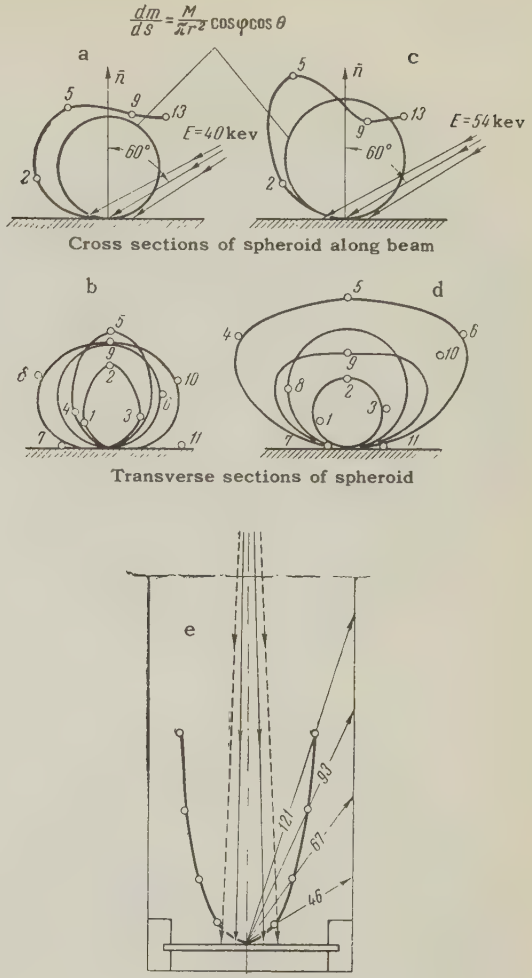

FIG. 5. Angular distribution of sputtered copper. a, b – E = 40 kev, $\alpha = 60°$, T = 150°C; c, d – E = 54 kev, $\alpha = 60°$, T = 240°C; e – E = 49 kev, $\alpha = 0°$, T = 100°C. The numerals on the curves denote the collecting foils as shown in Fig. 4.

4. SURFACE CONDITION

After each experiment it was almost always possible to observe four clearly defined regions. The granular structure at the center of the beam spot was visible even with the naked eye. After prolonged bombardment the copper begins to flake off in this area; strong etching separates the grains from the surface. The second region, which is a ring around the center, has the bright red color of reduced copper. The next ring is light red in color, while the peripheral region is covered with a translucent dark film. These regions result from the nonuniform lateral distribution of current density.

The targets were studied and photographed using a MS-51 comparator and a MIM-6 metallurgical microscope. Targets which were bombarded at $\alpha = 0°$ clearly showed the usual etch figures, cones and pits* (Fig. 6a). The numbers of cones and depressions increase with the ion current density. Estimates based on the sharpness of focusing and resolution of the microscope gave a cone vertex diameter of $\sim 3\mu$ and height $\sim 30\mu$. Targets positioned at 30° with respect to the beam exhibited grooves $\sim 5\mu$ wide and $\sim 30\mu$ long instead of cones and pits (Fig. 6b). The grooves indicate the direction of beam incidence and increase in number toward the beam center.

5. DISCUSSION OF RESULTS

The reduction of the sputtering ratio with increasing energy† can be accounted for by several

*The presence of pits was pointed out to the author by V. E. Yurasova.

† Indirect confirmation of this relationship can be found in the data obtained by B. V. Panin for the behavior of the ion-ion emission ratio, where a peak is observed at 8–10 kev (private communication), and also in reference 11.

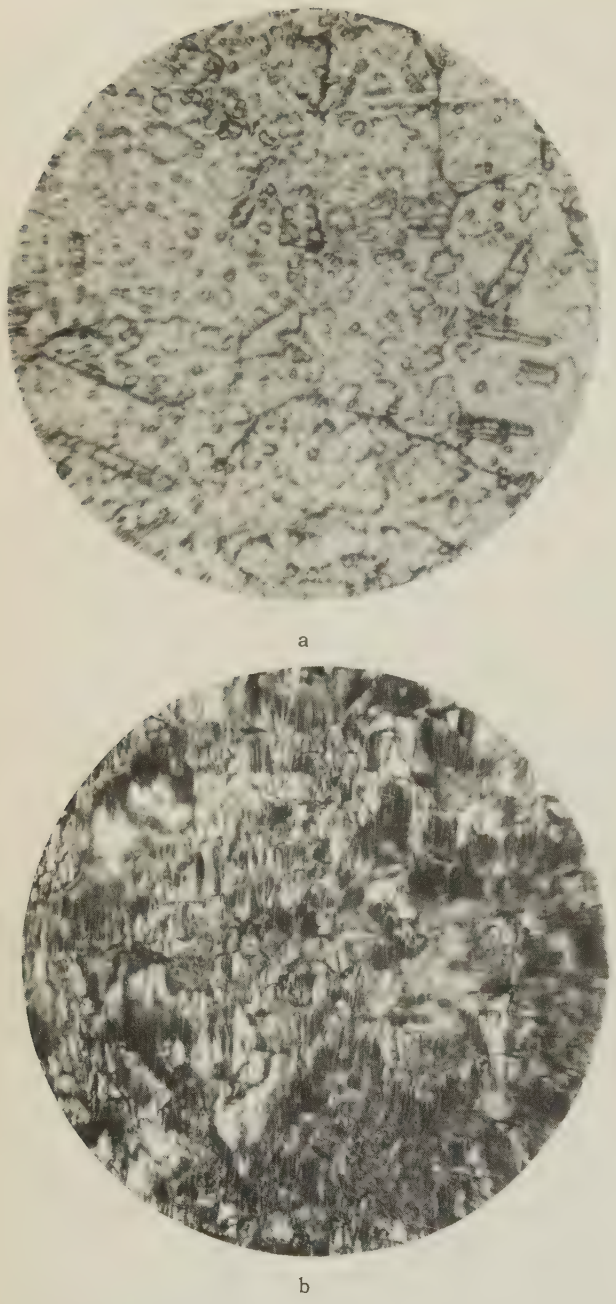

a

b

FIG. 6. Microrelief of copper surface after sputtering by hydrogen ions (×130); a – E = 30 kev, j = 1.6 ma/cm², t = 194 min; b – E = 14–54 kev, j = 0.07–0.8 ma/cm², t = 842 min.

factors, principally 1) increased ion range in the target material and the resulting greater depth from which the diffusion or ejection of displaced atoms occurs; 2) increased ion energy loss due to ionization and excitation in the region where the ion velocity is approximately equal to the velocity of orbital electrons. The sputtering curve peak was predicted by Keywell[5] while the monotonic decline following a $(\ln E)/E$ law was derived by Goldman and Simon[19] for ion energies above 50 kev.

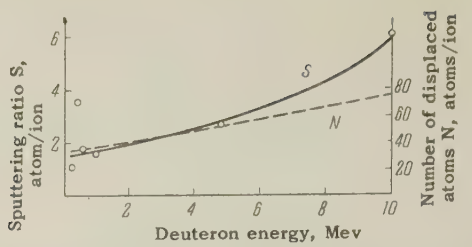

FIG. 7. Comparison of the number of displaced copper atoms with the number of sputtered atoms produced by deuterons with energies of 0.3–10 Mev.

Preliminary results for copper sputtering by 300 – 600 kev deuterons and in a cyclotron at 1 – 10 Mev indicated that the sputtering ratio increases with energy (Fig. 7). These data show that the theory of Goldman and Simon[19] for deuteron energies above 300 kev leads to results which are too low by 3 to 4 orders of magnitude and that their law is not correct in general.

At the present time the most widely accepted theory is that of Keywell,[5] which is based on the technique proposed by Seitz[20] for computing the number of displaced atoms, but which was developed only for energies up to 5 – 6 kev. We have therefore attempted to establish a relationship between the number of displaced atoms and the number of atoms sputtered by a single incident hydrogen or deuterium ion in the energy range 0.6 kev – 10 Mev. Data on the proton-stopping power of copper were taken from reference 21 and were extrapolated to the 0.6 – 6 kev region. The stopping power for deuterons was computed from Warshaw's data[22] for protons with the same velocities as the deuterons. Figures 7 and 8 show the results of the computations and preliminary runs, which indicate that about 5% of the displaced copper atoms are sputtered in the entire investigated energy range.

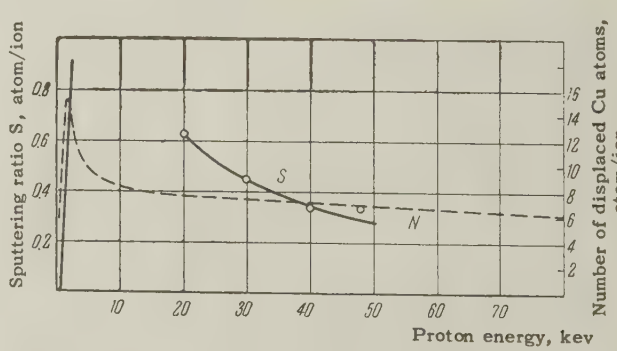

FIG. 8. Comparison of the number of displaced copper atoms with the number of sputtered atoms produced by protons up to 100 kev.

It is necessary to discuss the possible experimental errors. The composition of the beam was

known only very approximately because of the lack of a mass-spectrographic analysis. The beam included nitrogen and oxygen ions, resulting from charge exchange with hydrogen ions, which were able to induce additional sputtering; we shall now estimate the corresponding error. The charge-exchange cross sections for these vapors have been thoroughly investigated by a number of authors (see reference 23, for example) and the value $\sim 5 \times 10^{-16}$ cm^2 has been obtained for the maximum at 5 kev. In the univoltage electrostatic lens the mean free path of ions with this energy did not exceed 6 — 8 cm. It was easily computed that under the given working conditions N_2^+ and O_2^+ could not comprise more than 1% of the total beam current. This was confirmed experimentally by Orfanov,[24] who studied the mass spectrum of a beam in a similar gun. Under the given operating conditions of the ion source the beam was found to consist of H_2^+ (40 — 50%), H_1^+ (30 — 40%), H_3^+ (30 — 10%), N_2^+ and O_2^+ (1 — 3%). The sputtering ratio of copper by nitrogen ions is 2 atom/ion.[11] Therefore N_2^+ and O_2^+ should not produce an error greater than 6 — 10% in the value of S for hydrogen ions.

The author is deeply indebted to Professor B. K. Shembel' for suggesting this research and for his continued interest. He is also indebted to D. V. Karetnikov, S. N. Popov, I. F. Kvartskhava, and P. P. Dmitriev, who made it possible to perform the experiments using the ion gun and the cyclotron.

The author wishes to thank V. I. Lisovskiĭ for assistance in preparing and conducting some of the experimental runs; I. N. Slivkov for valuable discussions; and Professor N. D. Morgulis and M. I. Guseva for discussions of the results.

[1] L. N. Dobretsov and N. M. Karnaukhova, Dokl. Akad. Nauk S.S.S.R. **85**, 745 (1952).

[2] M. A. Eremeev and Ya. K. Éstrinov, J. Tech. Phys. (U.S.S.R.) **22**, 1552 (1952).

[3] R. Bradley, Phys. Rev. **93**, 719 (1954).

[4] F. Fairbrother and J. S. Foster, Vacuum **4**, 112 (1954).

[5] F. Keywell, Phys. Rev. **97**, 1611 (1955).

[6] J. R. Young, J. Appl. Phys. **26**, 1302 (1955).

[7] L. V. Zyrina and M. D. Yagudaev, Тр. Среднеазиатского университета (Trans. Central Asia University) **65**, 33 (1955).

[8] M. I. Guseva, Приборы и техника эксперимента (Instrum. and Meas. Engg.) **5**, 112 (1957).

[9] Moore, O'Briain, and Lindner, Ann. N.Y. Acad. Sci. **67**, 600 (1957).

[10] R. E. Honig, J. Appl. Phys. **29**, 549 (1958).

[11] Rol, Fluit and Kistemaker, Terzo congresso internazionale sui fenomeni d'ionizzazione nei gas tenuto a Venezia dall' 11 al 15 ginguo, Milano, 1957.

[12] M. Ardenne, Tabellen der Elektronenphysik, Ionenphysik und Übermikroskope, Berlin, 1956; Technik **2**, 3 (1956).

[13] D. V. Karetnikov, Dissertation, Inst. Chem. Phys., Acad. Sci. U.S.S.R., 1954; Egorov, Karetnikov and Popov, Приборы и техника эксперимента (Instrum. and Meas. Engg.) in press.

[14] L. P. Khavkin, J. Tech. Phys. (U.S.S.R.) **26**, 2356 (1956), Soviet Phys.-Tech. Phys. **1**, 2279 (1956).

[15] A. Guntherschulze and K. Meyer, Z. Physik **62**, 607 (1930).

[16] A. E. Ennos, Brit. J. Appl. Phys. **4**, 101 (1953); **5**, 27 (1954).

[17] R. Seeliger and K. Sommermeyer, Z. Physik **93**, 692 (1935).

[18] A. Guntherschulze, Z. Physik **119**, 79 (1942).

[19] D. T. Goldman and A. Simon, Bull. Am. Phys. Soc. Ser II, **3**, 40 (1958); Phys. Rev. **111**, 383 (1958).

[20] F. Seitz, Discussions Faraday Soc. **5**, 271 (1949).

[21] H. Batzner, Ann. Physik **25**, 233 (1938).

[22] S. D. Warshaw, Phys. Rev. **76**, 1759 (1949).

[23] P. M. Stier and C. F. Barnett, Phys. Rev. **103**, 896 (1956).

[24] I. V. Orfanov, Report Inst. Chem. Phys., Acad. Sci. U.S.S.R., 1959.

Translated by I. Emin
252

EFFECT OF TEMPERATURE ON THE VARIATION OF THE ISOTOPIC COMPOSITION OF LIQUID MERCURY IN THE ELECTRIC FIELD OF A CONSTANT CURRENT

I. V. BOGOYAVLENSKIĬ, V. N. GRIGOR'EV, and N. S. RUDENKO

Physico-technical Institute, Academy of Sciences, Ukrainian S.S.R.

Submitted to JETP editor June 16, 1959

J. Exptl. Theoret. Phys. (U.S.S.R.) **37**, 1241-1246 (November, 1959)

The temperature dependence of the change in the concentration of liquid mercury isotopes upon passage of a constant electric current through the liquid has been studied experimentally. In the stationary case the change in the concentration was found to be independent of the temperature. Some possible mechanisms of the phenomenon are discussed.

THE change in the isotopic composition of liquid metals in the passage through them of a constant electric current has recently been investigated for a whole series of metals: Hg,[1-4] Ga[5,6] K,[7] In,[8] Li,[9] Cd, Zn, Sn,[10] and Rb.[11] It is characteristic of all these metals that the heavy isotopes are always concentrated at the cathode and the lighter ones at the anode; the process of the change of concentration continues until a certain stationary state is reached that determines the equilibrium between the process of enrichment and the reverse one of diffusion; the coefficient of enrichment reaches several per cent per volt.

The phenomenological theory of the process, both in the stationary and non-stationary cases, has been developed by Bresler and Pikus.[12,13] and also in previously published researches of the authors.[3,4] This theory was completely substantiated in the previous work of the authors.[4]

The processes described by the nonlinear differential equation:

$$\frac{d}{dx}\left[c(1-c)\gamma\frac{\varepsilon_0 E}{kT}-\frac{dc}{dx}\right]=\frac{1}{D}\frac{dc}{dt}, \qquad (1)$$

where c is the concentration of one of the isotopes, D is the diffusion coefficient, E is the electric field intensity, T is the temperature, ϵ_0 is the electronic charge. Equation (1) preserves its form outside of the dependence on the assumed mechanism of separation; however, the constant γ entering into the equation will have a different physical meaning in each case.

Bresler and Pikus[12,13] assume two different mechanisms of separation. The first of these was based on the assumption that the reason for the separation was the difference in the mobilities of the heavy and light isotopes. In this case, the more mobile ions, carried along by the electric field, congregate about the cathode. Here, $\gamma = \Delta\mu/\mu$, where $\Delta\mu = \mu_1 - \mu_2$; μ_1 and μ_2 are the mobilities of ions of the one and the other isotope. To obtain the correct direction of the effect, it is necessary that the mobility of the ions of the heavy isotope be greater than those of the light.

The second mechanism takes into account the difference in the interaction of the electric current with ions of one or the other isotopes. If the probability of scattering of the electrons by ions of the different isotopes is characterized by the corresponding values of the electrical resistance, ρ_1 and ρ_2, and the scattering by each ion takes place independently, then the isotope possessing the larger electrical resistance is carried along in greater degree by the electric current and concentrates at the anode. In this case, $\gamma = \Delta\rho/\rho$, where $\Delta\rho = \rho_1 - \rho_2$. It follows from the direction of the effect that the electrical resistance of the light isotope must be greater than that of the heavy.

A thermodynamic consideration of the phenomenon of the change of concentration of isotopes in the stationary case was given by the author[3] under the assumption that the separation appears as a result of the different molar volumes of the isotopes, which leads to a difference in the charges of the ions of the different isotopes per unit volume. The separation of the ions in this case takes place in a way similar to the separation of particles of different mass in the gravitational field. Here $\gamma = \Delta V/V$, where $\Delta V = V_1 - V_2$; V_1 and V_2 are the molar volumes of the isotopes.

Gennes[14] also assumes that the separation is brought about by the presence of a strong interaction of the electronic current with the ion and, applying the relations for a solid for the micro-

scopic description, he obtains the value

$$\gamma = \frac{zC}{12}\left(\frac{\Theta}{T}\right)^2 \frac{\Delta M}{M},$$

for γ, where Θ is the Debye temperature, z = number of charges on a single ion, M = mass of the ion, $\Delta M = M_1 - M_2$, C = coefficient of the order of unity.

Thus there are several assumptions regarding the mechanism of the change in concentration of isotopes in an electric field of a constant current. However, the experimental data currently available do not make it possible to examine critically the assumptions that have been made. For such considerations additional experimental investigations are necessary.

One of the experimental possibilities is the study of the temperature dependence of the effect. Actually, the presence of such a dependence makes it possible to consider the assumptions from the point of view of the validity of the temperature dependence of the coefficient γ.

Unfortunately, the information in the literature on temperature dependence[6,8,10,11] is quite contradictory and unreliable because of its low accuracy, inasmuch as the authors of these papers used formulas for the computation of the quantity $\kappa = \gamma/(\Delta M/M)$ which do not take back diffusion into account. This compels them to carry out their investigations for short times of current transmission (at the beginning of the process), and consequently to use for mass spectrometric measurements slightly enriched specimens which have a strong influence on the accuracy of the measurements. An increase in the time of transmission of current increases the accuracy of the mass spectrometric measurements but lowers the accuracy of calculation of the value of κ because of lack of knowledge of back diffusion.

In the experiments described below, a method based on the phenomenological theory of Bresler and Pikus is employed which has already been used by the authors in reference 4.

EXPERIMENTS

The investigation of the temperature dependence of the change of the isotopic constitution of mercury in the passage through it of a constant current was carried out in glass capillaries of internal diameter 0.4 — 0.5 mm and external diameter 5 — 6 mm (Fig. 1). The sample consisted of two sections of capillary each of length 73 mm, joined together through a reservoir. Since the concentration of isotopes in the middle of the specimen remains unchanged, the presence there of a

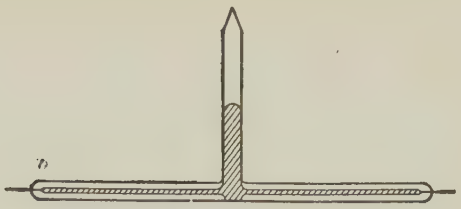

FIG. 1

mercury reservoir had no effect on the change of concentration. From the mathematical point of view, such a specimen corresponds to a homogeneous capillary of length 146 mm with closed ends at both electrodes.

The comparatively small length of the capillary was chosen for reasons of experimental convenience, because the time for establishing the stationary state in such a capillary amounted to about 20 days for the very low temperatures used in the experiments. The danger of the appearance of convection currents in the mercury for the short length of capillary was eliminated by the fact that the capillaries were horizontal at the time of the experiments (experiments carried out with capillaries in a vertical position showed that for such a length of capillary the convection currents appreciably lowered the value of the concentration change, beginning with a temperature of about 150° C).

The specimen was pumped out through the reservoir to a pressure of 10^{-6} mm mercury, heated and filled with mercury by means of distillation. A constant stabilized voltage maintained with an accuracy of 2 — 2.5 percent was applied to molybdenum electrodes soldered to the ends of the capillary. The decrease in the voltage on the specimens at a temperature of — 34° C amounted to about 1 volt, for all other temperatures, about 2 volts, and was measured separately for each specimen with an accuracy no worse than 0.5 percent.

For the maximum range of temperature of liquid mercury, a succession of baths were employed in which the specimens were submerged at the following temperatures (in degrees C): acetone, — 37 ± 1, water, 30 ± 5; lubricating oil, 105 ± 5; and tin, 210 ± 5, 250 ± 5, 300 ± 5. The drop in temperature between the bath and the mercury in the capillary was determined by means of a calculation in which the coefficient of thermal conductivity of the glass used for the specimens was measured for the corresponding temperature range. For a number of specimens, the temperature of the mercury was estimated by the change in the electrical resistance. The results of the measurements coincided with the computed data.

The parts of the capillary close to the electrodes, of length about 7 mm, were cut off after the lapse of a definite time of transmission of current between the specimens, and the mercury drawn off from the cut-off capillary was analyzed by a mass spectrometer. The coefficient of separation P existing at a difference of potentials of 1 volt was computed by the formula

$$P = (\Delta a / a_0) / U,$$

where $\Delta a = a_1 - a_2$; a_1, a_2, a_0 are the ratios of the concentration of Hg^{198} to the concentration of Hg^{204} in the mercury close to the anode, close to the cathode, and in standard mercury, respectively; U = voltage on the electrodes. For each temperature, the dependence of the coefficient P on time of transmission of the current was measured, and the coefficients of separation P_∞ corresponding to the stationary state ($t \to \infty$) were computed from these dependences, and also the coefficients $\gamma = (kT/\epsilon_0) P_\infty$.

From the equations describing the process, it is simple to obtain

$$P_\infty = \gamma \frac{\varepsilon_0}{kT} = P \left[1 - \sum_{n=0}^{\infty} \frac{8}{\pi^2 (2n+1)^2} \times \exp\left[- \frac{\pi^2 D (2n+1)^2}{4l^2} t \right] \right]^{-1}, \quad (2)$$

for $\gamma \ll 1$ and $\Delta a/a_0 \ll 1$, where ϵ_0 = electronic charge, l = length of the capillary (73 mm). Under such conditions, Eq. (2) is valid not only for a two component mixture, but also for any pairs of isotopes of a mixture consisting of many components.

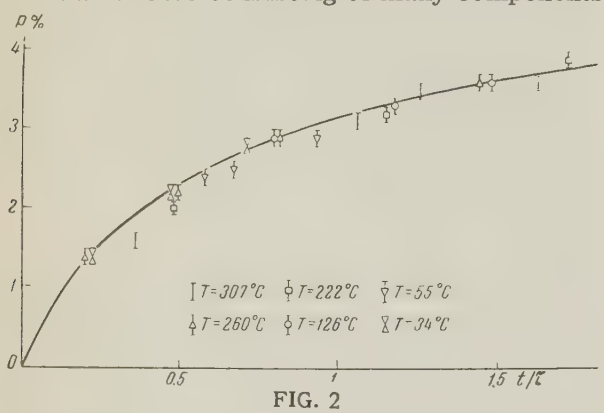

FIG. 2

The dependence of the change of concentration of Hg^{198} and Hg^{204} on the time of transmission of the current is plotted in Fig. 2 for different temperatures. The reduced time t/τ is plotted along the abscissa, where $\tau = 4l^2/\pi^2 D$ is the time required to establish the steady state. Here, the coefficient of self-diffusion D was computed according to the empirical formula[15]

$$D = 1.260 \cdot 10^{-4} \exp[-1160/RT].$$

It is seen from the graph that for equal times the coefficient P does not depend on the temperature. It also follows from the graph that the maximum change in the concentration (for large time of transmission of current) P_∞ remains constant for the whole temperature range of liquid mercury.

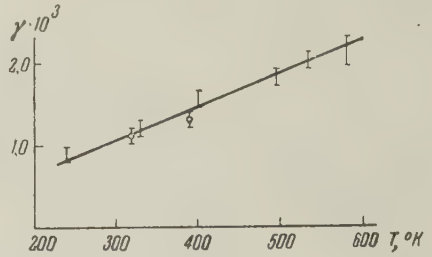

FIG. 3

The dependence of the coefficient γ on temperature is shown in Fig. 3. Points corresponding to temperatures 318°K and 388°K were obtained from the results of the previous work of the authors.[4*] As is seen from the graph the coefficient γ in which we are interested increases in proportion to the increase in temperature.

DISCUSSION OF RESULTS

The observed linear growth of γ with increase in temperature permits us to evaluate the assumptions of the nature of the process.

The temperature dependence that is obtained contradicts the assumption of Gennes inasmuch as it is necessary to assume that the product zC increases proportionally to T^3 in order that the condition $\gamma \sim T$ be satisfied. The density of charges per ion can increase with temperature; however, one does not have to rely on its rapid increase. The change of the coefficient C with temperature depends on the difference in activation energy of diffusion and viscosity and it is uncertain that it can depend so strongly on the temperature.

The assumption that the determining role in the process of concentration change is played by the difference in the molar volumes of the isotopes $\Delta V/V$ is also not capable of explaining the dependence $\gamma \sim T$. Although the molar volumes

*A mistake was made by the authors in reference 4. In Eq. (12) the quantity L/2 should appear for L/4 in front of the brackets. For this reason, the quantity $\varkappa$ computed for mercury from the results of the research and given in the Table is twice too large, and one must regard the values of L and $\Delta\mu/\mu$ as referring to the mercury isotopes Hg^{198} and Hg^{204}.

for metallic isotopes were not studied experimentally, experiments with isotopes of hydrogen and helium show a decrease, and not an increase, in the relative difference of molar volumes, with increase in temperature. Some further support can be found from the fact that the theoretical estimates of $\Delta V/V$ carried out with reference to the solid state also show a decrease in this quantity with increase in temperature.

The temperature dependence of the relative difference in mobilities $\Delta\mu/\mu$ is still not clearly established; however, there is an experimental fact which does not support the use of the assumption of $\Delta\mu/\mu$ as the reason for the effect. Lazarus and Okkerse[16] measured the coefficients of diffusion for two isotopes of iron Fe^{55} and Fe^{59} in silver and found that the light isotope of iron Fe^{55} possessed the greater mobility. At the same time, as was pointed out above, for a correct explanation of the direction of the change of concentration in the electric field of a constant current by such a mechanism, it is necessary that the lighter isotope possess a smaller mobility than the heavier. The fact that in one case we are talking about self diffusion in a liquid metal, and in the other about diffusion in a solid material is evidently not decisive for the sign of the difference of mobility of the isotopes.

An excellent opportunity of testing the assumptions connected with the difference in the electrical resistance of the isotopes is provided by a comparison of the value of $\Delta\rho/\rho$ and its dependence on temperature, obtained from experiments on the concentration change in the electric field of a current, with the value and temperature dependence of $\Delta\rho/\rho$ determined directly for the same isotopes. Such investigations, which also possess an interest in their own right, were carried out by the authors for the isotopes of mercury. The results of preliminary experiments do not eliminate the possibility of the explanation of the effect of the change of concentration in the electric field of a current by the presence of a difference in the electrical resistances of the isotopes.

In the present work we have not considered the mechanism proposed by Klemm,[17] inasmuch as the large number of parameters coming into consideration do not permit us to confirm this mechanism by an experimental test.

We can thus make the following comments regarding the assumptions discussed here. The assumption connected with the difference in the mobilities of the isotopes, the assumption on the difference in the molar volumes, and the consideration of Gennes, contradict the measured temperature dependence. The assumption connected with the difference in the specific electrical resistances of the isotopes represents the most probable of the mechanisms discussed; however, it requires further verification.

[1] E. Haeffner, Nature **172**, 775 (1953).

[2] Haeffner, Sjoborg, and Lindhe, Z. Naturforsch. **11a**, 71 (1956).

[3] Rudenko, Grigor'ev, Dolgopolov, and Bogoyavlenskiĭ, Works (Trudy) of the Session of the Academy of Sciences, Ukr. S.S.R. on the Peaceful Utilization of Atomic Energy, 1956. Acad. Sci. Press, 1958.

[4] Bogoyavlenskiĭ, Grigor'ev, Rudenko, and Dolgopolov, JETP **33**, 581 (1957); Soviet Phys. JETP **6**, 450 (1958).

[5] G. Nief and E. Roth, Compt. rend. **239**, 162 (1954).

[6] Goldman, Nief, and Roth, Compt. rend. **243**, 1414 (1956).

[7] Lunden, Reuterswärd, and Lodding, Z. Naturforsch. **10a**, 924 (1955).

[8] Lodding, Lunden, and Ubisch, Z. Naturforsch. **11a**, 139 (1956).

[9] Lunden, Lodding, and Fischer, Z Naturforsch. **12a**, 268 (1957).

[10] A. Lodding, Z. Naturforsch, **12a**, 569 (1957).

[11] A. Lodding, Z. Naturforsch. **14a**, 7 (1959).

[12] S. E. Bresler and G. E. Pikus, J. Tech. Phys. (U.S.S.R.) **26**, 109 (1956); Soviet Phys.-Tech. Phys. **1**, 102 (1956).

[13] S. E. Bresler and G. E. Pikus, J. Tech. Phys. (U.S.S.R.) **28**, 2282 (1958), Soviet Phys.-Tech. Phys. **2**, 2094 (1958).

[14] P. G. Gennes, J. phys. Rad. **17**, 343 (1956).

[15] R. E. Hoffman, J. Chem. Phys. **20**, 1567 (1952).

[16] D. Lazarus and B. Okkerse, Phys. Rev. **105**, 1677 (1957).

[17] A. Klemm, Z. Naturforsch. **9a**, 1031 (1954).

Translated by R. T. Beyer
253

ON THE PROBLEM OF THE MOTION OF CHARGES IN LIQUID HELIUM II

R. G. ARKHIPOV and A. I. SHAL'NIKOV

Institute for Physical Problems, Academy of Sciences, U.S.S.R.

Submitted to JETP editor June 19, 1959

J. Exptl. Theoret. Phys. (U.S.S.R.) 37, 1247-1251 (November, 1959)

The behavior of electrical charges produced in liquid helium with the aid of a β source has been investigated. An attempt has been made to observe "flushing" of the charges by a thermal current. The suggestion is advanced that the hysteresis effects observed arise from the presence of impurity particles suspended in the liquid helium.

THE behavior of charges in superfluid helium is of considerable theoretical interest. It can be assumed that due to the small polarizability of helium atoms an electron in liquid helium will interact weakly with the thermal excitations, and that its effective mass will be close to the mass of a free electron. In the case of positive charges two points of view are possible. It may turn out, for example, that positive charges in liquid helium move as "holes," and have, therefore, an effective mass close to that of negative charges. The possibility, however, cannot be excluded that, as a consequence of the appreciable binding energy of a positive charge, the helium ions may form about themselves "solvate" shells. In this case the interaction of the positive charges with the bulk of the superfluid liquid helium would naturally be considerably stronger. In particular, analogously to what occurs with a He^3 impurity, there should then be observed effects associated with the "flushing" of the charges by a thermal current.

In connection with the experimental investigations begun in 1954 by Shal'nikov to study the interaction of electrical charges with a thermal current in helium II, one of us[1] constructed a theory of the mobility of charged particles of small effective mass in superfluid helium. For the theory thus developed to be correct, in addition to the requirement of small effective mass $m^* \ll kT/S^2$, where S is the velocity of sound, the quasiclassicality conditions must be fulfilled — the impurity mean free path l must be much greater than the corresponding de Broglie wavelength ($l \gg \hbar/\sqrt{mkT} \sim 10^6$ cm), since in the alternative case it is impossible to write the kinetic equation for the problem, and the approach to the problem changes completely.

This quasiclassicality condition must absolutely be fulfilled for a sufficiently weak interaction of the impurities with the thermal excitations. However, the measurements published to date on the mobility of charged particles in superfluid helium sharply contradict the ideas presented above. The first publication on this problem was that of Williams,[2] who observed the current pulses arising in liquid helium in fields of 10 to 50 kV/cm under the action of a polonium source. The method employed by Williams, as is evident, is in practice quite unsuited to the measurement of ion mobility in the case of helium. In actuality, the ranges of the α particles in this low-density liquid are comparable with the distance between the electrodes of the pulse ionization chamber, the dimensions of which could not be further increased for a variety of reasons, which makes observation of even the pulses themselves impossible. Williams' results are insufficiently definitive, and not only by reason of the scatter in his experimental data; thus, for example, the mobility of the negative ions as determined in his experiments ($\mu^- = 2.0 \times 10^{-2}$ $cm^2/v\text{-}sec$) turned out to be less than the mobility of the positive ions ($\mu^+ = 8.8 \times 10^{-2}$ $cm^2/v\text{-}sec$), which seems to us in the highest degree improbable.

Unfortunately, we do not know all the details of the experiments of Careri et al. These authors also used an α -source, but the value of the mobility was obtained from the "flushing" of the charges by a thermal current. In a second communication by Careri et al.,[3] the agreement of their previous observations with Williams' results is confirmed.

In 1958, Meyer and Reif[4] published the results of mobility measurements obtained by them using the electric shutter method of Tyndall and Powell. They found that the mobility is independent of the magnitude of the electric field intensity for weak fields (50 - 200 v/cm), and confirmed again the closeness of the mobilities of the positive and negative carriers.

The results of Meyer and Reif seem to us

surprising in the highest degree. Most astonishing is the number (10!) of successive current maxima observed on the curve showing the dependence of the current upon the frequency of the voltage applied between the grids. It is known that even in gaseous helium at low pressures, at densities a hundred times smaller than the density of liquid helium, it has proven impossible to observe maxima of such high orders, as a consequence of scattering effects. The equidistant spacing of the maxima in the work of Meyer and Reif indicates, moreover, that the charge carriers in liquid helium have one single effective mass.

Although the experiments we have undertaken have not led us to any wholly definite conclusions, we think it appropriate to report them briefly, in view of the general obscurity of the problem of the motion of charges in liquid helium.

In our first experimental arrangement we proposed to observe the interaction of currents produced with the aid of a radioactive source with a thermal or mechanical current in liquid helium II. As an ion source we used a thin layer of Zr or Tl ($\sim 0.5\mu$), treated with tritium to obtain a compound of the type AT_2, and applied to a polished tungsten plate. The dielectric layer thus obtained was covered, by evaporation or by cathode sputtering, with a thin film of metal (Pt, $\sim 0.1\mu$), providing a good electrical contact between the surface layer of the emitter and the material of the substratum. Such a source (dia. ~ 3 mm) emits β particles having a maximum path in liquid helium $\sim 5\mu$ and allows 4.4×10^9 ion pairs/sec to be obtained.

In Fig. 2 is presented the dependence of current upon distance between the electrodes of apparatus a, illustrated in Fig. 1, on one of which is located the β-particle source, for various values of field intensity; Fig. 3 shows the dependence of current upon field for separations of 40 and 640μ. In these first measurements we encountered hysteresis effects which, it would seem, should not occur at all under the conditions of our experiments, and which were completely absent in gaseous helium. These hysteresis effects were partially present even when the most careful measures were taken to purify the helium, and were the more strongly evident, the weaker the currents being measured. In Fig. 4 are presented two voltage-current characteristics obtained, under conditions of maximum purity within our system, successively within 1.5 hours. The displacement of the characteristics is quite evident even for a current $\sim 10^{-11}$ amp.

Despite these complicating circumstances we nevertheless made an attempt to observe "flushing" of the charges by a thermal current in liquid helium, in the apparatus depicted in Fig. 1b. The idea of this experiment consisted of observation of the displacement of the voltage-current characteristic by a thermal current flowing in the liquid helium from the heater through the screen electrode into the surrounding bath. In the event that the charge current flowing in the space between the electrodes of the chamber was being entrained by the thermal current, we should have observed an effect opposite to the well-known ion "wind" effect. The instability

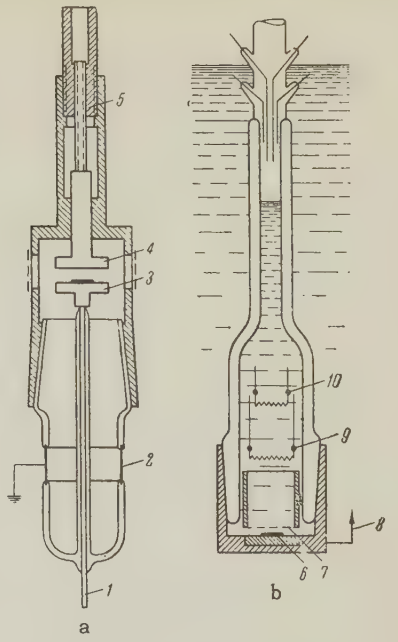

FIG. 1. Diagram of the apparatus: a) 1 – electrometer electrode, 2 – guard ring, 3 – electrode with β-particle source, 4 – electrode, 5 – differential screw; b) 6 – β source, 7 – grid electrode, 8 – electrometer electrode, 9, 10 – thermometer heaters.

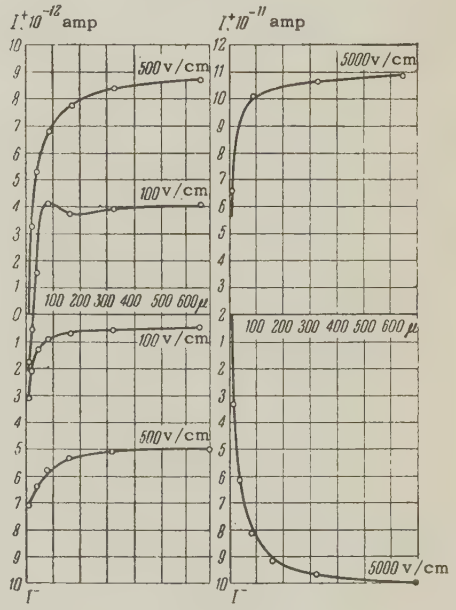

FIG. 2

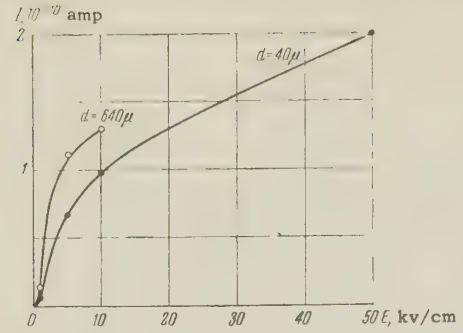

FIG. 3

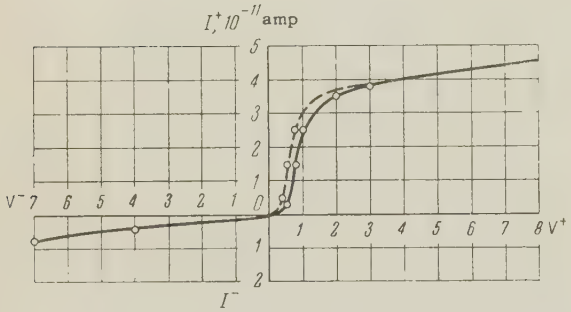

FIG. 4

of the characteristics of the system, however, arising from hysteresis in the region of limitingly small currents (for electric field intensities not exceeding tens of v/cm), prevented us from arriving at any definite conclusions.

Making use of the circumstance that in a sufficiently strong electric field, recombination of the ions virtually ceases at a certain distance from the emitting electrode (Fig. 2), we made yet another attempt to measure the mobility. For this purpose we placed in the apparatus 1a, at a distance of 300 μ from the emitting electrode, a grid, in the space beyond which we could work with a constant charge current of one or the other sign (depending upon the sign of the grid potential). From calculations,[1] the dependence of charge current upon field should be linear for small values of the electric field intensity, and then follow an $E^{1/2}$ law.

Plotting the dependence of the measured current upon field intensity on a log-log scale, it is possible to determine from the location of the break in the curve (field $E_0 \sim 3000$ v/cm), the quantity $1/m^{*1/2}$, which, from our data, amounts to 10^5 both for positive and for negative charges and indicates that the premises of the theory are not fulfilled.*

In addition to the experiments described above in which a β-source served as a source of charges, we used the extraction of electrons from the electrode surface with the aid of light to obtain negative charges. Using a ~ 50-watt low-pressure mercury lamp we were able to obtain currents of the order of 10^{-13} amp from one square centimeter of the surface of a zinc electrode, which, however, proved insufficient for the measurements, in particular as a result of the strong influence of hysteresis effects. An attempt to obtain large currents with the aid of a pulsed light source (a quartz lamp filled with helium) completely submerged in the liquid helium was likewise unsuccessful.

All of the above-cited experiments have forced us to the conclusion that the task of studying the motion of charges in liquid helium meets with serious difficulties, evidently arising from the presence of the suspended charged particles of solidified gases invariably present in liquid helium. The movement of these charged particles in the electric field and their deposition upon the electrodes leads to a variety of polarization and hysteresis effects. The presence of suspended solids in the liquid helium appears to be, not merely possible, but, apparently, certain. Actually, helium, liquified and subjected to adsorptive purification on charcoal at liquid nitrogen temperature, can contain up to 10^{-7}% of impurities, which thereafter remain in the liquid principally in the form of submicroscopic particles. If the dimensions of these particles are $\sim 10^{-6}\,\mu^3$, then their concentration can reach $10^8 - 10^9$ particles per cubic centimeter.

We were able to reduce significantly the hysteresis effects by condensing the helium directly into the apparatus through specially treated charcoal at liquid nitrogen temperature and at the same time employing special ultrafilters. Unfortunately, however, we did not succeed completely in avoiding the harmful action of the suspended particles.

It is impossible to doubt that the presence in liquid helium of a suspension of solid impurities was also manifested in the most decisive fashion in the previously-published experimental results.

We thank D. I. Vasil'ev and I. P. Shmelev for their aid in the experiments.

*The conductivity of liquid helium is naturally negligibly small, even in fields close to the breakdown value, which from our measurements, amounted to 700 kv/cm over a 10μ gap.

[1] R. G. Arkhipov, JETP **33**, 397 (1957), Soviet Phys. JETP **6**, 307 (1958).

[2] R. L. Williams, Can. J. Phys. **35**, 134 (1957).

[3] Careri, Reuss, Scaramuzzi, and Thomson, Proc. Fifth Internat. Conf. on Low Temperature Physics and Chemistry, p. 155, 1955.

[4] L. Meyer and F. Reif, Phys. Rev. **110**, 279 (1958).

Translated by S. D. Elliott
254

INVESTIGATION OF THE HIGH ENERGY μ-MESON FLUX IN EXTENSIVE ATMOSPHERIC SHOWERS

S. N. VERNOV, B. A. KHRENOV, and G. B. KHRISTIANSEN

Submitted to JETP editor June 22, 1959

J. Exptl. Theoret. Phys. (U.S.S.R.) **37**, 1252-1265 (November, 1959)

Experimental data on the possible existence of narrow beams of μ mesons (diameter in observation plane < 0.5 m) have been obtained with the aid of apparatus which permits one to study simultaneously extensive atmospheric showers on the surface of the earth and underground. Data on extensive atmospheric showers obtained at the surface of the earth can be used to construct a picture of generation of narrow μ meson beams.

INTRODUCTION

THE experimental study of μ meson flux of high energy in the composition of an extensive atmospheric shower is of great interest from the viewpoint of the study of nuclear interactions at super high energies. The μ mesons are themselves the "tracks" of nuclear interactions which reflect both the angular distribution of secondary particles and their energy spectrum. The connection of the quantitative characteristics of the μ-meson flux of high energy with the quantitative characteristics of the event of interaction of nuclear-active particles of an extensive atmospheric shower is simplified, since the decay of the high energy μ mesons plays almost no role, while the ionization losses in the atmosphere are small in comparison with the energies of the μ mesons.

This permits us to assume that the flux of high energy μ mesons belonging to the extensive atmospheric shower reflects at sea level the whole set of nuclear interactions which have taken place in the atmosphere in the development of the shower.

It can be expected that the separate acts of nuclear interaction can also leave a track in the lateral distribution of μ mesons of high energy. Actually, against the background of the equilibrium density fluctuations of μ mesons, irregularities can appear as the result of groups of μ mesons which maintain approximately the direction of the μ mesons given by the last nuclear interaction in the event. Thus the study of the lateral distribution of the μ-meson flux of high energy can give experimental information bearing on the events of nuclear interaction at super high energies.

We have carried out an investigation of the high-energy μ-meson flux underground on apparatus, which makes it possible to obtain simultaneously the identical data on the extensive atmospheric shower on the surface of the earth. The arrangement described below forms part of the installation at Moscow State University for the exhaustive investigation of extensive atmospheric showers. The work was carried out during 1957-1958.

The present work is devoted to a study of the peculiarities in the lateral distribution of high-energy μ mesons. Other problems will be taken up in subsequent papers.

DESCRIPTION OF THE APPARATUS

One of the most important difficulties in the simultaneous study of μ mesons of high energy underground and extensive atmospheric showers on the surface of the earth is the necessity of recording the extensive atmospheric shower over a large area. Actually, a large region of possible positions of the axis of the shower on the surface of the earth, the dimensions of which are determined by the angular distribution of the axes of the extensive atmospheric shower in the depths of the earth, corresponds to a fixed position of the axis of the shower under the earth. Therefore, apparatus which studies the showers individually and which possesses a sufficient aperture ratio should permit us to determine the axis and the number of particles in the shower over an area comparable with the area of the region indicated.

The arrangement we used on the surface of the earth made it possible to record the showers individually within a circle of radius 25 m. At a maximum depth in the earth of 40 m and with the location of the meson detector directly under the center of this circle one could effectively study the central region of showers with a number of particles from 10^4 to 10^6.

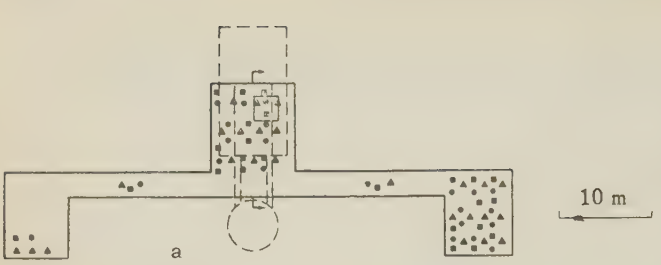

FIG. 1. Geometrical arrangement of the counters: a) on the surface of the earth, b) in the underground chamber. ▲ – group of 24 counters with counter area 330 cm², ■ – group of 24 counters with counter area of 100 cm², ● – group of 24 counters with counter area 24 cm². The dashed lines indicate the contours of the underground chambers. The open rectangles are banks of detectors of μ mesons of the type Fig. 3a.

For counting the extensive atmospheric shower and the meson flux in it we used the well-known method of correlated hodoscopes (see reference 1). The total number of Geiger-Müller counters contained in the hodoscope on the surface of the earth amounted to 1680. The geometry of the location of the counters on the earth's surface is shown in Fig. 1a. The underground chambers were along the vertical under the central chamber of Fig. 1a. The geometry of the position of the counters in the underground chamber is shown in Fig. 1b. The cross section of the arrangement along the vertical to the line ↑—↑ marked in Fig. 1a is shown in Fig. 2. The amount of material on the underground chamber was determined by a vertical profile of the ground and the building (the density of the ground amounted to 1.7 g/cm^3). Moreover, for the same purpose, controlled measurements of the vertical intensity of cosmic rays were carried out in the underground chambers with the aid of a telescope of counters separated by 10 cm of lead. The measured intensity amounted to $(1.5 \pm 0.05) \times 10^{-3}$ l/cm^2 sec. sterad in chamber 1 and $(0.8 \pm 0.1) \times 10^{-3}$ l/cm^2 sec. sterad in chamber 2.

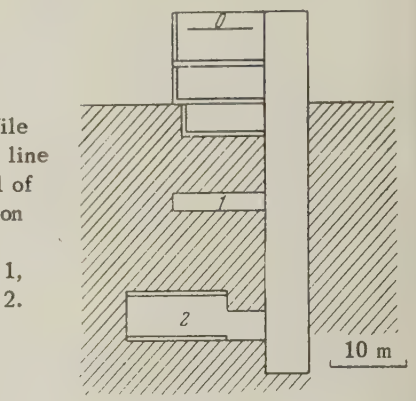

FIG. 2. Vertical profile of the chamber along the line ↑–↑ of Fig. 1a. 0 – level of position of the counters on the surface of the earth, 1 – underground chamber 1, 2 – underground chamber 2.

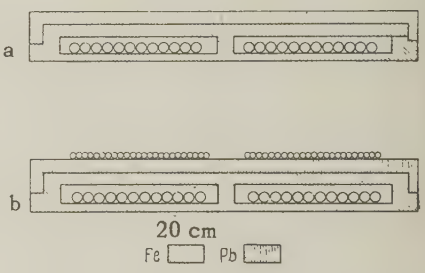

FIG. 3. Blocks of detectors of μ mesons.

The resultant intensities were compared with the data given in reference 2 on the dependence of the vertical intensity of cosmic rays on depth underground. The depth of the ground determined in this way amounted to: for chamber 1 — 20 m of water equivalent, for chamber 2 — 40 m of water equivalent along the vertical. The minimum energy of μ mesons necessary for penetration to this depth along the vertical amounts to 5 and 10 Bev.

Recording of mesons in the underground chambers was carried out by means of Geiger-Müller counters included in the hodoscope and screened by lead and iron. Figure 3a shows a group of counters which, together with the screen, forms a meson recording unit. The dimensions of the counters beneath the screen were 60 × 550 mm. The total number of counters was 120 in chamber 1 and 144 in chamber 2. In other setups the number of counters in chamber 2 was increased to 480.

An iron covering on the ceiling and walls of the chamber, the thickness of which amounted on average to 7.5 cm of iron or 4.7 t-units, served as an additional screen in chamber 2.

Hodoscopes with cold-cathode thyratrons of the Korablev type[3] were used in the research. The resolving time of the units in the underground chambers amounted to 15 — 20 microseconds; the number of random coincidences became comparable with the number of true ones at a meson density of 0.01 particles/m^2. This density was the lower limit of the recorded range of densities and made possible the study of the central region of the shower with a number of particles up to 5000. The upper limit was determined by the density at which the number of fired counters drew close to the total number of counters. For the total number of counters in the underground chamber this limit amounted to 100 particles/m^2, and for the chamber as a whole was not achieved experimentally throughout the whole time of operation of the apparatus. However, cases were observed in which the density at isolated points in the chamber exceeded this limit. During the entire period of operation of the apparatus, a control was maintained of the resolving time of the individual hodoscopic components and of the operation

of the counters. We also note that the possibility of parasitic coupling (induction) between the individual components of the applied hodoscope was eliminated.

Operation of the apparatus was carried out by various means. In the present paper experimental material is used which was obtained in the operation of the apparatus with coincidences of six groups of counters each of area 0.132 m^2. These groups of counters were located in the central chamber at ground level practically on the same vertical with the underground chambers. In the particular variant that is described the apparatus was operated over a period of 1740 hours.

METHOD OF RECORDING THE μ-MESON FLUX

The method of recording μ-meson flux with the use of Geiger-Müller counters that we have described possesses the advantage that it permits the use of a large area for the recording. However, the hodoscopic pictures thus obtained need special analysis for the separation of cases actually connected with the μ-meson flux. Unscreened counters can be triggered by the electron-photon component in equilibrium with the μ-meson. The former arises as a result of formation of δ electrons by μ mesons, and also due to the radiation retardation of μ mesons and to the direct creation by them of electron-positron pairs. The μ meson can therefore be accompanied (with a definite probability) by a current of electrons which is also recorded by the unscreened counters. The iron jacket of the ceiling in chamber 2 leads to an increase of particles in such a flow, although it decreases the mean energy of particles in it. Therefore, in the investigation of rare events (for example, the passage of the axis of the extensive atmospheric shower through the underground chamber) the frequency of which is comparable with the frequency appearance of δ showers, screening of the counters appears necessary.

Let us estimate the probability that a μ meson with energy W will have an electron-photon accompaniment, which passes through the filter we have used (12 t-units of lead and 4 t-units of iron). We obtain an upper estimate of this probability if we assume that the filter contains 16 t-units of lead. The probabilities of exciting an electron-photon shower capable of giving three particles under a filter with energies > 0 to one meson with energy W is equal to

$$C(W) = \int_0^W \frac{N^3(E)}{3!} \exp[-N(E)]\, U(W, E)\, dE,$$

where $N(E) = 3 \times 10^{-3} (E/\beta_{Pb})^{1.3}$ is the result of approximation for cascade showers in lead developed in reference 4; $N^3(E) \exp[-N(E)]/3!$ is the Poisson distribution; $U(W, E)$ is the equilibrium spectrum of electrons and photons accompanying a μ meson with energy W in iron; β is the critical energy:

$$U(W, E)\, dE \approx \int_E^W \{C_\delta(W, E')\, dE' + C_{h\nu}(W, E')\, dE' + C_e(W, E')\, dE'\} \frac{E'}{2.3\, E^2}\, dE.$$

Here $C_\delta(W, E')$, $C_{h\nu}(W, E')$ and $C_e(W, E')$ are the probabilities of transfer through one t-unit of energy E′ to a δ electron, Bremsstrahlung photon and an electron-positron pair, respectively. For a μ meson with energy $W = 10^{10}$ ev, we obtain $C \approx 3 \times 10^{-4}$ and for $W = 10^{13}$ ev, we obtain $C \approx 1$.

Thus, introduction of a screen above the counters permits a significant decrease in the probability of recording electrons and photons arising from the ground. But, on the other hand, μ mesons create δ electrons and δ showers in the screen itself, which can mask the groups of mesons. It is easy to differentiate such showers from groups of mesons if the mesons are recorded simultaneously above the screen by means of an additional row of counters. For μ mesons with $W \ll 10^{13}$ ev, the requirement of correspondence of the firing of the counters of the upper and lower rows practically eliminates the ambiguity in interpretation in the triggering of counters by mesons.

With the aim of investigating the pattern of the distribution of μ mesons in an individual shower, four units of type a of Fig. 3 were changed in chamber 2 to a two-row unit of type b of Fig. 3. In the upper row, counters were used with a smaller diameter (30 × 550). The frequency of appearance of δ electrons and δ showers under the screen classified according to the number of fired counters, was determined from the results of the action of units of type b and is plotted in Table I.

The frequency of appearance of δ showers was shown to be less than for particles which arise for detectors at the surface of the earth,[1] owing to the low altitude of the cavity of the block.

RESULTS

In the present work results are given of the work with the apparatus described, pertaining to the possible existence of irregular spatial distribution of μ-meson flux of high energy in an extensive atmospheric shower.

In eight hundred hours of operation of the two-

TABLE I

a	2	3	4	5	6
b	3800	3800	3800	3800	3800
c	105	23	8	4	3
d	4.0±0.4	0.6±0.1	0.2±0.08	0.1±0.05	0,08±0.05

a is the number of fired counters in the δ shower; b is the number of μ mesons which penetrate the unit, c is the number of δ showers, d is the percent of δ showers per meson.

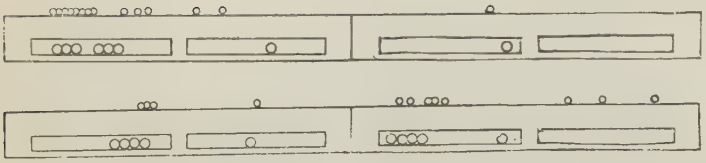

FIG. 4. Hodoscopic pictures for recording groups of μ mesons. Fired counters in units of the type of Fig. 3b are denoted by the circles.

row units of total area 3.1 m^2, we recorded 17 events of simultaneous firing of three and more counters in a line in an upper or lower row (see, for example, Fig. 4).

The readings of the upper row of counters establish the fact that the events recorded were not connected with electron-photon showers from the ground which are found close to the maximum of their development (the mean density of mesons obtained on the upper row of counters ρ_u and the density of mesons determined by the lower row ρ_l are the same: $\rho_u = 2.7 \pm 0.3$ particles/m^2 and $\rho_l = 2.2 \pm 0.3$ particles/m^2). It is possible that such events can be connected with very "young" electron-photon showers from the ground, perhaps with the simultaneous generation of a young shower in the ground and a second shower in the screen by a single meson. A precise estimate of the probability of appearance of such events is made difficult by the fact that the number of particles in the assumed δ showers is unknown experimentally. Moreover, data are lacking on the spectrum of μ mesons in the region $W > 10^{12}$ ev in the composition of extensive atmospheric showers. We shall consider below the set of experimental data which takes into account events that follow a group of μ mesons.

The following data can be compared for each group: 1) the minimum number of mesons in the group, equal to the number of counters of the upper row fired in the group; 2) the total amount of mesons recorded in a given shower in the underground chambers; 3) location of the axis of the shower on the surface of the earth and the number of particles in the shower. A summary of these data with respect to all recorded events is given in Table II.

The location of the axis and the number of particles in the shower was determined by the method suggested in reference 5, and with the aid of the arrangement of reference 6, which employs the knowledge of the spatial distribution function of the electrons in the shower. The accuracy of the determination of the axis and the number of particles in the shower were, respectively, 1 m and 20% close to and inside the surface chamber, and 4–5 m and 40% at distances of the order of 20 m from the surface chamber.

We shall show that the chosen groups of μ mesons cannot be the random accumulation of mesons connected with the Poisson statistical fluctuations of the particle flux. Bearing in mind that the characteristic phenomenon in the passage of a group of mesons is the successive firing of the counters in a row of unit b of Fig. 3, we shall consider each picture as consisting of group firings of the following classes: first class, o●o; second class,

TABLE II

№	a	b	c	d	e	f
1	$2 \cdot 10^5$	8	1	—	3	5
2	$5 \cdot 10^4$	13	1	—	3	2
3	$2 \cdot 10^5$	15	1	—	6	5
4	$2.5 \cdot 10^5$	12	1	—	5	3
5	$3 \cdot 10^5$	12	1	—	10	11
6	$2 \cdot 10^5$	25	1	—	9	2
7	$1 \cdot 10^5$	10	1	—	5	6
8	$2 \cdot 10^6$	11	2	1	5;4	18
9	$8 \cdot 10^5$	20	1	—	6	8
10	$5 \cdot 10^5$	20	1	—	6	11
11	$8 \cdot 10^5$	7	1	—	4	7
12	$1 \cdot 10^6$	25	1	—	5	11
13	$7 \cdot 10^5$	17	2	2	4;6	8
14	$3.5 \cdot 10^6$	15	2	1.5	4;5	14

a – number of particles in the shower; b – distance in meters from the axis of the shower on the earth's surface to the vertical passing through the point of observation of the group of mesons; c – number of groups of mesons in the shower; d – distance in meters between groups; e – number of fired counters in the vertical row of unit b of Fig. 3 at the point of passage of the group of mesons; f – number of mesons recorded in a given shower apart from the group of mesons (on an area of 4.35 m^2).

o●●o; third class, o●●●o, etc. We assume that of the total number n of counters, m were fired and the distribution of mesons in the plane of observation is uniform on the average. We shall calculate with what probability a given picture of fired counters can be observed if the trajectories of the mesons are independent.

A formula was derived in reference 7 for the probability which is of interest to us; it has the form

$$W(n, m, \nu, p) = \frac{C^p_{n-m+1}\, p!}{\prod_i \nu_i!\, C^m_n},$$

Here p is the number of groups of all classes in the given shower, ν_i is the number of groups of the i-th class. However, practical use of this formula is difficult because of the roughness of the calculations for large n. Moreover, we have it in mind to extend the same approach to the treatment of the data of single row units, making use of a knowledge of the frequency of appearance of δ showers. Therefore, we apply another approach to the determination of the probability of the given picture of fired counters by classes, based on a comparison of the theoretically expected number of groups of a given class with the experimental observations.

Under the observed conditions, the probability is m/n that a chosen counter fires, and $1 - m/n$ that it does not fire. Consequently, the probability of the event of first class is $(m/n)(1-m/n)^2$; of the second class, $(m^2/n^2)(1-m/n)^2$; of the third class, $(m^3/n^3)(1-m/n)^2$; etc. The appearance of an event of an arbitrary class, generally speaking, changes the probability of the remaining events, but if $m \ll n$, then the change is probably small. For $m \ll n$, the number of events of different classes is given by

$$M_1 = n\frac{m}{n}\left(1 - \frac{m}{n}\right)^2;$$

$$M_2 = n\frac{m^2}{n^2}\left(1 - \frac{m}{n}\right)^2 \text{ etc.}$$

For each shower, we have theoretical and experimental distributions of the events over the classes. Calculating the consistency criterion of Pearson

$$\chi^2 = \sum_i (M_{i\ \mathrm{exp}} - M_i)^2 / M_i .$$

we find the probability of appearance (connected with the statistical fluctuations) of a given picture of the distribution of mesons in the plane of observation.

Let us compare the frequency of appearance of pictures with groups of mesons (as a group of mesons we take events of third and higher classes) with the frequency of events expected because of statistical fluctuations. For this purpose, we analyze all pictures of fired counters in chamber 2 according to the total number of counters fired. The number of groups of mesons expected because of statistical fluctuations and the observed number of groups is shown in Table III.

TABLE III

a	5—8	9—14	15—26	>26
b	264	69	29	7
c	1	0,5	0.3	0.1
d	3	5	7	2

a – total number of discharge counters (m) under the screen in chamber 2; b – number of showers with given m; c – expected number of groups of mesons because of stati stical fluctuations; d – observed number of groups of mesons.

Comparison shows that the observed groups of μ mesons cannot be accounted for by statistical fluctuations in the meson distribution. Consequently, the observed groups of mesons are peculiarities of the lateral distribution of μ mesons of high energy.

We now attempt to determine the role of such groups in the general lateral distribution of mesons of high energy. It is seen from Table II that in showers with a number of particles $N \sim 10^5$, one group of mesons is observed, while in showers with $N \sim 10^6$ cases are encountered with two groups on an area of $3.1\,m^2$. It is possible that in showers with different N, the groups of mesons play different roles in the lateral distribution of the mesons. Therefore, let us consider separately showers with $N \sim 10^5$ and showers with $N \sim 10^6$. From Table II we can obtain the mean density of the meson accompaniment of a group of mesons for showers with $N < 5 \times 10^5$ and $N > 5 \times 10^5$:

$$\rho(\bar{N} = 2 \cdot 10^5) = (1.0 \pm 0.2) \text{ particles/m}^2$$

$$\rho(\bar{N} = 1.3 \cdot 10^6) = (2.3 \pm 0.3) \text{ particles/m}^2$$

It follows from the geometrical arrangement in chamber 2 (Fig. 1b) that these densities relate to a distance of $3 - 4$ m from the group of mesons. The densities of mesons measured by the same apparatus at a distance of 14 m from the axis of the extensive atmospheric shower (description of this experiment will be given in subsequent papers) amount to (0.22 ± 0.03) particle/m^2 and (1.6 ± 0.6) particles/m^2, respectively, for showers with $\bar{N} = 2 \times 10^5$ and with $\bar{N} = 1.3 \times 10^6$. It is thus seen

that in showers with $\bar{N} \sim 10^5$ a sharp increase in the density of μ mesons is observed upon approach to a group of mesons, while in showers with $N \sim 10^6$ this increase is less marked.

In this connection, it is of interest to compare the frequency of appearance of groups of μ mesons with the frequency of passage of the axes of the extensive atmospheric showers through the detector of μ mesons.

Let us now calculate the number of axes of extensive atmospheric showers with a different number of particles passing through the area of the double-row units in 800 hours of operation for the experimental setup that has been described. The intensity of the axes of extensive atmospheric showers with a number of particles N and with angles θ and φ in the underground chamber is equal to

$$(A / N^{\gamma+1})\, dN \cdot \cos^{\nu}\theta \sin\theta d\theta d\varphi.$$

The probability of recording such a shower at the surface of the earth is

$$[1 - \exp\{-kNf(r)\sigma\}]^6,$$

where $kNf(r)$ is the density of electrons at the surface of the earth in the extensive atmospheric shower, $\sigma = 0.132\,m^2$. The connection between the angle θ and r is the following: $r = H \tan\theta$, where H is the distance between the surface and underground chambers measured along the vertical. Then the number of axes passing through the area of the double row units is

$$I = \frac{A \cdot 3{,}1 \cdot 800}{N^{\gamma+1}}\, dN \int_0^{2\pi}\int_0^{\pi/2} \cos^{\nu}\theta \sin\theta d\varphi d\theta$$

$$\times [1 - \exp\{-kNf(H\tan\theta)\sigma\}]^6.$$

Taking $\nu = 8$ in accord with reference 8, and integrating numerically, we obtain the results shown in Table IV. It is seen from the table that the frequency of the groups in showers with $N \sim 10^5$ corresponds to the frequency of the axes of the showers while the frequency of the groups of mesons in showers with $N \sim 10^6$ is much greater than the frequency of axes of such showers.

It is quite probable that in showers with a number of particles $N < 10^5$, there are no groups of μ mesons of three or more mesons, for the mesons in these groups have a smaller lateral divergence.

Up to now we have been discussing data obtained by double-row units. If we analyze the data from single-row units, it is possible to broaden the statistical material for chamber 2 and obtain data on chamber 1 at a depth of 20 m under the screen. This permits us to trace the dependence of the number of groups of mesons on the depth. The simulation of groups of mesons by the δ showers from the screen serves as an obstacle to this course. However, the frequency of appearance of the δ showers is known from the experiment with double row units. We include the probability of appearance of the δ showers, determined experimentally, in the consideration of pictures of the discharge of counters in single-row units, similarly to what was done for double-row units. Then the probability of appearance of an event of the first class does not change, of the second class becomes $(m^2/n^2)(1-m/n)^2 + W_{\delta_2}$, where W_{δ_2} is the probability of appearance of the δ electron; for the third class, $(m^3/n^3)(1-m/n)^2 + W_{\delta_3}$, where W_{δ_3} is the probability of appearance of the δ shower with three discharge counters, etc. The values of W_{δ_2}, W_{δ_3}, W_{δ_4} are shown in Table I. Further, we obtain new theoretical values of M_i and find the probability of pictures of discharges for individual showers, just as for double-row units. Table V lists the results obtained from an analysis of the pictures in single-row units for chambers 1 and 2. As is seen from the table, the expected value of δ showers for pictures with $m \geq 9$ is small in comparison with the number of observed groups of discharges of counters, and at the same time the frequency of the groups of mesons determined according to double-row units corresponds to the frequency observed on single-row units. Consequently, in both cases we observe the groups of mesons (for $m \geq 9$). One can draw the conclusion from Table V that the ratio of the frequencies of appearance of groups of mesons at depths of 20 and 40 meters under the screen amounts to 1 ± 0.5. For groups of mesons observed in chamber 1, a mean density of mesons accompanying the groups for showers with $10^5 < N < 5 \times 10^5$ was obtained.

This density amounted to $\rho(\bar{N} = 2 \times 10^5)$

TABLE IV

a	$1 \cdot 10^4$—$1 \cdot 10^5$	$1 \cdot 10^5$—$5 \cdot 10^5$	$5 \cdot 10^5$—10^6	$> 10^6$
b	4;5	3	0.5	0.3
c	1	7	5	4

a — number of particles in the shower; b — expected number of axes of showers; c — number of observed groups of μ mesons.

TABLE V

	Chamber 1*				Chamber 2**			
Number of discharging counters in the chamber (m)	5—8	9—14	15—26	>26	5—8	9—14	15—26	>26
Number of showers with given m	400	120	30	20	450	170	37	22
Expected number of δ showers and groups of mesons connected with statistical fluctuations	3.4	1	0.3	0.2	4;5	1;2	0.4	0.2
Observed number of groups of discharged counters (class 4 and higher, see text)	4	7	5	5	4	9	10	6

*For chamber 1 the data are given on showers with $m < 26$ after 700 hours of operation, for showers with $m > 26$, after 1740 hours.

**For chamber 2, data are given for showers with $m < 26$ after 1070 hours of operation, and for showers with $m > 26$ after 1740 hours.

$= (0.9 \pm 0.1)$ particles/m^2 and is equal to the density of accompaniment of the groups in the same showers in chamber 2.

DISCUSSION OF RESULTS

Thus the study of the flux of high-energy μ mesons in extensive atmospheric showers points to the possible existence close to the axis of the showers of beams of μ mesons, the number of which increases with increase in the intensity of the shower.

Let us return to the problem of the possible nature of the observed phenomenon. First of all, we consider the possibility of generation of groups of μ mesons in the ground above the apparatus.

As a result of the nuclear-active components of high energy of the extensive atmospheric shower, formation of beams of π mesons in the ground is possible; these decay with finite probability with the formation of μ mesons.

The number of μ mesons is determined by the expression

$$n_\mu(\geqslant E) = \int_E^{E_{na}} \int_0^\infty n_\pi(x, E')\, dE' \frac{dx \lambda m_\pi c^2}{\rho \tau_0 c E'}, \qquad (1)$$

where $n_\pi(x, E')\,dE'$ is the number of π mesons in the shower at a depth x, expressed in path lengths for the interaction λ possessing energies from E′ to E′ + dE′, $\rho = 1.7$ g/cm^3 is the density of the earth, $\tau_0 = 2 \times 10^{-8}$ sec is the half-life of the π meson, and m_π is the mass of the π meson. The limit of integration of E for chamber 1 amounts to 5×10^9 ev, for chamber 2, 10^{10} ev. Consideration of the cascade process by the method of successive generations leads to the equation

$$n_\pi(E', x)\, dE' = \sum_{i=0}^{\infty} \frac{e^{-x}}{i!} x^i \Pi_i(E')\, dE',$$

where i is the number of the generation, Π_i is the spectrum of π mesons of the i-th generation. Substituting this expression in (1), we obtain

$$n_\mu(\geqslant E) = \int_E^{E_{na}} \sum_{i=0}^{\infty} \Pi_i(E')\, dE' \frac{\lambda m_\pi c^2}{\rho \tau_0 c E'}. \qquad (2)$$

In Appendix 1 it is shown that in the case of not too high an energy loss of the nuclear-active particles of the avalanche (which is evolved upon the formation of the electron-photon component), Eq. (2) has the form:

$$n_\mu = K E_{na} / E^2, \qquad (3)$$

where K is connected with the character of the acts of nuclear interaction in the avalanche. According to the estimate given in the Appendix, the energy of the nuclear-active particle responsible for a group of μ mesons of three particles must amount to 4×10^{13} ev. The experimental data on nuclear-active particles of high energy in extensive atmospheric showers at sea level show[9] that the appearance of such particles in showers with $N \sim 10^5$ is very unlikely. A comparison of experimental data at depths of 20 and 40 m below the screen also contradicts the picture we have given of the generation of μ-meson groups. Actually, if the energy E_{1na} which exists in showers with a number of particles N_1 suffices for the formation of a group of μ mesons with a given number of particles n_μ recorded at a depth of 40 m below the screen, then for the formation of a group observed at a depth of 20 m below the screen, the energy $E_{2na} = E_{1na}/4$ is sufficient [see Eq. (3)]; this exists in showers with $N_2 = N_1/4$. Then the frequency of appearance of groups at a depth of 20 m below the screen will exceed the frequency of appearance of groups at a depth of 40 m below the screen by a factor q, and this ratio will amount to (taking into account the spectrum of the showers in

terms of the number of particles and the effectiveness of the separation of the showers)

$$q=\frac{\int_{N_0}^{\infty}\int_{0}^{\pi/2}\frac{A}{N^{\gamma+1}}\cos^8\theta\sin\theta\,[1-\exp\{-kNf(H_1\tan\theta)\sigma\}]^6\,dN\,d\theta}{\int_{N_1}^{\infty}\int_{0}^{\pi/2}\frac{A}{N^{\gamma+1}}\cos^8\theta\sin\theta\,[1-\exp\{-kNf(H_2\tan\theta)\sigma\}]^6\,dN\,d\theta}\approx 4.$$

The ratio 1 ± 0.5 is observed experimentally (Table V), which contradicts the given picture of the generation of groups of μ mesons.

The observed group of μ mesons can also arise in the atmosphere because of decay of π and K mesons generated in acts of nuclear interaction. In this picture of the generation of groups of μ mesons, the character of the distribution of transverse momenta of secondary particles in the nuclear interaction is extremely important. Recent research[10,11] on the study of nuclear interaction in photoemulsions shows that the distribution of transverse momenta of secondary particles in nuclear interactions with energies $10^{12}-10^{13}$ ev can be represented in the form

$$\varphi(p_\perp)\,dp_\perp=\frac{dp_\perp}{9\cdot 10^8} \quad \text{and } 10^8\ \text{ev/c}\leqslant p_\perp\leqslant 10^9\ \text{ev}/c;$$

$$\varphi(p_\perp)=0 \quad \text{and } p_\perp>10^9\ \text{ev/c}.\quad p_\perp<10^8\ \text{ev}/c. \qquad (4)$$

It can also be shown (see Appendix 2) that with such a distribution of transverse momenta, the generation of a group of μ mesons of five particles, which cover a region with linear dimension $d = 0.5$ m at sea level in a single act of nuclear interaction, is highly improbable according to present-day representations. Let us therefore consider the possibility of the excitation of a group of μ mesons because of the decay of π mesons in the passage through the atmosphere of a complete nuclear avalanche of an extensive atmospheric shower. Such a group of μ mesons can be formed in the core of an extensive atmospheric shower. We shall find the number of μ mesons at sea level in an avalanche with primary energy E_0 which is diverging at a distance d from the axis of the shower:

$$n_\mu=\int_{x_0}^{1033}\int_{E_{min}}^{E_0}\int_{p_{\perp min}}^{p_{\perp max}} n_\pi(E_0,E,x)\,dE\,\frac{Bdx}{xE}\,\varphi(p_\perp)\,dp_\perp, \qquad (5')$$

where x is the depth of the atmosphere in g/cm^2, $n_\pi(E_0, E, x)$ is the differential spectrum of π mesons at a depth x, $B = 1.39 \times 10^{11}$ ev is the decay constant of the π mesons. Here it is assumed that the μ meson acquires a transverse momentum $p_\perp$ in the decay of the π meson, which up to this point preserved the direction of the primary particle. Such an approximation gives an upper bound to the number of μ mesons in the circle d. In the case of a distribution of transverse momenta according to Eq. (4), we have

$$n_\mu=\int_{x_0}^{1033}\int_{H(x)\cdot 10^8/d}^{E_0} n_\pi(E,x)\,dE\,\frac{dx}{x}\,B\,\frac{1}{9}\left(\frac{d}{H(x)\cdot 10^8}-\frac{1}{E}\right), \qquad (5'')$$

where H(x) is the distance above sea level corresponding to a depth x in the atmosphere.

For the calculation of n_μ according to Eq. (5″), it is necessary to give the energy spectra of the π mesons which have not yet been experimentally investigated with sufficient completeness. We shall consider only the theoretical models of the development of the nuclear cascade in the atmosphere which are considered in references 12 and 13. Numerical calculation carried out with the spectra of π mesons from the research of reference 12 according to Eq. (5″) gives the number of μ mesons in a circle with $d = 0.5$ m, $n_\mu = 0.2$ for $E_0 = 2 \times 10^{15}$ ev. However, we note that this model of the development of a nuclear cascade in the atmosphere does not give the number of nuclear-active particles of high energy at sea level corresponding to experiment. According to this model, $N_{na}(E > 10^{12}\ \text{ev})/N = 2 \times 10^{-6}$, while experiment[9] gives $N_{na}(E > 10^{12}\ \text{ev})/N = 2-5 \times 10^{-5}$. The calculation carried out in reference 13 gives better agreement with experiment on the number of nuclear-active particles of high energy at sea level in an extensive atmospheric shower [here $N_{na}(E > 10^{12}\ \text{ev})/N = 5 \times 10^{-5}$]. In this calculation the following assumptions were made: 1) In the collision of the nucleon with the nucleus of air, one-half of its energy goes into the formation of $n = 2(0.5E_0)^{1/4}$ secondary particles; 2) secondary particles obtain equal energy; 3) the π mesons interact according to the same model; 4) charged μ mesons consist of 70% of all π mesons; 5) the path for the interaction $\lambda = 90$ g/cm^2.

Using $n_\pi(E, x)$ calculated under these assumptions by Eq. (5″) for $E_0 = 2 \times 10^{15}$ ev, we obtain $n_\mu = 5$, which corresponds to observation of a group of μ mesons in the core of the shower. In this case 3 or 4 μ mesons in a group possess energies $E_\mu \sim 10^{11}$ ev and 1 or 2 μ mesons possess energies of $E_\mu \sim 10^{12}$ ev.

From the point of view of such a picture of the generation of groups of μ mesons, the appearance of several groups of μ mesons in showers with high primary energies corresponds to the appearance of additional π-meson cores in the extensive atmospheric shower. The energy contained in the additional core can be many times smaller than in the original. Actually, in the additional group

of μ mesons, for a shower with $E_0 \sim 10^{16}$ ev, as many mesons are observed as were in the fundamental group for showers with $E_0 \sim 10^{15}$ ev; therefore such an additional core can be connected with the emission of individual nuclear-active particles of high energy ($E_{na} \sim 10^{15}$ ev) from the original core. However, the observed distances between groups of μ mesons in showers with $E_0 \sim 10^{16}$ ev (~2 m) require very large transverse momenta for the nuclear-active particles generating the additional core:

$$p_\perp \approx \frac{2\ \text{m}}{2\cdot 10^4\ \text{m}} \cdot 10^{15}\ \text{ev/c} = 10^{11}\ \text{ev/c}.$$

Therefore, the existence of several groups of μ mesons in showers with $N \sim 10^6$ particles is improbable within the framework of the picture of the generation of μ mesons given here. The appearance of several groups of μ mesons in a single shower can be explained if it reduces the energy of the nuclear-active particle responsible for the group of μ mesons. It can be assumed that the total number of particles created in the act of nuclear interaction and also their energy and angle distributions undergo very large fluctuations. Then such acts of nuclear interactions are found which give narrow beams of π mesons, which yield in turn beams of μ mesons.

It can also be assumed that a process exists of much more rapid multiple production of μ mesons than the decay of π mesons (see, for example, reference 14). A substantially smaller energy of the nuclear-active particle ($E_{na} \ll 10^{15}$ ev) then suffices for the formation of the group of μ mesons. The rapid increase in the number of groups of μ mesons in a single shower in this case that is observed experimentally is explained by the increase in the flux of nuclear-active particles of the necessary energy ($N_{na} \sim E_0$). The fact that only a single group of μ mesons is observed in showers with $E_0 \sim 10^{15}$ ev means, in this interpretation, that the cross section of interaction with multiple production of μ mesons is significantly smaller than the total cross section of nuclear interaction.

The foregoing consideration shows that the final explanation of the nature of the particles which caused the events observed by us — the group discharge of counters screened by a filter under large thicknesses of earth in the passage of an atmospheric shower — is very important.

APPENDIX 1

For the calculation of the number of μ mesons observed underground and originating from π mesons reaching the ground, we consider a nuclear cascade process, in which the π mesons determine its development. We assume that in the collision of a nuclear-active particle with a nucleus of the earth, nπ mesons are produced while αn of them are nuclear active; in the collision of π mesons with the nuclei of the earth, nπ mesons are again produced, etc. Then

$$n_\pi(E, x) = \sum_{i=0}^{\infty} \frac{e^{-x}}{i!} x^i \Pi_i(E); \quad \Pi_i(E) = (\alpha n)^i \delta\left(E - \frac{E_{na}}{n^i}\right).$$

We are interested in the number of μ mesons from the decay of π mesons in the ground with energies > E. It is equal to

$$n_\mu(>E) = \int_E^{E_{na}} \int_0^{\infty} \sum_{i=0}^{\infty} (\alpha n)^i\, \delta\left(E' - \frac{E_{na}}{n^i}\right) \frac{dE' dx \lambda m_\pi c^2}{\rho\tau_0 c E'} \frac{e^{-x} x^i}{i!}$$

$$= \int_E^{E_{na}} \sum_{i=0}^{\infty} (\alpha n)^i\, \delta\left(E' - \frac{E_{na}}{n^i}\right) \frac{dE'}{E'} \frac{\lambda m_\pi c^2}{\rho\tau_0 c} = \frac{\lambda m_\pi c}{\rho\tau_0}$$

$$\times \sum_{i=0}^{k} (\alpha n)^i \frac{n^i}{E_{na}},$$

where k is determined from the relation $E = E_{na}/n^k$; $k = \log(E_{na}/E)/\log n$. Thus,

$$n_\mu(>E) = \frac{\lambda m_\pi c}{\rho\tau_0} \frac{[(\alpha n^2)^k - 1]}{E_{na}(\alpha n^2 - 1)} = \frac{\lambda m_\pi c}{\rho\tau_0} \left[\left(\frac{E_{na}}{E}\right)^{2+\log\alpha/\log n} - 1\right] \frac{1}{E_{na}(\alpha n^2 - 1)} \approx \frac{\lambda m_\pi c}{\rho\tau_0 E_{na}} \left(\frac{E_{na}}{E}\right)^{\gamma} \frac{1}{\alpha n^2},$$

where

$$\gamma = 2 + (\log\alpha/\log n).$$

It follows from the form of the dependence of n_μ on E that $n_\mu \sim KE_{na}/E^2$ for sufficiently small leakage of energy from the nuclear cascade process. If we take n = 5 (a value which was determined experimentally for energies $E_{na} \geq 10^{11}$ ev, see reference 10) and $\alpha = 0.7$, then a nuclear-active particle on the surface of the earth must possess energies of 4×10^{13} ev for the production of a group of μ mesons of three particles.

APPENDIX 2

For the act of nuclear interaction with energy of the nuclear-active particle E_0 which takes place at a depth H above the level of observation, we have

$$n_\mu = \int_{E_{min}}^{E_0} \int_{p_{\perp min}}^{p_{\perp max}} n_\pi(E)\, dE \varphi(p_\perp)\, dp_\perp \frac{L_{int}}{L_{int} + E\tau_0/m_n c} \times \left[1 - \exp\left(-\frac{H}{L_{eff}}\right)\right],$$

where $n_\pi(E)\,dE$ is the energy spectrum of π

mesons, $\varphi(p_\perp)\,dp_\perp$ is the distribution of transverse momenta of π mesons, L_{int} is the path length for the interaction of π mesons in centimeters,

$$1/L_{eff} = 1/L_{int} + m_\pi c^2/E\tau_0 c.$$

We assume that the distribution of transverse momenta of π mesons has the form (4). The energy spectrum of the π mesons produced in the act of nuclear interaction is given in two variants:

1. Interaction proceeds according to the Fermi-Landau theory; then the spectrum of π mesons has the form (see reference 19)

$$n_\pi(E)\,dE = \frac{n_0}{\sqrt{2\pi\mathscr{L}}}\exp\left\{-\frac{[\ln E/\bar{p}_\perp c]^2}{2\mathscr{L}}\right\}\frac{dE}{E},$$

$$n_0 = k(\bar{n}+1)(E_0/10^9)^{1/4}, \quad k\sim 1, \quad \bar{n}\sim 4,$$

$$\mathscr{L} = 0.56\ln(E_0/10^9) + 1.6\ln[2/(\bar{n}+1)] + 1{,}6,$$

$$\bar{p}_\perp c = 3\cdot 10^8 \text{ ev}.$$

2. The interaction proceeds according to the Heisenberg theory; then the spectrum of π mesons has the form

$$n_\pi(E)\,dE = E_0\left\{E^2\ln\frac{M}{m_\pi}\sqrt{\frac{E_0}{2Mc^2}}\right\}^{-1}dE \quad \text{for } m_\pi c^2 \times\sqrt{\frac{E_0}{2Mc^2}} < E < E_0.$$

Results of the calculation of n_μ are given in Table VI for three values of H and the maximum energy of nuclear-active particles appearing at these levels in showers with the number of particles at sea level $N \sim 10^5$.

TABLE VI

H	$E_0=10^{13}$ ev		$E_0=10^{15}$ ev
	100 m	500 m	10 km
First variant	0.15	0.08	0.1
Second variant	0.3	0.07	0.08

[1] Abrosimov, Goryunov, Dmitriev, Solov'eva, Khrenov, and Khristiansen, JETP **34**, 1077 (1958), Soviet Phys. JETP **7**, 746 (1958).

[2] Progress in Cosmic Ray Physics, edited by J. G. Wilson, vol. 1, North Holland Pub. Co., Amsterdam, 1952.

[3] L. N. Korablev, Приборы и техника эксперимента (Instrum. and Meas. Engg.) No. 2, 56 (1956).

[4] G. T. Zatsepin, Dokl. Akad. Nauk SSSR **63**, 243 (1948); I. P. Ivanenko, Dokl. Akad. Nauk **107**, 819 (1956), Soviet Phys.-Doklady **1**, 231 (1956).

[5] G. V. Kulikov and G. B. Khristiansen, JETP **35**, 635 (1958), Soviet Phys. JETP **8**, 441 (1959).

[6] G. V. Bogoslovskiĭ and B. A. Khrenov, Приборы и техника эксперимента (Instrum. and Meas. Engg.) (in press).

[7] G. B. Khristiansen, Dissertation, Moscow State Univ. 1952.

[8] Abrosimov, Goman'kov, Ivanovskaya, and Sarycheva, JETP **33**, 1110 (1957), Soviet Phys. JETP **6**, 856 (1958).

[9] Abrosimov, Dmitriev, Kulikov, Massal'skiĭ, Solov'ev, and Khristiansen, JETP **36**, 751 (1959), Soviet Phys. JETP **9**, 528 (1959).

[10] Edwards, Losty, Perkins, Pinkau, and Reynolds, Phil. Mag. **3**, 237 (1958).

[11] Minakawa, et al., Institute for Nuclear Study, Univ. Tokyo, p. 1 (1958).

[12] Fukuda, Ogita and Ueda, Progr. Theoret. Phys. **21**, 29 (1959).

[13] A. Ueda and H. Ogita, Progr. Theoret. Phys. **18**, 269 (1957).

[14] S. Higashi et al., Nuovo cimento **5**, 597 (1957).

[15] D. Kessler and R. Maze, Nuovo cimento **5**, 1540 (1957).

[16] M. Oda, Nuovo cimento **5**, 615 (1957).

[17] Barrett, Bollinger, Cocconi, Eisberg, and Greisen, Revs. Modern Phys. **24**, 133 (1952).

[18] G. A. Milekhin, JETP **35**, 1185 (1958), Soviet Phys. JETP **8**, 843 (1959).

[19] Vernov, Kulikov, Strugal'skiĭ, and Khristiansen, this issue, p. 848 (Russ. p. 1193).

Translated by R. T. Beyer
255

EMITTERS OF ALPHA PARTICLES WITH ENERGIES OF ABOUT 9 AND 12 Mev IN THE Po—Ra *REGION**

V. A. KARNAUKHOV, V. I. KHALIZEV, and G. N. FLEROV

Submitted to JETP editor June 22, 1959

J. Exptl. Theoret. Phys. (U.S.S.R.) **37**, 1266-1272 (November, 1959)

Lead was irradiated with accelerated oxygen and carbon ions. Isotopes emitting 11.8 ± 0.4 and 9.0 ± 0.3 Mev particles with half-lives of approximately one minute and 35 ± 10 seconds respectively were detected among the reaction products. Certain ideas are advanced concerning the identification of these isotopes.

IT has been noted many times that the use of accelerated heavy ions offers broad possibilities of obtaining new neutron-deficit isotopes of practically all elements.[2,3] For elements in the beginning and middle of the periodic table it is evidently possible to obtain the lightest isotopes, i.e., those near the boundary of the region of radioactive nuclei. Heavy ions are a particularly convenient means of obtaining and investigating the properties of light isotopes of elements from At to Ac. Many of these nuclei are difficult to prepare with the aid of beams of light particles (nucleons, deuterons, or α particles), since they do not have sufficiently stable isotopes capable of serving as targets. When heavy ions are used this difficulty is eliminated, for the target used can be an element (bismuth, lead, mercury, etc.) that differs greatly in atomic number from the final nucleus.

In the present investigation we studied unknown α emitters among the products of reactions caused by accelerated oxygen and carbon ions in lead.

1. EXPERIMENTAL PROCEDURE

The experiments were carried out with the 150-cm cyclotron of the U.S.S.R. Academy of Sciences. We had at our disposal intense beams of quintuply-charged ions of O^{16} and quadruply-charged ions of C^{12} and C^{13}, accelerated to 102.77 and 83 Mev respectively. To avoid overheating of the target, the particle beam intensity was kept below 0.2 or 0.3 μa. The irradiation took place inside the cyclotron chamber. The short-lived α-active reaction products were investigated with special apparatus shown schematically in Fig. 1, making use of the method of gathering recoil nuclei, as described in references 4 and 5. This method enabled us to use the same target in various experiments, which facilitated considerably the comparison of the results. The ion beam 1 was incident on a lead target 2, deposited on an aluminum foil (5 — 6 μ). The reaction products, with large momenta, were emitted from the target and struck a thin (~ 2 μ) aluminum receiver 3. After passing through the target and receiver, the bombarding particles were stopped by the current collector 4. The collector was connected to the current meter, so that the intensity of the beam could be monitored during the irradiation process and the total ion current through the target could be measured. The receiver was periodically moved, with the aid of kapron thread 5, two meters away from the target and placed near photographic plate 6, which registered the α decay of the reaction products. All these devices were placed in a vacuum container connected to the cyclotron chamber. The kapron thread was driven by an electric motor through a special seal, since the motor was outside the vacuum system. To estimate the half-lives of the nuclei, provision was made for measuring the times t_1, t_2, and t_3 during which the receiver was under

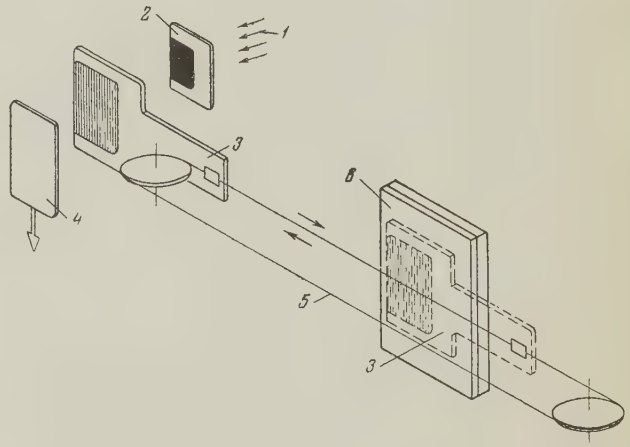

FIG. 1. Arrangement for the registration of α decay of the reaction products

*A brief report of the results of the present investigation is contained in a paper by G. N. Flerov.[1]

the target, near the emulsion, and in motion from the target to the emulsion, respectively. The time could be measured over a wide range. In our experiments the first two time intervals were chosen to be equal to each other and could be set at 10, 25, 50, 100 and 250 seconds. The value of t_3 could be set at 3, 10, 50, 100 and 250 seconds. In all the experiments the receiver moved from the photographic plate to the target within 3 — 5 seconds. Thus, the apparatus used was suitable for the investigation of α decay of nuclei with lifetimes from approximately one second and above. An electronic time relay was used to set the selected operating mode of the apparatus.

The lead targets were deposited on aluminum foil by precipitation from an aqueous solution of $Pb(NO_3)_2$ with addition of a certain amount of tetraethylene glycol.[6] The solution was dried for 5 — 6 hours under a lamp (500 watts) with gradual increasing of heating, after which the layer was roasted at approximately 500°, causing the lead nitrate to change to the lower oxide form. The targets thus obtained were sufficiently homogeneous and strong. The target thickness was 200 — 300 $\mu g/cm^2$. This thickness is evidently optimal when the recoil-nuclei gathering method is used. In the experiments described below we used targets of natural lead and targets containing essentially the isotopes Pb^{208} and Pb^{207}. The isotopic composition of the substance in the latter two cases is given in Table I.

TABLE I

Target	Isotopic composition, percent			
	204	206	207	208
Pb^{208}	0.1	0.1	0.6	99.3
Pb^{207}	0.1	0.1	97.4	2.6

We used NIKFI-T1 emulsions to register the α decay of the reaction products. These emulsions have good discrimination for α-particle and proton tracks and have low sensitivity to β and γ radiation, so that they could be used in the direct vicinity of the cyclotron for sufficiently long exposures.

II. RESULTS OF THE EXPERIMENTS

1. Experiments on Irradiation of Lead with O^{16} Ions

a) Figure 2 shows the α-particle spectrum obtained by irradiating a target of natural lead with O^{16} ions of ~ 97 Mev. In this experiment, $t_1 = t_2 = 10$ sec and $t_3 = 3$ sec. The spectrum was plotted after scanning a small part of the photographic plate.

Figure 3 shows the "hard" part of the α-particle spectrum, observed by irradiating lead with oxygen. This spectrum was obtained by selective scanning of photographic plates obtained in several experiments. For a better energy resolution we selected only the α-particle tracks that entered the emulsion at dip angles from 15 to 45°. The abscissas represent the ranges of the α particles in the emulsion and the corresponding particle energies. In the calculation of the α-particle energy we took into consideration the fact that the nuclei — the reaction products due to a certain "recoil" momentum — are distributed in depth in the receiver.

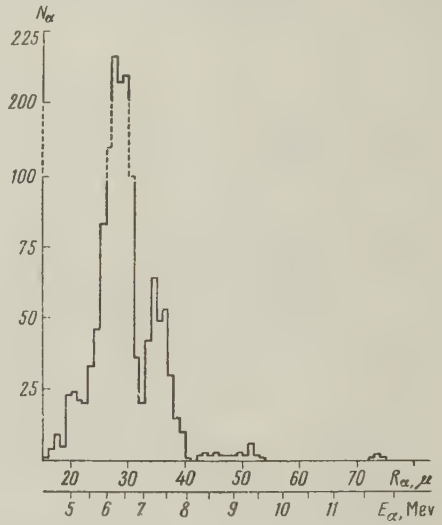

FIG. 2. Energy spectrum of α particles obtained by irradiating lead with oxygen ions.

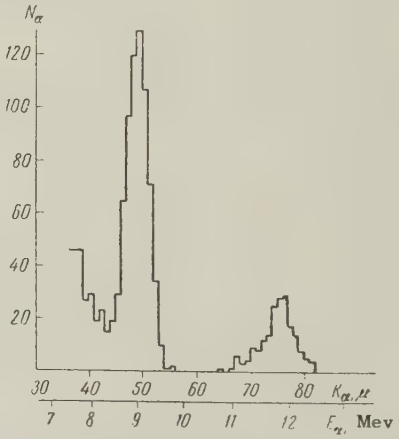

FIG. 3. α-particle spectrum, obtained by irradiating lead with oxygen.

Owing to the slowing down of the particle as it is scattered from the receiver, the measured energy is found to be less than the true one by an average of approximately 100 kev (experimental estimate).

The first to attract attention in the examination of the spectrum are the two groups of α particles,

one with a maximum at 9.0 ± 0.3 Mev and the second with a maximum at 11.8 ± 0.4 Mev. We note that the energy resolution of the method employed is not so great as to permit stating with assurance that each of these α-particle groups is connected with a single monochromatic line. The appearance of such radiation in our experiments is a somewhat unusual fact, since as a rule in the Po — Th region the lifetimes of α-active nuclei with decay energies exceeding 8 Mev is very short.

Another interesting fact is the magnitude of the energy of the second α-particle group — 11.8 Mev. Not in one case of the decay of the heretofore known radioactive nuclei were α particles of so high an energy registered. In the spectrum shown in Fig. 2, the most intense are the groups of α particles whose maxima lie near 6.2 and 7.3 Mev.

After extracting the target from the cyclotron, the half-life of the α emitter that produced the first group of particles was measured with an ionization chamber. This value was found to be approximately 25 minutes. In all probability this group is due to Em^{212}, produced in reactions of the type $Pb^{207-208}(O^{16}, x\alpha 3 \text{ or } 4n)(x = 0 \text{ to } 2)$.

The bulk of the α particles comprising the group near 7.3 Mev is obviously due to decay of an isotope with an approximate half-life of one minute.

b) The experiments described below were aimed essentially at an investigation of the properties and mechanism of formation of α emitters the decay of which leads to particles with energies ~11.8 and ~9 Mev.

Table II lists the results of the experiments performed to estimate the half-lives of these α emitters. The same lead target was used and the total current of the oxygen ions was the same. All that differed was the operating mode of the apparatus shown in Fig. 1. The third and fourth columns of the table list the total number of high energy α particles registered by the photographic plate. The calculation of the half-lives yields values of 35 ± 10 sec and ~1 min for the α emitters with $E_\alpha \approx 9$ Mev and $E_\alpha \approx 11.8$ Mev respectively.

TABLE II

Number of experiment	t_1 t_2—t_3	$N(E_\alpha \approx 9$ Mev)	$N(E_\alpha \approx 11.8$ Mev)
1	10	360	80
2	50	180	46
3	100	26	14
4	250	3	3

2. Experiments on Irradiation of Lead with Carbon Ions

a) The interaction between accelerated O^{16} ions and lead can give rise to unknown isotopes of the elements from At to Th. If carbon ions are used for the bombardment, the heaviest elements among the products can be Ra. Experiments on irradiation of lead with carbon were undertaken to establish whether the radiation of interest to us ($E_\alpha \approx 9$ Mev and $E_\alpha \approx 11.8$ Mev) is connected with the decay of Ac and Th. It was found that the α-particle spectrum obtained by irradiation of natural lead with C^{12} ions is similar to that observed in the case of oxygen ions. Thus, this radiation is not connected with the decay of Ac or Th. It has been established that on going to C^{13} ions the yield of α radiation of energy ≈ 9 Mev and ≈ 11.8 Mev increases.

b) To ascertain the type of reactions that lead to the appearance of the isotopes emitting the high energy α particles, separated lead isotopes were irradiated by C^{13} ions of different energies.

Figure 4 shows the total α-particle spectrum, obtained after a brief irradiation of Pb^{208} with C^{13} ions of ~70 Mev ($t_1 = t_2 = 25$ sec, $t_3 = 3$ seconds). A comparison of this spectrum with those of Figs. 2 and 3 indicates a substantial change in the ratio of the densities of the α-particle groups near 12 and 9 Mev: the former group has become more intense.

Figure 5 shows the cross sections for the production of high-energy α-particle emitters as a function of the C^{13}-ion energy in the irradiation of Pb^{208}. The relative course of the curves is determined by the statistical errors indicated in the diagram. The accuracy of the determination of the absolute values of the cross sections is not better than 50%. The energy of bombarding particles was measured by displacing the target along the radius of the cyclotron chamber (after first establishing the dependence of the ion energy on the radius). It is seen from Fig. 5 that, independent of the energy of the bombarding particles, the yield of α

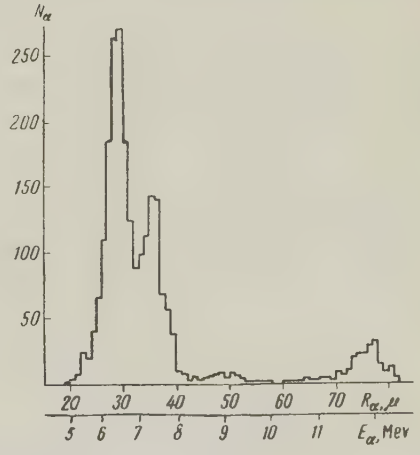

FIG. 4. Spectrum of α particles obtained by irradiating Pb^{208} with C^{13} ions.

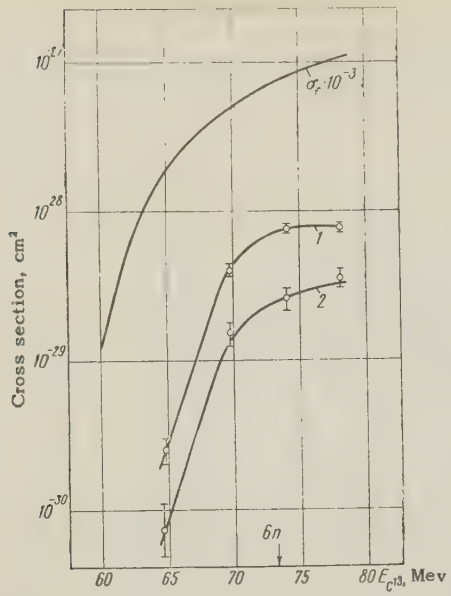

FIG. 5. Yield of α emitters with following particle energy: 1 – ~ 11.8 Mev, 2 – ~ 9 Mev, as a function of the energy of the C^{13} ions; σ_f – fission cross section, approximately equal to the cross section of production of the compound nucleus; the arrow indicates the threshold of reaction with emission of six neutrons.

particles of energies near 11.8 Mev is greater. Upon changing to a Pb^{207} target, the situation changes: for the maximum ion energy, the more probable reaction becomes the one that results in α radiation near 9 Mev (see Table III).

c) The comparatively longer lifetime of the α emitter of ~ 11.8-Mev particles has allowed us to perform an experiment to detect the α decay that is genetically related to this radiation. After a brief irradiation of a Pb^{208} with a beam of C^{13} ions, the receiver of the recoil nuclei was rapidly extracted from the cyclotron chamber and placed in prolonged contact with the emulsion surface. Against the background of a large number of particles with energies less than 8 Mev, six tracks from the first group of high-energy α particles ($E_\alpha \approx 9$ Mev) and 64 tracks belonging to the second group of particles ($E_\alpha \approx 11.8$ Mev) were registered. Not a single pair of correlated tracks was observed.

III. DISCUSSION OF THE RESULTS

1) On the basis of the Rasmussen and Perlman[7] classification of α emitters, it appears little likely for α particles of energy near 12 Mev to be emitted in the decay from the ground state of nuclei of elements from At to Ra. It is known that the energy of α decay increases with decreasing mass number, reaching a maximum for nuclei with N = 128 neutrons, and then rapidly decreases.

At the present time, two isotopes with N = 128 neutrons are known: Po^{212} ($E_\alpha = 8.78$ Mev, $T_{1/2} = 3 \times 10^{-7}$ sec) and At^{213} ($E_\alpha = 9.2$ Mev). Extrapolation of the dependence of the α-decay energy on the mass number for Em, Fr, and Ra shows that in these elements the maximum α-particle energy (at N = 128) evidently does not exceed 10 Mev. It appears most probable to us that the α radiation with energy ~ 11.8 Mev is emitted from the excited nucleus produced during the decay of a certain parent nucleus, i.e., we deal here with the so-called "long-range" α particles. An analysis of the properties of the isotopes that can be formed as a result of interaction of carbon ions with lead shows that the main competing processes in the decay of these nuclei are α decay and K capture. The negative result of the experiment on the detection of genetically-related α particles indicates that the emitter of particles with energy ~ 11.8 Mev cannot be produced by α decay. It is thus proposed that the parent nucleus experiences K decay, while the daughter nucleus is most probably in the excited state ($E^* \approx 2.5$ Mev) and decays with emission of a high-energy α particle. The half-life of the α activity is determined here by the lifetime of the parent nucleus. For the nuclei now known, the intensity of the "long-range" particles is many orders smaller than the intensity of α radiation from the ground state. This is due to the small probability of production of a nucleus in the excited state and with the fact that the decay of the excited nucleus with emission of a high-energy α particle takes place in a smaller fraction of cases (the nucleus experiences principally radiative transition to the ground state).

TABLE III

Target	$N_1(E_\alpha \approx 11.8$ Mev)	$N_2(E_\alpha \approx 9$ Mev)	N_1/N_2
Pb^{208}	589	235	2.5
Pb^{207}	96	148	0.65

In our case (see Fig. 4) the group of "long-range" α particles is more intense than the group with energy near 9 Mev; this can partially be ascribed to the decay of the same nucleus from the ground state. This circumstance can be explained by the fact that the probability of emission of an α particle increases very rapidly with energy. Estimates show that the lifetime of the Po – Ra nuclei relative to the "allowed" α decay with energy on the order of 12 Mev is 10^{-13} to 10^{-11} sec, i.e., in our case the decay of the excited state by emission of a high-energy α particle can compete successfully with radiative transition.

It is most probable that the parent nucleus is an

isotope with N = 127: At^{212}, Em^{213}, Fr^{214}, or Ra^{215}. The last two nuclei must be excluded from consideration in view of the fact that to produce them by bombardment of Pb^{208} with C^{13} ions we must have the reactions (C^{13}, p6n) and (C^{13}, 6n), which are energetically impossible at $E_{C^{13}} < 70$ Mev. In addition, the decay of Ra^{215} should lead to the appearance of two-pronged α-particle stars

$$Ra^{215} \xrightarrow{K} Fr^{215*} \xrightarrow[\sim 12\,\text{Mev}]{\alpha} At^{211} \xrightarrow{\alpha},$$

which has not been observed experimentally. The energy dependence of the cross section for the production of the α radiation of interest to us does not contradict the assumption of production of At^{212} [(C^{13}, p4n) reaction] and Em^{213} [(C^{13}, xα4n) reaction (x = 0, 1)]. There are still not enough grounds for giving preference to any of these isotopes.

It must also be assumed that these nuclei are produced in a metastable state — an assumption which is quite sensible, since the known nuclei with 127 neutrons (Bi^{210} and Po^{211}) have isomer levels. In the case of At^{212} this is necessary, if for no other reason than that the half-life of α particles of energy ~ 11.8 Mev does not coincide with the half-life of decay of At^{212} from the ground state (0.2 second). The metastability assumption allows us to explain the value of the excitation energy (~ 2.5 Mev) of the daughter nucleus and the small value of the cross section for its production. Let us consider the latter circumstance in greater detail for the case of Em^{213} production. The cross section of the (C^{13}, xα4n) reaction (x = 0, 1), which leads to the appearance of Em^{213} in the ground state, is $\sim 10^{-25}$ cm^2 at the maximum C^{13} ion energy (according to an estimate of the yield of Em^{212} from irradiation of Pb^{208} with C^{12} ions). The low yield of the daughter nucleus in the excited state (At^{213*}) could be related to the small probability of K capture of Em^{213} compared with α decay ($E_\alpha \approx 7.5$ Mev). In this case, however, the portion of the α-particle spectrum from 7 to 8 Mev should be hundreds of times more intense. In the case of Em^{213m} production the yield of the α-particle emitter will be determined not only by the "fork" in the Em^{213m} decay, but also by the probability of production of this nucleus and the (C^{13}, xα4n) reaction, which is less than that for Em^{213}.

The proposed mechanism for the appearance of "long-range" α particles is shown schematically in Fig. 6. This scheme should be considered as a working hypothesis, which will be verified and refined by further experiments.

2. The identification of the emitter of α particles of ~ 9 Mev is more difficult. This may be a

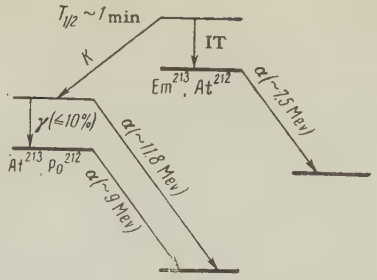

FIG. 6. Proposed scheme for a decay that leads to high-energy α particles; IT – isomer transition.

short-lived isotope in radioactive equilibrium with the parent nucleus, or else it may be a nucleus in the isomer state with a half-life 30 — 40 sec, which emits α particles of ~ 9 Mev (hindrance factor $\sim 10^7 - 10^8$). A known example of such a decay is the isomeric Po^{211} with a half-life of 25 sec, which emits 8.7-Mev α particles.[8] The production of this very isotope in our experiments [via the Pb^{208} (C^{13}, xα2n) reaction (x = 0 to 2)] is not to be excluded.

3. A study of the properties of emitters of high-energy α particles, resulting from the interaction of oxygen and carbon ions with lead is of particular interest for those engaged in the production and investigation of new transuranic elements. The point is that certain isotopes of the far transuranic elements may have radioactive properties similar to the α emitters described in the present paper. This means that lead impurities in targets may produce a substantial background if physical methods are used to identify the new elements. This circumstance was taken into account in experiments on the production of the 102nd element, carried out at the Institute of Atomic Energy of the U.S.S.R. Academy of Sciences in 1957 — 1958.[4,9] For a successful performance of these experiments a sensitive method was developed for activation analysis of lead impurities, and special measures were undertaken to purify the materials employed.

We note again that the interpretation of the results, suggested in Secs. 1 and 2, is tentative. Additional experiments, which are under preparation at the present time, will permit a more definite identification of the observed α emitters.

The authors express their gratitude to V. S. Zolotarev, for graciously supplying us with separated lead isotopes, and to A. M. Semchinova and D. M. Parfanovich for help with the work with the photoemulsions.

[1] G. N. Flerov, Proc. of 2nd U.N. Conf. on Peaceful Uses of Atomic Energy, **14**, p/2299, Geneva (1958).

[2] J. H. Fremlin, Physica, **22**, 1091 (1957).

[3] G. N. Flerov, Ядерные реакции при малых и энергиях, Тр. Всес. конф. 1957 г. (Trans. of 1957 All-union Conference on Nuclear Reactions at Low and Medium Energies) U.S.S.R. Acad. Sci., 1958, p. 489.

[4] G. N. Flerov et al., Dokl. Akad. Nauk SSSR 120, 73 (1958), Soviet Phys.-Doklady **3**, 546 (1959).

[5] A. Ghiorso, Proc. of the Conf. on Reactions between Complex Nuclei, Gatlinburg, 1958, p. 34.

[6] D. L. Hufford and B. F. Scott, The Transuranium Elements, NNES **2**, 1159 (1949).

[7] J. Rasmussen and J. Perlman, Handbuch der Physik, vol. 42, 1957.

[8] Jentschke, Inveland, and Kinsey, Phys. Rev. **96**, 231 (1954).

[9] G. N. Flerov et al., JETP **38**, 82 (1960), Soviet Phys. JETP **11**, in press.

Translated by J. G. Adashko
256

ELASTIC SCATTERING OF POSITIVE PIONS BY CARBON AT ENERGIES OF 5 — 22 Mev

V. G. KIRILLOV-UGRYUMOV, L. P. KOTENKO, E. P. KUZNETSOV, F. M. SERGEEV, and A. F. GRASHIN

Submitted to JETP editor June 23, 1959

J. Exptl. Theoret. Phys. (U.S.S.R.) **37**, 1273-1280 (November, 1959)

Elastic scattering of positive 5 — 22 Mev pions by carbon was investigated in a propane bubble chamber. Phase-shift analysis of the angular distribution shows that a repulsive potential acts on the meson in the S state in the nucleus.

INTRODUCTION

AN investigation of the scattering of very slow positive pions yields interesting data on the interaction between pions and nuclei practically in the S state, since the contribution of waves with $l \neq 0$ is found to be small at ~ 10 Mev. Analogous information for negative pions can be obtained when measuring the level shifts in π-mesic atoms. However, the pion energy does not exceed 0.13 Mev even at the K level of carbon and therefore, at energies greater than this value, a study of the scattering of pions by carbon is the only direct experimental method of investigating the interaction between pions and nuclei.

Investigations of the scattering of slow pions (with energies on the order of 20 Mev and greater) were undertaken with the aid of photoemulsions.[1-4] These papers give, in particular, data on the elastic and inelastic scattering cross sections. However the accuracy of the data given, together with the fact that there scattering by a mixture of heavy nuclei (for which the Coulomb scattering is large) takes place in the emulsion does not permit an analysis of the character of the pion-nucleon interaction in elastic scattering.

In an earlier paper[5] we reported preliminary data on the scattering of slow positive pions by carbon. The cross sections given in reference 5 include nuclear scattering and interference between the Coulomb and nuclear scattering.

In the present paper we give a data-reduction method and an analysis, based on greater statistical material, of the angular distributions of elastic scattering of positive pions at energies 5 — 22 Mev.

EXPERIMENTAL CONDITIONS

The scattering was investigated in a propane bubble chamber. Some of the material was obtained with the chamber described by Kotenko, Kuznetsov, and Popov.[6] Another portion of the material was obtained with the chamber described by Pershin,[7] and was graciously made available to us by the author, for which we take this opportunity to express our gratitude. The material obtained with these chambers was used earlier to determine the correlation in $\pi \to \mu \to e$ decay.[8,9] The chambers were irradiated in the pion beam of the Joint Institute for Nuclear Research, the pions were produced by the external proton beam on a polyethylene target 70 cm thick. The 170-Mev mesons emitted from the target at an angle of 70° were guided into the collimator by a deflecting magnet. In front of the chamber itself the pions were slowed down with an absorber so that most pions of the beam were stopped within the working volume of the chamber.

PROCESSING OF THE EXPERIMENTAL DATA

We investigated pions scattered and stopped in the chamber (the stopping of a positive pion was identified by the characteristic $\pi^+ \to \mu^+ \to e^+$ decay). In scanning the statistical material, an important role can be played by subjective errors, connected with miscounting of stopped positive pions. It can be stated that a positive pion stopped after prior scattering of the pion (particularly at a large angle) is observed in scanning more frequently than a stopping without scattering. Thus, the current of stopped particles may be underestimated and the scattering cross section may be artificially overestimated. To avoid this error as much as possible, half of the entire statistical material was scanned three times, the first two times being scanned only for the purpose of detecting the stopping of a positive pion as identified by the $\pi^+ \to \mu^+ \to e^+$ decay. The number of stopped positive pions after the first and second scannings was 5,306 and 6,670 respectively, i.e., the number of stoppings missed in the first scanning was 11.5%

TABLE I

Energy intervals, ΔE, Mev	Angular intervals, Δφ, deg	Observed number of scattering events, ΔN_{obs}	Number of scattering cases after introducing the correction, ΔN_c	dσ/dφ, mb/sterad				
				Experiment	Solutions I	Solutions II	Solutions III	Data of Byers[13]
					$\eta_0=-8°$, $\eta_1=-1°45'$	$\eta_0=33°$, $\eta_1=11°35'$	—	$\eta_0=-3°$, $\eta_1=1°$
5—8	15—20	25	20.8	3612±754	2702	1335	—	2303
	20—60	18	18.4	393±100	510	369	—	349
	60—120	9	9.5	141±47	72	157	—	39
	120—180	1	1.1	16±16	25	3	—	24
					$\eta_0=-7°30'$, $\eta_1=-1°$	$\eta_0=5°$, $\eta_1=-5°$	$\eta_0=20°$, $\eta_1=14°$	$\eta_0=-4°30'$, $\eta_1=2°40'$
8—15	15—20	24	20.5	853±181	835	987	539	727
	20—60	26	30.3	159±33	148	148	136	84
	60—120	4	6.2	22±12	29	5	28	15
	120—180	6	6.9	25±10	22	19	51	23
					$\eta_0=-4°$, $\eta_1=2°$	$\eta_0=12°$ $\eta_1=-0°45'$	$\eta_0=20°$, $\eta_1=0°45'$	$\eta_0=-6°20'$, $\eta_1=6°$
15—22	15—20	11	9.8	273±88	297	324	203	262
	20—60	7	10.5	36±15	46	60	27	22
	60—120	4	9.2	23±12	9	16	20	13
	120—180	3	4.5	11±7	11	15	19	29

will decay in flight, W_2 the probability that the positive muon will enter the investigated range of angles in the $\pi^+ \to \mu^+$ decay, and W_3 is the probability that the positive muon will imitate the $\pi^+ \to \mu^+$ decay at the end of its range (single scattering greater than 15°). W_1, W_2, and W_3 can be calculated.

c) Calculation of the error in the measurement of the angles and of the multiple scattering. In determining the limit of angle intervals and in plotting the angular distributions, it is very important to account correctly for the excess count of scatterings in a given angular interval due to the error in the measurement of the angles and due to multiple scattering. Assuming the distribution of the deviations in the angle measurement to be Gaussian within two standard deviations, the correction desired is obtained in the form

$$W_{ang} = \int_{\varphi_{lim}-2\sigma}^{\varphi_{lim}} F(\varphi)\, d\varphi \frac{1}{\sqrt{2\pi}} \int_{\varphi_{lim}-\varphi}^{\infty} e^{-t^2/2} dt - \times \int_{\varphi_{lim}}^{\varphi_{lim}+2\sigma} F(\varphi)\, d\varphi \frac{1}{\sqrt{2\pi}} \int_{\varphi-\varphi_{lim}}^{-\infty} e^{-t^2/2} dt, \quad (4)$$

where $F(\varphi)$ is the function that determines the projection of the Coulomb scattering on the plane of the film, $\sigma = \sqrt{\sigma_1^2 + \sigma_2^2}$; σ_1 is the mean-squared error in the measurement of the angle, σ_2 is the mean square of the projection of the angle of multiple scattering for a given energy interval. The integration was carried out numerically.

d) Calculation of the error in the measurement of the energy. The correction for the additional number of events within a given energy interval was allowed for in plotting the energy dependence of the scattering cross section by using a method similar to that described in case c). This correction was found to be negligibly small.

e) Scattering by hydrogen. The correction for Coulomb and nuclear scattering by the hydrogen contained in the propane was taken into account by the usual method used to determine the total cross section of scattering by a complex substance.

f) Inelastic scattering. In the investigation of scattering of positive pions by nuclei at low energies in a bubble chamber it is difficult to separate the elastic scattering from the inelastic one, since the positive pion has an increased track density long before stopping and a small (4 — 7 Mev) decrease in energy cannot be noticed. However, from experiments on scattering of positive pions by emulsion nuclei at our energies[1-4] and by carbon nuclei at energies greater than 30 Mev[11] it is known that the inelastic-scattering cross section diminishes rapidly with decreasing energy and is practically zero at energies less than 30 Mev. We therefore assume that the scattering measured by us is fully elastic.

ANALYSIS OF THE EXPERIMENTAL DATA

To plot the angular distributions, the energy interval investigated by us (5 — 22 Mev) was broken down into three smaller intervals: 5 — 8, 8 — 15, and 15 — 22 Mev.

The results of making all the corrections for the angular distributions are presented in Table I. We also list there the experimental cross sections by angle intervals (Coulomb plus nuclear).

It is known that the differential angular cross section for scattering by a nucleus of charge Z

of the number of cases observed in two scannings. The third scanning was to detect scattering of the previously found stopped positive pions. In this scanning, too, additional stoppings were observed, but their number was small compared with the total number of cases (less than 3% of the number found in the first two scannings). We believe that such a scanning of the material excludes the possibility of predominant observation of stopping plus scattering cases.

In the measurement of scattering we excluded from consideration stopped mesons with ranges less than 6 mm in the chamber prior to decay (the decay positive pion had a range of 3.15 mm), cases when the positive pion entered the chamber from the glass or at a large angle from the upper or lower walls of the chamber, and finally cases when the angle between the projection of the positive-pion momentum prior to stopping and the direction of the momentum of the decay positive pion was less than 15° — in these cases the admixture of positive pions produced outside the chamber is large.

In the third scanning we counted all single scatterings by more than 10° (projected on the plane of the film). Measurement of the projections of the angles allowed us to accelerate the data reduction and to decrease the error in the determination of the angle. The angles were measured accurate to ±1°.

All scattering cases were scanned two more times. In these scannings we selected carefully all cases of single scattering by angles greater than 15°. Such a selection was necessitated by the large value of the Coulomb scattering at our energies, and by the difficulty of separating single scatterings from multiple scatterings at smaller angles.

The second part of the statistical material was scanned carefully once more after the final reduction of the first part of the material (the two parts were approximately equal statistically). The results obtained with the second half of the material agreed, within the limits of statistical errors, with the results obtained in the reduction of the first half of the material. The statistics were then combined. Thus we selected 8,727 photographs of positive-pion tracks stopped in the chamber for our investigation of scattering.

The particle energy at the point of scattering was determined from the residual range. The errors in the measurements of the energy did not exceed 10% for the selected energy interval from 5 to 22 Mev. A total of 137 particles were scattered within the angle and energy intervals.

To proceed with the calculation of the cross sections and to determine the angular distributions of the scattering, it is necessary to introduce corrections for many factors, which we shall now discuss.

a) Geometric correction. The finite dimensions of the chamber cause some of the scattered particles to go into the walls of the chamber and become unobservable. The calculation of the correction for such omissions, owing to the rectangular form of the chamber, is similar to the problem of finding the probability that a segment of length l will fall in a random test on one of two parallel lines, the distance between which is a (see, for example, reference 10). Taking into account the features of the chamber geometry and of the particle scattering it is possible, using the solution to the above problem, to obtain the following value for the correction coefficient:

$$K_{\text{corr}} = \left[1 - \frac{2l\sin\theta}{\pi}\left(\frac{1}{a}+\frac{1}{b}\right) + \frac{l^2\sin^2\theta}{\pi}\right]^{-1}, \quad (1)$$

where θ is the three-dimensional angle of particle scattering, l the true length of the particle track after scattering, while a and b are the transverse dimensions of the chamber (in our case the height was equal to the depth). We used a correction coefficient of somewhat simpler form

$$K_{\text{corr}} = (1 - 2l\sin\varphi^*/\pi a)^{-1}, \quad (2)$$

where φ is the projection of the scattering angle on the plane of the film. This results in a slightly overvalued correction, but by an amount which is much smaller than the statistical error, and is therefore insignificant.

Corrections based on (1) and (2) are introduced for each individual scattering case and thus take automatically into account the spectrum of the scattered particles; (1) takes into account the distribution in space, while (2) takes into account the distribution in the projection on the emulsion plane.

The correction coefficients (1) and (2) disregard a certain inhomogeneity in the positive-pion current over the height and depth of the chamber, and also the dip angle of the entering positive-pion beam. Estimates show that these can be neglected in our case.

b) Corrections for positive-pion in-flight decay identified as scattering of positive pions. A positive pion can decay in flight and the positive decay muon, which experiences scattering shortly before stopping, may imitate a $\pi^+ \to \mu^+$ decay. Such cases can be mistaken for a positive-pion scattering.

The overall probability of registering a positive-pion decay as a scattering is

$$W = W_1 W_2 W_3, \quad (3)$$

where W_1 is the probability that the positive pion

is given, at small energies, by the following formula (see, for example, reference 12):

$$\frac{d\sigma}{d\Omega}=\frac{\alpha^2}{4k^2}\left|\frac{\exp\{-i\alpha\ln\sin^2(\theta/2)\}}{\sin^2(\theta/2)}+\frac{i}{\alpha}(e^{2i\eta_0^*}-1)\right.$$
$$\left.+\frac{3i}{\alpha}\frac{1+i\alpha}{1-i\alpha}(e^{2i\eta_1}-1)\cos\theta\right|^2, \qquad (5)$$

where $\alpha = Ze^2/\hbar v$, v the velocity of the incident particle, k the wave number, e the electron charge, θ the scattering angle, $\eta^* = \eta_0 + i\delta_0$ the complex phase shift of the S wave, and η_1 the phase shift of the P wave. It is assumed here that in the investigated energy region the principal contribution to the scattering is made by the S and P waves and that only the S wave is absorbed (see, for example, the paper by Byers[13]). Formula (5) is correct in the case of a target nucleus of infinite mass. In our case this condition is satisfied with high accuracy.

We reduced the data by projection, i.e., we measured the projections of the scattering angles of the positive pions on the plane of the emulsion. To compare the experimental angular distributions with the theoretical formula (5), the latter had to be projected on the plane passing through the primary direction of the particle track. In machine computation, the formula was projected exactly. Here we give an approximate value of the projected formula.

Omitting the intermediate computations, we can write for small phases η_0, δ_0, and η_1 (i.e., using the approximation $\sin\eta_1 = \eta_1$ and $\sin\delta_0 = \delta_0$)

$$\frac{d\sigma}{d\varphi_1}=\left[\frac{\alpha^2r_0^2}{4\beta^2}F_1(\varphi)+24\frac{r_0^2}{\beta^2}\eta_{i1}^2\cos^2\varphi\right.$$
$$\left.-\frac{\alpha r_0^2}{\beta^2}F_2(\varphi)-\frac{3\pi r_0^2}{\beta^2}\eta_1F_3(\varphi)+A\right]\text{rad}^{-1},$$

where $r_0 = \hbar/\mu c$, μ is the reduced mass, φ the projection of the scattering angle θ on the plane passing through the initial direction of the scattered particles,

$$F_1 = 16(\sin\varphi+(\pi-\varphi)\cos\varphi)/\sin^3\varphi.$$

is the projection of the Coulomb scattering,

$$F_2=4\frac{2(\pi-\varphi)-\pi\sin\varphi}{\cos\varphi\sin\varphi}[(1-C_1)(\eta_{i0}-2\delta_0\eta_{i0}+3\eta_{i1})$$
$$-C_2(\delta_0+\eta_{i0}^2+6\alpha\eta_{i1})],$$

$$F_3=\cos\varphi(C_1\alpha+2\alpha^2C_2-2\eta_{i0}),$$

$$A=\frac{4r_0^2}{\beta^2}[\eta_{i0}^2+\delta_0^2-C_1\alpha(\eta_{i0}-2\delta_0\eta_{i0}+6\eta_{i1})$$
$$-C_2\alpha(\delta_0+\eta_{i0}^2+12\alpha\eta_{i0})+6\alpha\eta_{i1}].$$

The constants C_1 and C_2 are determined from the conditions of approximate equality of the function used in the projection

$$\cos\left(\alpha\ln\sin^2\frac{\theta}{2}\right)=1-C_1\cos^2\frac{\theta}{2}, \qquad C_1=C_1(\alpha),$$
$$\sin\left(\alpha\ln\sin^2\frac{\theta}{2}\right)=C_2\cos^2\frac{\theta}{2}, \qquad C_2=C_2(\alpha).$$

A better agreement between the exact and approximate functions was obtained for C_1 at $\theta = 20°$ and, for C_2 at $\theta = 60°$ — the discrepancy in the remaining points did not exceed 10% in this case.

It can be shown that in the geometry of our experiment the conical projections of the scattering angles on the plane of the film differ very little from the orthogonal projections.[14]

From the plotted experimental angular distributions we found the phase shifts η_0 and η_1. To determine the shifts we used a somewhat modified least-squared method, which took into account the errors in the experimental values. The method was used in this form by Fermi[15] and consisted essentially of a method of estimating parameters by the minimum of χ^2 (reference 16). The phases were determined with a "Ural" digital computer, which evaluated the sum

$$\sum_i\left(\frac{\sigma_{ti}-\sigma_{ei}}{\varepsilon_i}\right)^2=N(\eta_{i0},\ \eta_{i1}). \qquad (6)$$

The value of N was calculated in the phase-shift range from +50 to −50°. This interval was specified on the basis of the values of the phase shifts calculated in the paper by Byers[13] for the scattering of negative pions by carbon and on the basis of analysis of mesic-atom data.

In Eq. (6), σ_{ei} is the experimental scattering cross section in the i-th angle interval, ϵ_i is the error in the determination of the experimental value of the cross section, and σ_{ti} is the theoretical value of the cross section in the given angle interval. The cross section σ_{ti} was calculated from the projected formula (5), neglecting also the absorption of the S wave. This assumption can be justified by the fact that the data on the absorption of positive pions in beryllium at 20 and 39 Mev,[17] and also the data on the measured width of the 1S level in the π-mesic atom from beryllium,[18] would lead us to expect that, in the investigated energy interval, the phase shifts corresponding to absorption δ_0 are one-third the scattering phase shifts η_0.[13] Allowance for absorption phase shifts of this order of magnitude changes the differential scattering cross section by not more than 5%, which is much less than the error in the cross-section measurements. This allows us to neglect absorption of the S-wave. Unfortunately, it is very difficult to determine experimentally in a bubble chamber the absorption cross section at energies 5 — 22 Mev.

In the indicated phase-shift interval we obtained for N three relative minima at 8 — 15 and 15 — 22

TABLE II. Relative minima of the values of N and the corresponding values of the phase shifts

ΔE, Mev	5—8		8—15			15—22		
Solution	I	II	I	II	III	I	II	III
η_0	—8°	33°	—7°30′	5°	20°	—4°	12°	20°
η_1	—1°45′	11°30′	—1°	—5°	14°	+2°	—0°45′	0°45′
N	5.6	9.2	0.6	2.5	6.9	2.0	2.3	2.1
P, %	80.0	0.05	99.0	90.0	3	87.0	4	50

Mev, and two minima at 5 — 8 Mev. The values of the phase shifts and the corresponding values of N are given in Table II. The sixth, seventh, and eighth columns of Table I give the cross sections corresponding to these solutions, calculated by formula (5).

Inasmuch as the differential elastic-scattering cross sections of zero-spin particles permit a unique determination of the scattering amplitude,[19] only one of the found solutions should be retained. The choice was made on the basis of an examination of the values of N, of the agreement levels for the Kolmogorov criteria, and of the stability of solution under variation of energy.

To avoid errors in the choice of a solution, which may be caused by insufficient statistics (which can lead in turn to a change in the profile of the function $N(\eta_0, \eta_1)$ in a repetition of the experiment), we estimated all pairs of solutions by the Kolmogorov agreement criterion. The agreement levels P for the Kolmogorov criteria are listed in Table II. Specifying, as usual, a 5% value level, we can discard solution II in the 5 — 8 Mev and 15 — 22 Mev intervals and solution III in the 8 — 15 Mev interval. Among the remaining solutions, solution I has in each energy interval a definite stability under a small change of energy of scattering particles, while the other solutions have no such stability. Obviously these solutions should be chosen as the true ones.

From the integrated cross sections for scattering at angles greater than 15° we estimated the statistical errors of the obtained phase shifts. Final data are summarized in Table III.

TABLE III

ΔE, Mev	5—8	8—15	15—22
η_0	$-8° \pm 4°$	$-7°30' \pm 2°$	$-4° \pm 3°$
η_1	$-1°45' \pm 4°$	$-1° \pm 3°$	$2° \pm 1°$

From the values of the phase shifts it is seen that in the scattering of 5 — 22 Mev positive pions the principal role is played by scattering in the S state, and that the phase shift of the S phase is negative, corresponding to the presence of repulsion in the S state. Since the P phase is small, it can be stated that in the investigated energy interval the nuclear forces between the carbon nucleus and the positive pion are repulsive in character, in other words, there is a positive effective potential between the nucleus and the positive pion.

This positive potential is in apparent contradiction with the results of an entire group of investigations of elastic scattering of pions by carbon nuclei in the energy range from 30 to 125 Mev.[20-24] The results obtained in these investigations (based on the optical model) indicate an attractive potential. However, there is no contradiction here since in the 30 — 125 Mev region P scattering predominates, with positive phase, and this yields an effective negative potential.*

TABLE IV. Phase shifts calculated with allowance for the Coulomb interaction, based on data for π-mesic atoms[13]

ΔE, Mev	5—8	8—15	15—22
η_0	—3°	—4°30′	—6°20′
η_1	+1°	+2°30′	+6°

Our result is qualitatively in agreement with data on the measurement of energy level shifts of negative pions in π-mesic atoms,[25] where the rise in the levels is evidence of a repulsive potential acting on the pion. Byers[13] calculated, from an analysis of the level shift in π-mesic atoms, the possible phase shifts in scattering of negative pions by carbon at 5 and 10 Mev. Using the results of this paper, we calculated (with allowance for the Coulomb interaction) the expected phase shifts for the scattering of positive pions by carbon at our energies. These phase shifts are listed in Table IV, and the corresponding cross sections are given in the last column of Table I. The cal-

*We can note in this connection that in the optical model the graph of the real part of the potential becomes positive at small energies, and does not vanish from the side of negative values, as shown by Frank et al.[26] (Fig. 2b).

culated phase shifts deviate somewhat from those we obtained experimentally, but we do not attach too great a significance to this since, firstly, the statistical errors in our experiments are large, and secondly the data on π-mesic atoms for the P wave are not reliable.

Assuming additivity of the pion-nucleus interaction potential, we can obtain from our phase shifts the connection between the phase shifts of the S waves in meson-nucleon scattering. Calculations yield $\delta_1 + 2\delta_3 < 0$ (where δ_1 and δ_3 are the phase shifts of the S wave at $T = \frac{1}{2}$ and $T = \frac{3}{2}$) in the entire energy interval under investigation. This agrees both with conclusions drawn from mesic-atom data and with direct measurements of meson-nucleon scattering.[27]

We note that an analysis of the experimental data on nuclear scattering at low energies is difficult because of the presence of a large Coulomb background, particularly at small angles, and the presence of interference between the Coulomb and nuclear scattering. The first difficulty can be eliminated by correct allowance for Coulomb scattering and by increasing the statistical material. Correct computation of the interference terms makes it desirable to obtain data on scattering of negative pions at the same energies.

In conclusion, we wish to express our gratitude to Professor V. P. Dzhelepov for enabling us to perform the experiments on the proton synchrotron, to Professor A. I. Alikhanyan for interest in the work and for useful discussions, to A. V. Samoĭlov and L. L. Sabsovich for computations with the computer, to V. P. Kuznetsov for useful discussions, and to A. A. Bednyakov for help in running the accelerator.

[1] B. Rankin and H. Brandner. Phys. Rev. **90**, 647 (1953).

[2] G. Bernardini. Phys. Rev. **84**, 610 (1951).

[3] L. Feretti and E. Manaresi, Nuovo cimento **1**, 512 (1957).

[4] M. Minguzzi and A. Minguzzi-Ranzi, Nuovo cimento **10**, 1100 (1958).

[5] Kirillov-Ugryumov, Kotenko, Kuznetsov, and Sergeev, JETP **35**, 1300 (1958), Soviet Phys. JETP **8**, 907 (1959).

[6] Kotenko, Kuznetsov, and Popov, Приборы и техника эксперимента (Instrum. and Meas. Engg.) No. 1, 36 (1957).

[7] I. I. Pershin, ibid. No. 1, 39 (1957).

[8] Alikhanyan, Kirillov-Ugryumov, Kotenko, Kuznetsov, and Popov, JETP **34**, 253 (1958), Soviet Phys. JETP **7**, 176 (1958).

[9] Barmin, Kanavets, Morozov, and Pershin, JETP **34**, 830 (1958), Soviet Phys. JETP **7**, 573 (1958).

[10] V. B. Gnedenko, Курс теории вероятностей (A Course in Probability Theory) GITTL, 1954, p. 38.

[11] L. M. Barkov and B. A. Nikol'skiĭ, Usp. Fiz. Nauk **61**, 341 (1957).

[12] J. Blatt and V. Weisskopf, Theoretical Nuclear Physics (Russ. Transl.) IIIL, 1954, p 265 (Wiley, N. Y., 1952).

[13] N. Byers, Phys. Rev. **107**, 843 (1948).

[14] Kotenko, Kuznetsov, Samoĭlov, and Sergeev, Материалы совещания по камерам Вильсона, диффузионным и пузырьковым камерам. (Proc. Conf. on Cloud, Diffusion and Bubble Chambers), No. 5, Dubna, 1958.

[15] Fermi, Metropolis, and Alei. Phys. Rev. **95**, 1581 (1954).

[16] See, e.g., H. Cramer, Mathematical Methods of Statistics, (Russ. Transl.) IIL, 1948, p 460 (Princeton, 1946).

[17] F. Tenney, and J. Tinlot, Phys. Rev. **92**, 974 (1953).

[18] D. West and E. Brandley, VI Rochester Conference, 1956.

[19] Puzikov, Ryndin, and Smorodinskiĭ, JETP **32**, 592 (1957), Soviet Phys. JETP **5**, 489 (1957).

[20] D. H. Stork. Phys. Rev. **93**, 868 (154).

[21] A. M. Shapiro. Phys. Rev. 84, 1063 (1951).

[22] Byfield, Kessler, and Lederman, Phys. Rev. **86**, 17 (1952).

[23] Isaacs, Sachs, and Steinberger, Bull. Amer. Phys. Soc. **26**, No. 6, 22 (1951).

[24] J. Kessler and L. Lederman. Phys. Rev. **94** 689 (1954).

[25] M. Stearns and M. B. Stearns. Phys. Rev. **103**, 1534 (1956).

[26] Frank, Gammel, and Wattson, Phys. Rev. **101**, 891 (1956).

[27] J. Orear, Phys. Rev. **96**, 176 (1954).

Translated by J. G. Adashko
257

TOPOLOGY OF THE FERMI SURFACE FOR GOLD

Yu. P. GAĬDUKOV

Institute for Physical Problems, Academy of Sciences, U.S.S.R.

Submitted to JETP editor June 24, 1959

J. Exptl. Theoret. Phys. (U.S.S.R.) 37, 1281-1291 (November, 1959)

The resistance anistropy of gold single crystals in a magnetic field has been investigated. It has been found that for certain directions of the magnetic field relative to the crystallographic axes of the single crystals the resistance increases as the square of the field, while for other directions it reaches complete saturation for values of the field $H \gg H_0$. It can thus be concluded that an open Fermi surface exists in the case of gold. A stereographic projection of preferred directions of the magnetic field has been constructed, and an analysis of it shows that the Fermi surface in the case of gold is a "spatial net" formed by "corrugated cylinders" whose axes are parallel to the [110] and [111] directions of the reciprocal lattice. The resistance of gold single crystals has been averaged over the angles. The values of the averaged resistance depend linearly on the magnetic field, thus explaining Kapitza's law.

1. INTRODUCTION

THE theory of galvanomagnetic phenomena based on the assumption of the quadratic form of the dispersion of the conduction electrons in a metal $\epsilon(\mathbf{p}) = \mathbf{p}^2/2m^*$ (ϵ is the energy, $\mathbf{p}$ is the quasi-momentum, m^* is the effective mass of electron[1,2]) was unable to explain such well known experimental facts as the linear increase in the resistance of polycrystalline samples (Kapitza's law[3]) and the pronounced resistance anisotropy of single crystals in a magnetic field.[4-6]

In 1955 I. Lifshitz, Azbel', and Kaganov[7] carried out a theoretical investigation of galvanomagnetic phenomena in metals with an arbitrary dispersion law. A very important aspect of this investigation was the treatment of the conduction electrons in the metal as a gas of quasi-particles with a complex anisotropic dispersion law $\epsilon(\mathbf{p})$ which may correspond to both closed and open isoenergetic surfaces $\epsilon(\mathbf{p}) = \zeta_0$. It was shown that in the region of strong magnetic fields $H \gg H_0$ (H_0 is the field for which $l/r = 1$, l is the mean free path, r is the radius of curvature of the electron trajectory in the magnetic field) the characteristic features of the galvanomagnetic properties of metals are determined by the topology of the Fermi surface $\epsilon(\mathbf{p}) = \zeta_0$ and do not depend on the interaction between the electrons and the lattice imperfections.

In the case of metals with open Fermi surfaces the theory[7] established in principle the possibility of saturation of the resistance of single crystals for some orientations of the magnetic field, and the quadratic increase of the resistance for other orientations. In the case of metals with closed Fermi surfaces we should not expect pronounced anisotropy of the resistance in a magnetic field, and, moreover, for metals with $n_1 \neq n_2$ (n_1 and n_2 are the densities of electrons and of "holes") the resistance will tend to saturation, while in the case $n_1 = n_2$ the resistance will increase quadratically with the magnetic field.

Thus, experimental study of galvanomagnetic phenomena enables us to obtain valuable information on the topology of Fermi surfaces in metals. However, this possibility was rendered doubtful as a result of the work of Chambers.[8] By extrapolating the experimental results to $H = \infty$ he concluded that the linear increase of resistance in the case of polycrystalline samples of Au, Cu, and Ag will occur only at very high values of the magnetic field; while, according to Lifshitz, Azbel' and Kaganov,[7] the resistance in this case must either increase quadratically with the field, or must be independent of the field.

It should be emphasized that Chambers carried out his measurements using polycrystalline samples. It appeared to us to be probable that an investigation of single crystals would lead to an essentially different picture. In connection with this we undertook an investigation of the resistance of single crystals of gold in a magnetic field, for which the linear growth of resistance in the case of polycrystalline samples[4] and the pronounced anisotropy of resist-

ance in the case of single crystals[9] have been established most clearly. A preliminary communication of the results obtained by us has been given earlier.[10]

2. SAMPLES AND THE MEASUREMENT METHOD

As we have noted already, the modern theory of galvanomagnetic phenomena in metals has been developed for the case of large fields $H \gg H_0$. In the case of monovalent metals H_0 may be estimated from the condition $l/r = H/\rho_0 nec = 1$, where e is the electron charge, n is the electron density, c is the velocity of light in vacuo, ρ_0 is the specific resistance at $H = 0$.

The validity of the condition $H \gg H_0$ improves as ρ_0 becomes smaller. Therefore, it is necessary to carry out the measurements at low temperatures utilizing samples of high purity.

a) Samples. The material used for the preparation of the samples was gold of purity 99.9999% (the impurities were Ag ≈ 0.00008% and Cu ≈ 0.00002%).

Gold single crystals were prepared by a method due to Bridgman.[11] The initial material in a quantity sufficient for obtaining one sample was melted under high vacuum in the wide portion of a quartz flask at the end of which there was a capillary of the required diameter and length (usually of 0.5 mm diameter and of length ~ 20 mm).

After melting and outgassing, the metal under a small pressure (≈ 1 atm) of gaseous helium was made to fill the capillary. The capillary was detached from the flask and was placed inside a quartz tube which could be pulled through an oven. The oven temperature was of the order of 1200° C. A clockwork mechanism pulled the oven along the quartz tube. The length of time that the sample remained in the oven was varied from 2 to 60 min.

After crystallization the quartz capillary was dissolved in hydrofluoric acid, and the sample was subjected to etching in aqua regia. A five minute etching period was sufficient to make the crystal sides produce sharp reflections, which permitted the optical method to be used for the determination of the orientation of the samples. The determination of orientations was carried out by means of a two-circle reflecting goniometer. As measurements have shown, in the case of gold which has a cubic face-centered lattice the planes giving the most intense reflections are the (111) planes. The shape of the reflected spots was that of three-pronged stars. Only the reflections from the (111) planes were used for the determination of the orientation. The accuracy of measurement was ~ 1°.

The determination of the orientation of a large number (~ 20) of single crystals showed that with such a method of preparation the axes of the samples were situated primarily in the binary plane of the crystal. In this plane the direction of the sample axes was random.

Eight samples were selected for the measurements. The characteristics of these samples are given in Table I (one can also infer the orientation of the samples from Fig. 5).

b) Mounting the samples. Particular attention was paid to the mounting of the samples. In reference 12 it was shown that the relative position of the sample electrodes may significantly affect the results of the measurements. It is also necessary to take precautions against the deformation of the samples.

We soldered the current electrodes (copper wire of 0.15 mm diameter) by means of Wood's alloy to the ends of the sample. The potential electrodes (copper or gold wire of 0.05 mm diameter) were mounted at a distance of $\frac{1}{3}$ of the sample length from its ends.

The wire encircled the sample by a single loop and was drawn tight. The ring formed in this manner was in tight contact with the sample and was then soldered.

The sample was then mounted in an ebonite holder which had the shape of a hollow half-cylinder. One end of the sample was glued to the inner wall of the half-cylinder while the other was completely free. A long metal needle could be inserted into the holder perpendicular to its axis (and to the sample axis), and a second determination of the directions of the crystallographic axes could be carried out with respect to it. By fixing the direction of the

TABLE I

Samples*	Au-1	Au-2	Au-3	Au-4	Au-5	Au-6	Au-7	Au-8
Orientation φ, ϑ', in degrees	23; 85	45; 90	45; 50	42; 4	45; 17	45; 28	40; 84	42; 84
$\rho(300°)/\rho(4°,2)$	1650	304	1456	945	1022	896	1178	1670
H_0, koe	1.4	7.6	1.56	2.44	2.25	2.6	1.95	1.38

*φ and ϑ' are polar coordinates of the sample axes in the stereographic projection of the gold lattice (Fig. 5); φ is the angle measured from the (010) plane, ϑ' is the angle between the [001] axis and the sample axis.

needle with respect to the magnetic field it was possible to determine the direction of the projections of the principal crystallographic axes on the plane in which the magnetic field was rotated and which was perpendicular to the sample axis. The error in determining the orientation with respect to the magnetic field could amount to not more than 2°.

c) Measurements. For the measurement of resistance we utilized a potentiometer KL-48 with a galvanometric two-stage photoelectric amplifier FEOU-15. The sensitivity of this arrangement was 1×10^{-9} V/(mm/m). The measuring current through the sample was usually equal to 0.5 amp.

To eliminate the effect of thermoelectric and Hall emfs both the measuring current and the magnetic field were chopped. The magnetic field was provided by means of an electromagnet which enabled us to obtain field intensities up to 24,000 oe in a 20 mm gap, and up to 34,000 oe in a 12 mm gap. Most of the measurements were carried out at T = 4.2° K, since when the temperature was lowered further the decrease in the resistance of the samples was insignificant.

3. RESULTS OF MEASUREMENTS

The dependence of the resistance $\rho(\vartheta)$ on the angle was measured for all eight single crystals in a constant magnetic field of H = 23,500 oe. The angle ϑ through which the magnetic field was rotated was varied from 0° to 180°, and the resistance was measured at intervals of 2.5°. Figures 1 — 4 show rotation diagrams for four gold single crystals:

$$\frac{\Delta\rho_H}{\rho_0} = \frac{\rho_H(\vartheta) - \rho_0}{\rho_0}.$$

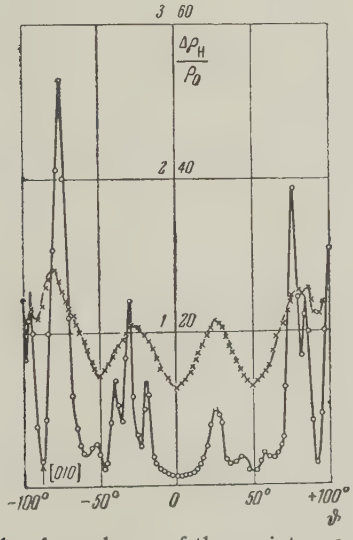

FIG. 1. Angular dependence of the resistance of the single crystal Au-1: H = 23,500 oe; o — T = 4.2°K (the values of $\Delta\rho_H/\rho_0$ are shown on the right); × — T = 20.4°K (the values of $\Delta\rho_H/\rho_0$ are shown on the left).

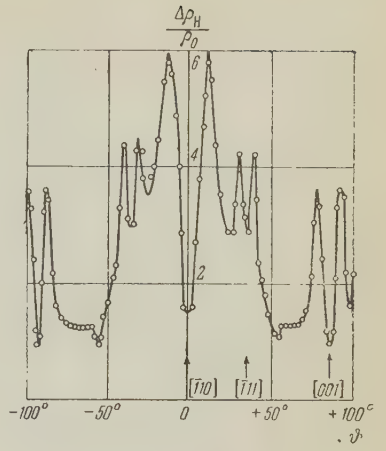

FIG. 2. Angular dependence of the resistance of the single crystal Au-2: H = 23,500 oe; T = 4.2°K.

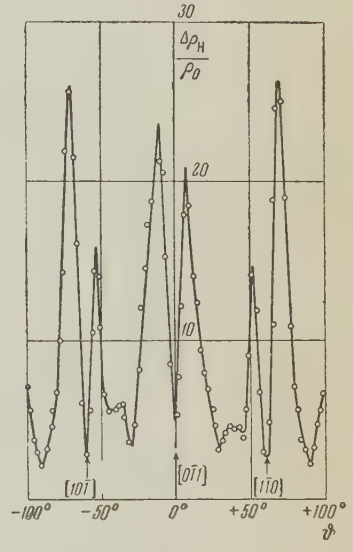

FIG. 3. Angular dependence of the resistance of the single crystal Au-3: H = 23,500 oe; T = 4.2°K.

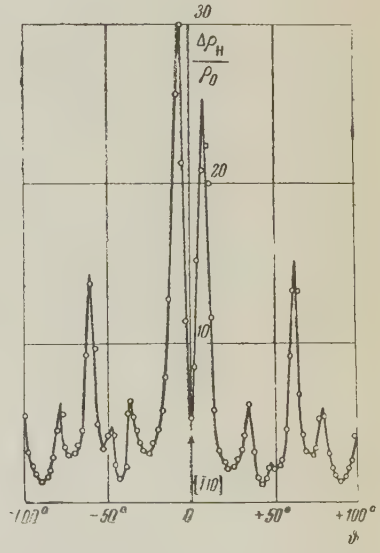

FIG. 4. Angular dependence of the resistance of the single crystal Au-5: H = 23,500 oe; T = 4.2°K.

A very sharp anisotropy characterizes the angular dependence of the resistance of gold single crystals. In the range of angles 5 — 10° the resistance varies by a factor of 10 or more. Very sharp maxima and minima occur in the rotation diagrams. Their position corresponds to the crystallographic symmetry of the samples.

The directions of the narrow minima coincide with the special crystal directions [001], [110], and [111]. Narrow maxima are situated symmetrically with respect to these directions at small distances from each other (not exceeding 26°). Very broad minima also occur (for example, in Fig. 1 at 0°). Considerable anisotropy showing all the characteristic features is also observed in the other gold samples. Table II gives the angular coordinates (with an accuracy of ± 0.5°) of all the maxima and the narrow minima occurring in the rotation diagrams.

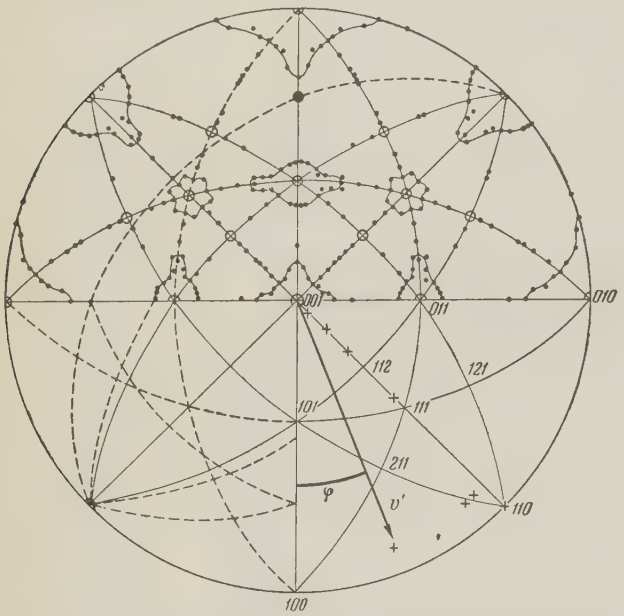

FIG. 5. The stereographic projection of the directions of the maxima (●) and of the narrow, deep minima (○), observed for all eight gold single crystals. Dotted lines show the traces of the planes of rotation of the magnetic field for some samples (Au-2, Au-3, and Au-6), + – orientations of the sample axes.

On the basis of all the rotation diagrams a stereographic projection was constructed of those directions of the magnetic field at which maxima occur (Fig. 5). The directions of the narrow minima are also indicated in the same diagram. Such a projection enables us to obtain a qualitative picture of the angular dependence of the resistance of a gold sample with an arbitrary crystallographic orientation. The experimental points on the projection are grouped in a twofold manner: the directions of the maxima of the first type are situated on lines which surround small regions in the stereographic projection. The centers of these regions coincide with the directions of the crystal axes [001], [110], and [111]. The basic dimensions of the regions are as follows: regions 001 and 110 — 26° and 15°, region 111 — 12° and 10°. The directions of the maxima of the second type lie in the (110) and (111) planes. The rotation diagram for the Au-1 sample (Fig. 1, $\vartheta = 0$) enables us to conclude that there are no maxima in directions lying in the (001) plane.

Two characteristic features of the stereographic projection should be noted: 1) if the directions of the current and of the magnetic field both lie in the binary plane then, instead of there being a maximum in the rotation diagram, a minimum occurs (for example, Fig. 4, $\vartheta = 90°$). It is quite likely that the same is also true for current and field directions lying in the (111) plane. 2) In the direction of the intersection of the (110) and (111) planes the maxima also disappear, and the minimum occurring in this case, in contrast to the minima in the directions [001], [110] and [111], is not surrounded by a line of maxima (Fig. 2, $\vartheta = +55°$ and Fig. 3, $\vartheta = \pm 30°; \pm 90°$).

The dependence of the resistance on the magnetic field was investigated for the directions corresponding to the minima and the maxima of the rotation diagrams.

As may be seen from Figs. 6 and 7, complete saturation of resistance is observed in the directions of the minima; in the directions of the maxima the resistance increases without limit: $\Delta\rho_H/\rho_0 \sim H^n$, where n varies from 1 to 1.8 for different maxima (cf. Table II).

Measurements in the region of low fields have shown that the difference in the character of the

TABLE II

Samples	Direction $\vartheta=0°$	Directions of the maxima in degrees. Brackets contain the power index n $\Delta\rho_H/\rho_0 \sim H^n$	Direction of the narrow, deep minima in degrees
Au-1	Intersection with the plane (001)	+85 (1.5); +78 (1.75); +58; +43 (1); +25 (1.25) −75 (1.8); −52; −40; −30 (1.5); −18 (1.35)	−87
Au-2	[$\bar{1}$10]	±13 (1.8)±30; +38: +82; −40; −81	0; ±35?; ±55;±90
Au-3	[0$\bar{1}$1]	±8; ±35; ±53; ±70	0; ±60
Au-4	[010]	+10; ±38; ±55; ±82; −7	0; ±45
Au-5	[$\bar{1}$10]	±8 (1.7); +35 (1)±48; ±60 (1.5); −37; ±80 (1)	0
Au-6	[$\bar{1}$10]	±7 (1.7); ±33 (1.15); ±50; +72; +78 (1.5)	0
Au-7	[$\bar{1}$10]	±7 (1.7); ±25; ±40; +55; ±82; −62	0; ±90
Au-8	[$\bar{1}$10]	+8; +30; +80; −15 (1.7); −32; ±40; ±63; −82	0; ±35

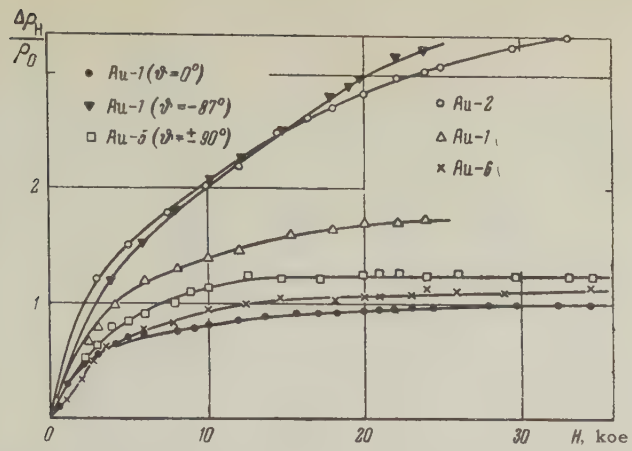

FIG. 6. Dependence of the resistance on the magnetic field in the direction of the minima in the rotation diagrams; ○ – $\vartheta = \pm 35°$, Δ – $\vartheta = -45°$, × – $\vartheta = \pm 42°$.

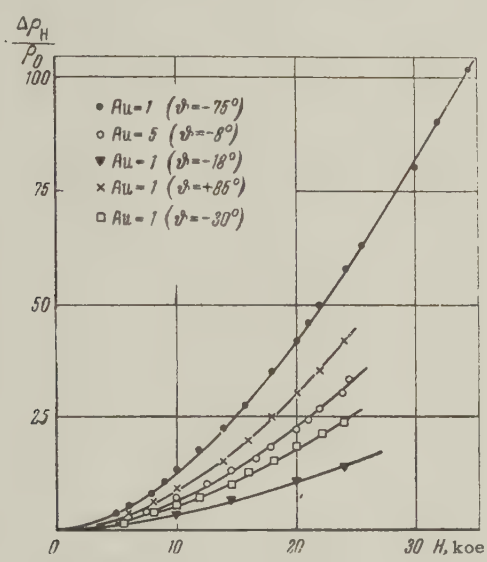

FIG. 7. Dependence of the resistance on the magnetic field in the direction of the maxima.

variation of the resistance corresponding to a minimum and a maximum sets in at fields close to H_0. It may also be seen from Fig. 8 that measurements at a temperature of 20.4° do not differ in any essential way from measurements carried out at 4.2°K (naturally, the measurements at higher temperatures are equivalent to measurements in smaller effective fields).

It was of interest to study the change in the shape of the maxima as the magnetic field was varied. From Fig. 9 it is seen that the width of a maximum of the first type decreases approximately as 1/H with increasing field. It was also established qualitatively that the width of the maxima of the second type also decreases as the magnetic field is increased.

The increase of resistance in a magnetic field in the direction of the maxima and a corresponding decrease in their width must lead to a decrease in

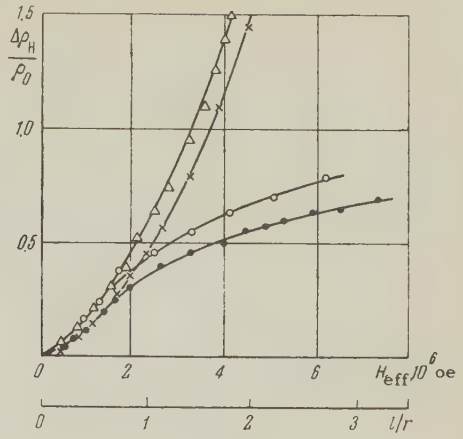

FIG. 8

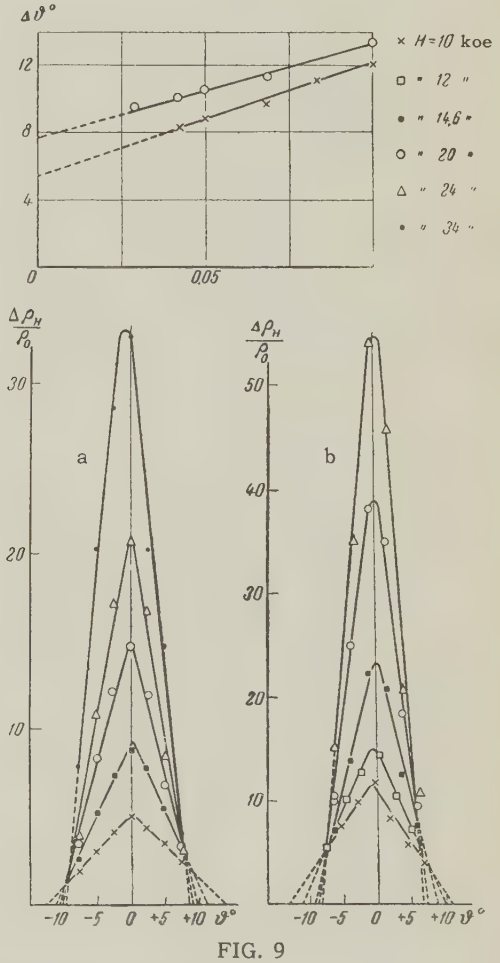

FIG. 9

the power of the dependence of the resistance on the field after averaging over the angle ϑ has been carried out. This was checked on samples Au-1 and Au-5. In the case of these samples rotation diagrams were obtained at several values of the magnetic field (from 5000 to 24,000 oe). For each value of the field the resistance was averaged over the angle ϑ. It turned out that the averaged resistance depends linearly on the magnetic field. The averaging of the resistance for an individual maxi-

mum of the first type (sample Au-1, $\vartheta = -75°$ in the interval from $-85°$ to $-69°$) also leads to a decrease in the power index n, however, we do not obtain a linear dependence as a result ($n \approx 1.4$). The results of averaging are shown in Fig. 10. Here are also given for purposes of comparison the curves for $\Delta\rho/\rho_0$ obtained by Kapitza[3] and Justi[4] for polycrystalline gold samples.

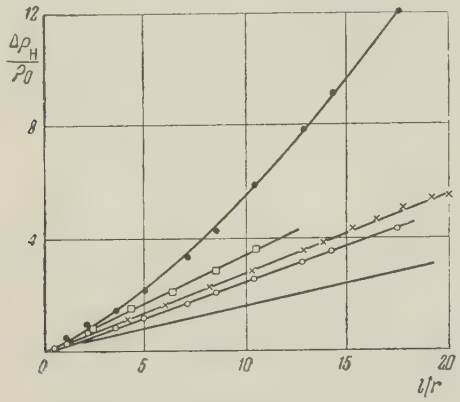

FIG. 10. Dependence on the magnetic field (in units of l/r) of the resistance averaged over the angle ϑ: ○ – Au-1 (from –87° to 93°); □ – Au-5 (from 0° to –106°); ● – Au-1 (maximum of the first type from –87° to –69°); × – Justi's results[4] for polycrystalline gold samples. The lowest straight line is an extrapolation of Kapitza's results[3] for polycrystalline gold samples.

4. DISCUSSION OF RESULTS

a) The Fermi surface for gold. A comparison of the results obtained by us with theory[7] shows that the Fermi surface for gold is open. This finds its expression in the fact that the resistance increases in the magnetic field in quite a different manner (quadratic increase and saturation) for the different crystallographic directions.

The galvanomagnetic properties of metals having open Fermi surfaces have been treated in the paper by Lifshitz and Peschanskiĭ.[13] One of the principal conclusions of this paper is that on the basis of an experimental study of the resistance anisotropy of a metal it is possible to determine those directions in which the Fermi surface is open.

Figure 11 gives a stereographic projection of the special directions of the magnetic field in the case of gold which was constructed on the basis of the projection of the maxima (Fig. 5). For the directions of the magnetic field lying within the two-dimensional regions I of this projection and in the (111) and (110) planes one should observe according to the theory[13] a quadratic increase in resistance

$$\Delta\rho_H/\rho_0 \sim H^2\cos^2\alpha, \qquad (1)$$

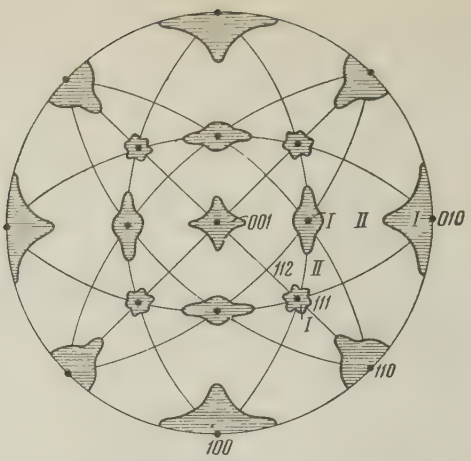

FIG. 11. The stereographic projection of special directions of the magnetic field for the Fermi surface for gold. The shaded regions (I) and the lines joining the regions I are directions for which the resistance increases quadratically with the magnetic field. In regions II the resistance does not depend on the field for $H \gg H_0$ (saturation). Points denote the directions of narrow deep minima.

where α is the angle between the current and the direction of the open sections of the Fermi surface. However, the dependence of the resistance on the field observed experimentally for these directions is somewhat less than quadratic. This circumstance may be explained by the averaging of the resistances associated with the narrow maxima as the result of the single crystals not being perfect, the magnetic field not being homogeneous, etc. As has been shown earlier, an averaging of this type leads to a decrease in the power dependence of the resistance on the field.

On taking this into account we may assume that the Fermi surface for gold, in accordance with the stereographic projection (Fig. 11), is represented (in a topological sense) by a "spatial net" formed by "corrugated cylinders" whose axes are parallel to the [110] and [111] axes of the reciprocal lattice. Indeed, the special directions situated in the (110) and (111) planes are formed by the "cylinders" [110] and [111]. The two-dimensional regions I arise as a result of the mutual intersection of these cylinders. Thus, the region 001 is formed by the cylinders [110] and [$\bar{1}$10] which intersect in the plane (001); the region 110 is formed by the cylinders [1$\bar{1}$0], [$\bar{1}$11], [1$\bar{1}$1], which intersect in the (110) plane; and, finally, the region 111 is formed by the cylinders [$\bar{1}$10], [0$\bar{1}$1] and [$\bar{1}$01], which intersect in the (111) plane. The dimensions and the shapes of the two-dimensional regions are chosen in accordance with the experimental data. The basic dimensions of the regions 001 and 110 are 15° and 26°, while the corresponding dimensions of the 111 region are 10° and 12°. (It is possible that the actual dimen-

sions of the regions are really somewhat larger, but in any case they cannot be smaller than the values indicated).

In accordance with reference 13, a very narrow minimum should appear for the central direction [001], [110] and [111] of the two-dimensional region in the diagram of the angular dependence of the resistance, and the resistance should tend to saturation in that direction. This finds good experimental confirmation. For all the other directions of the magnetic field (the broad regions II in Fig. 11) lying in the Fermi surface of the type indicated above a saturation of resistance should be observed. This is also confirmed by measurements (in the rotation diagrams broad minima correspond to these directions).

Let us now discuss the two peculiar features of the stereographic projections (Figs. 5 and 11) noted above.

1. Since the [112] direction is not surrounded by a two-dimensional region of special directions of the magnetic field (in contrast to the [001], [110] or [111] directions) we can conclude that some of the "corrugated cylinders" of the Fermi surface for gold do not intersect (for example, for the [112] direction such "cylinders" will be $[\bar{1}\bar{1}1]$ and $[\bar{1}10]$).

2. Expression (1) enables us to explain the absence of maxima in the rotation diagrams of samples Au-5 and Au-6 in the directions $\vartheta = 90°$, which are perpendicular to the axes of the "cylinders" $[1\bar{1}0]$. In the case of these samples the direction of the current, as well as the direction of the field, lies in the $(1\bar{1}0)$ plane. As a result of this angle $\alpha = 90°$, and minima should indeed arise in the rotation diagrams.

An investigation of the resistance anisotropy in a magnetic field enables us to draw conclusions only with respect to the direction of the open sections of the Fermi surface.

The shape of the Fermi surface for a metal can be constructed on the basis of results obtained by other experimental methods (oscillation of susceptibility, anomalous skin-effect, cyclotron resonance). Pippard[14] has constructed the Fermi surface for copper on the basis of a study of the anomalous skin-effect. Peschanskiĭ[15] has generalized the analytic expression for the Fermi surface for copper proposed in reference 16 and has investigated the possible types of open Fermi surfaces for metals with a face-centered cubic lattice. The stereographic projection of the special directions of one of the Fermi surfaces discussed by him agrees very well with the stereographic projection for gold. On taking into account the results of these papers it becomes natural to represent the Fermi surface for gold in the form of "cubes." In the space of the reciprocal lattice the "cubes" are joined at their vertices in such a way that open directions occur along the [111] and [110] axes, while the direction along the [001] axis remains closed.*

b) Kapitza's law. In the case of gold single crystals both a quadratic increase and a complete saturation of resistance in a magnetic field are observed. The resistance of polycrystalline samples of gold, as is well known,[3,9] depends on the field linearly. This forces us to conclude that Kapitza's law is a result of the averaging of the resistance over the variously oriented (with respect to the field) crystallites which make up the polycrystalline sample.[10] This conclusion is confirmed by averaging over the angle ϑ the resistance of the single crystal samples Au-1 and Au-5.

A theoretical explanation of Kapitza's law (using as an example a metal with a Fermi surface of the "corrugated cylinder" type) is given in reference 13. From the same paper it may also be seen that the resistance of the single crystals averaged over the angles lying in the two-dimensional region I (Fig. 11) will not depend linearly on the magnetic field ($\overline{\Delta\rho_H}/\rho_0$ must be proportional to H^2). A confirmation of this is provided by the results of averaging the resistance over a maximum of the first type ($n \approx 1.4$, Fig. 10).

Since the dimensions of the two-dimensional regions are relatively small, then in fields, which exceed H_0 by a factor of only several fold, their contribution to the averaged resistance is not significant. Therefore, averaging of the resistance for single crystals of gold which has a Fermi surface of the "spatial net" type is equivalent to averaging the resistance of single crystals of a metal with a Fermi surface of the "corrugated cylinder" type. However, in the region of very high fields the role played by the two-dimensional regions is significant, and the resistance of single crystals averaged over the whole rotation diagram will no longer depend linearly on the field.

For the reasons stated above one can expect that in the region of very high magnetic fields deviations from Kapitza's law will occur for gold polycrystalline samples (in contrast to the results of reference 8).

In conclusion the author considers it his pleasant duty to thank Academician P. L. Kapitza for

*If we assume that we can use Eq. (1) of reference 13 to estimate the smallest diameter of the "corrugated cylinder" [110], then it is possible to form some idea of the area of mutual intersection of the "cubes" of the Fermi surface for gold. For the [110] "cylinder" the smallest diameter (in units of the reciprocal lattice constant b) is equal to 0.1 b.

his close attention to this work and Prof. N. E. Alekseevskiĭ for constant guidance. The author is also grateful to Professor I. M. Lifshitz and V. G. Peschanskiĭ for discussion of the results obtained by him.

[1] H. Bethe and A. Sommerfeld, Electron Theory of Metals (Russ. transl.), Moscow-Leningrad, 1948.

[2] E. H. Sondheimer and A. H. Wilson, Proc. Roy. Soc. **A190**, 435 (1947).

[3] P. L. Kapitza, Proc. Roy. Soc. **A123**, 292 (1929).

[4] E. Justi, Physik Z. **41**, 563 (1940).

[5] Lazarev, Nakhimovich, and Parfenova, JETP **9**, 1169 (1939).

[6] E. S. Borovik, Dokl. Akad. Nauk S.S.S.R. **69**, 768 (1948).

[7] Lifshitz, Azbel', and Kaganov, JETP **31**, 63 (1956), Soviet Phys. JETP **4**, 41 (1957).

[8] R. G. Chambers, Proc. Roy. Soc. **A238**, 344 (1957).

[9] E. Justi, Physik Z. **41**, 486 (1940).

[10] N. E. Alekseevskiĭ and Yu. P. Gaĭdukov, JETP **35**, 554 (1958), Soviet Phys. JETP **8**, 383 (1959).

[11] P. W. Bridgman, Proc. Am. Acad. Arts Sci. **60**, 306 (1925).

[12] Alekseevskiĭ, Brandt, and Kostina, JETP **34**, 1339 (1958), Soviet Phys. JETP **7**, 924 (1958).

[13] I. M. Lifshitz and V. G. Peschanskiĭ, JETP **35**, 1251 (1958), Soviet Phys. JETP **8**, 875 (1959).

[14] A. B. Pippard, Phil. Trans. Roy. Soc. London **A250**, 325 (1957).

[15] V. G. Peschanskiĭ, Thesis, Khar'kov State University, 1959.

[16] F. G. Moliner, Phil. Mag. **3**, 207 (1958).

Translated by G. Volkoff
258

FRAGMENTATION ON BISMUTH NUCLEI

V. F. DAROVSKIKH, N. P. KOCHEROV, and N. A. PERFILOV

Radium Institute, Academy of Sciences, U.S.S.R.

Submitted to JETP editor June 30, 1959

J. Exptl. Theoret. Phys. (U.S.S.R.) **37**, 1292-1295 (November, 1959)

Fragmentation on bismuth nuclei induced by 660-Mev protons was investigated by imbedding small bismuth particles in a nuclear emulsion. Data are obtained on the cross section of the process, on the angular distribution (forward-backward ratio) of the fragments, and on the charge and energy distributions of multi-charged particles.

To explain the mechanism of fragmentation of heavy nuclei it is very important to know the dependence of many characteristics of this process on the atomic number of the target nucleus. Unfortunately, very little experimental data are available in this field. The cross sections for the production of heavy fragments when various elements are bombarded by high energy particles can be determined principally radiochemically. This method makes possible determination of the yields of several radioactive isotopes, the number of which is very limited in the region of small Z. Yet it is known[1-2] that in the fragmentation process there are produced essentially stable isotopes, which make the principal contribution to the yield of fragments of given charge. The ratio between the isotopes may vary in going from one target to another. Therefore the variation of the yield of certain nuclei cannot give a true idea of the variation of the fragmentation cross section with the Z of the target.

By counting the fragments produced in thick targets placed over an emulsion layer, Lozhkin[3] showed that the fragment yield increases with increasing atomic number of the target nucleus. For a more complete study of a fragmentation process on nuclei heavier than silver, it is necessary to introduce suitable elements in the emulsion if the photographic method is used.

Perfilov and Denisenko[4] determined the cross section for fragmentation on uranium, induced by 660-Mev protons. However, since the uranium was introduced into the emulsion by impregnation, cases of fragmentation on uranium were identified only when the residual nucleus was fissioned after the emission of the fragment. Thus, not all the fragments produced on the uranium were investigated. The value of $\sigma_{fr}(U)$ was calculated from the quantity $\sigma_{fis}(86)/\sigma_{nuc}(86)$ for the interaction between high energy protons and heavy nuclei. It was assumed here that the properties of nuclei with $Z = 86$, which are obtained on the average after the emission of the multiply-charged particle, are similar to the properties of nuclei with $Z = 86$ produced as a result of the ordinary cascade process. It may be that this assumption does not correspond well enough to reality.

We have attempted in this investigation to study the fragmentation phenomenon in pure form. Small grains of metallic bismuth (measuring $\sim 8-10\,\mu$) were deposited on an emulsion layer $100\,\mu$ thick, and a second emulsion layer of equal thickness was poured over the first. The plates prepared were bombarded by 660-Mev protons in the synchrocyclotron of the Joint Institute for Nuclear Research, developed, and scanned for cases of fragmentation on the bismuth grains. Simultaneously, all the cases of bismuth fission were counted, in order to determine the relative fragmentation cross section, σ_{fr}/σ_{fis}. In some plates we counted the stars on the bismuth inclusions; this was necessary to determine the size of the uncertainty zone around the bismuth granules. (The uncertainty zone is the emulsion layer around the bismuth granule, the disintegrations in which cannot be distinguished from the disintegrations on the bismuth itself.)

Fragments with charge $Z \geq 4$ and range $\geq 20\,\mu$ were registered. Since cases with a fragment-range ratio greater than 2 and with a total range greater than $30\,\mu$ are not encountered in practice in the fission of bismuth, this criterion excludes the possibility of attributing fission events to the fragments. Fragments with ranges less than $20\,\mu$ were attributed to fissions, even if the second fragment was missing, for it was assumed to be lost in the bismuth granule. In such an operation a certain number of fragments enters into the fission group, and the ratio σ_{fr}/σ_{fis} is underesti-

mated. There are grounds for assuming, however, that there will be few such fragments. Firstly, according to data on fragmentation on silver and bromine nuclei[2] and also on uranium nuclei,[4] much fewer fragments with range $< 20\mu$ are produced than fragments with range $\geq 20\mu$; in addition, the yield of fragments drops sharply with increasing fragment charge. Secondly, the energy of the fragments produced on the bismuth, with ranges < 20 and charges $Z = 4$ and $Z = 7$, is less than 0.34 and 0.46, respectively, of the magnitude of the nominal Coulomb barrier. Fragments of such energy have a negligibly small probability of penetrating through the Coulomb barrier, even if its true magnitude, as will be discussed below, is somewhat less than the nominal value.

The fragment charge was determined by measuring the integral width of the track.[5-6] The measurements were made with an MBI-8 microscope at a magnification of 4800, which increased the measurement accuracy considerably. The calibration was based on the hammer-like tracks found in the disintegrations of the silver and bromine nuclei in the same emulsions. These tracks can be readily divided into three groups: Li_3^8, Be_4^8, and B_5^8. In addition, we used the proportionality of the width of the track to the square root of the fragment charge, indicated by Nakagawa et al.[5]

Z	4	5	6	7
E_{exp}, Mev	13 15 23 23 26 27 30 39 63	28 29 34 35 58 70	28 45 57	40 54 80
E_{coul}, Mev	39	47	55	63

The resultant fragment charge distribution is given in the table, which lists also the value of the nominal Coulomb barrier E_{Coul} for fragments of various charges, calculated from the following formula

$$E_{coul} = (Z_0 - Z_p - Z_{fr})\, Z_{fr} e^2 / r_0 \,(A^{1/3} + a^{1/3}),$$

where Z_0, Z_p and Z_{fr} are respectively the charge of the polonium nucleus, the number of cascade protons penetrating the Po nucleus prior to the emission of the fragment, and the charge of the fragment. A is the mass number of the residual nucleus, a is the mass number of the fragment, and $r_0 = 1.47 \times 10^{-13}$ cm.

The table indicates also the energies of the obtained fragments, determined by range and by the range-energy curves[7] for the Ilford G-5 emulsion, which has the same stopping ability as the P-9 emulsion.

In determining the ranges of the fragments, a correction was introduced in each case for the fact that part of the fragment range $(\sim 2-4\mu)$ lies within the Bi granule. The point from which the fragment is emitted was determined by intersecting the prongs accompanying the fragmentation cases.

To determine the cross section for fragmentation on bismuth, a relative method was used: we determined the ratio of the number of the fragments on the bismuth granules to the number of fissions. With this method it was not necessary to know the bombarding proton current or the volume of the bismuth introduced into the emulsion. However, to calculate the fragmentation cross section it was necessary to estimate the fraction of the fragments actually originating on the bismuth, and how many fragments were produced on the emulsion grains in the uncertainty zone. To reduce the value of V_Z/V_{Bi} (the ratio of the volume of the zone to the volume of the bismuth granule) all the found fragmentation cases were reviewed in an emulsion wetted to increase its thickness seven-fold.[8] For fragments that remained on the granules, the size of the uncertainty zone was considerably reduced. Its value was determined from examination of the stars on the emulsion nuclei, which separated from the granules during the wetting. The resultant value was $V_Z/V_{Bi} = 0.7$.

To calculate the cross section for fragmentation on bismuth, we set up the following system of equations:

$$N_{fr.exp} = N_{fr.Bi} + N_{fr.z};$$
$$N_{fr.Bi} = N_0 \sigma_{fr}(\mathrm{Bi})\, N_{Bi} V_{Bi};$$
$$N_{fr.z} = N_0 [\sigma_{fr}(\mathrm{AgBr})\, N_{AgBr} + \sigma_{fr}(\mathrm{CNO})\, N_{CNO}]\, V_z;$$
$$N_{fis} = N_0 \sigma_{fis} N_{Bi} V_{Bi}.$$

Here $N_{fr.Bi}$, $N_{fr.z}$, $N_{fr.exp}$, and N_{fis} are the true number of fragments on the bismuth granules, on the emulsion grains in the uncertainty zone, the number of fragments obtained experimentally, and the number of bismuth fissions; $\sigma_{fr}(Bi)$, $\sigma_{fr}(AgBr)$, $\sigma_{fr}(CNO)$, and σ_{fis} are the cross sections of fragmentation on bismuth and on the heavy and light nuclei of the emulsion, and the bismuth fission cross section. N_0, N_{Bi}, N_{AgBr}, and N_{CNO} are the current of incident protons, the number of nuclei per cubic centimeter of bismuth, and the number of heavy and light nuclei per cubic centimeter of emulsion.

By solving this system of equations for $\sigma_{fr}(Bi)$, we obtain

$$\sigma_{fr}(Bi) = \sigma_{fis} N_{fr.exp} / N_{fis} - \sigma_0, \qquad (1)$$

where

$$\sigma_0 = \frac{V_z}{V_{Bi}} \frac{\sigma_{fr}(AgBr) N_{AgBr} + \sigma_{fr}(CNO) N_{CNO}}{N_{Bi}}.$$

We found 21 fragments in 132 bismuth fissions. Inserting these values in (1) together with $\sigma_{fr}(AgBr) = 10$ mb, $\sigma_{fr}(CNO) = 2$ mb, $\sigma_{fis} = 200$ mb, $N_{Bi} = 2.8 \times 10^{22}$ nuclei/cm^3, $N_{AgBr} = 2.04 \times 10^{22}$ nuclei/cm^3, $N_{CNO} = 2.83 \times 10^{22}$ nuclei/cm^3, and $V_z/V_{Bi} = 0.7$, we obtain $\sigma_{fr}(Bi) = 25$ mb. The possible error may amount to one-third of this quantity, since the result obtained agrees with the values of the cross section for fragmentation on uranium,[4] $\sigma_{fr}(U) = 22$ mb, and is approximately twice the cross section for fragmentation on the nuclei of silver and bromine for bombarding particles of the same energy.[3]

To compare data on the fragmentation on bismuth and on uranium[4] nuclei, we list several characteristics of this process:

	Bi	U
Fragmentation cross section, mb	25	22
Average number of protons and α particles in disintegrations with fragments	4.0	1.6
Average charge of fragment	5	6
Fragments with energy below the nominal Coulomb barrier, percent	71	82
Ratio of the number of fragments traveling with and against the beam	6	5

From an examination of these data it is seen that the characteristics of fragmentation on bismuth and uranium are remarkably identical. The discrepancy between the average number of protons and α particles in disintegrations with fragments on bismuth and on uranium is quite natural. Only approximately 30% of the fragments (accompanied by fission) are recorded in the case of uranium. Multiple-pronged events, in which the fission probability becomes smaller[9] because of the reduced charge and, apparently, because of the increase in the initial excitation energy of the nucleus, were for the most part left out.

The most characteristic feature of fragmentation on bismuth and on uranium is the large number of sub-barrier fragments. The fraction of fragments with $Z \geq 4$ having energies below the nominal Coulomb barrier is 71% for bismuth and 82% for uranium. Quantum-mechanical penetration through the barrier makes no noticeable contribution to these numbers. It must be assumed that the true Coulomb barrier is lower than the nominal one, amounting to approximately 0.6 of its value. A similar reduction in the Coulomb barrier was observed by Fulmer and Cohen[10] in an investigation of the $(p\alpha)$ reaction on heavy nuclei. Their results can be interpreted as the knock-out of an alpha particle from the diffuse region of the nucleus, where α groupings exist with considerable probability.[11] In our case, however, to explain the large fraction of sub-barrier particles it is not enough merely to account for the fact that the fragments can be knocked out from the diffuse region of the nucleus. Fragmentation of heavy nuclei, induced by high-energy particles, is apparently accompanied by considerable nuclear deformations as a result of the strong branching of the nuclear cascade.

[1] V. M. Sidorov and E. L. Grigor'ev, JETP **33**, 1179 (1957), Soviet Phys. JETP **6**, 906 (1958).

[2] O. V. Lozhkin, Dissertation, Radium Inst. U.S.S.R. Acad. Sci., 1957.

[3] O. V. Lozhkin, JETP **33**, 354 (1957), Soviet Phys. JETP **6**, 273 (1958).

[4] N. A. Perfilov and G. F. Denisenko, JETP **35**, 631 (1958), Soviet Phys. JETP **8**, 438 (1959).

[5] Nakagawa, Tamai, Huzita, and Okudairo, J. Phys. Soc. Japan. **11**, 191 (1956).

[6] V. I. Ostroumov and Yu. P. Yakovlev, JETP **35**, 1358 (1958), Soviet Phys. JETP **8**, 949 (1959).

[7] A. Papineau, Compt. rend. **242**, 2933 (1956).

[8] O. V. Lozhkin, J. Tech. Phys. (U.S.S.R.) **34**, 1341 (1955).

[9] Dostrovsky, Fraenkel, and Rabinovitz, Second United Nations International Conference on the Peaceful Uses of Atomic Energy, Geneva (1958).

[10] C. B. Fulmer and B. L. Cohen, Bull. Am. Phys. Soc. II, **3**, 56 (1958).

[11] V. I. Ostroumov and R. A. Filov, JETP **37**, 643 (1959), Soviet Phys. JETP **10**, 459 (1960).

Translated by J. G. Adashko
259

CONDITIONS FOR THE APPLICABILITY OF STATISTICAL FORMULAS TO A DEGENERATE FERMI GAS

Ya. B. ZEL' DOVICH and E. M. RABINOVICH

Submitted to JETP editor June 10, 1959

J. Exptl. Theoret. Phys. (U.S.S.R.) 37, 1296-1302 (November, 1959)

A degenerate ideal Fermi gas in an arbitrary potential field is considered. It is shown that a sufficient condition for the applicability of statistical formulas to the problem of the change of the density under the action of the potential $V(\mathbf{r})$ is that the motion of the particles with the maximum (Fermi limit) energy be a quasiclassical motion. This result is not invalidated by nonapplicability of the quasiclassical approximation to the motion of particles with smaller energies, and in particular, for $V < 0$, to that of bound particles. The corrections to the statistical formulas in the one-dimensional and three-dimensional problems have opposite signs.

1. INTRODUCTION

We shall examine the limits of applicability of the well known expressions for the density of a degenerate Fermi gas with boundary energy $\mathscr{E}$, in a potential field $V(\mathbf{r})$, for particles of spin $\frac{1}{2}$:

$$\rho_1 = 2K_m/\pi, \quad \Delta\rho_1 = \rho_1 - \rho_{10} = (2\sqrt{2}/\pi)\,[(\mathscr{E}-V)^{1/2} - \mathscr{E}^{1/2}] \tag{1.1}$$

in the one-dimensional case and

$$\rho_3 = \frac{8\pi}{3}\left(\frac{K_m}{2\pi}\right)^3, \quad \Delta\rho_3 = \frac{2\sqrt{2}}{3\pi^2}[(\mathscr{E}-V)^{3/2} - \mathscr{E}^{3/2}] \tag{1.2}$$

in the three-dimensional case, where K_m is the local boundary wave number (we take $\hbar = m = 1$)

$$K_m(\mathrm{r}) = \sqrt{2(\mathscr{E} - V(\mathrm{r}))}. \tag{1.3}$$

The textbook derivation of these expressions involves counting up the numbers of states per unit volume in regions with given values of $V(\mathbf{r})$. Let us think of a case with $V(\mathbf{r})$ negative in a restricted region of space and zero everywhere outside this region (potential well). Then it would seem that for the applicability of the formulas it is necessary for a large number of particles to be bound in the well. The question presents itself particularly sharply in the one-dimensional case. For $V \ll \mathscr{E}$ we find

$$\Delta\rho_1 = -\sqrt{2}V/\pi\sqrt{\mathscr{E}}. \tag{1.4}$$

For definiteness let us consider a well, i.e., the case $V < 0$, $\Delta\rho_1 > 0$. With increase of $\mathscr{E}$ the total change of the density of the gas over the well decreases. The meaning of this result is clear: in the one-dimensional case the well always has at least one bound level with $E < 0$, which makes a positive contribution to $\Delta\rho_1$. The free particles with $E > 0$ travel more rapidly when over the well than elsewhere, and consequently their density over the well is smaller. Therefore the quantity $\Delta\rho_1$ is the difference of the positive contribution of the bound particles (independent of $\mathscr{E}$) and the negative contribution of the free particles with $0 < E < \mathscr{E}$.

Can the formula be applied when there is a single bound state? For small $|V|$ the bound particle is localized in a region much larger than the well itself. What is the localization of $\Delta\rho_1$ in this case?

As will be shown below (Sec. 2), in the one-dimensional case the tendency of $\Delta\rho_1$ to zero as $\mathscr{E} \to \infty$ is an exact quantum-mechanical theorem, i.e., it is valid independently of the applicability of the statistical formula (1.4). This theorem is connected with the completeness of the system of eigenfunctions, both that in the unperturbed case ($V = 0$; ψ_0), and also the system of eigenfunctions in the field [$V(x)$; ψ_n]; from this property we have

$$\int_{-\infty}^{+\infty} |\psi_0(x, E)|^2\, dE = \int_{-\infty}^{+\infty} |\psi_n(x, E)|^2\, dE$$

(the integral is taken in the Stieltjes sense, including the discrete levels).

As a result of this theorem, the change of the density that comes from the inclusion of the particles with energies smaller than $\mathscr{E}$ is equal in magnitude and opposite in sign to the change of the density of all the particles with energies larger than $\mathscr{E}$.

If the quasiclassical approximation is valid for

the particles with energies equal to and greater than E in the field V(x), then from this it is easy to get the expression (1.4). Thus the expressions (1.1) and (1.4) can be obtained independently of the number of bound levels and of the character of the motion of the particles with energies less than $\mathscr{E}$. This argument also provides an approach (Sec. 3) to an estimate of the accuracy of Eqs. (1.1) and (1.4). In fact, considering the particles with energies larger than $\mathscr{E}$, we convince ourselves that for small V

$$\Delta\rho_1(x) = \int L(|x-y|)\,V(y)\,dy; \qquad (1.5)$$

the function $L(|x-y|)$ is different from zero in an interval of the order of $1/K_m$, where K_m is the wave number corresponding to the boundary energy $\mathscr{E}$.

The smearing out described by the function $L(|x-y|)$ does not change the total increase of the number of particles in the neighborhood of the region of action of the potential, and from Eq. (5) one gets

$$\int \Delta\rho_1(x)\,dx = -\frac{\sqrt{2}}{\pi\sqrt{\mathscr{E}}}\int V(x)\,dx \qquad (1.6)$$

in exact agreement with Eq. (1.4).

The deviation from the formula (1.6) is of higher order in V(x), whereas the deviations from the local formula (1.4) are of first order in V(x) and are due to the spatial distribution of V(x). Together with the leading correction term the expression (1.6) has the form [cf. Eq. (1.1)]

$$\int \Delta\rho_1(x)\,dx = 2\sqrt{2}\pi^{-1}\int[(\mathscr{E}-V)^{3/2}-\mathscr{E}^{3/2}]\,dx$$

$$+\,b\mathscr{E}^{-5/2}\int (dV/dx)^2\,dx.$$

Let us turn to the three-dimensional case (Sec. 4). From Eqs. (2) and (3) we get for small V

$$\Delta\rho_3 = -\sqrt{2}\pi^{-2}V(\mathbf{r})\,\mathscr{E}^{1/2}.$$

This expression increases without bound with increasing $\mathscr{E}$; from this it follows that for large $\mathscr{E}$ the main contribution comes from the change of the density of the free particles.

In the limit of small V the quantum-mechanical problem of the perturbation of the density of a plane wave is easy to solve in the Born approximation. Summing the contributions of all plane waves with energies smaller than E, we get the answer in the form

$$\Delta\rho_3(\mathbf{r}) = \int M(|\mathbf{r}-\mathbf{r}'|)\,V(\mathbf{r}')\,d\mathbf{r}'.$$

The function M found in this way also falls off at a distance of the order of $1/K_m$.

As is well known, in the three-dimensional case a sufficiently small well does not have any bound state at all. The application of the general arguments associated with the completeness of the system of eigenfunctions to the three-dimensional case requires an extremely careful definition of the procedure of passage to the infinite limit; thus this method is not an effective one. If, however, we have three-dimensional motion with a potential that allows separation of variables, for example a V(r) independent of θ and φ, or a V(x) independent of y and z, the completeness theorem can be unconditionally applied to each group of particles with fixed values of the conserved quantities — the angular momenta in the case of V(r), or k_y, k_z in the case of V(x). The completeness theorem then enables us to carry out the most difficult part of the calculation — the summation over k_r or k_x — by going over to the range of energies above the boundary energy and using the quasiclassical approximation. All told, by using different methods in the one-dimensional and three-dimensional problems, we are able in both cases to get an idea of the degree of accuracy of the statistical formulas and of the difference between the statistical expressions and the exact quantum-mechanical solutions.

The main result is that everything depends on the quasiclassical character of the motion of the particles with the boundary energy $\mathscr{E}$. For small V this result is a natural one, if we deal directly with the many-particle problem in the Fock representation in which the unperturbed eigenfunctions are antisymmetrized products, that is, Slater determinants, of plane waves. In such a treatment any perturbation V (including in particular a potential that has bound states) only causes transitions of the particles from the region $E < \mathscr{E}$ into the region $E > \mathscr{E}$. It seems to us, however, that only the examination we have made of the change of the one-particle states gives a completely intuitive picture of the realization of the statistical laws, and in particular gives a possibility of passing on easily to the case of a V that is comparable with the boundary energy $\mathscr{E}$, for which one cannot use just first-order perturbation theory.

2. THE COMPLETENESS THEOREM IN THE ONE-DIMENSIONAL PROBLEM

Let us consider the motion of particles in a field V(x) that has the eigenfunctions $\psi_n(x)$,

including both a discrete and a continuous spectrum.

Let us add to the potential a small perturbation δV (with arbitrary dependence on x) and find the changes of $\psi_n(x)$ and $\rho_n(x) = |\psi_n(x)|^2$ by first-order perturbation theory. To abbreviate the writing let us consider real nondegenerate functions; it is easy to verify that the results do not depend on this.

$$\delta\psi_n = \sum_m{}' \frac{\psi_m}{E_n - E_m} V_{mn}, \qquad \delta\rho_n(x) = \sum_m{}' A_{nm}(x), \quad (2.1)$$

$$V_{mn} = \int \psi_m(x)\,\delta V(x)\,\psi_n(x)\,dx, \qquad A_{nm} = \frac{2\psi_n\psi_m V_{mn}}{E_n - E_m}. \quad (2.2)$$

Let the index n be monotonically related to the energy. We consider the total change of the density of all the particles with $n < \nu$,

$$\delta\rho(n<\nu) = \sum_n^{\nu} \delta\rho_n = \sum_n^{\nu}\sum_m{}' A_{nm}. \quad (2.3)$$

We now make use of the fact that A_{nm} is antisymmetric, $A_{nm} = -A_{mn}$. Because of this the sum over all n from 0 to ∞ is identically zero. This means that

$$\delta\rho(n<\nu) + \delta\rho(n>\nu) = 0,$$
$$\delta\rho(n<\nu) = -\delta\rho(n>\nu) = -\sum_{n=\nu}^{\infty} \delta\rho_n. \quad (2.4)$$

Since Eq. (2.4) holds for an arbitrary small variation $\delta V(x)$, with an arbitrary and not small $V(x)$, the same relation also holds for an arbitrary change of $V(x)$, in particular for the change of V(x) from 0 to a given final $V(x)$.

For $V = 0$, $\rho(x) = \text{const} = \rho_0$, and consequently

$$\Delta\rho(n<\nu) = -\sum_{n=\nu}^{\infty} [\rho_n(x) - \rho_{0n}(x)]. \quad (2.5)$$

The meaning of this transformation is that the sum over $n < \nu$ gives the essential contribution of the discrete states, and also the contribution of states for which E is small and the wavelength is large; for each of these states individually a potential $V(x)$ that is different from zero in a small region of space causes changes of $\psi_n(x)$ and $\rho_n(x)$ at large distances, of the order of a wavelength.

By using Eq. (2.5) we go on to the examination of particles with energies larger than the boundary energy $\mathscr{E} \equiv E_\nu$. For particles with $E > \mathscr{E}$ the condition for the quasiclassical nature of the motion in the field $V(x)$ is much less restrictive. If it is satisfied, then for wave functions normalized in unit volume we have

$$\psi(x) = \sqrt{k_0/k}\exp\left\{i\int k\,dx\right\}, \qquad k(x) = \sqrt{k_0^2 - 2V(x)}, \quad (2.6)$$

$$\rho(x) - \rho_0 = -(k - k_0)/k_0, \quad (2.7)$$

$$\Delta\rho(k<k_m) = \frac{2}{\pi}\int_{k_{m1}}^{\infty} \frac{k-k_0}{k_0}\,dk_0. \quad (2.8)$$

From this we find

$$\Delta\rho(k<k_m) = 2(k_m - k_{m0})/\pi. \quad (2.9)$$

The unperturbed density is $\rho_0 = 2k_{0m}/\pi$, so that

$$\rho(k<k_m) = (2/\pi)\sqrt{k_0^2 - 2V} = 2k_m/\pi.$$

Thus the first point of the program stated in the introduction has been accomplished: an expression that agrees with the elementary formula (1.1) has been derived on the single assumption that the motion of particles whose energy exceeds the boundary energy is quasiclassical, although in reality we have to do with an assembly of particles whose energies are less than the boundary value, and whose motions may not be quasiclassical.

3. THE CORRECTIONS TO THE STATISTICAL FORMULA

To find the deviations from the elementary formulas (1.1) and (2.9) we can use two methods, in each of which we use the completeness theorem and make the calculations with wave functions for energies larger than the boundary energy.*

The first method is the use of the quasiclassical approximation

$$\psi_{k_0} = \sqrt{k_0/k}\exp\left\{-\sigma_3 + i\left[\int k\,dx - \sigma_2\right]\right\};$$
$$\sigma_2 = \frac{k'}{4k^2} + \frac{1}{8}\int\frac{k''}{k^3}\,dx, \qquad \sigma_3 = \frac{3}{16}\left(\frac{k'}{k^2}\right)^2 - \frac{k''}{8k^3}. \quad (3.1)$$

From this it follows that

$$\Delta\rho(k_0) = -\frac{2}{\pi}\int k_0\,dk_0\left[\frac{1}{k} - \frac{1}{k_0} - \frac{V''}{4k^5} - \frac{5V'^2}{8k^7}\right]. \quad (3.2)$$

Substituting in Eq. (2.5) and carrying out the integration, we get the answer in the form

$$\Delta\rho = \frac{2}{\pi}\left[(\sqrt{2(\mathscr{E}-V)} - \sqrt{2\mathscr{E}}) + \frac{V''}{12k_m^3} + \frac{V'^2}{8k_m^5}\right], \quad (3.3)$$

where the term in parentheses is the statistical formula, and the further terms give corrections to it. The problem of the quantum corrections to the statistical formulas has also been treated earlier by several writers.[1-3] We note that in the one-dimensional case the sign of the correction to the statistical formulas is opposite to that in the three-dimensional case (see Sec. 4 and references 1 – 3).

*For simplicity we confine ourselves to the case $V < \mathscr{E}$.

In the derivation of Eqs. (3.1) and (3.2) we neglect the amplitude of the reflected wave and consider only the deformation of the transmitted wave. As is well known, the amplitude of the reflected wave is proportional to the matrix element

$$\int V(x)\, e^{2ikx}\, dx. \tag{3.4}$$

For an analytic $V(x)$ without singularities on the real axis this matrix element $\sim \exp\{-2k \operatorname{Im}(x_0)\}$, where $\operatorname{Im}(x_0)$ is the imaginary part of the coordinate x_0 of a pole of $V(x)$. Such a term does not contribute to an expansion in powers of $1/k$, and therefore the expansion (3.3) is only an asymptotic expansion.

The second method is the use of the Born approximation. For a $V(x)$ that is of arbitrary form, but small, we find, again by using the completeness theorem,* that

$$\Delta\rho\,(k < k_m) = -\int_{k_m}^{\infty} dk \int_{-\infty}^{\infty} V(\xi)\, l(k,\ |x-\xi|)\, d\xi$$

$$= \int_{-\infty}^{+\infty} V(\xi)\, L(|x-\xi|)\, d\xi = \int_{k_m}^{\infty} j(x,\ k)\, dk,$$

$$L = \int l\, dk = -\frac{2}{\pi} \int_{2k_m}^{\infty} \frac{\sin t}{t}\, dt,$$

$$j(x,k) = \frac{2}{\pi} \int_{-\infty}^{+\infty} V(x') \frac{\sin 2k\,|x-x'|}{|x-x'|}\, dx'. \tag{3.5}$$

We note that $l(y)$ and $L(y)$ are even, but not analytic, functions; they have a singularity (discontinuity of all odd derivatives) at $y = 0$; therefore in the integral (3.5) the values of $V(\xi)$ at $x = \xi$ are singled out.

Equation (3.5) shows that $\Delta\rho$ is not zero outside the region of action of the potential, where $V = 0$. Then the integral

$$J = \int V(\xi)\, L(|x-\xi|)\, d\xi$$

comes entirely from the region where L has no singularities, and consequently according to the theory of the Fourier integral the value of J is determined by the singularities of $V(x)$, the discontinuities of $V(x)$ or of its derivatives and the poles of $V(x)$ in the complex plane.

For example, if $V(x) = a\delta(x-x_0)$, then $\Delta\rho = aL(|x-x_0|)$, so that in the region where $V = 0$ and $\Delta\rho$ is zero by the statistical formula we actually have $|\Delta\rho| \sim 1/k_m x$; when there is a discontinuity of the derivative of $V(x)$, $|\Delta\rho| \sim (k_m x)^2$, and so on.

The expression (3.5) brings out the fact that the scale of length in the solution is $\lambda_m = 1/k_m$, the wavelength of a particle moving with the boundary energy; on the other hand, the bound particles and low-energy particles, on which $V(x)$ acts especially strongly, have $\lambda \gg \lambda_m$. Consequently, there is effective mutual compensation of their contributions.

We note in conclusion that the formulas become inapplicable when $V(x)$ is small but has resonance properties, say $V \sim \sin k_m x$; as is well known, in this case the spectrum breaks up into zones; coincidence of a zone boundary with the boundary energy of the Fermi distribution decidedly changes the properties of the gas (in particular it turns a metal into a dielectric).

4. THREE-DIMENSIONAL MOTION

In the three-dimensional case a localized ($V(\mathbf{r}) = 0$ for $|\mathbf{r}| > R_0$) small potential V has no bound levels and the Born approximation applies for arbitrary energy, in particular for $E < V$, if $VR_0^2 \to 0$. For this reason we can do without the completeness theorem and integrate over the occupied states

$$\Delta\rho\,(\mathbf{r}) = \int L(k_m,\ R)\, V(\mathbf{r}')\, d\mathbf{r}',$$

$$L = \frac{\sin(2k_m R) - 2k_m R \cos(2k_m R)}{4R^4}. \tag{4.1}$$

Expanding $V(\mathbf{r})$ in a series in $\mathbf{r}-\mathbf{r}'$, we get the well known result

$$\Delta\rho = -\pi^{-2}\left(Vk_m + \frac{\nabla^2 V}{12k_m}\right). \tag{4.2}$$

The general character of the formulas (conservation of Δn, practical absence of effects at distances beyond $1/k_m$) does not differ from that of the corresponding formulas of the one-dimensional problem; the coefficient of V naturally correspond to the statistical formula. A nontrivial point, however, is the difference of the sign of the correction; in the one-dimensional case the coefficient of $\nabla^2 V$ was negative.

Let us now examine the special case of three-dimensional motion in a potential $V = V(x)$. In this case k_y and k_z are integrals of the motion, and for fixed k_y and k_z, according to Eq. (3.3),

$$\Delta\rho_1(k_y,\ k_z,\ x) = \frac{2}{\pi}\left\{\left(\sqrt{2(E_x - V)} - \sqrt{2E_x}\right) + \frac{V''}{12k_x^3} + \frac{V'^2}{8k_k^5} + \ldots\right\};$$

$$E_x = \mathcal{E} - (k_y^2 + k_z^2)/2, \qquad k_x = \sqrt{k_m^2 - k_y^2 - k_z^2}. \tag{4.3}$$

*Otherwise, integrating up to $\mathcal{E}$ from below, we would be confronted with the inapplicability of the Born approximation to the low-energy particles with $E \lesssim V_{max}$, and to the bound particles in the case $V < 0$.

We find the total change of the density by integrating over dk_y, dk_z. We note that in polar coordinates q, φ in the plane of k_y, k_z

$$dk_y dk_z = q dq\, d\varphi, \qquad k_x = \sqrt{k_m^2 - q^2}, \quad q dq = k_x dk_x,$$
$$\Delta\rho_3(x) = (2\pi)^{-1} \int \Delta\rho_1(k_x,\ x)\, k_x dk_x, \tag{4.4}$$

where the index 1 marks the solution for the one-dimensional motion, and the index 3 marks the desired solution for the three-dimensional motion. The expression (4.4) is exact if one uses the exact expression for $\Delta\rho_1(k_x, x)$, since the separation of the variables is exact.*

When, however, we substitute in Eq. (4.4) the quasiclassical expression for $\Delta\rho_1$ according to Eqs. (3.3) and (4.3), we encounter the fact that the integration starts from small k_x, where these quasiclassical formulas cannot be applied, and for all the terms except the first the integrals diverge in the region of small k_x.

Let us divide the range of integration over k_x in Eq. (4.4) into two parts. For $k_x < K$ (K is some boundary momentum) we integrate the exact, not quasiclassical, $\Delta\rho_1$. Above K we use the quasiclassical expression (3.3) and (4.3). Thus we have

$$\Delta\rho_3(k_m,\ x) = \Delta\rho_3(K,\ x) + (2\pi)^{-1} \int_K^{k_m} \Delta\rho_1(k_x,\ x)\, k_x dk_x. \tag{4.5}$$

It is natural to make the assumption that in the limit $k_m \to \infty$ the value of $\Delta\rho_3$ satisfies the statistical formula (1.2) without corrections,

$$\Delta\rho_3(k_x,\ x) \to (3\pi^2)^{-1} \{(k_m^2 - 2V)^{3/2} - k_m^3\} = \Delta\rho_3^0(k_m,\ x), \tag{4.6}$$

i.e., that the corrections go to zero for $k_m \to \infty$.

Comparing Eqs. (4.5) and (4.6), we find that (4.6) is just the integral of the first term of the one-dimensional expression [the term corresponding to Eqs. (1.1) and (2.9)]

$$(k_m^2 - 2V)^{3/2} - k_m^3 = \int_{\sqrt{2V}}^{k_m} (k_x^2 - 2V)^{1/2} k_x dk_x - \int_0^{k_m} k_x^2 dk_x, \tag{4.7}$$

and consequently to each successive (i-th) correction term in Eq. (4.3) there correspond two terms in Eq. (4.5), whose sum goes to zero for $k_m \to \infty$. From this we have

$$\Delta\rho_{3i}(x) = \Delta\rho_{3i}(K,\ x) + (2\pi)^{-1} \int_K^{k_m} \Delta\rho_{1i}(k_x,\ x)\, k_x\, dk_x$$
$$= -(\pi/2) \int_{k_m}^{\infty} \Delta\rho_{1i}(k_x,\ x)\, k_x\, dk_x. \tag{4.8}$$

Thus in the three-dimensional case the principle of carrying over the summation from the region below k_m to that above k_m can be applied to the corrections, although it is not applicable to the main statistical term.*

*For $V < 0$, when there is a bound level corresponding to $k_x^2 < 0$, it is understood that the integral in Eq. (4.4) also includes the sum over the discrete levels.

*We note that if we expand the main statistical term in powers of V and regard the terms in V^2, V^3, ... as corrections, then the principle of transferring the summation can also be applied to them, and their signs are also opposite in the one-dimensional and three-dimensional cases.

[1] A. S. Kompaneets and E. S. Pavlovskiĭ, JETP **31**, 427 (1956), Soviet Phys. JETP **4**, 328 (1957).

[2] D. A. Kirzhnits, JETP **32**, 115 (1957), Soviet Phys. JETP **5**, 64 (1957).

[3] S. Golden, Phys. Rev. **105**, 604 (1957).

Translated by W. H. Furry
260

DISTRIBUTION OF DENSITY OF PROTONS WITH GIVEN ANGULAR MOMENTUM IN THE NUCLEUS

L. P. RAPOPORT and S. G. KADMENSKIĬ

Voronezh State University

Submitted to JETP editor June 2, 1959

J. Exptl. Theoret. Phys. (U.S.S.R.) 37, 1303-1307 (November, 1959)

The density of protons of given angular momentum is computed from the experimental distribution of the total proton density. Spatial separation of nuclear shells is demonstrated using the distribution thus obtained.

1. METHOD OF CALCULATION

THE Thomas-Fermi statistical theory can be generalized so as to give the distribution of density of fermions with angular momentum.[1]

Expanding plane waves in eigenfunctions of the angular momentum, we have

$$\rho(r) = \lim_{r'\to r}\rho(r, r') = \lim_{r'\to r}\frac{2}{h^3}\int_0^{P_\mu(r)} \exp\left(i\mathbf{p}(\mathbf{r}-\mathbf{r}')/h\right) d\mathbf{p}$$

$$= \frac{1}{2\pi r}\sum_{l=0}^{\infty}(2l+1)\int_0^{K_\mu(r)} kJ^2_{l+1/2}(kr)\,dk,\quad K_\mu(r) = 2\pi P_\mu(r)/h, \tag{1}$$

where $P_\mu(r)$ is the Fermi momentum and l is the angular momentum quantum number.

From Eq. (1) it can be seen that if one introduces

$$\rho_l(r) = \frac{1}{2\pi r}(2l+1)\int_0^{K_\mu(r)} kJ^2_{l+1/2}(kr)\,dk, \tag{2}$$

such that

$$\rho(r) = \sum_{l=0}^{\infty}\rho_l(r), \tag{3}$$

then the $\rho_l(r)$ so defined is the density of fermions with given angular momentum l. From Eqs. (1) and (2) it is clear that knowing

$$K_\mu(r) = [3\pi^2\rho(r)]^{1/3} \tag{4}$$

from the distribution of total density $\rho(r)$, it is possible to calculate $\rho_l(r)$ for arbitrary $l = 0, 1, 2, \ldots$ Equation (2) can be used to calculate the distribution of protons with angular momentum in the nucleus if one takes for the density $\rho(r)$ the experimental values obtained from the experiments on electron scattering by nuclei.[2]

In this case, since we do not solve the complete dynamical problem of motion of nucleons in the nucleus, the difficult problem of the applicability of the Thomas-Fermi model to the nucleus can be partially avoided. The experimental density automatically takes into account all characteristics of proton motion in the nucleus (type of nuclear force, influence of neutrons, etc.). Considering that the expansion of the plane waves in Eq. (2) is in terms of the exact eigenfunctions of the angular momentum operator, one might expect the application of this formula in our calculation to be more successful than is the case in the usual statistical theory.

We compare, for example, Eq. (2) with the formula derived by Hellmann through generalizing the statistical model of the atom by means of grouping electrons according to orbital momentum.[3] Using Eq. (4), the formula of Hellmann for $\rho_l(r)$ has the form

$$\rho_l(r) = \frac{2l+1}{2\pi^2 r^2}\left[(3\pi^2\rho(r))^{2/3} - \frac{l(l+1)}{r^2}\right]^{1/2}. \tag{5}$$

In so far as imaginary values of $\rho_l(r)$ have no physical significance, for $l \neq 0$, $\rho_l(r)$ is nonzero in some interval $r_1 < r < r_2$, where r_1 and r_2 are roots of the quantity under the square root in Eq. (5). For the case of $l = 0$, we have

$$\rho_0(r) = (3\pi^2 p(r))^{1/3}/2\pi^2 r^2 = K_\mu/2\pi^2 r^2, \tag{6}$$

where for $r \to 0$ we have $\rho_0(r) \sim r^{-5/2}$ in the atomic case and $\rho_0(r) \sim r^{-2}$ in the nuclear case. In our case, for $l = 0$ the integration in Eq. (2) can be performed, and we have

$$\rho_0(r) = (2K_\mu r - \sin(2K_\mu r))/4\pi^2 r^3. \tag{7}$$

Thus, for $r \to 0$ we have $\rho_0(r) \to K_\mu^3/3\pi^2$, and comparison with Eqs. (3) and (4) shows that only protons with $l = 0$ can be at the origin, as should be the case. For large r, Eqs. (6) and (7) practically coincide. From analysis of Eq. (2) for $l \neq 0$, it follows that $\rho_l(r) \to 0$ for $r \to 0$ and

has finite real values for arbitrary $0 < r < \infty$ [in contradistinction to Eq. (5)]. This is in agreement with the behavior of $\rho_l(r)$ expected from quantum mechanical considerations.

2. DISTRIBUTION OF PROTON DENSITY WITH ANGULAR MOMENTUM AND SPATIAL DISTRIBUTION OF SHELLS IN THE NUCLEUS

We now apply Eq. (2) to calculate $\rho_l(r)$ for protons in a spherically symmetrical nucleus with $\rho(r)$ in the form of a Fermi distribution,

$$\rho(r) = \rho_0\left[1 + \exp\left(\frac{r-c}{b}\right)\right]^{-1}, \qquad (8)$$

where the coefficients c and b are determined from the experiments of Hofstadter et al.,[2]

$$c = (1.07 \pm 0.02)\, A^{1/3} \cdot 10^{-13} \text{ cm},$$

$$b = (0.5455 \pm 0.0682) \cdot 10^{-13} \text{ cm}, \qquad (9)$$

and ρ_0 is found by normalizing the total charge to Z protons in the nucleus.

From Eq. (2) we obtain for the number of protons Z_l in states with a given l

$$Z_l = 4\pi \int_0^\infty r^2 \rho_l(r)\, dr. \qquad (10)$$

Comparison of numerical values obtained by integrating Eqs. (2) and (10) with empirical values is shown in Table I for the particular case of Au^{197}_{79}. Instead of the parameters in Eq. (9) we here employ the actual experimental values of Hofstadter's parameters $\rho_0 = 0.68 \times 10^{38}$ cm^{-3}, $c = 6.38 \times 10^{-13}$ cm, $b = 0.528 \times 10^{-13}$ cm. The corresponding density distributions $\rho_l(r)$ are shown in Fig. 1.

From Table I it can be seen that the values of Z_l agree, in general, with the corresponding values from the shell model, making it possible to assess the correctness of the given $\rho_l(r)$. In the final column, the numbers of protons of given l present in the surface of the nucleus ($0.9\rho_0 \leq \rho(r) \leq 0.1\rho_0$) are given. From Fig. 1 it can be seen that the behavior found for $\rho_l(r)$ corresponds to that expected from quantum mechanical calculations. Analogous results have been obtained for other nuclei.

TABLE I. Number of protons Z_l with given l for Au^{197}_{79}

Angular momentum l	Z_l	Nearest integer	According to scheme of Mayer	Number of particles of given l in the surface layer
0	5.65	6	6	1.55
1	12.48	12	12	4.66
2	16.97	17	20	7.61
3	17.93	18	14	9.91
4	15.6	16	18	9.63
5	9.01	9	9	6.03
6	1.27	1	0	0.49

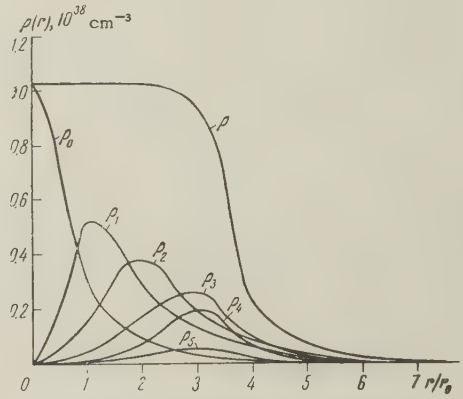

FIG. 1. Distribution of proton density $\rho_l(r)$ with angular momentum l for Au^{197}_{79}.

We now analyze how the distribution of radial proton density $\rho_l(r)\, r^2$ in states of given l changes with changing number of protons Z in the nucleus. The relevant curves for $l = 0$ and $l = 1$ are given in Figs. 2 and 3. Let us consider, for example, Fig. 3. Analysis of the change in density from Li^6_3 ($Z_1 = 1.05$) to S^{32}_{16} ($Z_1 = 6.12$) shows that the maximum density gradually increases, the maximum remaining at the same distance from the center, and the quantity $\rho_l(r)\, r^2/Z_l$ for arbitrary r does not depend upon

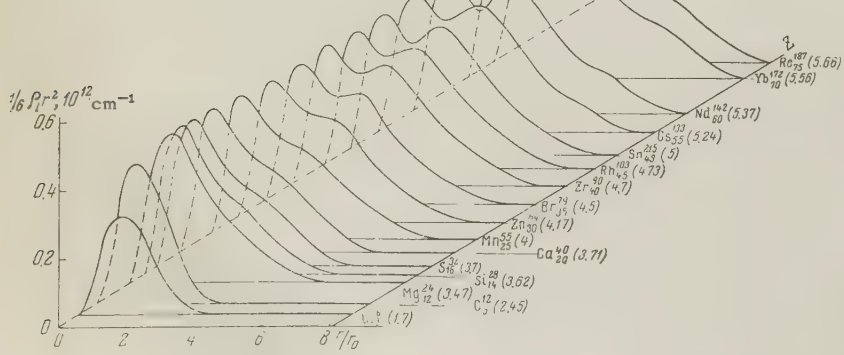

FIG. 2. Dependence of proton radial density $\rho_l(r)\, r^2$ on Z for $l = 0$. For light nuclei (up to Ca^{40}_{20}) the experimental parameters c and b were employed in Eq. (8) for $\rho(r)$. For heavy nuclei, c and b were obtained from Eq. (9). The numbers in parentheses after the nucleus give the number of protons found in the data with given l in the indicated nucleus.

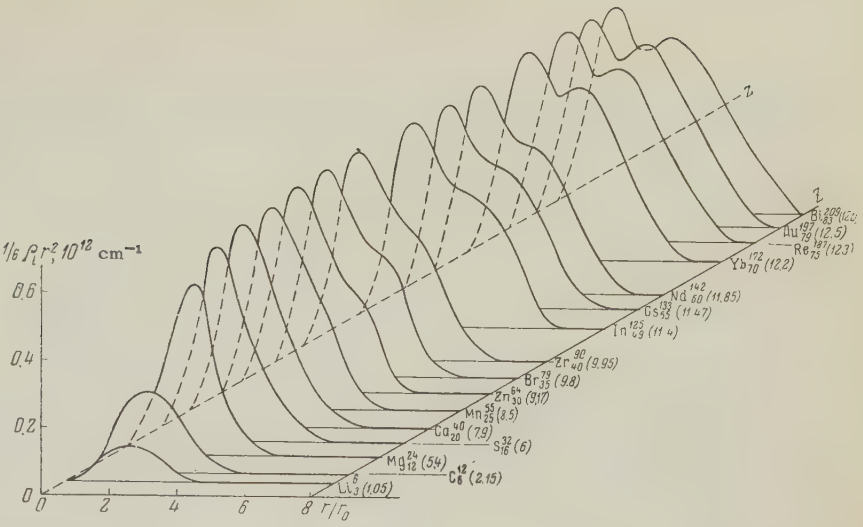

FIG. 3. Dependence of the proton radial density $\rho_l(r)r^2$ on Z for the case of $l = 1$.

TABLE II. Comparison of the number of protons Z_l in filled subshells with the Goeppert-Mayer scheme

	Z_l in this work		Z_l according to Mayer	
l	first subshell	second subshell	first subshell	second subshell
0	≈2	≈2	2	2
1	≈6	≈6	6	6

Z. After S_{16}^{32} the maximum stops growing with increasing Z, the left part of $\rho_l(r)r^2$ stops changing, and a deformation in the right part of the curve sets in. Such a behavior of the radial density indicates that the first subshell is filled in the region $Z = 15$ ($Z_1 \approx 6$). The deformation of the right part continues growing until near Nd_{60}^{142} ($Z_1 \approx 12$) a second maximum arises; i.e., a second subshell is apparently full. An analogous behavior of the curve continues further. The total numbers of protons in filled subshells, as follow from Figs. 2 and 3, and their comparison with the Goeppert-Mayer scheme are shown in Table II.

Thus, the semi-statistical way of considering the nucleus employed by us makes it possible not only to obtain information about the shell structure in the nucleus, but also to show the spatial distribution of the shells in the region of their principal maxima (by calculating the distribution curves for the preceding subshells). In particular, these distributions show that both the form and area of a completely filled subshell remain practically unchanged with the growth of further nucleon shells. Analyses of other distributions of total charge (for example, references 4 and 5) also show that shell structure arises; however, less satisfactory agreement with the Goeppert-Mayer scheme is obtained.

[1] S. Golden, Phys. Rev. **110**, 1349 (1958).

[2] R. Hofstadter, Revs. Modern Phys. **28**, 214 (1956).

[3] H. Hellmann, Acta Phys. Chem. URSS **4**, 225 (1936).

[4] L. P. Rapoport and V. A. Filimonov, JETP **27**, 243 (1954).

[5] F. Kligman, JETP **35**, 367 (1958), Soviet Phys. JETP **8**, 255 (1959).

Translated by G. E. Brown
261

SCATTERING OF ELECTRONS BY LIGHT NONSPHERICAL NUCLEI

E. V. INOPIN and B. I. TISHCHENKO

Physico-technical Institute, Academy of Sciences, Ukrainian S.S.R.

Submitted to JETP editor March 28, 1959; resubmitted June 26, 1959

J. Exptl. Theoret. Phys. (U.S.S.R.) 37, 1308-1318 (November, 1959)

The scattering of electrons by nonspherical nuclei is treated in the Born approximation. Expressions for the elastic and inelastic cross sections have been derived for the general case of oriented nuclei with arbitrary deformations. The theory is compared with the experiments on the inelastic scattering of electrons by light nuclei.

1. INTRODUCTION

A number of recently published papers[1-3] are devoted to the analysis of the experimental data on light nuclei ($4 \leq A \leq 30$). This analysis indicates that many of these nuclei are appreciably nonspherical. In particular, the data on the quadrupole moments in this region and also on the Coulomb excitation of the low-lying levels suggest that the nonsphericity of some light nuclei is more pronounced than in the well known rare earth region of deformed nuclei. It is highly probable that further investigation of the properties of the low-lying levels reveals the presence of rotational states in other light nuclei as well.

In this connection it is of interest to study in detail the effect of the nonsphericity of the light nuclei on the scattering of electrons with high energies. The investigation of this effect should add to our knowledge of the size of the light nuclei and of the distribution of the electric charge in them. Furthermore, the study of the excitation of the low-lying levels by electrons will be helpful in deciding which type of motion corresponds to any level under consideration (single particle, rotational, or vibrational motion).

The investigation of the nonsphericity of light nuclei by the scattering of electrons is less difficult than in the case of heavy nuclei, owing to the following circumstances: a) the nonsphericity of light nuclei is more pronounced, as already noted; b) the energy of the excited rotational levels is of the order 1 Mev (greater by an order of magnitude than in heavy nuclei), so that it is possible to separate the nonelastically scattered group of electrons, i.e., to observe the nonelastic scattering in its pure form; c) we can use the Born approximation, which greatly simplifies all calculations and makes it possible to obtain a number of simple and rather general results concerning the process under consideration.

In the present paper we study the effect of the nonsphericity of the nucleus on the elastic scattering of electrons, as well as the excitation of the rotational levels by electrons. A few results obtained earlier by Schiff[4] will be re-derived in the interest of clarity of presentation. To analyze the inelastic scattering we used a method which is a generalization of the usual method for the analysis of the elastic scattering of electrons. We also investigate further possibilities of studying the nonsphericity by using oriented nuclei.

2. GENERAL EXPRESSIONS FOR THE CROSS SECTIONS FOR ELASTIC AND INELASTIC SCATTERING OF ELECTRONS

In the calculation of the cross sections for the scattering of electrons by light nuclei we shall use the Born approximation. As is known, the condition of applicability of the Born approximation for a point charge is $Z/137 \ll 1$, which is well satisfied in the case of light nuclei ($Z = 10$ to 15). The finite extent of the charge removes the singularity of the Coulomb potential and therefore leads, generally speaking, to even better conditions for the applicability of perturbation theory. An exception to this are the neighborhoods of those scattering angles for which the cross section, as calculated in the Born approximation, reduces to zero. The comparison of the results of the exact calculations performed by Ravenhall for C^{12} and O^{16} (see reference 5) with those of the Born approximation permits a rough estimate of the extent of the region in which the Born approximation is not valid. It appears that this region is characterized by the quantity $\Delta q/q_0 \approx \pm 5\%$ (q is the momentum trans-

fer, and q_0 is that value of the momentum transfer for which the form factor goes to zero).

The cross section for a process in which the electron is scattered into the direction $\mathbf{n}$ and the nucleus goes from the state i to the state f is, in Born approximation, given by the formula

$$\sigma_{if}(\mathbf{n}) = \frac{1}{(2\pi)^2}\frac{p^2}{v^2}\left|\int \Psi_f^* V \Psi_i \, d\tau\right|^2. \qquad (2.1)$$

The wave functions Ψ_i and Ψ_f have the form

$$\Psi_i = u(\mathbf{p}_0)\, e^{i\mathbf{p}_0\mathbf{r}}\, \chi_K(\mathbf{X}_1, \ldots \mathbf{X}_A, \theta_s) \sqrt{(2I_0+1)/8\pi^2}\, D^{I_0}_{\mu_0 K}(\theta_s),$$

$$\Psi_f = u(\mathbf{p})\, e^{i\mathbf{p}\mathbf{r}}\, \chi_K(\mathbf{X}_1, \ldots \mathbf{X}_A, \theta_s) \sqrt{(2I+1)/8\pi^2}\, D^{I}_{\mu K}(\theta_s), \qquad (2.2)$$

where $\mathbf{p}_0$ and $\mathbf{p}$ are the initial and final momenta of the electron, $\mathbf{r}$ is the coordinate of the electron, $u(\mathbf{p}_0)$ and $u(\mathbf{p})$ are the spinor amplitudes, χ_K is the wave function describing the internal state of the nucleus, $\mathbf{X}_1, \mathbf{X}_2, \ldots, \mathbf{X}_A$ are the coordinates of the nucleons, θ_S are the Eulerian angles defining the orientation of the nucleus, I_0 and μ_0 are the total angular momentum of the nucleus and its projection in the ground state, I and μ are the same quantities in the excited rotational state, and K is the projection of the total angular momentum on the symmetry axis of the nucleus. It is assumed that the internal state of the nucleus, described by χ_K, does not change in the considered process; only its rotational state, described by the functions $D^{I_0}_{\mu_0 K}$ and $D^{I}_{\mu K}$, changes.

Substituting for V in (2.1) the expression for the Coulomb interaction of the electron with the protons of the nucleus and summing over the polarizations of the electron, we obtain

$$\sigma^{I\mu}_{I_0\mu_0}(\mathbf{n}) = S_{II_0}\,\sigma_c(\theta)\left|\int D^{I*}_{\mu K} F(\mathbf{q}, \theta_s)\, D^{I_0}_{\mu_0 K}\, d\theta_s\right|^2, \qquad (2.3)$$

where $\sigma_c(\theta)$ is the cross section for scattering from a point nucleus with charge Z;

$$S_{II_0} = (2I_0+1)(2I+1)/64\pi^4,$$

$$F(\mathbf{q}, \theta_s) = \int e^{i\mathbf{q}\mathbf{r}}\rho(\mathbf{r}, \theta_s)\, d\mathbf{r}$$

is a form factor corresponding to the density distribution (normalized to unity) of the protons in the nucleus,

$$\rho(\mathbf{r}, \theta_s) = \int |\chi_K(\mathbf{r}, \mathbf{X}_2, \ldots \mathbf{X}_A, \theta_s)|^2\, d\mathbf{X}_2, \ldots d\mathbf{X}_A$$

$$\mathbf{q} = \mathbf{p}_0 - \mathbf{p}.$$

According to the unified model of the nucleus, this distribution will have an axis of symmetry, whose orientation is given by the angle θ_S, and also a center of symmetry. It can therefore be expressed in the form of a sum,

$$\rho(\mathbf{r}, \theta_s) \equiv \rho(\mathbf{r}, \boldsymbol{\omega}) = \sum_L \rho_L(r)\, P_L\left(\frac{\mathbf{r}\boldsymbol{\omega}}{r}\right), \qquad (2.4)$$

which goes only over the even values of L; $\boldsymbol{\omega}$ is a unit vector defining the direction of the axis of symmetry of the nucleus.

In the general case the wave function of the nucleus in the initial state will be a superposition of the form

$$\varphi^l_{I_0} = \sum_m a^l_m\, D^{I_0}_{mK}. \qquad (2.5)$$

Furthermore, the ensemble of nuclei which make up the target will be a mixture of states of the type (2.5), in which each of these states will be present with a probability w_l. Replacing $D^{I_0}_{\mu_0 K}$ in (2.3) by the expression (2.5), summing over l with the weight w_l and also over the final states with different values μ, we obtain

$$\sigma^I_{I_0}(\mathbf{n}) = S_{I_0 I}\,\sigma_c(\theta) \sum_{mm'\mu} \rho_{mm'} F_{\mu m} (F_{\mu m'})^*, \qquad (2.6)$$

where

$$F_{\mu m} = \int D^{I*}_{\mu K} F(\mathbf{q}, \theta_s)\, D^{I_0}_{mK}\, d\theta_s, \qquad \rho_{mm'} = \sum_l w_l\, a^l_m\, a^{l*}_{m'}.$$

It is obvious that the quantities ρ_{mm} are elements of a $(2I_0+1)$-rowed density matrix describing the spin state of the ensemble of nuclei in the target.

It is known[6] that the density matrix ρ can be written in the form

$$\rho = \sum_{M=-J}^{J} \sum_{J=0}^{2I_0} \langle T^{JM+}\rangle\, T^{JM}. \qquad (2.7)$$

The matrices T^{JM} are given by their matrix elements in the following way:

$$T^{JM}_{mm'} = (-1)^{I_0+m'}(I_0 I_0 m - m' \,|\, JM), \qquad (2.8)$$

The quantities $\langle T^{JM+}\rangle$, the average values of the T^{JM+} (the plus sign denotes Hermitian conjugation), are parameters which define the orientation of the nuclei. In particular,

$$\langle T^{20}\rangle = (-1)^{2I_0}\left[\frac{5I_0(2I_0-1)}{(I_0+1)(2I_0+1)(2I_0+3)}\right]^{1/2} f_2, \qquad (2.9)$$

where f_2 is the quadrupole polarization:

$$f_2 = \frac{3\overline{m^2} - I_0(I_0+1)}{I_0(2I_0-1)}. \qquad (2.10)$$

It is obvious that $f_2 = 0$ for non-oriented nuclei, and $f_2 = 1$ for maximal orientation ($\overline{m^2} = I_0^2$).

After some simple transformations, which consist mainly in expanding the products of functions D^{I}_{MK} into a Clebsch-Gordan series and summing over the products of Clebsch-Gordan coefficients,

we obtain finally

$$\sigma^I_{I_0}(\mathbf{n}) = (2I+1)\,\sigma_c(\theta) \sum_{MJL_1L_2} (-1)^{I_0+I+1/2(J+L_1-L_2)} \langle T^{JM+}\rangle$$
$$\times (I_0IK-K\,|\,L_1 0)(I_0IK-K\,|\,L_2 0)\; Z(L_1 I_0 L_2 I_0;\, IJ)$$
$$\times F_{L_1}(q)\,F_{L_2}(q)\sqrt{4\pi/(2J+1)}\,Y_{JM}(\mathbf{q}/q), \qquad (2.11)$$

where

$$F_L(q) = \frac{1}{4\pi}\int P_L\left(\frac{\omega q}{q}\right) F(\mathbf{q},\omega)\,d\omega,$$
$$F(\mathbf{q},\omega) = \int e^{i\mathbf{q}\mathbf{r}}\,\rho(\mathbf{r},\omega)\,d\mathbf{r}. \qquad (2.12)$$

The most important case in practice is that of an axially symmetric external field which orients the nucleus. If the direction of this field, $\mathbf{e}$, is taken as the quantization axis, the only $\langle T^{JM}\rangle$ different from zero are those with $M = 0$. We then have

$$\sigma^I_{I_0}(\mathbf{n}) = (2I+1)\,\sigma_c(\theta) \sum_{JL_1L_2} (-1)^{I_0+I+1/2(J+L_1-L_2)} \langle T^{J0}\rangle$$
$$\times (I_0IK-K\,|\,L_1 0)(I_0IK-K\,|\,L_2 0)$$
$$\times Z(L_1 I_0 L_2 I_0;\, IJ)\,F_{L_1}(q)\,F_{L_2}(q)\,P_J(\mathbf{eq}/q). \qquad (2.13)$$

It is known[7] that $Z(L_1I_0L_2I_0;\,IJ) = 0$ if L_1+L_2+J is odd. The sum (2.13) contains only even values of L_1 and L_2; it follows from the property just mentioned that only terms with even J give a contribution to the cross section. In particular, the polarization of the target (which corresponds to $\langle T^{10}\rangle \neq 0$) does not affect the process under consideration at all.

If the nuclei are not oriented, then

$$\langle T^{J0}\rangle = \overline{(-1)^{I_0+m}(I_0\,I_0\,m-m\,|\,00)}\,\delta_{J0}$$
$$= (-1)^{2I_0}(2I_0+1)^{-1/2}\delta_{J0},$$
$$Z(L_1 I_0 L_2 I_0;\, I0) = \delta_{L_1L_2}(-1)^{I_0-I}(2I_0+1)^{1/2}$$

and (2.13) leads to

$$\sigma^I_{I_0}(\mathbf{n}) = \sigma_c(\theta)(2I+1)\sum_L |(I_0IK-K\,|\,L0)|^2 F_L^2(q). \qquad (2.14)$$

3. FORM FACTORS FOR ELASTIC AND INELASTIC SCATTERING

The cross sections for elastic and inelastic scattering are expressed in terms of form factors $F_L(q)$ which are defined by formulas (2.12). By a simple transformation we obtain

$$F_L(q) = i^L \int \rho(\mathbf{r},\omega)\,j_L(qr)\,P_L\left(\frac{\mathbf{r}\omega}{r}\right)d\mathbf{r}\,d\omega \qquad (3.1)$$

or, using (2.4),

$$F_L(q) = \frac{4\pi i^L}{2L+1}\int_0^\infty \rho_L(r)\,j_L(qr)\,r^2\,dr. \qquad (3.2)$$

The problem of the scattering of electrons by nonspherical nuclei consists in the determination of the functions $\rho_L(r)$ from the experimentally known functions $F_L(q)$. The problem is solved, in principle, by applying the Hankel transformation to (3.2), which leads to

$$\rho_L(r) = \frac{2L+1}{2\pi^2 i^L}\int_0^\infty F_L(q)\,j_L(qr)\,q^2\,dq. \qquad (3.3)$$

However, as is known from the analysis of the elastic scattering ($L = 0$), this expression is practically of no use, since the value of $F_L(q)$ is given with considerable error, and only in a limited interval of values q. A more practical method is therefore to take different expressions for ρ_L, substitute these in (3.2), and compare the calculated values of $F_L(q)$ with experiment. One then chooses that function ρ_L which gives best agreement with the experimental data.

After the well studied form factor for elastic scattering, $F_0(q)$, and the density $\rho_0(r)$, the most important quantities are the form factor $F_2(q)$ and the density $\rho_2(r)$.

Let us consider several general properties of the quantities $\rho_2(r)$ and $F_2(q)$. We note, first of all, that the quantity $\rho_2(r)$ cannot be given in an entirely arbitrary way, but has to satisfy definite requirements. Indeed, the obvious condition $\rho(\mathbf{r},\omega) > 0$ leads to $\rho_0(r) + \rho_2(r)P_2(\mathbf{r}\omega/r) > 0$, if we neglect the small terms with $\rho_4(r)$, $\rho_6(r)$, etc. We then have the inequalities

$$\rho_2(r) < 2\rho_0(r) \quad \text{for} \quad \rho_2(r) > 0, \qquad (3.4)$$
$$|\rho_2(r)| < \rho_0(r) \quad \text{for} \quad \rho_2(r) < 0. \qquad (3.5)$$

The quantity $\rho_2(r)$ can be related to the internal quadrupole moment of the nucleus,

$$Q_0 = Ze\int \rho(\mathbf{r},\omega)\,(3z^2-r^2)\,d\mathbf{r} = Ze\frac{8\pi}{5}\int_0^\infty r^4\rho_2(r)\,dr. \qquad (3.6)$$

It follows from (3.2) and (3.6) that for small q

$$F_2(q) \approx -\frac{1}{30}\frac{Q_0}{Ze}q^2. \qquad (3.7)$$

It can be shown in an entirely analogous fashion that the form factors with $L = 4$, 6, etc. are related to the higher multipole moments, so that the quantities $F_L(q)$ vanish rapidly with increasing L.

We now list the expressions for six densities of the simplest form and the corresponding form factors, using the following notation:

$$a^2 = \int \rho_2(r)\,r^2\,d\mathbf{r} \Big/ \int \rho_2(r)\,d\mathbf{r}$$

is the mean square radius of the nonspherical part of the charge distribution,

$$x = qa,\ y = r/a,\ \Lambda(y) = 4\pi a^5 Ze\rho_2(r)/125\,Q_0,$$
$$\Phi(x) = -30a^2 ZeF_2(q)/Q_0.$$

1. Uniform Model:

$$\Lambda(y) = \begin{cases} {}^1/_{10}\ ({}^5/_3)^{5/2}, & y \leqslant ({}^5/_3)^{1/2} \\ 0, & y = ({}^5/_3)^{1/2} \end{cases},$$
$$\Phi(x) = \frac{45}{z^2}\left\{\cos z - \frac{4\sin z}{z} + \frac{3\,\mathrm{Si}\,z}{z}\right\}, \qquad z = ({}^5/_3)^{1/2}x$$

2. Shell Model:

$$\Lambda(y) = {}^1/_{50}\,\delta(y-1), \qquad \Phi(x) = 15\,j_2(x).$$

3. Gaussian "Wine Bottle" Model:

$$\Lambda(y) = {}^1/_3\,(5/2\pi)^{1/2}\,y^2\exp(-{}^5/_2\,y^2),$$
$$\Phi(x) = x^2\exp(-x^2/10).$$

4. Exponential "Wine Bottle" Model I:

$$\Lambda(y) = {}^4/_3\,y\exp(-\sqrt{20}\,y),$$
$$\Phi(x) = x^2(1 + x^2/20)^{-3}.$$

5. Exponential "Wine Bottle" Model II:

$$\Lambda(y) = (3\sqrt{30}/4)\,y^2\exp(-\sqrt{30}\,y),$$
$$\Phi(x) = x^2(1 + x^2/30)^{-4}.$$

6. Parabolic Model:

$$\Lambda(y) = \begin{cases} {}^1/_{10}\ ({}^5/_7)^{5/2}\,y^2, & y \leqslant ({}^7/_5)^{1/2} \\ 0, & y \geqslant ({}^7/_5)^{1/2} \end{cases},$$
$$\Phi(x) = 75\,j_3(z)/z, \qquad z = ({}^7/_5)^{1/2}x.$$

In the case of the shell-like density the conditions (3.4) and (3.5) can, of course, not be fulfilled. However, the δ function may be interpreted as a function which is different from zero in a region of width Δ, with the constant value Δ^{-1}. This is possible if $q\Delta \ll 1$ in the considered region of momentum transfers q.

4. ELASTIC SCATTERING

Let us consider the effect of the nonsphericity of the nucleus on the elastic scattering. In the simplest case of elastic scattering from a nucleus with spin zero ($I = I_0 = 0$) we obtain

$$\sigma_0^0(\theta) = \sigma_c(\theta)\,F_0^2(q). \tag{4.1}$$

Since the quantity $\rho_0(r)$, which defines $F_0(q)$, is, according to (2.4), equal to

$$\rho_0(r) = \frac{1}{4\pi}\int \rho(\mathbf{r}, \omega)\,d\omega, \tag{4.2}$$

it is obvious that the elastic scattering from a nonspherical nucleus with spin zero and charge density $\rho(\mathbf{r}, \omega)$ is the same as the scattering from a spherical nucleus with density $\rho_0(r)$. In particular, if we take for the distribution a uniformly charged ellipsoid of revolution with semi-axes a and b, then

$$\rho_0(r) = \begin{cases} \rho_0, & 0 \leqslant r \leqslant b \\ \rho_0\,[1 - \sqrt{(r^2 - b^2)/(a^2 - b^2)}], & b \leqslant r \leqslant a \\ 0, & a \leqslant r \end{cases} \tag{4.3}$$

i.e., the nonsphericity appears in experiment as a smoothing out of the nuclear boundary.

Let us consider now a nonspherical nucleus with a density $\rho(\mathbf{r}, \omega)$ such that the surfaces of equal density are similar ellipsoids of revolution with the ratio of half-axes $a/b = \eta$. After a coordinate transformation which takes these ellipsoids into spheres of the same volume, $\rho(\mathbf{r}, \omega)$ goes over into $\rho_{\mathrm{sph}}(r)$. Let us compare the mean square radii of the nonspherical nucleus with density $\rho(\mathbf{r}, \omega)$ and of the spherical nucleus with density $\rho_{\mathrm{sph}}(r)$. It is easily seen that

$$\overline{r^2_{\mathrm{nonsph}}} = \frac{2 + \eta^2}{3\eta^{2/3}}\,\overline{r^2_{\mathrm{sph}}} \tag{4.4}$$

The factor $(2+\eta^2)/3\eta^{2/3}$ is equal to unity for $\eta = 1$ and greater than unity for any other value of η. Hence the nonsphericity leads to an apparent increase in the nuclear radius as compared to the spherical nucleus.

The elastic scattering from non-oriented nuclei with non-zero spin is given by the formula

$$\sigma^{I_0}_{I_0}(\theta) = \sigma_0^0(\theta) + \Delta_{I_0}(\theta), \tag{4.5}$$

where

$$\Delta_{I_0}(\theta) = \sigma_c(\theta)\,(2I_0 + 1)\sum_{L=2}^{\infty} |(I_0\,I_0\,K - K\,|\,L0)|^2\,F_L^2(\theta). \tag{4.6}$$

Obviously, $\Delta_{I_0} = 0$ not only for $I_0 = 0$, but also for $I_0 = \frac{1}{2}$.

We restrict ourselves to the first term in the sum (4.6) and assume $K = I_0$ (as is known, this relation can only be invalid for $K = \frac{1}{2}$), and obtain

$$\Delta_{I_0}(\theta) = \frac{5I_0^2(2I_0 - 1)}{(I_0 + 1)(2I_0 + 3)}\,\sigma_c(\theta)\,F_2^2(\theta). \tag{4.7}$$

The additional contribution to the cross section in the presence of nuclear spin is connected with the fact that in this case elastic scattering accompanied by a transfer of angular momentum L from the electron to the nucleus (according to the scheme $\mathbf{I}_0 + \mathbf{L} = \mathbf{I}_0$) becomes possible. Owing to the presence of a center of symmetry in the nucleus the odd values of L are excluded, and the lowest possible value is $L = 2$. This effect could possibly be observed in measurements of the ratio of the scattering cross sections for the nuclei Mg^{24} and Mg^{25}.

Let us consider now the effect of the orientation of nuclei on the elastic scattering. We restrict ourselves to the case of an axially-symmetric orienting field. In view of what was said above about the fast decrease of $F_L(\theta)$ with growing L, we may keep only terms containing F_0^2 and F_0F_2 in expression (2.4). With the help of (2.9) we then obtain

$$\sigma^{I_0}_{I_0}(\mathrm{n}) = \sigma^{I_0}_{I_0(\mathrm{nonorient})}(\theta) + f_2\,\gamma_{I_0}\,\sigma_c(\theta)\,F_0(\theta)\,F_2(\theta)\,P_2\left(\frac{eq}{q}\right), \tag{4.8}$$

where $\sigma^{I_0}_{I_0\,(\text{nonorient})}$ is the cross section for scattering from non-oriented nuclei, given by (4.5), and

$$\gamma_{I_0} = 10\frac{3K^2 - I_0(I_0+1)}{(I_0+1)(2I_0+3)}. \qquad (4.9)$$

The most striking feature of expression (4.8) is its dependence on the azimuthal angle, i.e., its azimuthal asymmetry. Evidently we observe the greatest asymmetry effect if we first measure the scattering with $\mathbf{e}\cdot\mathbf{q}/q = 1$ (the directions of the orienting field and of the momentum transfer are identical) and then with $\mathbf{e}\cdot\mathbf{q} = 0$ (the two directions are perpendicular to each other). We can therefore take the following quantity as a measure of the azimuthal asymmetry:

$$\delta_{I_0}(\theta) = \frac{\sigma^{I_0}_{I_0}(\mathbf{eq}/q=1) - \sigma^{I_0}_{I_0}(\mathbf{eq}/q=0)}{\sigma^{I_0}_{I_0}(\text{nonorient})(\theta)}. \qquad (4.10)$$

From (4.8) and (4.5) we obtain for the azimuthal asymmetry

$$\delta_{I_0}(\theta) = \frac{3}{2} f_2 \gamma_{I_0} \frac{F_0(\theta)F_2(\theta)}{F_0^2(\theta) + C^2_{I_0}F_2^2(\theta)},$$

$$C_{I_0} = \sqrt{5}\,(I_0 2K0 \mid I_0 K). \qquad (4.11)$$

The function $\delta_{I_0}(\theta)$ has extremal values at those angles θ for which $F_0 = \pm C_{I_0}F_2$. Since the quantity C_{I_0} is always close to unity, this condition can only be fulfilled in the neighborhood of the minimum of the elastic scattering. In particular, if the elastic scattering amplitude goes through zero at the angle θ_0, there will be a maximum and a minimum of the azimuthal asymmetry near θ_0. In the extremal points we obtain for δ_{I_0}

$$\delta_{I_0\,\text{extr}} = \pm\frac{3}{2}\left[\frac{5I_0(2I_0-1)}{(I_0+1)(2I_0+3)}\right]^{1/2}\nu(K) f_2. \qquad (4.12)$$

The sign in this expression has to be chosen such as to correspond to $F_0 = C_{I_0}F_2$ or $F_0 = -C_{I_0}F_2$, respectively. We see that the investigation of the scattering from oriented nuclei gives us the possibility to determine the sign of F_2 and, hence, of the quadrupole moment Q_0.

We have $\nu(K) = 1$ for $K = I_0$ and $\nu(K) = -1$ for $K = \frac{1}{2}$. Hence the sign of the asymmetry for $K = \frac{1}{2}$ is the opposite of that in the usual case, $K = I_0$. The factor in front of f_2 in (4.12) is of order unity and depends rather weakly on the spin of the nucleus. If $f_2 = 10\%$, the maximal asymmetry will be equal to 15% for a nuclear spin of $\frac{3}{2}$, and 20% for $I_0 = \frac{5}{2}$.

5. INELASTIC SCATTERING. COMPARISON WITH EXPERIMENT

In the consideration of the excitation of the rotational levels of non-oriented nuclei we keep in (2.14) only the terms containing F_2, and obtain

$$\sigma^I_{I_0}(\mathbf{n}) = 5\sigma_c(\theta)\,|(I_0 2K0 \mid IK)|^2 F_2^2. \qquad (5.1)$$

It follows from this formula that only the levels with the spins I_0+2, I_0+1, I_0-1, and I_0-2 can be excited. The levels with the spins I_0-1 and I_0-2 can, evidently, occur only if the level order in the rotational band is reversed. The levels with spins which differ from I_0 by more than two units can only be excited through the terms with $L \geq 4$ in the expression (2.14). These terms are smaller than the term with $L = 2$ by $1 \div 2$ orders of magnitude. The observation of the excitation of these levels is therefore very difficult.

From (5.1) we obtain for the relative probability of the excitation of the levels belonging to the same rotational band and having the spins I and I', the usual relation of the theory of the Coulomb excitation:

$$\sigma^I_{I_0}(\mathbf{n})/\sigma^{I'}_{I_0}(\mathbf{n}) = |(I_0 2K0 \mid IK)|^2/|(I_0 2K0 \mid I'K)|^2. \qquad (5.2)$$

If the nuclei are oriented, we obtain from (2.13), again keeping only the terms with $L = 2$,

$$\sigma^{\text{orient}}_{I_0 I}(\mathbf{n}) = \sigma^{\text{nonorient}}_{I_0 I}(\mathbf{n})\left\{1 + \frac{2}{3}\delta_{I_0 I}P_2(\mathbf{eq}/q)\right\}, \qquad (5.3)$$

where $\sigma^{\text{nonorient}}_{I_0 I}(\mathbf{n})$ is given by expression (4.1), and

$$\delta_{I_0 I} = -\frac{3}{2}\left[\frac{250\,I_0(2I_0-1)(2I_0+1)}{7(I_0+1)(2I_0+3)}\right]^{1/2} W(I_0 I 22 \mid 2I_0) f_2. \qquad (5.4)$$

It is obvious that the quantity $\delta_{I_0 I}$ determines the magnitude of the azimuthal asymmetry in a fashion analogous to (4.10). It is interesting to note that, in the inelastic scattering, this quantity is independent of the scattering angle and of the parameters describing the nuclear density. The values of the quantity $\delta_{I_0 I}/f_2$ are listed in Table I. We see that this quantity is in most cases close to unity, but can be either negative or positive. In particular, it is always negative for the levels with $I = I_0 + 2$, and positive for the levels with $I = I_0 + 1$.

TABLE I. Values of the quantity $\delta_{I_0 I}/f_2$

I_0 \ I	I_0+2	I_0+1	I_0-1	I_0-2
3/2	−3/7	15/14	−3/2	—
5/2	−75/98	255/196	−75/98	−15/7
7/2	−1	19/14	−5/14	−15/7
9/2	−90/77	15/11	−15/154	−15/7

Let us now turn to the available experimental data on the inelastic scattering of electrons from light nuclei. The excitation of the levels with spin 2^+ in the even-even nuclei Mg^{24}, Si^{28}, and S^{32} was studied by Helm;[8] Fregeau[9] investigated the C^{12}

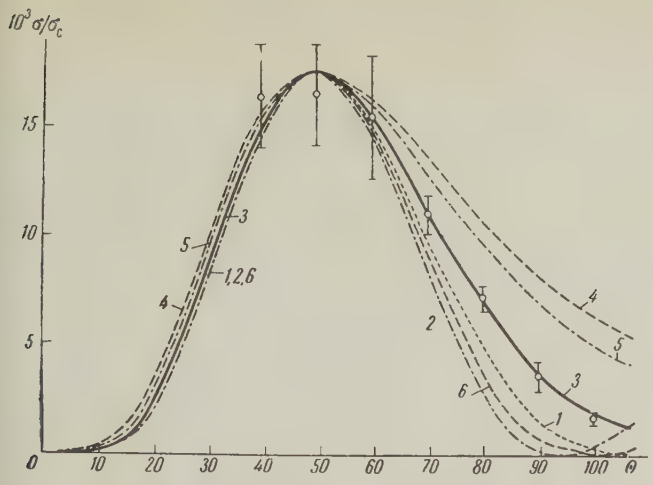

FIG. 1. Cross section for the inelastic scattering of electrons by the Mg^{24} nucleus with excitation of the 1.37-Mev level. The numbers of the calculated curves in this and the following figures correspond to the numbers of the models (see section 3).

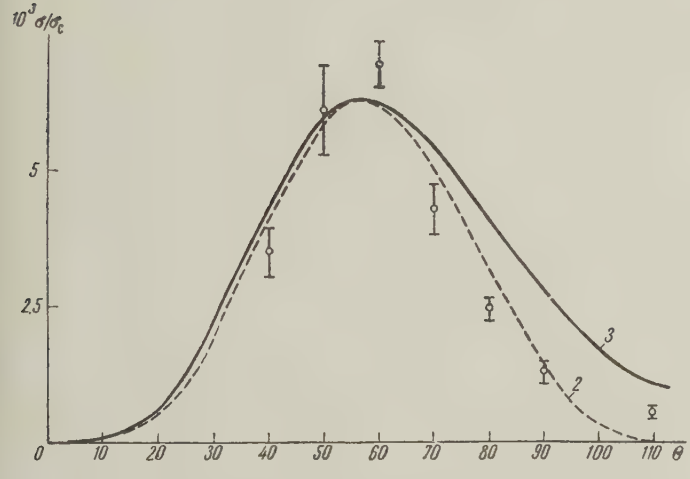

FIG. 2. Cross section for the inelastic scattering of electrons by the Si^{28} nucleus with excitation of the 1.79-Mev level.

nucleus. The levels Mg^{24} 0^+ ($E_0 = 0$), 2^+ ($E_2 = 1.37$ Mev), and 4^+ ($E_4 = 4.17$ Mev) can be regarded as a rotational band ($K = 0$), since they have the correct spins and parities, and also $E_4/E_2 \approx 3$, which is close to the value 3.33 required by the unified model. For the remaining of the above-mentioned nuclei the levels with spin and parity 4^+ have not yet been observed. But it is entirely possible that further investigation of the parities and spins of these nuclei will lead to their discovery. We shall regard these levels as rotational and attempt to draw conclusions on the distribution $\rho_2(r)$ in these nuclei by comparing the experimental data on the angular distribution of the inelastically scattered electrons with the results of the calculations.

TABLE II

Nucleus	Number of model	$a \cdot 10^{13}$ cm^{-1}	$Q \cdot 10^{24}$ cm^{-2}	η
C^{12}	3	2.73	0.200	1.5
Mg^{24}	1	3.93	0.822	
	2	4.16	0.801	
	3	3.94	0.898	1.8
	4	3.94	1.12	
	5	3.94	1.04	
	6	4.06	0.814	
Si^{28}	2	3.68	0.440	
	3	3.49	0.492	1.3
S^{32}	2	4.80	0.736	
	3	4.54	0.825	1.4

In Fig. 1 we make this comparison for Mg^{24}. We see, first of all, that widely different density distributions $\rho_2(r)$ lead to quite similar angular distributions. The parameters of these density distributions, listed in Table II, show that the values of the root mean square radii and of the quadrupole moments are also nearly identical for the different distributions. Apparently, the Gaussian "wine bottle" distribution gives the best agreement. Looking now at the criteria expressed by the relations (3.4) and (3.5), we see that these are not satisfied at all by the density distributions 1, 2, and 6, so that these types of distribution have to be discarded in the present case. For the remaining distribution types listed in Table I, relation (3.4), which corresponds to a positive quadrupole moment of the Mg^{24} nucleus, is well satisfied, but not relation (3.5). We have to except those large distances r, for which the values of $\rho_0(r)$ and $\rho_2(r)$ are so small that in this region the functions can be replaced by others (for which the above-mentioned relations are fulfilled) without affecting appreciably the value of the form factors in this region.

The value $Q_0 = 0.898$ for Mg^{24} obtained here is in satisfactory agreement with the value $Q_0 = 0.75$ which follows from the data of Alkhazov et al.[10] on the Coulomb excitation, and with the value $Q_0 = 0.70$ from the paper of Delyagin and Shpinel'[11] on the resonance scattering of γ rays.

The comparison of experiment and calculation for the remaining three nuclei is pictured in Figs. 2, 3, and 4. We see that the Gaussian "wine bottle" distribution is in good agreement with the experimental data for these nuclei as well. It gives a somewhat poorer fit in the case of the Si^{28} nucleus. The parameters of the distributions shown are given in Table II. The value $Q_0 = 0.492$ for Si^{28} obtained here is in agreement with the results of Alkhazov et al.[10] on the Coulomb excitation, which indicate that $Q_0 \leq 0.61$. The value $Q_0 = 0.2$ for

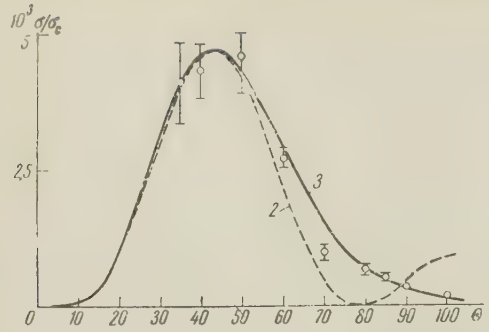

FIG. 3. Cross section of the inelastic scattering of electrons by the S^{32} nucleus with excitation of the 2.25-Mev level.

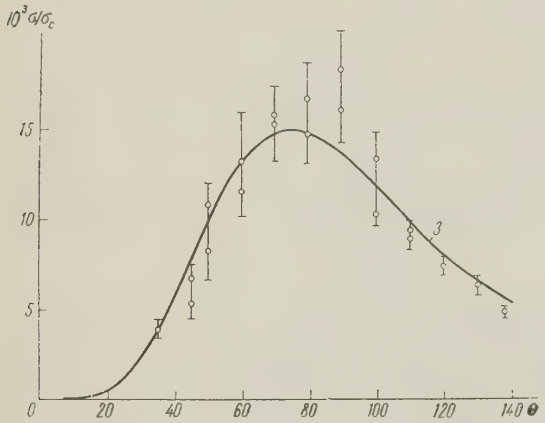

FIG. 4. Cross section of inelastic scattering of electrons by the C^{12} nucleus with excitation of the 4.43-Mev level.

C^{12} agrees well with the value $Q_0 = 0.3$ which follows from the data of Devons, Manning, and Towle,[12] if we take account of the low accuracy of their results.

The values of Q_0 obtained by us do not characterize directly the nonsphericity of the nuclei under consideration, because Q_0 depends not only on the nonsphericity but also on the size of the nucleus and on its charge. To obtain a criterion for the nonsphericity of the nucleus it is useful to introduce the concept of the equivalent ellipsoid: a uniformly charged nucleus with the shape of an ellipsoid of revolution with semi-axes a and b. This ellipsoid can be determined by the nonsphericity parameter $\eta = a/b$ and the mean square radius $\overline{r^2}_{\text{nonsph}} = \frac{3}{5}R^2$ (R is the radius of the equivalent sphere). It is easily shown, using relation (4.4), that this ellipsoid has the quadrupole moment

$$Q_0 = \frac{6}{5}\frac{\eta^2-1}{\eta^2+2}ZR^2. \qquad (5.5)$$

Using our values Q_0 and the values of R obtained from the experiments on the elastic scattering, we find the values of the nonsphericity parameter listed in the last column of Table II. We see that the nonsphericity for Mg^{24} is very large. Si^{28} has small nonsphericity. It is possible that in the case of a nucleus with such large nonsphericity the conditions for the validity of the strong coupling approximation in the unified model are violated to a considerable degree.

[1] Litherland, Paul, Bartholomew, and Gove, Phys. Rev. **102**, 208 (1956).

[2] Gove, Bartholomew, Paul, and Litherland, Nucl. Phys. **2**, 132 (1956/57).

[3] Gonchar, Inopin, and Tsytko, Тезисы 8-го совещания по ядерной спектроскопии (Reports of the Eighth Conference on Nuclear Spectroscopy) M.-L. (1958).

[4] L. I. Schiff, Phys. Rev. **96**, 765 (1954).

[5] R. Hofstadter, Ann. Rev. of Nucl. Science **7**, 231 (1957).

[6] U. Fano, Phys. Rev. **93**, 121 (1954). S. R. de Groot, Physica 18, 1201 (1952).

[7] Biedenharn, Blatt, and Rose, Revs. Modern Phys. **24**, 249 (1952).

[8] R. H. Helm, Phys. Rev. **104**, 1466 (1956).

[9] J. H. Fregeau, Phys. Rev. **104**, 225 (1956).

[10] Alkhazov, Grinberg, Gusinskiĭ, Erokhina, and Lemberg, Тезисы 9-го совещания по ядерной спектроскопии (Reports of the Ninth Conference on Nuclear Spectroscopy) M.-L. (1959).

[11] N. N. Delyagin and V. S. Shpinel', Dokl. Akad. Nauk SSSR **121**, 621 (1958), Soviet Phys.–Doklady **3**, 789 (1959).

[12] Devons, Manning, and Towle, Proc. Phys. Soc. **A69**, 173 (1955).

Translated by R. Lipperheide
262

A METHOD FOR THE CALCULATION OF PHASE VOLUMES

L. G. ZASTAVENKO

Joint Institute of Nuclear Research

Submitted to JETP editor March 31, 1959

J. Exptl. Theoret. Phys. (U.S.S.R.) 37, 1319-1323 (November, 1959)

A method for calculating phase volumes is developed for 2, 3, 4, and 5 particles. The error of the method increases with the number n of particles, but evidently does not exceed 5 percent for n = 5.

1. INTRODUCTION

PHASE volume is the name given to the quantity

$$\rho(E, M_1, M_2, \ldots, M_n) = \int d^3p_1 \int d^3p_2 \ldots \int d^3p_n \times \delta(\mathbf{p}_1 + \mathbf{p}_2 + \ldots \mathbf{p}_n)\, \delta\left(\sum_{i=1}^{n} \sqrt{M_i^2 + p_i^2} - E\right), \quad (1)$$

which is a function of the total energy E of the particles and of their masses M_i.

A knowledge of the phase volumes is needed in the Fermi statistical theory, so that methods for their calculation are dealt with in a number of papers. Fermi[1] calculated phase volumes for the case in which some of the particles are nonrelativistic and some are ultrarelativistic, with conservation of momentum not taken into account for the latter particles. In a paper by Maksimenko and Rozental'[2] these same phase volumes have been calculated with conservation of the total momentum taken into account.

Papers by Lepore and Stuart[3] and by Rozental'[4] give the expression for the phase volume when all the particles are ultrarelativistic (with total momentum conserved). Lepore and Stuart[3] have shown that the phase volume (1) can be represented in the form

$$\rho = \frac{4\pi (2\pi^2)^n \prod M_\alpha^2}{(2\pi)^4} \int_{-\infty-i\varepsilon}^{+\infty-i\varepsilon} d\lambda e^{i\lambda E} \lambda^n \times \int_{-\infty}^{+\infty} \sigma^2 d\sigma \frac{\prod_{\beta=1}^{n} H_2^{(1)}\left[-M_\beta \sqrt{\lambda^2 - \sigma^2}\right]}{[\sigma^2 - \lambda^2]^n}, \quad (2)$$

from which an expansion of ρ in powers of $1/E$ has been obtained,[2] useful in principle for the calculation of any phase volume, but which is inconvenient on account of its complication.

A paper by Fialho[5] proposes a simple method for calculating phase volumes by starting with Eq. (2) and using the method of steepest descents; this approach is useful for all energies E. We shall give a different method for calculating phase volumes, which is more accurate and convenient when the number n of particles involved is small.

2. THE PROPOSED METHOD

Our method is to calculate the function of the masses, $\rho(E, M_1, \ldots, M_n)$, for certain values of the masses M_i and then obtain the whole function of the variables $M_1, \ldots, M_n$ by interpolation.

Let us define a function $f(E, M_1, \ldots, M_n)$ by the formula

$$\rho(E, M_1, \ldots, M_n) = A_n E^{3n-4} f(E, M_1, \ldots, M_n), \qquad A_n = \frac{(\pi/2)^{n-1}(4n-4)!}{(3n-4)!\,(2n-1)!\,(2n-2)!}. \quad (3)$$

It follows from Eq. (1) that f is a homogeneous function of degree zero in its arguments. Thus if

$$x = E/\left(\sum_{\alpha=1}^{n} M_\alpha\right), \quad z_i = M_i/(\Sigma M_\alpha); \quad \sum_{i=1}^{n} z_i = 1,$$

then

$$f(E, M_1, \ldots, M_n) = f(x, z_1, \ldots, z_n). \quad (4)$$

By the formulas of Maksimenko and Rozental',[2] and also by formulas obtained in the Appendix, we have calculated tables of the functions ${}_nf_k(x)$:

$${}_nf_1(x) = f(x, 1, 0, \ldots, 0),$$

$${}_nf_2(x) = f(x, \tfrac{1}{2}, \tfrac{1}{2}, 0, \ldots, 0), \ldots,$$

$${}_nf_n(x) = f(x, 1/n, 1/n, \ldots, 1/n).$$

In order to get an approximate construction of the whole function $f(x, z_1, \ldots, z_n)$ from the ${}_nf_k(x)$,

$k = 1, 2, \ldots, n$, we have used the coefficients*

$$ {}_nC_k(z_1, z_2, \ldots, z_n) = \sum_{s=k}^{n} {}_sA_k \sum_{i_1>i_2\ldots>i_s} z_{i_1}z_{i_2}\ldots z_{i_s}, $$

$$ {}_sA_k = (-)^{s-k}sk^{s-1}(s!)\,[(k!)(s-k)!]^{-1}, \qquad (5) $$

which have the following properties which are basic for our interpolation:

$$ {}_nC_k(1, 0, 0, \ldots, 0) = 0, $$

$$ {}_nC_k\left(\tfrac{1}{2}, \tfrac{1}{2}, 0, \ldots, 0\right) = 0, \ldots $$

$$ \ldots \text{and only } {}_nC_k(\overbrace{1/k, 1/k, \ldots, 1/k}^{k \text{ times}}, 0, \ldots, 0) = 1 \qquad (6) $$

and which also satisfy the relation:

$$ \text{if } \Sigma z_i = 1, $$

then

$$ \sum_{k=n}^{n} {}_nC_k(z_1, z_2, \ldots, z_n) = 1. \qquad (7) $$

As an approximation to the phase volume we take the function

$$ \tilde{\rho}(E, M_1, \ldots, M_n) = A_nE^{3n-4} $$

$$ \times\left\{\sum_{k=1}^{n} {}_nC_k(z_1, \ldots, z_n)\,[{}_nf_k(x)]^{2/3}\right\}^{3/2}. \qquad (8) $$

Here z_i and x are expressed in terms of M_i and E by (4), the functions $[{}_nf_k(x)]^{2/3}$ are found from Table I in reference 8, the coefficients ${}_nC_k(z_1, \ldots, z_n)$ are defined by (5), and the coefficient A_n is defined by (3).

In virtue of (7) and the fact that for $x \to \infty$ all the functions ${}_nf_k(x)$ become the same, in the ultrarelativistic case $\tilde{\rho}$ no longer depends on the masses, as should be true of the phase volume. Since for $x \to 1$ the functions ${}_nf_n(x)$ are much larger than all the others, by Eq. (5) the function $\tilde{\rho}$ has the right dependence on the masses of the particles in the nonrelativistic case:

$$ \tilde{\rho} \sim \left(\prod_{\alpha=1}^{n} M_\alpha\right)^{3/2} $$

Thus our interpretation is confirmed by the agreement of $\tilde{\rho}$ with the known nonrelativistic and ultrarelativistic limits.

Equation (8) is indeed our final formula. We emphasize that the table of $[{}_nf_k(x)]^{2/3}$ in reference 8 has been constructed only for $n = 2, 3, 4, 5$.

*The writer is grateful to V. B. Magalinskiĭ for pointing out this unified formula for the ${}_nC_k$

To estimate the errors of the method we have made a comparison of the values of $\tilde{\rho}(E, M_1, M_2, \ldots)$ calculated from Eq. (6) with the exact values of the function $\rho(E, M_1, M_2, \ldots)$ found from the formulas of Maksimenko and Rozental' and of the Appendix, for certain values of E and M for 2, 3, and 5 particles (cf. Table II in reference 8).

The comparison gives a basis for the supposition that if the masses of any two particles do not differ by more than a factor 10, for numbers of particles up to and including 5 our method gives an error of not more than 5 percent (for $n = 2$ the largest error we have found in the method is 2.2 percent; it occurs when the mass m_1 of one of the particles goes to zero, and the total energy E goes to the rest mass m_2 of the second particle in such a way that $E - m_2 \approx 2m_1$).

In conclusion I express my deep gratitude to Professor M. A. Markov and to L. A. Chudov, V. I. Ogievetskiĭ, and G. I. Kopylov for the support they have given me and for a valuable consultation. The writer is also grateful to the staff of the computation laboratory directed by G. I. Kopylov for making the numerical calculations and to V. M. Maksimenko for making it possible for me to familiarize myself with his paper[2] before its publication.

APPENDIX

The expansions obtained by Maksimenko and Rozental'[2] were used for the calculation of the functions ${}_nf_k(x)$ for $x - 1 \gtrsim 1$. For $x - 1 \lesssim 1$ these expansions become inconvenient, and we found it necessary to obtain an expansion of the function ρ in powers of $x - 1$. For this purpose, in turn, we had to obtain a representation of the phase volume in the form of a single contour integral.

A. Transformation of the Integral (2)

In reference 2 the expression (2) is given in the form

$$ \rho = \frac{\pi^{n-3}}{2^{n+2}}\left(\prod_{\alpha=1}^{n} M_\alpha^2\right)\int_{-\infty-i\varepsilon}^{+\infty-i\varepsilon}\int dxdy e^{i(x+y)E} $$

$$ \times \frac{(x-y)^2}{(xy)^n} i^n (x+y)^n \times \prod_{\alpha=1}^{n}\left\{\frac{\pi}{i}H_2^{(2)}(2M_\alpha\sqrt{xy})\right\}. \qquad (A.1) $$

This expression can be written in the form (we write $\nu_\alpha = M_\alpha/E$)

$$ \rho = \frac{\pi^{n-3}}{2^{n+2}}\left(\frac{d}{dE}\right)^n E^{4n-4}\left(\prod_{\alpha=1}^{n}\nu_\alpha^2\right)\iint dxdy e^{i(x+y)}\frac{(x-y)^2}{(xy)^n} $$

$$ \times \prod_{\alpha=1}^{n}\left\{\frac{\pi}{i}H_2^2(2\nu_\alpha\sqrt{xy})\right\}. \qquad (A.2) $$

Substituting $x = t\tau$, $y = t/\tau$ in this formula, we get

$$U \equiv \iint dxdy \frac{e^{i(x+y)}}{(xy)^n} (x-y)^2 \prod_{\alpha=1}^{n} \left\{ \frac{\pi \nu_\alpha^2}{i} H_2^{(2)}(2\nu_\alpha \sqrt{xy}) \right\}$$

$$= \frac{8\pi}{i} 2^{2n-3} \int_{-\infty-i\varepsilon}^{+\infty-i\varepsilon} dt \frac{J_1(t)}{t^{2n-2}} \prod_{\alpha=1}^{n} \left\{ \frac{\pi}{i} \nu_\alpha^2 H_2^{(2)}(\nu_\alpha t) \right\}.$$

Thus we have

$$\rho(E, M_1, M_2, \ldots) = 2^{-n-2}\pi^{n-3}(d/dE)^n E^{3n-4} U, \quad \text{(A.3)}$$

and U contains only a single integral.

B. Expansion of the Function $\rho(E, M_1, M_2, \ldots)$ in Powers of $E-1$

We substitute in Eq. (A.3) the formula

$$-i\pi H_2^{(2)}(\nu t) = (2\pi/\nu t)^{1/2} \exp\{i(3\pi/4 - \nu t)\}\, {}_2F_0$$

$$\times \left(\tfrac{5}{2}, -\tfrac{3}{2}; -1/2i\nu t\right),$$

where (cf. reference 6)

$${}_2F_0\left(\tfrac{5}{2}, -\tfrac{3}{2}; x\right) = \sum_{k=0}^{\infty} \frac{\Gamma\left(\frac{5}{2}+k\right)\Gamma\left(-\frac{3}{2}+k\right)}{\Gamma\left(\frac{5}{2}\right)\Gamma\left(-\frac{3}{2}\right)k!} x^k. \quad \text{(B.1)}$$

For the values of α for which $\nu_\alpha = 0$, we must take $\nu^2 H_2^{(2)}(\nu t) = 4t^{-2}$. We get

$$U = \frac{8\pi}{i} 2^{(5n+3l-6)/2}\pi^{(n-l)/2} e^{3\pi i m/4} \prod_{\alpha=1}^{m} \nu_\alpha^{3/2} \sum_{k_1, k_2, \ldots=0}^{\infty} 2^{-k} e^{i\pi k/2}$$

$$\times \frac{a_{k_1} a_{k_2} \ldots a_{k_m}}{\nu_1^{k_1} \nu_2^{k_2} \ldots \nu_m^{k_m}} \int_{-\infty-i\varepsilon}^{+\infty-i\varepsilon} dt \cdot t^{-5n/2-k-3l/2} e^{-i\nu t} J_1(t),$$

$$\nu = \sum_{\alpha=1}^{m} \nu_\alpha, \quad k = \sum_{\alpha=1}^{m} k_\alpha. \quad \text{(B.2)}$$

Here l is the number of particles with mass zero, $m = n - l$, and a_k is the coefficient of x^k in Eq. (B.1). The integral in Eq. (B.2) is calculated by a procedure like that of reference 6, page 421; by use of quadratic identities for the hypergeometric functions it can be brought to the form

$$\int dt J_1(t) e^{-i\nu t} t^{2-k-5n/2-3l/2} = 2\pi i 2^{2-k-5n/2-3l/2}$$

$$\times \exp\left\{-i\frac{\pi}{2}\left(4-k-\frac{5n}{2}-\frac{3l}{2}\right)\right\} [2(1-\nu)]^{5n/2-3/2+k+3l/2}$$

$$\times \frac{F\left(\frac{3}{2}, -\frac{1}{2}; \gamma_k; (1-\nu)/2\right)}{\sqrt{\pi}\,\Gamma(\gamma_k)}. \quad \text{(B.3)}$$

Substituting the expression for U so obtained in Eq. (A.3), we find

$$\rho(E, M_1, M_2, \ldots, M_m, 0, 0, \ldots, 0) = 2^{2l}(2\pi)^{(3n-l-3)/2}$$

$$\times \left(\frac{d}{dE}\right)^n \left(\prod_{\alpha=1}^{m} M_\alpha^{3/2}\right) \sum \frac{a_{k_1} \ldots a_{k_m} (-)^k}{\nu_1^{k_1} \ldots \nu_m^{k_m} (2E)^k \Gamma(\gamma_k)}$$

$$\times \frac{(E-M)^{\gamma_k - 1}}{E^{3/2}} {}_2F_1\left(\frac{3}{2}, -\frac{1}{2}; \gamma_k; \frac{E-M}{2E}\right). \quad \text{(B.4)}$$

Here and in the preceding formula $\gamma_k = (5n + 3l - 3)/2 + k$.

To obtain formulas for the calculation of the functions we want we still have to perform the differentiation in Eq. (B.4). Let us define the numbers $\varphi_p^{(n)}$ by the relation

$$\left(\frac{d}{dE}\right)^n \frac{(E-M)^{\gamma-1}}{E^{3/2}} {}_2F_1\left(\frac{3}{2}, -\frac{1}{2}; \gamma; \frac{E-M}{2E}\right)$$

$$= \frac{(\gamma-1)(\gamma-2)\ldots(\gamma-n)}{\left(\frac{1}{2}+1\right)\left(\frac{1}{2}+2\right)\ldots\left(\frac{1}{2}+n\right)}$$

$$\times \sum_{p=0}^{\infty} \frac{\left(\frac{3}{2}\right)_p \left(-\frac{1}{2}-n\right)_p (E-M)^{\gamma+p-n}}{(\gamma-n)_p p!\, 2^p E^{p+3/2}} \varphi_p^{(n)},$$

$$(\alpha)_p \equiv \alpha(\alpha+1)\ldots(\alpha+p-1). \quad \text{(B.5)}$$

The $\varphi_p^{(n)}$ satisfy the obvious relation

$$2p\varphi_{p-1}^{(n)} - \left(p-n-\frac{3}{2}\right)\varphi_p^{(n)} = \varphi_p^{(n+1)}$$

and the relation

$$\varphi_{p+1}^{(n+1)} - \varphi_p^{(n+1)} = (n+1)\varphi_p^{(n)},$$

which is extremely convenient for their calculation.

Substituting Eq. (B.5) in Eq. (B.4), we get the final expression

$$\rho(E, M_1, M_2, \ldots M_m, 0, \ldots) = 2^{2l}(2\pi)^{[3(n-1)-l]/2}$$

$$\times \frac{(\Pi M_\alpha^{3/2})}{E^{3/2}} \frac{(E-M)^{[3(n+l)-5]/2}}{\Gamma([3(n+l)-3]/2)}$$

$$\times \sum \frac{(-)^k a_{k_1} \ldots a_{k_m} (E-M)^k \Gamma([3(n+l)-3]/2)}{2^k M_1^{k_1} \ldots M_m^{k_m} \Gamma([3(n+l)-3]/2+k)}$$

$$\times F_{nlk}\left(\frac{E-M}{2E}\right), \quad \text{(B.6)}$$

where

$$F_{nlk}(x) = \sum_{p=0}^{\infty} \frac{\left(\frac{3}{2}\right)_p \left(-\frac{1}{2}-n\right)_p \varphi_p^{(n)} x^p}{([3(n+l)-3]/2+k)_p\, p! \left(\frac{3}{2}\right)_p}$$

The basis functions ${}_n\rho_m(E)$ are obtained if in Eq. (B.6) we take $M_1 = M_2 = \ldots M_m = 1/m$.

[1] E. Fermi, Prog. Theor. Phys. **5**, 570 (1950).

[2] V. M. Maksimenko and I. L. Rozental', JETP **32**, 658 (1957), Soviet Phys. JETP **5**, 546 (1957).

[3] J. V. Lepore and R. N. Stuart, Phys. Rev. **94**, 1724 (1954).

[4] I. L. Rozental', JETP **28**, 118 (1955), Soviet Phys. JETP **1**, 166 (1955).

[5] G. E. A. Fialho, Phys. Rev. **105**, 328 (1957).

[6] G. N. Watson, A Treatise on the Theory of Bessel Functions (Russian Transl.), IIL, Moscow, 1949, Part 1, page 222. [Cambridge, 1944].

[7] E. T. Whittaker and G. N. Watson, A Course in Modern Analysis (Russian Transl.), Gostekhizdat, Leningrad-Moscow, 1944, Part II, page 83. [Cambridge, 1940].

[8] L. G. Zastavenko, Метод вычисления фазовых обьемов (A Method for the Calculation of Phase Volumes)(preprint, Joint Institutelof Nuclear Studies).

Translated by W. H. Furry
263

THE FARADAY EFFECT IN SEMICONDUCTORS DUE TO FREE CARRIERS IN A STRONG MAGNETIC FIELD

L. É. GUREVICH and I. P. IPATOVA

Institute for Technical Physics, Academy of Sciences, U.S.S.R., Leningrad

Submitted to JETP editor April 4, 1959

J. Exptl. Theoret. Phys. (U.S.S.R.) 37, 1324-1329 (November, 1959)

The dielectric constant tensor is determined for semiconductors with electrons with an anisotropic mass in a strong magnetic field. The Faraday effect is considered for the case of hexagonal crystals with an energy minimum in the center of the Brillouin zone and for a cubic crystal with a minimum which does not coincide with the center of the Brillouin zone. The refractive indices evaluated for different directions of the magnetic field relative to the main crystallographic directions in these crystals are found to depend strongly on the magnetic field direction. This enables us to determine the effective mass tensor by measuring the angle of rotation of the plane of polarization.

A large number of theoretical and experimental papers have been devoted in recent years to a study of the energy surfaces of the conduction electrons and to a determination of the effective mass tensor in semiconductors (see, for instance, reference 1).

One possible method of investigation is a study of the optical properties of semiconductors, in particular, the Faraday effect, i.e., the rotation of the plane of polarization in a magnetic field.

The Faraday effect in the microwave region can give information about the mobility of the conduction electrons;[2-4] the Faraday effect in the infrared region enables us, as was shown by Mitchell,[6] to determine directly the electron effective mass since one can in that region neglect the collisions between the electrons ($\omega\tau > 1$, where τ is the relaxation time). Experimental investigations by Moss, Smith, and Taylor[7] gave values for the effective mass for InSb which agreed with the results of Spitzer and Fan[8] who determined the effective mass from the coefficients of reflectivity and refraction.

The theoretical part of references 2 — 5 is based upon a classical model of free electrons with an isotropic mass in weak magnetic fields ($eH\tau/mc < 1$). Lax and Roth studied an electron with an anisotropic mass for the case of a magnetic field H in the [111] direction of a cubic crystal. This study referred, however, only to the case of a weak magnetic field. The phenomenon becomes essentially a quantum one in a strong magnetic field, showing up in a dependence of the chemical potential ζ on the magnitude and direction of the magnetic field. When there are several energy minima this leads to a non-equilibrium propagation of the electrons at those minima. The study by Lax and Roth is, however, insufficient even in the case of weak magnetic fields. The fact is that the frequency dependence of the Faraday effect depends in an important way on the direction of the magnetic field H. Generally speaking, the dielectric constant in a cubic crystal with several energy minima contains, for different directions of H, two resonance terms with sharp resonance frequencies. These frequencies coincide if the field is parallel to the [111] direction, and only this particular case was considered in reference 9.

It is the aim of the present paper to study the Faraday effect in the infrared region ($\omega\tau > 1$) for a conduction electron with an anisotropic mass and for different directions of a strong magnetic field.[10] We shall then obtain a solution of the problem of an electron with an anisotropic mass in a strong magnetic field which is considerably more convenient than Klinger and Voronyuk's solution.[11]

1. AN ELECTRON WITH AN ANISOTROPIC MASS IN A STRONG MAGNETIC FIELD

We take the magnetic field along the z axis and choose the vector potential in the form

$$\mathbf{A}^0 = (-Hy, 0, 0). \tag{1}$$

The Hamiltonian is then

$$\hat{H} = \frac{1}{2m} \mathrm{S} \mu_{jk} \left(p_j - \frac{e}{c} A_j^0\right)\left(p_k - \frac{e}{c} A_k^0\right), \tag{2}$$

where the μ_{jk} are the dimensionless components of the inverse mass tensor, and S is the symmet-

rization operator for non-commuting factors. We can use an effective mass representation since we are interested in the behavior of the electrons in a uniform field or in fields that vary sufficiently smoothly in space.[12]

The eigenfunctions and energy eigenvalues of the Hamiltonian (2) are of the form

$$\Psi^0_{np_xp_z} = \exp\left\{\frac{i}{\hbar}(p_x x + p_z z) - i\,\frac{\mu_{12}}{\mu_{22}}\,\frac{eH}{2\hbar c}(y-y_1)^2\right\}$$

$$\times \exp\left\{-\frac{m\Omega}{2\mu_{22}\hbar}(y-y_0)^2\right\}\mathcal{H}_n\left[\sqrt{\frac{m\Omega}{\mu_{22}\hbar}}(y-y_0)\right], \quad (3)$$

$$E(n,\ p_z) = \hbar\Omega\left(n+\frac{1}{2}\right) + \eta_1 p_z^2/2m. \quad (4)$$

Here $\mathcal{H}_n$ is the wave function of the harmonic oscillator with frequency

$$\Omega = (eH/mc)\sqrt{M_{33}} = \Omega_0\sqrt{M_{33}}, \quad (5)$$

$$y_1 = -(c/eH)(p_z\mu_{23}/\mu_{12} + p_x), \quad (6)$$

$$y_0 = -(c/eH)(p_z M_{31}/M_{33} + p_x), \quad (7)$$

$$\eta_1 = (M_{11}M_{33} - M_{13}^2)/\mu_{22}M_{33}, \quad (8)$$

where M_{jk} are the cofactors of the components of the inverse mass tensor.

We shall express the μ_{jk} in terms of the principal values of the inverse mass tensor μ_j (j = 1, 2, 3). To do this we perform a rotation from a coordinate system (xyz) where H is along the z axis to the system of the principal axes of the μ_{jk} tensor (XYZ). Such a transition can be realized, for instance, using two rotations: a) a rotation around Z through an angle φ such that $H_{Y'} = 0$ in the new coordinate system, and b) a rotation around Y′ through an angle φ' such that in the new coordinate system $H_X = 0$, $H_Y = 0$, $H_Z = H$ (see the figure). The table of rotational cosines can be written in terms of the angles φ_i between the direction of the magnetic field and the principal axes of the μ_{jk} tensor.

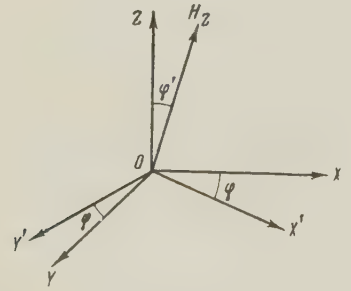

	X	Y	Z
x	$\cos\varphi_1\cot\varphi_3$	$\cos\varphi_2\cot\varphi_3$	$-\sin\varphi_3$
y	$-\cos\varphi_2/\sin\varphi_3$	$\cos\varphi_1/\sin\varphi_3$	0
z	$\cos\varphi_1$	$\cos\varphi_2$	$\cos\varphi_3$

Using this table Eqs. (5) and (8) can be rewritten in the form

$$\Omega = \Omega_0\left[\mu_1\mu_2\mu_3\left(\frac{\cos^2\varphi_1}{\mu_1} + \frac{\cos^2\varphi_2}{\mu_2} + \frac{\cos^2\varphi_3}{\mu_3}\right)\right]^{1/2}, \quad (9)$$

$$\eta_1 = \left(\frac{\cos^2\varphi_1}{\mu_1} + \frac{\cos^2\varphi_2}{\mu_2} + \frac{\cos^2\varphi_3}{\mu_3}\right)^{-1} \quad (10)$$

2. THE EVALUATION OF THE DIELECTRIC CONSTANT TENSOR

When light is propagated along the magnetic field, the perturbation energy is

$$\hat{H}' = -\frac{e}{2mc}\mu_{jk}\left[A_j^1\left(p_k - \frac{e}{c}A_k^0\right) + \left(p_k - \frac{e}{c}A_k^0\right)A_j^1\right], \quad (11)$$

where

$$\mathbf{A}^1 = \frac{c}{i\omega}\left[\mathbf{E}_0 e^{i(fz-\omega t)} - \mathbf{E}_0^+ e^{-i(fz-\omega t)}\right] \quad (12)$$

is the vector potential of the light wave.

The current density

$$(I_j)_n = \frac{e}{2m}\left\{\Psi^*_{n'}\mu_{jk}\left(p_k - \frac{e}{c}A_k^0\right)\Psi_n - \Psi_{n'}\mu_{jk}\left(p_k + \frac{e}{c}A_k^0\right)\Psi^*_{n'}\right\}$$
$$- \frac{e^2}{mc}\mu_{jk}A_k^1\Psi^*_{n'}\Psi_n \quad (13)$$

(n indicates here the set of values n, p_X, p_Z) evaluated using the first-order perturbation-theory wave functions, must be averaged over a statistical electron distribution $\exp\{(\zeta - E)/T\}$. Taking into account that $E(n, p_Z)$ is independent of p_X and that $f \ll p/\hbar$ and comparing the results of the averaging with the relation

$$I_j = i\omega E_k(\varepsilon_{jk} - \varepsilon^0_{jk})/4\pi, \quad (14)$$

which is well known from electrodynamics, we get for the dielectric-constant tensor

$$\varepsilon_{jk} = \varepsilon^0_{jk} + \frac{4\pi e^2 N}{m\omega^2}\,\frac{\omega^2\mu_{jk} - i\,(e/mc)\,\omega\delta_{jkl}M_{ls}H_s - (e/mc)^2\Delta H_j H_k}{(e/mc)^2 H_\alpha H_\beta M_{\alpha\beta} - \omega^2}, \quad (15)$$

where ϵ^0_{jk} is the dielectric-constant tensor caused by the bound charges, δ_{jkl} the antisymmetric unit tensor, and Δ the determinant of the inverse mass tensor. The conduction electron density $N = \exp(\zeta/T)Z/V$ must be determined from the neutrality condition. Here, ζ is the chemical potential and Z the partition function:

$$Z = Z_0\hbar\Omega/2T\sqrt{\mu_1\mu_2\mu_3}\sinh(h\Omega/2T),$$

$$Z_0 = 2(2\pi)^{-3}(2\pi mT/\hbar^2)^{3/2}. \quad (16)$$

One should note that Eq. (15) remains valid for an arbitrary orientation of the light wave relative to the magnetic field.

Hexagonal crystals. We shall consider the case where the bands are unconnected, where the energy minimum corresponds to the center of the Brillouin zone, and where the energy surface is an ellipsoid

of revolution. If the axis of revolution is along Z, we must put in (15) $\mu_1 = \mu_2$. In hexagonal crystals the principal axes of the ϵ_{jk} and the μ_{jk} tensor are the same. If there is no magnetic field ϵ^0_{jk} will have three non-vanishing components $\epsilon^0_{xx} = \epsilon^0_{yy} \neq \epsilon^0_{zz}$. We get from Eq. (16) and the neutrality condition for the electron density in an impurity semiconductor (in the limiting case $\hbar\Omega > T$)

$$N = \frac{e^{\zeta/T}Z}{V} = \left(\frac{Z_0}{2V}\frac{\hbar\Omega}{2T}\frac{1}{\mu_1\sqrt{\mu_3}}N_1\right)^{1/2}\exp\left\{-\frac{\Delta\epsilon}{2T}-\frac{\hbar\Omega}{4T}\right\}, \tag{17}$$

where N_1 is the impurity concentration and $\Delta\epsilon$ is the energy gap between the impurity level and the bottom of the conduction band.

Using the table we can write ϵ_{jk} in a coordinate system where the z axis is chosen along the magnetic field H and the optical axis of the crystal makes an angle φ_3 with H:

$$\varepsilon_{xx} = \left(\varepsilon^0_x + \frac{\nu^2\mu_1}{\Omega^2-\omega^2}\right)\cos^2\varphi_3 + \left(\varepsilon^0_z + \frac{\nu^2\mu_3}{\Omega^2-\omega^2}\right)\sin^2\varphi_3,$$

$$\varepsilon_{yy} = \left(\varepsilon^0_x + \frac{\nu^2\mu_1}{\Omega^2-\omega^2}\right),$$

$$\varepsilon_{zz} = \left(\varepsilon^0_x + \frac{\nu^2\mu_1}{\Omega^2-\omega^2}\right)\sin^2\varphi_3 + \left(\varepsilon^0_z + \frac{\nu^2\mu_3}{\Omega^2-\omega^2}\right)$$

$$\times\cos\varphi_3 - \frac{\nu^2\Omega_0^2\Delta}{\omega^2(\Omega^2-\omega^2)},$$

$$\varepsilon_{xy} = -i\nu^2\Omega^2/\Omega_0\omega(\Omega^2-\omega^2),$$

$$\varepsilon_{xz} = \left[\varepsilon^0_x + \frac{\nu^2\mu_1}{\Omega^2-\omega^2} - \varepsilon^0_z - \frac{\nu^2\mu_3}{\Omega^2-\omega^2}\right]\cos\varphi_3\sin\varphi_3,$$

$$\varepsilon_{yz} = -i\nu^2\Omega_0\mu_1(\mu_3-\mu_1)\cos\varphi_3\sin\varphi_3/\omega(\Omega^2-\omega^2), \tag{18}$$

where

$$\nu^2 = \frac{4\pi e^2 N}{m}, \qquad \Omega = \Omega_0\left[\mu_1^2\mu_3\left(\frac{\sin^2\varphi_3}{\mu_1}+\frac{\cos^2\varphi_3}{\mu_3}\right)\right]^{1/2}$$

We consider two cases:

a) $\varphi_3 = 0$, the magnetic field is along the optical axis. Then $\epsilon_{xx} = \epsilon_{yy}$; $\epsilon_{xz} = \epsilon_{yz} = 0$, $\Omega = \Omega_0\mu_1$. The refractive indices for left and right hand polarized light are $n^2_\pm = \epsilon_{xx} \pm i\epsilon_{xy}$ (see reference 13). The angle of rotation is determined by the formula

$$\varphi = \frac{\omega}{c}\left(\frac{n_+ - n_-}{2}\right)d, \tag{19}$$

where d is the thickness of the layer.

b) $\varphi_3 = 90°$, the magnetic field is perpendicular to the optical axis.

$$\varepsilon_{xx} \neq \varepsilon_{yy};\ \varepsilon_{xz} = \varepsilon_{yz} = 0, \qquad \Omega = \Omega_0\sqrt{\mu_1\mu_3}.$$

There are now two elliptically polarized waves with refractive indices

$$n^2_\pm = \frac{1}{2}(\varepsilon_{xx}+\varepsilon_{yy}) \pm \sqrt{\frac{1}{4}(\varepsilon_{xx}-\varepsilon_{xy})^2 + \varepsilon_{xy}\varepsilon_{yx}} \tag{20}$$

which pass through the crystal and we measure the angle between the major axis of the ellipse of the transmitted wave and the direction of the polarization of the incident wave.

Cubic crystals. To be specific, we shall consider the Faraday effect in silicon. It is well known from cyclotron resonance experiments[1] that the conduction electron energy surface in quasi-momentum space consists of six ellipsoids of revolution which are situated along the fourth order axes of the cubic crystal.

The dielectric constant tensor has the form (15) for each ellipsoid, if we put $\epsilon^0_{jk} = \epsilon^0\delta_{jk}$, $\mu_1 = \mu_2$ and determine the electron concentration from the neutrality condition:[11] $\Sigma N_i + N_0 = N_1$, where N_0 is the density of electrons in the impurity levels, N_1 the impurity concentration, and

$$N_i = \left(\frac{Z_0}{V}\frac{\hbar\Omega_0}{2T}N_1\right)^{1/2}(\sin^2\varphi_i/\mu_1 + \cos 2\varphi_i/\mu_3)\exp\left(-\frac{\hbar\Omega_i}{2T}\right)\Big/2$$

$$\times\sum_{t=1}^{3}(\sin^2\varphi_t/\mu_1 + \cos^2\varphi_t/\mu_3)^{1/2}\exp\left(-\frac{\hbar\Omega_t}{2T}\right)$$

is the electron density for the i-th ellipsoid.

Since the electromagnetic field cannot transfer electrons from one energy minimum to another because the wave vector is small, we get for the dielectric constant of a cubic crystal a sum over all ellipsoids taking their relative position in the Brillouin zone into account. We shall take the coordinate axes along the four-fold axes of the cubic crystal, and then

$$\varepsilon_{XX} = \varepsilon_0 + \frac{1}{3}\left\{\frac{\mu_1\nu_3^2}{\Omega_3^2-\omega^2} + \frac{\mu_1\nu_2^2}{\Omega_2^2-\omega^2} + \frac{\mu_3\nu_1^2}{\Omega_1^2-\omega^2} - \left(\frac{\Omega_0}{\omega}\right)^2\right.$$

$$\left.\times\Delta\cos^2\varphi_3\sum_i\frac{\nu_i^2}{\Omega_i^2-\omega^2}\right\},$$

$$\varepsilon_{XY} = -i\frac{\Omega_0}{3\omega}\left\{\frac{\mu_1^2\nu_3^2}{\Omega_3^2-\omega^2} + \frac{\mu_1\mu_3\nu_2^2}{\Omega_3^2-\omega^2} + \frac{\mu_1\mu_3\nu_1^2}{\Omega_1^2-\omega^2}\right\}\cos\varphi_3$$

$$-\frac{1}{3}\left(\frac{\Omega_0}{\omega}\right)^2\Delta\cos\varphi_2\cos\varphi_1\sum\frac{\nu_i^2}{\Omega_i^2-\omega^2}.$$

All other components of the ϵ_{jk} tensor can easily be written down from symmetry considerations. Here

$$\nu_i^2 = \frac{4\pi e^2 N_i}{m}, \qquad \Omega_i = \Omega_0\left[\mu_1^2\mu_3\left(\frac{\sin^2\varphi_i}{\mu_1}+\frac{\cos^2\varphi_i}{\mu_3}\right)\right]^{1/2}.$$

Using the rotation determined by the table we can write down ϵ_{jk} in the coordinate system where the z axis is taken along the magnetic field. We shall consider the following cases:

a) H ∥ [001], $\varphi_3 = 0$. We have then

$$\varepsilon_{xx} = \varepsilon_{yy} = \varepsilon_0 + \frac{1}{3}\left\{\frac{\mu_1 \nu_3^2}{\Omega_3^2 - \omega^2} + \frac{(\mu_1 + \mu_3)\nu_1^2}{\Omega_1^2 - \omega^2}\right\},$$

$$\varepsilon_{xy} = -\frac{i}{3\Omega_0\omega}\left\{\frac{\Omega_3^2\nu_3^2}{\Omega_3^2 - \omega^2} + \frac{2\Omega_1^2\nu_1^2}{\Omega_1^2 - \omega^2}\right\},$$

$$\varepsilon_{xz} = \varepsilon_{yz} = 0, \quad \Omega_1 = \Omega_0\sqrt{\mu_1\mu_3}, \quad \Omega_3 = \Omega_0\mu_1.$$

In this case the angle of rotation is given by Eq. (19).

b) $H \parallel [111]$, $\varphi_1 = \varphi_2 = \varphi_3$. Then

$$\varepsilon_{xx} = \varepsilon_{yy} = \varepsilon_0 + (2\mu_1 + \mu_3)\nu_3^2/3(\Omega_3^2 - \omega^2),$$
$$\varepsilon_{xy} = -(i/\Omega_0\omega)\Omega_3^2\nu_3^2/(\Omega_3^2 - \omega^2),$$
$$\varepsilon_{xz} = \varepsilon_{yz} = 0, \quad \Omega_3 = \Omega_0\left[\frac{1}{3}(2\mu_1\mu_3 + \mu_1^2)\right]^{1/2}.$$

Here again the angle of rotation is determined using (19) and the expressions for the refractive indices $n_\pm^2 = \epsilon_{XX} \pm i\epsilon_{XY}$ are the same as those found in reference 9.

c) $H \parallel [110]$, $\varphi_3 = 90°$. Then

$$\varepsilon_{xx} = \varepsilon_0 + \frac{1}{3}\left[\frac{\mu_3\nu_3^2}{\Omega_3^2 - \omega^2} + \frac{2\mu_1\nu_1^2}{\Omega_1^2 - \omega^2}\right],$$

$$\varepsilon_{yy} = \varepsilon_0 + \frac{1}{3}\left[\frac{\mu_1\nu_3^2}{\Omega_3^2 - \omega^2} + \frac{(\mu_1 + \mu_3)\nu_1^2}{\Omega_1^2 - \omega^2}\right],$$

$$\varepsilon_{xy} = -i\frac{1}{3\Omega_0\omega}\left[\frac{\Omega_3^2\nu_3^2}{\Omega_3^2 - \omega^2} + \frac{2\Omega_1^2\nu_1^2}{\Omega_1^2 - \omega^2}\right],$$

$$\varepsilon_{xz} = \varepsilon_{yz} = 0, \quad \Omega_1 = \Omega_0\left[\frac{1}{2}\mu_1(\mu_3 + \mu_1)\right]^{1/2}, \quad \Omega_3 = \Omega_0\sqrt{\mu_1\mu_3}.$$

The refractive indices are determined in this case from (20), and we measure the angle between the rotation of the ellipse of the transmitted wave and the direction of the polarization of the incident wave.

We see that in all cases considered, the dependence of the indices of refraction and thus also of the angle of rotation of the polarization ellipse on the frequency of the light has a resonance character, and that the magnitude of the resonance for the frequencies depends on the direction of the magnetic field. In the case $H \parallel [111]$ there is one resonance maximum. If, however, the field is parallel to the [001] or the [110] direction there are two resonance maxima. This makes it possible to determine the effective mass of conduction electrons both at the cyclotron resonance of the angle of rotation and also outside the resonance.

We need only take the quantum motion of the electrons into account for the evaluation of the electron concentration N_i, which leads to an exponential dependence of N_i on H.

In the limiting case of an isotropic mass our formulae go over into those of Rau and Caspari,[3] if we neglect in the latter the collision frequencies. In strong magnetic fields there is an additional exponential dependence of the electron concentration on the field.

[1] B. Lax, Revs. Modern Phys. **30**, 122 (1958).
[2] H. Suhl and G. L. Pearson, Phys. Rev. **92**, 858 (1953).
[3] R. R. Rau and M. E. Caspari, Phys. Rev. **100**, 632 (1955).
[4] R. Rau and P. H. Miller Jr., Phys. Rev. **98**, 1533 (1955).
[5] M. I. Klinger and M. M. Chaban, J. Tech. Phys. (U.S.S.R.) **26**, 938 (1956), Soviet Phys. Tech. Phys. **1**, 921 (1956).
[6] E. W. J. Mitchell, Proc. Phys. Soc. (London) **B68**, 973 (1955).
[7] Moss, Smith, and Taylor, J. Phys. Chem. Solids **8**, 323 (1959).
[8] W. G. Spitzer and H. Y. Fan, Phys. Rev. **106**, 882 (1957).
[9] B. Lax and L. M. Roth, Phys. Rev. **98**, 548 (1955).
[10] L. Landau, Z. Physik **64**, 629 (1930).
[11] M. I. Klinger and P. I. Voronyuk, JETP **33**, 77 (1957), Soviet Phys. JETP **6**, 59 (1958).
[12] J. M. Luttinger and W. Kohn, Phys. Rev. **97**, 869 (1955).
[13] M. Born, Optik (Russ. Transl.), 1937, part 1, Ch. V.

Translated by D. ter Haar
264

EXPANSION OF THE AMPLITUDE FOR A REACTION WITH PRODUCTION OF THREE LOW-ENERGY PARTICLES IN POWERS OF THE THRESHOLD MOMENTA

I. T. DYATLOV

Leningrad Physical and Technological Institute, Academy of Sciences, U.S.S.R.

Submitted to JETP editor May 16, 1959

J. Exptl. Theoret. Phys. (U.S.S.R.) 37, 1330-1336 (November, 1959)

It is shown that in the expansion near threshold of the amplitude for an arbitrary process in powers of the threshold momenta, the linear terms and the part of the quadratic terms that determines the angular distributions can be obtained from a consideration of the analytic properties of the amplitude.

1. As has been shown by Gribov,[1] the wave function of three low-energy particles whose interaction can be described by a potential that depends only on the distances between them differs from the wave function at zero energy by the factor

$$1 + ik_{12}a_{12} + ik_{13}a_{13} + ik_{23}a_{23},$$

$$k_{ik} = (\mathbf{p}_i m_k - \mathbf{p}_k m_i)/(m_i + m_k), \qquad (1)$$

where $\mathbf{p}_i$ and m_i are the momentum and mass of the i-th particle, and a_{ik} is the scattering amplitude of particles i and k at zero energy.

In the present paper this result is obtained for the amplitude of an arbitrary process in which the final state contains three low-energy particles with $|\mathbf{p}_i| \ll m$, where m is the minimum mass determining the radius of the interaction ($\hbar = c = 1$). The derivation is based on the analytic properties of the amplitude, which is represented as the combination of all possible Feynman diagrams. In addition it is shown that this method makes it possible to find the terms of second order in the threshold momenta $|\mathbf{p}_i|$ that determine the angular correlations of the particles produced in the reaction,[1] and to find the energy dependence of the amplitude in reactions of the type $a + A \to b + B$ near the threshold for production of particles of a third type $c + C$; this energy dependence has been considered by Baz'.[2]

The extension of the results to the case of reactions with more than three particles in the final state is obvious.

2. Let us consider the amplitude of a reaction in which the collision of two particles with the four-dimensional momenta p_1' and p_2' leads to the production of three particles with momenta p_1, p_2, p_3. For simplicity we shall suppose that the particles have no spin, charge, etc., and are characterized by their momenta and masses. None of them have resonance interactions with each other in the possible states ($a_{ik} \sim 1/m$).

The amplitude of such a process is a function of five invariants ($p^2 = \mathbf{p}^2 - p_0^2$)

$$T = T\{(p_1 + p_2)^2,\ (p_1 + p_3)^2,\ (p_2 + p_3)^2,$$
$$(p_1' - p_1)^2,\ (p_1' - p_2)^2\}$$
$$\left(S = 1 + i(2\pi)^4 \delta\left(\sum p_f - \sum p_i'\right) T\right). \qquad (2)$$

Near the threshold of the reaction, in the center-of-mass system $\mathbf{p}_1 + \mathbf{p}_2 + \mathbf{p}_3 = 0$, $|\mathbf{p}_i| \ll m$, so that the invariants in Eq. (2) can be expanded in powers of the threshold momenta:

$$-(p_i + p_k)^2 = (m_i + m_k)^2 + k_{ik}^2 m_i m_k/\mu_{ik}, \qquad (3)$$

$$-(p_1' - p_i)^2 = M_1'^2 + m_i^2 - 2\varepsilon_1 m_i + 2\mathbf{p}_1'\mathbf{p}_i + \varepsilon_1' p_i^2/m_i. \qquad (4)$$

Here $\mu_{ik} = m_i m_k/(m_i + m_k)$, and if T were an analytic function of the invariants, its expansion in powers of the threshold momenta would contain only terms of the types $\mathbf{p}_i\mathbf{p}_k/m^2$ and $\mathbf{p}_i\mathbf{p}_i'/m\varepsilon_i'$, that is, terms quadratic in the threshold momenta or terms that are linear but depend on the angle between a particle in the initial state and one in the final state.* For brevity we shall hereafter call both types quadratic terms, since a term $\mathbf{p}_i\mathbf{p}'$ makes a contribution to the cross-section integrated over the angle in question that is quadratic in the threshold momenta.

The amplitude T near threshold is not, however, an analytic function of its arguments, since the threshold point

*For example, the amplitude for the decay $\tau \to 3\pi$[1] does not depend on the invariants of the type $(p_i'' - p_i)^2$, and no terms $\mathbf{p}_i\mathbf{p}_i'$ occur in the expansion.

$$(p_i + p_k)^2 = -(m_i + m_k)^2,$$
$$(p_1 + p_2 + p_3)^2 = -(m_1 + m_2 + m_3)^2 \qquad (5)$$

is a branch point of T as a function of the invariants (5) [$(p_1+p_2+p_3)^2$, the square of the total energy in the center-of-mass system, is a combination of the invariants $(p_i+p_k)^2$]. The amplitude T depends on arguments of the type $I - I_0$, where I is some invariant or combination of invariants and I_0 is the value taken by this invariant or combination at some singular point. If the singularities (5) are the only ones close to the values I taken by the corresponding invariants (for the quantities (5) we have $I - I_0 \sim \mathbf{p}^2 \ll m^2$), then the appearance of terms other than quadratic in the expansion of T is due to the dependence of T on the quantities $(p_i + p_k)^2 + (m_i + m_k)^2$, $(p_1 + p_2 + p_3)^2 + (m_1 + m_2 + m_3)^2$, since (with $I' - I_0 \sim m^2$) the other arguments of T can lead only to terms of the types $\mathbf{p}_i \cdot \mathbf{p}_k/m^2$ and $\mathbf{p}_i \cdot \mathbf{p}'/m\epsilon'$ in the expansion.

The absence of any other nearby singularities in addition to (5) means, first, that the threshold for production of the particles with masses m_1, m_2, and m_3 is far from the thresholds for the production of any other groups of particles that are possible in the given reaction, that is*

$$(m_1 + m_2 + m_3)^2 - (m_1' + m_2' + m_3')^2 \approx m^2. \qquad (6)$$

Second, it is necessary that the singularities with respect to the invariants must lie far from the values taken by these invariants. These are invariants of the type of the momentum transferred, and for them the fact that this condition is satisfied follows, for example, from the analysis given by Landau[3] (for an amplitude represented as a sum of Feynman diagrams).

3. Thus, the terms other than quadratic ones in the expansion of T can be given only by the contribution from the diagrams that lead to singularities of the type (5). According to Landau a singularity with respect to $(p_i + p_k)^2$ at the value $-(m_i + m_k)^2$ arises in those diagrams that contain at least one pair of lines corresponding to virtual particles with the masses m_i and m_k and connecting the part of the diagram to which the momenta p_i and p_k are attached with the rest of the diagram (Fig. 1b and 1c). Similarly, for a singularity with respect to $(p_1 + p_2 + p_3)^2$ at the point $-(m_1 + m_2 + m_3)^2$ the diagram must be divisible into two parts connected only by three lines of virtual particles with the masses m_1, m_2, m_3, with the initial momenta attached to one part and the final momenta to the other (Fig. 1d and 1e).

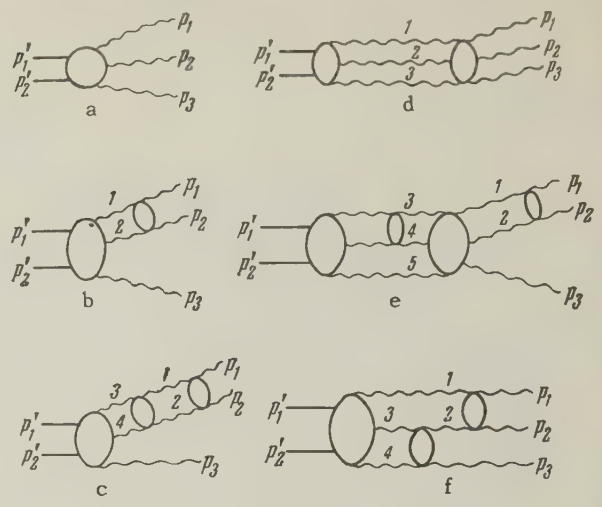

FIG. 2

We shall draw as a block the parts of the diagrams in which one cannot distinguish the lines of the specified types, the connecting lines. Then the diagrams of Fig. 1a have no singularities (5) and contribute only to the quadratic terms. In the other diagrams the treatment for finding the terms other than quadratic can be simplified to a remarkable extent. As is well known, the integral corresponding to an arbitrary diagram can be represented in the form (after integrating over all virtual momenta):

$$\int_0^1\int_0^1 \cdots \frac{d\alpha\, d\beta\, d\gamma\, d\delta \ldots \delta(\alpha + \beta + \gamma + \delta + \ldots - 1)}{(A\alpha + B\beta + C\gamma + D\delta + \ldots)^n}, \qquad (7)$$

where A, B, C, D, ... are the denominators corresponding to all the lines of the diagram:

$$A = q_A^2 + m_A^2, \qquad q_A \sim \sum_i \alpha_i P_i. \qquad (8)$$

Here P_i is the external momentum contained in the i-th line.

If A and B are the denominators corresponding to a pair of connecting lines, then at the point $(p_i + p_k)^2 = -(m_i + m_k)^2$ the denominator in Eq. (7) goes to zero for (cf. reference 3)*

$$A = B = 0, \qquad \alpha + \beta = 1, \qquad \gamma = \delta = \ldots = 0. \qquad (9)$$

At a point beyond the threshold, $(p_i + p_k)^2 = -(m_i + m_k)^2 + O(\mathbf{p}^2)$, the denominator in Eq. (7)

*The argument that follows will make it evident that this condition is not essential, and in each individual case one can figure out the changes that are introduced by the presence of another nearby threshold.

*We are considering the case in which there is only one pair of connecting lines in the diagram; an analogous treatment of more complicated diagrams leads to the same results.

can go to zero in a region $\gamma \sim \delta \sim \ldots \sim \mathbf{p}^2/m^2$, since $A \sim B \sim \mathbf{p}^2$ and C, D, and so on do not vanish at $\gamma = \delta = \ldots = 0$. But then in the region where the denominator $\sim \mathbf{p}^2$ and where we cannot expand in a series with respect to the threshold momenta (obviously this is the only region in which terms other than the quadratic terms can arise, since in regions where the denominator does not go to zero only quadratic terms appear), we can neglect the dependence on these momenta in all the lines except the connecting lines. In fact, in the region near the values (9) the denominators C, D, ... are multiplied by quantities $\gamma \sim \delta \sim \ldots \sim \mathbf{p}^2/m^2$, and in A and B the momenta of the other lines occur multiplied by the corresponding quantities $\gamma \sim \delta \sim \ldots \sim \mathbf{p}^2/m^2$.

Consequently, in expanding T in powers of the threshold momenta to obtain the terms different from $\mathbf{p}_i \cdot \mathbf{p}_k/m^2$ and $\mathbf{p}_i \cdot \mathbf{p}'/m\epsilon'$ we can neglect the threshold momenta everywhere in the diagrams that represent T, except in the denominators corresponding to the connecting lines.

4. To separate out the terms in which we are interested from an arbitrary diagram we must examine the dependence on the threshold momenta that arises only from the connecting lines; that is, we must examine the integrals over the virtual momenta belonging to the connecting lines. As will become evident from the further argument, each of these integrals can be considered independently of the presence of other connecting lines in the given diagram. For example, from the diagram of Fig. 1c we can separate out independently the contributions from the lines 1, 2 and 3, 4; from the diagram of Fig. 1e, those from lines 1, 2 and from 3, 4, 5; and so on. The only exception is the case in which the same line belongs to two different groups of connecting lines (line 5 in Fig 1e and line 1 in Fig. 1f). All such groups must be considered simultaneously.

The main types of connecting lines are shown in Fig. 2. The integral corresponding to the diagram of Fig. 2a is of the form

$$-(2\pi)^{-4}\int T_1(q)\frac{d^4q}{\left[(P_1+q)^2+m_1^2\right]\left[q^2+m_2^2\right]}T_2(q), \qquad (10)$$

where $P_1 = p_1 + p_2$, and $T_1(q)$ and $T_2(q)$ are the expressions corresponding to the blocks T_1 and T_2 in the diagram (they can also contain connecting lines). The factor

$$\frac{-1}{(2\pi)^4} = \frac{(-i)^2}{(2\pi)^8}(2\pi)^4$$

comes from the two connecting lines and the δ function from one of the blocks T_1 or T_2. The integration over dq_0 gives the sum of the integrals over d^3q of the various residues with respect to q_0. Of these only the one corresponding to $q_0 = -(m_2^2 + q^2)^{1/2}$ (we close the contour in the upper half of the q_0 plane) gives denominators that cannot be expanded in terms of the threshold momenta (the singular part). The residues of the integral over dq_0 that correspond to the denominators of the lines contained in $T_1(q)$ and $T_2(q)$ cannot contribute to the singular part, since a singularity of the type (5) arises only from the simultaneous vanishing of the denominators corresponding to a pair of connecting lines, i.e., the lines 1 and 2 in the case of Fig. 2a. Furthermore, contributions to the singular part come only from the free propagation functions, so that we have substituted in Eq. (10) only $\Delta_F^{(0)}$.

Then (with $\mathbf{p}_1 + \mathbf{p}_2 = -\mathbf{p}_3$) Eq. (10) can be written in the form

$$T'(0) + \frac{\pi i}{(2\pi)^4}\int \frac{T_1(q)\,d^3q\;T_2(q)}{\sqrt{m_2^2+\mathbf{q}^2}\left[\left(P_{10}-\sqrt{m_2^2+\mathbf{q}^2}\right)^2 - m_1^2 - (\mathbf{P}_3+\mathbf{q})^2\right]}$$

In $T'(0)$ the dependence of the connecting lines 1, 2 on the threshold momenta can give only quadratic terms (if T_1 and T_2 contain no connecting lines, then $T'(0)$ contains only quadratic terms in the expansion in terms of the threshold momenta). In the singular term the denominator goes to zero for $\mathbf{q} \sim \mathbf{p}$.

If we break up the integral over $|\mathbf{q}| = q$ into two integrals,

$$0 \leqslant q \leqslant \lambda \text{ and } \lambda \leqslant q, \qquad p \ll \lambda \ll m,$$

then the integral from λ to ∞ can be transferred to $T'(0)$, since in this integral the lines 1 and 2 give only quadratic terms. In the range from 0 to λ we can expand in terms of $|\mathbf{p}|$ and $|\mathbf{q}| \ll m$. In this region $T_i(\mathbf{q}) \sim T_i(0)$. We then have for the expression (10):

$$T(0) - \frac{i\pi\mu_{12}}{(2\pi)^4 m_1 m_2}T_1(0)\int_0^{\lambda}\frac{d^3q}{(\mathbf{q}+\mu_{12}\mathbf{p}_3/m_1)^2 - \mathbf{k}_{12}^2 - i\varepsilon}T_2(0), \qquad (11)$$

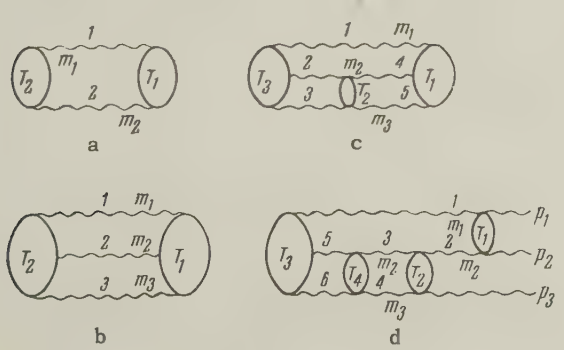

FIG. 2

or, putting the quadratic terms with $T(0)$,

$$T(0)+\frac{\mu_{12}}{16\pi m_1 m_2}|k_{12}|T_1(0)T_2(0)=T(0)+ik_{12}a_{12}^{(1)}\frac{T_2(0)}{2\sqrt{m_1m_2}}, \tag{12}$$

$$T_1(0)=(4\pi i(m_1+m_2)/\sqrt{m_1m_2})\,a_{12}^{(1)}. \tag{13}$$

If we are interested only in the terms linear in the threshold momenta, then in the second term of Eq. (12) we can set $p_i=0$ in $T_1(0)$ and $T_2(0)$. Then $a_{12}^{(1)}$ is the contribution of the diagram T_1 to the scattering amplitude of particles 1 and 2 at zero energy, and $T_2(0)/2(m_1m_2)^{1/2}$ is the contribution that the diagram T_2 makes to the amplitude of the process in question at the threshold energy of $T(0)$.

In just the same way we must separate off from the $T(0)$ in Eq. (12) the linear terms corresponding to the other connecting lines. It is then found that the connecting lines of the diagrams of Fig. 2b and c make the following contributions to the singular parts:

$$-\frac{\pi^2}{2m_1m_2m_3}T_2(0)\int_0^\lambda\frac{d^3q\,d^3q'}{q'^2/2\mu_{23}+q^2/2\mu_1-E-i\varepsilon}T_1(0) \tag{14}$$

for diagram 1b (sic!), and

$$\frac{i\pi^3}{2m_1(m_2m_3)^2}T_1(0)\times\int_0^\lambda\frac{d^3q\,d^3q'\,d^3q''\,T_2(0)\,T_3(0)}{(q'^2/2\mu_{23}+q^2/2\mu_1-E-i\varepsilon)(q''^2/2\mu_{23}+q^2/2\mu_1-E-i\varepsilon)} \tag{15}$$

for diagram 1c (sic!); here

$$1/\mu_1=1/m_1+1/(m_2+m_3),\quad E=k_{12}^2/2\mu_{12}+p_3^2/2\mu_3 \tag{16}$$

are the notations of Gribov's paper.[1]

It is easy to see that the expressions (14) and (15) do not contribute to the terms linear in the threshold momenta. In fact, for large q or q' (q'') each integral has no singular denominators and contains only E. A singularity arises for $q\sim q'\sim|p|$, but in this region the contribution to the integrals (14) and (15) is $\sim p^4$.

It can be shown that the contribution to the linear terms from a diagram of the type of Fig. 2d is given by the second term in Eq. (12), with appropriate values of $a_{12}^{(1)}$ and $T_2(0)$ (this contribution arises from lines 1 and 2 in Fig. 2d).

Thus terms linear in the threshold momenta are given only by diagrams of the type of Fig. 2a. The total contribution to the linear terms is obtained by summation of terms of the type (12) separated from all the connecting lines (of the type of Fig. 2a) of all possible diagrams. It can be shown that each product $a_{12}^{(1)}T_2(0)$ occurs in Eq. (12) only once. Therefore the sum of all the diagrams gives the expression

$$T=T(0)[1+ik_{12}a_{12}+ik_{23}a_{23}+ik_{13}a_{13}], \tag{17}$$

where $T(0)$ is the amplitude of the reaction in question when the threshold momenta are zero. The subsequent terms of the expansion in the threshold momenta contain either quadratic terms, or linear terms that depend on an angle between initial and final momenta, and thus make a quadratic contribution to the cross section integrated over this angle.

5. Neglect of the momenta in all the denominators except those of the connecting lines would mean neglect of terms of the types $p_i\cdot p_k/m^2$ and $p_i\cdot p'/m\epsilon'$.

There are also, however, quadratic terms of a different type: $|p_l|k_{ik}$ or $E^{1/2}k_{ik}$ (for the case of three particles no terms $k_{ik}k_{lm}$ appear in the final state). These differ from the former terms in that they determine angular correlations of the particles produced in the reaction in all orbital angular-momentum states, whereas the former terms give correlations only in states with relative orbital angular momentum 1 (cf. reference 1). If no state with relative orbital angular momentum 1 is possible, as is the case for the $\tau\to3\pi$ decay,[1] then the terms of first degree in the cosine of the angle between the momenta of the final particles must vanish in the final formulas, and to accuracy up to quadratic terms the angular correlations are completely determined by the terms $|p_l|k_{ik}$ and $E^{1/2}k_{ik}$. Just as in Eq. (17), these terms are determined by the dependences on the momenta in the connecting lines. They arise from the integrals of the diagrams of Fig. 2d on the integrations over the virtual momenta of lines 1, 2 and 1, 3, 4 or 1, 5, 6, etc., and only from these integrations.

For the singular part of these integrals we have an expression of the form [in Eq. (18) $T_3(0)$ is the contribution from T_3 and T_4 in the diagram of Fig. 2d when integrated over the momenta of lines 1 and 2, 3 and 4]

$$a_{12}^{(1)}a_{23}^{(2)}\frac{T_3(0)}{\sqrt{8m_1m_2m_3}}\frac{2\mu_{23}^{1/2}}{(2\pi)^4}\times\int_0^\lambda\frac{d^3q'}{q'^2/2\mu_{23}+q^2/2\mu_1-E-i\varepsilon}\frac{d^3q}{(q+\mu_{12}p_3/m_2)^2-k_{12}^2-i\varepsilon}. \tag{18}$$

From this we can separate out the quadratic terms of the type with which we are concerned,

$$\varkappa^2 a_{12}^{(1)}a_{23}^{(2)}T_3(0)J_{31}/\sqrt{8m_1m_2m_3}, \tag{19}$$

where

$$J_{31}=\frac{1}{3\pi}\frac{\varkappa\gamma_1^{1/2}}{\mu_{12}p_3}\left\{\left[1-\frac{(k_{12}+\mu_{12}p_3/m_2)^2}{\varkappa^2\gamma_1}\right]^{1/2}\cos^{-1}\frac{k_{12}+\mu_{12}p_3/m_2}{\varkappa\gamma_1^{1/2}}\right.$$

$$\left.-\left[1-\frac{(k_{12}-\mu_{12}p_3/m_2)^2}{\varkappa^2\gamma_1}\right]^{1/2}\cos^{-1}\frac{k_{12}-\mu_{12}p_3/m_2}{\varkappa\gamma_1^{1/2}}\right\};$$

$$\varkappa=\sqrt{2E\left(\frac{m_1m_2m_3}{M}\right)^{1/2}},\qquad \gamma_1=\left(\frac{\mu_1}{\mu_{12}}\right)^{1/2},$$

$$M=m_1+m_2+m_3. \tag{20}$$

Summation of the contributions from all the diagrams gives the angular correlations of the particles produced, with accuracy up to terms quadratic in the threshold momenta (terms depending on the angle between $\mathbf{p}_3$ and $\mathbf{k}_{12}$). When we include linear terms and the quadratic terms that determine the correlation of $\mathbf{p}_3$, $\mathbf{k}_{12}$, the amplitude is

$$T=T(0)[1+ik_{12}a_{12}+ik_{13}a_{13}+ik_{23}a_{23}+\varkappa^2a_{12}a_{23}J_{13}$$
$$+\varkappa^2a_{12}a_{13}J_{23}+\varkappa^2a_{13}a_{23}J_{12}+\varkappa^2a_{23}a_{13}J_{21}]+O(p^2/m^2); \tag{21}$$

J_{13} and so on are obtained from Eq. (20) by interchange of indices. The remaining terms quadratic in the threshold momenta do not depend on the angle between $\mathbf{p}_3$ and $\mathbf{k}_{12}$.

By a similar argument one can determine the energy dependence of the amplitude for reactions of the type $a + A \rightarrow b + B$ near the threshold for production of a pair of particles $c + C$.[2] Then we can separate out from diagrams of the type of Fig. 2a, with connecting lines corresponding to particles c and C, the term linear in

$$k=\{-(p_a+P_A)^2-(m_c+M_c)^2\}^{1/2}.$$

The amplitude will have the form

$$T_1(0)+ika_{aA\rightarrow cC}\,a_{cC\rightarrow bB}, \tag{22}$$

where $T_1(0)$ is the amplitude of the process $a + A \rightarrow b + B$ at energy equal to the threshold energy for the reaction $a + A \rightarrow c + C$. $a_{aA\rightarrow cC}$ and $a_{cC\rightarrow bB}$ are the amplitudes of the reactions in question at threshold. Below threshold $k \rightarrow -i|k|$.

Inclusion of spin and isotopic variables for the particles does not give rise to any difficulties, and means only that in the products $T(0)a_{ik}$ in Eq. (21) we must sum over all processes that are possible for the particles i and k at zero energy.

In conclusion the writer expresses his deep gratitude to V. N. Gribov for valuable discussions.

[1] V. N. Gribov, Nucl. Phys. **5**, 653 (1958).

[2] A. I. Baz', JETP **33**, 923 (1957), Soviet Phys. JETP **6**, 709 (1958).

[3] L. D. Landau, JETP **37**, 62 (1959), Soviet Phys. JETP **10**, 45 (1960).

Translated by W. H. Furry
265

OSCILLATIONS OF AN INHOMOGENEOUS PLASMA IN A MAGNETIC FIELD

L. I. RUDAKOV and R. Z. SAGDEEV

Submitted to JETP editor May 19, 1959

J. Exptl. Theoret. Phys. (U.S.S.R.) **37**, 1337-1341 (November, 1959)

Small oscillations of a hot plasma contained by a magnetic field are treated by means of the kinetic equation in the "drift" approximation without the collision integral.[1] Two waves can be excited when the propagation vector is in the plane perpendicular to the direction of the unperturbed magnetic field: a slow (drift) wave with a propagation velocity of the order of the mean drift velocity of the electrons (ions) in the unperturbed state, and a magneto-acoustic wave. The first is found in an inhomogeneous plasma only. If certain relations obtain between the zeroes of the magnetic field gradients, the plasma density, and the temperature, the drift current can cause amplification of these waves. Criteria for an instability of this kind are obtained.

1. INTRODUCTION. FORMULATION OF THE PROBLEM

In this paper, which is the first part of a work on oscillations in an inhomogeneous plasma, we consider the simplest geometric configuration for the unperturbed plasma: a straight pinch with an arbitrary distribution of longitudinal current.

We will consider oscillations at frequencies much higher than the collision frequency but smaller than the ion Larmor frequency. All characteristic dimensions are assumed to be large compared with the Larmor radius of the ions (electrons). Under these conditions it is convenient to describe the behavior of the plasma in terms of the drift approximation, using the kinetic equation.[1]

We introduce a cylindrical coordinate system for oscillations characterized by wave vectors which are transverse to the magnetic field (the magnetic field in the perturbed and unperturbed plasma is along φ).

The kinetic equation is

$$\frac{\partial f}{\partial t} + \nabla(\mathbf{v}_{dr} f) + \frac{\partial}{\partial v_\varphi}\frac{dv_\varphi}{dt} f = 0. \qquad (1)$$

Here $f(v_\varphi, u, r, t)$ is the electron (ion) distribution function, μ is the magnetic moment of the electron (ion) and v_{dr} is the drift velocity, which is

$$\mathbf{v}_{dr} = c\frac{[\mathbf{E}\times\mathbf{H}]}{H^2} + \frac{c}{e}\frac{\mu}{H^2}[\mathbf{H}\times\nabla H] + \frac{cm}{eH^2}\frac{v_\varphi^2}{r^2}[\mathbf{r}\times\mathbf{H}]. \qquad (2)$$

The first term in Eq. (2) corresponds to the electric drift, the second to the diamagnetic drift, and the third to the "centrifugal" drift.

The charge density and the current density are found from the distribution function

$$n = \int f d\mu dv_\varphi, \quad \mathbf{j} = c[\mathbf{H}\times\nabla p_\perp]/H^2 - \frac{c}{H}(p_\perp - p_\parallel)\operatorname{curl}\frac{\mathbf{H}}{H},$$

$$p = H\int \mu f d\mu dv_\varphi.$$

Maxwell's equations for the self-consistent field are

$$n_i = n_e \text{ (quasi-neutrality equation)} \qquad (3)$$

$$\operatorname{curl}\mathbf{H} = \frac{4\pi}{c}\mathbf{j} + \frac{4\pi n M}{H} c\frac{d}{dt}\frac{\mathbf{E}}{H}, \qquad \operatorname{curl}\mathbf{E} = -\frac{1}{c}\frac{\partial \mathbf{H}}{\partial t}. \qquad (4)$$

2. SMALL-OSCILLATION EQUATIONS

We investigate the time behavior of small departures from equilibrium.

The equilibrium state is given by the equation

$$\frac{1}{r}\frac{\partial}{\partial r} rH_0 = -\frac{4\pi}{H_0}\frac{d}{dr}\left(H_0\int \mu f_0 d\mu\right) \qquad (5)$$

The zeroth current term j_0 is due to the motion of electrons with velocity

$$(c/en_0)[\mathbf{H}_0\times\nabla(p_i + p_e)]H_0^{-2}.$$

The ions are assumed to be fixed (cf., for example, reference 2). We seek small corrections to the equilibrium quantities in the form

$$A = A(r)\exp\{i(kz - \omega t)\}.$$

The equation for the perturbed distribution function is

$$-i(\omega - kv_{dr}^0) f + \nabla(\mathbf{v}_{dr} f_0) - \frac{\partial}{\partial v_\varphi}\frac{v_\varphi}{r} c\frac{E_z}{H_0} f = 0. \qquad (6)$$

Here

$$v_{dr}^0 = -\frac{cm}{e}\frac{H_0'}{H_0} + \frac{cmv_\varphi^2}{eH_0 r} + c\frac{E_r^0}{H_0}, \qquad (7)$$

(primes denote differentiation with respect to r).

The correction to the distribution function is

$$f_1 = f_0 \frac{H}{H_0} + \left[\left(\frac{f_0}{H_0}\right)' - \frac{1}{r}\frac{v_\varphi}{H_0}\frac{\partial f_0}{\partial v_\varphi}\right]\frac{(kc\mu/e)H + icE_z}{\omega - kv_{dr}^0}. \quad (8)$$

Substituting f_1 in Maxwell's equations we obtain three equations for the three quantities H_φ, E_r, and E_z. By means of simple transformations we eliminate E_r and H_φ, obtaining a single second-order differential equation for E_z, which is given here without the intermediate steps:

$$\frac{d}{dr}\frac{c^2}{V_A^2}H_0\frac{(1+4\pi a/H_0)E_z' - i(\omega 4\pi b/cH_0)E_z}{(1+4\pi a/H_0) - \omega^2/k^2V_A^2} - \frac{k^2c^2}{V_A^2}H_0E_z + \frac{H_0}{r}\frac{(c^2/V_A^2)E_z' - i(k^2c4\pi b/\omega H_0)E_z}{(1+4\pi a/H_0) - \omega^2/k^2V_A^2} = 0, \quad (9)$$

where

$$a = \frac{2p_0}{H_0} + H_0\sum\int\left(\frac{f_0}{H_0}\right)'\frac{kc\mu^2/e}{\omega - kv_{dr}^0}d\mu dv_\varphi,$$

$$b = icH_0\sum\int\left(\frac{f_0}{H_0}\right)'\frac{\mu}{\omega - kv_{dr}^0}d\mu\, dv_\varphi,$$

$$V_A^2 = H_0^2/4\pi n_0 M. \quad (10)$$

The summation is taken over ions and electrons. The integrals over μ in Eq. (10) are taken along the real axis if $\mathrm{Im}(\omega) > 0$ and along a contour such that the pole of the integrand lies between the real axis and the contour if $\mathrm{Im}(\omega) < 0$, in agreement with the rules of analytic continuation.[3]

Thus, the problem of oscillations of an inhomogeneous plasma is reduced to that of finding the eigenvalues and eigenfunctions of a second-order differential equation with variable coefficients (9).

3. DRIFT WAVES

We consider oscillations whose frequencies satisfy the inequality $\omega \ll kH_0/\sqrt{4\pi n_0 M}$ (correspondingly, the phase velocity $\omega/k \ll V_A$).

Equation (9) can be simplified in this case:

$$\frac{c^2}{V_A^2}\frac{d^2E_z}{dr^2} - \frac{1}{r}\frac{4\pi k^2 cib}{\omega H_0}\frac{E_z}{1+4\pi a/H_0} = 0. \quad (11)$$

In Eq. (11) we have omitted the small parameter $\omega^2/(kV_A)^2$ in the coefficient of the second derivative.

Equation (11) is a generalized equation for the eigenvalues of a complex operator which is not self-adjoint.

We write this equation in the form

$$E'' - [U(x, \omega, k) + iV(x, \omega, k)]E = 0, \quad (12)$$

where U and V are real functions.

For solutions of Eq. (12) which converge in a bounded region of space we can write the integral conditions

$$\int |E'|^2 dx + \int U(x, \omega, k)|E^2|dx = 0,$$
$$\int V(x, \omega, k)|E|^2 dx = 0, \quad (13)$$

where the integration is taken over the entire region occupied by the plasma. The second of these conditions can be realized only if the quantity $V(x, \omega, k)$ passes through zero at some point in space.

We consider space localized solutions for which $U(x, \omega, k)$ passes through zero at the same point. The condition

$$U(x_0, \omega, k) + iV(x_0, \omega, k) = 0 \quad (14)$$

plays the role of a dispersion equation which relates ω and k.

Near this point Eq. (12) becomes an Airy equation with complex argument

$$E'' + (U_0' + iV_0')xE = 0.$$

We investigate the "high-gradient" case $(d/dr)_0 \gg 1/r$. In this case the "dispersion equation" is

$$b = icH_0\sum\int\left(\frac{f_0}{H_0}\right)'\frac{\mu d\mu dv_\varphi}{\omega - kcE_0/H_0 + kc\mu H_0'/eH_0} = 0. \quad (15)$$

It should be noted that although no curvature term appears in the dispersion equation, the derivation cannot be extended to the case $r \to \infty$ because terms of order ω/kV_A, which have been omitted in obtaining Eq. (11), become important at large values of r.

We now investigate Eq. (15). As an example we take $f_{0\mu}$ in the form $f_{0\mu} = n_0\delta(\mu - \mu_0)$. (All the particles at any point have the same magnetic moment.) Here we have already carried out the integration over the longitudinal velocity ($f_{0\mu} = \int f_0(\mu, v_\varphi)dv_\varphi$).

Integrating with respect to μ in Eq. (14) we have

$$\omega^2 = k^2 v_{dr}^{02}\left(1 - 2\frac{\mu_0}{\mu_0}\frac{n_0}{H_0}\Big/\left(\frac{n_0}{H_0}\right)'\right).$$

Whence, an instability develops if

$$\frac{\mu_0'}{\mu_0}\frac{n_0}{H_0}\Big/\left(\frac{n_0}{H_0}\right)' > \frac{1}{2}. \quad (16)$$

The case in which the Maxwellian distribution

$$f_0 = \frac{n_0 H_0}{T_0}e^{-\mu H/T_0}$$

is used in Eq. (15) has been investigated in reference 4. The instability criterion is of the form

$$0 < -\frac{H_0^2/8\pi n_0 T_0 + \partial \ln T_0/\partial \ln H_0}{1 - \partial \ln T_0/\partial \ln H_0} < 1. \quad (17)$$

4. MAGNETOACOUSTIC WAVES

We consider oscillations at frequencies $\omega \sim kV_A$. Omitting terms of order v_{dr}^0/V_A in Eq. (9) we obtain [for high gradients $(d/dr)_0 \gg 1/r$]:

$$\frac{d}{dr}\frac{c^2}{V_A^2}H_0\frac{(1+4\pi a/H_0)E_z' - i(\omega 4\pi b/cH_0)E_z}{(1+4\pi a/H_0)-\omega^2/k^2V_A^2} - \frac{k^2c^2}{V_A^2}H_0E_z = 0. \quad (18)$$

This is the equation for the magnetoacoustic waves. In the quasi-classical approximation ($E_z \sim \exp\{i\int k_r\,dr\}$, where k_r is a slowly varying function of r) we have

$$(k^2+k_r^2)(1+4\pi a/H_0)+\omega^2/V_A^2 = 0. \quad (19)$$

We consider oscillations close to the boundary of the stability region (small buildup). The real part of Eq. (19) determines the frequency of the oscillations and the imaginary part determines the increment factor ν ($\omega = \omega_1 + i\nu$).

For a given value of H_0' there is always a pole in one of the integrands. For small increments ($\nu \ll \omega_1$) we have

$$\int\frac{\mu^2(f_0/H_0)'\,d\mu}{\omega - k|v_{dr}^0|} = \int\frac{\mu^2(f_0/H_0)'\,d\mu}{\omega - k|v_{dr}^0|} + \pi i\,\mathrm{Res},$$

($\int$ is the integral in the sense of the principal value).

Separating real and imaginary parts in Eq. (19) we have

$$\omega^2 = (k_r^2+k^2)\left(V_A^2 + 2\frac{p_0}{n_0}\right),$$
$$\nu = \frac{3}{2}\pi\omega_1\left\{\mu^2\left(\frac{f_0}{H_0}\right)'\right\}_{\omega_1=kv_{dr}^0}\Big/\left(\frac{p_0}{H_0^2}\right)' \quad (20)$$

In evaluating the integrals we have taken into account that for the magnetoacoustic branch $\omega \gg k\overline{v_{dr}^0}$; $\overline{v_{dr}^0}$ is the mean drift velocity. Thus the instability criterion $\nu > 0$ is of the form

$$H_0'(f_0/H_0)' < 0. \quad (21)$$

For a Maxwellian distribution function:

$$\partial \ln T_0/\partial \ln H_0 > 1. \quad (22)$$

The physical nature of this instability and the instability in the drift branch may be described as follows.

Electrons which move with the unperturbed velocity v_{dr}^0, close to the phase velocity of the wave, drift towards points of zero gradient, acquiring energy by virtue of the interaction with the wave. If the condition in Eq. (21) is satisfied [or, correspondingly, the condition in Eq. (17)] this interaction leads to an instability (the electrons lose energy to the wave). The time required for the development of this instability is large because in the case being considered ($\omega \gg k\overline{v_{dr}}$) the number of particles in resonance with the wave is an exponentially small quantity.

The increments can become large when the mean velocity of the unperturbed electron drift is of the order of the velocity of the magnetoacoustic wave. This situation can arise if the gradients are large at equilibrium: $H_0^{-1}\partial H_0/\partial r > R_H^{-1}$ (R_H is the ion Larmor radius). However, in this case the drift approximation no longer applies for the ions.

A simplified analysis of this case can be carried out on the basis of a "cold" ion model ($T_i \ll T_e$). In this case, Eq. (18) with $T_i = 0$ is valid up to characteristic dimensions of the order of the electron Larmor radius and the increments are

$$\nu = \pi\omega_1\left\{\mu^2\left(\frac{f_0}{H_0}\right)'\right\}_{\omega_1=kv_{dr}^0}\Big/\left(\frac{p_0}{H_0^2}\right)'. \quad (23)$$

(In this we assume that $\nu \ll \omega_1$ since we are interested in the stability boundaries.) The plasma is unstable if

$$\frac{\partial \ln T_e}{\partial \ln H_0}\left(\frac{\mu_1 H_0}{T_e} - 2\right) > \frac{H_0^2}{8\pi n_0 T_e} + \frac{\mu_1 H_0}{T_e},$$
$$\mu_1 = |eV_A H_0/cH_0'|. \quad (24)$$

The authors wish to thank Academician M. A. Leontovich and Prof. L. A. Frank-Kamenetskiĭ for discussion of the problems considered in this paper.

[1] L. I. Rudakov and R. Z. Sagdeev, Coll. Физика плазмы и проблема управляемых термоядерных реакций (Plasma Physics and the Problem of a Controlled Thermonuclear Reaction) Academy of Sciences Press, U.S.S.R. 1958, Vol. 3, p. 268.

[2] L. Spitzer, The Physics of Fully Ionized Gases, Interscience, New York 1956, Russ. Transl. IIL, 1957.

[3] L. D. Landau, JETP **16**, 574 (1946).

[4] Yu. A. Tserkovnikov, JETP **32**, 69 (1957) Soviet Phys. JETP **5**, 58 (1957).

Translated by H. Lashinsky
266

ANOMALOUS MAGNETIC MOMENTS OF NUCLEONS IN THE CHEW METHOD

Yu. M. LOMSADZE, V. I. LEND' EL, and B. M. ÉRNST

Uzhgorod State University

Submitted to JETP editor May 21, 1959

J. Exptl. Theoret. Phys. (U.S.S.R.) **37**, 1342-1345 (November, 1959)

Corrected values of the anomalous magnetic moments of nucleons caused by virtual π-meson and nucleon currents are obtained by Chew's method. Contributions of strange particles and of the hypothetical ρ^0 meson are also taken into account, on various assumptions about their intrinsic parities.

1. INTRODUCTION

FROM the point of view of present quantum field theory, the main contribution to the anomalous magnetic moments μ_p and μ_n of nucleons must come from the virtual currents that arise on account of the coupling of the nucleon and π-meson fields — a coupling which is evidently the "strongest" of all known couplings. It can be expected that an appreciable contribution to μ_p and μ_n is also made by the strange particles, since the field of these particles is also coupled rather strongly with the nucleon field. In addition it is interesting to estimate the contribution to μ_p and μ_n that arises from the coupling of the nucleon field with the field of the hypothetical ρ^0 meson allowed by the Gell-Mann scheme;[1] there is lively discussion in the literature as to whether this particle exists.

Recently Gupta[2] has taken account of the contributions to μ_p and μ_n from both the strange particles and the ρ^0 meson, in the framework of ordinary perturbation theory. Owing to the fact, however, that he did not get agreement with experiment on any assumption about the intrinsic parities of the K and ρ^0 mesons, and also owing to the fact that perturbation theory is probably not applicable to these problems,[3] it is interesting to make analogous calculations by the more acceptable method of Chew.

It must be emphasized, however, that in the Chew method, based on the idea of a fixed nucleon source, the treatment we shall give of transitions from nucleon to hyperon and vice-versa is, strictly speaking, not consistent. Besides the fact that in this method recoil is neglected, in such a treatment we have to introduce a mixed nucleon-hyperon source, and the question at once arises as to its "size." Fortunately, the not very large difference of the masses and the equality of several other characteristics of nucleons and hyperons allows us to hope that also the size of such a mixed source will be close to the "size" of the nucleon source. In what follows we shall use the standard "cutoff" — $\omega_{max} = 5.6\, m_\pi$. We remark, however, that a change of this "cutoff" within reasonable limits makes only a slight change in our numerical results.

2. THE CONTRIBUTION OF THE π-MESON AND NUCLEON CURRENTS

In reference 4 calculations by the Chew method have been made on the magnetic moments of nucleons, with inclusion of only the meson current in the virtual state, and with the coupling constant $f^2 = 0.058$ the values found were* $\mu_p = 1.44$, $\mu_n = -1.44$.

In reference 5 the contribution of the virtual nucleon current has been taken into account, and an addition of -0.15 to the neutron magnetic moment was found. This treatment considered diagram 2 and its modifications in Chew's sense; these contribute only to the neutron magnetic moment (see diagram).

There is, however, one other diagram, namely diagram 1, that involves a nucleon current in the virtual state and gives a contribution to the magnetic moment of the proton. The contribution of diagram 1, corresponding to the emission of a π^0 meson, is smaller by a factor 2 than the contribution of diagram 2, which corresponds to the emission of a π^- meson. This follows from the fact that in the symmetrical theory the coupling of the charged meson field with the nucleon field contains an addition factor $2^{1/2}$. This same result can also easily be obtained formally, if we write

*Throughout this paper all values of magnetic moments are given in nuclear magnetons.

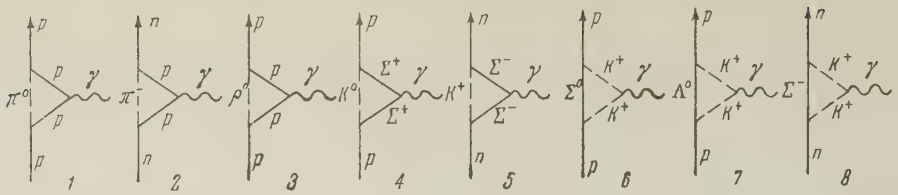

the Lagrangian for the interaction of the nucleon and electromagnetic fields (in the relativistic case) in the form

$$L = -ie : \bar{\Psi} {}^1/_2 (1 + \tau_3) \gamma_\nu \Psi A_\nu : . \qquad (1)$$

Here Ψ is the usual eight-component operator of the nucleon field, composed of the wave functions of proton and neutron, and $\tau_3 = \begin{pmatrix} 1 & 0 \\ 0 & -1 \end{pmatrix}$.

Owing to this the value calculated in reference 5 for the contribution to μ_n caused by diagram 2 must be doubled. The contribution to μ_p caused by diagram 1 is -0.15.

Thus with the coupling constant indicated above the values of the anomalous magnetic moments of the nucleons turn out to be $\mu_p = 1.29$ and $\mu_n = -1.74$.

Recently, however, a more logical analysis of the experimental data on the basis of dispersion relations has led to a decided increase of the coupling constant of the nucleon and π-meson fields. At present we must evidently take as the most acceptable value of this constant $f^2 = 0.1$.[6] The use of this constant leads to the following values of the anomalous magnetic moments of the nucleons

$$\mu_p = 2{,}51, \qquad \mu_n = -3{,}46. \qquad (2)$$

3. THE CONTRIBUTION OF STRANGE PARTICLES AND THE ρ^0 MESON

Since the intrinsic parities of the K and ρ^0 mesons are as yet unknown, we have made calculations both for scalar and for pseudoscalar K and ρ^0 mesons. On this basis the Hamiltonian now generally accepted for the interaction of the K and ρ^0 meson fields with the baryon field[7] can be written in the Chew approximation in the form

$$H = H_{N\Sigma K} + H_{N\Lambda^0 K} + H_{NN\rho^0}, \quad H_{N\Sigma K} = \sqrt{4\pi} \times \int dr\, \rho_{N\Sigma}(r)\, \tau \eta_K \varphi_K(r),$$

$$H_{N\Lambda^0 K} = \sqrt{4\pi} \int dr \rho_{N\Lambda^0}(r)\, \eta_K \varphi_K(r) + \text{Herm. adj.}$$

$$H_{NN\rho^0} = \sqrt{4\pi} \int dr \rho_{NN}(r)\, \eta_\rho \varphi_\rho(r), \qquad (3)$$

where $\eta_K = g'_K$ for scalar K mesons, $\eta_K = (f_K/m_K)\sigma\nabla$ for pseudoscalar K mesons, and similarly with η_ρ. In Eq. (3) it is assumed that the relative intrinsic parities of the nucleons and hyperons are the same.

In the calculations we have confined ourselves to the first nonvanishing approximation of the Chew method, since, as our calculations show and as could of course be foreseen, the next approximation gives a much smaller contribution.

For the process with which we are concerned there are six diagrams, 3 — 8. Using the Hamiltonian (3), we easily get the following matrix elements: for diagram 3 in the case of scalar ρ^0 mesons

$$M_3 = -\frac{e}{2m} \sigma \mathbf{H} \frac{g'^2_\rho}{\pi} \int \frac{dk k^2 v^2(k)}{\omega_k^3}, \qquad (4)$$

for diagrams 4 — 8 in the case of scalar K mesons

$$M_4 = -\frac{e}{2m} \sigma \mathbf{H} \frac{2m}{M} \frac{g'^2_K}{\pi} \int \frac{dk k^2 v^2(k)}{\omega_k^3},$$
$$M_5 = -M_4, \qquad M_6 = M_7 = M_8 = 0, \qquad (5)$$

for diagram 3 in the case of pseudoscalar ρ^0 mesons

$$M_3 = \frac{e}{2m} \sigma \mathbf{H} \frac{1}{3\pi} \frac{f^2_\rho}{m^2_\rho} \int \frac{dk k^4 v^2(k)}{\omega_k^3}, \qquad (6)$$

and for diagrams 4 — 8 in the case of pseudoscalar K mesons

$$M_4 = \frac{e}{2m} \sigma \mathbf{H} \frac{2}{3\pi} \frac{m}{M} \frac{f^2_K}{m^2_K} \int \frac{dk k^4 v^2(k)}{\omega_k^3}, \qquad M_5 = -M_4,$$

$$M_6 = M_7 = -\frac{e}{2m} \sigma \mathbf{H} \frac{4}{3\pi} \frac{m}{m_K} \frac{f^2_K}{m_K} \int \frac{dk k^4 v^2(k)}{\omega_k^4}, \quad M_8 = 2M_6. \qquad (7)$$

On the basis of reference 8 the coupling constant of the K-meson and baryon fields is taken to be $g'^2_K = 0.7$ for scalar K mesons and $g^2_K = (2m/m_\pi)^2 \times f^2_K = 2.6$ for pseudoscalar K mesons. To simplify the calculations we have neglected the difference of the hyperon masses, taking $M = 2300\, m_e$ for all the hyperons. Since at present there are no definite arguments regarding the value of the coupling constant of the ρ^0-meson and nucleon fields, we have taken for definiteness $g'^2_\rho = 1$ for the scalar ρ^0 meson and $f^2_\rho = 0.1$ for the pseudoscalar ρ^0 meson. As for the rest mass of the ρ^0 meson, we have considered two cases: $m_\rho = m_\pi$ and $m_\rho = 2m_\pi$.

With these assumptions we get the following values for the contributions to the magnetic moments of the nucleons from strange particles and ρ^0 mesons: from the hyperon and scalar K-meson currents +0.09 and −0.09; from the hyperon and pseudoscalar K-meson currents +0.002 and +0.003; from the coupling with the scalar ρ^0 meson +0.46 and 0 (for $m_\rho = m_\pi$) and +0.24 and 0 (for $m_\rho = 2m_\pi$); from the coupling with the pseudoscalar ρ^0 meson −0.17 and 0 (for $m_\rho = m_\pi$) and −0.02 and 0 (for $m_\rho = 2m_\pi$); the pairs of values are for μ_p and μ_n respectively.

4. DISCUSSION OF RESULTS

We note first of all that the so-called vector part of the magnetic moments of nucleons, caused by the couplings of the baryon field with the π and K meson fields, has been calculated recently by the method of dispersion relations.[3] The numerical results obtained in the present paper are in the main close to the results of reference 3, except for the case of the pseudoscalar K mesons, where the difference amounts to an order of magnitude. This last fact can be easily understood if we take note of the experimental fact that there is a large s-wave interaction between K mesons and nucleons (see reference 9, for example), which is automatically excluded for pseudoscalar K mesons in a calculation by the Chew method, which neglects the recoil effects. For scalar K mesons, on the other hand, this neglect evidently causes no large error.[10] An important point is that both the analysis on the basis of dispersion relations and the results we have obtained indicate that the strange particles make an extremely small contribution to the magnetic moments of nucleons.

The theoretical values of the anomalous magnetic moments of the nucleons given in Sec. 2 are in absolute value much larger than the experimental values, and, as has already been noted, inclusion of the contribution of strange particles cannot appreciably change this situation.

As for the ρ^0 mesons, our results show that only the pseudoscalar ρ^0 meson improves the theoretical value of μ_p (and only slightly, at least with the coupling constant we have chosen), but it leaves the value of μ_n unchanged.* In this respec our results are in contradiction with those of Gupta who is inclined to the idea of a scalar character fo the ρ^0 meson.

The writers express their deep gratitude to V. Ya. Faĭnberg for a number of very helpful comments.

[1] M. Gell-Mann, Phys. Rev. **106**, 1296 (1957).
[2] S. N. Gupta, Phys. Rev. **111**, 1436 (1958).
[3] Federbush, Goldberger, and Treiman, Phys. Rev. **112**, 642 (1958).
[4] M. H. Friedman, Phys. Rev. **97**, 1132 (1955).
[5] S. K. Kundu, Proc. Phys. Soc. **72**, 49 (1958).
[6] D. A. Geffen, Phys. Rev. **112**, 1370 (1958).
[7] A. Salam, Nucl. Phys. **2**, 173 (1957).
[8] P. T. Matthews and A. Salam, Phys. Rev. **110**, 569 (1958).
[9] Ascoli, Hill, and Yoon, Nuovo cimento **9**, 813 (1958).
[10] Komatsuzawa, Sugano, and Nogami, Progr. Theoret. Phys. **20**, 246 (1958).
[11] Lomsadze, Lend'el, and Krivskiĭ, Тр. Всесоюзно межвузовской конференции (Proc. All-Union Intercollegiate Conference) No. 2, 194, Uzhgorod, 1959.

Translated by W. H. Furry
267

*We note that the hypothesis that there exists a parity doublet of π mesons,[11] which provides a satisfactory explanation of the experiments on N–N scattering in the energy range 100–600 Mev, leads to additional contributions of +0.46 and +0.92 to μ_p and μ_n, respectively. This improves the value for μ_n, but makes the value for μ_p somewhat worse.

FIELD OF A CHARGED PARTICLE IN A MOVING MEDIUM

B. M. BOLOTOVSKIĬ and A. A. RUKHADZE

P. N. Lebedev Institute of Physics, Academy of Sciences, U.S.S.R.

Submitted to JETP editor May 25, 1959

J. Exptl. Theoret. Phys. (U.S.S.R.) **37**, 1346-1351 (November, 1959)

The field produced by the motion of a charge through a moving medium is considered. The energy losses of the charge due to Cerenkov radiation and excitation of plasma waves are determined.

1. The problem of determining the field of a charged particle in a moving medium has a long history. The "inverse" Cerenkov effect, i.e., the Cerenkov effect as seen in the rest system of the particle, was first considered by Tamm.[1] This question has also been considered in a number of later papers.[2] The interest in the inverse Cerenkov effect arises in connection with a suggestion made by Veksler[3] concerning the application of this effect in the acceleration of charged particles; Veksler's proposal is based on the use of a fast electron stream as the moving medium.

Below we consider certain properties of the field of a charge in a moving medium which have not been considered in the earlier analyses. The results which are obtained may be useful, for example, in experimental investigations of relativistic plasma beams and in the investigation of the interaction of beams of charged particles with plasma oscillations.

Following Ryazanov,[5] we use the phenomenological equations of classical electrodynamics for a moving medium which have been developed by Tamm.[4]

2. Let $\epsilon(\omega)$ and $\mu(\epsilon)$ be the dielectric constant and the permeability of the medium in the system in which it is at rest. We introduce the quantity

$$\varkappa = \varepsilon\mu - 1. \tag{1}$$

Now suppose that the medium moves with the 4-velocity u_i:

$$u_{1,2,3} = u_{x,y,z}/\sqrt{1-u^2/c^2} \qquad u_4 = c/\sqrt{1-u^2/c^2},$$

where $\mathbf{u}$ is the three-dimensional velocity of the medium. The dielectric-magnetic permeability tensor is then written in the form

$$\varepsilon_{ikst} = \mu^{-1}(\delta_{is} + \varkappa c^{-2} u_i u_s)(\delta_{kt} + \varkappa c^{-2} u_k u_t) \tag{2}$$

Maxwell's equations assume the form

$$\partial_l F_{ke} + \partial_k F_{le} + \partial_e F_{lk} = 0, \qquad \partial_k H_{ik} = -(4\pi/c) j_i,$$
$$H_{ik} = \varepsilon_{ikst} F_{st}, \tag{3}$$

where $\partial_i(-\nabla, \partial/c\partial t)$ is the four-dimensional gradient, F_{ik} is a field tensor (electric field and magnetic induction field) and H_{ik} is a field tensor (magnetic field and electric induction field). The product of two 4-vectors A_i and B_i is written in the form

$$(AB) = A_i B_i = A_4 B_4 - A_1 B_1 - A_2 B_2 - A_3 B_3.$$

Introducing the 4-potential A_i in accordance with the relation $F_{ik} = \partial_i A_k - \partial_k A_i$ and imposing the following supplementary condition on the components:

$$(\partial_k + \varkappa c^{-2} u_k u_i \partial_i) A_k = 0,$$

we find a simple equation for the potentials:

$$\mu^{-1}[\partial_k^2 + \varkappa c^{-2}(u_k \partial_k)^2](\delta_{st} + \varkappa c^{-2} u_s u_t) A_t = -(4\pi/c) j_s. \tag{4}$$

In a medium which is at rest ($\mathbf{u} = 0$) and in vacuum ($\kappa = 0$) Eq. (4) becomes the well-known relation.

We may note that if the quantity κ in Eq. (1) is a function of frequency in the medium at rest, in the moving medium κ will depend on the four-dimensional product (uk), where k ($\mathbf{k}$, ω/c) is the four-dimensional wave vector.

3. We now consider the solution of Eq. (4). We multiply both sides by u_s and sum over s. Introducing the notation

$$L = \partial_k^2 + \varkappa c^{-2}(u_k \partial_k)^2, \tag{5}$$

we have

$$L(Au)(1+\varkappa) = -\frac{4\pi}{c}(ju). \tag{6}$$

On the other hand, from Eq. (4) it follows that

$$LA_s = -(4\pi\mu/c) j_s - u_s c^{-2} L\varkappa (Au). \tag{7}$$

Substituting the value of (Au) from Eq. (6) in Eq. (7) we have

$$A_s = -\frac{4\pi}{c} L^{-1}\left[\delta_{st} - \frac{\varkappa}{c^2(1+\varkappa)} u_s u_t\right]\mu j_t. \qquad (8)$$

Equation (8) determines the field in the moving medium produced by an arbitrary source. To this same expression we can add the electromagnetic field in a medium at rest, using the appropriate Lorentz transformation.

4. We now assume that a point charge q with a velocity **v**, moves through a medium which itself is moving with velocity **u**. The current density and charge density are written in the form:

$$\mathbf{j} = \mathbf{v}q\delta(\mathbf{x} - \mathbf{v}t), \qquad \rho = q\delta(\mathbf{x} - \mathbf{v}t), \qquad (9)$$

We use the Fourier expansion of the δ function and obtain the following solutions for the vector and scalar potentials:

$$\mathbf{A} = \frac{q}{2\pi^2}\int\left[\frac{\mathbf{v}}{c} - \frac{\varkappa}{1+\varkappa}\frac{\mathbf{u}}{c}\frac{1 - \mathbf{uv}/c^2}{1 - u^2/c^2}\right] \times \frac{\mu \exp\{i\mathbf{k}(\mathbf{x} - \mathbf{v}t)\}\, d\mathbf{k}}{(\mathbf{kv})^2/c^2 - k^2 + (\varkappa/c^2)(\mathbf{ku} - \mathbf{kv})^2/(1 - u^2/c^2)},$$

$$\varphi = \frac{q}{2\pi^2}\int\left[1 - \frac{\varkappa}{1+\varkappa}\frac{1 - \mathbf{uv}/c^2}{1 - u^2/c^2}\right] \times \frac{\mu \exp\{i\mathbf{k}(\mathbf{x} - \mathbf{v}t)\}\, d\mathbf{k}}{(\mathbf{kv})^2/c^2 - k^2 + (\varkappa/c^2)(\mathbf{ku} - \mathbf{kv})^2/(1 - u^2/c^2)} \qquad (10)$$

5. The energy loss of the charge in the moving medium is given by

$$\frac{dW}{dx} = q\frac{\mathbf{Ev}}{v}\Big|_{\mathbf{x}=\mathbf{v}t} = -\frac{q_l}{2\pi^2 v}\int\left[1 - \frac{v^2}{c^2} - \frac{\varkappa}{1+\varkappa}\frac{(1 - \mathbf{uv}/c^2)^2}{1 - u^2/c^2}\right] \times \frac{\mu(\mathbf{kv})\, d\mathbf{k}}{(\mathbf{kv})^2/c^2 - k^2 + (\varkappa/c^2)(\mathbf{ku} - \mathbf{kv})^2/(1 - u^2/c^2)} \qquad (11)$$

It should be kept in mind that the quantity $\kappa = \epsilon\mu - 1$ is a function of the scalar product

$$(uk) = (\mathbf{kv} - \mathbf{ku})/(1 - u^2/c^2)^{1/2}.$$

When the sign of the wave vector **k** changes, the integrand in Eq. (11) becomes the complex conjugate expression. Hence the integration is limited to values of **k** for which $\mathbf{k}\cdot\mathbf{v} > 0$ and the real part which is obtained is multiplied by two.

If the velocity vector of the charge **v** does not coincide in direction with the velocity of the medium **u**, a deflecting force acts on the charge in addition to the decelerating force.

6. We consider the integrand in Eq. (11). It is pure imaginary if we consider a transparent medium (ϵ and μ real). A contribution to the real part of the integral can be obtained only from poles along the path of integration. As is apparent from Eq. (12), poles will exist if one of the following conditions is satisfied:

$$1 + \varkappa = 0, \quad \text{i.e.,} \quad \varepsilon(k_l u_l) = 0, \qquad (12)$$

or

$$\frac{(\mathbf{kv})^2}{c^2} - k^2 + \frac{\varkappa}{c^2}\frac{(\mathbf{ku} - \mathbf{kv})^2}{1 - u^2/c^2} = 0. \qquad (13)$$

The first equation determines the losses which are the analog of the longitudinal losses in a medium at rest. When $\mathbf{u} = 0$, from Eq. (11) we obtain the usual condition, $\epsilon(\omega) = 0$. The second equation determines the Cerenkov loss. This equation will now be investigated in detail.

7. We take

$$\mathbf{kv} = \omega = ck/n, \qquad \mathbf{ku} = ku\cos\psi. \qquad (14)$$

Then, from Eq. (13) we obtain an equation which determines the phase velocity c/n for waves which propagate at an angle ψ with respect to the direction of motion of the medium:

$$c^2/n^2 - c^2 + \eta(c/n - u\cos\psi)^2 = 0. \qquad (15)$$

The solution of this equation is

$$\frac{c}{n_{1,2}} = \frac{\eta u\cos\psi \pm \sqrt{c^2 + \eta(c^2 - u^2\cos^2\psi)}}{1+\eta}, \qquad (16)$$

where

$$\eta = \varkappa/(1 - u^2/c^2) = (\epsilon\mu - 1)/(1 - u^2/c^2). \qquad (17)$$

We now plot the "surface of normals": In any direction, at an angle ψ, with respect to the velocity of the medium **u**, we lay off the segment $c/n(\psi)$. The ends of these segments then form the surface of normals. In other words, if there is a radiation pulse at the origin, the surface of constant phase for waves of a given frequency (after unit time) is the surface of normals. It is apparent from Eq. (16) that the surface of normals is a surface of rotation with axis along **u**. Furthermore, Eq. (16) defines one surface rather than two because

$$c/n_1(\pi - \psi) = -c/n_2(\psi), \qquad (18)$$

i.e., both solutions describe one surface (if 1/n is negative, we assume that the phase velocity of the wave is opposite to the direction of the wave vector).

It is apparent from Eq. (16) that the properties of the surface of normals are determined by the parameter $\sqrt{\epsilon\mu}\, u/c$. The entrainment of the radiation of the moving medium appears in the fact that when $\epsilon\mu > 1$ the surface of normals is displaced in the direction of the moving medium (with respect to the origin). If $\epsilon\mu < 1$ the surface is displaced in the opposite direction.

From the surface of normals c/n we can go over to a surface of refractive indices n. When $\epsilon\mu u^2/c^2 < 1$ this surface is an ellipsoid, when $\epsilon\mu u^2/c^2 = 1$ it is a parabaloid, and when $\epsilon\mu u^2/c^2 > 1$ it is a hyperboloid of rotation.

8. Equation (13) indicates a remarkable property of media for which

$$\varepsilon\mu = 1 + \text{const}/\omega^2. \tag{19}$$

In media of this kind the surface of normals is a sphere of fixed radius in any system of coordinates, regardless of the velocity of the medium. An example of a medium for which (19) is satisfied is an isotropic electron plasma.

We may also note that if the velocity of the moving medium is large $(1-u^2/c^2 \ll 1)$ the argument of ϵ and μ, $(\omega - \mathbf{k}\cdot\mathbf{u})/(1-u^2/c^2)^{1/2}$, becomes large and the asymptotic expressions can be used for ϵ and μ:

$$\mu = 1, \qquad \varepsilon = 1 - 4\pi nc^2/m\omega^2. \tag{20}$$

In this case the propagation relation is the same as for an electron plasma [cf. Eq. (19)]. It should be noted, however, that when $\omega = \mathbf{k}\cdot\mathbf{u}$ this statement no longer applies. In the latter case the c/n surface is a sphere whose diameter is the vector $\mathbf{u}$, laid off from the origin.

9. From the definition of the refractive index (14) it follows that the vector $\mathbf{k}$, which satisfies Eq. (13), forms an angle ϑ with the velocity of the particle $\mathbf{v}$; this angle is given by the familiar relation

$$\cos\vartheta = c/vn(\psi). \tag{21}$$

Real waves can be emitted only when $c^2/v^2n^2(\psi) \leq 1$. This is the familiar Cerenkov radiation condition.

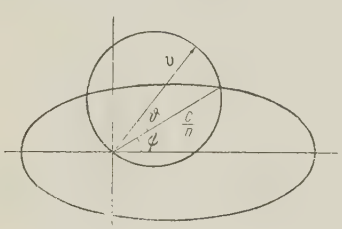

10. If the surface of normals is known the Cerenkov cone can be determined graphically. From the center of the surface of normals we lay off the vector corresponding to the particle velocity $\mathbf{v}$; on $\mathbf{v}$, we lay off a sphere with the vector as a diameter (cf. figure). In general this sphere intersects the surface of normals in some closed curve. A normal which connects the center of the surface with a point on the intersection curve gives the possible direction of the wave vector associated with the Cerenkov radiation while a line which connects the intersection point with the end of the vector $\mathbf{v}$ gives the wave front. If the intersection curve is traversed the normal describes the wave-vector cone while the line connecting the ends of the vector with the intersection curve describes the wave-front cone. In certain directions it may be impossible for radiation to be excited if the electric vector of the wave is perpendicular to the velocity of the charge.

11. We consider several simple cases of radiation of a charge in a moving medium. Let the velocity of a charge be parallel to the velocity of the medium. Then, from Eq. (11) we obtain the following expression for the Cerenkov radiation of the charge:

$$\frac{dW}{dx} = \frac{q^2}{v^2}\int\left[1 - \frac{v^2}{c^2} - \frac{\varkappa}{1+\varkappa}\frac{(1-uv/c^2)^2}{1-u^2/c^2}\right]\mu\omega d\omega, \tag{22}$$

where the integration extends over frequency regions which satisfy the inequality

$$1 - v^2/c^2 - \eta(v-u)^2/c^2 < 0, \qquad \eta = \varkappa/(1-u^2/c^2). \tag{23}$$

The radiation cone is circular, with a uniform distribution of intensity over the geneatrices. The opening angle of the cone is given by the relation

$$\tan^2\vartheta = v^2/c^2 + \eta(u-v)^2/c^2 - 1. \tag{24}$$

If the velocity of the particle is parallel to the velocity of the medium the quantity κ is a function of the argument $\omega(1-u/v)/(1-u^2/c^2)^{1/2}$.

12. Let the velocity of the charge form an arbitrary angle with the velocity of the medium. Since the Cerenkov losses are given by Eq. (13), Eq. (11) can be written in the form

$$\frac{dW}{dx} = \frac{q^2}{\pi v^2}\int\limits_{\mathbf{kv}>0}\left[1 - \frac{v^2}{c^2} - \frac{\varkappa}{1+\varkappa}\frac{(1-\mathbf{uv}/c^2)^2}{1-u^2/c^2}\right]$$

$$\times\,\mu\mathbf{kv}\delta\left\{\frac{(\mathbf{kv})^2}{c^2} - k^2 + \frac{\varkappa}{c^2}\frac{(\mathbf{ku}-\mathbf{kv})^2}{(1-u^2/c^2)}\right\}d\mathbf{k}. \tag{25}$$

In k-space we introduce a cylindrical coordinate system with its k_z axis along the velocity of the charge. We take $\mathbf{k}\cdot\mathbf{v} = \omega$, $k^2 = \omega^2/v^2 + \sigma^2$, $\sigma = \mathbf{k} - \mathbf{v}(\mathbf{k}\cdot\mathbf{v})/v^2$. It will be apparent that

$$d\mathbf{k} = \sigma d\sigma d\varphi d\omega/v,$$

where φ is the angle in the plane perpendicular to $\mathbf{v}$. Carrying out the integration over σ, we have

$$\frac{dW}{dx} = \frac{q^2}{\pi v^2}\int\left[1 - \frac{v^2}{c^2} - \frac{\varkappa(\sigma_0)}{1+\varkappa(\sigma_0)}\frac{(1-\mathbf{uv}/c^2)^2}{1-u^2/c^2}\right]$$

$$\times\,\frac{\mu(\sigma_0)\,\sigma_0}{F_\sigma'(\omega,\varphi,\sigma_0)}\omega d\omega d\varphi, \tag{26}$$

where $F(\omega, \varphi, \sigma)$ is the argument of the δ function in Eq. (25) and σ_0 is the value of σ for which $F = 0$. Since σ_0 depends on ω and φ, Eq. (26) gives the distribution of Cerenkov radiation over angle and frequency. The radiated waves form an

angle ϑ with the velocity of the charge where

$$\tan \vartheta = v\sigma_0/\omega. \quad (27)$$

It is apparent that the radiation cone is not circular, but has a complicated shape (since σ_0 depends on φ). It also follows from Eq. (26) that the radiation intensity is not uniform over the geneatrices.

13. We may also consider the polarization losses of the charge in the medium. Carrying out calculations similar to those in Section 12, we have

$$\frac{dW}{dx} = -\frac{q^2}{\pi v^2}\frac{(1-\mathbf{uv}/c^2)^2}{1-u^2/c^2} \times \sum \int \frac{\sigma_0 \mu(\sigma_0)}{\left|\varkappa'_\sigma(\omega, \varphi, \sigma_0)\right|} \frac{\omega d\omega d\varphi}{(\omega/v)^2(1-v^2/c^2)+\sigma_0^2+\omega_s^2/c^2}, \quad (28)$$

where σ_0 is the value of $\sigma(\omega, \varphi)$ for which $1 + \kappa = 0$ and ω_S is the root of the equation $\epsilon(\omega_S) = 0$. The summation is taken over all roots ω_S. The polarization losses are determined by the equation

$$(\mathbf{kv} - \mathbf{ku})/(1-u^2/c^2)^{1/2} = \omega_s. \quad (29)$$

It is interesting to note that the group velocity of the polarization waves is equal to the velocity of the medium **u**, i.e., the energy of these waves is "frozen" in the medium.

The relativistic Doppler shift in the frequency of the excited longitudinal oscillations of the medium can be used for measuring its velocity.

The authors wish to thank V. L. Ginzburg and I. M. Frank for valuable discussions.

[1] I. E. Tamm, J. Phys. (U.S.S.R.) **1**, 439 (1939).

[2] B. M. Bolotovskiĭ, Usp. Fiz. Nauk **62**, 201 (1957).

[3] V. I. Veksler, Атомная энергия (Atomic Energy) **2**, 427 (1957).

[4] I. E. Tamm, J. Russ. Phys. Chem. Soc. **56**, 248 (1924).

[5] M. I. Ryazanov, JETP **32**, 1244 (1957), Soviet Phys. JETP **5**, 1013 (1957). (Coll. Некоторые вопросы теоретической физики (Certain Problems in Theoretical Physics), Atomizdat, 1958, p. 75.

Translated by H. Lashinsky
268

EQUILIBRIUM OF A PLASMA WITH HELICAL SYMMETRY

B. B. KADOMTSEV

Submitted to JETP editor May 26, 1959

J. Exptl. Theoret. Phys. (U.S.S.R.) **37**, 1352-1354 (November, 1959)

A simple example of plasma equilibrium in a magnetic field with helical symmetry is considered.

THE problem of equilibrium of a plasma in a magnetic field involves the solution of the system of equations:

$$\operatorname{div}\mathbf{H}=0, \qquad \nabla p=[\operatorname{curl}\mathbf{H}\times\mathbf{H}]/4\pi. \tag{1}$$

In this note we consider the case of helical symmetry, in which the plasma pressure p and the magnetic field components H_r, H_φ, H_z in a cylindrical coordinate system, depend only on r and $\zeta = kz - m\varphi$ (m is an integer and $\lambda = 2\pi/k$ is the period of the variation in p and **H** along the z axis). As has been shown by Johnson et al.[1] in this case the system of equations in (1) can be reduced to a single nonlinear equation. From the equation

$$\operatorname{div}\mathbf{H}=\frac{1}{r}\frac{\partial}{\partial r}(rH_r)+\frac{\partial}{\partial\zeta}\left(-\frac{m}{r}H_\varphi+kH_z\right)=0$$

it follows that*

$$H_r=\frac{1}{r}\frac{\partial\psi}{\partial\zeta}, \qquad \frac{m}{r}H_\varphi-kH_z=\frac{1}{r}\frac{\partial\psi}{\partial r},$$

where ψ is an arbitrary function of r and ζ. Furthermore, from the relation $\mathbf{H}\cdot\nabla p=0$ it follows that p is a function of ψ only, while from the equation $\nabla p\cdot\operatorname{curl}\mathbf{H}=0$ it follows that $mH_z + krH_\varphi = I$, where I is an arbitrary function of ψ. By means of these relations the component of the equilibrium equation (1) along $\nabla\psi$ can be transformed as follows:

$$\frac{1}{r^2}\frac{\partial^2\psi}{\partial\zeta^2}+\frac{1}{r}\frac{\partial}{\partial r}\left(\frac{r}{k^2r^2+m^2}\frac{\partial\psi}{\partial r}\right)+4\pi\frac{dp}{d\psi}+\frac{I}{k^2r^2+m^2}\frac{dI}{d\psi}+\frac{2kmI}{(k^2r^2+m^2)^2}=0. \tag{2}$$

If the functional dependence of p and I on ψ is given and Eq. (2) is solved, in principle it is possible to obtain all possible equilibrium configurations characterized by helical symmetry. However, the problem of solving the nonlinear equation is extremely difficult. It is only in the simplest case, in which I and $dp/d\psi$ are linear functions of ψ, that Eq. (2) is linear and can be solved by separation of variables.

Here we consider a still simpler example of the equilibrium configuration: I = const, $p = p_0 + (a/4\pi)\psi$. In this case Eq. (2) becomes

$$\frac{1}{r^2}\frac{\partial^2\psi}{\partial\zeta^2}+\frac{1}{r}\frac{\partial}{\partial r}\left(\frac{r}{k^2r^2+m^2}\frac{\partial\psi}{\partial r}\right)=-a-\frac{2kIm}{(k^2r^2+m^2)^2}. \tag{3}$$

Whence we find

$$\psi=-\frac{ar^2}{8}(k^2r^2+2m^2)-\frac{kr^2I}{2m}+A\left(\frac{k^2r^2}{2}+m^2\ln r\right)+\psi_1, \tag{4}$$

where A = const, and $\psi_1(r,\zeta)$ is an arbitrary solution of the homogeneous equation.

From the known function ψ we find the plasma pressure and the magnetic field:

$$p=p_0+\frac{a}{4\pi}\left\{-\frac{ar^2}{8}(k^2r^2+2m^2)-\frac{kr^2I}{2m}+A\left(\frac{k^2r^2}{2}+m^2\ln r\right)+\psi_1\right\}, \tag{5}$$

$$H_r=\frac{1}{r}\frac{\partial\psi}{\partial\zeta}=H_{1r}, \tag{6}$$

$$H_\varphi=\frac{1}{m^2+k^2r^2}\left(m\frac{\partial\psi}{\partial r}+krI\right)=-\frac{mar}{2}+\frac{mA}{r}+H_{1\varphi}, \tag{7}$$

$$H_z=\frac{1}{m^2+k^2r^2}\left(-kr\frac{\partial\psi}{\partial r}+mI\right)=\frac{I}{m}-kA+\frac{akr^2}{2}+H_{1z}, \tag{8}$$

where $\mathbf{H}_1$ is the curl-free magnetic field, given by the function ψ_1.

It is apparent that the magnetic field is composed of the uniform magnetic field along the z axis, the field of the uniform longitudinal current (j_z = const) and the longitudinal current concentrated at the z-axis ($J_0 \sim A$), the field due to the azimuthal current j_φ, which increases linearly with r, and the arbitrary curl-free field $\mathbf{H}_1$ characterized by helical symmetry.

*If this relation is integrated over the volume bounded by the surface ψ = const and the planes z = 0 and $z = 2\pi/k$, we obtain

$$\psi=\frac{k}{2\pi}(m\Phi_\varphi-\Phi_z),$$

where

$$\Phi_z(\psi)=\int_0^{2\pi}\int_0^{r(\psi)}H_z\,r\,dr\,d\varphi, \qquad \Phi_\varphi(\psi)=\int_0^{2\pi/k}\int_0^{r(\psi)}H_\varphi\,dr\,dz.$$

In this case (I = const) it can be shown that $j_\varphi = (kr/2\pi m) j_z$, i.e., the current flows along the helical lines $\zeta = \text{const}$ (this feature explains the possibility of applying an arbitrary field $\mathbf{H}_1$ with the same symmetry without disturbing the condition $\mathbf{j} \cdot \nabla p = 0$).

For simplicity we limit our analysis to the particular case in which

$$\psi_1 = \sin\zeta \cdot kr\,(BI'_m(kr) + CK'_m(kr), \qquad (9)$$

where A = const, B = const, I_m is a Bessel function of imaginary argument and K_m is the Macdonald function. The general solution of the equation for ψ_1 can be given in the form of a series of functions such as (9).

If we require that the pressure p and the function ψ be regular as $r \to 0$, we must set A = C = 0 and ψ becomes

$$\psi = -(ar^2/8)(k^2r^2 + 2m^2) - kr^2I/m + B\sin\zeta \cdot krI'_m(kr). \qquad (10)$$

Let $a > 0$ and $I > 0$; then, for small values of B (or if $m > 2$, for any value of B, but small values of r) close to the z axis there is a region in which ψ and the pressure p fall off with radius. This solution can be interpreted as characterizing equilibrium of a plasma inside a chamber whose walls coincide with the surface $\psi = -4\pi p_0/a$, where the plasma pressure vanishes. When m = 2, for example, the pressure distribution assumes the form shown in the figure, in which the pattern of the lines of constant pressure in the planes z = const ($p_0 = 1$) is shown.

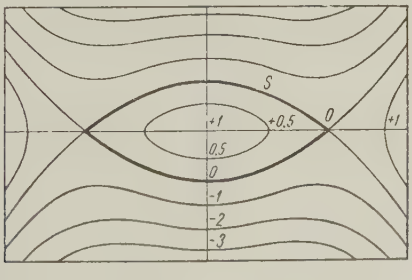

It is apparent from Eq. (10) that if the coefficient B becomes larger, i.e., if the magnetic field $\mathbf{H}_1$ produced by the external helical winding is increased, the equilibrium situation is worse; in particular, there is a reduction in the limiting pressure p_0 for which a plasma with zero pressure at the walls of the chamber can still be in equilibrium. In addition, the transverse dimension of the region in which $p > 0$ becomes smaller. This phenomenon is explained by the fact that the increase $\mathbf{H}_1$ causes a large curvature in the lines of force, resulting in a reduction of the region in which the lines of force do not extend to infinity in a radial direction. (In the figure this region is enclosed by the boundary marked S).

We consider another particular case: that in which $a > 0$ and $I < -am^3/4k$. If B is small, when $B > 0$ the function ψ will have a maximum $\psi = \psi_0$ at some helical line $r = r_0$, $\sin\zeta = 1$. Since ψ falls off with distance from this line, at low pressures there is an equilibrium state of the plasma in which the pressure vanishes along some helical tube $\psi = \text{const} < \psi_0$ which surrounds the line $r = r_0$, $\sin\zeta = 1$. Thus, this solution represents the simplest representation of the equilibrium states of a plasma in a chamber in the form of a helical tube. We may note that in the analysis of equilibrium in chambers of this type the constants A and C may be taken different from zero, allowing some extension of the family of simple solutions of this kind.

[1] Johnson, Oberman, Kusrud, and Frieman, Proceedings of the Second International Conf. on the Peaceful Uses of Atomic Energy, Geneva 1958, P/1875.

Translated by H. Lashinsky
269

A POSSIBILITY FOR INVESTIGATING THE STRUCTURE OF NUCLEONS AND NUCLEI

N. G. BIRGER and Yu. A. SMORODIN

P. N. Lebedev Physics Institute, Academy of Sciences, U.S.S.R.

Submitted to JETP editor June 1, 1959

J. Exptl. Theoret. Phys. (U.S.S.R.) **37**, 1355-1360 (November, 1959)

It is shown that in the interaction of high energy particles the sum of the quantities $(E - p\cos\vartheta)$ for all particles emitted after the interaction is equal to the mass of the target particle which effectively participates in the interaction. Thus the distribution of $\Sigma(E - p\cos\vartheta)$ is determined by the structure of the target particle. Application of this type of analysis to the experimental data shows that interactions with the part of the target which has a mass close to that of the π meson are dominant.

1. In reference 1 we derived a form of conservation laws for energy and momentum, proposed by S. N. Vernov, which is convenient for the kinematic analysis of interactions in which a high energy particle generates secondary particles.

If the target particle is at rest, we can write for sufficiently fast primary particles $(E_0 - p_0 = M_0^2/2p_0 \ll M_{tg})$

$$\sum (E_i - p_i \cos\vartheta_i) = M_{tg}. \qquad (1)$$

Here E, p, ϑ, and M are the total energy, the momentum, the angle of emission, and the mass of the particle. The index 0 denotes the primary particle, i the particle after the interaction, and tg the target particle. The summation in (1) goes over all particles emitted after the interaction.

If the particles emitted after the interaction are sufficiently fast, we can write (1) in the form

$$M_{tg} = \sum \left(\frac{M_i^2}{2p_{\perp i}} \sin\vartheta_i + p_{\perp i} \tan\frac{\vartheta_i}{2} \right). \qquad (2)$$

In this form of writing the physical meaning of expression (1) becomes clear: it gives a connection between the mass of the target and the values of the angles and transverse momenta of the particles emitted after the interaction.

2. Let us generalize relation (1) to the case when the target particle moves.

With the notation $E_i - p_i \cos\vartheta_i = \Delta_i$, we obtain

$$\sum \Delta_i = M_{tg} + T_{tg} - p_{tg}\cos\vartheta_{tg}, \qquad (3)$$

where T_{tg} is the kinetic energy of the target particle, and $p_{tg}\cos\vartheta_{tg}$ is the projection of its momentum before the collision on the direction of motion of the incoming particle.

We assume further that the target particle is bound to some heavier particle. Let us consider, for example, the interaction with a nucleon inside the nucleus. The potential energy of the nucleon in the nucleus, u_n, is small in comparison with the mass of the nucleon. After the emission of the nucleon the residual nucleus $M_{nuc\,0}$ receives an impulse on the order of u_n, which causes it to recoil slightly. In studying the interaction with a definite moving nucleon, one must take account of the fact that the residual nucleus is not at rest before the interaction, but has a momentum which is equal and opposite to that of the nucleon in the nucleus. The quantity $\Delta_{nuc\,0} = E - p\cos\vartheta$ for the residual nucleus can be written in the form $\Delta_{nuc\,0} = M_{nuc\,0} - p_{nuc\,0}\cos\vartheta_{nuc\,0} + T_{nuc\,0}$. Neglecting $T_{nuc\,0}$ and using $p_{nuc\,0} = -p_n + \alpha$, we obtain $\Delta_{nuc\,0} = M_{nuc\,0} + p_n\cos\vartheta_n - \alpha$, where α is a quantity of the same order as u_n.

We write relation (1) for the initial nucleus M_{nuc} in the form

$$\sum \Delta_i + \Delta_{nuc\,0} = M_{nuc},$$

where $M_{nuc} = M_{nuc\,0} + M_n + T_n - u_n$, and obtain

$$\sum \Delta_i = M_n + T_n - (u_n - \alpha) - p_n\cos\vartheta_n. \qquad (4)$$

Relation (4) takes account of the recoil of the residual nucleus. If the recoil is neglected, we have

$$\sum \Delta_i = M_n + T_n - u_n - p_n\cos\vartheta_n. \qquad (5)$$

The distribution of the quantities $\Sigma\Delta_i$, which we shall call M_t in the following, is given in this case by a line with a maximum at the value $M_n + (\overline{T_n - u_n})$ (the average $\overline{p_n\cos\vartheta_n} = 0$, in any case for unpolarized nuclei). The width of the line is determined by the quantity p_n, the Fermi momentum of the nucleon in the nucleus.

3. Let us now consider the interaction of a sufficiently fast particle with a nucleus of mass M_{nuc}.

If there are interactions with one, two, or more nucleons, the spectrum of the quantities M_t will, according to the foregoing, have lines near the values of one, two, etc. nucleon masses.

In the region of target masses close to M_{nuc} the spectrum of the quantities M_t will be smeared out and appear to become continuous. Since the recoil of the residual nucleus cannot be neglected in this region, the position and the width of the line do not any more have the clear classical meaning expressed by relation (5). Even in this case, however, the form of the spectrum of M_t will reflect the structure of the nucleus.

Since in any case

$$\sum \Delta_i + \Delta_{\text{nuc }0} = M_{\text{nuc}}, \qquad (6)$$

where $\Delta_{\text{nuc }0} = E - p\cos\vartheta$ for the recoiling residual nucleus as a whole or for its fission products, it should be noted that the distribution of the quantities $\Delta_{\text{nuc }0}$ will simply reflect the distribution of the quantities $\Sigma\Delta_i$. A preference for either one of these quantities has to be based on experimental considerations.

4. This method can also be applied to the study of the structure of the nucleon by considering the interaction of the nucleon with particles whose wavelength is small compared with the dimensions of the nucleon.

In this case we extract from the sum of all Δ_i the term which corresponds to the recoil nucleon: $\Delta_\delta = E_\delta - p_\delta \cos\vartheta_\delta$. It follows from the analog of relation (4) that the value of $M_t = \Sigma\Delta_i$ will correspond to the value of the "effective masses" of those parts of the target nucleon which participate in the interaction.

The value of the quantities M_t obtained in this way will determine the relative probability of interaction with various regions of the nucleon.

If the nucleon has no structure, the spectrum of M_t should not have separate lines. If such lines are observed in experiment, it indicates that the nucleon is made up of separate structures. In the opinion of the authors, the question whether the experimentally observed structure is real or virtual is to be decided by the relative width of the lines in the distribution of M_t. From this point of view there is no physical borderline which separates a real particle from a virtual one; one can only speak of the degree of reality of a particle.

5. Since $\Sigma\Delta_i + \Delta_\delta = M_n$, we can obtain the distribution of M_t from $\Sigma\Delta_i$ or from the quantities Δ_δ for the recoil nucleon, whichever is more convenient from the experimental point of view.

In the region of small energies, where the identification of the recoil protons is possible, it is obviously more convenient experimentally to study the recoil nucleons.

In experiments with high energy particles, on the other hand, a number of circumstances are favorable for an exact determination of $\Sigma\Delta_i$ for the generated particles.

We emphasize, first of all, that $\Sigma\Delta_i$ and Δ_δ can be calculated without knowing the energy and the mass of the incoming particle, which appreciably simplifies the experimental procedure.

According to (2), the particles that give the greatest contribution to the sum are those emitted under relatively large angles with relatively small momenta. This circumstance allows us to relax the accuracy requirements with respect to the measurement of the momenta.

For sufficiently high energies of the secondary particles and sufficiently high number of generated π mesons, the error arising from the impossibility of identifying the fast nucleon is insignificant. If, in forming $\Sigma\Delta_i$, we treat the slow nucleon like a π meson with the same momentum, then Δ_δ will be automatically excluded from the sum of the Δ_i.

It can be shown that in the sum $\Sigma\Delta_i$ the errors in the measurement of the angles and momenta are averaged out in first approximation. An increase in the number of the π mesons generated in the shower leads, therefore, to an increase in the accuracy of the calculation of $\Sigma\Delta_i$.

Since the second term of the sum (2) gives the main contribution to the sum of the Δ_i, a small admixture of heavy mesons will not affect the value of $\Sigma\Delta_i$ appreciably.

6. We calculated $M_t = \Sigma\Delta_i$ from the available data on the following interactions of high energy particles with nucleons and nuclei: 1) proton-proton interaction with proton energy 3.7 Bev;[2] 2) interaction of cosmic ray protons with Be nuclei with an average proton energy of about 5 Bev;[1] 3) pion-proton interaction ($\pi^- + p$) with pion energies of about 5 Bev;[3] 4) generation of π mesons by μ mesons in lead nuclei, which was treated by Kessler and Maze[4] like the photoproduction of μ mesons by photons with energies of about 17 Bev; 5) interaction of 10^{11}-ev cosmic-ray particles* with LiH nuclei; 6) interaction of cosmic ray particles with energies $10^{12}-10^{13}$ ev with nuclei

*The authors express their deep gratitude to the workers of the cosmic ray laboratories of the Physics Institute of the Academy of Science and the Institute of Nuclear Physics of the Moscow State University, N. A. Dobrotin, N. L. Grigorov, S. A. Slavatinskiĭ, V. S. Murzin, V. V. Guseva, K. S. Kotel'nikov, and S. I. Ryabikov for giving us the opportunity to become acquainted with their experimental results before publication. It was this opportunity which stimulated the present paper.

"Jets" in photoemulsions*

Type of star	E_0, eV	M_t/M_n	Remarks	Reference
2+16 p	$5\cdot10^{12}$	0.33	The $p\beta$ of the ionizing particles was determined	[5]
2+15 p	$2\cdot10^{13}$	0.16	" " "	[6]
1+39 p	$5\cdot10^{12}$	1.05	" " "	[8]
0+14 α	$\sim10^{14}$	0.08	The energy of the π^0 mesons was determined	[7]
0+7 p	10^{12}	0.10	The $\pi^{\pm}$ and π^0 mesons were measured	[9]

*In the table we list the high energy "jets" in which the angles and momenta of the secondary particles have been measured. The energy was estimated by the authors of the references on the basis of the angular distribution. In these cases the energy of the interaction given by the authors of references 5, 6, 7, and 9 is apparently much too high. The very poor sampling of the interactions does not allow us to make conclusions about the true contribution from the interactions with small M_t.

in photoemulsions, leading to the formation of so-called "jets," in those cases where data on the momenta of the particles exist.[5-9]

The calculated distributions of M_t are given in the table and in Figs. 1 to 5, the captions of which contain all the necessary notes.

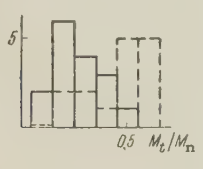

FIG. 1

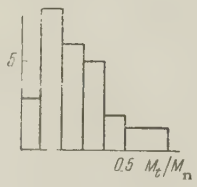

FIG. 2

FIG. 3

FIG. 4

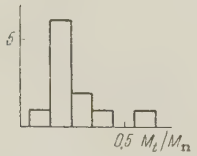

FIG. 5

FIG. 1. Interaction p + p, E_0 = 3.7 Bev. M_t was determined as the difference $M_n - \Delta_\delta$. The quantities Δ_δ were measured for the nucleons in the interactions $p + p \to p + N + \pi^+$ (solid line) and $p + p \to p + N + \pi^+ + \pi^0$ (dotted line), which could be reliably identified. The method of identification could lead to a distortion of the distribution in the region of large M_t. The comparison of the distributions of the two above-mentioned reactions shows, however, that the occurrence of a maximum in the region of small M_t for the reaction in which one pion is produced cannot be explained by the sampling. The absence of the maximum for the reaction leading to the production of two pions is connected with the small value of the center of mass energy (E = 500 Mev).

FIG. 2. Interaction p + Be, $\bar{E}_0$ = 5 Bev. M_t is, in most cases, determined as the difference $M_n - \Delta_\delta$. In the remaining cases it is measured directly as the sum of the Δ_i.

FIG. 3. Interaction π^- + p, E_0 = 5 Bev. M_t is determined as the difference $M_n - \Delta$. Dotted lines: reliably identified protons; solid lines: all events. The dotted curve shows the effect of the sampling in the region $M_t > 0.5$. The character of the sampling is analogous to that in the case of the interactions shown in Figure 1.

FIG. 4. Photoproduction of pions, $h\nu$ = 17 Bev. The figure shows the distribution of M_t for the penetrating showers generated by μ mesons of high energy incident on lead nuclei. M_t is computed by formula (2) with the value $\overline{p_{\perp i}} = 4.2 \cdot 10^8$ ev.

FIG. 5. Interaction of cosmic ray particles with LiH, $E_0 \approx 10^{11}$ ev. The angles and momenta of the particles are measured in the Wilson chamber. $M_t = 1.5 \sum_{\text{charged}} \Delta_i$; the factor 1.5 corrects for the generation of π^0 mesons.

The experimental data used to obtain the distributions of M_t do not have sufficient statistical accuracy to lead to conclusive quantitative results. Nevertheless, it can be assumed that more abundant experimental material will lead to the following conclusions.

A. For nucleon-nucleon interactions in a large energy interval the distribution has a maximum in the region $M_t \approx 0.2\, M_n$. An analogous maximum is observed for interactions of photons with nucleons. The occurrence of this maximum indicates that the interaction with an "effective mass" close to the mass of the π meson plays the predominant role.

B. Let us assume that in the nucleon-nucleon

interaction the number of cases in which the fast nucleon interacts with $M_t \approx M_\pi$ is equal to the number of cases in which the target is a nucleon and the incident nucleon interacts only through a part of itself, whose mass is close to M_π. Then the observed distributions of M_t can be interpreted by assuming that the cross section for the interaction of the "core" with π mesons is a few times larger than the cross section for the interaction of the nucleon "cores" with each other ($\sigma(N', \pi) \approx 4\sigma(N', N')$).

C. For the interaction of π mesons with nucleons the distribution of M_t does not have a maximum in the neighborhood of the π meson mass. This indicates that the cross section for the π-π interaction for energies of 5 Bev is relatively small ($\sigma(\pi, \pi) < \frac{1}{3}\sigma(\pi, N)$).

These results on the distribution of M_t for the interactions (N, N) and (π, N) permit us to estimate[1] the energy losses in the interaction of nucleons with energies $10^{10}-10^{11}$ ev with other nucleons and to explain the fact, established in cosmic-ray experiments, that the energy losses in the interaction of nucleons of about 10^{10} ev with light nuclei are small,[10] and the energy dependence of the energy losses is weak.[11]

7. From the standpoint of our method, the most fruitful experiments for the study of the structure of the nucleon appear to be the following:

1) Investigation of the photo production of π mesons by photons of high energy in nucleons and light nuclei. The distribution of M_t reflects, in this case, directly the relative frequency of the interaction with various parts of the target nucleon.

2) Comparison of the Δ spectra for the interactions $p+p$ and $\pi+p$ with similar effective energies. These experiments make it possible to separate the $\pi-\pi$ interaction.

3) Experiments at such energies of the particles that there are no energetical limitations on interactions with small M_t. These experiments lead to a more accurate determination of the character of the tail of the Δ spectrum and allow us to solve the problem of the coupling and, in the last analysis, of the degree of reality of the π meson in the nucleon.

There is no doubt that this classical treatment of the Δ spectra is rather crude for the nucleon. One should, obviously, get a deeper insight by treating the interactions quantum-theoretically.

The authors are deeply grateful to E. L. Feĭnberg and D. S. Chernavskiĭ for valuable advice and fruitful discussions, and also to S. N. Vernov, N. L. Grigorov, G. T. Zatsepin, I. L. Rozental', S. A. Slavatinskiĭ, and F. L. Shapiro for participating in the critical discussion of the results.

[1] N. G. Birger and Yu. A. Smorodin, JETP **36**, 1159 (1959), Soviet Phys. JETP **9**, 823 (1959).

[2] Block, Harth, Cocconi, Hart, Fowler, Shutt, Thorndike, and Whittemore, Phys. Rev. **103**, 1484 (1956).

[3] Maenchen, Fowler, Powell, and Wright, Phys. Rev. **108**, 850 (1957).

[4] D. Kessler and M. Maze, Nuovo cimento **5**, 1540 (1957).

[5] Boos, Vinitskiĭ, Takibaev, and Chasnikov, JETP **34**, 622 (1958), Soviet Phys. JETP **7**, 430 (1958).

[6] Glasser, Haskin, Schein, and Lord, Phys. Rev. **99**, 1555 (1955).

[7] Ciok, Danysz, Gierula, Jurak, Miesowiez, Pernegr, Vrana, and Wolter, Nuovo cimento **6**, 1409 (1957).

[8] Debenedetti, Garelli, Tallone, and Vigone, Nuovo cimento **4**, 1142 (1956).

[9] Hopper, Biswas, and Darby, Phys. Rev. **84**, 457 (1951).

[10] N. L. Grigorov, Dokl. Akad. Nauk SSSR **94**, 835 (1954).

[11] Vernov, Grigorov, Zatsepin, and Chudakov, Izv. Akad. Nauk SSSR, Ser. Fiz. **19**, 493 (1955), Columbia Tech. Transl. p. 445.

Translated by R. Lipperheide
270

APPLICATION OF THE DISPERSION RELATIONS METHOD IN QUANTUM ELECTRODYNAMICS

V. Ya. FAĬNBERG

Submitted to JETP editor June 1, 1959

J. Exptl. Theoret. Phys. (U.S.S.R.) **37**, 1361-1371 (November, 1959)

An approximate set of dispersion equations for the Green's function of the photon and vertex part has been derived in quantum electrodynamics on the basis of the dispersion relations and unitarity conditions. The "nonsubtraction" procedure is employed in the asymptotic investigation of the solutions of the equation. Agreement with the renormalized perturbation theory when the fine structure constant tends to zero has been used as the boundary condition. It is shown that the vertex function decreases asymptotically with increase in the square of the photon 4-momentum $q^2 = (p_+ + p_-)^2$ for $p_+^2 = p_-^2 < m^2$ where p_-, p_+ are the electron and positron 4-momenta. This leads to finite renormalization of the charge in the approximation under consideration.

1. INTRODUCTION

THE method of dispersion relations, based on very general requirements of covariance, causality, positiveness of the energy spectrum (spectrality), and unitarity has been developed intensively in recent years in quantum field theory.

This method permits us to express the Green's function (for the amplitudes of processes) in terms of invariant spectral functions which can in turn be connected with the Green's function of other processes by means of the unitarity conditions. Thus a set of equations for the Green's function can be obtained in principle. This set of equations possesses important advantages over the usual approach. First, it contains only renormalized quantities and consequently does not lead to the appearance of expressions that diverge at high momenta, the latter effect being characteristic for perturbation theory and the Schwinger-Dyson equation; second, it interrelates the amplitudes of various processes on the energy surface.

Serious hopes of avoiding the well-known difficulties attached to the approximate solutions of the Schwinger-Dyson equation[1-3] are connected with the method of dispersion relations.

A whole series of papers has appeared in which the method of dispersion relations is used for the derivation of approximate equations for the Green's function, Thus, Mandel'shtam[4] obtained an approximate equation from the dispersion relations for the amplitude of scattering of a meson by a nucleon. In the work of Drell and Zachariasen,[5] an attempt was undertaken at the determination of the approximate equation for the vertex part in quantum electrodynamics following from the dispersion relations (form factor of the electron). However, the basic results obtained in this research have raised objections.*

In the present research an attempt has been made at a more systematic analysis of quantum electrodynamics from the point of view of the dispersion relations. Inasmuch as spectral representations have been well studied only for the simplest Green's function, and also because of the extraordinary difficulties which arise in the calculation of higher Green's functions, we have limited ourselves to a discussion of the lowest approximation in the dispersion equations which contains only the Green's function of the photon and vertex part. The principal unsolved question today in such an approach is thus the consideration and estimation of the contribution of higher approximations, i.e., two-particle and more complicated Green's functions.

The choice of quantum electrodynamics is not accidental. First, there enters only a single constant here — the renormalized charge of the electron and the well-known boundary conditions — agreement with perturbation theory at low energies. Second, in the first stage of the investigation we can consider the interaction of photons only with the electron-positron field and disregard other particles (the "pure" quantum electrodynamics).

In the setting up of the dispersion relations,

*For details see below, Sec. 3..

we start out from the "nonsubtraction" procedure.* A formulation is given in Sec. 2 of the dispersion relations and the boundary conditions in quantum electrodynamics. In Sec. 3, we have investigated the asymptotic solution of a set of equations for the photon Green's function and vertex part in the simplest approximation. A discussion of the results obtained is given in Sec. 4. Appendices are included at the end of the paper.

2. DERIVATION OF THE DISPERSION RELATIONS

Derivation of the dispersion relations can be divided conditionally into three steps: I — the fundamental dispersion relations; II — an expression of the anti-Hermitian part of the spectral functions in terms of other amplitudes; III — the finding of reasonable boundary conditions.

It is natural to begin this process with the simplest single particle Green's function. The dispersion relations for the Green's function of the photon (the Källen-Lehman theorem[6]) are well known:†

$$D(q^2) = -\frac{1}{q^2} + \int_0^\infty \frac{\rho(q'^2)\,dq'^2}{q'^2 - q^2 - i\varepsilon}. \qquad (1)$$

The longitudinal part of $D_{\mu\nu}(q)$ is chosen equal to zero; in this case,

$$D_{\mu\nu}(q) = (\delta_{\mu\nu} - q_\mu q_\nu / q^2)\, D(q^2). \qquad (2)$$

By making use of the equation for the Heisenberg operators

$$\Box A_\mu(x) = j_\mu(x)$$

and decomposition over the whole set‡ (unitarity) one can express the spectral function $\rho(q^2)$ in terms of the amplitude of other processes.

$$\rho(q^2) = \frac{(2\pi)^3}{3}\,\mathrm{Sp}\left(\frac{1}{q^2}\right)^2 \sum_n \langle 0|j_\mu(0)|n\rangle\langle n|j_\nu(0)|0\rangle\,\delta(p_n - q). \qquad (3)$$

Equations (1) and (3) give the desired equation for $D_{\mu\nu}$.

Similarly, one can write down the dispersion relation for the Green's function of the electron. However, we shall not do this, inasmuch as it is not needed in what follows.

In order to extend the chain of equations, it is necessary to write down the dispersion relation for the matrix elements $\langle 0|j_\mu(0)|n\rangle$, which are on the right side of (3). The matrix element $\langle|j_\mu(0)|p_+, p_-\rangle$, where $|p_+, p_-\rangle$ is the state electron + positron, can be represented in the form

$$\langle 0|j_\mu(0)|p_+, p_-\rangle = \bar{u}_+(\mathbf{p}_+)\,\Lambda_\mu(p_+, p_-)\,u_-(\mathbf{p}_-),$$
$$\Lambda_\mu(p_+, p_-) = \gamma_\mu F_1(q^2) + \sigma_{\mu\nu}q_\nu F_2(q^2), \qquad q = p_+ + p_-. \qquad (4)$$

from consideration of relativistic and gauge invariance. Here, $u_\pm$ are solutions of the Dirac equation for the positron and electron, respectively;

$$(\hat{p} \pm m)\,u_\pm(\mathbf{p}) = 0, \qquad \gamma = \beta\alpha, \qquad \gamma_0 = \beta$$
$$p_0 = E(\mathbf{p}) = +(\mathbf{p}^2 + m^2)^{1/2}, \qquad \sigma_{\mu\nu} = (\gamma_\mu\gamma_\nu - \gamma_\nu\gamma_\mu);$$

$F_1(q^2)$ and $F_2(q^2)$ are invariant functions which characterize the charge distribution and the magnetic moment of the electron. The quantity Λ_μ is connected with the vertex function Γ_ν for $p_+^2 = p_-^2 = m^2$:

$$\bar{u}_+\Lambda_\mu(p_+, p_-)\,u = -\bar{u}_+\Gamma_\nu(p_+, p_-\ u_-\cdot D_{\mu\nu}(q)\,q^2. \qquad (5)$$

We emphasize that there is no necessity of taking Γ_μ into consideration. First, $\rho(q^2)$ [see Eq. (3)] is easily expressed* directly in terms of Λ_μ; second, inasmuch as Γ_μ in x space is not directly connected with the T product of the Heisenberg operators, the anti-Hermitian part of the vertex function can only be expressed indirectly in terms of the amplitude of other processes.

Up to the present time the dispersion relations for $F_i(q^2)$ have not been rigorously established. In the general case they can be shown in terms of q^2 under the condition $p_\pm^2 < 0$.† In the physical region $p_\pm^2 \to m^2$ ($p_\pm^2 \le m^2$) there is a proof of the dispersion relations in any approximation of perturbation theory.[7] We shall start out from the validity of the following dispersion relation (for $p_\pm^2 \le m^2$):

$$F_i(q^2) = \frac{1}{\pi}\int_0^\infty \frac{\mathrm{Im}\,F_i(q'^2)\,dq'^2}{q'^2 - q^2 - i\varepsilon}. \qquad (6)$$

In the derivation of (6), in addition to a knowledge of the analytic properties of $F_i(q^2)$ with respect to q^2, it is assumed that $F_i(q^2) \to 0$ for $|q^2| \to \infty$.‡ In this assumption is included the basic idea of the nonsubtraction procedure of Chew in the theory of dispersion relations. We note that the vanishing of $F_i(q^2)$ is the necessary condition for the finiteness of the charge renormaliza-

*In connection with the "nonsubtraction" procedure see, for example, reference 5 (see also below).

†These dispersion relations are obtained by starting out from the "nonsubtraction" procedure, i.e., under the assumption that $D(q^2) \to 0$ for $|q^2| \to \infty$. In our research the metric $q^2 = q_0^2 - q^2$ is used throughout.

‡By way of the entire system one can with equal right make use of the states $|n_{in}\rangle$ and $|n_{out}\rangle$, which correspond to incident and diverging waves.

*See also Sec. 4.

†The difficulty with analytic continuation in the "physical" region $p_\pm^2 \to m^2$ has not been overcome.[8]

‡In the opposite case (if $F_i(q^2) = \mathrm{const}$, or increases more slowly than $|q^2|$ for $|q^2| \to \infty$) the dispersion relations will be:

$$F_i(q^2) - F_i(0) = (q^2/\pi)\int_0^\infty \mathrm{Im}\,F_i[q'^2(q'^2(q'^2 - q^2 - i\varepsilon))]^{-1}\,dq'^2.$$

tion (i.e., the convergence of the integral $\int \rho(q^2)\,dq^2$).

The expression for $\mathrm{Im}\, F_1(q^2)$, which plays the role of spectral functions, can be found in the following fashion. We write:

$$\langle 0|j_\mu(0)|p_+,\ p_-\rangle = -\int \bar{u}_+(p_+)(i\hat{\nabla}_x - m)$$
$$\times \langle 0|T\psi(x)\bar{\psi}(x')j_\mu(0)|0\rangle (i\hat{\nabla}_{x'} + m)u_-(p_-)$$
$$\times \exp(-ip_+x - ip_-x')\,d^4x d^4x' \ldots \quad (7)$$

The corresponding expression for $\Lambda_\mu(p_+, p_-)$ is obtained if we omit the "coverings" $\bar{u}_+$ and u_- in (7). Noting that

$$\gamma_0\Lambda_\mu^*(-p_-, -p_+)\gamma_0 = -\int (i\hat{\nabla}_x - m)\langle 0|T\psi(x)\bar{\psi}(x')$$
$$\times j_\mu(0)|0\rangle (i\hat{\nabla}_{x'} + m)\exp(-ip_+x - ip_-x')\,d^4x d^4x', \quad (8)$$

where $\tilde{T}$ denotes the anti-product, and $\psi(x)$ is the Heisenberg operator of the electric field, we find

$$(2i)^{-1}\bar{u}_+(p_+)(\Lambda_\mu(p_+,\ p_-) - \gamma_0\Lambda_\mu^*(-p_-, -p_+)\gamma_0)$$
$$\times u_-(p_-) = \bar{u}_+(p_+)(\gamma_\mu \mathrm{Im}\, F_1(q^2)$$
$$+ \sigma_{\mu\nu}q_\nu \mathrm{Im}\, F_2(q^2))u_-(p_-) = \tfrac{1}{2}\int \bar{u}_+(p_+)(i\hat{\nabla}_x - m)$$
$$\times \langle 0|[j_\mu(0),\ \psi(x)]_-|p_-\rangle \exp(-ip_+x)d^4x$$
$$= \tfrac{1}{2}(2\pi)^4 \sum_n \delta(p_n - p_+ - p_-)\langle 0|j_\mu(0)|n\rangle$$
$$\times \langle n|\bar{u}_+(p_+)\eta(0)|p_-\rangle,$$
$$\eta(x) \equiv (i\hat{\nabla} - m)\psi(x). \quad (9)^*$$

Equations (6) and (9) are the desired dispersion equations for $\langle 0|j_\mu(0)|p_+, p_-\rangle$.

Equations (1), (3), (6) and (9) should be supplemented by dispersion equations for the more complicated matrix elements $\langle 0|j_\mu|n\rangle$ and $\langle n|\bar{u}_+\eta(0)|p_-\rangle$, which appear on the right hand side of (3) and (9). In principle, an infinite set of equations is obtained for all possible amplitudes. The difficulties that arise in this course were already noted in the introduction. In practice one always deals with a "broken" system of equations, in which amplitudes with a number of particles greater than some given value are discarded.† In the solution of such a system, the problem arises as to reasonable boundary conditions. In quantum electrodynamics, it is natural to assume for the boundary conditions

$$F_1(0) = e, \qquad F_2(0) = -\frac{1}{4\pi}\left(\frac{e^2}{4\pi}\right)\frac{e}{2m} = -\frac{1}{2}\Delta\mu, \quad (10)$$

where e is the renormalized charge and $\Delta\mu$ is the anomalous magnetic moment of the electron. It is seen that in the lowest approximation, which was considered in the present work (see Sec. 3), the condition (10) is insufficient for a unique determination of the solution [because of the homogeneity of the equation for $F_1(q^2)$].

As an additional condition we shall require agreement with perturbation theory for $e^2 \to 0$.

3. INVESTIGATION OF THE SIMPLEST APPROXIMATION

We shall neglect on the right side of (3) and (9) all matrix elements with a number of particles in the intermediate state greater than two. Then

$$\rho(q^2) = \frac{1}{3(2\pi)^3}\mathrm{Sp}\int d^4q_+ d^4q_-\,\theta(q_+^0)\,\theta(q_-^0)\,\delta(q_+^2 - m^2)\,4q_+^0 q_-^0$$
$$\times \delta(q_-^2 - m^2)\,\delta(q_+ + q_- - q)$$
$$\times \langle 0|j_\mu(0)|q_+,\ q_-\rangle\langle q_-,\ q_+|j_\nu(0)|0\rangle.., \quad (11)$$

$$\bar{u}_+(p_+)\{\gamma_\mu \mathrm{Im}\, F_1(q^2) + \sigma_{\mu\nu}q_\nu F_2(q^2)\}u_-(p_-) =$$
$$= \frac{1}{2(2\pi)^2}\int d^4q_+ d^4q_-\,\theta(q_+^0)\,\theta(q_-^0)\,\delta(q_+^2 - m^2)$$
$$\times \delta(q_-^2 - m^2)4q_+^0 q_-^0\,\delta(q_+ + q_- - p_+ - p_-)$$
$$\times \langle 0|j_\mu(0)|q_+,\ q_-\rangle\langle q_-,\ q_+|\bar{u}_+\eta(0)|p_-\rangle. \quad (12)$$

Together with (1) and (6), these relations form the simplest set of dispersion relations in which, in addition to the Green's function of the photon $D_{\mu\nu}$ and the matrix element $\langle 0|j_\mu|q_+, q_-\rangle$, there also enters into (12) the exact matrix element $\langle q_-, q_+|\bar{u}_+(p_+)\eta(0)p_-\rangle$ of the scattering of the electron by a positron. In order to obtain a closed system, it is necessary to attempt to express $\langle q_-, q_+|\bar{u}_+\eta|p_-\rangle$ in terms of $D_{\mu\nu}$ and $\langle 0|j_\mu|q_+, q_-\rangle$. This can be done approximately if we limit ourselves in the expression for $\langle q_-, q_+|\bar{u}_+\eta|p_-\rangle$ to the first irreducible Feynman diagram, pictured in the drawing, where the corresponding exact vertex functions Γ_μ are inserted at the junction, while the wavy line corresponds to $D_{\mu\nu}$.

We note that the conditions (9) are violated, generally speaking, in the approximate equation (12). Satisfaction of these conditions in each given approximation can be guaranteed if in (12), in place of the right hand part, we take the half sum of the matrix elements corresponding to solutions with diverging and converging waves (see footnote ‡ on page 969).

*The second term of the anticommutator does not make any contribution, since $p_-^0 = +(p_-^2 = m^2)^{1/2} > 0$.

†In the nonrelativistic region in mesodynamics, a similar device is used in the derivation of the Low equation.[9] Here there is also a formal analogy with the Tamm-Dancoff method,[10] where the cutoff is by the number of virtual particles.

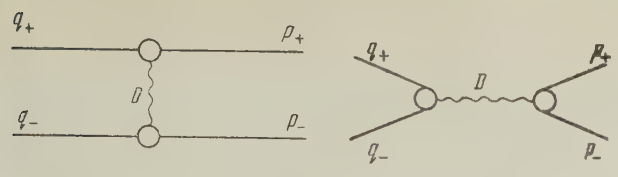

Applying this rule to (12), and taking (5) into account, we obtain in the given approximation

$$\bar{u}_+(\mathbf{p}_+)\,(\gamma_\mu \operatorname{Im} F_1(q^2) + \sigma_{\mu\nu}q_\nu \operatorname{Im} F_2(q^2))\,u_-(\mathbf{p}_-) = \frac{1}{8\pi^2}$$
$$\times \int d^4q_+ d^4q_- \theta(q_+^0)\,\theta(q_-^0)\,\delta(q_+^2 - m^2)\,\delta(q_-^2 - m^2)$$
$$\times \delta(q_+ + q_- - q)\cdot \bar{u}_+(\mathbf{p}_+)\{[\Lambda_\nu \mathrm{Sp}\ (\Lambda_\mu(-\hat{q}_+ + m)$$
$$\times \gamma_0 \Lambda_\nu^* \gamma_0 (\hat{q}_- + m)) + \Lambda_\nu^+ \mathrm{Sp}\,(\Lambda_\mu^+(-\hat{q}_+ + m)\,\Lambda_\nu(-\hat{q}$$
$$\times (\hat{q}_- + m))]\,(q^2 D(q^2)\,q^2)^{-1} - \widetilde{\Lambda}_\nu(-\hat{q}_+ + m)$$
$$\times \operatorname{Re}\Lambda_\mu \cdot (\hat{q}_- + m)\gamma_0 \widetilde{\Lambda}_\nu^* \gamma_0 (k^2 D(k^2)\,k^2)^{-1}\}\,u_-(\mathbf{p}_-), \qquad (13)$$

where the notation used is

$$\operatorname{Re}\Lambda_\mu \equiv \gamma_\mu \operatorname{Re} F_1(q^2) + \sigma_{\mu\nu}q_\nu \operatorname{Re} F_2(q^2),$$
$$\widetilde{\Lambda}_\nu \equiv \gamma_\nu F_1(k^2) + \sigma_{\mu\nu}k_\nu F_2(k^2),$$
$$\Lambda_\mu^+ \equiv \gamma_\mu F_1^*(q^2) + \sigma_{\mu\nu}q_\nu F_2^*(q^2),$$
$$k = p_+ - q_+ = q_- - p_-. \qquad (14)$$

In the work of Drell and Zachariasen,[5] the approximate equation for the spectral functions $F_i(q^2)$ was investigated. This corresponds to consideration only of the Born term in the matrix element $\langle q_-, q_+ | \bar{u}_+ \eta(0) | p_- \rangle$ of the scattering of the electron by a positron. However, it is not difficult to establish the fact that the expression obtained by them for $\operatorname{Im} F_i(q^2)$ is wrong. Actually, setting $\widetilde{\Lambda}_\nu = e\gamma_\nu$ and $D(q^2)\,q^2 = -1$ in (14), and carrying out the necessary integrations, we find (omitting the "coverings")

$$\gamma_\mu \operatorname{Im} F_1(\lambda) + \sigma_{\mu\nu}q_\nu \operatorname{Im} F_2(\lambda) = \left(\frac{e^2}{4\pi}\right)\left(1 - \frac{2}{\lambda}\right)^{1/2}$$
$$\times \left\{\left(\operatorname{Re} F_1(\lambda) + \operatorname{Re} F_2(\lambda)\frac{q_\nu}{m}\right)\cdot \frac{1}{2}\left(\frac{\lambda - 1}{\lambda - 2}\right)\int_\xi^{\lambda - 2}\frac{d\mu}{\mu}\right.$$
$$- ((13/12)\operatorname{Re} F_1(\lambda)\,\gamma_\mu + \operatorname{Re} F_2(\lambda)\,\sigma_{\mu\nu}q_\nu/m)$$
$$- \gamma_\mu(3\lambda)^{-1}\operatorname{Re} F_1(\lambda) - {}^1/_2(\lambda - 2)^{-1}(\operatorname{Re} F_1(\lambda)$$
$$\left. + 8\operatorname{Re} F_2(\lambda))\,(\gamma_\mu + \sigma_{\mu\nu}q_\nu/4m)\right\}, \qquad (15)$$

where for convenience the dimensionless quantity $\lambda = q^2/2m^2$ has been introduced; $F_i(q^2) \equiv F_i(\lambda)$; $F_2(q^2)\,m = F_2(\lambda)$; $\xi \approx (m^2 - p^2)/2m^2$; $p_+^2 = p_-^2 = p^2 \lesssim m^2$. Equation (15) differs from the similar equation (22) in reference 5 in that here the integral $\int_\xi^{\lambda-2} d\mu/\mu$ appears in the first term on the right hand side instead of $\int_{-1}^{+1} \frac{d\mu}{1-\mu}$ in the expression of Drell and Zachariasen.[5] The reason for this divergence is most simply understood from the example of perturbation theory. If we compute $\operatorname{Im} F_1$ in the first approximation of perturbation theory, then, because of the presence of the infrared catastrophe, we obtain different expressions depending on its capability for correction (see Appendix A); if we define $\operatorname{Im} F_1(\lambda)$ as the limit of $\operatorname{Im} F_1(\lambda, p^2)$ for $p^2 \to m^2$ in the region $p^2 < m^2$, then we get (15). As $p^2 \to m^2$ from the region $p^2 > m^2$, we obtain Eq. (22) of reference 5.* However, for $p^2 \gtrsim m^2$, $\operatorname{Im} F_1(\lambda)$ does not vanish everywhere in the spatially similar region $\lambda < 0$. Thus we can draw the important conclusion that the dispersion relations for $F_i(\lambda)$ in quantum electrodynamics in form (6) exist only for p_+^2 and $p_-^2 \lesssim m^2$. In the opposite case, integration in (6) must be carried out over all q^2 from $-\infty$ to $+\infty$. This completes our proof, inasmuch as Drell and Zachariasen on the one hand use dispersion relations in the form (6) and on the other hand calculate $\operatorname{Im} F_1(q^2)$, essentially as the limit of the region $p^2 > m^2$.† The absence of a solution vanishing at infinity for $F_1(q^2)$ (i.e., in contradiction with the nonsubtraction procedure) and the negative value for the mean square of the radius of the distribution of charge of the electron in reference 5 were brought about in just this way. It is also necessary to emphasize that the approximation corresponding to replacement of $\langle q_-, q_+ | \bar{u}_+ \eta | p_- \rangle$ by the Born term [i.e., use of (15)] is scarcely valid. In this case, substitution of (15) in (6) leads to an integral equation for $F_1(q^2)$ which has a solution (corresponding to the perturbation theory for $e^2 \to 0$) which falls off for $q^2 \to \infty$ as $(q^2)^{-1/2}$ (see Appendix B). Such a behavior points up the essential role of $F_1(q^2)$ in the neglected terms in the matrix element $\langle q_-, q_+ | \bar{u}_+ \eta | p_- \rangle$ and the necessity of their calculation. Equation (13) again corresponds to an attempt to consider in first approximation the change in the Born term as $q^2 \to \infty$ because of $F_i(q^2)$ and $D_{\mu\nu}(q)$.

We now investigate the asymptotic solution of the set of integral nonlinear equations (1), (3), (6) and (9) as $q^2 \to \infty$. For this purpose we make the

*In order to find the first approximation of perturbation theory it is necessary in (15) and (22) of reference 5 to set $\operatorname{Re} F_1 = e$; $\operatorname{Re} F_2 = 0$.

†In fact, the infrared divergence of $\operatorname{Im} F_i(q^2)$ is removed in reference 5 by the elimination of the scattering of the electron by the positron at small angles under the assumption that the minimum obtainable angle in the center-of-mass system does not depend on q^2. However, such a situation is qualitatively equivalent to the calculation of $\operatorname{Im} F(q^2)$ in the region $p^2 \gtrsim m^2$.

assumption, first, that $|D(q^2)q^2|$ differs slightly from unity over the whole region of variation of q^2; second,* that $F_2(q^2)$ falls off as $|q^2| \to \infty$ not more slowly than $(q^2)^{-1}$. Then, neglecting terms in (11) and (13) which contain $F_2(q^2)$, we find†

$$\rho(\lambda) = \frac{\theta(\lambda-2)}{1-\pi^2\lambda^2}\left(1-\frac{2}{\lambda}\right)^{1/2}(1+\lambda)|F_1(\lambda)|^2, \quad \rho(\lambda) \equiv 2m^2\rho(q^2), \tag{16}$$

$$\operatorname{Im} F_1(\lambda) = \operatorname{Re} F_1(\lambda)\left\{-\pi\lambda\rho(\lambda) + \frac{1}{4\pi}\left(1-\frac{2}{\lambda}\right)^{1/2}\left(\frac{1}{2}\left(\frac{\lambda-1}{\lambda-2}\right)\right.\right.$$
$$\left.\left.\times I_0(\lambda) - \left(\frac{\lambda}{\lambda-2}\right)I_1(\lambda) + \frac{\lambda+4}{4(\lambda-2)}I_2(\lambda)\right)\right\}, \quad \lambda > 2 \tag{17}$$

where

$$I_0(\lambda) = \int_\xi^{\lambda-2} |F_1(-\mu)|^2 \frac{d\mu}{\mu}, \quad I(\lambda) = \frac{1}{\lambda-2}\int_0^{\lambda-2} |F_1(-\mu)|^2 d\mu, \tag{18}$$
$$I_2(\lambda) = \frac{2}{(\lambda-2)^2}\int_0^{\lambda-2} |F_1(-\mu)|^2 \mu d\mu.$$

Substituting (17) in (6), we obtain an integral equation for $F_1(\lambda)$:

$$F_1(\lambda) = \frac{1}{\pi}\int_2^\infty \frac{\operatorname{Re} F_1(\lambda')\, g(\lambda')\, d\lambda'}{\lambda'-\lambda-i\varepsilon}, \tag{19}$$

where $g(\lambda) = \operatorname{Im} F_1(\lambda)/\operatorname{Re} F_1(\lambda)$ is obtained from (17).

The formal, general solution of (19), which is finite at $\lambda = 0$, has the form[11]

$$F_1(\lambda) = P(\lambda)(\lambda-2)^{-n}\exp(\varphi(\lambda)), \tag{20}$$

$$\varphi(\lambda) = \frac{\lambda}{\pi}\int_2^\infty \frac{\tan^{-1} g(\lambda')\, d\lambda}{\lambda'(\lambda'-\lambda-i\varepsilon)}, \tag{21}$$

where $P(\lambda)$ is a polynomial and n is an integer. Agreement with the renormalized perturbation theory for $e^2 \to 0$ is achieved by the choice $n = 0$ and $P(\lambda) = e$.

It is seen from (21) that if $g(\lambda)$ is a nonvanishing function for $\lambda \to -\infty$, then

$$\lim_{\lambda\to-\infty}\varphi(\lambda) \to -\pi^{-1}\tan^{-1} g(|\lambda|)\ln|\lambda|. \tag{22}$$

Therefore, if $\tan^{-1} g(\lambda) \to \text{const} > 0$ for $|\lambda| \to \infty$, then, in accord with (20), we obtain a vanishing solution for $F_1(\lambda)$ with the asymptotic value

$$F_1(\lambda) \sim e\exp[-\pi^{-1}\tan^{-1} g(|\lambda|)\ln|\lambda|]. \tag{23}$$

On the other hand, it follows from (17) and (18) that if $F_1(\lambda) \to 0$ as $|\lambda| \to \infty$, then

$$g(\lambda) \to \frac{1}{8\pi}\int_\xi^\lambda |F_1(-\mu)|^2 \frac{d\mu}{\mu} \to \text{const} > 0, \tag{24}$$

since in this case the terms $\sim I_1$, I_2 and $\lambda\rho(\lambda)$ tend to zero with increase in λ.

Now it is easy to find the asymptotic value of $g(\infty)$. We assume that $g(\infty) \ll 1$, we replace $\tan^{-1} g(\infty)$ in (23) by $g(\infty)$, and then substitute (23) in (24). We obtain

$$g^2(\infty) = (e^2/16)(2/\xi)^{(2/\pi)\, g(\infty)}. \tag{25}$$

The divergence in (25) as $\xi \to 0$ (the infrared catastrophe) arises from the fact that the scattering amplitude $\langle q_-, q_+|\bar{u}_+\eta|p_-\rangle$ of the electron on the positron becomes infinitely great for forward scattering. Strict elimination of the infrared divergence in the method of dispersion relations lies outside the framework of our present article, and will be investigated separately.* Assuming that $(2/\pi)g(\infty)\ln\xi^{-1} \ll 1$, we have from (25)

$$g(\infty) \approx {}^1/_2 (e^2/4)^{1/2} \ll 1. \tag{26}$$

The neglected terms have a maximum order of magnitude equal to $(2/\pi)g(\infty)\ln\xi^{-1}$ and are small for $(2/\pi)g(\infty)\ln\xi^{-1} \ll 1$ and $(2/\pi) \times g(\infty)\ln\lambda \gg 1$.

Finally, we obtain the following asymptotic solution of Eq. (19) for $(2/\pi)g(\infty)\ln\lambda \gg 1$.

$$F_1(\lambda) \approx e\lambda^{-\frac{1}{2}(e^2/4)^{1/2}}. \tag{27}$$

The most characteristic property of the vanishing asymptote is the nonanalytic dependence on e^2 for $\pi^{-1}(e^2/4)^{1/2}\ln\lambda \gg 1$. We note also that in the region $\lambda \gg 1$, and $(e^2/8\pi^2)(\ln\lambda)^2 \ll 1$, $F_1(\lambda)$ differs slightly from e and one can replace $\tan^{-1} g(\lambda)$ by $g(\lambda)$; in this case, $\varphi(\lambda)$ in (21) coincides with $F_1(\lambda)$, computed by perturbation theory (with accuracy to e^3) and, consequently, the dependence of $F_1(\lambda)$ on λ in (20) is obtained in the same way as in the research of Abrikosov.[12]

4. DISCUSSION OF RESULTS

We shall first investigate Eqs. (1) and (16) on the basis of (27) for $D(\lambda) \equiv 2m^2 D(q^2)$. Substitution of (27) in (16) gives the following behavior for $\rho(\lambda)$ in the region $\pi^{-1}(e^2/4)^{1/2}\ln\lambda \gg 1$:

$$\rho(\lambda) \approx (e^2/12\pi^2\lambda)\exp\{-(e^2/4)^{1/2}\ln\lambda\}. \tag{28}$$

The convergence of the integral $\int_0^\infty \rho(\lambda)\, d\lambda$ then follows, and consequently the finiteness of the con-

*For justification of the second assumption we can introduce the same arguments as in reference 5, which are still more forceful in our case because of the presence of a vanishing asymptotic value for F_1 (see below).

†Inasmuch as the set of equations with account of F_2 is rather cumbersome and is not analyzed in the present work, we shall not write it out.

*It is of interest to observe that in the approximation that we have considered, a solution also exists in the limiting case $\xi \to 0$.

stant of charge renormalization Z_3^{-1} $= (1 + \int_0^\infty \rho(\lambda)\, d\lambda)$ in the given approximation. Estimating Z_3 by means of the asymptotic expression (28) for ρ, we find

$$Z_3^{-1} \approx 1 + (3\pi)^{-1} (e^2/4)^{1/2}. \qquad (29)$$

It is also not difficult to establish the fact that $\rho(\lambda)$ in this approximation does not have any resonance at $(e^2/12\pi^2) \ln \lambda \sim 1$, in contrast to the results of references 13 and 14 (see also below).

As is well known from the dispersion relations (1) for $D(\lambda)$, it follows that $|\lambda D(\lambda)|$ as $\lambda \to -\infty$ is smaller than Z_3^{-1}. We have obtained for Z_3^{-1} the finite value (29) which differs slightly from unity, justifying the initial assumption that $|\lambda D(\lambda)| \sim 1$ for $|\lambda| \to \infty$.*

It is interesting to compare our results with the results of other researchers. Lehman, Symanzik and Zimmermann,[15] starting out from the dispersion relations for $D(\lambda)$, found an important condition which must be satisfied by the quantity

$$M(\lambda) = \rho(\lambda) / |D(\lambda)|^2. \qquad (30)$$

As is easy to prove, $M(\lambda)$ is connected with the imaginary part of the polarization operator $\Pi_{\mu\nu}(q)$. Thus

$$\pi M(\lambda) = \lambda \operatorname{Im} \pi(\lambda), \qquad \Pi_{\mu\nu}(\lambda) = (\delta_{\mu\nu} q^2 - q_\mu q_\nu)\, \pi(\lambda).$$

They have shown that if one considers (30) and (1) as the equation relative to $\rho(\lambda)$ for a given function $M(\lambda)$, then the solution of this equation exists only if

$$\int_0^\infty \lambda^{-2} M(\lambda)\, d\lambda \leqslant 1. \qquad (31)$$

In the lowest approximation, $M(\lambda)$ in quantum electrodynamics is expressed in terms of the vertex parts

$$M(\lambda) = (e^2/12\pi^2)\, \theta(\lambda - 2)(1 - 2/\lambda)^{1/2} \{(1+\lambda)|\Gamma_1(\lambda)|^2 + 4\lambda(\lambda+4)|\Gamma_2(\lambda)|^2 - 6\lambda(\Gamma_1(\lambda)\Gamma_2^*(\lambda) + \Gamma_1^*(\lambda)\Gamma_2(\lambda))\}, \qquad (32)$$

where $\Gamma_i(\lambda)$ are determined from the relation

$$\bar{u}_+(\mathbf{p}_+)\Gamma_\mu(p_+, p_-)u_-(\mathbf{p}_-) = \bar{u}_+(\mathbf{p}_+)(\gamma_\mu\Gamma_1(\lambda) + \sigma_{\mu\nu} q_\nu \Gamma_2(\lambda))u_-(\mathbf{p}_-).$$

On the basis of (31) and (32), the authors of reference 15 drew a fundamental conclusion on the necessity of the vanishing of the vertex part with increase in λ for internal self-consistency of the theory. Inasmuch as $F_1(\lambda) = D(\lambda)\lambda\Gamma_1(\lambda)$ [see (5)] and for $\lambda \to -\infty$ $|\lambda D(\lambda)| \to Z_3^{-1}$, we conclude that, in the approximation that we have considered, $\Gamma_1(\lambda)$ falls off with increase of λ according to the same law as $F_1(\lambda)$. This guarantees satisfaction of the condition (31).

In the works of Redmond and Uretsky[13] and Bogolyubov, Logunov, and Shirkov,[14] a combination approach to the method of dispersion relations was employed, in which, besides the dispersion relations for obtaining a series of quantities in quantum field theory, series determined by perturbation theory were summed. The combination approach in the form in which it was formulated in these works, i.e., within the framework of single particle Green's functions only, possesses great ambiguity. The reasons for this ambiguity are discussed in reference 16; it is brought about principally by the fact that satisfaction of the dispersion relations for single particle Green's function is not a sufficient condition for fulfilling the requirements of causality and unitarity in the theory.

The concrete results of references 13 and 14 did not differ materially from ours. In the first place, although $D(\lambda)$ in references 13 and 14 does not possess non-physical poles, $\rho(\lambda)$ maintains a resonance character of behavior in the region of the former pole $[(e^2/12\pi^2) \ln \lambda \sim 1]$. In the second place, the specific non-analytic dependence of the superconducting type in $D(\lambda)$ in references 13 and 14 comes about from the use of the expression for $\rho(\lambda)$ outside the region of its applicability.

It is not without interest to note that if we set $\Gamma_1(\lambda) = 1$ in (32), and $\Gamma_2(\lambda) = 0$, then the formal solution of Eqs. (1) and (30) gives an expression for $\rho(\lambda)$ which coincides with that found in the work of Landau, Abrikosov, and Khalatnikov.[1]

In conclusion, we emphasize once more (see Sec. 1) that the most important problem in the investigation of "broken" dispersion equations (and in equal degree in the combination approach) is the calculation or even qualitative estimation of the role of higher approximations which include the more complicated matrix elements. In spite of the fact that corrections to the free Green's function of the photon in the simplest approximation turn out to be $\sim (e^2/4\pi)^{1/2}$ [see (29)], it is still impossible to say anything definite about the presence of a small parameter of expansion in such an approach. It appears to us that the solution of these questions permits us to shed additional light on the problem of the internal closed nature of quantum electrodynamics, and also to explain in what measure the method of dispersion relations is an escape from the framework of the Lagrangian formulation of quantum field theory. In equal measure this ap-

*This permits us, in place of the set of equations for $D(\lambda)$ and $F_1(\lambda)$, to limit ourselves to the initially asymptotic investigation of the equation only for $F_1(\lambda)$.

plies to all other interactions.

APPENDIX A

Let us consider $\bar{u}_+(p_+)\Gamma_\mu(p_+, p_-)u_-(p_-)$ according to perturbation theory. For simplicity, we set $p_+^2 = p_-^2 = p^2 \neq m^2$, $q = p_+ + p_-$;

$$\Gamma_\mu(p_+, p_-) = \frac{e^3}{i(2\pi)^4}\int \frac{\gamma_\nu(-\hat{p}_+ + \hat{k} + m)\gamma_\mu(\hat{p}_- + \hat{k} + m)\gamma_\nu d^4k}{[(p_+ - k)^2 - m^2 + i\varepsilon)]\,[(p_- + k)^2 - m^2 + i\varepsilon]\,(k^2 + i\varepsilon)}. \quad (A.1)$$

Transforming the numerator with account of the "coverings" $\bar{u}_+$ and u_-, we get

$$\bar{u}_+\gamma_\nu(-\hat{p}_+ + \hat{k} + m)\gamma_\mu(\hat{p}_- + \hat{k} + m)\gamma_\nu u_- = \bar{u}_+[(-2q^2 + 4p^2)\gamma_\mu - 2\hat{k}\gamma_\mu\hat{k} - 2\gamma_\mu\hat{k}\hat{p}_+ + 2\hat{p}_-\hat{k}\gamma_\mu]u_-. \quad (A.2)$$

Infrared divergence occurs only in the first term on the right in (A.2). We limit ourselves to the consideration of the contribution of this term alone. Carrying out integration over d^4k in (A.1), we find

$$\Gamma_\mu(p_+, p_-) = e^3\gamma_\mu\frac{q^2 - 2p^2}{16\pi^2}\int_0^1 dx\int_0^1 dy \times [x(p^2 - q^2(1-y)y) - (p^2 - m^2) - i\varepsilon]^{-1}.$$

If we set $\Gamma_\mu(p_+, p_-) \equiv \gamma_\mu\Gamma_1(q^2, p^2)$, then for real q^2 and p^2,

$$\operatorname{Im}\Gamma_1(q^2, p^2) = e^3\frac{q^2 - 2p^2}{16\pi}\int_0^1 dx\int_0^1 dy\,\delta \times (x[p^2 - q^2(1-y)y] - (p^2 - m^2)) = \frac{e^3}{8\pi}\left(\frac{\lambda-1}{\lambda-2}\right)\left(1 - \frac{2}{\lambda}\right)^{1/2}\ln\frac{\lambda-2}{\xi} \quad \text{for } p^2 \to m^2.$$

It is immediately seen from this expression that for $p^2 < m^2$, $\operatorname{Im}\Gamma_1(q^2, p^2)$ vanishes if $q^2 < 4m^2$, and for $p^2 > m^2$ and $q^2 < 0$,

$$\operatorname{Im}\Gamma_1(q^2, p^2) = \frac{e^3}{8\pi}\frac{q^2 - 2p^2}{16\pi|q^2|}\left(1 - \frac{4m^2}{q^2}\right)^{-1/2}\ln\frac{(1 - 4p^2/q^2)^{1/2} + 1}{(1 - 4p^2/q^2)^{1/2} - 1},$$

i.e., it is different from zero and finite for $p^2 \to m^2$ throughout the spatially similar region $q^2 < 0$. Consequently, the dispersion relations in the form (6) exist only for $p^2 < m^2$, which also supports our statement in Sec. 3.

APPENDIX B

Let us find the asymptote of $F_1(\lambda)$ from (15). Neglecting $F_2(\lambda)$ and substituting in (21) for $g(\lambda)$ the asymptotic value for $|\lambda| \to \infty$: $g(\lambda) \approx (e^2/8\pi^2)\ln(\lambda/\xi)$, we find

$$F_1(\lambda) \approx \frac{\lambda}{\pi}\int_2^\infty \frac{\tan^{-1}(e^2/8\pi^2)\ln(\lambda'/\xi)\,d\lambda'}{\lambda'(\lambda' - \lambda - i\varepsilon)}.$$

For $(e^2/8\pi^2)\ln(\lambda/\xi) \gg 1$ and $|\lambda| \to \infty$, the fundamental role in the integral (B.1) is played by $\lambda' \sim \lambda$. Therefore

$$F_1(\lambda) \to e\exp(-{}^1/_2\ln(\lambda/2)) = e(\lambda/2)^{-1/2},$$

Since

$$\tan^{-1}(e^2/8\pi^2)\ln(\lambda/\xi) \to \pi/2 \quad \text{for } \lambda \to \infty.$$

[1] Landau, Abrikosov, and Khalatnikov, Dokl. Akad. Nauk SSSR **95**, 497, 773, (1954); **96**, 261 (1954).

[2] E. S. Fradkin, JETP **29**, 258 (1955); Soviet Phys. **2**, 361 (1956).

[3] L. D. Landau and I. Ya. Pomeranchuk, Dokl. Akad. Nauk SSSR **102**, 489 (1955); see also, L. D. Landau, Niels Bohr and the Development of Physics, London, 1955.

[4] S. Mandel'shtam, Phys. Rev. **112**, 1344 (1958).

[5] S. D. Drell and F. Zachariasen, Phys. Rev. **111**, 1727 (1958).

[6] G. Källen, Helv. Phys. Acta **25**, 417 (1952); H. Lehmann, Nuovo cimento **11**, 342 (1954); M. Gell-Mann and F. E. Low, Phys. Rev. **95**, 1300 (1954).

[7] Y. Nambu, Nuovo cimento **6**, 1064 (1957); K. Symanzik, Progr. Theor. Phys. **20**, 690 (1958).

[8] Bremermann, Oehme and Taylor, Phys. Rev. **109**, 2178 (1958); R. Oehme, Phys. Rev. **111**, 1430 (1958).

[9] F. E. Low, Phys. Rev. **97**, 1392 (1955).

[10] I. E. Tamm, J. Phys. (U.S.S.R.) **9**, 449 (1945); S. M. Dancoff, Phys. Rev. **78**, 382 (1950).

[11] N. I. Muskhelishvili, Сингулярные интегральные уравнения (Singular Integral Equations)(Gostekhizdat, 1946), Sec. 79. R. Omnes, Nuovo cimento **8**, 316 (1958).

[12] A. A. Abrikosov, JETP **30**, 96 (1956); Soviet Phys. JETP **3**, 71 (1956).

[13] P. J. Redmond, Phys. Rev. **112**, 1404 (1958). P. J. Redmond and J. L. Uretsky, Phys. Rev. Lett. **1**, 147 (1958).

[14] Bogolyubov, Logunov, and Shirkov, Метод дисперсионных соотношений и теория возмущений (Method of Dispersion Relations and Perturbation Theory)(preprint) Dubna, 1959.

[15] Lehmann, Symanzik, and Zimmermann, Nuovo cimento **2**, 425 (1955).

[16] Kirzhnits, Faĭnberg, and Fradkin, JETP, in press.

Translated by R. T. Beyer
271

INELASTIC COLLISIONS BETWEEN FAST POLARIZED PARTICLES AND ATOMS

V. V. BATYGIN and I. N. TOPTYGIN

Leningrad Polytechnical Institute

Submitted to JETP editor June 6, 1959

J. Exptl. Theoret. Phys. (U.S.S.R.) 37, 1372-1378 (November, 1959)

The differential cross section for scattering of electrons, positrons and μ mesons on atoms is derived in the Born approximation as a function of the polarization of the particles in the initial and final states. The change in the polarization vector from the scattering of the particles by free unpolarized electrons is also obtained.

1. INTRODUCTION

THE behavior of polarized electrons, positrons and μ mesons has recently been the subject of many experiments. In this connection it is of interest to calculate the cross sections for various processes involving the interactions of polarized particles with matter, in particular elastic and inelastic scattering of such particles by atoms in matter. Coulomb scattering of electrons including polarization effects was discussed in the review article by Tolhoek[1] and in a number of other papers.[2-5] Ivanter[6] obtained radiative corrections to the Coulomb scattering cross section of polarized electrons and μ mesons. Polarization effects in scattering of Dirac particles on free electrons were also considered by a number of authors.[7-12] However in reality the electrons in matter are not free. Effects due to the binding of electrons in matter are important for small angle scattering. This region of angles is particularly relevant when depolarization due to multiple scattering and bremsstrahlung of polarized particles is studied, since in these processes mainly small angle deviations are involved.

In this paper we study inelastic collisions between polarized particles and atoms. We obtain, in the Born approximation, the differential cross section $d\sigma_n(\theta, \zeta_1, \zeta_2)$ for scattering of the particle through an angle θ with excitation of the n-th level of the atom and change in polarization $\zeta_1 \to \zeta_2$, as well as the angular distribution of the inelastically scattered particles independently of the energy loss. We also study the change in polarization upon scattering by free unpolarized electrons. The calculations are performed for the general case of arbitrary polarization of one of the particles in the initial and final states.

2. SCATTERING ON ATOMS

The scattering of a relativistic unpolarized electron on an atom was first discussed by Bethe.[13] He found, in the Born approximation without taking into account exchange effects, the following expression for the cross section for a collision resulting in the atom making a transition to the n-th level:

$$d\sigma_n = 4\left(\frac{e}{\hbar c}\right)^4 \frac{\varepsilon\varepsilon'}{[q^2-(\Delta\varepsilon/\hbar c)^2]^2}\frac{p'}{p}|F_{n0}|^2 d\Omega, \qquad (1)$$

$$F_{n0} = \int \psi_n^* \Big[ZA_0 + \sum_{j=1}^{z} e^{i\mathbf{q}\mathbf{r}_j}(-A_0 + \mathbf{A}\alpha_j)\Big]\psi_0 d\tau. \qquad (2)$$

Here ϵ, $\mathbf{p}$, ϵ', and $\mathbf{p}'$ are the total energy and momentum of the particle before and after scattering respectively, $\Delta\epsilon = \epsilon - \epsilon' = E_n - E_0$ is the energy transfer, $\hbar\mathbf{q} = \mathbf{p} - \mathbf{p}'$ is the momentum transfer, ψ_0 and ψ_n are the wave functions of the atom in the initial and final state, and α_j is a Dirac operator acting on the spin variables of the j-th atomic electron. The particle undergoing scattering is described by a plane wave with a spinor factor $u(\zeta)$ and $u(\zeta')$ for the initial and final states respectively, where ζ and ζ' describe the particle polarization in its rest frame, u and u' are normalized to unity. At that

$$A_0 = (u'^*, u), \quad \mathbf{A} = (u'^*, \alpha u). \qquad (3)$$

The expression for the transition matrix element

$$F_{n0} = \int \psi_n^* \Big\{ZA_0 + \sum_{j=1}^{z} e^{i\mathbf{q}\mathbf{r}_j}\Big[-A_0 + \frac{1}{c}\hat{\mathbf{v}}_j A + (\hbar/2mc)\,\mathbf{A}\,(\mathbf{q} + i[\sigma_j \times \mathbf{q}])\Big]\Big\}\psi_0 d\tau. \qquad (4)$$

on which the following discussion is based, is obtained by going over in Eq. (2), in a conventional manner, to the nonrelativistic approximation for the atomic electrons. Here $\mathbf{v}_j$ is the velocity

operator for the j-th atomic electron and σ_j is a Pauli matrix.

Since Eq. (4) is rather complicated in the general case, we shall evaluate the matrix element F_{n0} in the dipole approximation, i.e., we assume that $qa \ll 1$, where a is the radius of the atom. This corresponds[14] to small scattering angles $\theta \ll p_0/p$ and not too large atomic excitation energies $\Delta\epsilon \ll p_0 v$, where p_0 is of the order of magnitude of the average momentum of the atomic electrons and v is the velocity of the particle. In this approximation, with $\exp(i\mathbf{q}\cdot\mathbf{r}_j)$ replaced by $1+i\mathbf{q}\cdot\mathbf{r}_j$ and leaving terms proportional to q in Eq. (4), we find

$$F_{n0} = (i/e)[(\Delta\varepsilon/\hbar c)\mathbf{A}\mathbf{d}_{n0} - A_0\mathbf{q}\mathbf{d}_{n0}], \qquad \mathbf{d}_{n0} = e\int \psi_n^* \sum_j \mathbf{r}_j \psi_0 d\tau. \tag{5}$$

Here $\mathbf{d}_{n0}$ is the matrix element of the electric dipole moment. If the atoms in the initial and final states are unpolarized then $|F_{n0}|^2$ should be averaged over the initial and summed over the final states corresponding to different values of the projection of the angular momentum of the atom. Denoting this averaging and summing by a bar we obtain

$$\overline{|F_{n0}|^2} = \tfrac{1}{3}\overline{|\mathbf{d}_{n0}|^2}\{q^2|A_0|^2 - 2(\Delta\varepsilon/\hbar c) \times \mathrm{Re}(\mathbf{q}\mathbf{A})A_0 + (\Delta\varepsilon/\hbar c)^2|\mathbf{A}|^2\}. \tag{6}$$

For calculational purposes it is convenient to express the bispinor expressions appearing in Eq. (6) in terms of traces of certain 2×2 operators. This method was used by Olsen.[15] Consider, for example, the calculation of $|A_0|^2$. We express the bispinor amplitudes involved in A_0 in the form

$$u = \sqrt{\frac{\varepsilon+m}{2\varepsilon}}\begin{pmatrix} 1 \\ \sigma p/(\varepsilon+m)\end{pmatrix} V, \quad u' = \sqrt{\frac{\varepsilon'+m}{2\varepsilon'}}\begin{pmatrix} 1 \\ \sigma p'/(\varepsilon'+m)\end{pmatrix} V', \tag{7}$$

where V, V′ are spinors describing the initial and final polarization states. With the help of Eq. (3) we obtain

$$A_0 = (V'^{+}TV).$$

Here T is a certain 2×2 operator whose explicit form follows from Eq. (7). Introducing the projection operator onto a state with polarization ζ

$$P(\zeta) = \tfrac{1}{2}(1+\zeta\sigma), \tag{8}$$

we find

$$|A_0|^2 = \tfrac{1}{4}\mathrm{Sp}\{T^+(1+\zeta'\sigma)T(1+\zeta\sigma)\}. \tag{9}$$

In the following we shall measure q in units of $mc/\hbar$ and will use the abbreviations $\gamma = \epsilon/mc^2$ and $\beta = v/c$. When obtaining an explicit expression for $d\sigma_n$ it is necessary to keep in mind that in the range of validity of the dipole approximation $\Delta\gamma$ and θ are small quantities. We therefore expand the right hand side of Eq. (1) in a series and keep only the leading terms in q^2 and $(\Delta\gamma)^2$. These terms may be of the same order in the extreme relativistic limit; in the nonrelativistic limit the terms with $(\Delta\gamma)^2$ are negligibly small. We obtain the following final expression for the differential scattering cross section:

$$\frac{d\sigma_n}{d\Omega} = \frac{e^2}{3r^2c^4}\overline{|\mathbf{d}_{n0}|^2}\frac{\gamma^2}{[q^2-(\Delta\gamma)^2]^2}\{[2q^2 - 2(\Delta\gamma/\gamma)^2(\gamma^2+1)] \times (1+\zeta_1\zeta_2) + [-q^2(\gamma-1)^2/\gamma^2 + (\Delta\gamma/\gamma)^2(\gamma-1) \times (\gamma-3)]\cdot[(\mathbf{n}_1\zeta_1)(\mathbf{n}_1\zeta_2) + (\mathbf{n}_2\zeta_1)(\mathbf{n}_2\zeta_2)] + [q^2(\gamma-1) \times (3\gamma-1)/\gamma^2 + (\Delta\gamma/\gamma)^2(\gamma-1)(-3\gamma+5)/\gamma^2] \times (\mathbf{n}_1\zeta_1) \times (\mathbf{n}_2\zeta_2) + [-q^2\beta^2 + (\Delta\gamma/\gamma)^2(\gamma^2-1)](\mathbf{n}_2\zeta_1)(\mathbf{n}_1\zeta_2)\}, \tag{10}$$

where $\mathbf{n}_1$ and $\mathbf{n}_2$ are unit vectors in the direction of the particle momentum before and after scattering. As can be seen from Eq. (10), an initially unpolarized beam remains unpolarized after scattering. However if transitions between states with definite projection of the angular momentum of the atom are registered, then terms linear in ζ, ζ' will appear in Eq. (10). This means that the initially unpolarized beam becomes polarized after scattering.

Now let us determine the angular distribution of the polarized particles in inelastic scattering by the atom, independent of the energy loss:

$$d\sigma(\theta, \zeta, \zeta') = \sum_{n\neq 0} d\sigma_n. \tag{11}$$

It is shown in reference 14 that if the scattering angle satisfies the condition $\theta \gg p_0 v_0/pv$, where v_0 is the average velocity of the atomic electrons, then q is independent of n and the summation in Eq. (11) may be carried out in a general form by using rules of matrix multiplication. The term $(\Delta\epsilon/\hbar c)^2$ in Eq. (1) may be neglected in comparison with q^2. The sum over n entering into Eq. (11) is transformed as follows:

$$\sum_{n\neq 0}|F_{0n}|^2 = (FF^+)_{00} - |F_{00}|^2. \tag{12}$$

The operator F in Eq. (12) may be taken in the form

$$F = \Big(Z - \sum_{l=1}^{Z}\exp\{i\mathbf{q}\mathbf{r}_l\}\Big)A_0; \tag{13}$$

the remaining terms will contain, after averaging over the ground state of the atom, an additional factor of order $(v_0/c)^2$ and may be neglected. Substituting Eq. (13) into Eq. (12) we obtain

$$\sum_{n\neq 0}|F_{0n}|^2 = ZS(q)|A_0|^2, \tag{14}$$

where S(q) is the "incoherent scattering function" introduced by Heisenberg[16] and tabulated by Bewilogua.[17]

$$S(q) = 1 - \frac{1}{Z}F_0^2(q) + \frac{1}{Z}\sum_{j\neq k}\exp\{i\mathbf{q}(\mathbf{r}_j - \mathbf{r}_k)\}, \quad (15)$$

where F(q) is the atomic form factor. From Eqs. (14), (11), and (1) we obtain the following expression for the angular distribution of polarized particles in inelastic scattering through a small angle ($\theta \ll 1$):

$$d\sigma/d\Omega = 2Z(e^2/pv)^2 S(q)\theta^{-4}\{1 + \zeta_1\zeta_2 - \tfrac{1}{2}\beta^2(\mathbf{n}_2\zeta_1)(\mathbf{n}_1\zeta_2) + \left[\tfrac{1}{2}\beta^2 + (\gamma-1)^2/\gamma^2\right](\mathbf{n}_1\zeta_1)(\mathbf{n}_2\zeta_2) - [(\gamma-1)^2/2\gamma^2][(\mathbf{n}_1\zeta_1)(\mathbf{n}_1\zeta_2) + (\mathbf{n}_2\zeta_1)(\mathbf{n}_2\zeta_2)]\}. \quad (16)$$

The dependence of the cross section on polarization is precisely the same as that obtained in Coulomb scattering of electrons in the Born approximation. This is explained by the fact that the neglect of $\Delta\epsilon$ is equivalent to going over from inelastic to elastic scattering in a certain spherically symmetric field.

Equations (10) and (16) are valid for electrons, positrons, and μ mesons. Exchange effects, which exist in the scattering of electrons and positrons and which were not taken into account, are unimportant in the region of validity of these formulas ($\theta \ll 1$).

3. SCATTERING ON FREE ELECTRONS

If the scattering angle satisfies the condition $\theta \gg p_0/p$ (which means that the energy transfer is much larger than the binding energy) then the binding effects of the atomic electrons may be neglected. In this region inelastic scattering by an atom is equivalent to scattering by free electrons. The change in the polarization vector of electrons and positrons in scattering by free electrons was calculated for certain special cases in a number of papers. Ford and Mullin[8] obtained the change in the polarization of a longitudinally polarized electron when scattered by an electron. Mukhtarov and Perov[12] calculated the longitudinal component of positron polarization after scattering (the initial polarization being assumed to be also longitudinal). Lastly, Kresnin and Rozentsveĭg[7] determined the polarization of an initially unpolarized electron beam after scattering by polarized electrons. Since the results in reference 7 are given in the center of mass system one could derive from them an expression for the polarization vector of an electron beam deflected by an angle θ after scattering by unpolarized electrons, by replacing θ by $\pi - \theta$ in formulas (23) — (27) of that paper. However there apparently are mistakes in the indicated formulas since, for example, it follows from Eq. (26) that in the nonrelativistic limit in scattering through an angle $\theta = 0$ the polarization is reduced four fold which is obviously false. From Eq. (27) one obtains the information that in the scattering of a longitudinally polarized electron in the extreme relativistic limit its spin keeps its original direction independent of the scattering angle, which is also false. Therefore we give here expressions for the polarization of an electron beam after scattering by unpolarized electrons, obtained by the conventional method of projection operators:

$$\zeta_2(d\sigma/d\Omega) = A_1\zeta_1 + [A_2(\mathbf{n}_2\zeta_1) + A_4(\mathbf{n}_1\zeta_1)]\mathbf{n}_1 + [A_3(\mathbf{n}_1\zeta_1) + A_4(\mathbf{n}_2\zeta_1)]\mathbf{n}_2. \quad (17)$$

In this formula ζ_1 and ζ_2 refer, as before, to the rest system of the electron; however $\mathbf{n}_1$ and $\mathbf{n}_2$ now indicate the momentum direction before and after scattering in the center of mass system; $d\sigma/d\Omega$ is the Möller scattering cross section of unpolarized electrons

$$\frac{d\sigma}{d\Omega} = \frac{r_0^2}{4}\frac{(2\gamma^2-1)^2}{\gamma^2(\gamma^2-1)^2}\left[\frac{4}{\sin^4\theta} - \frac{3}{\sin^2\theta} + \frac{(\gamma^2-1)^2}{(2\gamma^2-1)^2}\left(1 + \frac{4}{\sin^2\theta}\right)\right]. \quad (18)$$

Here $r_0 = e^2/mc^2$, and γ and θ are the energy and deflection angle of the electron in the center of mass system. The energy is measured in units of mc^2. The coefficients A_i are given by

$$A_i = [r_0^2/2\gamma^2(\gamma^2-1)^2]\,a_i,$$
$$a_1 = (2\gamma^2-1)^2(1+\cos\theta)/\sin^4\theta - (2\gamma^4-1)/\sin^2\theta,$$
$$a_2 = -(\gamma^2-1)[(2\gamma^2-1) + 2\gamma^2\cos\theta]/\sin^4\theta,$$
$$a_3 = (\gamma-1)[(2\gamma^2-1)(3\gamma+1) + 2(3\gamma^3+\gamma^2-2\gamma-1)\times\cos\theta]/\sin^4\theta - (\gamma-1)^2(2\gamma^2-1)(1+\cos\theta)/\sin^2\theta,$$
$$a_4 = (\gamma-1)[-2\gamma^3+2\gamma+1-\gamma(2\gamma^2-1)\cos\theta]/\sin^4\theta - (\gamma-1)(2\gamma^2-1)/\sin^2\theta. \quad (19)$$

In the nonrelativistic limit we obtain

$$\zeta_2 = \frac{2(1+\cos\theta)\cos\theta}{1+3\cos^2\theta}\zeta_1. \quad (20)$$

In this case the spin does not turn since there is no spin-orbit interaction, however the degree of polarization is reduced due to exchange effects. In the extreme relativistic case we obtain

$$\zeta_2 = 4(3+\cos^2\theta)^{-2}\{(1+\cos\theta)^2\zeta_1 - (1+\cos\theta)(\mathbf{n}_2\zeta_1)\mathbf{n}_1 + (1+\cos\theta)(3-\sin^2\theta)(\mathbf{n}_1\zeta_1)\mathbf{n}_2 - (1+\cos\theta+\sin^2\theta)\times[(\mathbf{n}_1\zeta_1)\mathbf{n}_1 + (\mathbf{n}_2\zeta_1)\mathbf{n}_2]\}. \quad (21)$$

If the initial polarization is longitudinal then after scattering through a small angle ($\theta \ll 1$) $\zeta_2 = \zeta_1\mathbf{n}_1$,

i.e., the polarization remains longitudinal.

The polarization of final state positrons in the scattering of a polarized positron beam by electrons may also be expressed in the form of Eq. (17). However $d\sigma/d\Omega$ now stands for the scattering cross section of unpolarized positrons by electrons

$$\frac{d\sigma}{d\Omega} = \frac{r_0^2}{16\gamma^2}\left[\frac{(2\gamma^2-1)^2}{(\gamma^2-1)^2\sin^4(\theta/2)} - \frac{8\gamma^4-1}{\gamma^2(\gamma^2-1)\sin^2(\theta/2)} + \frac{12\gamma^4+1}{\gamma^4} - \frac{4(\gamma^2-1)(2\gamma^2-1)}{\gamma^4}\sin^2\frac{\theta}{2} + 4\frac{(\gamma^2-1)^2}{\gamma^4}\sin^4\frac{\theta}{2}\right]. \quad (22)$$

In this case the coefficients A_i are

$$A_1 = \frac{r_0^2}{16\gamma^2}\left[\frac{(2\gamma^2-1)^2}{(\gamma^2-1)\sin^4(\theta/2)} - \frac{8\gamma^4-1}{\gamma^2(\gamma^2-1)\sin^2(\theta/2)} + \frac{4(\gamma^2+1)}{\gamma^2}\right],$$

$$A_2 = \frac{r_0^2}{32\gamma^2}\left[-\frac{4\gamma^2-1}{(\gamma^2-1)\sin^4(\theta/2)} + \frac{4}{\sin^2(\theta/2)}\right],$$

$$A_3 = \frac{r_0^2}{32\gamma^2}\left[\frac{12\gamma^3+4\gamma^2-7\gamma-3}{(\gamma+1)^2(\gamma-1)^2\sin^4(\theta/2)} - \frac{4(7\gamma^4+4\gamma^3-3\gamma^2+1)}{\gamma^2(\gamma+1)^2\sin^2(\theta/2)} + \frac{16(\gamma-1)(2\gamma^2-1)}{\gamma^2(\gamma+1)} - \frac{16(\gamma-1)^2}{\gamma^2}\sin^2\frac{\theta}{2}\right],$$

$$A_4 = \frac{r_0^2}{32\gamma^2}\left[-\frac{(2\gamma+1)^2}{(\gamma+1)^2\sin^4(\theta/2)} + \frac{2(2\gamma^3-4\gamma^2-\gamma+1)}{\gamma^2(\gamma+1)\sin^2(\theta/2)} + \frac{8(\gamma-1)}{\gamma^2}\right]. \quad (23)$$

In the nonrelativistic limit the positron polarization is not changed by the scattering, i.e., $\zeta_1 = \zeta_2$. This is explained by the fact that exchange effects are absent in positron-electron scattering in the nonrelativistic limit.

In the extreme relativistic limit we obtain

$$\zeta_2 = \cos^2\frac{\theta}{2}\left\{\cos^2\frac{\theta}{2}\,\zeta_1 - \frac{1}{2}[(\mathbf{n}_2\zeta_1)(\mathbf{n}_1+\mathbf{n}_2) + (\mathbf{n}_1\zeta_1)\mathbf{n}_1] + \left(1+\frac{1}{2}\cos^2\theta\right)(\mathbf{n}_1\zeta_1)\mathbf{n}_2\right\} \times\left[\sin^4\frac{\theta}{2} + \left(1+\sin^4\frac{\theta}{2}\right)\cos^4\frac{\theta}{2}\right]^{-1}. \quad (24)$$

In the scattering of a longitudinally polarized positron through a small angle we have, as in the electron case, $\zeta_2 = \zeta_1\mathbf{n}_2$.

In the scattering of μ mesons by electrons the exchange effects are absent and the masses of the colliding particles are different. Meson polarization after scattering is given by Eq. (17) in which $d\sigma/d\Omega$ now stands for the scattering cross section of unpolarized mesons

$$\frac{d\sigma}{d\Omega} = \left(\frac{e^2}{c^2}\right)^2 \frac{p^4\cos^2\theta + p^2(1+2\gamma\varepsilon+\Delta^2)\cos\theta + p^2(3\gamma^2+2\gamma\varepsilon-2) + \Delta^2(\gamma^2+1)}{8(\varepsilon+\gamma)^2 p^4\sin^4(\theta/2)}, \quad (25)$$

where $\Delta = m/\mu$. The coefficients A_i are:

$$A_i = \left(\frac{e^2}{\mu c^2}\right)^2 a_i\left[8(\varepsilon+\gamma)^2 p^4\sin^4\frac{\theta}{2}\right]^{-1},$$

$$a_1 = p^2(2\gamma^2+2\gamma\varepsilon-1+\Delta^2)\cos\theta + p^2(2\gamma^2+2\gamma\varepsilon-1) + \Delta^2(\gamma^2+1),$$

$$a_2 = -2p^4 - p^2(2\gamma\varepsilon+\Delta^2),$$

$$a_3 = p^2(\gamma-1)^2\cos^2\theta + 2(\gamma-1)^2[(\gamma+1)\times(\gamma+2\varepsilon)+\Delta^2]\cos\theta + 3p^4 + 2p^2\gamma\varepsilon + p^2\Delta^2,$$

$$a_4 = p^2(\gamma-1)\cos\theta - p^2(\gamma-1)(2\gamma+1) - 2p^2\varepsilon(\gamma-1) - (\gamma-1)^2\Delta^2. \quad (26)$$

In Eqs. (25) and (26) γ and ϵ denote the total energy of the meson and electron respectively measured in units of μc^2, and p is the momentum in units of μc where μ is the meson mass. If the meson is longitudinally polarized then the probability of the spin flipping with respect to its initial direction is given for low meson velocities by the formula*

$$Q = \left(\frac{m}{\mu}\right)^2\beta_L^2\sin^2\frac{\theta}{2}\left(1+\sin^4\frac{\theta}{2}\right), \quad (27)$$

where β_L is the meson velocity in the laboratory system in units of c. In the extreme relativistic case we find

$$\zeta_2 = \{4(1+\cos\theta)\zeta_1 - 4(\mathbf{n}_2\zeta_1)\mathbf{n}_1 + (\cos^2\theta+6\cos\theta+5)\times(\mathbf{n}_1\zeta_1)\mathbf{n}_2 - 4[(\mathbf{n}_1\zeta_1)\mathbf{n}_1 + (\mathbf{n}_2\zeta_1)\mathbf{n}_2]\}\times(\cos^2\theta+2\cos\theta+5)^{-1}. \quad (28)$$

For a longitudinally polarized meson Eq. (28) becomes

$$\zeta_2 = \zeta_1\mathbf{n}_2.$$

The authors are grateful to A. Z. Dolginov for suggesting the research project of which the present paper is a part, and for valuable discussions.

Note added in proof (October 5, 1959). After this paper was submitted to the editor, G. V. Frolov has shown us his unpublished work which is a continuation of his previous work.[18] Our formulas (25) – (27) are special cases of Frolov's results.

*In the paper by Ford and Mullin[8] the analogous formula (20) contains an superfluous term $-\sin^4(\theta/2)$.

[1] H. A. Tolhoek, Revs. Modern Phys. **28**, 277 (1956).

[2] F. Gursey, Phys. Rev. **107**, 1734 (1957).
[3] G. Passatore, Nuovo cimento **6**, 850 (1957).
[4] H. Banerjee, Acta Phys. Austriaca **12**, 70 (1958).
[5] Bernardini, Brovetto, and Ferroni, Nucl. Phys. **8**, 294 (1958).
[6] I. G. Ivanter, JETP **36**, 325 (1959), Soviet Phys. JETP **9**, 224 (1959).
[7] A. A. Kresnin and L. N. Rozentsveĭg, JETP **32**, 353 (1957), Soviet Phys. JETP **5**, 288 (1957).
[8] G. W. Ford and C. J. Mullin, Phys. Rev. **108**, 477 (1957).
[9] A. M. Bincer, Phys. Rev. **107**, 1434, 1467 (1957).
[10] J. M. C. Scott, Phil. Mag. **2**, 1472 (1957).
[11] Bockmann, Kramer, and Theis, Z. Physik **150**, 201 (1958).
[12] A. I. Mukhtarov and Yu. S. Perov, Изв. высш. уч. завед., физика (News of the Higher Inst. of Learning, Physics), No. 3, 48 (1958).
[13] H. Bethe, Z. Physik **76**, 293 (1932); Quantum Mechanics of the One- and Two-Electron System. (Russ. Transl.) ONTI (1935).
[14] L. D. Landau and E. M. Lifshitz, Квантовая механика (Quantum Mechanics), Gostekhizdat, 1948 [Engl. Transl., Pergamon, 1958].
[15] I. Olsen Haakon, Kgl. norske vid, selskabs forhandl, **31**, No. 11, 11a, 1 (1958).
[16] W. Heisenberg, Physik. Z. **32**, 737 (1931).
[17] L. Bewilogua, Physik. Z. **32**, 740 (1931).
[18] G. V. Frolov, JETP **34**, 764 (1958), Soviet Phys. JETP **7**, 525 (1958).

Translated by A. M. Bincer
272

DISPERSION RELATIONS FOR INELASTIC K-MESON PROCESSES

Yu. VOL' F

Joint Institute for Nuclear Research

Submitted to JETP editor June 7, 1959

J. Exptl. Theoret. Phys. (U.S.S.R.) **37**, 1379-1384 (November, 1959)

Dispersion relations for a process of the type $\widetilde{K} + N \to Y + \pi$ are written down. The structure of the amplitude for scalar and pseudoscalar K mesons is described.

1. Amati and Vitale[1] considered nonrelativistic dispersion relations for inelastic K-meson processes; relativistic dispersion relations for $\pi + N \to Y + K$ (Y means Λ or Σ) and $\gamma + N \to Y + K$ were studied by Polivanov and Okubo.[2] In the present work the processes $\widetilde{K} + N \to Y + \pi$ are considered, in particular $K^- + p \to \Sigma^0 + \pi^0$. Because of the difference in the M_Λ and M_Σ masses, which particles also occur in intermediate states, the energy spectra are different for each process.

2. We make use here of a complex field for $K^\pm$ and a real field for π^0 which directly represent the physical K and π particles.

Using the notation of Bogolyubov and Shirkov[3] for a complex scalar field and the definitions

$$j_K(x) = i\frac{\delta S}{\delta \varphi_K^*(x)} S^+,$$

$$j_\pi(x) = i\frac{\delta S}{\delta \varphi_\pi(x)} S^+,$$

we get for $K^- + p \to \Sigma^0 + \pi^0$, dropping the factor

$$\delta(q + p - p' - q') \Big/ \sqrt{2q_0 q_0'},$$

$$\langle p' | S + S^+ | p \rangle = i\,[T^{ret}(k) - T^{adv}(k)] = iT(k),$$

where $|p\rangle$ is a state of momentum p, and p' and p are the momenta of the hyperon and nucleon, while q' and q are the pion and K-meson momentum, where

$$(p')^2 = M_Y^2, \quad (p)^2 = M^2, \quad (q')^2 = m_\pi^2, \quad (q)^2 = m_K^2.$$

Here, using the Bogolyubov causality condition[4]

$$T^{ret}(k) = \int d\eta e^{i(k\eta)} \left\langle p' \left| \frac{\delta j_K(-\eta/2)}{\delta \varphi_\pi(\eta/2)} \right| p \right\rangle = \int d\eta e^{i(k\eta)} F^{ret}(\eta),$$

$$T^{adv}(k) = \int d\eta e^{i(k\eta)} \left\langle p' \left| \frac{\delta j_\pi(\eta/2)}{\delta \varphi_K^*(-\eta/2)} \right| p \right\rangle = \int d\eta e^{i(k\eta)} F^{adv}(\eta),$$

where $k = \frac{1}{2}(q' - q)$ and $(k\eta) = k_0\eta_0 - \mathbf{k}\boldsymbol{\eta}$. In getting the second term we use the condition $SS^+ = 1$ and the invariance of the vacuum and one-particle states.

Later we shall work with the Fourier transforms

$$T(k) = 2iA(k) = \int d\eta e^{i(k\eta)} F(\eta),$$

$$D(k) = \int d\eta e^{i(k\eta)} \bar{F}(\eta),$$

where

$$F(\eta) = i\langle p' | [j_K(-\eta/2),\ j_\pi(\eta/2)] | p \rangle$$

and

$$\bar{F}(\eta) = {}^1/_2 [F^{ret}(\eta) + F^{adv}(\eta)],$$

which represent the antihermitian part A(k) and the Hermitian part D(k) of the retarded matrix $T^{ret}(k)$.

3. We introduce the coordinate system in which $p_0 = p_0'$ and $q_0 = q_0'$. We put $\mathbf{p}' = a\mathbf{p}$; the condition $p_0 = p_0'$, $\sqrt{\mathbf{p}^2 + M^2} = \sqrt{a^2\mathbf{p}^2 - M_Y^2}$ gives

$$a = \pm\sqrt{1 - \Delta/\mathbf{p}^2} = \pm\alpha,$$

where $\Delta = (M_Y^2 - M^2)$. The sign of α is determined below from the condition that there is a break in the energy spectrum, and it turns out to be positive. Therefore

$$\mathbf{p}' = \alpha\mathbf{p}.$$

Using momentum conservation and the definition $\mathbf{k} = \frac{1}{2}(\mathbf{q}' + \mathbf{q}) = \lambda\mathbf{e} - \gamma\mathbf{p}$, we get from the conditions $\mathbf{ep} = 0$ and $\mathbf{e}^2 = 1$

$$\gamma = -\delta/2(1 - \alpha)\mathbf{p}^2, \quad \delta = (m_K^2 - m_\pi^2), \quad \lambda^2 = q_0^2 - E_\tau,$$

where

$$E_\tau^2 = {}^1/_4(1 - \alpha)^2\mathbf{p}^2 + \gamma^2\mathbf{p}^2 + m,$$

and $m = \frac{1}{2}(m_K^2 + m_\pi^2)$.

Therefore, for $k = \frac{1}{2}(q' + q)$, where $k_0 = \frac{1}{2}(q_0' + q_0)$, we get

$$k = (E;\ \mathbf{k}) = (E;\ \lambda\mathbf{e} - \gamma\mathbf{p}),$$

$$\lambda = \pm\sqrt{E^2 - E_\tau^2}.$$

Here E_τ is the threshold energy in our coordinate system.

4. We thus have

$$T(E) = \int d\eta \exp\{iE\eta_0 - i\lambda\eta\mathbf{e} + i\gamma\eta\mathbf{p}\} F(\eta). \quad (4.1)$$

For the process $\pi^0 + p \to \Sigma^0 + K^+$ we get

$$T_c(E) = -\int d\eta \exp\{iE\eta_0 - i\lambda\eta\mathbf{e} - i\gamma\eta\mathbf{p}\} F(-\eta). \quad (4.2)$$

Expanding the members of the commutator in the complete system of intermediate states we find that the first member in T(E) contains the state

$$|\nu\rangle = p,\ p + \pi^0, \ldots$$

and the second

$$|\mu\rangle = \Lambda,\ \Sigma^0 + \pi, \ldots,$$

i.e., from baryon and strangeness conservation we have a nucleon branch $|\nu\rangle$ and a hyperon branch $|\mu\rangle$.

Integrating over η, we get

$$T(E) = i(2\pi)^4 \left\{ \sum_\nu \langle p'|j_K(0)|p_\nu\rangle\langle p_\nu|j_\pi(0)|p\rangle \delta(E - p_0 + p_0^\nu) - \sum_\mu \langle p'|j_\pi(0)|p_\mu\rangle\langle p_\mu|j_K(0)|p\rangle \delta(E + p_0 - p_0) \right\} \quad (4.3)$$

and the momenta of the intermediate states, determined by the delta-functions

$$\mathbf{p}_\nu = {}^1/_2(1+\alpha)\mathbf{p} - \mathbf{k} = [(1+\alpha)/2 + \gamma]\mathbf{p} - \lambda\mathbf{e},$$

$$\mathbf{p}_\mu = {}^1/_2(1+\alpha)\mathbf{p} + \mathbf{k} = [(1+\alpha)/2 - \gamma]\mathbf{p} - \lambda\mathbf{e}. \quad (4.4)$$

The delta-functions determine the spectrum of the nucleon branch

$$-2p_0E_\nu = (M_\nu^2 - M^2 - m) - \mathbf{p}^2(1-\alpha) - \frac{\delta}{2}\left(\frac{1+\alpha}{1-\alpha}\right). \quad (4.5')$$

and the hyperon branch

$$2p_0E_\mu = (M_\mu^2 - M^2 - m) - \mathbf{p}^2(1-\alpha) + \frac{\delta}{2}\left(\frac{1+\alpha}{1-\alpha}\right). \quad (4.5'')$$

Here M_ν and M_μ mean the mass of the intermediate states. The spectrum has the form given in the figure.

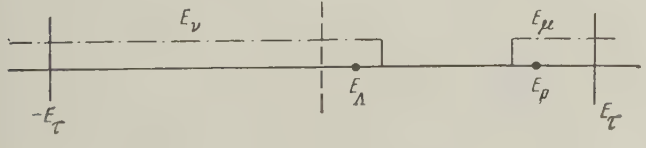

Form of the spectrum for the process $K^- + p \to \Sigma^0 + \pi^0$

5. Examination shows that the two regions of the continuous spectrum are not joined for all values of $\mathbf{p}^2$ within the limits

$$1.04\,\Delta < \mathbf{p}^2 < \infty$$

(Δ is the minimum $\mathbf{p}^2$ value).

We see that here the continuous spectrum in the unobservable region takes up an even greater area than it does in the K-meson scattering case, where we also have a continuous spectrum even for forward scattering. In this case the reaction $K^- + p \to Y + \pi$ contributes in the unphysical region, since $M + m_K > M_Y + m_\pi$ always. For dispersion relations in the K-scattering case, Galzenati and Vitale[5] got reasonable results, in the sense of comparisons with experiment, by neglecting the integrals over the unphysical region; lowest order perturbation theory for $K^- + N \to Y + \pi$ shows[6] that the introduction of an amplitude below the threshold is smooth for the case of a pseudoscalar K meson.

In all reactions of the $K^- + p \to Y + \pi$ type, there is a contribution in the unphysical region from the reactions $\pi_1 + Y_1 \to Y_2 + \pi_2$ and $\pi_1 + N_1 \to N_2 + \pi_2$; estimating these contributions is made more difficult by the fact that both branches still contain states of the type $(p + 2\pi)$ or $(Y + 2\pi)$ and so on, corresponding to different processes of the strong pion interaction.

6. The spectrum of the function $T_c(E)$ for the reaction $\pi^0 + p \to \Sigma^0 + K^+$ is reflection symmetric relative to the spectrum of the function T(E).

From (4.1) and (4.2), we have

$$S_eT(-E) = -S_eT_c(E),$$
$$\mathfrak{A}_eT(-E) = +\mathfrak{A}_eT_c(E), \quad (6.1)$$

where S_e, $\mathfrak{A}_e$ mean symmetrization with respect to e, which excludes the doublevaluedness of λ (see reference 7). The expression (6.1) corresponds to the "crossing symmetry" and affords the possibility of excluding the negative-energy region in dispersion relations.

Dispersion relations can be obtained by substituting the Cauchy integral formula in the function T(E); the contour of integration is evident from the figure. Under the same conditions as in reference 7, we get the relation between D(E) and A(E):

$$S_eD(E) = \frac{1}{\pi}\mathrm{P}\int_0^\infty d\varepsilon \left[\frac{S_eA(\varepsilon)}{\varepsilon - E} + \frac{S_eA_c(\varepsilon)}{\varepsilon + E}\right],$$

$$\mathfrak{A}_eD(E) = \frac{1}{\pi}\mathrm{P}\int_0^\infty d\varepsilon \left[\frac{\mathfrak{A}_eA(\varepsilon)}{\varepsilon - E} - \frac{\mathfrak{A}_eA_c(\varepsilon)}{\varepsilon + E}\right]. \quad (6.2)$$

Combining equal relations for $T_c(E)$ we can write the symmetric expressions

$$S_e\{D(E) - D_c(E)\} = \frac{2E}{\pi}\mathrm{P}\int_0^\infty \frac{d\varepsilon}{\varepsilon^2 - E^2}\{S_eA(\varepsilon) - S_eA_c(\varepsilon)\},$$

$$\mathfrak{A}_e\{D(E) - D_c(E)\} = \frac{2}{\pi}\mathrm{P}\int_0^\infty \frac{\varepsilon\, d\varepsilon}{\varepsilon^2 - E^2}\{\mathfrak{A}_eA(\varepsilon) - \mathfrak{A}_eA_c(\varepsilon)\}, \quad (6.3)$$

where the subtraction of the amplitudes plays a "cutoff" role at high energies.

7. For pseudoscalar K mesons the amplitude of the process is scalar.

Then

$$T^{ret} = \delta_{s's} T^0 + i\lambda [\mathbf{e} \times \mathbf{p}] \langle \sigma \rangle_{s's} T^1, \qquad (7.1)$$

where s' and s are the spin states of the hyperon and the nucleon. The other possible invariant **ep** is equal to zero in our coordinate system, so that T^0, T^1 do not depend on the sign of **e** or **p**. Separating T^0 and T^1 into hermitian and antihermitian parts, corresponding to T^0_c and T^1_c we get from (6.3), applying the symmetrizations S_e and $\mathfrak{A}_e$

$$D^1(E) - D^1_c(E) = \frac{2}{\pi} P \int_0^\infty \frac{\varepsilon\, d\varepsilon}{\varepsilon^2 - E^2} \{A^1(\varepsilon) - A^1_c(\varepsilon)\},$$

$$D^0(E) - D^0_c(E) = \frac{2E}{\pi} P \int_0^\infty \frac{d\varepsilon}{\varepsilon^2 - E^2} \{A^0(\varepsilon) - A^0_c(\varepsilon)\} \qquad (7.2)$$

For scalar K mesons the amplitude is pseudoscalar. The only non-vanishing pseudoscalars are $\sigma \cdot \mathbf{p}$ and $\sigma \cdot \mathbf{e}$, which expresses the fact that we have here only the spin-flip amplitudes; the spin flip compensates for the change in internal parity.

Therefore

$$T^{ret} = \{\langle \sigma \rangle_{s's} \mathbf{p}\}\, T^{(p)} + \{\langle \sigma \rangle_{s's} \mathbf{e}\}\, T^{(e)}. \qquad (7.3)$$

This gives, together with (6.3), the relationship between the hermitian and antihermitian part of the amplitudes $T^{(p)}$ and $T^{(e)}$

$$D^{(p)}(E) - D^{(p)}_c(E) = \frac{2}{\pi} P \int_0^\infty \frac{d\varepsilon}{\varepsilon^2 - E^2} \{A^{(p)}(\varepsilon) - A^{(p)}_c(\varepsilon)\},$$

$$D^{(e)}(E) - D^{(e)}_c(E) = \frac{2}{\pi} P \int_0^\infty \frac{\varepsilon\, d\varepsilon}{\varepsilon^2 - E^2} \{A^{(e)}(\varepsilon) - A^{(e)}_c(\varepsilon)\}. \qquad (7.4)$$

8. Let us examine the contribution of the poles. The first terms in $A(E)$ for one nucleon or one hyperon in the intermediate state give the amplitudes

$$a_p = |1 - E_p/p^0| \sum_{s''} \langle p' | j_K(0) | p_\nu, s'' \rangle \times \langle p_\nu, s'' | j_\pi(0) | p \rangle \delta(E - E_p),$$

$$a_\Lambda = |1 - E_\Lambda/p^0| \sum_{s''} \langle p' | j_\pi(0) | p_\mu, s'' \rangle \times \langle p_\mu, s'' | j_K(0) | p \rangle \delta(E + E_\Lambda).$$

They contain the the coupling constants $(gg_{\Sigma Kp})$ and $(g_{\Sigma\Lambda\pi} g_{\lambda pK})$ where g is the pion-nucleon coupling constant. We note, however, that the energy E_p corresponding to a pole is not the same as the pole contribution for pion-nucleon scattering.

In both the scalar and pseudoscaler K-meson cases, the contributions from the poles are

$$(gg_{\Sigma Kp}) \frac{E}{(2\pi)^2 (E_p^2 - E^2)} \{+ E_p F(\mathbf{p}^2) + f(\mathbf{p}^2)\} - (g_{\Sigma\Lambda\pi} g_{\Lambda pK}) \frac{E}{(2\pi)^2 (E_\Lambda^2 - E^2)} \{E_\Lambda \Phi(\mathbf{p}^2) + \varphi(\mathbf{p}^2)\}, \qquad (8.2')$$

and

$$(gg_{\Sigma Kp}) \frac{E_p}{(2\pi)^2 (E_p^2 - E^2)} \Psi(\mathbf{p}^2) + (g_{\Sigma\Lambda\pi} g_{\Lambda pK}) \frac{E}{(2\pi)^2 (E_\Lambda^2 - E^2)} \Psi(\mathbf{p}^2), \qquad (8.2'')$$

corresponding to the first and second equations in (7.2) and (7.4).

The functions $F(\mathbf{p}^2)$, $\Phi(\mathbf{p}^2)$, etc depend on our coordinate system and we do not give their general form.

9. It has already been remarked that these relations contain integrals over the unphysical regions, even more than the K-scattering case. According to perturbation theory results[6] or to the dispersion relations for K scattering, this difficulty may not be so serious for scattering; but this question is still open.

In our case the possibility of estimating the coupling constants is reduced by the existence of the nucleon branch of the pion-nucleon coupling.

As an approximation, as for example a one-meson approximation, we can express the amplitudes $\langle \Sigma, \pi | j_\pi | Y \rangle$, for which there are no experimental data, in terms of other amplitudes by making some assumptions about strong interaction symmetries.

I express my thanks to A. A. Logunov for suggesting the problem and to M. K. Polivanov for valuable discussions.

[1] D. Amati and B. Vitale, Nuovo cimento **10**, 1282 (1957).

[2] M. K. Polivanov, Dokl. Akad. Nauk SSSR **118**, 679 (1958), Soviet Phys.-Doklady **3**, 114 (1958). F. Oubo, Progr. Theoret. Phys. Japan **19**, 43 (1957).

[3] N. N. Bogolyubov and D. V. Shirkov, Введение в теорию квантованных полей (Introduction to the Theory of Quantized Fields), Fizmatgiz (1957).

[4] N. N. Bogolyubov, Izv. Akad. Nauk SSSR, Ser. Fiz. **19**, 237 (1955), Columbia Tech. Transl. p. 215.

[5] E. Galzenati and B. Vitale, Preprint.

[6] San-Fu Tuan, Preprint. P. T. Matthews and A. Salam, Phys. Rev. **110**, 565 (1958).

[7] Bogolyubov, Medvedev, and Polivanov, Вопросы теории дисперсионных соотношений (Questions in the Theory of Dispersion Relations), Fizmatgiz (1958).

Translated by W. Ramsay
273

REDUCED WIDTHS FOR NUCLEON ASSOCIATIONS IN THE SHELL MODEL OF THE NUCLEUS

V. V. BALASHOV, V. G. NEUDACHIN, Yu. F. SMIRNOV, and N. P. YUDIN

Institute of Nuclear Physics, Moscow State University

Submitted to JETP editor June 8, 1959

J. Exptl. Theoret. Phys. (U.S.S.R.) **37**, 1385-1389 (November, 1959)

A method is considered which can be employed to calculate the reduced widths of compound-nucleus levels decaying with emission of deuterons, tritons, and α particles. The analysis is based on the shell model of the nucleus.

IT has been pointed out several times that the shell model and the α particle model are not mutually exclusive. For example, it can be easily shown[1,2] that, using oscillator functions, the wave functions for the lowest states 0^+, 2^+, and 4^+ of the Be^8 nucleus are the same in the shell model with LS coupling and in the α particle model. This is an illustration of the fact that the α association of the nucleons is compatible with the Young scheme of the orbital part of the wave function if this scheme contains the maximal number of four-groups.[3] An essential part of the features of the α particle model is, therefore, already contained in the symmetry properties of the wave functions of the lowest states of nuclei with shell structure, as has been noted earlier.[4]

It should be mentioned that by basing the analysis of the α association in the nucleus on the shell model, we can not only make a formal comparison between the models as mentioned above, but also obtain for the first time the possibility to calculate all those effects in which the α association (or the d, t, and other associations) plays the principal role. This means we can use the experimental data immediately to test the correctness of the approach to this problem. One of these effects is the decay of the compound nucleus under emission of d, t, He^3, or α. The probability of the decay through one of these channels is determined by the corresponding reduced level width γ^2, which, in the instance of α particles, is given by[5,6]

$$\gamma = \binom{A}{4}^{1/2} \frac{\hbar}{\sqrt{2\mu}} \sum_{M, M_1} (J_1 M_1 \Lambda M \mid J_0 M_0) \times \int X_\lambda^* \psi_1 \psi_\alpha Y_{\Lambda M}(\mathbf{R}_1 - \mathbf{R}_\alpha)\, d\sigma \qquad (1)$$

where $|\mathbf{R}_1 - \mathbf{R}_\alpha| = a$. X_λ is the wave function for the level λ of the compound nucleus; ψ_1 and ψ_α are the functions of the final state of the nucleus and of the α particle, respectively; $Y_{\Lambda M}(\mathbf{R}_1 - \mathbf{R}_\alpha)$ is the angular part of the wave function describing the relative motion of the recoiling particles with the orbital angular momentum Λ and its projection M; μ is the reduced mass of the recoiling particles;

$$\binom{A}{m} = A!/m!\,(A-m)!;$$

a is the channel radius; J_0, M_0 and J_1, M_1 are the angular momenta and their projections of the initial and final states of the nucleus, respectively; $(J_1 M_1 \Lambda M \mid J_0 M_0)$ are Clebsch-Gordan coefficients; the integration is to be taken over the internal variables of the recoiling particles and over the angular coordinates of their relative motion.

Using oscillator functions to describe the relative motion of the nucleons in the states X_λ, ψ_1, and ψ_α, we can connect the internal functions of X_λ, ψ_1, and ψ_α with the shell model functions X_λ^{sh}, ψ_1^{sh}, and ψ_α^{sh}, corresponding to the lowest energy state for the center of mass of these nuclei. According to the theorem of Elliot and Skyrme,[4] we have for states with one unfilled state,

$$X_\lambda^{sh} = \psi_{00}(\mathbf{R})\, X_\lambda = |\beta, l^n [f] TSL\rangle, \qquad (2a)$$

$$\psi_1^{sh} = \psi_{00}(\mathbf{R}_1)\psi_1 = |\beta, l^{n-4}[f_1] T_1 S_1 L_1\rangle, \qquad (2b)$$

$$\psi_\alpha^{sh} = \psi_{00}(\mathbf{R}_\alpha)\psi_\alpha = |s^4 [4] 000\rangle, \qquad (2c)$$

where $\psi_{00}(\mathbf{R})$ is an oscillator function describing the motion of the center of mass of the nucleus with the quantum numbers $N = 0$ and $L = 0$ [N is the principal quantum number: $E_{NL} = \hbar\omega(N + 3/2)$] β is a symbol denoting all closed shells, and n is the number of nucleons in the unfilled shell.

With the help of the technique of fractional parentage coefficients a group of four nucleons can be separated out of the function X_λ^{sh}. We

shall be interested only in the fractional parentage coefficient

$$\langle \beta, l^n [f] TSL | \beta, l^{n-4} [f_1] TSL_1; l^4 [4] 00\Lambda \rangle,$$

corresponding to the separation of four nucleons in the state with $T = 0$, $S = 0$, and the same Young scheme $[f_2] = [4]$ as for ψ_α^{sh}. For these coefficients we have the following relation:

$$\langle \beta, l^n [f] TSL | \beta, l^{n-4} [f_1] T_1 S_1 L_1; l^4 [f_2] T_2 S_2 L_2 \rangle = \binom{n}{4}^{1/2} \times \binom{A}{4}^{-1/2} \langle l^n [f] TSL | l^{n-4} [f_1] T_1 S_1 L_1; l^4 [f_2] T_2 S_2 L_2 \rangle. \quad (3)$$

The function $| l^4 [4] 00\Lambda \rangle$ contains the state $\psi_3 = \psi_{N\Lambda}(\mathbf{R}_\alpha)\psi_\alpha$ with the coefficient

$$K(N\Lambda) = \langle l^4 [4] 00\Lambda | \psi_{N\Lambda}(\mathbf{R}_\alpha)\psi_\alpha \rangle,$$

for which (2c) gives the expression

$$K(N\Lambda) = \left\langle l^4 [4] 00\Lambda \left| \frac{\psi_{N\Lambda}(\mathbf{R}_\alpha)}{\psi_{00}(\mathbf{R}_\alpha)} \right| s^4 [4] 000 \right\rangle. \quad (4)$$

If we integrate in the right-hand side of (1) not only over the angular variables of the vector $\mathbf{R}_1 - \mathbf{R}_\alpha$, but also over the radial variable, we can rewrite the expression for γ in the following form:

$$\gamma = R_{N\Lambda}(|\mathbf{R}_1 - \mathbf{R}_\alpha| = a)\binom{A}{4}^{1/2} \frac{\hbar}{\sqrt{2\mu}} \times \int X_\lambda^* \psi_1 \psi_\alpha \psi_{N\Lambda}(\mathbf{R}_1 - \mathbf{R}_\alpha)\, d\sigma d(|\mathbf{R}_1 - \mathbf{R}_\alpha|). \quad (5)$$

(ψ_1 and $\psi_{N\Lambda}$ are coupled in the state J_0, M_0).

Let us consider the integral

$$I = \int X_\lambda^{sh*} \psi_1^{sh} \psi_3\, d\sigma\, d(|\mathbf{R}_1 - \mathbf{R}_\alpha|)\, d\mathbf{R} = \binom{n}{4}^{1/2} \binom{A}{4}^{-1/2} \times \langle l^n [f] TSL | l^{n-4} [f_1] TSL_1; l^4 [4] 00\Lambda \rangle K(N\Lambda). \quad (6)$$

Separating the relative motion of the recoiling particles and their center of mass motion with the help of the Talmi transformation[8] and using expression (5), we can write this integral in the form

$$I = \gamma \left\langle \begin{matrix} 0\,0 \\ N\Lambda \end{matrix} \middle| A-4.4 \middle| \begin{matrix} N\Lambda \\ 0\,0 \end{matrix} \right\rangle [R_{N\Lambda}(|\mathbf{R}_1 - \mathbf{R}_\alpha| = a)]^{-1} \binom{A}{4}^{-1/2}$$

$$\left\langle \begin{matrix} 0\,0 \\ N\Lambda \end{matrix} \middle| A-4.4 \middle| \begin{matrix} N\Lambda \\ 0\,0 \end{matrix} \right\rangle = \int \psi_{00}^*(\mathbf{R}_1)\psi_{N\Lambda}^*(\mathbf{R}_\alpha)\psi_{00}(\mathbf{R})\psi_{N\Lambda} \times (\mathbf{R}_1 - \mathbf{R}_\alpha)\, d\mathbf{R}_1 d\mathbf{R}_\alpha = \left(\frac{A-4}{A}\right)^{N/2}. \quad (7)$$

Hence

$$\gamma = \frac{\hbar}{\sqrt{2\mu}} \left(\frac{A}{A-4}\right)^{N/2} \binom{n}{4}^{1/2} \langle l^n [f] TSL | l^{n-4} [f_1] TSL_1; l^4 [4] 00\Lambda \rangle \times K(N\Lambda) R_{N\Lambda}(|\mathbf{R}_1 - \mathbf{R}_\alpha| = a). \quad (8)$$

Assuming that at the nuclear boundary $\frac{1}{2} a^3 R_{N\Lambda}^2(a) = 1$ (reference 5), we obtain for the reduced width for the decay of the compound nucleus under emission of an α particle

$$\gamma^2 = \frac{\hbar^2}{\mu a}\left(\frac{A}{A-4}\right)^N \binom{n}{4} \langle l^n [f] TSL | l^{n-4} [f_1] TSL_1; l^4 [4] 00\Lambda \rangle^2 K^2(N\Lambda). \quad (9)$$

This formula can be generalized to the case where a cluster with an arbitrary number of nucleons m and with spin $S_2 \neq 0$ is emitted:

$$\gamma^2_{m\Lambda J_0 J_1} = \frac{\hbar^2}{\mu a}\left(\frac{A}{A-m}\right)^N \binom{n}{m} \sum_{L_2 J_2} \langle l^n [f] TSL | l^{n-m} [f_1] T_1 S_1 L_1; l^m [f_2] T_2 S_2 L_2 \rangle^2 K^2(N\Lambda, L_2) U^2 \times (SL_1 J_0 L_2 : J_2 L) U^2 (L_1 S_1 J_2 S_2 : J_1 S), \quad (10)$$

where J_0 and J_1 are the total angular momenta of the initial and final states, respectively, J_2 is the channel spin, $U(ABCD:EF)$ is a Racah coefficient,[9] and

$$K(N\Lambda, L_2) = \left\langle l^m [f_2] T_2 S_2 L_2 \left| \frac{\psi_{N\Lambda}(\mathbf{R}_2)}{\psi_{00}(\mathbf{R}_2)} \right| \psi_2^{sh} \right\rangle.$$

For the deuteron we take $\psi_2^{sh} = | s^2 [2] 010 \rangle$, and for the triton, $\psi_2^{sh} = | s^3 [3] \frac{1}{2}\frac{1}{2}0 \rangle$. Here we assume that the internal wave function of the recoiling particles is not changed appreciably during the transition in the external region. Rough estimates support this assumption. According to the shell model we describe the states of the nuclei H^3, He^3, and He^4 by the configurations s^3 and s^4 with oscillator wave functions. To obtain the correct binding energies for these nuclei, we must set $\hbar\omega = 16$ Mev (the "width of the well" is $r_0 = \sqrt{\hbar/m\omega} = 1.6 \times 10^{-13}$ cm). This value is very close to that used in the description of the p shell nuclei in the framework of the intermediate coupling model. Thus the internal wave functions of the three-nucleon and four-nucleon clusters, corresponding to the states $| s^n [f] TS_0 \rangle$ and $| p^n [f] TSL \rangle$, are close to one another. If we recall that in general the same form of potential for the nucleon interaction is used to calculate the binding energy of t, He^3, and α as well as the binding energies and level energies of p shell nuclei, we find that in these nuclei the binding energies of the t and α clusters (and of He^3 as well) agree with good accuracy (5 — 10%) with the experimental binding energies for the corresponding free particles. This gives rise to the hope that our "algebraic" separation of the

Reduced widths for the d, t, and α decays of levels of light nuclei

Nucleus	E* Mev	J, T	$2T+1, 2S+1L[f]$	Type of decay	Λ	$2\mu a\gamma^2/3\hbar^2$		$a \cdot 10^{13}$cm
						Theory	Experiment	
He^5	2.0	3/2,1/2	^{22}P [1]	$He^4 + n$	1	5/6	1[11]	
Li^6	2.189 4.52	3,0 2,0	^{13}D [2]	$He^4 + d$	2	3/4	0.5[12] 0.6	4.0
Be^7	4.65	7/2,1/2	^{22}F [3]	$He^4 + He^3$	3	$\frac{343}{432}$	0.3[13]	4.4
Be^8	2.9	2,0	^{11}D [4]	$He^4 + \alpha$	2	1	1[12]	5.0

three- and four-nucleon complexes in the framework of the shell model reproduces the most essential features of this association. In the case of deuterons the situation is somewhat worse. It should further be noted that the smallness of the binding energy of the deuteron and the triton may lead to an additional factor smaller than unity in the corresponding formulas for the reduced widths, as a result of the action of the nuclear boundary on the internal function of the emitted particle. At the same time one might think that our method of calculation will satisfactorily reproduce the relative values of the reduced widths for the emission of d and t for the different levels of the same nucleus. The results of this work are given in the table (E* is the excitation energy of the level).

Mang,[10] in his calculation of the α decay of heavy nuclei, also used oscillator functions for the separation of the internal motion of the nuclei and the α particles.

In conclusion it is of interest to anticipate the appearance of those effects of the peculiarities of the α association which are due to the correlations between the nucleons which are not taken account of in the shell model.

1. One might think that, if we use nucleon interaction parameters that reproduce the energies of nuclear states which do not admit of α association (for example, the levels with T = 1 in Be^8) to compute the levels which do admit of α association, i.e., which are characterized by a Young scheme with maximal number of 4-groups, the latter will lie above the corresponding experimental levels as a consequence of the additional energy connected with forming the four-nucleon complex.

2. The α associations should involve LS coupling, i.e., the states of the nuclei admitting α associations should be more adequately described by the LS coupling scheme than is the case in the intermediate coupling model. (Thus, for example, the Be^8 core in the nuclei of the type B^{10} is apparently better described by LS coupling, while the outer nucleons should conform to jj or intermediate coupling.) Correlations in the α associations which are not considered in the shell model can also show up in the β decay. Thus, these additional correlations can lead to a higher value of ft for the decay B^{12}-C^{12} than is obtained in the usual shell model theory with intermediate coupling

3. As another consequence of these additional correlations, the fractional parentage expansion of the true wave function of, for example, the Be^9 nucleus should contain the α associated states Be^8 with a greater statistical weight than that given by the fractional parentage coefficients of the shell model wave function.

[1] K. Wildermuth and Th. Kanellopoulos, Nucl. Phys. 7, 150 (1958); Nucl. Phys. 9, 449 (1959).
[2] J. K. Perring and T. H. Skyrme, Proc. Phys. Soc. 69, 600 (1956).
[3] B. F. Bayman and A. Bohr, Nucl. Phys. 9, 596 (1958).
[4] A. I. Baz', JETP 31, 831 (1956); Soviet Phys. JETP 4, 704 (1957).
[5] A. M. Lane, Proc. Phys. Soc. A66, 977 (1953).
[6] R. G. Thomas, Phys. Rev. 88, 1109 (1952).
[7] J. P. Elliot and T. H. R. Skyrme, Proc. Roy. Soc. A232, 561 (1955).
[8] I. Talmi, Helv. Phys. Acta 25, 185 (1952).
[9] H. A. Jahn, Proc. Roy. Soc. A205, 192 (1951).
[10] H. J. Mang, Z. Physik 148, 582 (1957).
[11] R. Adair, Phys. Rev. 86, 155 (1952); D. Dodder and H. Gammel, Phys. Rev. 88, 520 (1952).
[12] F. Ajzenberg and T. Lauritsen, Revs. Modern Phys. 27, 77 (1955).
[13] Ph. Miller and G. Phillips, Phys. Rev. 112, 2048 (1958).

Translated by R. Lipperheide
274

RAMAN SCATTERING OF ELECTROMAGNETIC WAVES IN FERROMAGNETIC DIELECTRICS

F. G. BASS and M. I. KAGANOV

Institute of Radiophysics and Electronics, Academy of Sciences, Ukrainian S.S.R.; Physico-technical Institute, Academy of Sciences, Ukrainian S.S.R.

Submitted to JETP editor June 10, 1959

J. Exptl. Theoret. Phys. (U.S.S.R.) **37**, 1390-1393 (November, 1959)

A phenomenon of Raman scattering of electromagnetic waves by fluctuations of the magnetic moment is predicted. The coefficient of extinction for the scattered radiation is calculated.

RAMAN scattering — that is, the appearance of shifted frequencies in the spectrum of the scattered radiation — is connected with an interaction of the incident electromagnetic wave with the characteristic oscillations of the scattering object. A ferromagnetic dielectric possesses an additional branch of oscillations, produced by propagation of spin waves. The magnetic field of the incident wave interacts with the oscillations of the magnetic moment (with the spin wave), and this also should lead to characteristic Raman scattering. The present communication is devoted to the theoretical elucidation of this phenomenon.

We consider the case in which the frequency ω_0 of the incident wave is much larger than the characteristic frequencies of the ferrodielectric. The discussion applies to waves in the millimeter range or in the far infrared part of the spectrum, since a ferromagnetic dielectric is transparent at these frequencies. It is true, of course, that this can be the case only at sufficiently low temperatures, where the semiconducting properties of the ferrites are not exhibited. Then the system of equations that describes the scattered field in the medium has the form

$$\operatorname{curl} \mathbf{H}_{sc} - \frac{\varepsilon}{c}\frac{\partial \mathbf{E}_{sc}}{\partial t} = 0, \qquad \operatorname{curl} \mathbf{E}_{sc} + \frac{1}{c}\frac{\partial \mathbf{B}_{sc}}{\partial t} = 0,$$

$$\mathbf{B}_{sc} = \mathbf{H}_{sc} + 4\pi \mathbf{M}_{sc}, \quad \partial \mathbf{M}_{sc}/\partial t = g\,[\mathbf{M}_{sp} \times \mathbf{H}_{inc}]. \quad (1)$$

Quantities related to the scattered wave are distinguished by the index "sc"; $\mathbf{M}_{sp}$ is the oscillating part of the magnetic moment, due to the spin wave; $\mathbf{H}_{inc}$ is the magnetic field intensity of the incident wave. $\mathbf{H}_{inc}$ satisfies the linear Maxwell equations for a ferromagnetic dielectric.

Since by hypothesis the frequency of the incident wave is large, the magnetic permeability of the ferrite can be set equal to unity, i.e., $\mathbf{M}_{inc} = 0$. This has permitted omission, in the equation for $\mathbf{M}_{sc}$, of all terms containing $\mathbf{M}_{inc}$. Omitted also are terms $g[\mathbf{H}_{eff} \times \mathbf{M}_{sc}]$, with $\mathbf{H}_{eff} = \mathbf{H}_0 + \beta \mathbf{M}_0$ ($\mathbf{H}_0$ is a constant field applied to the ferrite along its axis of easiest magnetization; $\mathbf{M}_0$ is the saturation magnetic moment; β is the anisotropy constant), since by hypothesis $\omega_0 \gg g\mathbf{H}_{eff}$.

From the system (1) we have

$$\Delta \mathbf{E}_{sc} - \frac{\varepsilon}{c^2}\frac{\partial^2 \mathbf{E}_{sc}}{\partial t^2} = \frac{4\pi g}{c} \operatorname{curl} [\mathbf{M}_{sp} \times \mathbf{H}_{inc}]. \quad (2)$$

We expand $\mathbf{M}_{sp}$ as a Fourier integral in time:

$$\mathbf{M}_{sp} = \int_{-\infty}^{\infty} \mathbf{M}_{\Omega} e^{-i\Omega t}\, d\Omega. \quad (3)$$

Since the magnetic field of the incident wave is proportional to $e^{-i\omega_0 t}$ ($\mathbf{H}_{inc} = \mathbf{H}_{\omega_0} e^{-i\omega_0 t}$), we get from (2) for the Fourier component $\mathbf{E}_{\omega}$ of the scattered field, where $\omega = \omega_0 + \Omega$,

$$\mathbf{E}_{\omega}(\mathbf{r}) = -\frac{g}{c}\int \operatorname{curl}' [\mathbf{M}_{\Omega}(\mathbf{r}') \times H_{\omega_0}(\mathbf{r}')] \frac{e^{ikR}}{R}\, dv'. \quad (4)$$

where

$$k^2 = \omega^2 \varepsilon(\omega)/c^2. \qquad R = |\mathbf{r} - \mathbf{r}'|. \quad (5)$$

On taking into account that the distance to the point at which the field is sought is much larger than the linear dimensions of the scattering body (the ferrite), we find from (4)

$$\mathbf{E}_{\omega} = -g\frac{e^{ikR_0}}{R_0 c}\int \operatorname{curl} [\mathbf{M}_{\Omega}(\mathbf{r}') \times \mathbf{H}_{\omega_0}(\mathbf{r}')] e^{-i\mathbf{k}\mathbf{r}'}\, dv', \quad \mathbf{k} = k\mathbf{r}/r. \quad (6)$$

Since $\mathbf{H}_{\omega_0}(\mathbf{r}') = \mathbf{H}_{\omega_0} e^{i\mathbf{k}_0\mathbf{r}'}$, where $k_0^2 = \omega_0^2 \epsilon(\omega_0)/c^2$, it is easy to obtain from the last expression

$$E_{\omega} = -ig\frac{e^{ikR_0}}{cR_0}\int \{\mathbf{M}_{\Omega}(\mathbf{r}')(\mathbf{k}\mathbf{H}_{\omega_0}) - \mathbf{H}_{\omega_0}(\mathbf{k}\mathbf{M}_{\Omega}(\mathbf{r}'))\} e^{-i\mathbf{q}\mathbf{r}'}\, dv', \quad (7)$$

where $\mathbf{q} = \mathbf{k} - \mathbf{k}_0$.

We are interested in the scattering of an electromagnetic wave by thermal fluctuations of magnetic

moment; that is, by spin waves of random amplitude. Naturally the mean value of the scattered field in this case is zero, since $\langle M_\Omega \rangle = 0$. Here and hereafter, $\langle f \rangle$ denotes the statistical mean of the quantity f.

For description of the properties of the scattered radiation, it is convenient to introduce the tensor

$$I_{lk} = \langle E_l E_k \rangle_\omega, \tag{8}$$

which according to (6) is equal to

$$I_{\alpha\beta} = g^2 \frac{k^2 V}{R_0^2 c^2} \Big\{ H_z^2 \int \langle M_\alpha M_\beta \rangle_\Omega e^{-iq\rho}\, dv_\rho - H_\beta H_z \int \langle M_\alpha M_z \rangle_\Omega e^{-iq\rho} dv_\rho - H_\alpha H_z \int \langle M_\beta M_z \rangle_\Omega e^{-iq\rho} dv_\rho + H_\alpha H_z \int \langle M_z M_z \rangle_\Omega e^{-iq\rho} dv_\rho \Big\} \qquad (\alpha, \beta = x, y) \tag{9}$$

(V is the volume of the scattering body; $H_i = (H\omega_0)_i$).

In obtaining the last formula we have made use of the facts that: (1) in the tensor I_{ik} only the x and y components differ from zero, if the z axis is taken along the vector k; (2) $\langle M_i(\mathbf{r}) M_k(\mathbf{r}') \rangle_\Omega \equiv \langle M_i M_k \rangle_\Omega$ depends only on $\rho = \mathbf{r} - \mathbf{r}'$.

It is clear from formula (9) that the tensor components $I_{\alpha\beta}$ are determined by the Fourier transforms $\langle M_i M_k \rangle_{\Omega, q}$ (because of the smallness of the correlation distance as compared with the dimensions of the body, the integration in (9) is extended over all space). If we neglect spatial dispersion of the magnetic susceptibility, then by proceeding as was done, for example, in reference 1, one can obtain

$$\langle M_l M_k \rangle_{\Omega, q} = \langle M_l M_k \rangle_{\Omega, 0} = \frac{\hbar}{2\pi} \chi''_{ik}(\Omega) \coth \frac{\hbar\Omega}{2T},$$

$$\chi''_{ik}(\Omega) = (1/2i)\{\chi_{ik}(\Omega) - \chi^*_{kl}(\Omega)\}. \tag{10}$$

Here $\chi_{ik}(\Omega)$ is the magnetic susceptibility tensor of the ferrite.

Neglect of spatial dispersion is legitimate if the incident wavelength satisfies the following condition:

$$\lambda \gg a\sqrt{I/g\hbar H_{\text{eff}}} \sim (30 \text{ to } 100)\, a, \tag{11}$$

where I is the exchange integral ($I \sim 10^{-13}$ erg) and a is the interatomic distance. This condition shows that up to ultraviolet frequencies the incident wave interacts chiefly with the uniform oscillation of the magnetic moment. From (10) and (9) we have

$$I_{\alpha\beta} = g^2 \frac{k^2 \hbar H^2 V}{2\pi R_0^2 C^2} \coth \frac{\hbar\Omega}{2T} \{e_z^2 \chi''_{\alpha\beta} - e_\beta e_z \chi''_{\alpha z} - e_\alpha e_z \chi''_{\beta z} + e_\alpha e_\beta \chi''_{zz}\}. \tag{12}$$

We assume that the incident wave is linearly polarized. The vector $\mathbf{e} = \mathbf{H}/H$ is its polarization unit-vector.

By definition, the extinction coefficient h is equal to

$$h = (R_0^2/VH^2) \iint I_{\alpha\alpha}(\Omega)\, do\, d\omega, \qquad \omega = \omega_0 + \Omega, \tag{13}$$

where do is an element of solid angle (the integration is extended over all directions of the wave vector of the scattered wave). On substituting (12) in (13) and carrying out the integration, we get

$$h = \frac{4}{3} g^2 \frac{k^2 \hbar}{c^2} \int \coth \frac{\hbar\Omega}{2T} \{\chi'_{jj} - (\mathbf{e}, \hat{\chi}''\mathbf{e})\}\, d\omega, \tag{14}$$

where $\hat{\chi}''\mathbf{e}$ is the vector with components $\chi''_{ik}e_k$.

If $\chi''_{ik} = \chi''\delta_{ik}$, that is, if the anisotropy of the tensor χ''_{ik} can be neglected, then

$$h = (8g^2k^2\hbar/3c^2) \int \chi''(\Omega) \coth(\hbar\Omega/2T)\, d\Omega. \tag{15}$$

If the incident radiation is unpolarized, then the expression (14) must be averaged over all orientations of the vector e. The result of the averaging is

$$h = 2g^2 \frac{k^2\hbar}{c^2} \left(1 - \frac{1}{3}\cos^2\theta\right) \int \chi'_\perp \coth \frac{\hbar\Omega}{2T}\, d\omega. \tag{16}$$

In the averaging we assumed that $\chi''_{11} = \chi''_{22} = \chi''_\perp$ and that $\chi_{j3} = \chi_{3j} = 0$ for $j = 1, 2, 3$; θ is the angle between axis 3 and the direction of propagation of the scattered wave, $\mathbf{k}_0/k_0$.

The tensor χ''_{ik} that was used is characteristic of ferrites (with axis 3 pointed along an axis of easiest magnetization) if we suppose that we have to do with a ferrite magnetized to saturation. Under these conditions, the magnetic susceptibility is determined by rotation of the magnetic moment under the influence of the external field.

The expression (16) determines the total intensity (at all frequencies) of the scattered radiation. The integrand is the density of radiation in the frequency interval $(\omega, \omega + d\omega)$. Since $\chi_\perp(\omega)$ has a resonance character, the scattered radiation is concentrated near the frequencies $\omega = \omega_0 \pm \omega_r$, where $\omega_r = gH_{\text{eff}}$ is the ferromagnetic resonance frequency:*

$$h = \int I_\omega \delta(\omega \pm \omega_r)\, d\omega,$$

$$I_\omega = \pi(1 - {}^1/_3\cos^2\theta)\, g^3 (k^2\hbar M/c^2) \coth(\hbar\omega_r/2T). \tag{17}$$

In the derivation of the last formula, we used

*$\omega_r = gH_{\text{eff}}$ is the frequency of uniform ferromagnetic resonance for an infinite ferrite or a specimen in the form of a sphere. For specimens of more complicated shape, the resonance frequency depends on the demagnetizing factors. The possibility of neglecting the shape of the specimen is based on the fact that representative dimensions L of the specimen are large ($L \gg c/\omega_r \sim 1$ cm).

the expression for $\chi_{\perp}''(\omega)$ known from the theory of ferromagnetic resonance:

$$\chi_{\perp}^{*}(\Omega) = \lim_{\eta \to 0} \frac{1}{4} \eta \frac{gM\omega_r}{(\omega_r \pm \Omega)^2 + \eta^2 \omega_r^2}. \quad (18)$$

Here we have neglected the finite width of the ferromagnetic resonance line. If we take account of the line width, then according to (16) and (18) we get

$$h = \frac{1}{2}\left(1 - \frac{1}{3}\cos^2\theta\right) \frac{g^3 k^2 \hbar M \omega_r}{c^2} \eta \int_0^{\infty} \frac{\operatorname{curl}(\hbar\Omega/2T)\, d\Omega}{(\Omega \pm \omega_r)^2 + \eta^2 \omega_r^2}, \quad (19)$$

where $\eta = \lambda/gM$; λ is the relaxation constant in the equation of motion of the magnetic moment.

In order to estimate the magnitude of the extinction coefficient, we may use formula (17). If we assume $\hbar\omega_r \ll 2T$ and take the incident wavelength equal to 1 mm, then $h \approx 10^{-16}$. Such extinction coefficients are easy to measure by modern methods of radio technology. Study of the dependence of I_ω on frequency provides a possibility of determining the resonance frequencies (and line shapes) of a ferromagnetic dielectric.

In closing, we mention that the radiation scattered by a ferrite possesses peculiar polarization properties. Because of the gyrotropy of the scattering medium, the scattered radiation is a mixture (superposition) of two circularly polarized beams, with the relative intensity different in different directions.

[1] L. D. Landau and E. M. Lifshitz, Электродинамика сплошных сред (Electrodynamics of Continuous Media), Fizmatgiz, 1958.

Translated by W. F. Brown, Jr.
275

VELOCITY DISTRIBUTION OF ELECTRONS IN A STRONG ELECTRIC FIELD*

L. M. KOVRIZHNYKH

Submitted to JETP editor June 12, 1959

J. Exptl. Theoret. Phys. (U.S.S.R.) **37**, 1394-1400 (November, 1959)

A method is developed for finding a nonstationary solution of the Boltzmann equation in the case of strong electric fields. An expression is derived for the electron distribution function in a completely ionized plasma located in a strong electric field. It is shown that in the first approximation the distribution is a Maxwellian one superimposed on the general translational motion of the electron gas. In the first approximation the translational velocity increases proportionally with time, whereas the temperature remains constant.

In the solution of the problem of the velocity distribution of electrons in an electric field usually the investigation is restricted to the stationary case. Moreover, the method of successive approximations is used, which is based on expanding the distribution function $f_e(\mathbf{v})$ in spherical harmonics in velocity space.[1,2] However, this method is justified only when the anisotropic part of the distribution function is much smaller than its isotropic part, or, which is the same thing, when the mean directed velocity is smaller than the thermal velocity. In the stationary case this condition, as a rule, is fulfilled, as a consequence of the small exchange of energy ϵ between the electrons and the gas atoms ($\Delta\epsilon/\epsilon \sim 2m/M \ll 1$). However, for times shorter than the relaxation time, the mean directed velocity may exceed the thermal velocity, and thus the above solution method turns out, generally speaking, to be inapplicable to the description of the processes leading to the establishment of a steady state. In a number of cases, however, such processes are of an essentially nonstationary character. Thus, for example, it can be shown that if the cross section for the collision of electrons with heavy particles falls off faster than $1/v$, then no stationary state exists at all in the presence of a constant electric field. The nonexistence of a stationary distribution is associated with the appearance of so-called "run-away" electrons.[3-5] The "run-away" phenomenon consists of the following. The energy lost by an electron per unit time is proportional to the collision frequency $\nu(v)$. Evidently if $\nu(v)$ falls off with the velocity faster than $1/v$, then when the electron velocity exceeds a certain critical value the increase in the electron energy under the action of the external electric field becomes larger than the energy losses due to collisions, and therefore, the electron energy will continuously increase with time.*

This effect is most pronounced in the case of fully ionized gases,† when the particles are subject to a Coulomb interaction and, consequently, the collision frequency is given by $\nu(v) \sim v^{-3}$. However, in the case of weak fields and not very high temperature, the number of such electrons is very small, although it does increase with time. Therefore for limited time intervals in a number of problems one can still utilize the stationary solution for the distribution function, if one formally cuts it off at large velocities (of the order of several times the thermal velocity). But if the electric field is sufficiently large, so that even over one mean free path the electrons acquire sufficient energy to enter the state of continuous acceleration, then the number of "run-away" electrons is large, the mean directed velocity may considerably exceed the thermal velocity, and the usual method of solution becomes inapplicable. In this case it is natural to utilize another method of obtaining an asymptotic solution, which consists in expanding the distribution function in inverse powers of the electric field, taking for the first approximation the solution of the Boltzmann equation without collisions.

As an illustration of the application of the method

*Reported at the IV International Conference on Ionization Phenomena in Gases (Upsala, August 1959).

*An attempt at a theoretical investigation of this phenomenon on the assumption that the ratio of the ion mass to the electron mass is infinite ($m/M = 0$) was made by Dreicer,[4] who reported the results of a numerical integration of the Boltzmann equations for the case of a fully ionized plasma.

†Strictly speaking the "run-away" electrons are present at any degree of ionization, even when collisions with neutral atoms play the dominant role, since at sufficiently high velocities the screening becomes unimportant, and the electrons are, in fact, scattered by the atomic nuclei. However, in this case the number of such electrons is very small and, as a rule, they need not be considered.

outlined above we shall obtain the velocity distribution of electrons in a fully ionized homogeneous plasma situated in a strong electric field. Let us first consider the case when the electric field is constant in time.

The equation from which the electron distribution function $f_e(\mathbf{v}, t)$ may be determined has the following form

$$\frac{\partial f_e}{\partial t} + \gamma \frac{\partial f_e}{\partial \mathbf{v}} = \mathrm{St}\{f_e\},$$
$$\mathrm{St}\{f_e\} = \mathrm{St}_{ee}\{f_e f_e\} + \mathrm{St}_{ei}\{f_e f_i\}, \tag{1}$$

where $\boldsymbol{\gamma} = -e\mathbf{E}/m$, the terms $\mathrm{St}_{ee}\{f_e f_e\}$ and $\mathrm{St}_{ei}\{f_e f_i\}$ take into account the electron-electron and electron-ion collisions, while $f_i(\mathbf{v})$ is the ion distribution function.

By following the procedure outlined above and by setting

$$f_e(\mathbf{v}, t) = f_e^{(1)}(\mathbf{v}, t) + f_e^{(2)}(\mathbf{v}, t) + \ldots, \tag{2}$$

we obtain

$$\frac{\partial f_e^{(1)}}{\partial t} + \gamma \frac{\partial f_e^{(1)}}{\partial \mathbf{v}} = 0,$$
$$\frac{\partial f_e^{(n)}}{\partial t} + \gamma \frac{\partial f_e^{(n)}}{\partial \mathbf{v}} = \mathrm{St}\{f_e^{(n-1)}\}, \quad n = 2,3,\ldots \tag{3}$$

From this equation, letting $f_0(\mathbf{v})$ denote the initial distribution function

$$f_0(\mathbf{v}) = f_e(\mathbf{v}, t)|_{t=0},$$

we obtain

$$f_e^{(1)}(\mathbf{v}, t) = f_0(\mathbf{v} - \gamma t),$$
$$f_e^{(n)}(\mathbf{v}, t) = \int_0^t dt' \int \mathrm{St}\{f_e^{(n-1)}(\mathbf{v}', t')\}\, \delta(\mathbf{v}' - \mathbf{v} - \gamma[t' - t])\, d\mathbf{v}'. \tag{4}$$

We note that from the relation

$$\int \mathrm{St}\{f_e\}\, d\mathbf{v} = 0$$

it follows that

$$\int f_e^{(n)}(\mathbf{v}, t)\, d\mathbf{v} = 0 \qquad (n = 2, 3, 4, \ldots) \tag{5}$$

and, thus, the normalizing factor is determined just by the first approximation to the function.

In order to calculate $f_e^{(n)}(\mathbf{v}, t)$ we must know the collision operator $\mathrm{St}\{f_e\}$. The expression for this operator is given by Landau.[6] It has the following form

$$\mathrm{St}_{ee}\{f_e f_e\} = -\alpha \frac{\partial}{\partial v_k} \int \left[f_e \frac{\partial f_e'}{\partial v_n'} - f_e' \frac{\partial f_e}{\partial v_n} \right] V_{kn}(\mathbf{v}, \mathbf{v}')\, d\mathbf{v}', \tag{6}$$

$$\mathrm{St}_{ei}\{f_e f_i\} = -\alpha \frac{\partial}{\partial v_k} \int \left[\delta f_e \frac{\partial f_i'}{\partial v_n'} - f_i' \frac{\partial f_e}{\partial v_n} \right] V_{kn}(\mathbf{v}, \mathbf{v}')\, d\mathbf{v}', \tag{7}$$

where summation over n, k = 1, 2, 3 is implied;

$$f_e' = f_e(\mathbf{v}', t), \quad f_i' = f_i(\mathbf{v}', t), \quad \delta = m/M,$$
$$V_{kn} = (u^2\delta_{kn} - u_k u_n)/u^3, \quad u_k = v_k - v_k', \quad \alpha = 2\pi e^4 \lambda / m^2,$$

while λ is a slowly varying function of the particle velocity. The expression for λ obtained by Landau is applicable only to a low temperature plasma ($e^2/\hbar v > 1$). In our case we must use a different expression given by Landshoff.[7] Since λ is insensitive to the choice of the values of the density and the velocity we will in future suppose that $\lambda = \text{const}$.

Let us suppose for the sake of simplicity that the ions have a Maxwellian distribution corresponding to the temperature T_0, i.e.,*

$$f_i(\mathbf{v}) = N(\beta_i/2\pi)^{3/2} \exp(-\beta_i v^2/2),$$
$$f_0(\mathbf{v}) = N(\beta_e/2\pi)^{3/2} \exp(-\beta_e v^2/2), \tag{8}$$

where $v^2 = v_1^2 + v_2^2 + v_3^2$, while $\beta_e = \delta\beta_i = m/kT_0$. We choose the z axis in the direction opposite to the electric field vector $\mathbf{E}$. Then it follows from (4) that

$$f_e^{(1)}(\mathbf{v}, t) = N(\beta_e/2\pi)^{3/2} \exp\left\{-\tfrac{1}{2}\beta_e[v_1^2 + v_2^2 + (v_3 - \gamma t)^2]\right\}, \tag{9}$$

where $\gamma = |\gamma|$.

We substitute expressions (8) and (9) into (7) and integrate over the velocities. Then, on taking into account the fact that $\mathrm{St}_{ee}\{f_e^{(1)} f_e^{(1)}\} = 0$, and neglecting quantities of order δ compared to unity, we obtain

$$\mathrm{St}\{f_e^{(1)}\} = -\alpha\beta_e\beta_i f_e^{(1)}(\mathbf{v}, t)[v_3 \Psi(v\sqrt{\beta_i/2}) - \delta\gamma t \chi(\mathbf{v})]\, v^{-1}\gamma t, \tag{10}$$

where

$$\Psi(z) = z^{-2}(\Phi(z) - z\partial\Phi/\partial z), \quad \Phi(z) = \frac{2}{\sqrt{\pi}} \int_0^z e^{-y^2}\, dy,$$
$$\chi(\mathbf{v}) = (1 - v_3^2/v^2)[\Phi(v\sqrt{\beta_i/2}) - \tfrac{1}{2}\Psi(v\sqrt{\beta_i/2})]$$
$$+ (v_3^2/v^2)\Psi(v\sqrt{\beta_i/2}). \tag{11}$$

Now on substituting the expression obtained for $\mathrm{St}\{f_e^{(1)}\}$ into (4), and on integrating, we obtain to the same order of accuracy after introducing the notation $v_r^2 = v_1^2 + v_2^2$, $v_z = v_3$:

*In general, the ion distribution function in strong fields need not have the form (8). However, in the case under consideration at present the specific form of $f_i(v)$ has only a small effect on the final result.

$$f_e^{(2)}(\mathbf{v}, t) = \frac{2\alpha N\beta_e}{\gamma} f_e^{(1)}(\mathbf{v}, t)\left\{\frac{\beta_e v_r^2 (v_z-\gamma t)\,[(v_z-\gamma t)^2 + v_r^2 + 2/\beta_i]}{2\,(v_r^2+2/\beta_i)\,(v^2+2/\beta_i)^{1/2}}\right.$$

$$-\gamma t\,\frac{2/\beta_i + v_r^2 + {}^1/_2\beta_e v_r^2\,[(v_z-\gamma t)^2 - v_r^2]}{(v_r^2+2/\beta_i)\,(v^2+2/\beta_i)^{1/2}}$$

$$-\frac{\beta_e v_r^2\,(v_z-\gamma t)\,[(v_z-\gamma t)^2 + v_r^2 + 2/\beta_i]^{1/2}}{2\,(v_r^2+2/\beta_i)}$$

$$\left.-\left(1-\frac{\beta_e v_r^2}{2}\right)\ln\frac{(v^2+2/\beta_i)^{1/2}+v_z}{[(v_z-\gamma t)^2+v_r^2+2/\beta_i]^{1/2}+(v_z-\gamma t)}\right\}.$$

By proceeding in a similar manner we can, in principle, determine $f_e(\mathbf{v}, t)$ to any predetermined degree of accuracy. However, since the successive approximations are of no fundamental interest, while the expressions obtained for them are rather awkward, we shall limit ourselves to the second approximation. In this case we have

$$f_e(\mathbf{u}, \tau) = N\left(\frac{\beta_e}{2\pi}\right)^{3/2} e^{-u^2}\left\{1-\varepsilon\left[\frac{u_z u_r^2 (u^2+\delta)^{1/2}}{u_r^2+\delta}\right.\right.$$

$$-\frac{\varepsilon u_z u_r^2 (u^2+\delta) + \tau\,[\delta + u_r^2(1+u_z^2-u_r^2)]}{\varepsilon\,(u_r^2+\delta)\,[(u_z+\tau/\varepsilon)^2+u_r^2+\delta]^{1/2}}$$

$$\left.\left.+(1-u_r^2)\ln\frac{[(u_z+\tau/\varepsilon)^2+u_r^2+\delta]^{1/2}+u_z+\tau/\varepsilon}{(u^2+\delta)^{1/2}+u_z}\right]\right\}, \qquad (12)$$

where the following dimensionless variables have been introduced

$$u^2 = {}^1/_2\beta_e v^2, \quad u_r^2 = {}^1/_2\beta_e v_r^2, \quad u_z^2 = {}^1/_2\beta_e (v_z-\gamma t)^2, \quad \tau = \nu_0 t,$$

$$\nu_0 = \sqrt{2}\alpha N\beta_e^{3/2}, \quad \varepsilon = \gamma_k/\gamma, \quad \gamma_k = eE_k/m = 2\alpha N\beta_e. \qquad (13)$$

By comparing the successive terms of the expansion (2) we can easily obtain a sufficiency criterion for the applicability of the method outlined above. It has the form

$$E \gg E_k \ln(4\tau E/\delta E_k),$$

where in accordance with the definition [cf. (13)]

$$E_k = 2\cdot 10^{-12} N/T_0 \ \text{v/cm},$$

if the temperature T_0 is expressed in electron-volts. We note that if we are interested only in the calculation of averages, then it is sufficient to require that the series (2) should converge only for velocities which in order of magnitude are equal to the thermal velocity. In this case the condition for convergence is somewhat relaxed and assumes the following form

$$E \gg E_k \ln(2\tau E/E_k). \qquad (14)$$

By utilizing the expression (12) obtained above for $f_e(\mathbf{v}, t)$ we can determine the time dependence of the average directed velocity $\mathbf{z}(\tau)$ $= ({}^1/_2\beta_e)^{1/2}\bar{\mathbf{v}}$, and of the square of the components of the mean squared relative velocity along and at right angles to the electric field: $w_{\parallel}(\tau) = {}^1/_2\beta_e(\overline{v_z^2} - \bar{v}_z^2)$ and $w_{\perp}(\tau) = {}^1/_2\beta_e\overline{v_r^2}$. However, it is simpler to proceed directly from equations (3). On multiplying each of them by $\mathbf{v}$, adding them, and integrating over the velocities, we obtain after neglecting, as was done previously, quantities of order δ compared to unity

$$\mathbf{z}(\tau) = (\gamma/\gamma_k)\{\tau - (\varepsilon^2/\sqrt{\pi})[1 - {}^1/_2\tau^{-1}\varepsilon\sqrt{\pi}\Phi(\tau/\varepsilon)]\}. \qquad (15)$$

Similarly we obtain

$$w_{\perp}(\tau) = 1 + \varepsilon\left\{\left[\Phi\left(\frac{\tau}{\varepsilon}\right) - \frac{3}{2}\Psi\left(\frac{\tau}{\varepsilon}\right)\right]\ln\left(\frac{\tau}{\varepsilon}\right)\right.$$

$$\left.-3\int_0^{\tau/\varepsilon}\left[\frac{\Psi(x)}{x} - \frac{4}{3\sqrt{\pi}}e^{-x^2}\right]\ln x\,dx\right\}, \qquad (16)$$

$$w_{\parallel}(\tau) = \frac{1}{2} + \varepsilon\left\{\frac{3}{2}\int_0^{\tau/\varepsilon}\frac{\Psi(x)}{x}\,dx - \Phi\left(\frac{\tau}{\varepsilon}\right)\right.$$

$$\left.-\frac{\varepsilon}{\pi}\left[1 - \frac{\varepsilon\sqrt{\pi}\Phi(\tau/\varepsilon)}{2\tau}\right]^2\right\}, \qquad (17)$$

i.e., $w_{\perp}$ increases logarithmically with time, while $w_{\parallel}$ remains practically constant.

The figure shows the contours of the distribution function for different instants of time in terms of the dimensionless variables u_r, u_z for the case $\epsilon = 5\times 10^{-2}$. It is interesting to note that in the region of small u_r the distribution function has a dip which increases with time, i.e., the number of particles with zero radial velocity continuously diminishes. It is also characteristic that the distribution function is asymmetric in the direction of the electric field. The physical reason for this asymmetry lies in the difference in the initial conditions for particles which have different directions of velocities at the instant when the field is switched on. Thus, for example, the velocity of those electrons, which have been moving against the field at the initial instant of time, will continually increase, and, consequently, the probability of their colliding with ions will decrease, while the velocity of electrons with negative values of v_z will at first decrease, and the probability of collision will increase. In general, the particles at the trailing edge of the distribution function ($u_z < 0$), undergo a larger number of collisions than the particles at the leading edge ($u_z > 0$), and this leads to the asymmetry indicated above. The fact that the distribution function has a "gap" is apparently also related to the previously mentioned dependence of the collision frequency ν on the velocity. Indeed, those electrons which have a low radial velocity have a greater probability of colliding than electrons with

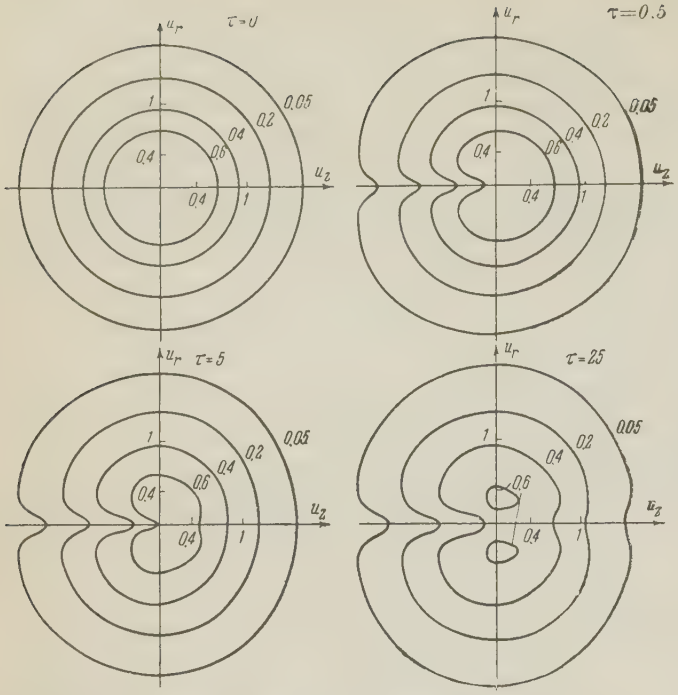

Lines of constant values of the distribution function $N^{-1}[\beta_e/2\pi]^{-3/2} f_e(\mathbf{u}, \tau)$.

the same longitudinal velocity v_z, but with a larger value of v_r, as a result of which the number of particles with small values of v_r decreases continually.

Thus we see that in a strong electric field the electron velocity distribution stays close to the initial distribution (with the exception of a small range of u_r close to zero) superimposed on the average translational velocity $\mathbf{z}(\tau)$, and merely spreads slowly with time in the direction perpendicular to the electric field vector.

In the above discussion we assumed that the electric field $\mathbf{E}$ was constant in time. However, this assumption is not essential, and the method of solution outlined above may be easily generalized to the case when the electric field depends on the time. Indeed, on setting $\mathbf{E}(t) = \mathbf{E}\varphi(t)$, where $\mathbf{E}$ is constant, and on taking into account the fact that the replacement of the variable t by $x(t) = \int_0^t \varphi(\xi)\, d\xi$ brings the equation

$$\frac{\partial f_e}{\partial t} + \varphi(t)\gamma \frac{\partial f_e}{\partial \mathbf{v}} = \mathrm{St}\{f_e\} \qquad (1')$$

into the form (1), we evidently obtain in place of (4)'

$$f_e^{(1)}(\mathbf{v}, t) = f_0(\mathbf{v} - \gamma x(t)),$$

$$f_e^{(2)}(\mathbf{v}, t) = \int_0^t dt' \int \mathrm{St}\{f_e^{(1)}(\mathbf{v}', t')\}\, \delta(\mathbf{v}' - \mathbf{v} - \gamma[x(t') - x(t)])\, d\mathbf{v}'. \qquad (4')$$

If, moreover, the initial distribution is Maxwellian, we have

$$\mathrm{St}\{f_e^{(1)}\} = -\alpha\beta_e\beta_i f_e^{(1)}(\mathbf{v}, t) \times \frac{\gamma x(t)}{v}\left[v_3 \Psi\left(v\sqrt{\frac{\beta_i}{2}}\right) - \delta\gamma x(t)\chi(\mathbf{v})\right] \qquad (10')$$

and the problem of finding the second approximation to the function reduces, as before, to a single integration. Finally, the expressions for the average directed velocity $\mathbf{z}(\tau)$, $w_\perp(\tau)$, and $w_\parallel(\tau)$ may be obtained in the same way as in the case $\varphi(t) = 1$. After a few simple transformations we find

$$\mathbf{z}(\tau) = \frac{\gamma}{\gamma_k}\left\{\nu_0 x(\tau/\nu_0) - \frac{\varepsilon\nu_0}{2}\int_0^{\tau/\nu_0} \Psi\left(\frac{\nu_0 x(\zeta)}{\varepsilon}\right) d\zeta\right\}, \qquad (15')$$

$$w_\perp(\tau) = 1 + \varepsilon\int_0^{\tau/\nu_0}\left[\Phi\left(\frac{\nu_0 x(\zeta)}{\varepsilon}\right) - \frac{3}{2}\Psi\left(\frac{\nu_0 x(\zeta)}{\varepsilon}\right)\right]\frac{d\zeta}{x(\zeta)}, \qquad (16')$$

$$w_\parallel(\tau) = \frac{1}{2} + \nu_0\frac{\gamma}{\gamma}\int_0^{\tau/\nu_0} \mathbf{z}(\nu_0\zeta)\,\Psi\left(\frac{\nu_0 x(\zeta)}{\varepsilon}\right) d\zeta - \varepsilon\int_0^{\tau/\nu_0}\left[\Phi\left(\frac{\nu_0 x(\zeta)}{\varepsilon}\right) - \frac{3}{2}\Psi\left(\frac{\nu_0 x(\zeta)}{\varepsilon}\right)\right]\frac{d\zeta}{x(\zeta)}, \qquad (17')$$

where the functions $\Phi(z)$ and $\Psi(z)$ are defined in accordance with (11). The criterion for the applicability of these formulas may be obtained from the condition that the correction terms in formulas (16'), (17') should be small compared to the principal terms. It has the following form

$$w_\perp(\tau) - 1 \ll 1. \qquad (14')$$

We note that in the case when the electric field increases monotonically with time, it follows from expressions (16') and (17') that the quantities $w_\perp(\tau)$ and $w_\parallel(\tau)$ remain bounded, i.e., in contrast to the case $\varphi(t) = 1$ the electron "temperature" tends to a certain constant value which is equal to

$$T_{max} = {}^2/_3 T_0 [w_\perp(\infty) + w_\parallel(\infty)].$$

In conclusion we note that if we do not make the assumption that the initial electron temperature T_e is equal to the ion temperature T_0, then for $\delta T_0/T_e \ll 1$ the formulas obtained earlier for f_e, $\mathbf{z}$, $w_\perp$, and $w_\parallel$ remain valid if in them we replace T_0 by T_e, and δ by $\delta T_0/T_e$.

The author is indebted to M. S. Rabinovich for useful discussions.

Note added in proof (October 21, 1959). In this paper we have assumed that the ion distribution function is given. The simultaneous solution of equations for the electrons and the ions shows that the results referring to the electrons remain unal-

tered. Analogous expressions are obtained for the ions, with the expansion parameter ϵ remaining the same, i.e., the concept of a strong field is the same both in the cases of ions and electrons.

[1] B. I. Davydov, JETP **6**, 463 (1936).
[2] B. I. Davydov, JETP **7**, 1069 (1937).
[3] R. G. Giovanelli, Phil. Mag. **40**, 206 (1949).
[4] H. Dreicer, On the Theory of Run-away Electrons. Proc. of Geneva Conference, 1958.
[5] Bernstein, Chen, Heald, and Kranz, Phys. Fluids **1**, 430 (1958).
[6] L. D. Landau, JETP **7**, 203 (1937).
[7] R. Landshoff, Phys. Rev. **76**, 940 (1949).

Translated by G. Volkoff
276

ONE POSSIBILITY OF CONSTRUCTING A SYSTEM OF THE "ELEMENTARY" PARTICLES

I. V. CHUVILO

Joint Institute for Nuclear Research

Submitted to JETP editor June 13, 1959

J. Exptl. Theoret. Phys. (U.S.S.R.) **37**, 1401-1406 (November, 1959)

A possibility is discussed for setting up a system of the baryons and mesons based on the postulate that there is a single "elementary" baryon and a single "elementary" meson, with a strong interaction between them. The "elementary" particles chosen are an isotopic singlet baryon Ω^- with strangeness -3 and an isotopic doublet of mesons K^+, K^0 with strangeness $+1$. Conclusions are obtained that agree qualitatively with the known experimental data on processes that involve "strange particles." Some qualitative results on form factors are obtained.

As the result of the great achievements of experimental high-energy physics, during the last decade a number of new unstable particles have been discovered — the hyperons and K mesons. The foundations of the systematics of these particles have been laid in the well known papers of Gell-Mann and Nishijima (the G-N scheme).[1] But such a large number of "elementary" particles is in some respects surprising. Therefore doubts as to their elementary nature arise from time to time. This gives rise to attempts to represent the known particles as some sort of composite structures, so as to diminish the number of "elementary" particles, and also to restrict the set of the interactions.

We present here one more possibility, which we believe has not been discussed so far; retaining all the baryons and mesons that are known and predicted by the G-N scheme, we can nevertheless decidedly diminish the number of "elementary" particles.

It would be extremely attractive to leave in the systematics only one "elementary" baryon and only one "elementary" light particle. Remaining within the framework of the G-N scheme, we can limit our choice to the isotopic singlets Ω^-, Λ^0, and Z^+, with the respective strangenesses -3, -1, and $+1$. The most interesting possibilities are obtained with Ω^- and Z^+, with which we can associate as the "elementary" light particles the isotopic doublets (K^+K^0) and $(K^-\bar{K}^0)$, respectively. The sets Ω^-, K^+, K^0 and Z^+, K^-, $\bar{K}^0$ are symmetric with each other. An explanation of the various effects can be given with either one or the other type of theory. In what follows we shall use the type with Ω^-, K^+, K^0, since it seems to us that it corresponds more to the known experimental data.

Thus we shall assume that there exist only electrically neutral and singly charged baryons and K mesons.

We shall suppose that the "elementary" baryon is the hypothetical negatively charged Ω^- hyperon of the G-N scheme, an isotopic singlet ($I = 0$) with strangeness $S = -3$ and usual baryon spin (s = half-integral number).

We assume that the "elementary" light particle is the isotopic doublet (K^+, K^0), $I = \frac{1}{2}$, which is a boson in ordinary space (s = integer) and has strangeness $S = +1$. The antiparticles of our chosen particles will be $\bar{\Omega}^+$ and $(K^-\bar{K}^0)$, respectively.

We define a strong ΩK interaction and begin the construction of the series of baryons with the isotopic doublet of the Ξ hyperons; we define their structure by combining Ω^- with each of the two K mesons we have postulated, i.e., in the form*

$$\Xi^0 = (\Omega^- K^+), \qquad \Xi^- = (\Omega^- K^0).$$

We then define the structure of the sequence of Σ hyperons, an isotopic triplet, by combining two K mesons with the Ω^- in the three possible ways, namely

$$\Sigma^+ = (\Omega^- K^+ K^+), \qquad \Sigma^0 = (\Omega^- K^+ K^0), \qquad \Sigma^- = (\Omega^- K^0 K^0).$$

It is known that the Σ^0 hyperon cannot exist long and goes over into a Λ^0 hyperon by a fast electromagnetic transition. This could be explained by assuming that it is not possible for the K^+K^0 pair to exist together near the Ω^-, and that through a strong K^+K^0 interaction (in an isotopic singlet state) it forms a bound state $\omega^+ = (K^+K^0)$, which could be understood as a meson with the strange-

*In the type of theory with Z^+, K^-, $\bar{K}^0$ the construction begins with the isotopic doublet of the nucleons, according to the scheme $p = (Z^+\bar{K}^0)$, $n = (Z^+K^-)$.

ness $S = +2$, isotopic singlet, predicted by the G-N scheme.

Thus the structure of the isotopic singlet Λ^0 hyperon can be written in the form $\Lambda^0 = (\Omega^-\omega^+)$. Continuing with the addition of K^+ and K^0 mesons, we get the structure of the isotopic doublet of the nucleons in the form

$$p = (\Omega^-\omega^+K^+), \qquad n = (\Omega^-\omega^+K^0).$$

Now, in virtue of our original assumptions, there remains only one possible structure $Z^+ = (\Omega^-\omega^+\omega^+)$, which corresponds to a hyperon that is an isotopic singlet with strangeness $S = +1$, which is also contained in the G-N scheme.

From the pairs of particles (K^+K^0) and antiparticles (K^0K^-); in combination with a $\bar{\Omega}\bar{\Omega}^+$ pair we can construct four isobosons with schemes of the type $(K\bar{K}\Omega\bar{\Omega})$.

We can identify the charged systems with the π^+ and π^- mesons, and from the neutral systems we can construct the third component of the isotopic triplet (π^+, π^0, π^-) and a neutral isotopic singlet, which is contained in the G-N scheme as the ρ^0 meson.

Thus, by postulating only two elementary particles we have been able to construct all the particles of the G-N scheme. The attraction of the scheme under discussion is that we can get along with only two particles both in ordinary and in isotopic space, and also with only two types of interaction. Furthermore we can identify the π mesons with the quanta of the field that gives the (ΩK) coupling.

Using the proposed scheme, we can get from the measured masses of the known hyperons estimates of masses for the predicted hyperons. The differences $m_{\Sigma^-} > m_{\Sigma^0} > m_{\Sigma^+}$ and $m_n > m_p$ are very probably a consequence of the fact that $m_{K^0} > m_{K^+}$ (cf. reference 2). Then we may suppose that the Ξ^0 particle must be lighter than the Ξ^- by an amount of the order of $5m_e$ (cf. reference 3).

For the absolute magnitude of the energy of coupling of the K mesons with the Ω^- one gets a value of the order of $1200 - 1300\, m_e$. It follows from this that the Ω^- hyperon is $250 - 350\, m_e$ heavier than the Ξ particle. This means that obviously the Ω^- hyperon should decay by the schemes (if we accept the rule $|\Delta S| = 1$)

$$\bar{\Omega} \to \Xi^0 + \beta^- \quad \text{or} \quad \Omega^- \to \begin{matrix} \Xi^0 + \pi^- \\ \Xi^- + \pi^0. \end{matrix}$$

An interesting situation occurs in the estimate of the mass of the Z^+ hyperon. If we begin with: 1) the masses of the proton and the K meson and their binding energy, or 2) with the mass of the Λ^0 particle and the mass and binding energy of the ω^+, both routes lead to the conclusion that the mass of Z^+ must be of the order of $1500\, m_e$. With such a mass, however, the Z^+ hyperon cannot be observed, since we know of no ways in which it can be converted into a stable baryon or nucleon, since it is lighter than the latter. The question of the existence of the Z^+ hyperon, the value of its mass, and the manner of its decay is extremely interesting.

The scheme developed here provides possibilities for explaining a large number of known experimental facts about the production and interactions of hyperons and K mesons. We shall examine only some of them.

It seems most natural to explain a reaction of the type

$$\pi + N \to Y + K,$$

by a process of dissociation of the π meson in the field of the Ω^- particle into a pair of mesons $(K, \bar{K})$, followed by annihilation of the $\bar{K}$ meson so formed with one of the K mesons around the Ω^- (with annihilation of a pair K^+K^- or $K^0\bar{K}^0$). In this scheme the Λ^0 particles produced in reactions

$$\pi + N \to \Lambda^0 + K,$$

will be produced predominantly "backward" in the center-of-mass system, since in this case the K meson leaves the composite system practically without interaction, moving in the "forward" direction, and the $\bar{K}$ meson interacts only with the K meson, without touching the ω^+ system.

The charged hyperons from the reactions

$$\pi^- + p \to \Sigma^- + K^+, \qquad \pi^+ + n \to \Sigma^+ + K^0$$

will have a sharp "forward" directionality in the center-of-mass system, since now both the K^- and the $\bar{K}$ meson interact with the $K\omega^+$ system in the nucleon.*

On the other hand, in the reactions

$$\pi^- + p \to \Sigma^0 + K^0, \qquad \pi^- + n \to \Sigma^- + K^0,$$
$$\pi^+ + n \to \Sigma^0 + K^+, \qquad \pi^+ + p \to \Sigma^+ + K^+$$

both of the channels that have been mentioned can take part. Therefore it seems that the angular distributions of these reactions should be more nearly isotropic in the center-of-mass system, possibly with some preference for emergence of the Σ particles in the "backward" direction. It would be interesting to check these arguments for the reaction

*For experimental data on this point see reference 4.

$$\pi^+ + p \to \Sigma^+ + K^+,$$

for which the experimental data known so far[4] contradict the consequences of our scheme.

With increase of the energy of the incident π meson a $K\bar{K}$ pair that is produced may leave the compound system; this leads to the production of K^+K^- and $K^0\bar{K}^0$ meson pairs. With the same total cross section for production of strange particles this can lead to a decrease of the cross section for production of YK pairs as compared with its value up to the threshold for production of $K\bar{K}$ pairs (at π-meson kinetic energy 1.34 Bev).* An analysis shows that reactions of the type

$$\pi^- + N \to N + K^- + K^0, \quad \pi^+ + N \to N + \bar{K}^0 + K^+,$$

that go in one step are preferred over the reactions

$$\pi^- + p \to n + K^+ + K^-, \quad \pi^+ + n \to p + K^0 + \bar{K}^0,$$

which require a further step of charge transfer $K^+ \rightleftarrows K^0$.

Let us now consider the question of the interaction of $\bar{K}$ mesons with nucleons. We first note the smallness of the charge-transfer effect in the reaction $K^- + p \to \bar{K}^0 + n$, which is due to the necessity for this process to go through a link $K^-K^+ \to K^0\bar{K}^0$.†

Of all the reactions of the type‡ $K^- + N \to Y + \pi$, the most probable is the reaction $K^- + n \to \Lambda^0 + \pi^-$, since it goes through the process $K^-K^0 \to \pi^-$ without the participation of the $\Omega^-\omega^+$ system.

Another curious point that we note is that in interactions of $\Sigma^\pm$ hyperons with nucleons, reactions of the type

$$\Sigma^\pm + N^{+}_{0} \to \Sigma^0 + N^{+}_{0},$$

are more probable than reactions of the type

$$\Sigma + N \to \Lambda^0 + N,$$

since the former go only through the charge-transfer process $K^+ \rightleftarrows K^0$.

Is the observation of the ω^+ particle possible? If it can actually exist, then the most convenient way to produce it is by the reactions $K + N \to \Lambda^0 + \omega^+$. If $m_\omega < 2m_K$, the threshold for these reactions must be at a K-meson kinetic energy less than 1.23 Bev. Decay of this particle is possible through the schemes $\omega^+ \to K + \pi$ or $\omega^+ \to \pi^+ + \pi^0$. So far there are no definite experimental indications of reactions and decays of these types. The observation of the ω^+ particle is one of the basic problems of the scheme we are discussing.*

We now go on to the problem of the production of the cascade particles $\Xi^{-,0}$ and Ω^-. It is obvious that the simplest way of producing the Ξ^- hyperon will be by reactions with neutrons, since they go only through the $\bar{K}\omega^+$ interaction:

$$\bar{K} + n \to \Xi^- + K, \quad \pi + n \to \Xi^- + K + K.$$

On the other hand reactions of the types

$$K^- + p \to \Xi^- + K^+, \quad \pi^- + p \to \Xi^- + K^+ + K^0$$

are less probable, since for them an additional redistribution of energy between the K^+ and ω^+ mesons is required. The production of the Ξ^0 hyperon is possible only in reactions with protons,

$$\bar{K} + p \to \Xi^0 + K, \quad \pi + p \to \Xi^0 + K + K.$$

Reactions of the type $\bar{K} + n \to \Xi^0 + K$ are less probable. Thus the observation of Ξ^0 is possible in liquid-hydrogen bubble chambers, and the production of Ξ^- is difficult.

As is well known, the Alvarez group[3] has observed the Ξ^0 hyperon in a liquid-hydrogen bubble chamber and has not observed the Ξ^- hyperon. Thus the facts are in agreement with the consequences of our scheme. For the reasons indicated the reaction $\pi^- + p \to \Xi^- + \omega^+$ is also unsuitable for the observation of the ω^+ meson.

The process of production of the Ω^- hyperon is still more difficult to observe. In this case all the possible reactions of the type

$$\bar{K} + N \to \Omega^- + K + K, \quad \pi + N \to \Omega^- + K + K + K$$

involve more than one stage, and their yields must be very limited.

We must also note the interesting possibility of explaining the decay properties of hyperons by the mechanism of production of a virtual $K\bar{K}$ pair followed by decay of the $\bar{K}$ meson. This gives results in qualitative agreement with existing experimental data.

Finally, we can try to draw some qualitative conclusions about the electric form-factors of nucleons. In our scheme they have the structures

$$p = (\Omega^-\omega^+)K^+, \quad n = (\Omega^-\omega^+)K^0.$$

From this it can be seen that since the system $(\Omega^-\omega^+)$ is very tightly packed the core of the nucleon must be electrically neutral.† Because the

*Such a behavior of the cross-sections for the YK and $K\bar{K}$ reactions has been suggested by Wang Kang-Ch'ang on other considerations.

†In the Z^+, K^-, $\bar{K}^0$ scheme this reaction is allowed, which is clearly in contradiction with experiment.

‡In the Z^+, K^-, $\bar{K}^0$ scheme the treatment has to be in terms of a virtual $K\bar{K}$ pair around the Z^+.

*The same is true of the reaction $K^- + p \to Z^+ + \omega^-$ for the Z^+, K^-, $\bar{K}^0$ scheme.

†A similar picture was suggested by V. I. Veksler on the basis of an analysis of the angular distributions of hyperons from $\pi + p$ reactions.

outer "shells" of the proton and neutron have respectively a K^+ and a K^0 meson, we can suppose that these particles mainly determine the natures of the electric form-factors of the respective nucleons. It seems to us that this picture corresponds to the known experimental facts.[5]

A question that could be discussed is that of the mean radius of the electric charge distribution in the proton. It may perhaps be somewhat smaller (by a factor of about $m_K/m_\pi \sim 3$) than is believed. A possibility that seems more attractive, however, is obtained by introducing the $K\Omega$ coupling by means of π mesons. Then the electric radius of the proton will be that corresponding to the π meson, and the magnetic moments of nucleons will be given by the sum of the Dirac moment of the Ω particle and the additional moment of the π-meson "coat," with a mean radius of the order of that of the π-meson cloud.

We have here dealt only with effects associated with the existence of the "strange" particles. We believe that within the framework of our model there are interesting possibilities for explaining many questions of the structure of nucleons (isobars, etc.), and a number of effects associated with them (photomesonic processes, etc.).

The writer is grateful to Academician V. I. Veksler and to Chou Kuang-Chao, and V. N. Ogievetskiĭ for interesting discussions of this subject.

[1] M. Gell-Mann, Phys. Rev. **92**, 833 (1953) [see also Probl. Sovr. Fiz. **11**, 28 (1956)]; K. Nishijima, Progr. Theoret. Phys. **12**, 107 (1954); **13**, 285 (1955).

[2] Crawford, Cresti, Good, Stevenson, and Ticho, Phys. Rev. Letters **2**, 112 (1959). Rosenfeld, Solmitz, and Wojcicki, Phys. Rev. Letters **2**, 110 (1959).

[3] Alvarez, Eberhard, Good, Graziano, Ticho, and Wojcicki, Phys. Rev. Letters **2**, 215 (1959).

[4] J. Steinberger, Annual International Conf. on High Energy Physics at CERN, 1958, p. 147.

[5] R. Hofstadter, Nuovo cimento **12**, 63 (1959).

Translated by W. H. Furry
277

THEORY OF SUPERCONDUCTING ALLOYS IN A STRONG MAGNETIC FIELD NEAR THE CRITICAL TEMPERATURE

L. P. GOR'KOV

Institute for Physical Problems, Academy of Sciences, U.S.S.R.

Submitted to JETP editor June 17, 1959

J. Exptl. Theoret. Phys. (U.S.S.R.) 37, 1407-1416 (November, 1959)

The equations of the phenomenological Ginzburg-Landau theory near T_c have been deduced from the Bardeen-Cooper-Schrieffer (BCS) theory. As in the case of pure superconductors, a double charge is encountered in the equations. The relation between the constant κ of the alloy with κ_0 of the pure superconductor has been found under the assumption that the shift in T_c is small. For a sufficiently "impure" alloy, κ depends only on the coefficient in the linear law for the electronic specific heat of the metal. Agreement between the theory and experiments has been found to be satisfactory.

It has been shown by us[1] that it follows from the superconductivity theory of Bardeen, Cooper and Schrieffer (BCS)[2] that, close to the critical temperature, the behavior of pure superconductors in a magnetic field is described by the equations of the phenomenological theory of Ginzburg-Landau.[3] Below we shall carry out a similar consideration for superconducting alloys. As usual, we assume the concentration of the impurity to be so small that we can neglect any change in the critical temperature. This can be done, for while the shift of T_c is a comparatively slow effect, the magnetic properties of the superconducting alloys depend very strongly on the concentration of the impurity.

The role of the impurities in a superconductor, as is well known, lies in the fact that the scattering of the electrons by the atoms of the impurity leads to the disappearance of the correlation between electrons which is established in the transition to the superconducting state. For appreciable concentration of impurity, the role of the correlation length will be played by the mean free path. For sufficiently "impure" superconductors, the penetration depth is greater than the mean free path; consequently, its behavior in the magnetic field will be described by local "London" equations. As is known, one can distinguish two groups among pure conductors which differ, according to their properties, in a weak magnetic field.[2,4] The so-called "London" superconductors are characterized by the fact that for them the penetration depth over the whole temperature range is larger than the characteristic correlation parameter of superconducting interaction. Such a parameter in the BCS theory is the size of the pair coupling $\xi_0 \sim \hbar v/kT_c$. To this case there correspond the electrodynamics of London. A "Pippard" metal represents the opposite limiting case. For such superconductors, at almost all temperatures, the penetration depth is much smaller than ξ_0. Most of the known superconductors belong to the Pippard type and to the intermediate type. The ordinary Pippard metal has a London interval of temperatures only in the immediate vicinity of the critical temperature. This region is very small. A superconducting alloy like a London or intermediate metal has a much larger region of temperatures close to T_c where their properties in a magnetic field (as is shown) can be described by equations corresponding completely to the equations of the Ginzburg-Landau theory.

As in reference 1, we shall in the derivation begin with the equations[5] for the Fourier components of the thermodynamic Green's function:

$$\left\{i\omega_n + \frac{1}{2m}\left(\frac{\partial}{\partial \mathbf{r}} - ie\mathbf{A}(\mathbf{r})\right)^2 + V(\mathbf{r}) + \mu\right\} \times \mathfrak{G}_\omega(\mathbf{r}, \mathbf{r}') + \Delta(\mathbf{r})\,\mathfrak{F}_\omega^+(\mathbf{r}, \mathbf{r}') = \delta(\mathbf{r} - \mathbf{r}'), \quad (1)$$

$$\left\{-i\omega_n + \frac{1}{2m}\left(\frac{\partial}{\partial \mathbf{r}} + ie\mathbf{A}(\mathbf{r})\right)^2 + V(\mathbf{r}) + \mu\right\} \times \mathfrak{F}_\omega^+(\mathbf{r}, \mathbf{r}') - \Delta^*(\mathbf{r})\,\mathfrak{G}_\omega(\mathbf{r}, \mathbf{r}') = 0,$$

$$\Delta^*(\mathbf{r}) = gT\sum_n \mathfrak{F}_\omega^+(\mathbf{r}, \mathbf{r}), \qquad \omega = \pi T(2n+1),$$

$\mathbf{A}(\mathbf{r})$ is the vector potential (below we shall use everywhere the standard div $\mathbf{A} = 0$), $V(\mathbf{r})$ is the potential energy of interaction with all atoms of the impurity:

$$V(\mathbf{r}) = \sum_a u(\mathbf{r} - \mathbf{r}_a), \quad (2)$$

where the sum runs over all atoms of the impurity arbitrarily distributed over a lattice. The smallness of the concentration means that the mean distance between atoms of the impurity is large in comparison with the interatomic distances in the lattice.

Repeating the derivation of reference 1, expanding $\mathfrak{G}$ and $\mathfrak{F}^+$ near T_c in powers of $|\Delta|$, we obtain the following equation:

$$\Delta^*(\mathbf{r}) = gT\sum_n \int \tilde{\mathfrak{G}}_{V\omega}(\mathbf{r}, \mathbf{r}')\,\tilde{\mathfrak{G}}_{V-\omega}(\mathbf{r}, \mathbf{r}')\,\Delta^*(\mathbf{r}')\,d^3\mathbf{r}' - gT$$
$$\times \sum_n \iiint \tilde{\mathfrak{G}}_{V\omega}(\mathbf{s}, \mathbf{r})\,\tilde{\mathfrak{G}}_{V-\omega}(\mathbf{s}, \mathbf{l})\,\tilde{\mathfrak{G}}_{V\omega}(\mathbf{m}, \mathbf{l})\,\tilde{\mathfrak{G}}_{V-\omega}(\mathbf{m}, \mathbf{r})$$
$$\times \Delta(\mathbf{s})\,\Delta^*(\mathbf{l})\,\Delta^*(\mathbf{m})\,d^3\mathbf{s}d^3\mathbf{m}d^3\mathbf{l}. \qquad (3)$$

This equation differs from Eq. (8) of reference 1 by the fact that the Green's function $\tilde{\mathfrak{G}}_{V\omega}$ appearing in it represents the Green's function of electrons in a normal metal in the absence of impurity atoms. The corresponding quantity in the pure metal $\tilde{\mathfrak{G}}_\omega$, as was found in reference 1, depends on the magnetic field in simple fashion:

$$\tilde{\mathfrak{G}}_\omega(\mathbf{r}, \mathbf{r}') = \exp\{ie(\mathbf{A}(\mathbf{r}),\ \mathbf{r}-\mathbf{r}')/c\}\,\mathfrak{G}_\omega(\mathbf{r}-\mathbf{r}'), \qquad (4)$$

where $\mathfrak{G}_\omega(\mathbf{r}-\mathbf{r}')$ is the Green's function of normal electrons in the absence of a field. The dependence of $\tilde{\mathfrak{G}}_{V\omega}$ on the field has precisely the same form

$$\tilde{\mathfrak{G}}_{V\omega}(\mathbf{r}, \mathbf{r}') = \exp\{ie(\mathbf{A}(\mathbf{r}),\ \mathbf{r}-\mathbf{r}')/c\}\,\mathfrak{G}_{V\omega}(\mathbf{r}, \mathbf{r}'), \qquad (4')$$

where $\mathfrak{G}_{V\omega}(\mathbf{r}, \mathbf{r}')$ is the Green's function in the normal metal in the absence of impurities, but without a magnetic field. Actually, the twisting of electrons in a magnetic field is very small, the radius of twisting being much larger than the free path length. Therefore, scattering on impurities takes place independent of the motion in the magnetic field.

Equation (3) should be averaged over the position of each atom of the impurities at distances large in comparison with interatomic distances. The function $\Delta(\mathbf{r})$ is slowly changing since the functions $\mathfrak{G}_{V\omega}$ oscillate rapidly at atomic distances ($\sim 1/p_0$); therefore, averaging in (3) leads to an average of the corresponding combinations of functions $\tilde{\mathfrak{G}}_{V\omega}(\mathbf{r}, \mathbf{r}')$.

In accordance with what has been said about the dependence on a magnetic field, one can take the phase multipliers in (4') out from under the averaging sign. After averaging, Eq. (3) has a much simpler form. Getting ahead of ourselves, we can point out that the essential distances in the integration will be distances of the order of the free path length l if $l \ll \xi_0 = \hbar v/2\pi k T_c$, and of the order ξ_0 if $l \gg \xi_0$. Further, close to T_c the change of Δ and of the field takes place at distances much larger than when the same quantity Δ is small. Repeating the discussions of reference 1, we can, for example, take all Δ and Δ^* in terms of third order in (3) out from under the integral at the point $\mathbf{r}$ and neglect the dependence on the field (4'), after which it is shown to be necessary to compute the constant

$$B = T_c \sum_n \iiint \overline{\tilde{\mathfrak{G}}_{V\omega}(\mathbf{s}, \mathbf{r})\,\tilde{\mathfrak{G}}_{V-\omega}(\mathbf{s}, \mathbf{l})\,\tilde{\mathfrak{G}}_{V\omega}(\mathbf{m}, \mathbf{l})\,\tilde{\mathfrak{G}}_{V-\omega}(\mathbf{m}, \mathbf{r})}$$
$$\times d^3\mathbf{s}d^3\mathbf{m}d^3\mathbf{l}, \qquad (5)$$

in this term, where the bar indicates averaging over the position of the impurity atoms.

If we introduce the notation

$$Q(\mathbf{r}-\mathbf{r}') = T\sum_n \overline{\tilde{\mathfrak{G}}_{V\omega}(\mathbf{r}, \mathbf{r}')\,\tilde{\mathfrak{G}}_{V-\omega}(\mathbf{r}, \mathbf{r}')}, \qquad (6)$$

then, by consideration of (5) and (6), we can write Eq. (3) in the form

$$g^{-1}\Delta^*(\mathbf{r}) = \int Q(\mathbf{r}-\mathbf{r}')\exp\{2ie(\mathbf{A}(\mathbf{r}), \mathbf{r}-\mathbf{r}')/c\}$$
$$\times \Delta^*(\mathbf{r}')\,d^3\mathbf{r}' - B|\Delta(\mathbf{r})|^2\Delta^*(\mathbf{r})$$

Expanding the expression under the integral in the second term on the right side in terms of second order in $\mathbf{r}-\mathbf{r}'$, we get

$$g^{-1}\Delta^*(\mathbf{r}) = \Delta^*(\mathbf{r})\int Q(R)\,d^3\mathbf{R} + \frac{1}{6}\left(\frac{\partial}{\partial \mathbf{r}} + 2ie\mathbf{A}(\mathbf{r})\right)^2\Delta^*(\mathbf{r})$$
$$\times \int Q(R)\,R^2 d^3\mathbf{R} - B|\Delta(\mathbf{r})|^2\Delta^*(\mathbf{r}). \qquad (7)$$

To obtain the constants in (7) it is consequently necessary to calculate the average in (5) and (6).

A diagram technique has been developed in the work of Abrikosov and the author, and also in that of Edwards,[6] by means of which it is convenient to perform the averaging over the location of the impurity atoms. Each scattering of an electron by an impurity atom leads to a factor $u(\mathbf{q}) \times \exp\{i\mathbf{q}\cdot\mathbf{r}_a\}$ in the expression for the Green's function in the momentum representation, where $\mathbf{q}$ is the forward momentum, and $u(\mathbf{q})$ is the Fourier component of the potential of the impurity atom. In averaging over $\mathbf{r}_a$, inasmuch as $|\mathbf{q}| \sim p_0$ essentially, this factor vanishes only if there is no term in the averaged expression corresponding to scattering by this very atom, but with $\mathbf{q}' = -\mathbf{q}$; in this case there appears $|u(\mathbf{q})|^2$ — a quantity proportional in the Born approximation to the probability of scattering with exchange of momentum $\mathbf{q}$. Thus, in the averaging, it is necessary to throw away pairwise all scatterings by identical atoms. If we represent scattering by each atom by a cross on the diagram,

then in the averaging it is necessary to connect two crosses, corresponding to scattering by identical atoms, by a line. In the matrix element $n|u(q)|^2$ corresponds to such a line, where n is the number density of the impurity atoms. According to reference 6, if the dotted line on the diagram includes a vertex with a large transfer of momentum, then the corresponding contribution from this diagram is small ($\sim 1/p_0 l$) and it can be discarded.

Averaging of the Green's function itself leads to the factor $\exp\{-|\mathbf{r}-\mathbf{r}'|/2l\}$, which must be multiplied by the Green's function of the pure metal. Here the mean free path $l = v\tau$ in the Born approximation is directly connected with the potential of the impurity atom:

$$\frac{1}{\tau} = \frac{nmv^2}{(2\pi)^2}\int |u(\mathbf{q})|^2\, do.$$

Averaging of the product of several functions, which takes place in (5) and (6), is somewhat more complicated. Let us first consider the averages:

$$K_\omega(\mathbf{r}-\mathbf{s}, \mathbf{r}'-\mathbf{s}) = \overline{\mathfrak{G}_{V\omega}(\mathbf{r}, \mathbf{s})\,\mathfrak{G}_{V-m}(\mathbf{r}', \mathbf{s})}. \qquad (8)$$

We introduce the Fourier components

$$K_\omega(\mathbf{x}, \mathbf{y}) = (2\pi)^{-6}\iint e^{ip_1 x + ip_2 y} K_\omega(\mathbf{p}_1, \mathbf{p}_2)\, d^3\mathbf{p}_1 d^3\mathbf{p}_2.$$

The product of the two Green's functions in (8)

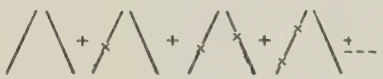

FIG. 1

is shown graphically in Fig. 1, where the crosses, as indicated above, express scattering by individual impurities. In the averaging, in correspondence with the program that we have outlined, we shall connect the crosses with one another pairwise in all processes by dotted lines, which corresponds to scattering by one and the same impurity atom.

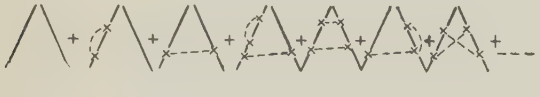

FIG. 2

In Fig. 2 diagrams are shown of lower orders which arise as a result of such averaging. As has been pointed out, diagrams with an intersection of dotted lines are not important in this group. All dotted lines joining points together that are located on a single electron line evidently give the following Green's function for the corresponding line:

$$\mathfrak{G}_\omega^\tau(\mathbf{r}-\mathbf{r}') = \exp\{-|\mathbf{r}-\mathbf{r}'|/2l\}\,\mathfrak{G}_\omega(\mathbf{r}-\mathbf{r}'). \qquad (9)$$

Taking this into account, it is easy to write down the integral equation which $K_\omega(\mathbf{p}_1, \mathbf{p}_2)$ satisfies:

$$K_\omega(\mathbf{p}_1, \mathbf{p}_2) = \mathfrak{G}_\omega^\tau(\mathbf{p}_1)\,\mathfrak{G}_\omega^\tau(\mathbf{p}_2)$$
$$\times\left[1 + \frac{n}{(2\pi)^3}\int |u(\mathbf{p}_1 - \mathbf{p}_1')|^2 K_\omega(\mathbf{p}_1', \mathbf{p}_2')\, d^3\mathbf{p}_1'\right], \qquad (10)$$

where $\mathbf{p}_1 + \mathbf{p}_2 = \mathbf{p}_1' + \mathbf{p}_2' = \mathbf{q}$. This equation sums the set of diagrams shown in Fig. 3, where the electron line must now be compared with the average Green's function $\mathfrak{G}_\omega^\tau(\mathbf{p})$.

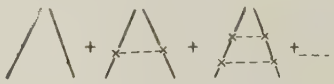

FIG. 3

The kernel $Q(\mathbf{r}-\mathbf{r}')$, in terms of which the first two coefficients in Eq. (7) are expressed, is evidently connected with (8). We write down the expression for the Fourier component $Q_\mathbf{q}$ in terms of $K_\omega(\mathbf{p}_1, \mathbf{p}_2)$:

$$Q_\mathbf{q} = T(2\pi)^{-3}\sum_\omega \int K_\omega(\mathbf{p}, \mathbf{p}-\mathbf{q})\, d^3\mathbf{p};$$

Then, as is seen from (7), the constant which we must determine is simply

$$Q_0 = \int Q(R)\, d^3\mathbf{R}, \qquad -\partial^2 Q_q/\partial q_i^2|_{q=0} = \int Q(R)\, R^2 d^3\mathbf{R}.$$

Therefore, in the calculation of $K_\omega(\mathbf{p}, \mathbf{p}-\mathbf{q})$ we must consider $\mathbf{q}$ to be small and limit ourselves in the expression for $K_\omega(\mathbf{p}, \mathbf{p}-\mathbf{q})$ to terms of second order in $\mathbf{q}$.

For the solution of Eq. (10), it is useful to introduce the notation

$$L_{\omega, \mathbf{q}, \mathbf{p}} = n(2\pi)^{-3}\int |u(\mathbf{p}-\mathbf{p}')|^2 K_\omega(\mathbf{p}', \mathbf{p}'-\mathbf{q})\, d^3\mathbf{p}'.$$

The equation for this quantity is obtained in obvious fashion after multiplying (10) by $n(2\pi)^{-3} \times |u(\mathbf{1}-\mathbf{p})|$ and integration over $\mathbf{p}$:

$$L_{\omega, \mathbf{q}, \mathbf{p}} = n(2\pi)^{-3}\int |u(\mathbf{p}-\mathbf{p}')|^2 \mathfrak{G}_\omega^\tau(\mathbf{p}')\,\mathfrak{G}_{-\omega}^\tau(\mathbf{q}-\mathbf{p}')$$
$$\times [1 + L_{\omega, \mathbf{p}', \mathbf{q}-\mathbf{p}'}]\, d^3\mathbf{p}'. \qquad (11)$$

In accordance with reference 6, we have the following simple expression for the components of the Green's function $\mathfrak{G}_\omega^\tau(\mathbf{p})$:

$$\mathfrak{G}_\omega^\tau(\mathbf{p}) = [i\eta\omega - \xi]^{-1}; \qquad \xi = v(p-p_0), \quad \eta = 1 + 1/2\tau|\omega|$$

The product of the two Green's functions under the integral in (11) quickly falls off upon increasing distance from the Fermi surface. Integration over ξ can easily be completed. It is evident that because of the slow dependence of $u(\mathbf{p}-\mathbf{p}')$ on the quantity $\mathbf{p}$, only the dependence on the direc-

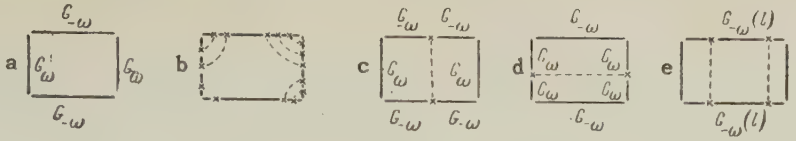

FIG. 4

tion of the vector $\mathbf{p}$ ($|\mathbf{p}| \approx p_0$) enters into $L_{\omega,\mathbf{q},\mathbf{p}}$. The equation takes the form

$$L_{\omega,\mathbf{q},\mathbf{p}} = nv\int (d\sigma/do_{\mathbf{p}'})\,\nu_{\omega,\mathbf{q},\mathbf{p}'}\,[1 + L_{\omega,\mathbf{q},\mathbf{p}'}]\,do_{\mathbf{p}'} \qquad (12)$$

where

$$\nu_{\omega,\mathbf{q},\mathbf{p}} = (2|\omega\eta|)^{-1}\,[1 - \mathbf{qp}/2im\omega\eta]^{-1} \qquad (12')$$

is the result of integration of the product of two $\mathfrak{G}$ functions in (11) over ξ.

We limit ourselves only to calculation of Q_0. In (11), $\mathbf{q} = 0$, $\nu_{\omega,0,\mathbf{p}'} = \frac{1}{2}|\omega\eta|$ and $L_{\omega,0,\mathbf{p}} = \frac{1}{2}\tau|\omega|$. Then, in accord with (10),

$$K_\omega(\mathbf{p},\mathbf{p}) = \eta_i \mathfrak{G}^\tau_\omega(\mathbf{p})\,\mathfrak{G}^\tau_{-\omega}(\mathbf{p}). \qquad (13)$$

In the calculation of Q_0, before summing over all frequencies in the expression

$$Q_0 = T\sum (2\pi)^{-3}\int d^3\mathbf{p}\,\mathfrak{G}^\tau_\omega(\mathbf{p})\,\mathfrak{G}^\tau_{-\omega}(\mathbf{p})\,\eta$$

we must satisfy ourselves, by integrating the difference $\mathfrak{G}^\tau_\omega(\mathbf{p})\,\mathfrak{G}^\tau_{-\omega}(\mathbf{p})\,\eta - \mathfrak{G}_\omega(\mathbf{p})\,\mathfrak{G}_{-\omega}(\mathbf{p})$, that Q_0 for alloys coincides with the corresponding integral for the pure metal:

$$Q_0 = T\sum_\omega (2\pi)^{-3}\int d^3\mathbf{p}\,\mathfrak{G}_\omega(\mathbf{p})\,\mathfrak{G}_{-\omega}(\mathbf{p}) = \frac{mTp_0}{2\pi^2}\sum_\omega\int\frac{d\xi}{\omega^2+\xi^2}$$

$$(\omega = \pi T(2n+1)).$$

Completing the summation, we find

$$Q_0 = \frac{mp_0}{4\pi^2}\int d\xi\frac{\tanh(\xi/2T)}{\xi}$$

The divergence in this integral for large ξ must be eliminated by a cut corresponding to the fact that only electrons found in a layer within a distance $\tilde{\omega}$ from the Fermi surface interact in the model under consideration.[2] In accordance with reference 2.

$$Q_0 = \frac{mp_0}{2\pi^2}\ln\frac{2\tilde{\omega}\gamma}{\pi T} = \frac{mp_0}{2\pi^2}\left(\frac{1}{g} + \ln\frac{T_c}{T}\right).$$

No difficulty arises in finding $-\partial^2 Q_{\mathbf{q}}/\partial q_i^2|_{\mathbf{q}=0}$; differentiating Eqs. (10) and (12) with respect to $\mathbf{q}$, we obtain, after some calculation,

$$-\partial^2 Q_{\mathbf{q}}/\partial q_i^2|_{\mathbf{q}=0} = (mp_0/2\pi^2)(\pi v^2 T/2)\sum_\omega \omega^{-3}\eta_{tr}^{-1},$$

where

$$\eta_{tr} = 1 + 1|2\tau_{tr}|\omega|, \qquad \tau_{tr}^{-1} = nv\int (d\sigma/do)\,(1-\cos\theta)\,do.$$

Finally, the average (5) is computed in the following fashion. The product of the four Green's functions in the integral (5) is drawn in Fig. 4. Their average over the position of the impurity atoms, in accord with the method employed, leads first to the diagram of Fig. 4a, in which now the average Green's functions appear. There will be other diagrams such as those in Fig. 4b, for example. These diagrams represent a modification of the corresponding vertices and are summed by means of Eqs. (10) and (12). In addition, there are two types of diagrams shown in Figs. 4c and 4d. It is not necessary to consider other diagrams, inasmuch as the diagrams with the intersection of dotted lines make a small contribution, according to the results of reference 6, while diagrams such as those shown in Fig. 4e contribute nothing in the integration over the internal momentum l, since the product of two $\mathfrak{G}$ functions appearing under the integral has a pole for ξ only in a single halfplane.

FIG. 5

Figure 5 shows the final form of the diagrams which are to be computed; the heavy dots at the vertices correspond to summation of all corrections to the vertex according to Fig. 3. Inasmuch as the momentum $\mathbf{q} = \mathbf{p}_1 + \mathbf{p}_2 = 0$ in Eq. (5) at all vertices, this means that the heavy dot corresponds to the factor η, as was found in (13). The integral and sums over the frequencies are easily computed:

$$B = (mp_0/2\pi^2)\,(7\zeta(3)/8\,(\pi T_c)^2),$$

where $\zeta(x)$ is the Riemann function, $\zeta(3) = 1.202$.

Substituting the results obtained above in Eq. (7), we find the following equation:

$$\left\{\frac{1}{2m}\left(\frac{\partial}{\partial\mathbf{r}} - 2ie\mathbf{A}(\mathbf{r})\right)^2 + \frac{1}{\lambda_\tau}\left[\frac{T_c - T}{T_c} - \frac{7\zeta(3)}{8\,(\pi T_c)^2}|\Delta(\mathbf{r})|^2\right]\right\}\Delta(\mathbf{r}) = 0,$$

which differs from the corresponding equation of reference 1 only in the expression for λ_τ:

$$\lambda_\tau = \lambda_0\chi(\rho), \qquad (14)$$

where λ_0 is the corresponding coefficient for a pure superconductor, $\lambda_0 = 7\zeta(3)\,\epsilon_F/12\pi^2 T_c^2$, and

$$\chi(\rho) = \frac{8}{7\zeta(3)} \sum_0^\infty \frac{1}{(2n+1)^2 [2n+1+\rho]} \cdot \frac{8}{7\zeta(3)} \left(\frac{1}{\rho}\right) \left[\frac{\pi^2}{8} + \frac{1}{2\rho}\left\{\psi\left(\frac{1}{2}\right) - \psi\left(\frac{1}{2}+\rho\right)\right\}\right] \quad (15)$$

(for $\rho \to 0$, $\chi(\rho) \to 1$, while for $\rho \to \infty$, $\chi(\rho) \approx \pi^2/7\zeta(3)\rho$). Here, $\rho = \frac{1}{2}\pi T_c \tau_{tr}$, $\psi(x)$ is the logarithmic derivative of the Γ function.

For the determination of the value of the electromagnetic current, it is necessary to know the contribution of second order in $|\Delta|$ to the Green's function. Repeating the derivation given in reference 1, we obtain

$$\delta\mathfrak{G}_\omega(r, r') = -\int \tilde{\mathfrak{G}}_{V\omega}(r, s)\,\Delta(s)\,\tilde{\mathfrak{G}}_{V\omega}(l, r') \times \Delta^*(l)\,\tilde{\mathfrak{G}}_{V-\omega}(l, s)\,d^3l\,d^3s. \quad (16)$$

As above, the averaging over the sites of the impurity atoms of a combination of three Green's functions of the normal metal does not show any dependence of the integrand on the magnetic field.

In the determination of the current,

$$j(r) = + \left[\frac{ie}{m}(\nabla_r - \nabla_{r'})\,G(x, x') + \frac{2e^2}{mc}A(r)\,G(xx')\right]_{r=r',\, t'=t+0} \quad (17)$$

a Green's function appears with coinciding arguments; therefore, in the averaging of (16), it is sufficient to limit ourselves to this case. Considering the field to be weak, and $\Delta(r)$ to be of the order of l, changing slowly with distance, we carry out the corresponding simplification in (16) and (17). We shall not linger over the calculations, limiting ourselves only to the scheme of averaging over the impurity in Fig. 6, which represents the corresponding diagram which must be summed.

FIG. 6

We note that the corrections to the vertex into which enter two Green's functions with the same frequency are absent, inasmuch as such corrections lead to the integration of products of two $\mathfrak{G}$ functions with poles located in one halfplane. After computation we obtain the following expression for the current:

$$j(r) = \left\{\frac{ie}{m}\left(\Delta(r)\frac{\partial\Delta^*(r)}{\partial r} - \Delta^*(r)\frac{\partial\Delta(r)}{\partial r}\right) - \frac{4e^2}{mc}A(r)\,|\Delta(r)|^2\right\}\chi(\rho)\frac{7\zeta(3)N}{16\pi^2 T_c^2}.$$

If we introduce the "wave function" $\psi(r)$ connected with $\Delta(r)$ by the relation

$$\psi(r) = [\chi(\rho)\,7\zeta(3)\,N/16\pi^2 T_c^2]^{1/2}\,\Delta(r),$$

then the resultant system of equations can be written in a form corresponding to the equations of the phenomenological theory of Ginzburg-Landau:[3]

$$\left\{\frac{1}{2m}\left(\frac{\partial}{\partial r} - 2ieA(r)\right)^2 + \frac{1}{\lambda_\tau}\left[\frac{T_c - T}{T_c} - \frac{2}{N\chi(\rho)}|\psi(r)|^2\right]\right\}\psi(r) = 0,$$

$$j(r) = \frac{ie}{m}\left(\psi\frac{\partial\psi^*}{\partial r} - \psi^*\frac{\partial\psi}{\partial r}\right) - \frac{4e^2}{mc}A(r)\,|\psi|^2. \quad (18)$$

The most interesting part of this result is the two-fold charge which figures in the equations. The existence of bound pairs of electrons in the BCS theory makes this result entirely understandable. In this light, the meaning of the wave function $\psi(r)$ of the Ginzburg-Landau theory as a quantity proportional to the wave function of a bound pair (more precisely, the coordinates of its center of mass) becomes clarified. An identical result was obtained by us for a pure superconductor.[1]

The difference of alloys from the case of a pure metal lies, as is well known, in the constant κ which appears in the phenomenological theory of Ginzburg-Landau, and which is determined (with consideration of the double charge) by the relation

$$\varkappa = \sqrt{2}\,2eH_{cT}\delta_T^2/\hbar c, \quad (19)$$

where H_{cT} is the critical field, and δ_T is the penetration depth close to T_c which is temperature dependent.

The equations (18) permit us to find the connection of the constant κ for alloys with κ_0 of a pure superconductor, and to express it in terms of the parameters of the BCS theory. The constant κ for alloys is equal to

$$\varkappa = \varkappa_0/\chi(\rho),$$

where the function $\chi(\rho)$ has been introduced above in (15), while κ_0 for a pure metal is expressed (according to reference 1) in the following form:

$$\varkappa_0 = (3\pi T_c mc/e)\sqrt{2\pi m/7\zeta(3)\,p_0^5} \qquad (\zeta(3) = 1.202). \quad (20)$$

In the relations that have been obtained and in the determination of $\rho = \frac{1}{2}\pi T_c \tau_{tr}$, four parameters generally appear: T_c, m, p_0 for the pure metal, and the "transport" time of the free flight τ_{tr}. For pure superconductors of the London type and for intermediates, i.e., such for which throughout the whole temperature range the penetration depth is larger or comparable to the correlation length $\xi_0 = hv/2\pi T_c$, an appreciable temperature region close to T_c exists where one can use the relations (19) with the experimental values of H_c and δ_0 for the determination of κ_0. The theoretical expression[2] for δ_0 close to T_c has the form

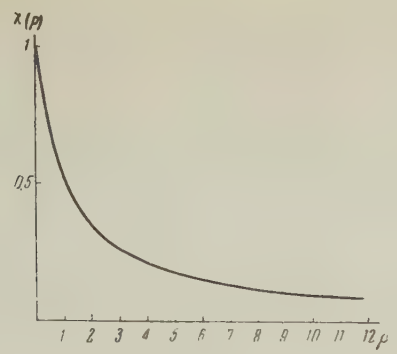

FIG. 7

$$\delta_0 = \delta_{0L}/\sqrt{2(1-T/T_c)} \qquad (\delta_{0L} = \sqrt{mc^2/4\pi Ne^2}) \quad (21)$$

In the isotropic model under consideration, the time between collisions τ_{tr} can be expressed in terms of δ_{0L} and the conductivity σ:

$$\tau_{tr} = 4\pi\sigma\delta_{0L}^2/c^2. \quad (22)$$

In terms of these quantities

$$\rho = \hbar c^2/8\pi^2 kT_c\sigma\delta_{0L}^2. \quad (23)$$

The function $\chi(\rho)$ is shown graphically in Fig. 7. We also give the formula which connects the penetration depth of a weak magnetic field for an alloy with the penetration depth for the pure superconductor

$$\delta = \delta_0/\sqrt{\chi(\rho)}. \quad (24)$$

If the quantity of impurity is sufficiently large, so that $l \ll \xi_0$, the equations are simplified. In this case, κ for alloys can be expressed only in terms of the parameters of the normal metal: the coefficient in the linear law for the heat capacity γ and the conductivity σ:

$$\varkappa = (ec\gamma^{1/2}/\sigma k\pi^3)\sqrt{21\zeta(3)/2\pi} = 0.065ec\gamma^{1/2}/\sigma k \quad (25)$$

For metals of the Pippard type, i.e., those for which at low temperatures the penetration depth is much smaller than the parameter ξ_0, chief interest lies in the latter formula. This is connected with the fact that for a pure superconductor of the Pippard type, the London region of temperatures close to T_c, where the Ginzburg-Landau equations hold, is very narrow (for aluminum, $\Delta T/T_c \sim 10^{-4}$). The presence of impurities enlarges this region. In order that this region be experimentally accessible, it is necessary that $l \ll \xi_0$.

Equations (20) and (25) permit us to determine the critical concentration of impurities for which the superconductor in a strong field begins to reveal the characteristic peculiarities of alloys. As is well known, the surface energy on the boundary of separation between the normal and superconducting phases vanishes for $\kappa_{cr} = 1/\sqrt{2}$. At the same time, the critical field of supercooling is made equal to the critical thermodynamic field, while for large κ it exceeds it. Therefore, for $\kappa > 1/\sqrt{2}$, the transition in the magnetic field from the normal to the superconducting state begins at fields larger than the critical field H_{cT} of the pure superconductor, namely at the field $H_{c1} = \sqrt{2}\,\kappa H_{cT}$. This peculiarity of alloys was pointed out by Abrikosov.[7] For Pippard superconductors, $\kappa = 1/\sqrt{2}$ is achieved at such concentrations of impurities that $l \ll \xi_0$; therefore, it follows from (25) that for the critical amount of impurities, the residual conductivity is connected only with the coefficient γ in the linear law for electronic specific heat $\sigma_{cr} = 0.092\,ec\gamma^{1/2}/k$.

The linear dependence of H_{cT}/H_{c1} on the path length l for contaminated alloys on the basis of phenomenological considerations was first pointed out by Pippard.[8] For $l \ll \xi_0$, the formula for the penetration depth was obtained in the work of Abrikosov and the author.[6]

We note that, as experiment has shown,[8,9] the actual region $\kappa \sim 0.7$ corresponds, for example, in the case of an alloy of tin and indium, to $l \sim 5 \times 10^{-6}$ cm (or a concentration of indium ~ 3 percent). For such concentrations of impurities, there is a certain insignificant shift in the temperature[9] ($\Delta T_c/T_c \sim 5$ percent). We shall neglect this effect, assuming the number of impurities to be so small that we do not have to take into consideration their effect on the fundamental lattice. At high concentrations, it appears that such an approximation is improper. However, it is possible to assume, that the relation (25) will still hold in such alloys, inasmuch as there appear in it only quantities which refer to the normal metal. The coefficient in the linear law for the specific heat γ must be introduced in this case for the alloy itself.

The available experimental data refer to tin.[8,9] In the work of Dodge,[9] the transition in a magnetic field from a normal phase to the superconducting phase was studied for an alloy of tin and indium. For concentrations of indium of about 3 percent, this transition has the usual character; for higher concentrations, the appearance of the superconducting phase occurs at fields larger than the critical thermodynamic field. The ratio H_{cT}/H_{c1}, i.e., the value $\chi(\rho)/\sqrt{2}\,\kappa_0$ is plotted in Fig. 8 as a function of the mean free path length l. (We have made use of the result of the research of Chambers[10] for tin: $\sigma/l = 8.5 \times 10^{22}$, by means of which one can express ρ in terms of the mean free path length: $\rho = 2 \times 10^{-5}/l$.) For pure tin, $\kappa_0 = 0.158$,[11] the value of κ of the alloy (0.707) corresponds

in the calculations to $l \sim 5.5 \times 10^{-6}$ cm, while the experimental value is somewhat less than 8×10^{-6} cm.

Taking into account the known crudeness in the determination of $\delta_0 L$ (we have used $\delta_0 L = \delta_{00}/\sqrt{2}$, where δ_{00} is the coefficient in the law for the skin depth

$$\delta = \delta_{00}/\sqrt{1-(T/T_c)^4},$$

is equal to $\delta_{00} = 5.1 \times 10^{-6}$ cm), one can consider the agreement to be excellent.

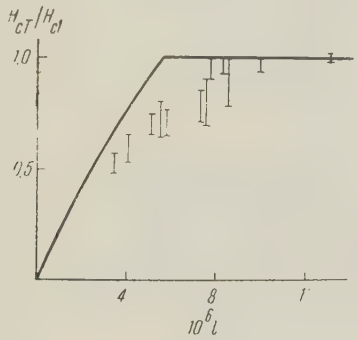

FIG. 8

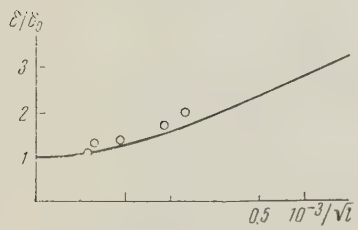

FIG. 9

Results are shown in Fig. 9 of a comparison of the formula (24) for the skin depth with the results of Pippard,[8] which apply to an alloy of indium and tin with a concentration up to 3 percent of indium. We note that the proportionality of the penetration depth $l^{-1/2}$ is still not attained for such concentrations.

In conclusion I express my deep gratitude to Acad. L. D. Landau for his interest in the work and for the comments that he has made.

[1] L. P. Gor'kov, JETP **36**, 1918 (1959), Soviet Phys. JETP **9**, 1364 (1959).

[2] Bardeen, Cooper, and Schrieffer, Phys. Rev. **108**, 1175 (1957).

[3] V. L. Ginzburg and L. D. Landau, JETP **20**, 1064 (1950).

[4] A. A. Abrikosov and I. M. Khalatnikov, Usp. Fiz. Nauk **65**, 551 (1958).

[5] L. P. Gor'kov, JETP **34**, 735 (1958), Soviet Phys. JETP **8**, 505 (1958).

[6] A. A. Abrikosov and L. P. Gor'kov, JETP **35**, 1558 (1958); **36**, 319 (1959); Soviet Phys. JETP **8**, 1090 (1959); **9**, 220 (1959).

[7] A. A. Abrikosov, JETP **32**, 1442 (1957), Soviet Phys. JETP **5**, 1174 (1957);

[8] A. B. Pippard, Proc. Roy. Soc (London) **A216**, 547 (1953).

[9] P. R. Dodge, Phil. Trans. Roy. Soc. (London) **A248**, 553 (1956).

[10] R. G. Chambers, Proc. Roy. Soc. (London) **A215**, 481 (1952).

[11] V. L. Ginzburg, JETP **36**, 1930 (1959); Soviet Phys. JETP **9**, 1372 (1959).

Translated by R. T. Beyer
278

MAGNETOHYDRODYNAMICS OF WEAKLY CONDUCTING LIQUIDS

S. I. BRAGINSKIĬ

Submitted to JETP editor June 23, 1959

J. Exptl. Theoret. Phys. (U.S.S.R.) **37**, 1417-1430 (November, 1959)

The approximate form of the magnetohydrodynamic equations has been obtained for a fluid of low electrical conductivity (small magnetic Reynolds number) in an external magnetic field. Several characteristic problems which illustrate the physical behavior of such a liquid in a strong magnetic field are examined.

1. GALVANIC APPROXIMATION

As is well known (cf. for example, references 1 — 3), in magnetohydrodynamics there are additional characteristic dimensional quantities beyond those in ordinary hydrodynamics: the Alfvén velocity, $c_A = B(4\pi\mu\rho)^{-1/2}$, and the magnetic field diffusion coefficient, $D_m = c^2/4\pi\mu\sigma$. Here, B is the magnetic induction, ρ is the density, σ the electrical conductivity, and μ the magnetic permeability of the liquid, while c is the velocity of light. To these correspond two additional dimensionless similitude criteria, the magnetic analogs of the Mach number, v/c_A, and of the Reynolds number, $R_m = lv/D_m$ or $R_m = l^2\omega/D_m$ (l, v, and ω are respectively the characteristic linear dimension, the velocity, and the frequency). The magnetic Reynolds number characterizes the entrainment of the magnetic lines of force by the liquid in its motion. If $R_m \gg 1$, the lines of force behave as though frozen in the material — this is the case which is usually considered in magnetohydrodynamics, astrophysics, etc. We consider the other limiting case: $R_m \ll 1$. The equations used below can be obtained from the equations of magnetohydrodynamics by an expansion in powers of R_m, but it is more convenient to introduce them directly.

The volume density of the electromagnetic forces **f** is

$$\mathbf{f} = c^{-1}[\mathbf{j}\times\mathbf{B}], \tag{1.1}$$

where **j** is the current density. The currents which arise in the liquid are proportional to its electrical conductivity (small), but may result in the appearance of rather large forces if the liquid is located in an external magnetic field. This is the case which is considered here.

Because of its motion, an emf of order $(v/c)B$ and a current of order $\sigma(v/c)B$ are produced in the liquid. The magnetic field due to this current is of order $B_1 \sim R_m B$ and can be neglected when $R_m \ll 1$. The variation of B_1 produces an induced electric field $E_1 \sim R_m(vB/c)$ which is always unimportant when $R_m \ll 1$. Thus, in the approximation being used here it may be assumed that the magnetic field is given and equal to the external field. This field satisfies the equations div **B** = 0 and curl **B** = 0 (we assume that μ is independent of the coordinates or is approximately unity).

In determining the force **f** it is sufficient to consider only the currents which are produced in the liquid; the fields produced by these currents can be neglected. This approximation may be called the "galvanic" or non-induction approximation.

The current density in the moving liquid is

$$\mathbf{j} = (\sigma/c)\{[\mathbf{v}\times\mathbf{B}] - \nabla\varphi - \partial\mathbf{A}/\partial t\}, \tag{1.2}$$

where φ is the scalar potential (in magnetic units, i.e., $\varphi = c\varphi_{abs}$), **A** is the vector potential of the magnetic field (external) and curl **A** = **B**. We use the gauge condition div **A** = 0. As in "galvanostatics" the equation for φ is obtained from the condition that the charge is neutralized.

$$\operatorname{div}\mathbf{j} = 0. \tag{1.3}$$

For a uniform liquid this condition yields

$$\Delta\varphi = \mathbf{B}\operatorname{curl}\mathbf{v}. \tag{1.4}$$

If the conductivity is a function of coordinates, however, we have

$$\Delta\varphi = \mathbf{B}\operatorname{curl}\mathbf{v} - c(\mathbf{j}\nabla)\sigma^{-1}. \tag{1.4'}$$

Equation (1.1) for the volume forces assumes the form

$$\mathbf{f} = \frac{\sigma}{c^2}\left\{[[\mathbf{v}\times\mathbf{B}]\times\mathbf{B}] - [\nabla\varphi\times\mathbf{B}] - \left[\frac{\partial\mathbf{A}}{\partial t}\times\mathbf{B}\right]\right\} \tag{1.5}$$

This force appears in the equation of motion of the liquid

$$\rho(\partial\mathbf{v}/\partial t + (\mathbf{v}\nabla)\mathbf{v}) = -\nabla p + \rho\mathbf{g} + \eta\nabla^2\mathbf{v} + \mathbf{f}. \tag{1.6}$$

Here p is the pressure, **g** is the acceleration of

gravity, the viscosity force is written for an incompressible liquid, and the viscosity is $\eta = \rho\nu$.

In the galvanic approximation, in addition to the equation of motion of the liquid it is necessary to have one scalar equation (1.4), which does not contain differentiation with respect to time; on the other hand, in true magnetohydrodynamics it is necessary to add a vector equation for $\partial\mathbf{B}/\partial t$.

We assume that the magnetic field is constant, $\partial\mathbf{A}/\partial t = 0$. If the currents produced by the induced emf $c^{-1}(\mathbf{v}\times\mathbf{B})$ can flow freely, the interaction of the liquid with the magnetic field results in an anisotropic "friction force" $\mathbf{f} = -(\sigma B^2/c^2)\mathbf{v}_\perp$, where $\mathbf{v}_\perp = \mathbf{v} - (\mathbf{v}\cdot\mathbf{B})\mathbf{B}/B^2$. If however $\operatorname{div}(\mathbf{v}\times\mathbf{B}) = \mathbf{B}\cdot\operatorname{curl}\mathbf{v} \neq 0$, in accordance with Eq. (14), charges will be produced and will create an electric field $-\nabla\varphi$. Charges and an electric field are also produced if the boundary conditions are such that the currents $(\sigma/c)\mathbf{v}\times\mathbf{B}$ cannot flow freely. In these cases the interaction of the liquid with the magnetic field does not produce magnetic friction and is not localized but, as before, the force $\mathbf{f}$ is a linear function of velocity. Since φ is linear in $\mathbf{v}$ (if the boundary conditions are linear), in the general case $\mathbf{f}$ is a linear function of the velocity taken at the same instant of time.

We may note that the magnetic field and the conductivity appear in $\mathbf{f}$ only in the combination σB^2. In the galvanic approximation this is the only additional dimensional parameter which appears beyond the usual hydrodynamic quantities.

In our analysis we shall consider a uniform incompressible liquid in a uniform magnetic field. In this case it is possible to obtain a convenient equation for the force $\mathbf{f}$ directly. Assuming that $\operatorname{div}\mathbf{v} = 0$, from Eq. (1.2) we find

$$\operatorname{curl}\mathbf{j} = (\sigma/c)(\mathbf{B}\nabla)\mathbf{v} - (\sigma/c)\,\partial\mathbf{B}/\partial t \qquad (1.7)$$

and, using Eqs. (1.1) and (1.3)

$$\operatorname{curl}\operatorname{curl}\mathbf{f} = (\sigma B^2/c^2)(\mathbf{b}\nabla)^2\mathbf{v}, \qquad (1.8)$$

where $\mathbf{b} = \mathbf{B}/B$ is a unit vector in the direction of the magnetic field. It is apparent that in the interaction of the liquid with the field there is a considerable change in the velocity component in the direction of the field.

Viscosity effects and the Joule heating effects cause dissipation of energy; this energy is given by

$$Q_\eta = (\eta/2)(\partial v_i/\partial x_k + \partial v_k/\partial x_i)^2,$$

$$Q_\sigma = j^2/\sigma = (\sigma/c^2)([\mathbf{v}\times\mathbf{B}] - \nabla\varphi)^2. \qquad (1.9)$$

If $\nabla\varphi = 0$, the Joule dissipation can be regarded as the result of magnetic friction:

$$Q_\sigma = -\mathbf{fv} = (\sigma B^2/c^2)\mathbf{v}_\perp^2.$$

In order-of-magnitude terms the ratio of the magnetic force to the viscosity force and the ratio of the corresponding dissipations are determined by the dimensionless Hartmann number, $M = \kappa l$, where

$$\varkappa^2 = \sigma B^2/\eta c^2. \qquad (1.10)$$

The ratio of the magnetic force to the inertia force is determined by the dimensionless number

$$N = \gamma_m/\omega = \gamma_m l/v = M^2R^{-1},$$

where R is the Reynolds number,

$$\gamma_m = \sigma B^2/\rho c^2. \qquad (1.11)$$

Which terms predominate in the equation of motion depends on the relative magnitudes of the quantity σB^2, the velocity, and the linear dimensions.

1. If σB^2 is very small, so that $M \ll 1$, the magnetic field has only a small effect on the motion of the liquid which, in the first approximation, is the same as in ordinary hydrodynamics. The chief new effects are the production of currents and potentials which, for a given velocity distribution, are determined by Eqs. (1.2) and (1.4). These effects can be used, for example, for measuring velocities. From a knowledge of the current one can find the force $\mathbf{f}$; then, substituting in Eq. (1.6) if necessary, it is possible to determine the small corrections to the velocity and pressure. This case is typical for electrolytes; for example for a 25% solution of NaCl in water $\sigma = 2\times10^{11}$ and for $B = 10^3$ gauss, $\kappa = 0.15\ \text{cm}^{-1}$. For liquid metals under laboratory conditions it is easy to make $M \gg 1$.

All the numerical examples below are given for mercury: the pertinent parameters are as follows: $\sigma = 0.95\times10^{16}\ \text{sec}^{-1}$, $\rho = 13.6\ \text{g-cm}^{-3}$, $\eta = 1.56\times10^{-2}\ \text{g-cm}^{-1}\ \text{sec}^{-1}$, $\nu = \eta/\rho = 1.15\times10^{-3}\ \text{cm}^2\ \text{sec}^{-1}$, $D_m = c^2/4\pi\sigma = 0.75\times10^4\ \text{cm}^2\ \text{sec}^{-1}$. For $B = 10^3$ gauss, $\kappa = 26\ \text{cm}^{-1}$, $\gamma_m = 0.78\ \text{sec}^{-1}$. The ratio $R/R_m = D_m/\nu = 1.5\times10^7$ so that the galvanic approximation applies for values of the Reynolds number up to $R \lesssim 10^7$.

2. At large values of the Reynolds number it is possible to have $M \gg 1$, but $N \ll 1$. In this case the magnetic forces are small compared with the inertial forces and the behavior of the liquid is approximately that of an ideal liquid. If the motion is laminar the magnetic forces play an important role in the dissipation of energy (damping of oscillations etc.). Furthermore, the magnetic forces change the nature of the boundary layers and this, in turn can change the flow as a whole and the stability conditions as, for example, in flow in tubes.

Flow between parallel planes has been shown theoretically[4] and experimentally[5] to be stable in a transverse magnetic field up to $R \sim 10^3 M$. If a turbulence develops, however, the effect of the magnetic field is small. For motion on the basic scale the magnetic forces are small compared with the inertial forces since $N \ll 1$; however, the frequencies of the turbulent motions increase with a reduction in scale and in all smaller scales it is certainly true that $N = \gamma_m/\omega \ll 1$. When $\lambda_0 \sim lR^{-3/4}$, however, where the basic dissipation occurs (cf. reference 2, §32), the viscosity dominates: $\kappa\lambda_0 \sim N^{1/2}R^{-1/4} \ll 1$ so that the magnetic forces are also unimportant in dissipation.

3. The effect of the magnetic field is most pronounced when $M \gg 1$, $N \gg 1$, in which case the force $\mathbf{f}$ dominates. The high Joule dissipation characteristic of this case has a stabilizing effect on the flow. Stuart[6] has shown, for example, that Poiseuille flow between plates is stabilized by a longitudinal magnetic field when $N \gtrsim 0.1$. However, the stabilizing effect of the Joule dissipation may be insufficient if the production of the instability is associated with small-scale high frequency motions, for which N is already small. This is the case, for example, in the experiment carried out by Lehnert.[7] Turbulent motion for $M \gg 1$ and $N \gg 1$ is also subject to a strong effect of the magnetic field, which plays a decisive role in motion of large-scale vortices and may change the entire motion pattern.

At small Reynolds numbers, if $\operatorname{curl}(\mathbf{v}\cdot\nabla)\mathbf{v} = 0$, because of symmetry, from Eqs. (1.6) and (1.8) we can obtain the following equation for stationary flows; this equation determines the "leakage" of the fluid through the magnetic field:

$$\Delta\Delta v - \varkappa^2(\mathbf{b}\nabla)^2 v = 0. \qquad (1.12)$$

From Eqs. (1.4) and (1.6), $\operatorname{curl}\mathbf{f} = c^{-1}(\mathbf{B}\cdot\nabla)\mathbf{j}$ and Eq. (1.2) we obtain the same equation for φ:

$$\Delta\Delta\varphi - \varkappa^2(\mathbf{b}\nabla)^2\varphi = 0. \qquad (1.12')$$

Equation (1.12) for $\operatorname{curl}\mathbf{v}$ has already been obtained by Lehnert[8] for stationary small perturbations by linearization of the equations of magnetohydrodynamics with an arbitrary conductivity.

Suppose that a characteristic dimension of the system in the direction perpendicular to the field is l, and along the field is $l_{\|}$. When $M = \kappa l \gg 1$ both terms in Eq. (1.12) may be of the same order if $l_{\|} \sim \kappa^{-1} \ll l$ or $l_{\|} \sim \kappa l^2 \gg l$. An example of a solution of the first type, which describes a perturbation transverse to the field, gives the boundary layer formed in the Hartmann[9] analysis of flow between plane plates in a perpendicular magnetic field:

$$v = v_0[\cosh \varkappa h - \cosh \varkappa(h-y)]/\cosh \varkappa h. \qquad (1.13)$$

The magnetic field is along y, the velocity along z, and the distance between the plates is $2h$.

A solution of the second type describes perturbations which are along the magnetic field. For example, they may act like tangential discontinuities. Equation (1.12) is satisfied by the expressions $\mathbf{v} = c_+\mathbf{v}_+ + c_-\mathbf{v}_-$, where $\mathbf{v}_\pm$ represents solutions of the equation

$$\{\Delta \mp \varkappa(\mathbf{b}\nabla)\}\mathbf{v}_\pm = \text{const}_\pm.$$

Let $B = B_y$, $v = v_z$ and $\partial/\partial z = 0$. If we neglect $\partial^2/\partial y^2$ compared with $\partial^2/\partial x^2$ in the Δ operator, the curly brackets will contain the same operators as those in the usual thermal-conductivity equation so that we can write the approximate solution immediately:

$$v_+ = \frac{v_0}{2}\Phi\left(\sqrt{\frac{\varkappa}{4(y_0+y)}}(x-x_0)\right), \quad \Phi(\xi) = \frac{2}{\sqrt{\pi}}\int_0^\xi e^{-t^2}dt. \qquad (1.14)$$

This solution describes the velocity jump from $-v_0/2$ to $+v_0/2$ at $x = x_0$. The effective half width of the discontinuity δ is

$$\delta = \sqrt{4(y_0+y)/\varkappa}. \qquad (1.15)$$

If $\kappa(y_0 + y) \gg 1$, $\partial^2/\partial y^2$ can be neglected compared with $\partial^2/\partial x^2$.

We now compute the current. From the equilibrium equation $f_z + \eta\Delta v = 0$, we obtain $j_x = -(c/B) \times \eta\Delta v$; however, $\Delta v = \kappa\partial v/\partial y$ so that $j_x = -\sqrt{\sigma\eta} \times \partial v/\partial y$. Then, integrating Eq. (1.3) we have $j_y = \sqrt{\sigma\eta}\,\partial v/\partial x$. Thus, $\sqrt{\sigma\eta}\,v(x, y)$ is a function of the current for the vector $\mathbf{j}$. The "surface" current flowing along the discontinuity is $J_y = \int j_y dx = \sqrt{\sigma\eta}\,v_0$ or

$$\mathbf{J}_+ = -\sqrt{\sigma\eta}([\mathbf{n}\times\mathbf{v}]_1 + [\mathbf{n}\times\mathbf{v}]_2); \qquad (1.16)$$

the subscripts 1 and 2 refer to the left and right side of the discontinity, $\mathbf{n}_{1,2}$ corresponds to the corresponding inward normals. Knowing the current, it is easy to find the potential gradient $\partial\varphi/\partial y = -(B/\kappa)\partial v/\partial x$, $\partial\varphi/\partial x = -vB + (B/\kappa)\partial v/\partial y$. Whence it is apparent that there is a tangential discontinuity in the charge and the discontinuity in the electric field is

$$(\partial\varphi/\partial x)_2 - (\partial\varphi/\partial x)_1 = -v_0 B. \qquad (1.17)$$

These same results apply if there is a fixed pressure gradient $\partial p/\partial z = -\Gamma$; it is only necessary to add the constant terms $j_x(\infty) = -c\Gamma/B$ and $c^2\Gamma/\sigma B$, to j_x and $\partial\varphi/\partial x$.

The tangential discontinuity may also be regarded as a jet of electric current along the magnetic field. In the "galvanostatics" of solid conductors such jets are not possible because the

current tends to flow along the line of least resistance and diverges to a large cross section; in a liquid, however, the force due to the j_x component produces a velocity v_z, which in turn results in an emf which supports the current in the jet.

Changing the sign in front of y in Eq. (1.14) we obtain the solution v_-, which corresponds to the current J_- and differs from Eq. (1.16) only in sign.

It will be shown below that in the motion of a liquid the current frequently appears only in thin layers and has a surface density $\sqrt{\sigma\eta}\,v$. In these cases the region of applicability of the galvanic approximation can be expanded since the magnetic field which is produced is of order $B_1 \sim (4\pi\mu/c) \times \sqrt{\sigma\eta}\,v \sim (R_m/M)B$ rather than R_mB.

2. SMALL OSCILLATIONS

In small oscillations we can neglect the quadratic term $(\mathbf{v}\cdot\nabla)\mathbf{v}$. The equation of motion is written in the form

$$\partial\mathbf{v}/\partial t = \nu\nabla^2\mathbf{v} + \mathbf{F}, \quad \operatorname{div}\mathbf{v} = 0, \tag{2.1}$$

where $\mathbf{F} = -\nabla p'/\rho + \mathbf{f}/\rho$ and p' is the deviation of the pressure from the equilibrium value p_0. In accordance with Eq. (2.1), div $\mathbf{F} = 0$, and from Eq. (1.8) we have

$$\Delta\mathbf{F} = -\gamma_m(\mathbf{b}\nabla)^2\mathbf{v}. \tag{2.2}$$

Volume waves. We consider a plane wave in which all quantities are proportional to $\exp(i\mathbf{k}\cdot\mathbf{r} - i\omega t)$. From Eqs. (2.1) and (2.2) we find that the possible motions for a plane wave are two slipping motions $\mathbf{v}\perp\mathbf{k}$, which are damped with the same decrement

$$\omega = -i(\nu k^2 + \gamma_m(\mathbf{bn})^2), \tag{2.3}$$

where $\mathbf{n} = \mathbf{k}/k$. The magnetic damping is due only to the field component parallel to the gradient. The perturbation of the motion is found from div $\mathbf{F} = 0$; the quantities $\mathbf{j}$ and φ are found from Eq. (1.7) and Eq. (1.4):

$$\frac{p'}{\rho} = -\frac{i\gamma_m}{k^2}(\mathbf{bk})(\mathbf{bv}), \qquad \mathbf{j} = -\frac{\sigma B^2}{ck^2}(\mathbf{bk})[\mathbf{k}\times\mathbf{v}],$$

$$\varphi = -\frac{iB}{k^2}([\mathbf{b}\times\mathbf{k}]\mathbf{v}). \tag{2.4}$$

Thus, in the galvanic approximation magnetohydrodynamic waves are not possible. The small conductivity leads to the appearance of an additional mechanism but, in contrast with the high-conductivity case, there is no elastic restoring force. When $\omega \sim \gamma_m$, $R_m = \gamma_m/D_mk^2$; this result has been obtained by Lundquist;[10] the galvanic approximation applies if R_m is small. For mercury with $B = 10^4$ gauss, $k = 1\ \text{cm}^{-1}$ and $R_m = 10^{-2}$.

If the compressibility of the liquid is taken into account we find that in addition to the damped slipping motion it is also possible to have longitudinal sound waves with frequencies given by $\omega = c_sk$. The acoustic velocity is large (for mercury $c_s = 1.5 \times 10^5$ cm/sec) so that it is not very sensitive to the magnetic field ($\gamma_m \ll \omega$); however, the damping of the acoustic wave may be a strong function of magnetic field. The current $(\sigma/c)\mathbf{v}\times\mathbf{B}$ flows freely along $\mathbf{k}\times\mathbf{B}$ so that the Joule dissipation can be regarded as the result of magnetic friction. The mean dissipation rate is $\sigma B^2/c^2\overline{v_\perp^2} = \gamma_m(\mathbf{b}\times\mathbf{n})^2\rho\overline{v^2}$, where $\rho\overline{v^2}$ is the energy density of the wave and the magnetic damping is

$$\gamma_{\text{mag}} = [\mathbf{b}\times\mathbf{n}]^2\gamma_m/2. \tag{2.5}$$

We note that this quantity is anisotropic and independent of frequency. Equation (2.5) applies only when $R_m = c_s^2/\omega D_m \ll 1$, i.e., for high (and not low!) frequencies; for example, $\omega \gg 10^6$ for mercury. The ratio of the magnetic damping to viscosity is of order $\gamma_m/\nu k^2 = \kappa^2k^2$; with $\omega \sim 10^6\ \text{sec}^{-1}$, $k \sim 10\ \text{cm}^{-1}$ and $B = 10^4$ gauss, this ratio is approximately 10^3.

Surface waves. Suppose that the z axis is vertical and the x axis is in the direction of propagation, so that all quantities vary as $\exp(ikx - i\omega t)$. The unperturbed surface is given by $z = 0$ and the perturbed surface by $z = \zeta = \zeta_0 \times \exp(ikx - i\omega t)$. The unperturbed pressure is $p_0 = -\rho gz$. We limit ourselves, for simplicity, to the case in which viscosity can be neglected $k^2 \ll \kappa^2$. In this case the boundary conditions at $z = 0$ (with surface tension taken into account) assume the form (cf. reference 2, §61)

$$v_z(z=0) = -i\omega\zeta, \quad p'(z=0) = (\rho g + \alpha k^2)\zeta, \tag{2.6}$$

where α is the surface tension coefficient. An additional condition at the surface is $j_z = 0$.

It is apparent that it is sufficient to consider the velocity components v_x and v_z, taking $v_y = 0$. In this case the force $\mathbf{F}$, as follows from Eq. (2.2), has no y component; curl $\mathbf{v}$ and the current density $\mathbf{j}$ are along the y axis so that the condition $j_z(z = 0) = 0$ is satisfied trivially. Thus, B_y of the magnetic field has no effect on the wave.

We seek a solution proportional to e^{mz} and introduce the complex vector $\mathbf{q}(k, 0, -im)$. From Eqs. (2.1) and (2.2) we find the condition which must be satisfied for a non-trivial solution

$$i\omega q^2 = \gamma_m(\mathbf{bq})^2, \tag{2.7}$$

and also $\mathbf{q}\cdot\mathbf{v} = 0$. The quadratic equation (2.7) determines m; we must take values which give

damping inside the liquid, Re m > 0. The expression for p′ can be obtained by replacing **k** by **q** in Eq. (2.4). Using $\mathbf{q}\cdot\mathbf{v} = kv_x - imv_z = 0$, we can express v_x and p′ in terms of v_z:

$$p'/\rho = (i\omega/k)(\mathbf{bq})^{-1}(mb_x - ikb_z)v_z. \qquad (2.8)$$

Here we have also made use of Eq. (2.7). Substituting Eq. (2.8) in Eq. (2.6), we obtain the relation for the frequency:

$$\omega^2(mb_x - ikb_z) = \omega_0^2(bq), \qquad (2.9)$$

where ω_0 is the frequency in the absence of the magnetic field:

$$\omega_0^2 = gk + \alpha k^3/\rho. \qquad (2.10)$$

After some elementary algebraic transformations, we obtain from Eqs. (2.7) and (2.9)

$$m/k = (\omega_0^2 b_x + \omega^2 ib_z)(\omega^2 b_x + \omega_0^2 ib_z)^{-1}, \qquad (2.11)$$

$$\omega^4 - \omega_0^4 + \omega^3 i\gamma_m(b_x^2 + b_z^2) = 0. \qquad (2.12)$$

If $\gamma_m \ll \omega$, damped oscillations are possible:

$$\omega = \omega_0 - (i\gamma_m/4)(b_x^2 + b_z^2). \qquad (2.13)$$

The motion in this case is approximately potential motion, $m \approx k$, as is to be expected for $N \ll 1$. However, if $\gamma_m \gg \omega$ the perturbations of the surface are damped aperiodically:

$$\omega = -i\gamma_m(b_x^2 + b_z^2). \qquad (2.14)$$

These results agree with the experimental data. It has been found in reference 8 that in a field of 10^4 gauss surface oscillations in mercury are completely suppressed. Under these conditions $\gamma_m = 78$ and the oscillations are damped rapidly; when $k < 4$ cm^{-1}, generally speaking it is impossible to have oscillations at all.

3. FLOW ALONG A TUBE

We consider stationary flow of a liquid in a long tube transverse to the magnetic field. We take the z axis along the axis of the tube: $v = v_z$ and $B = B_y$. All quantities are independent of z except for the pressure, which has a constant derivative in this direction.* This problem has been solved by Shercliff[11] for a non-conducting tube with cross section symmetric with respect to the x axis. The solution in reference 11 was obtained by substitution of variables; for the case of a conducting tube or an asymmetric tube this procedure is not quite as effective. Below a more general case is considered.

Projecting Eqs. (1.1), (1.2), and (1.6) on the z axis we have

$$\Gamma + \eta\Delta v + f_z = 0,$$

$$f_z = c^{-1}j_x B = -(\sigma B^2/c^2)(v + B^{-1}\partial\varphi/\partial x). \qquad (3.1)$$

Here $\Gamma = -\partial p/\partial z$ and for an inclined tube $\Gamma = -\partial p/\partial z + \rho g \sin\alpha$, where α is the angle of inclination with respect to the horizontal.

When $M \ll 1$, viscosity predominates and the flow is approximately the same as ordinary Poiseuille flow. We consider the opposite limiting case, $M \gg 1$. In this case viscosity is important only in the thin layers close to the walls of the tube.

Boundary layer. We will approximate a small section of a wall as a plane and introduce the coordinates s, along the periphery of the cross section, and r, along the normal **n**. Taking derivatives with respect to r only we obtain the solution (1.12) corresponding to the Hartmann layer $v = v_0 \times [1 - \exp(-\kappa_n r)]$, where $\kappa_n^2 = \kappa^2(\mathbf{b}\cdot\mathbf{n})^2$. By v_0 we mean the value of the velocity obtained from the solution for the inner region for a given point of the periphery.

Let the wall be insulating; then, close to the wall $j = j_S$. Using Eq. (1.7) we have

$$j_s = (\sigma B_n/c)\exp(-\varkappa_n r) + j_{s\infty}.$$

The "surface" current in the layer is

$$J_s = \int (j_s - j_{s\infty})\,dr = \sqrt{\sigma\eta}\,v_0$$

or

$$\mathbf{J} = \sqrt{\sigma\eta}\,[\mathbf{n}\times\mathbf{v}_0](\mathbf{bn})/|(\mathbf{bn})|. \qquad (3.2)$$

If $j_{S\infty} \ll j_S$, using Eq. (1.9) it is possible to compute the energy dissipation in the Hartmann layer. The viscous loss and Joule dissipation are the same and their sum per unit surface is

$$Q_1 = \sqrt{\sigma\eta}\,c^{-1}|B_n|v_0^2. \qquad (3.3)$$

If the conditions in the layer change slowly and a current **j** flows toward the insulating wall, it is possible to write an equation for conservation of charge for the layer

$$dJ_s/ds + (\mathbf{jn}) = 0. \qquad (3.4)$$

Let the wall of the tube be highly conducting; in this case it assumes a fixed potential φ_0. If the electric field outside the layer is much smaller than the field inside we can write the potential drop in the layer $\varphi_\infty - \varphi_0$.

Using Eq. (1.4) we have

$$\varphi = \varphi_0 + B_s v_0 \varkappa_n^{-1}[1 - \exp(-\varkappa_n r)].$$

The potential discontinuity in the layer is

*In the liquid there are induced currents in the xy plane; the magnetic field in the z direction due to these currents has no effect on the force f_z since there are no time variations so that for an infinite tube length it is not necessary that R_m be small.

$$\varphi_\infty - \varphi_0 = (B/\varkappa_n)(\mathbf{b}[\mathbf{n}\times\mathbf{v}_0]). \quad (3.5)$$

The relations in Eqs. (3.3) – (3.5) serve as the effective boundary conditions for the equations inside the region.

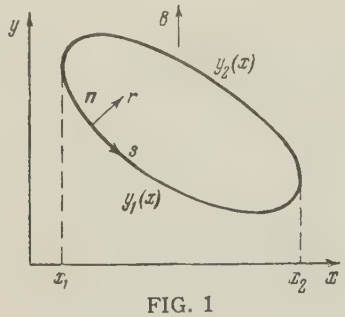

FIG. 1

It should be noted that this picture of the layer is valid only when $\kappa_n l \gg 1$; if, however, $B_n \to 0$, the relations which have been obtained no longer hold. This situation pertains, for example, to the regions near the points x_1 and x_2 (Fig. 1). If the wall of the tube is parallel to the magnetic field a longitudinal surface layer of the type considered by Shercliff[11] is formed; this is similar in structure to the tangential discontinuity (1.14). The layer thickness is of order $\sqrt{l/\kappa}$ [cf. Eq. (1.15)].

Viscosity can be neglected in the inner part of the tube and Eq. (1.12) yields $\partial^2 v/\partial y^2 = 0$, $\partial^2\varphi/\partial y^2 = 0$. Whence

$$v(x,y) = v_0(x) + v_1(x)\,y, \quad \varphi(x,y) = \varphi_0(x) + \varphi_1(x)\,y, \quad (3.6)$$

where φ_0 and φ_1 are related to v_0 and v_1 in accordance with Eq. (3.1). In the inner region, from Eq. (3.1) j_x is constant and since div $\mathbf{j} = 0$, j_y depends on x and is determined by Eq. (1.7)

$$j_x = -(c\Gamma/B), \quad dj_y/dx = (\sigma B/c)\,v_1(x). \quad (3.7)$$

Tube with insulating walls. Let the cross section of the tube be given by two single-valued curves $y_1(x)$ and $y_2(x)$ (cf. Fig. 1). The effective boundary conditions (3.2) at these boundaries can be written in the form

$$J_1 = \sqrt{\sigma\eta}\,v(x,y_1), \quad J_2 = -\sqrt{\sigma\eta}\,v(x,y_2). \quad (3.8)$$

In terms of the difference of these quantities, using Eq. (3.6) it is easy to express the total flow of liquid V through the cross section of the tube:

$$V = \int v\,dx\,dy = 2^{-1}(\sigma\eta)^{-1/2}\int_{x_1}^{x_2}(J_1 - J_2)(y_2 - y_1)\,dx.$$

Now, making use of Eq. (3.4) and taking account of the fact that $n_y\,ds = dx$ and $n_x/n_y = -dy/dx$, we obtain

$$d(J_1 - j_x y_1)/dx = -j_y, \quad d(J_2 - j_x y_2)/dx = -j_y. \quad (3.9)$$

Subtracting the second equation from the first and integrating, we have

$$J_1 - J_2 = -j_x(y_2 - y_1) = (c\Gamma/B)(y_2 - y_1).$$

Thus, the flow of liquid in a tube of arbitrary cross section with non-conducting walls is

$$V = (c\Gamma/B\sqrt{\sigma\eta})\int_{x_1}^{x_2}[y_2(x) - y_1(x)]^2\,dx. \quad (3.10)$$

Summing Eq. (3.9), taking account of Eqs. (3.7) and (3.8), and neglecting the term of order $1/\kappa l$, we have

$$j_y = -(c\Gamma/2B)\,d(y_1 + y_2)/dx. \quad (3.11)$$

If the tube is symmetric with respect to the x axis $j_y = 0$, $v_1 = 0$ and Eq. (3.10) coincides with the result which has been obtained by Shercliff. If the shape is not symmetric, then $j_y \sim j_x$ but the velocity shows almost no change along the field $v_1 y \ll v_0$. Actually, from Eq. (3.10) $v \sim c\Gamma l/B\sqrt{\sigma\eta}$ whereas from Eq. (3.7) $v_1 l \sim (c/\sigma B)\,j_y \sim v/\kappa l$.

Tube with highly conducting walls. A completely different picture obtains if the walls of the tube are highly conducting. In this case, the current can flow freely across the magnetic field, being closed in the walls of the tube, the potential of which may be assumed constant. In the zeroth approximation the interaction of the liquid with the field leads to magnetic "friction" and the term associated with the production of a potential difference is small, approximately M^{-1}. In this approximation, for the entire inner region we have

$$v = c^2\Gamma/\sigma B^2, \quad j = j_x = \sigma B v/c, \quad \varphi = 0. \quad (3.12)$$

The corrections associated with the next approximation can also be found easily. As before, in the inner region we can neglect viscosity since $\eta\Delta v \sim M^{-2}$ so that v and φ inside are of the form given in Eq. (3.6). The electric field inside ($\sim \varphi/l$) is much smaller than in the layer ($\sim \kappa\varphi$) so that we can use the effective boundary condition in (3.5). If $y = y_1$ and $y = y_2$, this condition becomes

$$\varphi(x,y_1) = (Bv/\varkappa)\,dy_1/dx, \quad \varphi(x,y_2) = -(Bv/\varkappa)\,dy_2/dx.$$

The quantities φ_0 and φ_1 are determined by the conditions:

$$\varphi_0(x) = (Bv/\varkappa)(y_2 - y_1)^{-1}\,d(y_1 y_2)/dx,$$
$$\varphi_1(x) = -(Bv/\varkappa)(y_2 - y_1)^{-1}\,d(y_2 - y_1)/dx. \quad (3.13)$$

Tubes with electrodes. Comparing the velocity in tubes with conducting walls and nonconducting walls, we see that for a given Γ, the velocity in the first case is approximately M times smaller

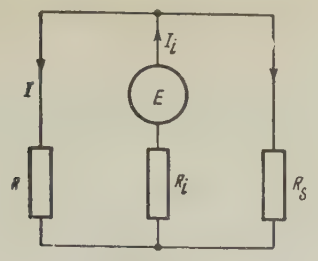

FIG. 2

than in the second. If the walls of the tube are insulating, but the upper and lower walls have electrodes which are connected through an external resistance R, it is possible to obtain a continuous transition between the two cases. The equivalent electric circuit of this tube is shown in Fig. 2. The current I_i produced by the induction emf $\mathcal{E}$ flows across the tube through the liquid (R_i) part of it returning through the resistance R and part through the liquid in the boundary layer (R_S).

We consider in greater detail a tube of rectangular cross section ABCD in which the sides AB = CD = l, perpendicular to the magnetic field, are insulating and the sides AC = BD = h, parallel to the field, are highly conducting and connected through an external resistance. The length of the tube is L. On sides AB and CD Hartmann layers are formed; on walls AC and BD longitudinal boundary layers similar to the Shercliff layer are formed. Since the thickness of the longitudinal layers [cf. Eq. (1.15)] is approximately $(h/\kappa)^{1/2} \sim M^{1/2}\kappa^{-1}$ and is much thicker than the Hartmann layers, the resistance of these layers is much smaller and the role they play in dissipation is not important. In general they need not be considered. From Eq. (3.6) and the symmetry conditions, over the entire inner region of the tube $\varphi = \varphi(x)$; consequently, $j_y = 0$. Whence it follows that the currents in the layers are constant and, in accordance with Eqs. (3.2) and (3.6), the velocity v is constant over the entire inner region. For this case of uniform flow it is easy to find the current which issues from the tube:

$$I = j_x hL + 2J_s L = -c\Gamma hL/B + 2\sqrt{\sigma\eta}\,vL,$$

and the difference of potentials between the conducting walls

$$ld\varphi/dx = -lvB + lc^2\Gamma/\sigma B.$$

On the other hand, $l\,d\varphi/dx = cIR$ so that

$$v = \frac{c^2\Gamma}{\sigma B^2}\left(1+\frac{R}{R_i}\right)\left(1+\frac{R}{R_s}\right)^{-1}, \qquad (3.14)$$

where we have used the notation

$$R_i = l/\sigma hL, \quad R_s = \varkappa l/2\sigma L, \quad \mathcal{E} = (v/c)\,Bl. \qquad (3.15)$$

The meaning of Eq. (3.14) is simple. When $R \gg R_S$, the electromagnetic force IBl/c vanishes since $I \approx 0$. The magnetic field is found to have only an indirect braking effect, producing a thin layer in which the friction force is $\eta\kappa v$; hence $v = \Gamma h/2\eta\kappa$ is approximately M times smaller than in Poiseuille flow. If $R \ll R_S$, the basic retardation effect is due to the force IBl/c, where $I = \mathcal{E}(R + R_i)^{-1}$ so that $v = (c^2\Gamma/\sigma B^2)(1 + R/R_i)$.

For other cross sections the circuit (Fig. 2) is still valid but Eq. (3.14) is accurate only to an order of magnitude. We may note that if the side walls are inclined rather than parallel to the field, Hartmann layers will also be formed on them. This means a certain increase in resistance; on the other hand there is an increase in the stability of flow at high velocities since the effective Reynolds number $R_\delta = v\delta/\nu$ is reduced (δ is the thickness of the layer).

Self-excited dynamo. If the current flowing out of the tube I is used for producing the magnetic field in the tube, under certain conditions it is possible to obtain a self-excited system. In this case the magnetic field is proportional to the current B = KI, where $K \sim 4\pi n/ch$ and n is the number of turns of the coil which produces the field. Assuming that $\mathcal{E} = (v/c)\,Bl$, we obtain the equation which determines the current:

$$L\,dI/dt + R_{\text{eff}} I = 0,$$

$$R_{\text{eff}} = R + R_i R_s (R_i + R_s)^{-1} - R_s (R_i + R_s)^{-1} Klv/c, \qquad (3.16)$$

where L is the self-inductance of the coil. The criterion for self-excitation is $R_{\text{eff}} < 0$ or $v > v_{\text{exc}}$ where $v_{\text{exc}} \sim (c^2 h/4\pi ml)[R_i + R(1 + R_i/R_S)]$. At small fields $R_S \sim R_i$. In order to increase K it is convenient to increase the number of turns of the coil; conversely R can be reduced by reducing the number of turns. In a system without iron the turns are wound along the tube $R \sim n^2 L/\sigma_c S$, where σ_c is the conductivity of the wire in the coil, S is the total cross section of the turns ($S \lesssim hl$). The most favorable conditions are obtained when $R \sim R_i$ or $n^2 \sim \sigma_c S/\sigma L^2$. When $\sigma_c/\sigma = 60$ (copper and mercury) this condition gives $n \sim 3-4$. For mercury, with L = 10 cm an estimate yields $v_{\text{exc}} \sim 10^3$ or several times 10^2 cm/sec. If a ferromagnetic material is used in the electromagnet, it is possible to reduce the dimensions of the turns and a greater number of turns can be used for the same R. With n = 10 and L = 10 cm, for example, for mercury we obtain $v_{\text{exc}} \sim 10^2$ cm/sec.

After excitation the field grows so long as its retarding effect does not reduce the velocity in such a way that $R_{\text{eff}} = 0$ or $4\pi nlv/c^2 h = R + R_i$.

Substituting this criterion in Eq. (3.14) we find the magnetic field $B^2 = 4\pi\delta p$, where $\delta p = \Gamma L$ is the pressure difference in the gap with the magnetic field present. With $\delta p \sim 1$ atmos, values of several kilogauss are obtained. If iron is used, the field can be limited by saturation; this causes a reduction in K.

This scheme represents an example of the transformation of mechanical energy of a liquid into magnetic energy although, obviously, it is not a "true" hydromagnetic dynamo since solid conductors and insulators are used.

Flow along a channel (trough). If the tube is symmetric with respect to the x axis, in the median plane the boundary conditions for a free surface $j_y = 0$ and $\partial v/\partial y = 0$ are satisfied; hence the problem of a channel reduces to the problem of a tube with $\Gamma = -g\rho \sin \alpha$. For example, the flow of a liquid layer of thickness h along an inclined plane is the same as the flow (1.13) between plates with a spacing 2h. When $\kappa h \gg 1$ the flow velocity along an insulating inclined plane is κh times smaller than along a conducting plane.

The damping of surface waves has been considered in Section 2 for short wave lengths, i.e., $kh \gg 1$. On the other hand, if $kh \ll 1$ it is possible to have (cf. reference 2, §13) long gravitational waves with propagation velocities $\sqrt{gh}$. In these waves the velocity is essentially parallel to the bottom. We now find the damping of these waves (assuming that it is small and that $\kappa h \gg 1$) in the presence of a vertical magnetic field. If the trough is conducting, the currents flow freely and the damping is computed in exactly the same way as for the acoustic waves. The decrement is $\gamma = \gamma_m/2$ [cf. Eq. (2.5)]. If the trough is insulating, dissipation takes place chiefly in the boundary layer at the bottom. According to Eq. (3.3) the mean dissipation per unit surface is $\sqrt{\sigma\eta}\,(B/c)\overline{v^2}$; comparing this with the energy of the wave $h\rho\overline{v^2}$, we find

$$\gamma = \sqrt{\sigma\eta}B/2h\rho c = \gamma_m/2\varkappa h. \qquad (3.17)$$

For a channel of arbitrary cross section the damping can be determined by using Eq. (3.10) to compute the resistance of a corresponding symmetric tube.

4. ROTATION OF A LIQUID

We introduce the cylindrical coordinates r, φ and z. We assume that $\partial/\partial\varphi = 0$, that the magnetic field is vertical, $B = B_z$, and that the velocity of rotation $v_\varphi = v(r, z)$. We will also assume that $v_r, v_z \ll v$ and neglect curl $(\mathbf{v}\cdot\nabla)\mathbf{v}$ so that Eq. (1.12) can be used. We will also neglect the meniscus at the free surface; at small rotation velocities this procedure is valid.

Rotation of a Liquid Caused by Rotation of the Bottom of the Container

A. Insulating Bottom. Let the annular region $R_1 \le r \le R$ at the bottom be rotated with a constant angular velocity Ω. The boundary conditions are of the following form: on the bottom $z = 0$, $v = v_d$ ($v_d = \Omega r$ for $R_1 \le r \le R$, $v_d = 0$ for $r < R_1$ and $r > R$), $j_z = 0$ or $\partial\varphi/\partial z = 0$; at the free surface $z = h$, $\partial v/\partial z = 0$, $j_z = 0$ or $\partial\varphi/\partial z = 0$. In a strong magnetic field, $M \gg 1$, only the layer of liquid above the rotating part of the bottom rotates. It is easy to construct the approximate solution (1.12) in this case. At $r = R_1$ and $r = R$ there are tangential discontinuities in the velocity $v = \Omega R_1(\frac{1}{2} + \bar{\Phi})$ and $v = \Omega R(\frac{1}{2} - \bar{\Phi})$, where [cf. Eq. (1.14), $x = r - R_1$ or $x = r - R$]

$$\bar{\Phi} = {}^1/_4[\Phi(\sqrt{x/4hx}) + \Phi(\sqrt{x/4(2h-z)}\,x)], \qquad (4.1)$$

and between the discontinuities the liquid rotates as a whole, together with the bottom, with velocity Ωr. In this case, Eq. (1.4) (with the boundary conditions in (1.17) at the charge discontinuities) gives $\partial\varphi/\partial r = B\Omega r = vB$, whence $j_r = 0$ so that no tangential force acts on the liquid. The centrifugal force $\rho v^2/r$ is equalized by the pressure gradient. Across the rotating liquid there is a potential difference $(B\Omega/2)(R^2 - R_1^2)$. When $R_1 = 0$ there is no inner discontinuity.

We consider the velocity discontinuity in greater detail, for example, at $r = R$. Equation (4.1) is a superposition of solutions for current jets which flow upward and downward; for $z = h$, one is easily convinced, this equation yields $j_z = 0$, a current jet which behaves as though reflected from the free surface. At the bottom the current is closed by the Hartmann layer, which is formed at the interface of the rotating and fixed portions of the bottom at $r = R$. In accordance with Eq. (4.1), the velocity distribution at the interface of these layers is given by the relation

$$v_0 = (\Omega R/4)[3 - \Phi(\sqrt{x/8hx})], \quad x < 0;$$

$$v_0 = (\Omega R/4)[1 - \Phi(\sqrt{x/8hx})], \quad x > 0. \qquad (4.2)$$

The current entering the layer is $j_z = \sqrt{\sigma\eta}\,\partial v_0/\partial x$, and the current in the layer is given by Eq. (3.2), where, in place of v_0 we substitute $v_0 - v_d$. It is apparent that the equation of continuity (3.4) is satisfied; at $x = 0$ from the right and left there flow currents whose sum is exactly equal to the current in the jet which diverges from this "point." The only place at which the indicated solution does not

apply is in a region of dimensions given roughly by κ^{-1} at $x = 0$, $z = 0$, which is a singularity point.

Integrating the friction expression $\eta\kappa(v_0 - \Omega R)$, we can compute the moment of the friction force M_z which acts on the rotating bottom:

$$M_z = \Omega\eta\sqrt{2\pi\kappa h}(R^3 + R_1^3). \qquad (4.3)$$

B. Conducting Bottom (Lehnert experiment[7]). In place of the condition $\partial\varphi/\partial z = 0$ at the bottom, here we have $\partial\varphi/\partial r = vB$ or $j_r = 0$. As in the preceding case, in the annular region $R_1 \leq r \leq R$ the liquid rotates with the bottom; $v = \Omega r$, $\partial\varphi/\partial r = vB$ and at $r = R_1$ and $r = R$ there are velocity discontinuities. However, in this case no Hartmann layer can be formed; hence the solution for the tangential discontinuity, although qualitatively similar to the earlier solution, is not made up of self-similar solutions (4.1). We may assume, from Eq. (4.2), that the half-width of the discontinuity is given by

$$\delta = \sqrt{8h/\kappa}. \qquad (4.4)$$

Under the conditions of the Lehnert experiment ($h = 0.6$ cm., $R_1 + R = 7$ cm, $R - R_1 = 1$ cm., $\Omega = 0.2$ rev/sec) the rotating ring of liquid starts to form at approximately $B = 600$ gauss; this result is in qualitative agreement with Eq. (4.4) which, for this field, yields $\delta = 0.55$ cm.

The experiments carried out by Lehnert indicate that the tangential discontinuity is not stable and that a vortex path of cylindrical vortices, which behave like the rollers in a roller bearing, is formed under the rotating ring. As has been indicated by Lehnert, this effect is to be associated with the influence of the magnetic field on the form of flow. The velocity profile in the tangential "jump" has an inflection point and flow patterns of this kind, as is well known from the theory of stability in ordinary hydrodynamics,[12] become unstable at Reynolds numbers of the order of several tens. For the highest field which was used ($B = 8000$ gauss), however, a calculation made on the basis of Eq. (4.4) gives $R_\delta = v\delta/\nu = 570$. Correspondingly, $N_\delta = \gamma_m\delta/v = 1.7$; this value is insufficient for stabilization since an instability may develop completely in regions with dimensions appreciably smaller than δ. It is reasonable to expect that with a several-fold reduction of the rotation velocity (so that the ratio $R/N = v^2/\nu\gamma_m$ is of the order of ten) the flow would be stable.

The value of N is rather large for the rotating liquid ring as a whole; for $l = R - R_1 = 1$ cm we find $N = 14$, $R = 3.8 \times 10^3$. In the experiment carried out by Lehnert the stabilizing effect of the magnetic field is felt and instead of the development of turbulent motion in the jet there is a proper vortex row with a relatively small number of large vortices.

Rotation of a Liquid by a Transverse Current

Let a container with liquid, a cylindrical condenser with inner radius R_1, outer radius R, and height h, be placed in a strong magnetic field $B = B_z$. The faces of the container are insulators while the side walls are cylindrical coaxial electrodes. If a current flows between these walls the liquid is set into rotation. At the electrodes there are longitudinal boundary layers with thickness of the order of δ in Eq. (4.4); Hartmann layers are formed at the bases, In the inner region the viscosity can be neglected in accordance with Eq. (1.12) and, in this region, $\partial^2 v/\partial z^2 = 0$ and $\partial^2\varphi/\partial z^2 = 0$. Invoking the symmetry conditions we have $v = v(r)$ and $\varphi = \varphi(r)$ so that $j_z = 0$. Thus, the total current in each of the Hartmann layers $2\pi r J_s$ is independent of radius and, since $J_s \sim v$, we have $v \sim r^{-1}$. In the inner region there is a potential flow. When $v \sim r^{-1}$ the viscosity force is exactly equal to zero and consequently there is no radial current. The longitudinal electric field here is compensated by the induction emf $\partial\varphi/\partial r = vB$. The total current I flows in layers at the faces ($I = 2 \cdot 2\pi r\sqrt{\sigma\eta}\, v$), whence

$$v = I(4\pi\sqrt{\sigma\eta}r)^{-1} \qquad (4.5)$$

In ordinary hydrodynamics, flow between cylinders is stable when $v \sim r^{-1}$; since the magnetic field increases the stability, one may expect that the flow will also be stable in the case considered here.

It is interesting to note that the velocity is independent of magnetic field although the rotational moment is proportional to the field. The point is that friction at the faces is also proportional to the field since the reciprocal thickness of the layer $\kappa \sim B$. It can be shown that the resistance to rotation arises at the intersection of the magnetic lines of force at the faces of the container. This flow pattern applies if the longitudinal layers (thickness of order $(h/\kappa)^{1/2}$) are thin enough, i.e., if $h \ll \kappa R^2$. If, for example, $h \sim R \sim 10$ cm this means that $B \gg 4$ gauss. For $h \to \infty$[13] the friction force is of order $\eta v/R$ and the rotational force is approximately jB/c so that $v \sim I_1 BR/2\pi c\eta$, where I_1 is the current per unit height. In a real cylinder of height h this relation applies only when $h > \kappa R^2$. In rotation of a gas of low density the thickness of the layer κ^{-1} may be smaller than the mean free path, in which case the gas does not adhere to the faces and the velocity again increases with field.

As long as the mode of rotation is not established the current flows over the entire cross section and communicates to the liquid a velocity given approximately by $(I/2\pi Rh)\,B/c\rho$; hence, for a constant current the time for establishing the velocity (4.5) is of order $t_0 = h(\nu\gamma_m)^{-1/2}$. For example, with $h = 10$ cm and $B = 5 \times 10^3$ gauss, $t_0 = 1$ min.

The rotation of the liquid produces a radial pressure gradient $\partial p/\partial r = \rho v^2$. In the layers at the faces the liquid has a smaller velocity than in the remaining part of the container so that the motion is characterized by circulation in the meridian planes; the liquid in the layers moves towards the axis while the liquid in the center part moves away from the axis. The azimuthal currents can flow freely and there is a radial magnetic friction force $-(\sigma B^2/c^2)v_r$ which equilibrates the pressure gradient. In this case the radial velocity in the layers is of order $v_r \sim v^2c^2/\sigma B^2 r = vN^{-1}$ while the velocities v_r and v_z in the center part are smaller by a factor of κh or κR. Above we have neglected $(\mathbf{v}\cdot\nabla)\mathbf{v}$ terms in the azimuthal velocity equations as compared with the term $\nu\Delta\mathbf{v}$. The ratio of the neglected terms to those which have been considered is of order $(v/\gamma_m R)^2 = N^{-2}$; for example, with $v = 10^2$ cm sec^{-1} and $B = 10^4$ gauss, we have $N^{-2} = 2 \times 10^{-2}$.

I am indebted to M. A. Leontovich and E. P. Velikhov for discussions.

[1] L. D. Landau and E. M. Lifshitz, Электродинамика сплошных сред (Electrodynamics of Continuous Media), Gostekhizdat 1957 Chap. 8.

[2] L. D. Landau and E. M. Lifshitz Механика сплошных сред (Mechanics of Continuous Media), Gostekhizdat 1954.

[3] T. G. Cowling, Magnetohydrodynamics, Interscience, New York 1957.

[4] R. C. Lock, Proc. Roy. Soc. (London) **A233**, 105 (1955).

[5] W. Murgatroyd, Phil. Mag. **44**, 1348 (1953).

[6] J. T. Stuart, Proc. Roy. Soc. (London) **A221**, 189 (1954).

[7] B. Lehnert, Proc. Roy. Soc. (London) **A233**, 299 (1955), Пробл. совр. физ. (Problems of Contemporary Physics) No. 7, (1957).

[8] B. Lehnert, Arkiv Fysik, **5**, 69 (1952).

[9] J. Hartmann, Kgl. Danske Videnskab Selskab, Mat.-fys. Medd. **15**, 6 (1937).

[10] S. Lundquist, Arkiv Fysik, **5**, 297 (1952), Пробл. совр. физ. (Prob. Contemp. Physics) No. 2, (1954).

[11] J. A. Shercliff, Proc. Cambridge Phil. Soc. **49**, 136 (1953).

[12] C. C. Lin, Theory of Hydrodynamic Stability, Russ. Transl. IIL (1958).

[13] G. V. Gordeev and A. N. Gybanov, J. Tech Phys. (U.S.S.R.) **28**, 2046 (1958), Soviet Phys.-Tech Phys. **3**, 1880 (1959).

Translated by H. Lashinsky
279

THE CONTRIBUTION OF THREE-PARTICLE FORCES TO THE BINDING ENERGIES OF HYPERNUCLEI

V. A. LYUL'KA and V. A. FILIMONOV

Moscow State University; Institute of Nuclear Physics, Electronics, and Automation of the Tomsk Polytechnic Institute

Submitted to JETP editor June 23, 1959

J. Exptl. Theoret. Phys. (U.S.S.R.) **37**, 1431-1433 (November, 1959)

The three-particle Λ-nucleon potential is calculated in the lowest order of meson theory. It is shown that the contribution of this potential to the potential energy of a Λ particle in a hypernucleus is positive and of insignificant amount. The estimates so obtained do not confirm Spitzer's[1] conclusion that three-particle forces play a large part in hypernuclei.

ASSUMPTIONS that many-particle forces can play a large part in the interactions of Λ particles with nucleons have been put forward repeatedly.[2-5] The absence of interaction between a Λ particle and a nucleon through the exchange of a single π meson has the result that the radius of action of the pair forces is of the order of $1/2m_\pi$. At the same time, on the assumption of charge independence of the forces the exchange of single π mesons is allowed in three-particle interactions (see figure). This leads to forces with a radius of action of the order $1/m_\pi$. Therefore it might be expected that three-particle forces are of more importance in Λ-nucleon than in nucleon-nucleon interactions.

Spitzer[1] has calculated the three-particle forces in the lowest order of perturbation theory and found that these forces make a very large negative contribution to the potential energy of the Λ particle. This result is somewhat unexpected, since such forces do not play any important part in nucleon-nucleon interactions.[6] The study of these forces is continued in the present paper.

The eight diagrams of the type shown in the figure lead to the following expression for the potential-energy operator of the interaction between a Λ particle and a system of A nucleons:

$$V_3 = -\frac{f^4}{m_\pi^4}\frac{4M_N^2}{M_\Lambda^2}\sum_{i\neq j}^{A}\frac{(\tau_i\tau_j)}{(2\pi)^4}\iint\frac{(k_1k_2)(\sigma_ik_1)(\sigma_jk_2)}{\omega_1^2\omega_2^2}$$

$$\times\{\exp[ik_1(\mathbf{x}-\mathbf{x}_i)+ik_2(\mathbf{x}-\mathbf{x}_j)]\}\,v^2(k_1)v^2(k_2)\,d\mathbf{k}_1\,d\mathbf{k}_2; \quad (1)$$

$\mathbf{x}_i$ and $\mathbf{x}_j$ are the coordinates of the nucleons, $\mathbf{x}$ is the coordinate of the Λ particle, and $v(k)$ is the cutoff function.

In the calculation of the potential we have neglected the mass difference $\Delta = M_\Sigma - M_\Lambda$ and have assumed that the parities of the Λ and Σ particles

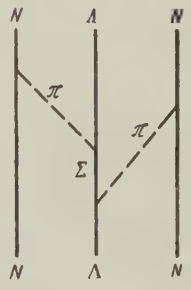

are the same as for nucleons. It must be noted that if the parities of Λ and Σ are different, then in the adiabatic approximation the forces of the type in question are zero.

The potential (1) does not contain the spin operator of the particle. In both the singlet and the triplet symmetric S state of a pair of nucleons the operator $(\tau_i\tau_j)(\sigma_ik_1)(\sigma_jk_2)$ has the value:

$$\langle(\tau_i\tau_j)(\sigma_ik_1)(\sigma_jk_2)\rangle = -(k_1k_2). \quad (2)$$

Therefore in the case of light hypernuclei the contribution to the potential energy of the Λ particle from the forces (1) is proportional to the number of pairs of nucleons in the core nucleus.

To obtain an estimate of the potential energy of the Λ particle in a light hypernucleus the distribution of nucleons in the core nucleus was taken to be a Gaussian distribution:

$$\rho(r) = a\exp\{-r^2/\gamma^2r_\pi^2\}, \quad (3)$$

$r_\pi = 1/m_\pi$ is the Compton wavelength of the π meson, and a is a normalization constant (we take $\hbar = c = 1$). The parameter γ was chosen to make the density distribution in the core nucleus agree with the data on the scattering of electrons by light nuclei (taking account of the size of the proton).

The distribution of the Λ particle in the hypernucleus was also taken to be Gaussian:

$$\rho_\Lambda(r) = a_\Lambda \exp\{-r^2\eta^2/\gamma^2 r_\pi^2\}. \quad (4)$$

The variation parameter η characterizes the deviation of the distribution of the Λ particle from that of the nucleons. Using Eqs. (3), (4), and (2), we get the following expression for the potential energy of the Λ particle in a light hypernucleus, with the central part of the force fixed by Eq. (1):

$$U = f^4 \frac{8}{3\pi^2} \frac{M_N^2}{M_\Lambda^2 \gamma_2^6} m_\pi \frac{1}{2} A(A-1) F(\gamma^2, \gamma_1^2, \gamma_2^2), \quad (5)$$

$$F(\gamma^2, \gamma_1^2, \gamma_2^2) = \int_0^{x_m}\int_0^{x_m} \frac{(\gamma_2^4 x_1^3 x_2^3 - \gamma_2^2 x_1^2 x_2^2 + {}^1/_2 x_1 x_2)}{(x_1^2+1)(x_2^2+1)^{3/2}}$$

$$\times \exp[-\gamma_1^2 (x_1 - x_2)^2 - {}^1/_2 \gamma^2 x_1 x_2]\, dx_1 dx_2,$$

$$\gamma_1^2 = {}^1/_4 \gamma^2 (1+\eta^{-2}), \qquad \gamma_2^2 = (4\gamma_1^2)^{-1},$$

$$x = k/m_\pi, \qquad x_m = k_m/m_\pi, \quad (6)$$

k_m is the cutoff momentum (a rectangular cutoff is used). The function $F(\gamma^2, \gamma_1^2, \gamma_2^2)$ was calculated numerically for $x_m = 6$. The values of the variation parameter were found from the condition that the binding energy of the Λ particle be a minimum, as calculated by means of the two-particle potentials of the meson theory.[7] The constants in these potentials were taken to have the values given in reference 7. The table shows the values of γ^2 and η^2 that were used, and the potential energies calculated from Eq. (5) ($f^2 = 0.083$). The last line shows for comparison the potential energies for the pair forces caused by the exchange of two π mesons. The comparison shows that the contribution of the three-particle forces is insignificant.

Hypernucleus	H^3_Λ	H^4_Λ, He^4_Λ	He^5_Λ
γ^2	1.00	0.80	0.88
η^2	0.33	0.42	0.25
Three-particle forces, Mev	0.1	0.3	0.5
Pair forces, Mev	—8	—14	—18

From (5) it can be seen that as the number of particles in the core nucleus increases the contribution of the three-particle forces increases as A^2. In heavy hypernuclei, however, owing to the short-range nature of the forces, the contribution to the potential energy will be determined not by the number of particles in the core nucleus, but by the density of the nuclear matter. We can estimate the contribution of the potential (1) to the potential of a Λ particle in a heavy hypernucleus if we regard the nucleons as a degenerate Fermi gas and describe them by a wave function ψ that is a determinant made up of plane waves, taking account of the spin and isotopic spin of the nucleons. In this case the technique of calculation used earlier to find the contribution of the pair forces[8,9] leads to the following expression for the potential energy of a Λ particle in a heavy hypernucleus owing to the forces (1):

$$U = \langle\psi, V_3\psi\rangle = f^4 \frac{24}{\pi^2} m_\pi \frac{M_N^2}{M_\Lambda^2} \int_0^{2x_F} (x^2+1)^{-5/2}$$

$$\times \left(\frac{2}{3} x_F^3 x^6 - \frac{1}{2} x_F^2 x^7 + \frac{1}{24} x^9\right) dx, \quad (7)$$

$x_F = k_F/m_\pi$, and k_F is the maximum momentum of the nucleons in the nucleus. (In obtaining the expression (7) we have assumed that the number of protons is equal to the number of neutrons.) For nuclear radius $R = 1.2 A^{1/3}$ F, $x_F = 1.77$. With this value of x_F and $f^2 = 0.08$ we get from Eq. (7) U = 2.6 Mev. This result is to be compared with the contribution of the pair forces from interchange of two π mesons, which is $U^{(2\pi)} = -78$ Mev.[8] Thus the contribution from three-particle forces of the type under consideration is positive and of negligible size both for light and also for heavy hypernuclei. The results of these calculations do not support the conclusion of reference 1, that three-particle forces play a large part.

There can also be three-particle forces between a Λ particle and nucleons owing to the exchange of K and π mesons

$$N + \Lambda + N \to N + \tilde{K} + N + \pi + N \to \Lambda + N + N,$$

$$N + \Lambda + N \to \Lambda + K + \Lambda(\Sigma) + \pi + N \to \Lambda + N + N.$$

Estimates show that forces of this type make a negative contribution to the potential energy, but here also it is negligibly small both in light and in heavy hypernuclei.

In conclusion the writers thank Professor D. D. Ivanenko and N. N. Kolesnikov for their interest in the work and for a helpful discussion of the results, and Kh. A. Khachartyan for making the numerical computations.

[1] R. Spitzer, Phys. Rev. **110**, 1190 (1958).
[2] E. M. Henley, Phys. Rev. **106**, 1083 (1957).
[3] V. I. Ogievetskiĭ, JETP **33**, 546 (1957), Soviet Phys. JETP **6**, 427 (1958).
[4] R. Dalitz and B. W. Downs, Phys. Rev. **111**, 967 (1958).

[5] R. Dalitz, Proc. Annual Conf. on High Energy Physics, CERN, 1958.

[6] Brueckner, Levinson, and Mahmoud, Phys. Rev. **95**, 217 (1954).

[7] V. A. Lyul'ka and V. A. Filimonov, JETP **35**, 1026 (1958), Soviet Phys. JETP **8**, 717 (1959).

[8] V. A. Filimonov, JETP **36**, 1569 (1959), Soviet Phys. JETP **9**, 1113 (1959).

[9] V. A. Filimonov, All-union Intercollegiate Conference on Quantum Field Theory and the Theory of Elementary Particles, Uzhgorod, 1958 (in press).

Translated by W. H. Furry
280

EXCITATION OF VIBRATIONAL LEVELS IN NUCLEI BY CHARGED PARTICLES

A. D. PILIYA

Leningrad Physico-technical Institute, Academy of Sciences, U.S.S.R.

Submitted to JETP editor June 25, 1959

J. Exptl. Theoret. Phys. (U.S.S.R.) **37**, 1434-1440 (November, 1959)

The excitation of the first vibrational level of an even-even nucleus by charged particles with energies close to the height of the Coulomb barrier is considered.

IN an earlier paper[1] the author considered the excitation of the rotational levels of nuclei by charged particles with energies close to the height, B, of the Coulomb barrier. The excitation of the vibrational levels can be discussed in an entirely analogous fashion. If the energy of the incoming particle is $E \sim B$, the basic process leading to collective excitations is, besides the ordinary Coulomb excitation, the direct nuclear interaction. Compound nucleus formation should play only a secondary role, since the compound nucleus can decay in a very great number of ways, out of which only one gives a contribution to the reaction under consideration. This is true especially in the case when the incoming particle is complex (α particle, deuteron, etc.).

Since the internal structure of the nucleus is not affected by the excitation of the collective levels, it is natural to describe the direct interaction with the help of the optical model, which is modified in such a way as to take into account the collective degrees of freedom in the nucleus. This modification consists of regarding the parameters specifying the shape of the complex nuclear potential as dynamical variables in the Schrödinger equation for the system consisting of the target nucleus and the incoming particle. Thus, if the nuclear potential has the form

$$V_n(\mathbf{r}) = V_n\left[\frac{r - R(\theta,\varphi)}{d}\right], \tag{1}$$

where

$$R = R_0\left[1 + \sum_{\lambda\mu}\alpha_{\lambda\mu}Y_{\lambda\mu}(\theta,\ \varphi)\right], \tag{2}$$

one conveniently chooses for these collective coordinates the coefficients $\alpha_{\lambda\mu}$. The Hamiltonian of the system can then be written in the form

$$H = H_{vib}(\alpha) - (\hbar^2/2m)\nabla^2 + Z_1Z_2e^2/r + V_n(\mathbf{r},\alpha) + V_c(r,\alpha), \tag{3}$$

where α is the set of coordinates $\alpha_{\lambda\mu}$, $\mathbf{r} = \mathbf{r}(r, \theta, \varphi)$ is the radius vector of the incoming particle, $V_c(\mathbf{r}, \alpha)$ is the non-central part of the electrostatic interaction leading to the Coulomb excitation, and $H_{vib}(\alpha)$ is the collective Hamiltonian of the nucleus:[2]

$$H_{vib}(\alpha) = \sum_{\lambda\mu}\left[\tfrac{1}{2}B_\lambda|\alpha_{\lambda\mu}|^2 + \tfrac{1}{2}C_\lambda|\alpha_{\lambda\mu}|^2\right] \tag{4}$$

We are interested in a solution of the Schrödinger equation

$$H\Psi(\mathbf{r},\alpha) = E\Psi(\mathbf{r},\alpha), \tag{5}$$

which, for large r, has the form

$$\Psi(\mathbf{r},\alpha) \to \varphi_{n_0}^{I_0\mu_0}(\alpha)\exp\{i\mathbf{k}_0\mathbf{r} + i\eta_{l_0}\ln(kr - \mathbf{kr})\} + \sum_{l,\mu,n} r^{-1}f_{l\mu n}(\theta,\varphi)\,\varphi_n^{l\mu}(\alpha)\exp\{ik_nr - i\eta_{ln}\ln k_nr\}. \tag{6}$$

Here $\varphi_n^{I\mu}(\alpha)$ are the wave functions of the stationary states of the nucleus, satisfying the equation

$$H_{vib}\varphi_n^{l\mu} = E_n\,\varphi_n^{l\mu}. \tag{7}$$

The oscillatory levels of the nucleus are characterized by the value of the total moment I, its projection μ, and the number of phonons n. The quantities k_n and η_n in (6) are the wave number and the Coulomb parameter $Z_1Z_2e^2/\hbar v$ of the incoming particle with energy $E - E_n$, respectively.

In the following we shall consider only the quadrupole ($\lambda = 2$) oscillations of even-even nuclei ($I_0 = \mu_0 = n_0 = 0$) with respect to the spherical equilibrium shape. Estimates show that the term $V_c(\mathbf{r}, \alpha)$ can here be regarded as a perturbation, as in the usual theory of the Coulomb excitation.

Our first task, therefore, is to solve the equation

$$H_0\Psi_0 = E\Psi_0, \tag{8}$$

where the Hamiltonian H_0 differs from the complete Hamiltonian (2) by the absence of the term $V_c(\mathbf{r}, \alpha)$.

We introduce the system of orthonormal functions

$$\Phi_{lin}^{JM} = \sum_\mu C_{l\mu,\,lM-\mu}^{JM}\,\varphi_n^{l\mu}(\alpha)\,Y_{l,M-\mu}(\theta,\varphi); \tag{9}$$

these are the eigenfunctions of the total moment of

the system J, its projection M, the moment of the nucleus I, and the moment of the particle l.

The function Ψ_0 is conveniently expressed in a form analogous to that used in ordinary scattering theory:

$$\Psi_0 = \sqrt{4\pi}\sum_l (kr)^{-1} i^{l+1}\sqrt{2l+1}\,\Psi_l^{(0)}(r,\alpha), \qquad (10)$$

where the functions $\Psi_l^{(0)}$ at $r\to\infty$ have the form

$$\Psi_l^{(0)} \to \Phi_{0l_0}^{l_0}\sin(k_0 r - l\pi/2 + \delta_l - \eta_0 \ln 2k_0 r) + \sum b_{0l_0,I'l'n'}^{(0)}\Phi_{I'l'n'}^{l_0}\exp\{ik_{n'}r - i\eta_{n'}\ln 2k_{n'}r\}. \qquad (11)$$

If the energy of the incoming particle is close to the height of the Coulomb barrier, the function $\Psi_l^{(0)}$ changes relatively slowly outside the nucleus for $r\sim R_0$, while it oscillates strongly inside the nucleus. This means that at the nuclear surface

$$\Psi_l^{(0)} \ll \partial\Psi_l^{(0)}/\partial(kr) \qquad (12)$$

so that we can make the approximation

$$\Psi_l^{(0)}[R(\theta,\varphi,\alpha)] = 0. \qquad (13)$$

The inequality (12) is not satisfied for certain resonance values of the energy; however, all these resonances lie above the Coulomb barrier and are therefore not important to us.

Outside the range of the nuclear forces the functions $\Psi_l^{(0)}$ can be expressed in the form

$$\Psi_l^{(0)} = F_l(k_0 r)\Phi_{0l_0}^{l_0} + \sum_{I'l'n'} b_{0l_0,I'l'n'}^{(0)}[G_{l'}(k_{n'}r) + iF_{l'}(k_{n'}r)]\Phi_{I'l'n'}^{l_0}, \qquad (14)$$

where $G_{l'}$ and $F_{l'}$ are the radial Coulomb functions, which for large r have the asymptotic forms

$$F_l \sim \sin(kr - l\pi/2 + \delta_l - \eta\ln 2kr),$$
$$G_l \sim \cos(kr - l\pi/2 + \delta_l - \eta\ln 2kr); \qquad (15)$$

the $b^{(0)}$ are certain unknown amplitudes. Condition (13) allows us to determine these amplitudes without considering the solution in the internal region at all. This condition can be rewritten in the form

$$F_l(k_0R)\Phi_{0l_0}^{l_0} + \sum_{I'l'n'} b_{0l_0,I'l'n'}^{(0)}[G_{l'}(k_{n'}R) + iF_{l'}(k_{n'}R)]\Phi_{I'l'n'}^{l_0}(\theta,\varphi,\alpha) = 0, \qquad (16)$$

where $R = R(\theta,\varphi,\alpha)$ is given by (2). Equation (16) must be satisfied for all values of θ, φ, α. The amplitudes $b^{(0)}$ are now found in exactly the same way as in the problem of the excitation of the rotational levels.[1]

By analogous methods we obtain

$$\beta_{0l_0,I'l'n'}^{(0)} = I_{0l_0,I'l'n'} - i\sum_{l'',I'',n''}\beta_{0l_0,I''l''n''}^{(0)} I_{I''l''n'',I'l'n'}F_{l''}(k_{n''}R_0)/G_{l''}(k_{n''}R_0), \qquad (17)$$

where

$$\beta_{0l_0,I'l'n'}^{(0)} = -b_{0l_0,I'l'n'}^{(0)}F_{l'}(k_0R_0)/G_{l'}(k_{n'}R_0), \qquad (18)$$

$$I_{Iln,I'l'n'} = \int \Phi_{I'l'n'}^{l_0*}\frac{f_{Iln}}{\gamma_{I'l'n'}}\Phi_{Iln}^{l_0}\,d\Omega\,d\alpha, \qquad (19)$$

$$f_{Iln} = F_l[k_nR(\theta,\varphi,\alpha)]/F_l(k_nR_0);$$
$$\gamma_{Iln} = G_l[k_nR(\theta,\varphi,\alpha)]/G_l(k_nR_0). \qquad (20)$$

As in reference 1, we have neglected in (17) all integrals which differ from (19) in that f is replaced by γ. Since in all known cases the distance between vibrational levels is ~ 1 Mev, we have $F_l(k_nR_0)/G_l(k_nR_0) \ll 1$ for $E \lesssim B$ and $n > 0$. In the sum over n'' in (17) we may therefore keep only the terms with $n'' = 0$. In the following we shall be interested in the excitation of the first vibrational level ($n' = 0$, $I' = 2$); for the corresponding amplitude we have

$$b_{0l_0,2l'1}^{(0)} = -\frac{F_l(k_0R_0)}{G_{l'}(k_1R_0)}\frac{I_{0l_0,2l'1}}{1 + i[F_l(k_0R_0)/G_l(k_0R_0)]I_{0l_0,0l_0}} \qquad (21)$$

The integrals $I_{Iln,I'l'n'}$ can be calculated by expanding the logarithm of the function f/γ in powers of the quantity $\sum\alpha_{2\mu}Y_{2\mu}$, keeping only the linear term:

$$\frac{f_{ln}}{\gamma_{l'n'}} \to \exp\left\{k_0R_0\left[\frac{F_l'(k_0R_0)}{F_l(k_0R_0)} - \frac{k_1G_{l'}'(k_1R_0)}{k_0G_{l'}(k_1R_0)}\right]\sum_\mu \alpha_{2\mu}Y_{2\mu}\right\} \qquad (22)$$

(the prime denotes differentiation of the function with respect to its argument). Using the equations satisfied by the functions F_l and G_l and formulas (32) and (33), it is easily shown that the neglected terms have the order $1/\eta$. Substituting (22) in (19), we obtain

$$I_{0l_0,0l_0} = a_{l_0,l_0};\quad I_{0l_0,2l'1} = a_{l_0,l'1}\alpha_0\varkappa_{l_0,l'1}\sqrt{5/4\pi}C_{l_020}^{l'0}; \qquad (23)$$

$$\varkappa_{ln,l'n'} = k_nR_0[F_l'(k_nR_0)/F_l(k_nR_0) - k_{n'}G_{l'}'(k_{n'}R_0)/k_{n'}G_{l'}(k_{n'}R_0)],$$
$$\alpha_0 = \hbar/\sqrt{2BC},\quad a_{ln,l'n'} = \exp\{(5\alpha_0^2/16\pi)\varkappa_{ln,l'n'}^2\}. \qquad (24)$$

Formulas (23), (24), and (20) solve the first part of the problem.

The exact amplitude b is connected with the amplitude found above, $b^{(0)}$, by the known relation

$$b_{Iln,I'l'n'} = b_{Iln,I'l'n'}^{(0)} + b_{Iln,I'l'n'}^{(c)}, \qquad (25)$$

$$b_{Iln,I'l'n'}^{(c)} = -\frac{2m}{k\hbar^2}\int\Psi_l^{(-)*}V_c\Psi_l^{(0)}\,dr\,d\alpha, \qquad (26)$$

where $\Psi_l^{(-)}$ is the l-th component in the expansion of the exact wave function $\Psi^{(-)}$, analogous to (10); for large r, $\Psi_l^{(-)}$ consists of an incident plane wave and an incoming spherical wave.

As already indicated, we regard V_c as a perturbation, and we can therefore replace the exact function $\Psi_l^{(-)}$ in (26) by $\Psi_l^{(-)(0)}$. It is easily seen

that we can also neglect the diverging wave in (26) which is due to the scattering by the nucleus. This leads to a small error in the total cross sections which is connected with the fact that the nuclear amplitudes $b^{(0)}$ decrease much faster with increasing l than the Coulomb amplitudes $b^{(C)}$.

Retaining in (26) only the "incoming" waves and assuming for simplicity that the charge density in the nucleus is constant, we find

$$b^{(c)}_{0l_0,2l'_1} = -(6\gamma/5)\, k_0 k_1 R_0^2 \alpha_0 \sqrt{5/4\pi}\, C^{l'0}_{l020}\, M^{-3}_{ll'}, \qquad (27)$$

where $M^{-3}_{ll'}$ is a radial matrix element defined by

$$M^{-3}_{ll'} = \frac{1}{k_0 k_1} \int_0^\infty F_{l'}(k_1 r)\, r^{-3} F_l(k_0 r)\, dr. \qquad (28)$$

For the total cross section for the excitation of the first vibrational level we now have

$$\sigma_{0\to 1} = \sigma^{(c)}_{0\to 1} + \sigma^{(n)}_{0\to 1} + \sigma^{(nc)}_{0\to 1},$$

where

$$\sigma^{(c)}_{0\to 1} = 4\pi k_0^{-2} \sum_{ll'} (2l+1)\, |b^{(c)}_{ll'}|^2 =$$

$$(45/16\pi^2) k_0^{-2} \gamma_1^2 (k_1/k_0)\, R_0^2 \alpha_0^2 (R_0/a)^2 f_{E2}(\eta, \xi), \qquad (29)$$

$$\sigma^{(n)}_{0\to 1} = 4\pi k_0^{-2} \sum_{ll'} (2l+1) |b^{(0)}_{0l_0,2l'_1}|^2, \qquad (30)$$

$$\sigma^{(nc)}_{0\to 1} = 8\pi k_0^{-2} \sum_{ll'} (2l+1)\, \mathrm{Re}[b^{(c)}_{0l_0,2l'_1}\, b^{(0)*}_{0l_0,2l'_1}]. \qquad (31)$$

Here $a = Z_1 Z_2 e^2/2E$, $\xi = \eta_0 - \eta_1$, and $f_{E2}(\eta, \xi)$ is a dimensionless function known in the theory of Coulomb excitation (tables for this function can be found, for example, in the review article by Alder et al.[3]).

To calculate $\sigma^{(n)}$ and $\sigma^{(nc)}$ it is necessary to know the Coulomb functions $F_l(kr)$ and $G_l(kr)$ near the classical turning point $kr = 2\eta$. In this region these functions are given with good accuracy by the expressions[4]

$$F_l = (2\eta_l)^{1/6} v\left[\frac{\eta + \sqrt{\eta^2 + l(l+1)} - kr}{(2\eta)^{1/3}}\right], \qquad (32)$$

$$G_l = (2\eta_l)^{1/6} u\left[\frac{\eta + \sqrt{\eta^2 + l(l+1)} - kr}{(2\eta)^{1/3}}\right], \qquad (33)$$

where u and v are Airy functions in the Fock notation.[5] These functions are related to the Bessel functions of order $1/3$ in the following way:

$$\begin{matrix} u(t) \\ v(t) \end{matrix} = \sqrt{\frac{\pi}{3}}\, t \left\{ I_{-1/3}\left(\frac{2}{3} t^{3/2}\right) \pm I_{1/3}\left(\frac{2}{3} t^{3/2}\right) \right\} \qquad t > 0,$$

$$\begin{matrix} u(t) \\ v(t) \end{matrix} = \sqrt{\frac{\pi}{3}}\, t \left\{ J_{-1/3}\left(\frac{2}{3} |t|^{3/2}\right) \mp J_{1/3}\left(\frac{2}{3} |t|^{3/2}\right) \right\} \qquad t < 0$$

[the upper sign refers to the function u(t)].

The important values of l in the sums (30) and (31) are $l \sim (2\eta)^{2/3}$. If the incoming particle is a proton, a typical value of η is $\eta \sim 3$. In this case it is easy to carry out the summations in (30) and (31) immediately. To evaluate the radial matrix elements $M^{-3}_{ll'}$ in (31), it is convenient to use the approximate quasi-classical expressions for them, which are quite accurate for $\eta > 1$:

$$M^{-3}_{ll'} = I_{2\mu}(\theta, \xi)/4\eta_l^2, \qquad \mu = l - l',$$

$$\theta = 2\sin^{-1}[1 + l(l+1)\eta^{-2}]^{-1/2},$$

where $I_{2\mu}(\theta, \xi)$ is a classical orbital integral known in the theory of Coulomb excitation.[6] Tables of the function $I_{2\mu}(\theta, \xi)$ are given, for example, in reference 3.

If the excitation of the nucleus is due to α particles, then $\eta \gg 1$ ($\eta \sim 10$) and the summation in (30) and (31) can be carried out analytically (with an accuracy up to terms of order $1/\eta$). Let us first consider the sum (30). It is seen from the expression (21) for the amplitudes $b^{(0)}_{ll'}$ that for $\eta \gg 1$ only the Clebsch-Gordan coefficient $C^{l'0}_{l020}$ depends strongly on the value l' for a given l; in the other factors we may set $l' = l$.

Since the Airy function is quite sensitive to changes of its argument of order unity, the root in (32) and (33) may be expanded in terms of powers of $l(l+1)/\eta^2$, keeping only the linear term. Furthermore, we can replace the summation over l in (30) by an integration over the variable $x = l(l+1)/(2\eta)^{4/3}$. We then obtain for $\sigma^{(n)}$

$$\sigma^{(n)} = 5(2\eta)^{1/3} R_0^2 \alpha_0^2 \int_0^\infty \left\{ a^2(z_0, z_1, x) \left[\frac{k_1 u'(x+z_1)}{k_0 u(x+z_1)} - \frac{v'(x+z_0)}{v(x+z_0)}\right]^2 \right.$$

$$\left. \times \frac{u^2(x+z_0)\, v^2(x+z_0)}{u^2(x+z_1)[u^2(x+z_0) + a^2(z_0, z_0, x)\, v^2(z_0+x)]} \right\} dx,$$

where

$$z_n = (2\eta_n - k_n R_0)/(2\eta_n)^{1/3},$$

$$a(z_n, z_p, x) = \exp\left\{ \frac{5\alpha_0^2}{16\pi} (k_n R_0)^2 \left[\frac{k_p u'(z_p+x)}{k_n u(z_p+x)} - \frac{v'(z_n+x)}{v(z_n+x)}\right]^2 \right\}$$

The integrand can now be written in the form

$$\left\{ a^2(z_0, z_1, x) \frac{v(z_0+x)\, u^3(z_0+x)}{u^2(z_1+x)} \left[\frac{k_1 u'(z_1+x)}{k_0 u(z_1+x)} - \frac{v'(z_0+x)}{v(z_0+x)}\right]^2 \right\}$$

$$\times \left\{ \frac{v(z_0+x)}{u^3(z_0+x)[1 + a^2(z_0, z_0, x)\, v^2(z_0+x)/u^2(z_0+x)]} \right\}$$

For all values of the excitation energy of the first vibrational level occuring in real cases, the first factor depends very weakly on x as compared to the second factor (in a typical case, $\eta_0 = 10$, $k_0 R_0 = 2\eta_0$ and $\eta_1 = 9.5$, it varies by less than 20%, whereas the second factor changes by more than two orders of magnitude). This comes from the fact that in the considered region of values of the arguments, the Airy functions change monotonically, while the logarithmic derivatives u'/u and v'/v, the products v(x)u(x),

and the ratios $u(x+a)/u(x+b)$ vary slowly (not exponentially) in comparison with expressions of the type u^{-2} or v/u.

The first factor can therefore be pulled out from under the integral sign, with $x = 0$. To calculate the remaining integral it is convenient to change to a new variable of integration, $t = v(z_0+x)/u(z_0+x)$; by virtue of the relation $u'v - uv' = 1$ we have

$$dx / u^2(z_0 + x) = dt.$$

The slowly varying quantity $a(z_0, z_0, x)$ must be regarded as a constant, setting $x = 0$.

As a result we obtain

$$\sigma^{(n)} = {}^5/_2 R_0^2 (2\eta)^{2/3} \alpha_0^2 \frac{a^2(z_0, z_1, 0)}{a^2(z_0, z_0, 0)} \frac{v(z_0) u^3(z_0)}{u(z_1)} \times \left[\frac{k_1 u'(z_1)}{k_0 u(z_1)} - \frac{v'(z_0)}{v(z_0)}\right]^2 \ln\left[1 + a^2(z_0, z_0, 0) \frac{v^2(z_0)}{u^2(z_0)}\right]. \quad (34)$$

The summation in expression (31) for $\sigma^{(nc)}$ can be carried out in an entirely analogous fashion. The factor $I_{2\mu}(\theta, \xi)$ can be taken out of the integral with $\theta = \pi$ (i.e., $l = 0$).

We finally obtain for $\sigma^{(nc)}$:

$$\sigma^{(nc)} = 6(k_1 R_0) R_0^2 \alpha_0^2 \left[\frac{k_1 u'(z_1)}{k_0 u(z_1)} - \frac{v'(z_0)}{v(z_0)}\right] \frac{a(z_0, z_1, 0)}{a(z_0, z_0, 0)} \times \frac{v(z_0) u^2(z_0)}{u(z_1)} I_{20}(\pi, \xi) \tan^{-1}\left\{a(z_0, z_0, 0) \frac{v(z_0)}{u(z_0)}\right\}. \quad (35)$$

We note that all quantities $a(z, z, 0)$ are very close to unity for the parameter values occuring in reality.

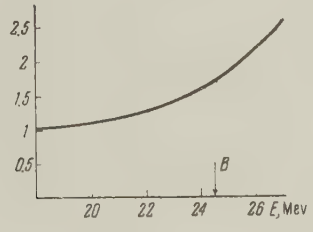

The figure shows the ratio of the total cross section for the excitation of the first vibrational level over the cross section for Coulomb excitation by α particles for the nucleus $_{52}Te^{120}$ ($E_1 = 0.56$ Mev).

In the case of protons the nuclear corrections are more important.

We note in conclusion that in the case of α particles we can replace the boundary condition (12) by the condition of complete absorption, accounting for the presence of a diffuse boundary in the same way as was done in the discussion of the excitation of the rotational levels. Our discussion is easily generalized to the case $I_0 \neq 0$, $\lambda \neq 2$. The excitation of higher vibrational levels ($n > 1$) has to be considered together with terms of higher orders in V_C. This is connected with great difficulties, since the adiabatic approximation is not applicable in this case.

[1] A. D. Piliya, JETP **37**, 583 (1959), Soviet Phys. JETP **10**, 413 (1960).

[2] A. Bohr, Kgl. Danske Videnskab. Selskab, Mat.-fys. Medd. **26**, No. 14 (1952).

[3] Alder, Bohr, Huus, Mottelson, and Winther, Revs. Modern Phys. **28**, 432 (1956).

[4] Biedenharn, Gluckstern, Hull, and Breit, Phys. Rev. **97**, 542 (1955).

[5] V. A. Fock, Таблицы функций Эйри (Tables of Airy Functions), M. 1946.

[6] K. A. Ter-Martirosyan, JETP **22**, 284 (1952).

Translated by R. Lipperheide
281

*RELATIVISTIC SPHERICAL FUNCTIONS. II.**

A. Z. DOLGINOV and I. N. TOPTYGIN

Leningrad Physico-technical Institute, Academy of Sciences, U.S.S.R..

Submitted to JETP editor June 25, 1959

J. Exptl. Theoret. Phys. (U.S.S.R.) **37**, 1441-1451 (November, 1959)

Properties of infinite-dimensional representations of the Lorentz group are considered which are of interest for the solution of problems in relativistic elementary particle theory. Infinite-dimensional representations are applied to an analysis of the amplitude of the reaction $a + b \rightarrow c + d$.

1. INTRODUCTION

A study of the symmetry properties of a system of particles enables one to draw a number of important conclusions with respect to the behavior of the system even in the case when the nature of the interaction between the particles is unknown. The conditions of invariance of a problem under different groups of transformations impose strong limitations on possible types of solutions. These restrictions are widely used in the analysis of the processes of interaction between particles. Particularly wide use is made of the symmetry properties of a system with respect to the group of rotations and reflections of three-dimensional space. In contrast to the representations of the three-dimensional group the representations of the Lorentz group are utilized comparatively infrequently. This refers particularly to the infinite-dimensional representations of this group. But they may turn out to be useful both in the phenomenological analysis of processes involving relativistic particles, and also in the development of field theory.

One of the reasons for this insufficient utilization of the irreducible representations of the Lorentz group is the lack of mathematical apparatus similar to the one available in the case of the three-dimensional group. For finite-dimensional representations of the Lorentz group such a formalism was developed in an article by one of the authors.[1] The present paper is a continuation of the earlier one.[1] In the present paper a study is made of the infinite-dimensional representations of the Lorentz group in connection with their applications to different problems of the relativistic theory of elementary particles. A discussion is given of the possibility of utilizing the basis functions of this group for the solution of the equations of quantum field theory. The reaction $a + b \rightarrow c + d$ is discussed. The amplitude of this reaction is expanded in terms of the basis functions of the infinite-dimensional representation. The coefficients of such an expansion depend only on the nature of the interaction between the particles, and not on the kinematics of the process. For high-energy particles the method of analyzing the reaction amplitudes outlined here is simpler and more convenient than the usual phase analysis.

Infinite-dimensional representations of the Lorentz group have been utilized by a number of authors. Ginzburg and Tamm,[2] Gel'fand and Yaglom,[3] Dirac[4] and others have used them for the development of a theory of elementary particles with a spectrum of spins and masses, E. M. Lifshitz[5] has used them for the solution of the problem of the stability of an expanding universe, I. S. Shapiro[6] has used them for a relativistically-invariant classification of the states of elementary particles, etc. The results of the present paper may be applied to the problems enumerated above. One of the main methodological advantages of our method of investigating the infinite-dimensional representations as compared with the investigations of other authors is the possibility of utilizing the techniques of Clebsch-Gordan, Racah, and Fano which have become widespread in physics.

2. THE BASIS FUNCTIONS OF THE UNITARY INFINITE-DIMENSIONAL REPRESENTATIONS OF THE LORENTZ GROUP

The representations of the Lorentz group are determined by the eigenvalues of two invariants which can be constructed from the components of the operator for the infinitesimal rotation $M_{\alpha\beta}$ in four-dimensional space. If **H** is the space-like,

*This is a continuation of a paper by one of the authors,[1] published in JETP under the same title.

and $\mathbf{F}$ is the time-like part of $M_{\alpha\beta}$ then the invariants are given by $M^2 = H^2 - F^2$ and $(\mathbf{HF})$. If $M_{\alpha\beta}$ operates on functions which depend only on the coordinates and do not contain any spin variables, then the second invariant is equal to zero and the representation is determined by specifying the eigenvalue of M^2.

The basis functions of the irreducible finite-dimensional representations given in reference 1 for the time-like case ($t = \rho \cosh \alpha$, $r = |\rho| \times \sinh \alpha$, $0 \leq \alpha \leq \infty$, $-\infty \leq \rho \leq \infty$) are of the following form

$$\Psi_{nlm}(\alpha, \vartheta, \varphi) = \Pi_l(n, \alpha) Y_{lm}(\vartheta, \varphi), \tag{1}$$

$$\Pi_l(n, \alpha) = \frac{\sinh^l \alpha}{\sqrt{n^2(n^2-1^2)(n^2-2^2)\ldots(n^2-l^2)}} \frac{d^{l+1}\cosh n\alpha}{d\cosh^{l+1}\alpha} \tag{2}$$

By replacing n in (2) by iN, where N is a real number which takes on all values in the range $0 \leq N \leq \infty$, we obtain the basis functions of the principal series of the unitary irreducible infinite-dimensional representations of the Lorentz group:

$$\Psi_{Nlm}(\alpha, \vartheta, \varphi) = \Pi_l(N, \alpha) Y_{lm}(\vartheta, \varphi)$$

$$= \frac{\sinh^l \alpha}{M_l} \frac{d^{l+1}\cos N\alpha}{d\cosh^{l+1}\alpha} Y_{lm}(\vartheta, \varphi),$$

$$M_l = \sqrt{N^2(N^2+1^2)\ldots(N^2+l^2)}. \tag{3}$$

In the papers of Gel'fand and Naĭmark[7] it is shown that the basis functions of the Lorentz group must satisfy the following relations:

$$H_\mu \Psi_{Nlm} = \sqrt{l(l+1)}\, C^{lm+\mu}_{lm1\mu} \Psi_{Nlm+\mu},$$

$$F_\mu \Psi_{Nlm} = i \sum_{l'} C^{Nl}_{l'} C^{l0}_{l'010} C^{l'm+\mu}_{lm1\mu} \Psi_{Nl'm+\mu},$$

$$C^{Nl}_{l-1} = -\sqrt{N^2+l^2}, \quad C^{Nl}_{l+1} = \sqrt{N^2+(l+1)^2}; \tag{4}$$

$$\mathbf{H} = -i[\mathbf{n}\times\nabla^\omega], \quad \mathbf{F} = -i[\mathbf{n}\,\partial/\partial\alpha + \coth\alpha\nabla^\omega]. \tag{5}$$

Here $\mathbf{rn} = \mathbf{r}$, ∇^ω is the angular part of the operator ∇, and H_μ and F_μ are the cyclic components* of $\mathbf{H}$ and $\mathbf{F}$.

Formulas (4) define the basis functions of an infinite-dimensional irreducible unitary representation for which $k_0 = 0$, $c = iN$, where $c^2 - 1$ and k_0 are the eigenvalues of the two invariants of the group in the notation of reference 7. One can easily show by means of a direct substitution that (4) is valid for the function (3).

*The cyclic components of a vector $\mathbf{a}$ are related to its Cartesian components by the equations $a_{\pm1} = \pm(a_x \pm ia_y)\sqrt{2}$, $a_0 = a_z$; our definition of the spherical harmonics $Y_{lm}(\vartheta, \varphi)$ is the same as the one used by Bethe,[8] and differs by the factor $(-1)^m$ from the functions listed by Condon and Shortley.[9]

From (4) we may obtain recurrence relations for $\Pi_l(N, \alpha)$:

$$d\Pi_l/d\alpha = -(l+1)\coth\alpha\Pi_l - \sqrt{N^2+l^2}\,\Pi_{l-1},$$
$$d\Pi_l/d\alpha = l\coth\alpha\Pi_l + \sqrt{N^2+(l+1)^2}\,\Pi_{l+1}, \tag{6}$$

which lead to the following second order equation

$$\frac{d^2\Pi_l}{d\alpha^2} + 2\coth\alpha\frac{d\Pi_l}{d\alpha} - \frac{l(l+1)}{\sinh^2\alpha}\Pi_l + (N^2+1)\Pi_l = 0. \tag{7}$$

The function $\Pi_l(N, \alpha)$ may also be expressed in terms of the following integral

$$\Pi_l(N, \alpha) = (-1)^{l+1}\frac{M_l}{\sinh^{l+1}\alpha}\int_0^\alpha \cos N\beta \frac{(\cosh\alpha - \cosh\beta)^l}{l!}\,d\beta. \tag{8}$$

It can be easily verified that (8) satisfies (6), and reduces to (3) when $l = 0$. This proves the identity of expressions (8) and (3). The normalization of $\Pi_l(N, \alpha)$ is such that

$$\int_0^\infty \Pi_l(N, \alpha)\Pi_l(N', \alpha)\sinh^2\alpha d\alpha = \frac{\pi}{2}\delta(N - N'). \tag{9}$$

Π_l has no singularities over the whole range of values of α and satisfies the condition $\Pi_l(N, 0) = -N\delta_{l_0}$.

Relations analogous to (6) — (8) were obtained by Fock[10] for the four-dimensional spherical harmonics in Euclidean space.

To obtain the recurrence relations and the equation for the space-like case ($t = \rho\sinh\alpha$, $r = \rho\cosh\alpha$, $-\infty \leq \alpha \leq \infty$, $0 \leq \rho \leq \infty$), one should replace in (6) and (7) $\sinh\alpha$ by $\cosh\alpha$ and vice versa. As we have already noted in reference 1, the space-like function Ψ_{Nlm} can be obtained from (3) for the time-like case by means of replacing α by $\alpha \pm i\pi/2$. For our two linearly independent functions we may choose

$$\Psi^{\pm}_{Nlm}(\alpha, \vartheta, \varphi) = i^l\frac{\cosh\alpha}{M_l}\frac{d^{l+1}\cos N(\alpha \pm i\pi/2)}{d\sinh^{l+1}\alpha} Y_{lm}(\vartheta, \varphi). \tag{10}$$

These functions are orthogonal and are normalized by the condition

$$\int_{-\infty}^{\infty}\cosh^2\alpha d\alpha \int d\Omega\, \Psi^*_{N_1l_1m_1}(-\alpha, \vartheta, \varphi)\Psi_{N_2l_2m_2}(\alpha, \vartheta, \varphi)$$
$$= \pi\delta_{l_1l_2}\delta_{m_1m_2}\delta(N_1 - N_2). \tag{11}$$

3. MATRICES FOR THE ROTATION OPERATOR IN FOUR-DIMENSIONAL PSEUDO-EUCLIDEAN SPACE

Every proper Lorentz transformation may be represented in the form of three successive transformations: a) a spatial rotation, defined by the Eulerian angles $\varphi_1 = \Phi$, $\vartheta = \theta$, and $\varphi_2 = 0$; b) a transformation to a coordinate system which

has the velocity $v = \tanh\psi$ along the new z axis ($0 \le \psi \le \infty$, the velocity of light is $c = 1$), while the direction of the velocity is determined in the initial system by the polar angles θ and Φ;
c) a second spatial rotation, defined by the angles φ_1, ϑ, and φ_2.

To obtain the matrix elements of the rotation operator we have to construct the matrices for each of the three rotations a), b), c) and multiply them together. The Cayley-Klein coefficients for the spatial rotation have the following form

$$\alpha = \delta^* = \exp\left\{\frac{1}{2} i (\varphi_1 + \varphi_2)\right\} \cos\frac{\vartheta}{2},$$
$$\beta = -\gamma^* = -\exp\left\{-\frac{1}{2} i (\varphi_1 - \varphi_2)\right\} \sin\frac{\vartheta}{2}. \quad (12)$$

A rotation through the angle ψ in the (z, t) plane is specified by the quantities

$$\alpha = \exp(-\psi/2), \quad \delta = \exp(\psi/2), \quad \beta = \gamma = 0. \quad (13)$$

Let $U^{Jj}_{M\mu}$ be the basis function of an irreducible finite-dimensional representation of dimension $(2J+1)(2j+1)$, where J and j are defined by the eigenvalues of the two group invariants. In the notation of Gel'fand and Naĭmark[7] $k_0 = |J - j|$, $c = n = J + j + 1$. The transformation of $U^{Jj}_{M\mu}$ under four-dimensional rotations is defined by the following equation

$$U^{Jj}_{M\mu}(A) = \sum_{M'\mu'} D^{Jj}_{M\mu M'\mu'}(\Omega_2, \psi, \Omega_1)\, U^{Jj}_{M'\mu'}(A'), \quad (14)$$

where $U^{Jj}_{M\mu}(A)$ is taken in the original, and $U^{Jj}_{M'\mu'}(A')$ in the new coordinate system. The matrix elements of the four-dimensional rotation operator $D^{Jj}_{M\mu M'\mu'}(\Omega_2, \psi, \Omega_1)$ were given in reference 1 for the case $\Omega_2 = 0$. With the aid of (12) and (13) we can obtain, in a manner analogous to that used in reference 1, the general expression for the rotation matrix

$$D^{Jj}_{M\mu\, M'\mu'}(\Omega_2, \psi, \Omega_1) = \sum_{ll'\varkappa} (-1)^{\mu-\mu'} C^{lm}_{J-Mj\mu} C^{l'm'}_{J-M'j\mu'} D^{l}_{m\varkappa}$$
$$\times (\Phi, \theta, 0)\, D^{l'}_{\varkappa m'}(\varphi_1, \vartheta, \varphi_2)\, Q^{ll'}_{Jj\varkappa}(\psi). \quad (15)$$

$$Q^{ll'}_{Jj\varkappa}(\psi) = \sum_{\Lambda\lambda} C^{l\varkappa}_{J-\Lambda j\lambda} C^{l'\varkappa}_{J-\Lambda j\lambda} \exp\{(\Lambda + \lambda)\psi\}. \quad (16)$$

$D^{l}_{mm'}$ are the well-known matrix elements of the three-dimensional rotation operator:[11]

$$D^{l}_{mm'}(\varphi_1, \vartheta, \varphi_2) = \sum (-1)^k$$
$$\times \frac{[(l+m)!\,(l-m)!\;\;(l+m')!\,(l-m')!]^{1/2}}{(l+m'-k)!\,(l-m-k)!\,(m-m'+k)!\,k!}$$
$$\times e^{im\varphi_1} \left(\cos\frac{\vartheta}{2}\right)^{2l+m'-m-2k} \left(\sin\frac{\vartheta}{2}\right)^{2k-m'+m} e^{im'\varphi_2}. \quad (17)$$

In accordance with our definition of the angles of rotation the following equalities hold:

$$Y_{lm}(\theta, \Phi) = \sum_{m'} D^{l}_{mm'}(\varphi, \vartheta, \varphi_2)\, Y_{lm'}(\theta', \Phi'),$$
$$Y_{lm}(\vartheta, \varphi) = \sqrt{(2l+1)/4\pi}\, D^{l}_{m0}(\varphi, \vartheta, \varphi_2). \quad (18)$$

The function $D^{Jj}_{M\mu M'\mu'}$ transforms according to the $(2J+1)(2j+1)$-dimensional irreducible representation of the Lorentz group.

The rotation matrices for the functions Ψ_{nlm} can be easily obtained with the aid of (15) and formula (22) of reference 1. If

$$\Psi_{nlm}(\alpha, \vartheta, \varphi) = \sum_{l'm'} T^{n}_{lml'm'}(\Omega_2, \psi, \Omega_1)\, \Psi_{nl'm'}(\alpha', \vartheta', \varphi'), \quad (19)$$

then we have

$$T^{n}_{lml'm'}(\Omega_2, \psi, \Omega_1) = \sum_{\varkappa} D^{l}_{m\varkappa}(\Phi, \theta, 0)\, Q^{ll'}_{n\varkappa}(\psi)\, D^{l'}_{\varkappa m}(\varphi_1, \vartheta, \varphi_2), \quad (20)$$

where

$$Q^{ll'}_{n\varkappa} \equiv Q^{ll'}_{JJ\varkappa}, \quad n = 2J + 1.$$

On setting in (19) $\alpha' = \vartheta' = \varphi' = 0$, we obtain

$$\Psi_{nlm}(\alpha, \theta, \Phi) = (n/\sqrt{4\pi})\, T^{n}_{lm00}(\Omega_2, \alpha, \Omega_1) \quad (21)$$

and, in particular,

$$\Pi_l(n, \alpha) = (n/\sqrt{2l+1})\, Q^{l0}_{n0}(\alpha). \quad (22)$$

The matrices which transform the basis functions of the infinite-dimensional unitary representation will differ from (20) only by the form of the function $Q^{ll'}_{N\kappa}(\psi)$, since the spatial parts of Ψ_{nlm} and Ψ_{Nlm} are the same. In order to determine $Q^{ll'}_{N\kappa}(\psi)$, we must find the explicit form of the operator corresponding to the infinitesimal rotation **F**. This operator will depend on six variables θ, Φ, ψ, φ_1, ϑ, and φ_2. The result of its operation on $T^{N}_{lml'm'}$ is defined by a formula analogous to (4),

$$F_\mu T^{N}_{LMlm} = i \sum_{L'} C^{NL}_{L'} C^{L0}_{L'010} C^{L'M+\mu}_{LM1\mu} T^{N}_{L'M+\mu lm}. \quad (23)$$

We need not consider the operator **H**, since it does not operate on ψ. The explicit form of F_μ can be found by means of the well-known method of constructing the operators for an infinitesimal rotation.[7] We obtain

$$iF_\mu = n_\mu \frac{\partial}{\partial\psi} + \coth\psi \nabla^{\Omega}_{\mu} + \frac{1}{\sinh\psi}$$
$$\times \{D^{1}_{\mu-1}(\Phi, \theta, 0)\, L_{-1} - D^{1}_{\mu 1}(\Phi, \theta, 0)\, L_1\}. \quad (24)$$

Here $n_\mu(\theta, \Phi)$ is a unit vector; ∇^{Ω}_{μ} is the operator which under rotations transforms in the same way as the gradient

$$\nabla^{\Omega}_{\pm 1} = \pm \frac{e^{\pm i\varphi_1}}{\sqrt{2}} \left[\cos\theta \frac{\partial}{\partial\theta} \pm \frac{i}{\sin\theta} \frac{\partial}{\partial\Phi} \mp \cot\theta \frac{\partial}{\partial\varphi_1} \right],$$

$$\nabla^{\Omega}_{0} = -\sin\theta \frac{\partial}{\partial\theta}; \qquad (25)$$

L_μ is the operator of an infinitesimal rotation operating on the angles φ_1, ϑ, and φ_2:

$$L_{\pm 1} = \pm \frac{e^{\pm i\varphi_1}}{\sqrt{2}} \left[\pm \frac{\partial}{\partial\vartheta} + i\cot\vartheta \frac{\partial}{\partial\varphi_1} - \frac{i}{\sin\vartheta} \frac{\partial}{\partial\varphi_2} \right],$$

$$L_0 = -i \frac{\partial}{\partial\varphi_1}. \qquad (26)$$

On substituting T^N_{LMlm} into (3), and on separating the factors that depend on the spatial angles, we obtain three recurrence relations which interrelate the functions $Q^{Ll}_{N\kappa}(\psi)$ corresponding to different values of L and κ:

$$C^{L'\varkappa}_{L\varkappa 10}(dQ^{Ll}_{N\varkappa}/d\psi + \gamma^L_L \coth\psi Q^{Ll}_{N\varkappa}) + C^{NL}_{L'} C^{L0}_{L'010} Q^{L'l}_{N\varkappa} = \frac{\sqrt{l(l+1)}}{\sinh\psi}$$

$$\times (C^{l\varkappa}_{l\varkappa-111} C^{L'\varkappa}_{L\varkappa-111} Q^{Ll}_{N\varkappa-1} - C^{l\varkappa}_{l\varkappa+11-1} C^{L'\varkappa}_{L\varkappa+11-1} Q^{Ll}_{N\varkappa+1}); \qquad (27)$$

$$L' = L,\ L \pm 1, \quad \gamma^{L-1}_L = L+1,$$

$$\gamma^L_L = 1, \quad \gamma^{L+1}_L = -L,$$

$C^{NL}_{L'}$ is defined by formula (4).

The recurrence relations (27) completely define the function $Q^{Ll}_{N\kappa}(\psi)$. For $l = 0$ they reduce to (6). At the same time $\Pi_L(N, \alpha) = -(N/\sqrt{2L+1}) \times Q^{L0}_{N0}(\psi)$. If we construct the invariant operator $M^2 = H^2 - F^2$, which depends on the six angles, then from the equation

$$M^2 T^N_{LMlm} = -(N^2+1) T^N_{LMlm} \qquad (28)$$

we can obtain a system of second-order differential equations for $Q^{Ll}_{N\kappa}$:

$$\frac{d^2 Q^{Ll}_{N\varkappa}}{d\psi^2} + 2\coth\psi \frac{dQ^{Ll}_{N\varkappa}}{d\psi} - \frac{L(L+1)+l(l+1)}{\sinh^2\psi} Q^{Ll}_{N\varkappa}$$

$$+ \varkappa^2 \frac{(\cosh\psi - 1)^2}{\sinh^2\psi} Q^{Ll}_{N\varkappa} + (N^2+1) Q^{Ll}_{N\varkappa}$$

$$+ 2\sqrt{L(L+1)\,l(l+1)} \frac{\cosh\psi}{\sinh^2\psi} \sum_\mu C^{l\varkappa-\mu}_{l\varkappa 1-\mu} C^{L\varkappa-\mu}_{L\varkappa 1-\mu} Q^{Ll}_{N\varkappa-\mu} = 0. \qquad (29)$$

We note that for $N = -in$, where n is an integer, (27) and (29) will define the rotation matrix for the basis functions ψ_{nlm} of the finite-dimensional representations; for complex values of N we shall obtain the rotation matrix for the basis functions of the infinite-dimensional nonunitary representations.

We can verify directly that the recurrence relations (27) and the equations (29) will be satisfied by the function $Q^{Ll}_{N\kappa}(\psi)$ which is obtained by means of analytic continuation of (16) into the region of purely imaginary values of $n = 2J+1 = iN$, $J = j$.

On taking into account the fact that $\Pi_l(n, \alpha)$ may be represented in the following form[1]

$$\Pi_l(n, \alpha) = \sum_\mu C^{J\mu}_{J\mu l0} e^{2\mu\alpha}, \quad n = 2J+1, \qquad (30)$$

and on utilizing the explicit form (16) of $Q^{ll'}_{n\kappa}$, we obtain

$$Q^{ll'}_{n\varkappa}(\psi) = (-1)^\varkappa e^{\varkappa\psi} \sqrt{(2l+1)(2l'+1)/n} \times$$

$$\times \sum_s \sqrt{2s+1}\, C^{s0}_{l\varkappa l'-\varkappa} W(lJl'J; Js) \Pi_s(n, \psi). \qquad (31)$$

W(abcd; ef) is the Racah function.[12] It may be expressed in terms of the Γ function and the generalized hypergeometric function ${}_4F_3$ (see reference 13), which are defined both for real and for complex values of their arguments. This enables us to go over from (31) to the case of an infinite-dimensional representation. To achieve this, we must replace n in expression (31) by a complex number. In particular, for the case of an infinite-dimensional unitary representation we must replace n by iN. We then obtain

$$Q^{ll'}_{N\varkappa}(\psi) = e^{\varkappa\psi} \sum_s (2s+1) C^{l'\varkappa}_{l\varkappa s0} F(Nll's) \Pi_s(N, \psi), \qquad (32)$$

$$F(Nll's) = -(-i)^{l+l'+s} \sqrt{i(2l+1)/N}\, W$$

$$\times \left(\frac{iN-1}{2}\, l\, \frac{iN-1}{2}\, l';\ \frac{iN-1}{2}\, s \right) = \frac{(-1)^{l+l'+s} Nl!\ l'!\, s!}{M_l M_{l'} M_s}$$

$$\times \sqrt{\frac{(2l+1)(l+l'-s)!\,(l+s-l')!\,(l'+s-l)!}{(l+l'+s+1)!}}\, w(Nll's), \qquad (33)$$

$$w(Nll's)$$

$$= i \sum_k \frac{(-1)^k \Gamma(l+l'+1-k+iN)}{\Gamma(-s-k+iN)(l-k)!(l'-k)!(l+l'-s-k)!\, k!(s-l+k)!(s-l'+k)!}.$$

We note several symmetry properties of the function $Q^{ll'}_{N\kappa}$. It follows from (3), (27), and (32) that

$$Q^{ll'}_{N\varkappa}(\psi) = (-1)^{l+l'} Q^{l'l}_{N\varkappa}(\psi) = Q^{ll'}_{N,-\varkappa}(\psi) = (-1)^{l+l'} Q^{ll'}_{N\varkappa}(-\psi). \qquad (34)$$

The normalizing constant for T^N_{LMlm} can be calculated by utilizing (20) and the explicit form $Q^{ll'}_{N\kappa}$. On introducing the notation $d\Omega_1 = (1/4\pi)\sin\theta\, d\theta\, d\Phi$, $d\Omega_2 = (1/8\pi^2)\sin\vartheta\, d\vartheta\, d\varphi_1\, d\varphi_2$, we obtain

$$\int_0^\infty \sinh^2\psi d\psi \int T^{N'*}_{L'M'l'm'} T^N_{LMlm}\, d\Omega_1 d\Omega_2$$

$$= \frac{\pi}{2N^2} \delta(N - N') \delta_{LL'} \delta_{ll'} \delta_{MM'} \delta_{mm'}. \qquad (35)$$

The addition theorem for Π_l in the finite-dimensional case follows from formula (19):

$$\sum_l (2l+1) \Pi_l(n, \alpha) \Pi_l(n, \beta) = n\Pi_0(n, \alpha+\beta). \qquad (36)$$

The analogous formula for the infinite-dimensional representation has the following form

$$\sum_l (-1)^{l+1} (2l+1) \Pi_l(N, \alpha) \Pi_l(N, \beta) = N\Pi_0(N, \alpha+\beta). \qquad (37)$$

4. THE CLEBSCH-GORDAN EXPANSION FOR THE INFINITE-DIMENSIONAL REPRESENTATIONS OF THE LORENTZ GROUP

In reference 1 we have obtained the Clebsch-Gordan expansion for the finite-dimension representations:

$$\Psi_{n_1 l_1 m_1}\Psi_{n_2 l_2 m_2}=\sum_{n,l}\sqrt{n_1 n_2/4\pi n}\,A(n_1 l_1 n_2 l_2 nl)\,C^{lm}_{l_1 m_1 l_2 m_2}\Psi_{nlm},$$

$$A(n_1 l_1 n_2 l_2 nl)=n\sqrt{(2l_1+1)(2l_2+1)}\,X(J_1 J_1 l_1, J_2 J_2 l_2, JJl), \tag{38}$$

X(abc, def, ghs) are the Fano functions whose explicit form together with tables of particular values are given by Matsunobo and Takebe.[14] The coefficients A satisfy the following orthogonality relations:

$$\sum_{l_1 l_2} A(n_1 l_1 n_2 l_2 nl)\,A(n_1 l_1 n_2 l_2 n'l)=\delta_{nn'},$$

$$\sum_{n} A(n_1 l_1 n_2 l_2 nl)\,A(n_1 l_1' n_2 l_2' nl)=\delta_{l_1 l_1'}\delta_{l_2 l_2'}. \tag{39}$$

With the aid of (38) and (39) we may obtain the Clebsch-Gordan expansion

$$T^{n_1}_{l_1 m_1 l_1' m_1'}T^{n_2}_{l_2 m_2 l_2' m_2'}=\sum_{nll'}A(n_1 l_1 n_2 l_2 nl)$$
$$\times A(n_1 l_1' n_2 l_2' nl')\,C^{lm}_{l_1 m_1 l_2 m_2}C^{l'm'}_{l_1' m_1' l_2' m_2'}T^{n}_{lml'm'} \tag{40}$$

and the inverse expansion

$$T^{n}_{lml'm'}=\sum A(n_1 l_1 n_2 l_2 nl)\;A(n_1 l_1' n_2 l_2' nl')$$
$$\times C^{lm}_{l_1 m_1 l_2 m_2}C^{l'm'}_{l_1' m_1' l_2' m_2'}T^{n_1}_{l_1 m_1 l_1' m_1'}T^{n_2}_{l_2 m_2 l_2' m_2'} \tag{41}$$

In (41) the summation is carried out over all the allowable values of l_1, l_2, l_1', l_2', m_1, m_2, m_1', m_2'.

In accordance with reference 15 we shall seek the Clebsch-Gordan expansion of the product of basis functions Ψ_{Nlm} of the infinite-dimensional representation in the following form

$$\Psi_{N_1 l_1 m_1}\Psi_{N_2 l_2 m_2}=(1/\sqrt{4\pi})\sum_{l}$$
$$\times\int_0^\infty dN B(N_1 N_2 N)\,C(N_1 l_1 N_2 l_2 Nl)\,C^{lm}_{l_1 m_1 l_2 m_2}\Psi_{Nlm}, \tag{42}$$

and we shall require that $C(N_1 0 N_2 0 N 0)=-1$. By making use of the orthogonality of the functions Ψ_{Nlm} we obtain

$$B(N_1 N_2 N)=\pm\tfrac{1}{4}\sinh\pi N_1\sinh\pi N_2\sinh\pi N$$
$$\times\Big[\cosh\tfrac{\pi}{2}(N_1+N_2+N)\cosh\tfrac{\pi}{2}(N_1+N_2-N)$$
$$\times\cosh\tfrac{\pi}{2}(N+N_2-N_1)\cosh\tfrac{\pi}{2}(N+N_1-N_2)\Big]^{-1}. \tag{43}$$

The plus sign corresponds to the time-like, and the minus sign to the space-like case. To determine the expansion coefficient $C(N_1 l_1 N_2 l_2 Nl)$, we apply to both sides of (42) the operator F_μ (24), and then expand products of the type $\Psi_{N_1 l_1 m_1}\times\Psi_{N_2 l_2' m_2+\mu}$, which will appear in the left hand side of the equation, again by utilizing (42). By equating coefficients of Ψ_{Nlm} on both sides of the equation, and by utilizing the orthogonality properties of the coefficients $C\begin{smallmatrix}\cdot\cdot\cdot\\ \cdot\cdot\cdot\end{smallmatrix}$, we obtain the following recurrence relations

$$C(N_1 l_1 N_2 l_2 Nl')\,C^{Nl}_{l'0}C^{l'0}_{l010}$$
$$=\sum_{l_1'}C(N_1 l_1' N_2 l_2 Nl)\,C^{N_1 l_1}_{l_1'}C^{l_1 0}_{l_1 010}\,U(l_1 l_2 1l;\ l'l_1')$$
$$+\sum_{l_2'}C(N_1 l_1 N_2 l_2' Nl)C^{N_2 l_2}_{l_2'}C^{l_2 0}_{l_2 010}\,U(l_2 l_1 1l;\ l'l_2'),\quad l'=l,l\pm 1,$$
$$U(abcd;\ ef)=\sqrt{(2e+1)(2f+1)}\,W(abcd;\ ef). \tag{44}$$

The relations (44) enable us to define the function $C(N_1 l_1 N_2 l_2 Nl)$ for arbitrary l_1, l_2 and l. It has the following symmetry properties:

$$C(N_1 l_1 N_2 l_2 Nl)=C(N_2 l_2 N_1 l_1 Nl)$$
$$=(-1)^{l_2}\sqrt{\frac{2l+1}{2l_1+1}}\,C(N_2 l_2 Nl N_1 l_1), \tag{45}$$

$C(N_1 l_1 N_2 l_2 Nl)=0$ if l_1+l_2+l is an odd integer. These properties become obvious if we express $C(N_1 l_1 N_2 l_2 Nl)$ in terms of an integral of the product of three $\Pi_l(N,\alpha)$, by utilizing (42).

We shall seek the expansion which is the inverse of (42) in the form

$$\Psi_{Nlm}=(N\sqrt{4\pi}/N_1 N_2)\sum_{l_1 m_1 l_2 m_2}\tilde{C}(N_1 l_1 N_2 l_2 Nl)$$
$$\times C^{lm}_{l_1 m_1 l_2 m_2}\Psi_{N_1 l_1 m_1}\Psi_{N_2 l_2 m_2}. \tag{46}$$

On setting $\alpha=0$ in both sides of this equation we obtain $\tilde{C}(N_1 0 N_2 0 N 0)=-1$. The recurrence relations between $\tilde{C}$ and different values of l_1, l_2, and l can be obtained in the same way as for C. They are identical with (44), from which it follows that $\tilde{C}(N_1 l_1 N_2 l_2 Nl)$ coincides with $C(N_1 l_1 N_2 l_2 Nl)$.

From (42) and (46) we obtain the orthogonality relation*

$$\int_0^\infty N dN B(N_1 N_2 N)\,C(N_1 l_1 N_2 l_2 Nl)\,C(N_1 l_1' N_2 l_2' Nl)$$
$$=N_1 N_2\delta_{l_1 l_1'}\delta_{l_2 l_2'},$$

$$NB(N_1 N_2 N)\sum_{l_1 l_2}C(N_1 l_1 N_2 l_2 Nl)\,C(N_1 l_1 N_2 l_2 N'l)$$
$$=N_1 N_2\delta(N-N'). \tag{47}$$

The coefficients $C(N_1 l_1 N_2 l_2 Nl)$ defined by the recurrence relations (44) are identical, up to a constant factor, with the Fano function of complex arguments:

*We note that in reference 15 the factor $B(n_1 n_2 n)$ has been omitted in the right hand sides of (7) and (8); the factor $-\frac{1}{4}$ is lacking in the expression for $B(n_1 n_2 n)$ [formula (6)].

$$C(N_1l_1N_2l_2Nl) = i^{l-l_1-l_2}\sqrt{iNN_1N_2(2l_1+1)(2l_2+1)}$$

$$\times X(J_1J_1l_1,\ J_2J_2l_2,\ JJl).$$

$$J_k = {}^1/_2(iN_k - 1). \tag{48}$$

To calculate the particular values of the Fano function in (48), we can use the usual formula

$$X(J_1J_1l_1,\ J_2J_2l_2,\ JJl) = \sum_\lambda (2J_2 + 2\lambda + 1)\, W(JlJ_1J_2;\ JJ_2{+}\lambda)$$

$$\times W(l_1lJ_2J_2;\ l_2J_2 + \lambda)\, W(JJ_2J_1l_1,\ J_1J_2 + \lambda), \tag{49}$$

in which λ must take on all integral values from $-l_0$ to $+l_0$, where l_0 is the smallest of the three numbers l_1, l_2, and l.

The explicit form of the functions W and others, which was obtained by Racah for real values of J_k, is also preserved in the case of complex $J_k = \frac{1}{2}(iN_k - 1)$ if all the factorials are replaced by the corresponding Γ functions of complex argument. In order not to lose a phase factor in this process, we must in the process of squaring and of extracting the square root retain all the factors i, and only in the very last stage can we put -1 for the i^2 which are outside the radical.

From (42) and (46) we obtain the Clebsch-Gordan expansion

$$T^{N_1}_{l_1m_1l_1'm_1'}T^{N_2}_{l_2m_2l_2'm_2'} = \frac{1}{N_1N_2}\sum_{ll'}\int_0^\infty NdNB(N_1N_2N)$$

$$\times C(N_1l_1N_2l_2Nl)\, C(N_1l_1'N_2l_2'Nl')\, C^{lm}_{l_1m_1l_2m_2}C^{l'm'}_{l_1'm_1'l_2'm_2'}T^N_{lml'm'}. \tag{50}$$

The inverse expansion may be obtained by utilizing the orthogonality properties of the coefficients $C(N_1l_1N_2l_2Nl)$. It has the following form

$$(N/N_1N_2)\, B(N_1N_2N)\sum C(N_1l_1N_2l_2Nl)\, C(N_1l_1'N_2l_2'N'l')$$

$$\times C^{lm}_{l_1m_1l_2m_2}C^{l'm'}_{l_1'm_1'l_2'm_2'}T^{N_1}_{l_1m_1l_1'm_1'}T^{N_2}_{l_2m_2l_2'm_2'} = T^N_{lml'm'}\delta(N - N'). \tag{51}$$

All the formulas of this section, with the exception of (47), hold for both the time-like and the space-like case. In (47) a minus sign will appear in the right hand sides if $B(N_1N_2N)$ is negative (space-like case).

5. APPLICATION OF THE INFINITE-DIMENSIONAL REPRESENTATIONS TO THE STUDY OF RELATIVISTIC PROCESSES

1. The infinite-dimensional representations of the Lorentz group can be utilized for the spectral representation of the reaction amplitude. As an example we consider the reaction $a + b \to c + d$, and assume that the particles are spinless. Then the reaction amplitude will depend on the masses of the particles, and on three independent momenta, p_a, p_b, and p_c. To describe the angular and the energy distributions of the particles, the reaction amplitude is usually expanded in terms of spherical harmonics of the angles that specify p_i, and the energy dependence of the coefficients of these functions is then obtained. Such an expansion is inconvenient for relativistic processes since the convergence of the expansion becomes worse as the energy increases. The reaction amplitude, regarded as a function of the variables p_a, p_b, p_c, depends not only on the nature of the interaction, but also on the kinematics of the process. Since the amplitude is a scalar, it contains only invariant combinations of the momenta. Along with $p_i^2 = m_i^2$, we can choose as such combinations, for example, the two scalar products (p_ap_b) and (p_cp_d).

In order to characterize the process independently of the kinematics, and to describe the angular distribution without expanding in terms of spherical harmonics, we can utilize the expansion of the amplitude in terms of the infinite-dimensional representations of the Lorentz group. We denote the reaction amplitude by $A(m_i^2, p_i)$. The expansion of the amplitude in terms of the basis functions of the infinite-dimensional representation has the following form

$$A(m_i^2,\ p_i) = \int_0^\infty\int_0^\infty dN_1dN_2A(m_i^2, N_1, N_2)\,\Pi_0(N_1, \gamma_1)\,\Pi_0(N_2, \gamma_2). \tag{52}$$

Here we have

$$\Pi_0(N, \gamma) = -\sin N\gamma/\sinh\gamma,\ \cosh\gamma_1 = \cosh\alpha_a\cosh\alpha_b$$

$$-\sinh\alpha_a\sinh\alpha_b\cos\theta_{ab},$$

$$(p_ap_b) = m_am_b\cosh\gamma_1 = E_aE_b - p_ap_b,\ (p_cp_d) = m_cm_d\cosh\gamma_2.$$

The interaction process will be completely described by the quantity

$$A(m_i^2, N_1, N_2) = (4/\pi^2)\int d\omega_1d\omega_2A(m_i^2, p_i)\,\Pi_0(N_1, \gamma_1)\,\Pi_0(N_2, \gamma), \tag{53}$$

where $d\omega = \sinh^2\gamma\, d\gamma\, d\Omega$.

The whole angular and energy dependence of the amplitude is contained in the known functions $\Pi_0(N, \gamma)$. The expansions (52) and (53) hold for functions which are quadratically integrable over $d\omega$. If $A(m_i^2, p_i)$ is not such a function, then one can always separate the invariant factor in such a way that the remaining part will have the required properties.

If the particles that participate in the reaction have spin, then the amplitude will contain spin operators with factors that depend on the momenta and transform according to a finite-dimensional representation. The product of these factors and $\Pi_0(N, \gamma)$ can be expanded in terms of the infinite-

dimensional unitary representations and, thus, an expansion for the reaction amplitude can be obtained in the general case.

2. The infinite-dimensional representations can be utilized for the solution of equations of quantum field theory. As an example let us consider the simplest case — the D'Alembert equation. It can be easily seen that in this case the basis functions $\Psi_{Nlm}(\alpha, \vartheta, \varphi)$ enable us to separate variables. Indeed, in accordance with reference 15, we have

$$\partial_{\alpha\beta} G_N(\rho)\Psi_{Nlm}(\alpha,\vartheta,\varphi) = \pm\sum_{Lxf} i^{l-L}\left[\frac{\partial}{\partial\rho} - \varkappa\frac{iN-\varkappa}{\rho}\right]$$
$$\times G_N(\rho)\sqrt{\frac{N(2f+1)}{2\nu}}\, C^{1/2\alpha}_{1/2\beta f-\sigma} C^{L\Lambda}_{lmf\sigma} A(Nl\,2f\,\nu L)\Psi_{\nu L\Lambda}(\alpha,\vartheta,\varphi), \tag{54}$$

$i\nu = iN + \kappa$, $\kappa = \pm 1$, $G_N(\rho)$ depends only on ρ, while

$$\partial_{\pm 1/2 \pm 1/2} = \partial/\partial t \mp \partial/\partial z, \qquad \partial_{\pm 1/2 \mp 1/2} = \pm(\partial/\partial x \mp i\partial/\partial y).$$

The $\pm$ signs in (54) refer respectively to the cases $t^2 - r^2 > 0$ and $t^2 - r^2 < 0$. By applying the operator $\partial_{\alpha\beta}$ twice we obtain

$$\Box G_N(\rho)\Psi_{Nlm}(\alpha,\vartheta,\varphi) = -\tfrac{1}{2}\sum_{\alpha\beta}\partial^{\alpha\beta}\partial_{\alpha\beta} G_N(\rho)\Psi_{Nlm}(\alpha,\vartheta,\varphi)$$
$$= \left\{\frac{\partial^2}{\partial\rho^2} + \frac{3}{\rho}\frac{\partial}{\partial\rho} + \frac{N^2+1}{\rho^2}\right\} G_N(\rho)\Psi_{Nlm}(\alpha,\vartheta,\varphi). \tag{55}$$

For equations of a more complicated type, for example, the Bethe-Salpeter equation, a chain of equations in the variable ρ is obtained.

[1] A. Z. Dolginov, JETP **30**, 746 (1956), Soviet Phys. JETP **3**, 589 (1956).

[2] V. L. Ginzburg and I. E. Tamm, JETP **17**, 227 (1947).

[3] I. M. Gel'fand and A. M. Yaglom, JETP **18**, 703 (1948).

[4] P. A. M. Dirac, Proc. Roy. Soc. **A183**, 284 (1945).

[5] E. M. Lifshitz, J. Phys. **10**, 116 (1946).

[6] I. S. Shapiro, Dokl. Akad. Nauk S.S.S.R. **106**, 647 (1956), Soviet Phys.-Doklady **1**, 91 (1956).

[7] I. M. Gel'fand and M. A. Naĭmark, Izv. Akad. Nauk S.S.S.R., Ser. Mat. **11**, 411 (1947). M. A. Naĭmark, (Linear Representationsof the Lorentz Group), Moscow, 1958.

[8] H. Bethe, Quantum Mechanics of the One- and Two-Electron Systems (Russ. Transl.), M-L, 1935.

[9] E. U. Condon and G. H. Shortley, Theory of Atomic Spectra, Cambridge, 1944 (Russ. Transl., Moscow, 1949).

[10] V. A. Fock, Z. Physik **98**, 148 (1935).

[11] E. Wigner, Gruppentheorie, Braunschweig, 1931.

[12] G. Racah, Phys. Rev. **62**, 438 (1942).

[13] M. E. Rose, Multipole Fields, Wiley, N.Y., 1955 (Russ. Transl., Moscow, 1957).

[14] H. Matsunobo and H. Takebe, Progr. Theoret. Phys. (Kyoto) **14**, 1589 (1955).

[15] A. Z. Dolginov and I. N. Toptygin, JETP **35**, 794 (1958), Soviet Phys. JETP **8**, 550 (1959).

Translated by G. Volkoff
282

THE ZONE ENERGY SPECTRUM IN THE PRESENCE OF A MAGNETIC FIELD

G. E. ZIL' BERMAN

Khar'kov Aeronautical Engineering Military College

Submitted to JETP editor June 24, 1959

J. Exptl. Theoret. Phys. (U.S.S.R.) **37**, 1452-1454 (November, 1959)

Eigenfunctions (in the **k**-representation) are derived which describe the motion of an electron with an arbitrary dispersion law in a magnetic field, account being taken of two zones (and in particular of overlapping ones). A criterion for the applicability of the one-zone approximation is obtained.

THE state of an electron moving in the periodic field of a crystal is described, as is well known, by the wave vector **k** and by the number of the allowed energy zone s. If the crystal is placed in an external field, electric or magnetic, the eigenfunction of the electron is generall described in the form of an expansion

$$\psi = \sum_s \int g_s(\mathbf{k})\,\psi_{\mathbf{k}s}\,dk, \qquad (1)$$

covering all zones. However, if the external field satisfies the conditions for quasi-classical behavior (in the case of a magnetic field, this means that the minimum radius of rotation of the electron $\alpha_0 = \sqrt{\hbar c/eH}$ must be significantly larger than the lattice constant a), then a single zone can play the principal role in the expansion (1), as before. The aim of the present note is the clarification of the condition of admissibility of such a single zone approximation and the discovery of the eigenfunction (1) for this case. For simplicity of description, we shall consider only two zones, s and r.

We give the name "jump at a given point" to the energy difference $E_s(\mathbf{k}) - E_r(\mathbf{k})$ at a given point of **k**-space. Such a discontinuity can exist even in the presence of zones overlapping in energy. Inasmuch as $E_s(\mathbf{k})$ and $E_r(\mathbf{k})$ are different functions of **k**, the discontinuity at the point as a rule exists although the case of coincidence of E_s and E_r for some **k** can occur (degenerate zones). It will be shown below that the condition for admissibility of the single zone approximation in the magnetic field is the existence of a sufficiently large discontinuity at points lying on a given isoenergetic surface.

The problem of taking neighboring zones into account was considered previously by the author,[1] and also, in a much less general form, by Adams,[2] and Luttinger and Kohn.[3] In the presence of a magnetic field directed along the z axis and described by the vector potential $A_x = -Hy$, $A_y = A_z = 0$, it is expedient to write the expansion (1) in Bloch eigenfunctions, as was shown by the author:[4,1]

$$\psi_{\mathbf{k}s} = \sum_{\mathbf{h}} b_{\mathbf{h}s}(k_1, k_2, k_3)\, e^{i(\mathbf{k}+2\pi\mathbf{h})\mathbf{r}}, \qquad (2)$$

in which k_1 is replaced by $k_1 + y/\alpha_0^2$. We use Eq. (I) of reference 1 for $g_s(\mathbf{k})$, setting the potential of the electric field in it equal to zero, keeping the non-diagonal (interzone) "magnetic terms" of order α_0^{-2}, and leaving out two zones. Equation (I) can be described in the case under consideration in the form of a set of equations

$$\hat{E}_s g_s - \alpha_0^{-2}\hat{H}_{sr} g_r = E g_s, \qquad \hat{E}_r g_r - \alpha_0^{-2}\hat{H}_{rs} g_s = E g_r. \qquad (3)$$

Here (see, for example, references 4 and 1) $\hat{E}_s$ is the operator obtained from $E_s(k_1, k_2, k_3)$ by the substitution $k_1 \to k_1 - (1/i\alpha_0^2)\,\partial/\partial k_2$ and $\hat{H}_{sr}$ is an operator of the same type as $\hat{E}_s$, $\hat{E}_r$, depending, however, not only on the dispersion law of the electron in the crystal, but also on the wave functions in the zones s and r.

Those states are of interest to us in which g_r is small in comparison with g_s. We satisfy the system (3) by setting

$$g_r = \alpha_0^{-2}\Phi(\mathbf{k})\, g_s. \qquad (4)$$

Discarding terms of order α_0^{-4}, we obtain for g_s the "single zone" equation $\hat{E}_s g_s = E g_s$, the solution of which, as shown in reference 4, has the form

$$g_s = \left(\frac{\partial E_s}{\partial \varkappa_{1s}}\right)^{-1/2} \exp\left\{ + i\alpha_0^2 k_1 k_2 - i\alpha_0^2 \int_0^{k_2} \varkappa_{1s}\, dk_2 \right\},$$

$\varkappa_{1s}$ is the solution of the equation $E_s(\varkappa_{1s}, k_2, k_3) = E$.

Substituting (4) in the second equation of (3), we find $\Phi(\mathbf{k})$ (we can remove this quantity from

under the operator $\hat{E}_r$ since it is slowly changing). The action of the operator $\hat{H}_{rs}$ on g_s reduces after transformation to multiplication of g_s by the function $F_{rs}(\mathbf{k})$, which depends on the dispersion law and the wave functions in both zones [see (2)]:

$$F_{rs}(\mathbf{k}) = \sum_{\mathbf{h}} b_{\mathbf{h}r}(\mathbf{k}) \left\{ \frac{\hbar^2}{m}(k_2 + 2\pi h_2) \frac{\partial b_{\mathbf{h}s}}{\partial k_1} - \frac{\partial b_{\mathbf{h}s}}{\partial k_2} \frac{\partial E_s}{\partial k_1} \right\}. \quad (5)$$

The final form of g_r will be

$$g_r(\mathbf{k}) = \frac{i\alpha_0^{-2} F_{rs}(k)}{E_r(\varkappa_{1s}, k_2, k_3) - E_s(\varkappa_{1s}, k_2, k_3)} g_s(\mathbf{k}). \quad (6)$$

Consequently, the criterion for the admissibility of the single zone approximation has the form

$$|E_r(\mathbf{k}) - E_s(\mathbf{k})| \gg \alpha_0^{-2} F_{rs}. \quad (7)$$

The quantity F_{rs} is of order $\hbar^2/m^*$, where m^* is the effective mass in the basic zone (s); therefore, the inequality (7) can be written in the form

$$|E_r(\mathbf{k}) - E_s(\mathbf{k})| \gg \mu^* H. \quad (8)$$

It must be kept in mind that the inequalities (8) and (7), in accord with (8), must hold at points in $\mathbf{k}$-space lying on a surface of constant energy $E_s(\mathbf{k}) = E$.

Without calculation, we write down the corresponding criterion for an electron placed in crossed homogeneous magnetic H and electric F fields [it is assumed that the principal reason for the appearance of interzone terms is the electric field; in other words, we have the criterion (8)]:

$$|E_r(\mathbf{k}) - E_s(\mathbf{k})| \gg eFam/m^* \quad (9)$$

(a is the lattice constant). In the absence of a magnetic field, as was shown in reference 1, the inequality (9) holds again; however, in the presence of a magnetic field, only those points of $\mathbf{k}$-space enter into (9) which lie on a surface of constant energy.

The author takes this occasion to thank I. M. Lifshitz for discussions of the problem.

[1] G. E. Zilberman, JETP **36**, 1465 (1959), Soviet Phys. JETP **9**, 1040 (1959).

[2] E. Adams, Phys. Rev. **89**, 63 (1953).

[3] J. Luttinger and W. Kohn, Phys. Rev. **97**, 869 (1955).

[4] G. E. Zil'berman, JETP **32**, 296 (1957); **33**, 387 (1957); Soviet Phys. JETP **5**, 208 (1957); **6**, 299 (1958).

Translated by R. T. Beyer
283

Letters to the Editor

MEASUREMENT OF THE ENERGY LOSSES OF FAST ELECTRONS IN MATTER

I. A. GRISHAEV, A. N. FISUN, A. S. LITVINENKO, V. M. GRIZHKO, B. I. SHRAMENKO, and I. N. ONISHCHENKO

Physico-technical Institute, Academy of Sciences, Ukrainian S.S.R.

Submitted to JETP editor June 5, 1959

J. Exptl. Theoret. Phys. (U.S.S.R.) **37**, 1455-1456 (November, 1959)

ELECTRONS lose energy in passing through matter. The energy loss is due to the interaction of the electrons with nuclei and with shells of atoms of the stopping material. For electrons of intermediate energy the most probable energy losses are due to ionization of atoms of the material.

Using the Landau theory,[1] taking account of the Fermi corrections[2] for polarization of the medium, we can write the most probable energy loss for a relativistic electron as follows:[3]

$$-\Delta W = 0.1537 \frac{\Sigma Z}{\Sigma A} D \left(19.43 + \ln \frac{D}{\rho}\right) \text{Mev},$$

where Z is the atomic number of the stopping materials, A is the mass number, ρ is the density, and D is the surface density.

In the present note we describe results of experiments carried out to determine the most probable energy losses of 18-Mev electrons. The experimental arrangement is shown in Fig. 1.

By means of a 90° magnetic monochromator the primary electron beam is made monoenergetic to within ±0.2% (~± 40 kev). The energy losses are determined from the displacement of the maxima in the energy spectra obtained by means of the magnetic analyzer 4 with the sample placed in front of the beam in the experimental chamber 3 and with the sample removed. The accuracy of the measurements is ±40 kev.

Typical curves are shown in Fig. 2. In this case

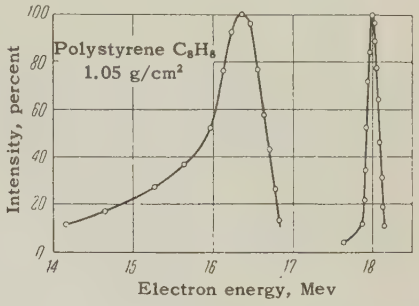

FIG. 2

the samples are targets of aluminum, polystyrene $(C_8H_8)_n$ and Plexiglas $(C_4H_8O_2)_n$. The results of the measurements are shown in the table, where we compare our data with the results obtained by Goldwasser[3] and with theory. Here ΔW is the loss predicted by the Landau theory with the Fermi correction, $(\Delta W)_G$ is the loss measured by Goldwasser, and $(\Delta W)_0$ is the result obtained in present experiment.

	Al	$(C_8H_8)_n$	$(C_4H_8O_2)_n$
D	0.81	1.055	0.559
ρ	2.694	1.055	1.130
ΔW	1.09	1.65	0.96
ΔW_G	0.99	1.61	—
ΔW_0	1.04	1.65	0.92

An examination of these results indicates good agreement between the theoretical and experimental values.

[1] L. Landau, J. Phys. (U.S.S.R.) **8**, 204 (1944).
[2] E. Fermi, Phys. Rev. **57**, 485 (1940).

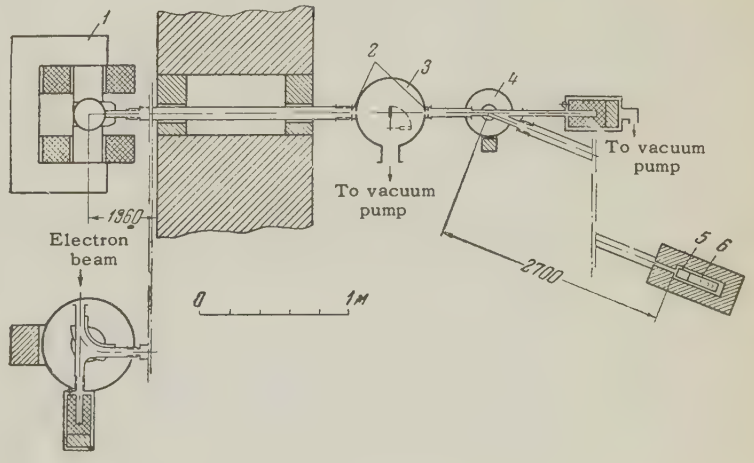

FIG. 1. 1 – magnetic monochromator, 2 – lead collimators, 3 – experimental chamber, 4 – magnetic analyzer, 5 – Cerenkov radiator, 6 – photomultiplier.

[3] Goldwasser, Mills, and Hanson, Phys. Rev. **88**, 1137 (1952).

Translated by H. Lashinsky
284

MEASUREMENT OF THE INTENSITY RATIO OF THE TRANSITIONS TO THE FIRST EXCITED LEVELS OF DAUGHTER NUCLEI IN THE DECAY OF U^{238} AND U^{234}

A. A. VOROB'EV, A. P. KOMAR, and V. A. KOROLEV

Leningrad Physico-technical Institute, Academy of Sciences, U.S.S.R.

Submitted to JETP editor June 12, 1959

J. Exptl. Theoret. Phys. (U.S.S.R.) **37**, 1456-1457 (November, 1959)

THE ratio of the intensities of the transitions to the first excited levels was measured by us with a pulse ionization chamber with a screen connected for coincidence with a scintillation counter with a NaI crystal. The latter registered the x-rays accompanying the α decay to the first excited levels of the daughter nuclei. In plotting the α spectra without coincidences, the lines corresponding to the transitions to the first excited level and to the ground state are incompletely resolved. Data on the transition intensities[1] obtained in this manner are therefore insufficiently accurate. Transitions to the ground state are not registered if coincidences with x-ray L-quanta are introduced, so that it becomes possible to determine reliably the relative intensities of the transitions to the first excited levels.

The α spectrum of a natural mixture of uranium isotopes, plotted in coincidence with x-ray L radiation, yielded the following information: 1) the number of pulses N_1 corresponding to the transition of U^{234} to the first excited level of Th^{230} is 1815; 2) the number of pulses N_2 corresponding to the transition of U^{238} to the first excited level Th^{234} is 1640. It is necessary to subtract from N_2 approximately 30 pulses, due to the decay of U^{235}. The calculations performed have shown that the errors in the intensities, due to the presence of two conversion lines L_{II} and L_{III} (different absorption, Auger effect, etc.) and to conversions on the M and N shells, are quite insignificant and result in a total correction of 0.7%. Taking this correction into account, we obtain for the intensity ratio $N_2/N_1 = 0.91 \pm 0.04$. The populations of the same levels were investigated previously by Teillac[2,3] by a method in which the conversion electrons were registered in thick photoemulsions. These measurements yielded a value of 0.75 for N_2/N_1. However, owing to the poor distribution of the groups of α particles and the small number of registered events, the accuracy of this ratio was small ($\sim 25\%$).

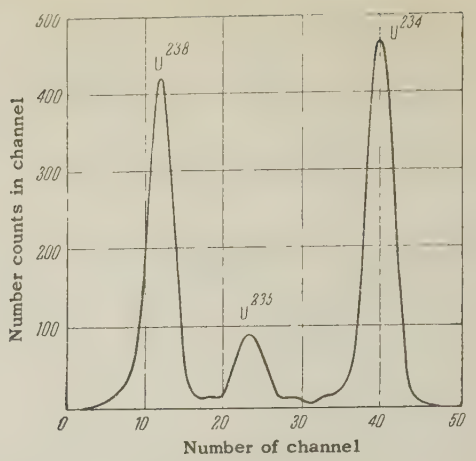

The intensity of the transition to the first excited level in the decay of U^{234}, measured with a magnetic spectrometer, amounts to 28%.[4] We therefore obtain a value of 25.5% for the intensity of the analogous transition in the decay of U^{238}. (The accuracy of this value is determined essentially by the accuracy of the measurements made by Gol'din, Tret'yakov, and Novikova,[4] which, unfortunately, was not stated by the authors.) Investigations in which the photoemulsion method was used[3,5] yielded a value of $(23 \pm 3)\%$. It can be shown that in these investigations the number of conversion electrons due to the U^{235} decay was incorrectly computed. This value should have been computed, since the U^{235} line was not separated from the U^{238} line. It was thought that each U^{235} decay was accompanied by a conversion electron. Investigations performed recently in our laboratory and in others on the α decay of U^{235} make it possible to state that the number of conversion electrons of energy within U^{234} conversion-electron energy range is only approximately half the number of the U^{235} decays. Taking this into account, the results of references 3 and 5 can be reduced to a value of $(25 \pm 3)\%$.

[1] Kocharov, Komar, and Korolev, JETP **36**, 68 (1959), Soviet Phys. JETP **9**, 48 (1959).

[2] J. Teillac, Compt. rend. **230**, 1056 (1950).

[3] J. Teillac and G. Albouy, Compt. rend. **236**, 829 (1952).

[4] Gol'din, Tret'yakov, and Novikova, U.S.S.R. Acad. Sci. Session on Peaceful Uses of Atomic Energy, July 1955.

[5] B. Zajac, Phil. Mag. **43**, 264 (1952).

Translated by J. G. Adashko
285

INVESTIGATION OF THE X-RAY SPECTRA OF THE SUPERCONDUCTING COMPOUND CuS

I. B. BOROVSKIĬ and I. A. OVSYANNIKOVA

Institute of Metallurgy, Academy of Sciences, U.S.S.R.

Submitted to JETP editor June 16, 1959

J. Exptl. Theoret. Phys. (U.S.S.R.) **37**, 1458-1460 (November, 1959)

IN the formation of a chemical compound there is always a rearrangement of the electron energy spectrum of the elements that enter into the composition. These changes are accurately determined from the fine structure of the x-ray emission and absorption spectra.

In the case of superconducting compounds of nonsuperconducting elements, according to the presently developing concepts,[1] the fine structures of the x-ray spectra of the metals will change so as to come closer to the fine structures of the spectra of a superconducting metal, whose position in the periodic table is close to that of the metal under consideration (in the same period).

We report in the present paper the results of an investigation of the fine structure of x-ray absorption and emission K spectra of sulfur and copper in the pure elements and in the compound CuS. These results confirm the foregoing point of view. Sulfur and copper are nonsuperconducting elements, while CuS is a superconductor with a transition temperature 1.62°K. The CuS lattice is of space group D_{6h}^4 (reference 2).

The investigations were carried out in an x-ray vacuum spectrograph with bent quartz crystal (radius of curvature 500 mm, Kapitza-Johann focusing). Photographic registration was used. The sulfur spectra were obtained in reflection from the $(10\bar{1}1)$ plane, those of copper from the $(13\bar{4}0)$ plane. The accuracy of measurement of the position of the sulfur edge was 0.4 xE, that of copper — 0.15 xE, and that of the positions of the maxima of the emission lines of sulfur was 0.2 xE. The emission K spectrum of sulfur was studied by a secondary method.

The diagram shows the average microphotograms of the resultant spectra; the curves are arranged in such a way that the inflection points of the long-wave portion of the S and Cu edges coincide in the CuS. This point, accurate to the width of the initial state, determines the position of the Fermi surface of the energy spectrum of the compound. All the curves that represent the fine structures of the spectra are arranged about this point in equal energy scale.

The experimental results obtained allow us to note the following (see table):

1. The sulfur spectrum in CuS does not have a discontinuity between the center of the short-wave branch of the last emission line and the point of inflection of the long-wave portion of the edge. This corresponds to a metallic character of the conductivity of the CuS compound.

2. In the absorption spectrum of the sulfur in CuS a maximum, which is new compared with the spectrum of pure sulfur, appears for the absorption coefficient in the long wave portion of the edge abc (see diagram).

3. The intensity ratio J_{β_X}/J_{β_1} of the sulfur spectrum in the CuS is reduced to one half the value in the pure sulfur spectrum.

4. The absorption edge of copper in CuS has lost completely the fine structure that is characteristic of the edge of pure copper. The form of the edge exhibits great similarity with the K edge of Zn or Ga.

5. There is a similarity in the form of the Cu and S edges in CuS (the maxima of the absorption coefficients A and A′ or B and B′ are located at approximately equal distances from the point F; the regions def and d′e′f′ have the same

Wavelengths of different elements of the fine structure

Fine-structure element	In the pure element		In the compound		Shift $\Delta\lambda$, ev
	xE	ev	xE	ev	
Start of sulfur absorption edge	5008.0	2470.1	5012.4	2467.9	—2.2
Maximum of $K\beta_1$ sulfur line	5019.8	2464.3	5021.6	2463.4	—0.9
Maximum of $K\beta_x$ sulfur line	5013.7	2467.3	5013.4	2467.4	—0.1
Start of copper absorption edge	1377.94	6515.1	1377.55	6516.9	+1.8
Maximum of $K\beta_5$ copper line	1378.22	6512.8	1378.20	6513.9	+1.1
Maximum of $K\beta_1$ copper line	1389.65	6405.7	1389.26	6904.3	+3.6

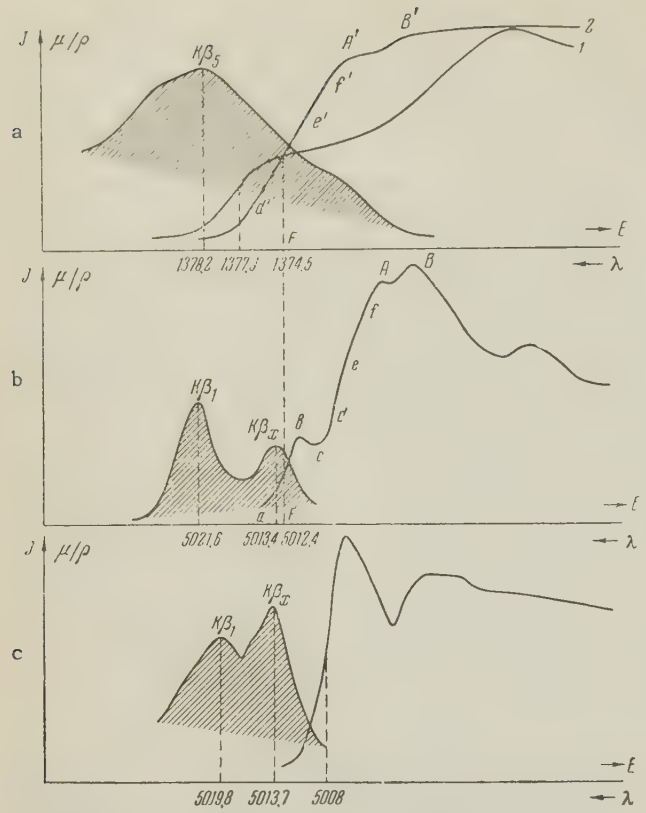

Dependence of the emission-line intensity J and of the coefficient of mass absorption μ/ρ on the wavelength: a – spectra of Cu: curve 1 – copper metal, curve 2 – copper in CuS; b – spectra of sulfur in CuS; c – spectra of pure sulfur. The emission lines are shown shaded. The energy scale is 0.86 ev per division, corresponding to 0.13 xE in the region of wavelengths of the copper edge and to 1.74 xE in the region of wavelengths of the sulfur edge.

curvature relative to the abscissa axis).

6. An investigation of the $K\beta_1$ line of copper by the ionization method has shown that the spectrum of metallic copper has a satellite $K\beta'$, which is absent from the spectrum of copper in CuS, or from the spectrum of Zn.

The following is a possible interpretation of the results obtained: the electron configuration of copper (free atoms) is $3s^2 3p^4$. The shortest emission lines of sulfur, $K\beta_1$ and $K\beta_X$, are due to transitions of electrons from the filled portion 3p of the band to the 1s level. The reduction in the intensity of the $K\beta_X$ line of the S spectrum in CuS and the appearance of an additional long-wave structure in the absorption spectrum are evidence that in the CuS compound a portion of the 3p electrons of the sulfur has gone over to a different state, making it possible to excite electrons in previously-occupied states. The absorption spectrum of copper in the compound has changed in a way as to approach the zinc spectrum. It follows from this that on the average one sulfur electron has gone from the 3p state to the 4s state of copper. Actually this electron belongs to the conduction band of the entire compound, with metallic properties, the same as the "proper" 4s electron of copper, given up by each copper atom to the conduction band. The structure of the ionic residue of copper is $3d^{10}$. The absence of a satellite $K\beta'$ in the spectrum of copper in CuS is an additional argument in favor of the above.

In light of these facts, it becomes necessary to revise the structure of covellin,[3] which is considered an ionic type compound. X-ray-spectral data indicate that CuS is a compound of the intermetallic type, in which the atoms of both components give up electrons to the conduction band. This agrees with the physical properties of CuS — metallic character of conductivity and diamagnetism.

[1] I. B. Borovskiĭ, Тр. инст. металургии АН СССР, (Trans. Inst. of Metallurgy, Acad. Sci. U.S.S.R.), vol. 6. U.S.S.R. Acad. Sci. 1959.

[2] Strukturberichte, Leipzig, **2**, 10, 229 (1937).

[3] N. V. Belov, Структуры ионных соединений и металлических фаз, (Structures of Ionic Compounds and Metal Phases), U.S.S.R. Acad. Sci. 1947.

Translated by J. G. Adashko
286

ANGULAR DISTRIBUTIONS OF ALPHA PARTICLES FROM THE REACTION C^{12} (p, p'3α)

S. S. VASIL'EV, V. V. KOMAROV, G. V. KOSHELYAEV, and A. M. POPOVA

Institute of Nuclear Physics, Moscow State University

Submitted to JETP editor July 3, 1959

J. Exptl. Theoret. Phys. (U.S.S.R.) **37**, 1460-1461 (November, 1959)

WE investigated the angular distributions of α particles that result from the decay of C^{12}, induced by fast protons with energies 22 ± 1 and 29 ± 1 Mev. The decay of the C^{12} nuclei was observed in the form of five-pronged stars (three α particles and the incident and scattered protons), formed in nuclear photoemulsions Ya2 and D-NIKFI, bombarded by protons in the proton synchrotron of the Research Institute for Nuclear Physics of the Moscow State

University. The bombardment was carried out simultaneously with several proton beams of different energies, separated by a system of diaphragms from the beam of the protons scattered by a wedge-like target inside the proton-synchrotron chamber.

At the present time, after an analysis of more than 500 stars, we counted 113 stars produced by protons of the foregoing energies. The diagram shows the angular distributions of the α particles in these stars (c.m.s.). It is seen from the diagram that whereas the angular distribution is symmetrical about 90° for the 22-Mev incident protons, the symmetry is violated for the 29-Mev protons, with emission of α particles in the forward hemisphere predominating.

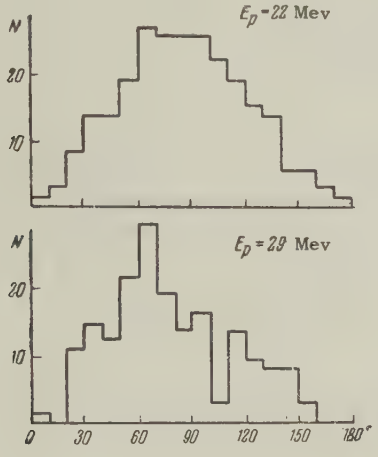

The angular distribution shown indicates that for 29 ± 1 Mev incident protons interact directly with the α particle of the C^{12} nucleus.

It should be noted that for 22-Mev incident protons we observed individual cases of C^{12} decay, which can be classified as direct knock-out of an α particle by a proton inelastically scattered by this particle. These cases are characterized by relatively large energies of the knocked-out α particles, compared with the energies of the two other particles and with the scattering direction of the products (taking excitation energies of the possible intermediate nuclei into account).

Direct interaction of the p—α type with decay of the C^{12} nucleus into three α particles were observed for 180 and 340 Mev incident protons.[1] Our results deduce the presence of a noticeable admixture of type p—α direct interactions for 29 Mev protons and the presence of individual cases of such interactions for 22-Mev protons.

[1] A. Samman and P. Cuer, J. phys. radium **19**, 13 (1958).

Translated by J. G. Adashko
287

SUPERCONDUCTIVITY OF BERYLLIUM AND ITS LOW-TEMPERATURE POLYMORPHISM

B. G. LAZAREV, A. I. SUDOVTSEV, and E. E. SEMENENKO

Physico-Technical Institute, Academy of Sciences, Ukrainian S.S.R.

Submitted to JETP editor July 7, 1959

J. Exptl. Theoret. Phys. (U.S.S.R.) **37**, 1461-1463 (November, 1959)

IT has been reported previously[1] that beryllium, in the form of a film condensed on a substrate at liquid helium temperature, becomes superconducting at ~ 8° K. In this note we present the results of a more accurate determination of the transition temperature. The existence of low-temperature modifications of a number of metals, including bismuth and beryllium, has recently been discovered[2] and in this connection it was especially interesting to examine the superconductivity and electrical conductivity of these beryllium films.

The films were formed by the well-known method.[1,3-5] Measurements were made on the superconducting transition and the temperature dependence of electrical resistance over a wide temperature range. The results on the superconducting transition are shown in Fig. 1. The various curves refer to different films. Some difference in the transition curves is probably related to the conditions of formation of the films and their thickness. All films examined which had a thickness between 400 and 2,500 A behaved in a similar way and became superconducting in the region between 7 and 9° K, over which the resistivity increased from zero to its maximum value.

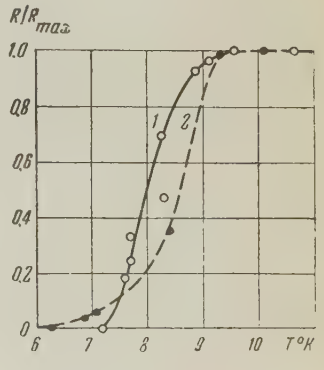

FIG. 1. Plots of the superconducting transition for beryllium films: 1 – film thickness 400 A, R_{max} = 360Ω; 2 – thickness 2300 A, R_{max} = 480Ω.

The detailed temperature variation of resistivity was studied in order to decide about a transition to a low-temperature form. Figure 2 shows this temperature variation up to about 400° K.

All films show, in common, a temperature re-

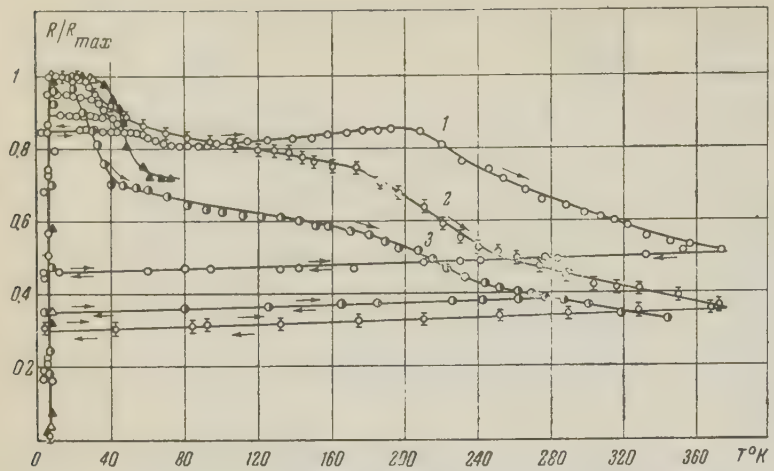

FIG. 2. Temperature variation of electrical resistance of beryllium films: 1 – film thickness 700 A, R_{max} = 200Ω; 2 – thickness 1800 A, R_{max} = 1070Ω; 3 – thickness 400 A, R_{max} = 360Ω; ▲ – data for thickness 500 A, R_{max} = 300Ω (film condensed at 20°K).

gion (up to 20 – 30°K) in which the superconducting modification exists. If heated up to this temperature, the films become superconducting again on subsequent cooling. Heating to temperatures above this leads to an incomplete superconducting transition on cooling again: some resistivity remains, which increases with increasing temperature of heating. Superconductivity is completely lost if heating is carried on above 60°K. This limiting temperature is somewhat lower if the heating time is increased.

We can presume that the first sharp drop on the heating curves is determined by the transition of the film into a different (non-superconducting) modification.

Further on, up to ~ 200°K the resistivity changes little. Around ~ 200°K the resistivity drops again and this is connected either with the transition to yet another form, appropriate to bulk beryllium, or with recrystallization of the film.

Structural investigation will enable a more precise opinion to be given on these transitions.

We have shown that by condensing beryllium from the vapor onto a cold substrate a new modification is formed with different properties from normal beryllium, in particular it shows superconductivity. It is possible that this is the same modification which is obtained by plastic deformation at temperatures below 20°K.[2] This seems likely in view of the analogous behavior of bismuth: superconductivity is found in the low temperature modification of bismuth obtained by plastic deformation[6] at a temperature close to the superconducting transition temperature of freshly condensed films.

[1] Lazarev, Sudovtsev, and Smirnov, JETP **33**, 1059 (1957), Soviet Phys. JETP **6**, 816 (1958).

[2] Gindin, Lazarev, Starodubov, and Khotkevich, JETP **35**, 802 (1958), Soviet Phys. JETP **8**, 558 (1959).

[3] N. V. Zavaritskiĭ, Dokl. Akad. Nauk S.S.S.R. **86**, 687 (1952).

[4] W. Buckel and R. Hilsch, Proc. Int. Conf. Low Temp. Phys., Oxford, 1951, p. 119; Z. Physik **138**, 109 (1954).

[5] A. I. Shal'nikov, Nature **142**, 74 (1938); JETP **10**, 630 (1940). N. E. Alekseevskiĭ, Dokl. Akad. Nauk S.S.S.R. **24**, 27 (1939); JETP **10**, 1392 (1940).

[6] Gindin, Lazarev, Starodubov and Khotkevich, VI All-Union Conference on the Physics of Low Temperatures, Sverdlovsk, 1959.

Translated by R. Berman
288

THE MOTION OF A CHARGED PARTICLE IN A ROTATING MAGNETIC FIELD

A. P. KAZANTSEV

Institute of Radiophysics and Electronics, Siberian Branch, Academy of Sciences U.S.S.R.

Submitted to JETP editor July 11, 1959

J. Exptl. Theoret. Phys. (U.S.S.R.) **37**, 1463-1464 (November, 1959)

IN plasma physics a discussion of the problem of the possibility of localizing a charged particle by a variable electromagnetic field within a certain region of space is of some interest. This question has been discussed by Trubnikov[1] and by Gaponov and Miller.[2] The behavior of a charged particle in a variable electromagnetic field was also discussed by Vedenov and Rudakov.[3] In the present note we show that the localization of a particle is possible in principle by means of a rotating magnetic field

under definite quite restrictive conditions.

We assume that the rotating magnetic field is produced, as usual, by two crossed coils situated along the x and y axes, while a constant magnetic field H is applied along the z axis. If the phases of the alternating currents are suitably chosen, an electromagnetic field with the following components (in the quasi-stationary approximation) is produced in the region of space formed by the intersection of the two cylinders

$$\mathbf{E}\left\{-\frac{h\omega}{2c}z\cos\omega t,\ -\frac{h\omega}{2c}z\sin\omega t,\ \frac{h\omega}{2c}(x\cos\omega t+y\sin\omega t)\right\},$$
$$\mathbf{H}\{h\cos\omega t,\ h\sin\omega t,\ H\}, \qquad (1)$$

where h is the amplitude of the rotating magnetic field, and ω is the frequency of rotation.

The equations of motion for the particle may be conveniently written in the following matrix form:

$$\ddot{\mathbf{r}} = \hat{m}_H\dot{\mathbf{r}} + \hat{m}_E\mathbf{r}. \qquad (2)$$

The explicit expression for the matrices $\hat{\mathrm{m}}$ may be easily found from (1). In the rotating system of coordinates in which the vector $\mathbf{h}$ is at rest (2) reduces to the following equation with constant coefficients:

$$\ddot{\mathbf{R}} = \hat{\mu}_1\dot{\mathbf{R}} + \hat{\mu}_2\mathbf{R}. \qquad (3)$$

If $\mathbf{R} = \hat{\mathrm{M}}(t)\mathbf{r}$, where $\hat{\mathrm{M}}(t)$ is the matrix representing a rotation about the z axis, then the matrices $\hat{\mu}$ and $\hat{\mathrm{m}}$ are related by the following equations

$$\hat{\mu}_1 = \hat{M}\hat{m}_H\hat{M}^{-1} - 2\hat{M}d\hat{M}^{-1}/dt,$$
$$\hat{\mu}_2 = \hat{M}\hat{m}_E\hat{M}^{-1} + \hat{M}\hat{m}_H d\hat{M}^{-1}/dt - \hat{M}\,d^2\hat{M}^{-1}/dt^2. \qquad (4)$$

We introduce the following notation: $\Omega = eH/mc$, $\omega_h = eh/mc$. Then with the aid of (4) the matrices μ may be written in the following form

$$\hat{\mu}_1 = \begin{pmatrix} 0 & \Omega-2\omega & 0 \\ 2\omega-\Omega & 0 & \omega_h \\ 0 & -\omega_h & 0 \end{pmatrix},\quad \mu_2 = \begin{pmatrix} \omega^2+\omega\Omega & 0 & -\omega_h\omega/2 \\ 0 & \omega^2+\omega\Omega & 0 \\ -\omega\omega_h/2 & 0 & 0 \end{pmatrix}. \qquad (5)$$

We note that in the rotating coordinate system the electric field has the potential

$$U = -\frac{eH\omega}{c}(X^2+Y^2) + \frac{\omega eh}{2c}XZ$$

(the X axis is chosen in the direction of the vector $\mathbf{h}$). On substituting $\mathrm{R} = \mathrm{R}_0\exp(i\sqrt{kt})$ into (3) we obtain the following characteristic equation:

$$k^3 - \{\omega_h^2+\Omega^2-6\omega\Omega+2\omega^2\}k^2 + \{\omega^2(\omega+\Omega)^2 - {}^{13}/_4\omega^2\omega_h^2\}k$$
$$-{}^1/_4\omega^3\omega_h^2(\Omega+\omega) = 0.$$

The particle motion is stable (finite) only

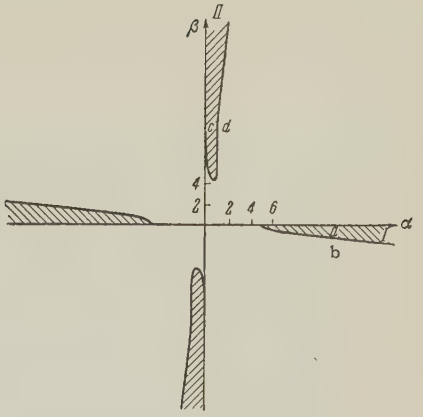

when the roots of this equation are positive and are different. The ranges of parameters for which this condition is fulfilled are shown in the diagram (by shaded areas). Region I is bounded by the curve a which (for $\alpha \gg \beta$ and $\alpha \gg 1$, $\alpha = 2\omega/\omega_h$, $\beta = H/h$) asymptotically approaches the horizontal axis, and by the curve b which asymptotically approaches the straight line $9\beta + \alpha = 0$. For $\beta = 0$ the boundary of the region I is given by $\alpha_{cr} \approx 5$. The region II is bounded by the curve c which coincides for $\beta \gg \alpha$, $\beta \gg 1$ with the hyperbola $\alpha\beta = 2$, and by the curve d which has the asymptote $\beta - 9\alpha = 0$.

The regions I and II are symmetric with respect to the origin in the different quadrants.

In conclusion I wish to express my gratitude to A. M. Dykhne, V. L. Pokrovskiĭ, S. K. Savvinykh, and B. L. Zhelnov for their advice and discussions.

[1] B. A. Trubnikov, Behavior of Plasma in a Rapidly Varying Magnetic Field, Coll. Физика плазмы и проблема управляемых термоядерных реакций (Plasma Physics and the Problem of Controlled Thermonuclear Reactions) vol. IV, Acad. of Sci. U.S.S.R., 1958.

[2] A. V. Gaponov and M. A. Miller, JETP **34**, 242 (1958), Soviet Phys. JETP **7**, 168 (1958).

[3] A. A. Vedenov and L. I. Rudakov, On the Motion of a Charged Particle in Rapidly Varying Fields, loc. cit. ref. 1.

Translated by G. Volkoff
289

ANGULAR ASYMMETRY IN (πN) COLLISIONS AND ($\pi\pi$) INTERACTION

V. S. BARASHENKOV

Joint Institute for Nuclear Research

Submitted to JETP editor July 13, 1959

J. Exptl. Theoret. Phys. (U.S.S.R.) **37**, 1464-1466 (November, 1959)

A model of "central" and "peripheral" collisions was proposed[1,2] to interpret experiments with inelastic (NN) collisions at energies E > 1 Bev.

This model can also be used to explain the angular distributions of particles generated in inelastic (πN) collisions. The figure shows the diagram of a central (πN) collision (a), and also possible variants of peripheral collisions (b, c, and d). In one of these the nucleus, losing the peripheral pion, goes into an excited state, which then decays (model with isobar). In the calculations we have assumed values of $^3/_2$ for the spin and the isotopic spin of the isobar. The peripheral collisions are due to ($\pi\pi$) interactions.

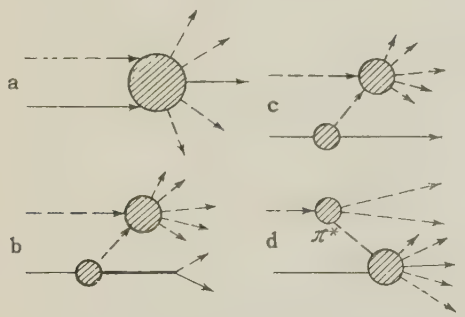

Numerical calculations have been made for (π^-p) collisions at E = 5 Bev. The results can be compared with the experimental data of reference 3. The central collisions for this energy have been considered in reference 4. We used the statistical theory of multiple production to calculate the inelastic (πp) and ($\pi\pi$) collisions.

The table lists the average numbers of particles created in peripheral collisions of type b and c and emitted, in the c.m.s. of the colliding negative pion and proton, into the forward ($\vec{n}^p$) or rear ($\overleftarrow{n}^p$) hemisphere relative to the velocity vector of the primary negative pion. As can be seen, the particles produce here a considerable angular asymmetry, $A = \vec{n}/\overleftarrow{n} \neq 1$.*

A calculation of the type-d collisions is less unambiguous, since little is known at present concerning the structure of the meson. From a comparison of various assumptions with experiment it is possible to obtain, in principle, information

Generated particles	Model with isobar		Model without isobar	
	$\vec{n}^p$	$\overleftarrow{n}^p$	$\vec{n}^p$	$\overleftarrow{n}^p$
p	0	0.78	0	0.33
n	0	0.22	0	0.67
π^+	1.15	0.79	1.0	0.34
π^-	1.0	0.39	1.0	0.34
π^0	0.95	0.59	0.86	0.34

on the structure of the pion.† However, if collisions with small momentum transfer are considered, the results of the table do not change qualitatively and change very little quantitatively within the framework of sensible assumptions concerning the peripheral meson.

Taking central (π^-p) collisions into account, the angular asymmetry of the particles generated in (π^-p) collisions is of the form

$$A = \vec{n}/\overleftarrow{n} = \left(\vec{n}^c + \vec{n}^p \frac{\xi}{1+\xi}\right) \Big/ \left(\overleftarrow{n}^c + \overleftarrow{n}^p \frac{\xi}{1+\xi}\right),$$

where $\xi = \sigma^p_{\pi N}/\sigma^{in}_{\pi N}$, $\vec{n}^c \simeq \overleftarrow{n}^c \simeq n^c/2$ is the number of particles of a given kind, produced in the central collisions: $n^c_p \simeq 0.4$, $n^c_n \simeq 0.6$, $n^c_{\pi^+} \simeq n^c_{\pi^-} \simeq n^c_{\pi^0} \simeq 1.2$.

Qualitatively, both models (with and without the isobar) explain the experimental values of the angular asymmetry, but the model with the isobar is in better agreement with the experiment. In this case the experimental data for protons and pions can be reconciled with the theory if $\xi \gtrsim 0.2$. To reconcile the angular asymmetry of the neutrons with experiment we must have $\xi \gtrsim 0.5$, but the experimental data obtained in reference 3 for neutral particles are less reliable than those for charged ones.

If the cross section $\sigma_{\pi\pi}$ of the ($\pi\pi$) interactions, like the cross sections $\sigma_{\pi N}$ and σ_{NN}, changes little with energy at E > 1 Bev, then the cross section for the peripheral (πN) and (NN) interactions is

$$\sigma^p_{NN} \equiv \eta \sigma^{in}_{NN} = 2\int \sigma_{\pi N}(\varepsilon)\, q_N(\varepsilon)\, d\varepsilon \simeq 2\sigma_{\pi N} n_N,$$

$$\sigma^p_{\pi N} \equiv \xi \sigma^{in}_{\pi N}$$

$$= \int \sigma_{\pi\pi}(\varepsilon)\, q_N(\varepsilon)\, d\varepsilon + \int \sigma_{\pi N}(\varepsilon)\, q_\pi(\varepsilon)\, d\varepsilon \simeq \sigma_{\pi\pi} n_N + \sigma_{\pi N} n_\pi,$$

where $\sigma_{\pi N}$ and $\sigma_{\pi\pi}$ are the total interaction cross sections, q_N and q_π are the spectra of the peripheral mesons, and n_N and n_π are their number (~ 0.05 to 0.1, cf. reference 2).

Since $\sigma^{in}_{\pi N} \sim \sigma^{in}_{NN}$ and $\eta \gtrsim 0.2$ (see reference 2), we have

$$\sigma_{\pi\pi} = 2\sigma_{\pi N}(\xi - n_\pi \sigma_{\pi N}/\sigma^{in}_{\pi N})/\eta \sim \sigma_{\pi N}.$$

This estimate is confirmed also by an optical

analysis of the experimental angular distributions of elastic (π^-p) interactions at E > 1 Bev.‡

I am grateful to D. I. Blokhintsev for discussions.

*It was assumed here that, in the case of (πN) and (NN) collisions at E > 1 Bev, the cross section of diffraction ($\pi\pi$) scattering $\sigma^{d}_{\pi\pi} \simeq 1/3\sigma^{in}_{\pi\pi}$, where $\sigma^{in}_{\pi\pi}$ is the cross section of all inelastic ($\pi\pi$) interactions. Calculations have shown that the numbers in the table vary little with $\sigma^{d}_{\pi\pi}$.

†This question will be considered in detail in another paper.

‡Approximately half of the (π^-p) collisions occurs at impact parameters $\rho \gtrsim (0.5 \text{ to } 0.6) \times 10^{-13}$ cm, which can be explained only by assuming $r_\pi \sim r_N \sim 0.5 \times 10^{-13}$ cm, i.e. $\sigma_{\pi\pi} \sim 4\pi r^2_\pi \sim \sigma_{\pi N}$ (see reference 5).

[1] I. E. Tamm, Nucl. Phys., in press.

[2] Barashenkov, Maltsev, and Mihul, Nucl. Phys., in press.

[3] Maenchen, Fowler, Powell, and Wright, Phys. Rev. **108**, 850 (1957).

[4] V. S. Barashenkov and V. M. Maltsev, Acta Phys. Polonica **17**, 177 (1958); JETP **37**, 884 (1959), Soviet Phys. JETP **10**, 630 (1960).

[5] Barashenkov, Belyakov, Wang, Glagolev, Dolhadzov, Kirillova, Lebedev, Maltsev, Markov, Tolstov, Tsyganov, Shafranova, and Jao, Nucl. Phys., in press.

Translated by J. G. Adashko
290

DETECTION OF Eu^{++} *IONIZATION IN THE* SrS-Eu, Sm *PHOSPHOR BY THE PARAMAGNETIC ABSORPTION METHOD*

V. V. ANTONOV-ROMANOVSKIĬ, V. G. DUBININ, A. M. PROKHOROV, Z. A. TRAPEZNIKOVA, and M. V. FOCK

P. N. Lebedev Physics Institute, Academy of Sciences, U.S.S.R.

Submitted to JETP editor July 13, 1959

J. Exptl. Theoret. Phys. (U.S.S.R.) **37**, 1466-1467 (November, 1959)

IN the phosphor SrS-Eu, Sm (without flux) we discovered a decrease in the paramagnetic absorption of Eu^{++} upon excitation of this phosphor with light in the absorption band of Eu^{++} ($\lambda \sim 440$ mμ). This decrease was found to be dependent on the degree of the phosphor stimulation. At the moment of excitation the decrease of paramagnetic absorption is ~15%, and ~10 minutes after cessation of excitation this decrease amounts to ~8%. This agrees with the decrease in the self-absorption coefficient of Eu^{++} in phosphor during excitation. Measurements made some 10 — 20 minutes after cessation of excitation showed that the coefficient of activator absorption in the excited phosphor was less by ~11%. At the same time, measurements of the total number of quanta emitted by the excited phosphor were made starting 10 — 20 minutes after cessation of excitation. The measurements yielded 6.5×10^{15} quanta, proving that not less than 4% of the Eu^{++} became ionized. Assuming that the quantum yield of the radiation at recombination is ~½ and that the full amount of the activator was used for the formation of luminescence centers (Eu^{++}) we can state that about 8% of the Eu^{++} ions became ionized.

Thus, three independent methods gave compatible results. This allows us to state that ionization of the activator (Eu$^{++} \rightarrow$ Eu^{+++}) takes place upon excitation of the phosphor SrS-Eu, Sm.

The cause of the non-detection of ionization in the previous[1] work remains unclear. It is probably connected with the lower stability of the radiation spectroscope or with stray excitation of the luminophore in the resonator.

[1] Manenkov, Prokhorov, Trapeznikova, and Fock, Оптика и спектроскопия (Optics and Spectroscopy) **2**, 470 (1957).

Translated by Z. Scheidlinger
291

SCATTERING OF A LOW-ENERGY ELECTRON BY A SHORT-RANGE POTENTIAL IN A STRONG MAGNETIC FIELD

V. G. SKOBOV

Leningrad Physico-technical Institute, Academy of Sciences U.S.S.R.

Submitted to JETP editor July 17, 1959

J. Exptl. Theoret. Phys. (U.S.S.R.) **37**, 1467-1469 (November, 1959)

WE study the question of the scattering of an electron with energy E by a potential V(**r**) in a homogeneous magnetic field **H**, assuming that the radius of action of the scattering potential

$r_0 \ll \lambda = (2mE)^{-1/2}$ (the system of units is employed in which $\hbar = c = 1$).

The Hamiltonian of the electron without consideration of the scattering potential is $H_0 = (p - eA)^2/2m$, where curl $A = H$. Let $H_0\varphi_\alpha = E_\alpha\varphi_\alpha$, α is the total set of quantum numbers for an electron in a magnetic field. The exact wave function of the electron $\Psi(r)$ satisfies the integral equation[1]

$$\Psi_\alpha(r) = \varphi_\alpha(r) + \int G(r, r';\ E_\alpha)\, V(r')\, \Psi_\alpha(r')\, d^3r', \qquad (1)$$

$$G(r, r'; E) = \sum \varphi_\nu(r)\, \varphi^*_\nu(r') / (E - E_\nu + i\delta). \qquad (2)$$

According to Lippmann and Schwinger, the scattering is completely determined by the matrix elements $T_{\beta\alpha} = (\varphi_\beta | V | \Psi_\alpha)$, i.e., for the solution of the problem, one needs to know the form of $\Psi_\alpha(r)$ at distances of the order r_0. Taking the vector A in the form $A_x = A_z = 0$, $A_y = Hx$, and summing, in (2) over the x coordinates of the center of rotation of the electron, we obtain

$$G(r, r';\ E) = \Phi(r, r')\, S(r - r'; E),$$

$$S(r, E) = \frac{\gamma}{4\pi^2} \int_{-\infty}^{+\infty} dk \exp(ikz - \gamma\rho^2/4) \sum_{n=0}^{\infty} \frac{L_n(\gamma\rho^2/2)}{E - E_n(k) + i\delta},$$

$$\Phi(r, r') = \exp\{i\gamma(x + x')(y - y')/2\}, \qquad (3)$$

where

$$\rho^2 = x^2 + y^2, \qquad E_n(k) = [2\gamma(n + 1/2) + k^2]/2m, \qquad \gamma = eH;$$

$L_n(u)$ are the Laguerre polynomials normalized to unity.

We introduce the notation $E = (N + 1/2 - \epsilon)\gamma/m$, where $0 < \epsilon \leq 1$, and separate the first N terms from the sum over n in the formula (3). Then $S(r, E) = S_N(r) + S'(r)$, where

$$S_N(r) = -i\gamma \frac{m}{2\pi} \sum_{n=0}^{\Lambda} k_n^{-1} L_n(\gamma\rho^2/2) \exp(ik_n z - \gamma\rho^2/4),$$

$$k_n = \sqrt{2\gamma(N - \varepsilon - n)}.$$

We note that the condition $r \ll \lambda$ now has the form $r \ll (2\gamma N)^{-1/2}$. It can be shown that for $r \ll \lambda$

$$S'(r) = -(m/2\pi)(1/r + \gamma_{i1}\sqrt{2\gamma} + \gamma_{i2}\, 2\gamma N r),$$

where $|\eta_{1,2}| < 1$ for all ϵ. Thus the asymptotic solution of the Green's function G for $r, r' \ll \lambda$ has the form ($\Phi(r, r') \approx 1$)

$$G(r, r'; E) \approx S(r - r'; E) \approx -(m/2\pi)[|r - r'|^{-1} + iK(E)],$$

$$K(E) = \gamma \sum_{n=0}^{N} (k_n)^{-1}. \qquad (4)$$

We now write down Eq. (1) in the region $r \ll \lambda$:

$$\Psi_\alpha(r) = \varphi_\alpha(0) - \frac{m}{2\pi} \int \left(\frac{1}{|r - r'|} \int + iK \right) V(r')\, \Psi_\alpha(r')\, d^3r'. \qquad (5)$$

It is easy to see that the solution of this equation has the form

$$\Psi_\alpha(r) = \frac{\varphi_\alpha(0)}{1 + iKf} \Psi_0(r), \qquad (6)$$

where $\Psi_0(r)$ is determined by the equation

$$\Psi_0(r) = 1 - (m/2\pi) \int |r - r'|^{-1} V(r')\, \Psi_0(r')\, d^3r',$$

$$f = (m/2\pi) \int V(r)\, \Psi_0(r)\, d^3r;$$

f represents the scattering amplitude of a free electron with zero energy in a potential V. It follows from (6) that

$$T_{\beta\alpha} = \frac{2\pi f}{m} \frac{\varphi^*_\beta(0)\, \varphi_\alpha(0)}{1 + iK(E_\alpha) f}. \qquad (7)$$

With the aid of (7), it is easy to find the total scattering probability per unit time, averaged over the positions of the center of rotation of the electron in the initial state:

$$W(E) = \frac{4\pi}{\Omega} \frac{f^2 K'(E)/m}{(1 + K''f)^2 + (K'f)^2}; \qquad (8)$$

We introduce here the notation $K = K' - iK''$, Ω is the normalized volume.

Let us investigate the expression (8) in the case $1 \ll N \ll 1/2\, \gamma f^2$. Here,

$$K'(E) = \sqrt{2mE} + \eta_1(\varepsilon)\sqrt{2\gamma/(1 - \varepsilon)},$$

where $|\eta(\epsilon)| \lesssim 1$ for all ϵ. If $K'f \ll 1$ and $K''f \ll 1$, i.e., $(1 - \epsilon) \gg \gamma f^2/2$ and $\epsilon \gg \gamma f^2/2$, then the formula (8) yields

$$W(E) = \frac{4\pi f^2}{\Omega} \sqrt{\frac{2E}{m}} \left[1 + \frac{\eta_1(\varepsilon)}{\sqrt{N(1 - \varepsilon)}} \right] \qquad (9)$$

In the case $E \to (N + 1/2)\gamma/m$,

$$W(E) = \begin{cases} \frac{4\pi}{\Omega} \frac{1}{m\eta} \sqrt{\frac{1 - \varepsilon}{2\gamma}} & \text{for } (1 - \varepsilon) \ll \gamma f^2/2, \\ \frac{8\pi}{\Omega} \sqrt{\frac{2E}{m}} \frac{\varepsilon}{\gamma} & \text{for } \varepsilon \ll \gamma f^2/2. \end{cases} \qquad (10)$$

Equation (8) for $W(E)$ has a maximum value for $K'f \sim 1$, i.e., for $(1 - \epsilon) \sim \gamma f^2/2$, whence

$$W_{max} \sim 2\pi f/\Omega m.$$

It follows from Eqs. (9) and (10) that the width of these resonant peaks is of the order $\Delta E = \gamma^2/4m^2E$.

The energy levels of the electron have a finite width Γ, and δ in Eq. (2) should be replaced by $\Gamma/2$. As a consequence, $K(E)$ is finite for all ϵ, and $W(E)$ does not vanish for any E. However, $W(E)$ will, as before, have resonance maxima if $\Gamma/2 \ll \Delta E$.

I express my gratitude to L. É. Gurevich for his constant attention to the work and also to V. N. Gribov, S. V. Maleev, and L. P. Pitaevskiĭ for useful discussions.

[1] B. A. Lippmann and J. Schwinger, Phys. Rev. **79**, 469 (1950).

Translated by R. T. Beyer
292

CERTAIN EXPERIMENTS WITH METASTABLE LIQUIDS IN AN X-RAY BEAM

G. A. ASKAR'YAN, L. P. KOTENKO, E. P. KUZNETSOV, and A. V. SAMOĬLOV

P. N. Lebedev Physics Institute, Academy of Sciences, U.S.S.R.

Submitted to JETP editor July 17, 1959

J. Exptl. Theoret. Phys. (U.S.S.R.) **37**, 1469-1470 (November, 1959)

To establish the sensitivity of metastable liquids to low-energy electrons and the extent of this sensitivity, and also to carry out test experiments on the photography in a beam of penetrating radiation with the aid of metastable liquids, we placed a 0.75-liter propane bubble chamber in the beam of the URS-70 x-ray structural-analysis apparatus. To reduce the absorption of soft x-rays, an inlet hole 5 mm in diameter was made in the wall of the bubble chamber and was covered with a bakelite layer 3 mm thick. Owing to the pulsations in the tube electrode voltage and to the short sensitivity time of the chamber (on the order of several milliseconds), several pictures were taken for each set of conditions, from which we selected the cases of maximum intensity of action and associated them with the maximum value of the current and voltage in the tube. We observed that bubbles were produced at 10 kev and above (see Figs. 1 and 2), but the sharp change in the penetrating ability and the spectrum of the x-ray beam at low tube voltages does not allow us to draw more definite quantitative conclusions concerning the electron threshold energy necessary to initiate bubbling.

We attempted to photograph an object in an x-ray beam penetrating to the side glass of the chamber. The use of an illuminated layer of metastable (superheated or gassed) liquid as a converter and registrator for the image of objects in the transmitted beam of penetrating radiation (x-rays, γ rays, or neutrons) is of interest because of the extremely high

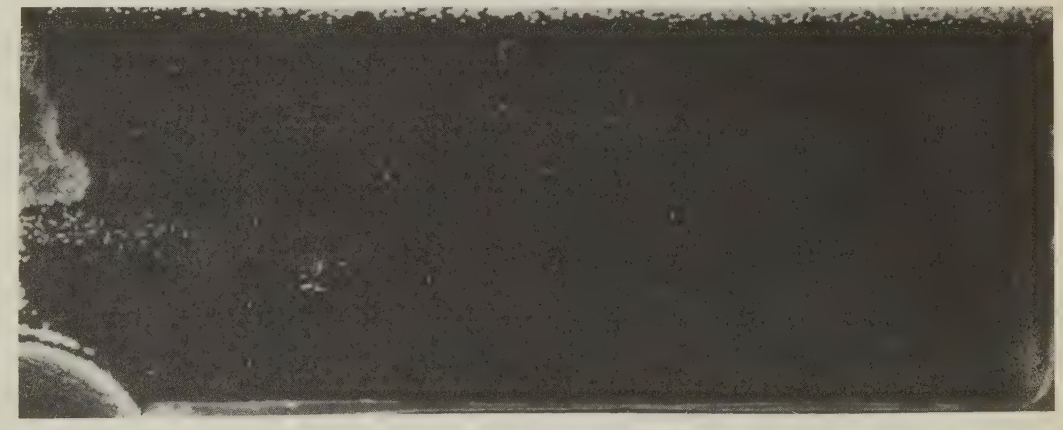

FIG. 1. Formation of bubbles by x-ray beams at x-ray-tube voltage 10 kv and a current of 10 ma. The input window of the chamber was 30 cm from the anticathode of the tube.

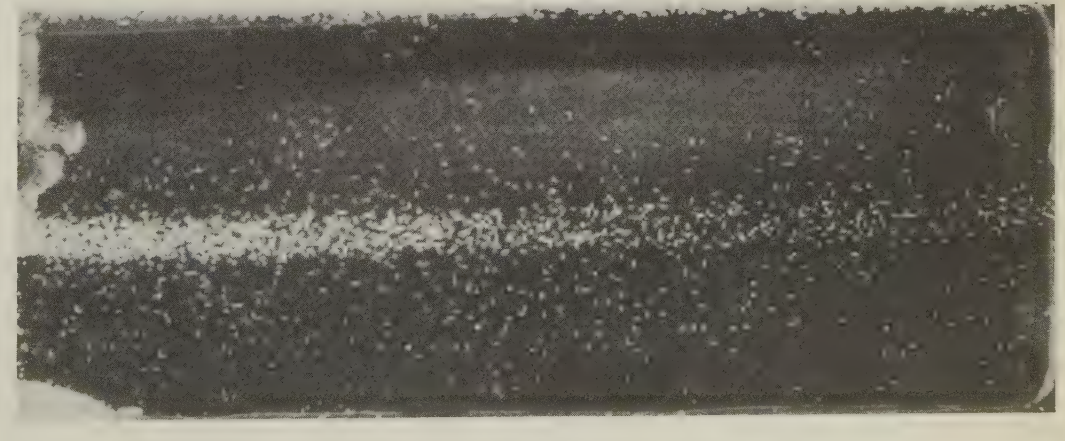

FIG. 2. The same at 30 kv and 1 ma, in the presence of a 9 cm paraffin absorber in front of the entrance window of the chamber.

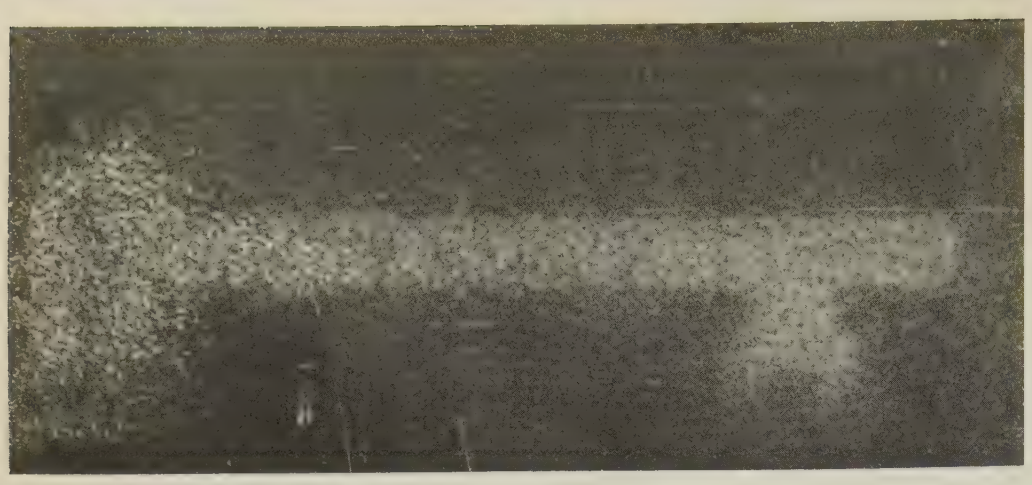

FIG. 3. Image of a key placed 20 cm in front of the chamber, with the chamber exposed through the glass window. The tube operated at 50 kv and 10 ma. The actual exposure was less than the sensitivity time of the chamber (on the order of a millisecond).

sensitivity of such systems to penetrating radiations. Actually, the production of ionizing particles in a liquid under the influence of a penetrating beam has a high probability because of the large density of the liquid, where the ionizing particles form bubbling centers which generate visible bubbles measuring from 1 micron to a fraction of a millimeter, depending on their growth time prior to the illumination flash. The intense scattering of light by such bubbles, the density of which depends on the local intensity of the penetrating beam passing through the object, produces an image of the object in reflected or transmitted light.

By varying the intensity of bubbling of the liquid and the time of illumination, it is possible to vary the sharpness of the image over a wide range. Image distortion due to the ionizing-particle track lengths can be made negligibly small at quantum energies up to several hundreds kev and neutron energies up to several Mev, owing to the smallness of the transverse projections of the paths of the secondary electrons and the recoil protons.

The use of a high-speed cyclic bubble chamber (see, for example, reference 1) makes possible either high-speed intermittent or continuous visual examination of objects. (When the cycle frequency exceeds 10 cps, the eye perceives a continuous image).

We have obtained the first test photographs of a key (see Fig. 3), using the same bubble chamber at 50 kv and 10 ma (the actual exposure time is less than the sensitivity time of the chamber, which is on the order of several milliseconds).

In spite of the very inconvenient conditions (great thickness of the chamber and of the glass, poor geometry, and large distance to the object because the key was placed outside the case in which the chamber and the illuminating lamps were installed), even the first photographs yielded relatively satisfactory image contrast. It is interesting to note that both negative and positive shadow images can be obtained, depending on the placement of the illuminating lamps and the degree of intensity of the scattering.

In conclusion, we consider it our pleasant duty to thank Yu. I. Skanavi and A. I. Demeshina for graciously permitting us to use the x-ray apparatus, and also thank K. V. Filippova, V. N. Mikhalenko, and A. F. Nalgranyan for useful advice.

[1] Kuznetsov, Lomanov, Blinov, and Huan, JETP **31**, 911 (1956), Soviet Phys. JETP **4**, 773 (1957).

Translated by J. G. Adashko
293

CAPTURE OF POLARIZED μ^- MESONS BY DEUTERONS

A. P. BUKHVOSTOV and I. M. SHMUSHKEVICH

Leningrad Physico-technical Institute, Academy of Sciences, U.S.S.R.

Submitted to JETP editor July 17, 1959

J. Exptl. Theoret. Phys. (U.S.S.R.) **37**, 1471-1473 (November, 1959)

THE capture of polarized μ^- mesons in deuterium has been investigated theoretically by Überall and Wolfenstein.[1] However, it is assumed in their work that the polarized μ^- meson is captured by an unpolarized nucleus. Actually, because of the long lifetime of the μ^- meson in the K shell, the nucleus is also polarized in this case;[2] the calculations for the capture in hydrogen with account of this circumstance were given in reference 3.

For μ-mesodeuterium, it is necessary to con-

sider separately the capture from states with total momentum $F = 3/2$ and $F = 1/2$. Corresponding density matrices have the form:

$$\rho_+ = \frac{1}{4}\left[1 + \frac{3}{5}\lambda_+ \mathbf{j}(\sigma_1 + \sigma_2 + \sigma_\mu)\right]\frac{4 + \sigma_\mu(\sigma_1 + \sigma_2)}{6}\,\frac{3 + \sigma_1\sigma_2}{4},$$

$$\rho_- = \frac{1}{2}[1 + \lambda_- \mathbf{j}(\sigma_1 + \sigma_2 + \sigma_\mu)]\frac{2 - \sigma_\mu(\sigma_1 + \sigma_2)}{6}\,\frac{3 + \sigma_1\sigma_2}{4}. \quad (1)$$

Here σ_1, σ_2 and σ_μ are the spin operators of the nucleons and the μ meson. In comparison with the formulas set forth in reference 2, there is in (1) the additional factor $(3 + \sigma_1\sigma_2)/4$, which is a projection operator on the state of the system of two nucleons with spin 1 (deuteron).

In what follows we start from the Hamiltonian of interaction in the form of Lee and Yang,[4] but with the wave functions of the electron replaced by the functions of the μ^- meson, and we employ the notation adopted in reference 1. For the probability of emission of a neutron in the energy range dE and solid angle $d\Omega$, we have

$$dW = p_+ dW_+ + p_- dW_- = \frac{M^2 dE d\Omega}{(2\pi)^4 \pi a^3} I_0 [1 - A\cos(\mathbf{j}, \mathbf{p})], \quad (2)$$

$$I_0 = I_{tt}\, a_{FF} + [I_{tt} + 3p_-(I_{tt} + I_{ss})](a_{GG} - \tfrac{2}{3} a_{GP}) + (1 - 3p_-) I_{tt} \cdot 2\,\mathrm{Re}\left(a_{GF} - \tfrac{1}{3} a_{GP}\right), \quad (3)$$

$$I_0 A = I_{tt}'[(p_+\lambda_+ - \tfrac{1}{3} p_-\lambda_-) b_{FF} + (p_+\lambda_+ - \tfrac{4}{3} p_-\lambda_-) \times (b_{GG} - 2\,\mathrm{Re}\, b_{GP}) + (p_+\lambda_+ + \tfrac{2}{3} p_-\lambda_-) \cdot 2\mathrm{Re}(b_{GF} - b_{FP})] + I'_{ss}\, p_-\lambda_-(3b_{GG} + \tfrac{4}{3}\,\mathrm{Re}\, b_{GP}). \quad (4)$$

Here dW_+ and dW_- are the respective capture probabilities from the quadruplet and doublet states of mesodeuterium; p_+ and p_- are the probabilities of formation of these states. In these formulas, as in those of reference 1, terms proportional to $|C_P|^2$ are neglected. The polarization of the neutron $\langle\sigma\rangle$ when pseudoscalar interaction is neglected is shown to be the following:

$$I_0[1 - A\cos(\mathbf{j}, \mathbf{p})]\langle\sigma\rangle = -a\frac{\mathbf{p}}{p} + c\mathbf{j} - d\left[\frac{\mathbf{p}}{p}, \mathbf{j}\right],$$

$$-a = I'_{tt}\left(p_- - \tfrac{1}{3}\right) b_{FF} + \left[\left(3p_- - \tfrac{1}{3}\right) I'_{tt} + 4p_-\,\mathrm{Re} I'_{st}\right] b_{GG} - 2\mathrm{Re}\left\{\left[\left(p_- + \tfrac{1}{3}\right) I'_{tt} + p_- I'_{st}\right] b_{GF}\right\}, \quad (5)$$

$$c = I_{tt}\left(p_+\lambda_+ + \tfrac{2}{3} p_-\lambda_-\right) a_{FF} + \left[\left(p_+\lambda_+ + \tfrac{8}{3} p_-\lambda_-\right) I_{tt} - 4p_-\lambda_- \times \mathrm{Re}\, I_{st}\right] a_{GG} + 2\mathrm{Re}\left\{\left[\left(p_+\lambda_+ - \tfrac{4}{3} p_-\lambda_-\right) I_{tt} + p_-\lambda_- I_{st}\right] a_{GF}\right\},$$

$$-d = p_-\lambda_- \cdot 2\,\mathrm{Im}[(2b_{GG} - b_{GF}) I_{st}']. \quad (6)$$

In the case of universal V—A interaction[5] and neglect of the renormalization of constants on account of strong interaction ($C_S = C'_S = C_P = C'_P = C_T = C'_T = 0$; $C_V = -C'_V = -C_A = C'_A = G/\sqrt{2}$) the probability of capture from the quadruplet state is shown to be equal to zero* and the formulas become simplified

$$I_0 = 3G^2 p_-(3I_{tt} + I_{ss}), \qquad I_0 A = 3G^2 p_-\lambda_-(I'_{tt} - I'_{ss}); \quad (7)$$

$$-a = -6G^2 p_-(I'_{tt} + \mathrm{Re}\, I'_{st}), \qquad c = 6G^2 p_-\lambda_-(I_{tt} - \mathrm{Re}\, I_{st}),$$

$$-d = -6G^2 p_-\lambda_-\,\mathrm{Im}\, I'_{st}. \quad (8)$$

These equations are consistent with those obtained from the formulas of Überall and Wolfenstein under similar assumptions (V—A interaction and absence of renormalization of the constants). In this case an additional factor $3p_-$ appears in the expression for capture probability (in contrast with reference 1); the distribution of neutrons with respect to energy can be obtained by summing the graphs F and G in Fig. 1 of reference 1 and by multiplication of the result by $3p_-$. In the parameter of asymmetry and polarization, the difference consists in replacing the polarization of the μ meson P by $-3\lambda_-$. Account of strong interactions leads to renormalization of the constants (strictly speaking, these will also be form factors depending on the energy of the neutrino, but in the fundamental region, i.e., for ν close to μ, they are approximately constant) and effectively to the appearance of pseudoscalar coupling;[7] in this case the deviation from reference 1 appears to be more significant.

Making use of the completeness of the wave functions of the system of two neutrons, we find the distribution over direction of the emergent neutrino dW and the mean asymmetry of flight of the neutrons $\langle \mathbf{p}\cdot\mathbf{j}\rangle$:

$$dW_\nu = \frac{\bar{\nu}^2}{(2\pi)^2 \pi a^3} d\Omega_\nu I_D [1 - B\cos(\mathbf{j}, \nu)], \quad (9)$$

$$I_D = \xi\left[a_{FF} + (1 - 3p_-)\cdot 2\mathrm{Re}\left(a_{GF} - \tfrac{1}{3} a_{FP}\right)\right] + (\xi + 3p_-)\left(a_{GG} - \tfrac{2}{3}\mathrm{Re}\, a_{GP}\right), \quad (10)$$

$$I_D B = \xi\left[\left(p_+\lambda_+ - \tfrac{1}{3} p_-\lambda_-\right) b_{FF} + (p_+\lambda_+ + \tfrac{2}{3} p_-\lambda_-) \times 2\mathrm{Re}(b_{GF} - b_{FP}) + (p_+\lambda_+ - \tfrac{4}{3} p_-\lambda_-)(b_{GG} - 2\mathrm{Re}\, b_{GP})\right] + (1 - \xi) p_-\lambda_-\left(3b_{GG} + \tfrac{4}{3}\mathrm{Re}\, b_{GP}\right), \quad (11)$$

$$\langle \mathbf{pj}\rangle = \tfrac{1}{6} B\bar{\nu}; \qquad \xi = \tfrac{1}{2}\left(1 - \int |\psi_d|^2 \cos \nu r dr\right); \quad (12)$$

for $\psi_d = \left(\frac{\alpha}{2\pi}\right)^{1/2} \frac{e^{-\alpha r}}{r}$ we obtain $\xi = \frac{1}{2}\left(1 - \frac{2\alpha}{\bar{\nu}} \tan^{-1}\frac{\nu}{2\alpha}\right)$

≈ 0.11 ($\bar{\nu} = 94$ Mev.)

For V--A interaction and neglect of renormalization of the constants, we have

$$I_D = 3G^2 p_- (2\xi + 1), \qquad B = (2\xi - 1)/(2\xi + 1).$$

We now write down the expression for the probability dW_1 of capture with the formation of two slow neutrons with energies E_1 and E_2 (E_1, E_2, $\lesssim 10$ Mev):

$$dW_1 = \frac{\nu M^2}{(2\pi)^4 \pi a^3} dE_1 dE_2 d\Omega_1 I_1 [1 + C\cos(j, p_1)]; \quad (13)$$

$$I_1 = |J_t|^2 a_{FF} + [|J_t|^2 + 3p_-(|J_t|^2 + |J_s|^2)](a_{GG} - \tfrac{2}{3} a_{GP}) + (1 - 3p_-)|J_t|^2 \cdot 2\mathrm{Re}(a_{GF} - \tfrac{1}{3} a_{FP}); \quad (14)$$

$$I_1 C = \frac{\bar{\nu}^2 - p_1^2 - p_2^2}{\bar{\nu} p_1} \{|J_t|^2 [(p_+\lambda_+ - \tfrac{1}{3} p_-\lambda_-) b_{FF} + (p_+\lambda_+ - \tfrac{4}{3} p_-\lambda_-)(b_{GG} - 2\mathrm{Re}\, b_{GP}) + (p_+\lambda_+ + \tfrac{2}{3} p_-\lambda_-) \times 2\mathrm{Re}(b_{GF} - b_{FP})] + p_-\lambda_- |J_s|^2 (3b_{GG} + \tfrac{4}{3}\mathrm{Re}\, b_{GP})\}. \quad (15)$$

The authors express their gratitude to V. N. Gribov for useful discussions.

*A similar effect was noted in the capture of hydrogen from the triplet state.[6]

[1] H. Überall and L. Wolfenstein, Nuovo cimento **10**, 136 (1958).

[2] I. M. Shmushkevich, JETP **36**, 953 (1959), Soviet Phys. JETP **9**, 673 (1959).

[3] I. M. Shmushkevich, Nucl. Phys. **11**, 419 (1959).

[4] T. D. Lee and C. N. Yang, Phys. Rev. **104**, 254 (1956).

[5] E. C. Sudarshan and R. E. Marshak, Phys. Rev. **109**, 1860 (1958); R. P. Feynman and M. Gell-Mann, Phys. Rev. **109**, 193 (1958).

[6] Ya. B. Zel'dovich and S. S. Gershteĭn, JETP **35**, 821 (1958). Soviet Phys. JETP **8**, 570 (1959).

[7] M. L. Goldberger and S. B. Treiman, Phys. Rev. **111**, 354 (1958); L. Wolfenstein, Nuovo cimento **8**, 882 (1958).

[8] A. P. Rudik, Dokl. Akad. Nauk SSSR **92**, 739 (1953).

Translated by R. T. Beyer
294

CYCLOTRON RESONANCE IN LEAD

M. S. KHAĬKIN

Institute for Physical Problems, Academy of Sciences, U.S.S.R.

Submitted to JETP editor July 23, 1959

J. Exptl. Theoret. Phys. (U.S.S.R.) **37**, 1473-1476 (November, 1959)

THE phenomenon of cyclotron resonance predicted by Azbel' and Kaner[1] was observed in the case of lead by a number of authors.[2-4] The graphs of the dependence of the ratio $R(H)/R(0)$ on the intensity of the magnetic field H show[2-3] a shallow minimum near 1000 oe of width ~ 1000 oe defined by several experimental points. The record of the quantity $dR(H)/dH$ given in the brief communication by Kip et al[4] also contains only one broad minimum in the field range up to 2000 oe and, in addition to that, approximately ten minima for values of $H = 2000 - 5000$ oe.

In the present work, due to the utilization of a highly sensitive method of measurement — a resonator with rectilinear high frequency currents flowing in the sample, and very pure lead used for the preparation of the sample — several tens of cyclotron resonance minima have been observed for different orientations of the magnetic field (of intensity $150 - 3000$ oe) with respect to the crystallographic directions. In our experiments the dependence of the quantity $X^{-1}\partial X/\partial H$ on $1/H$ was measured, where X is the surface reactance of the metal. The sample was a single crystal of lead characterized by the resistance ratio $\bar{\rho}_{20°C}/\bar{\rho}_{3.75°K} = 1.4 \times 10^5$ (reference 5, sample No. 6), which yields the value for the parameter $\omega\tau \approx 50$; the measurements were carried out at 2.4° K at a frequency of 9.4×10^9 cps. The single crystal grown from melt in a glass container had the shape of a rectangular plate of dimensions $13 \times 6 \times 1$ mm^3; its surface was untreated. The tetragonal crystal axis is directed along the plate, the binary axes parallel to its two smaller dimensions. The high frequency currents flow along the plate, the magnetic field vector may rotate in the plane of the plate.

The method is based on measuring the frequency modulation of the signal from an oscillator using a traveling-wave tube the resonator of which contains the sample, resulting from modulation of the magnetic field applied to the sample. The frequency F of this measuring oscillator is compared with the frequency of a similar standard oscillator stabilized by a superconducting lead resonator of high quality factor;[6] the frequency stability of the comparison oscillator is better than 10^{-9}.

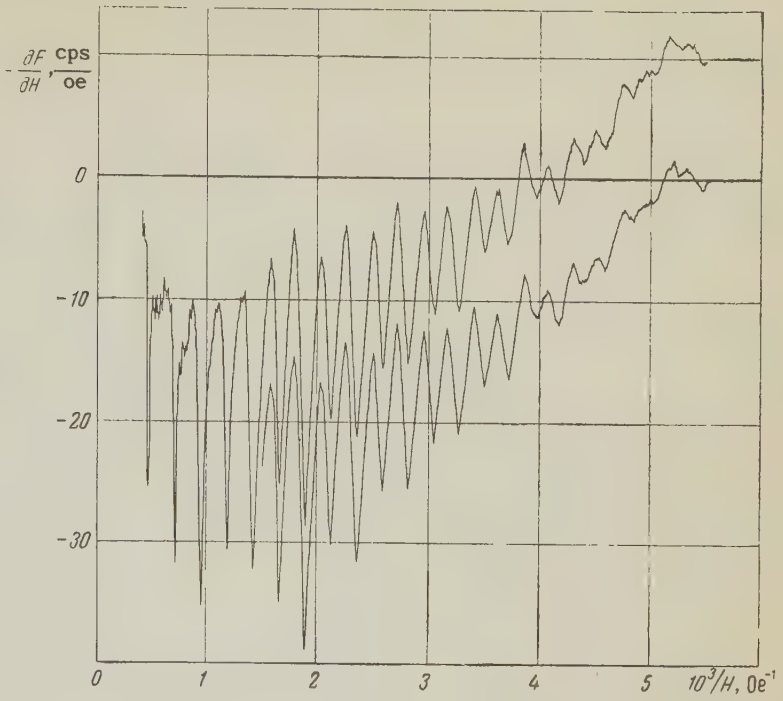

FIG. 1. Spectrum of cyclotron resonances in a magnetic field directed along the bisector of the angle between the tetragonal and the binary axes of a lead crystal (in the table $\psi = 45°$). The displaced lower curve is another record illustrating the reproducibility of observations. The temperature is 2.4°K, the frequency is 9.4×10^9 cps.

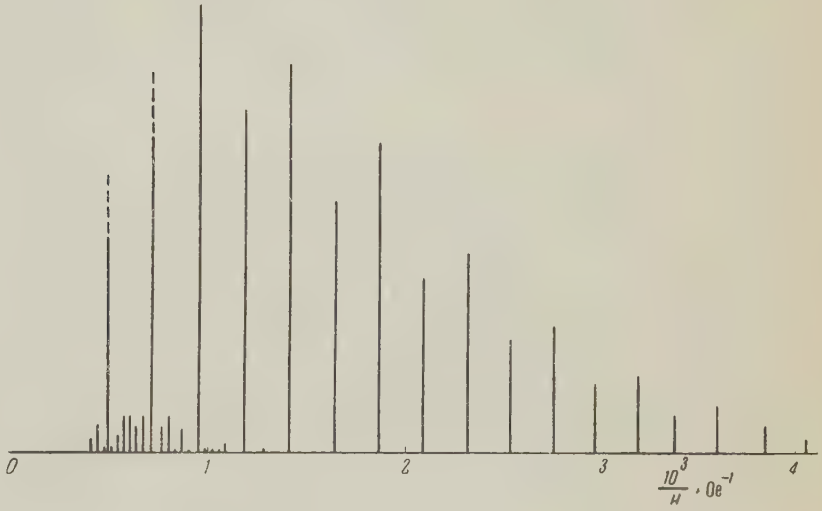

FIG. 2. Schematic representation of a part of the spectrum of Fig. 1; the height of a line representing a resonance is proportional to its depth.

Figure 1 shows a sample record of the quantity $-\partial F/\partial H$ (which is proportion to $X^{-1}\,\partial X/\partial H$) as a function of 1/H. The observed resonances are so sharp that the position of their peaks may be determined with an accuracy of ~1000 oe. The sensitivity of the method, determined from the smallest resonances which can be reliably reproduced on repeated recordings, amounts to $\sim 10^{-5}$ expressed in terms of the quantity dX/X, which is approximately 10^3 times less than the scatter of the points in the graphs of R(H)/R(0) given by Fawcett[2] and by Bezuglyĭ and Galkin[3] (a comparison with reference 4 is not possible since there is no scale given in their figure). Apparently in the work of the authors cited above only some average variation in the resistance of the metal in the magnetic field was observed; probably this also applies to the work of Kip et al.[4]

The spectra obtained for other orientations of the field have a different appearance, however a main sequence of deep equidistant resonances is always apparent, while smaller peaks may be separated into 1 to 3 additional series having other periods of $\Delta(H^{-1})$. A schematic representation of a part of the spectrum of Fig. 1, which enables us to decipher it, is shown in Fig. 2; a series of small peaks is partially noticeable in Fig. 1, but it is indicated in Fig. 2 on the basis of a different record made on a larger scale.

The preliminary results of the analysis of several spectra are given in the table. The periods $\Delta(H^{-1})$ have been determined from the minima

ψ°	n	k	$10^3 \cdot \Delta(H^{-1})$, Oe^{-1}	m^*/m	ψ°	n	k	$10^3 \cdot \Delta(H^{-1})$, Oe^{-1}	m^*/m
0	12	12	0.47	0.60	67.5	6	6	0.95	0.30
	6	5	0.36	0.78		15	7	0.19	2.4
	5	4	0.52	0.54		8	5	0.31	0.91
	5	4	0.60	0.47		4	4	1.06	0.27
22.5	13	13	0.40	0.70	90	12	10	1.04	0.27
	2	2	0.34	0.83		12	7	0.32	0.88
45	24	23	0.23	1.2		8	5	1.10	0.26
	34	19	0.033	8.5					

ψ is the angle between the field vector and the tetragonal crystal axis, n is the highest order of resonance observed in a given series, k is the number of identified resonances of the given series.

of $X^{-1}\partial X/\partial H$, however they must coincide with the periods in the variation of X(H). The effective masses of the electrons have been computed by means of the following formula

$$m^*/m = (e/mc\omega)/\Delta(H^{-1}).$$

For each orientation ψ we have first tabulated the main series of deep resonances. The quantity m*/m is determined with an error of $\lesssim$ 2%, primarily as a result of the inaccuracy in the measurement of H. The error in the values of ψ amounts to $\sim 2°$.

An analysis of the shapes and amplitudes of the resonance peaks is for the time being still premature due to a number of experimental reasons (inexact adjustment of the field, uneven surface of the single crystal etc.). However, certain regularities are apparent: for example in Fig. 1 the even resonances are deeper than the odd ones, which, possibly, may be explained by the effective mass being equal to exactly one-half. An investigation of these regularities will undoubtedly be useful in constructing the Fermi surfaces.

The author is grateful to P. L. Kapitza and A. I. Shal'nikov for unfailing interest in and attention to his work, and to G. S. Chernyshev for technical aid.

[1] M. Ya. Azbel' and É. A. Kaner, JETP **30**, 811 (1956); Soviet Phys. JETP **3**, 772 (1956). M. Ya. Azbel' and É. A. Kaner, JETP **32**, 896 (1957); Soviet Phys. JETP **5**, 730 (1957).

[2] E. Fawcett, Phys. Rev. **103**, 1582 (1956).

[3] P. A. Bezuglyĭ and A. A. Galkin, JETP **33**, 1076 (1957); Soviet Phys. JETP **6**, 831 (1958). P. A. Bezuglyĭ and A. A. Galkin, JETP **34**, 236 (1958); Soviet Phys. JETP **7**, 163 (1958).

[4] Kip, Langenberg, Rosenblum, and Wagoner, Phys. Rev. **108**, 494 (1957).

[5] V. B. Zernov and Yu. V. Sharvin, JETP **36**, 1038 (1959); Soviet Phys. JETP **9**, 737 (1959).

[6] M. S. Khaĭkin, Thesis, Inst. Phys. Prob. Acad. Sci. U.S.S.R., 1952.

Translated by G. Volkoff
295

MEASUREMENT OF ANGULAR DISTRIBUTIONS OF NEUTRONS ELASTICALLY SCATTERED FROM He^3

A. I. ABRAMOV

Submitted to JETP editor August 1, 1959

J. Exptl. Theoret. Phys. (U.S.S.R.) **37**, 1476-1478 (November, 1959)

To measure the angular distributions of neutrons elastically scattered from He^3 nuclei, we used a miniature spherical ionization chamber, filled with a mixture of 25% He^3 and 75% argon to a total pressure of 11 atmos.[1] As is well known, in elastic scattering the energy of the recoil nucleus ($E_{r.n}$) is linearly dependent on the cosine of the scattering angle of the neutron in the center-of-mass system

$$E_{r.n} = {}^1/_2 E_{max}(1 - \cos\theta),$$

where E_{max} is the maximum energy that can be transferred to the recoil nucleus. Therefore the energy distribution of the recoil nuclei is proportional to the differential scattering cross section in the c.m.s. and consequently the spectrum of the pulses due to the recoil nuclei yields directly the angular distribution curve for the argument $\cos\theta$. The angular distribution of elastic scattering of neutrons from He^4 was measured in an analogous manner. In the case of He^3 the measurements are made more difficult by the exothermal reaction $He^3(n, p)T^3$ (Q = 770 kev) which proceeds in paral-

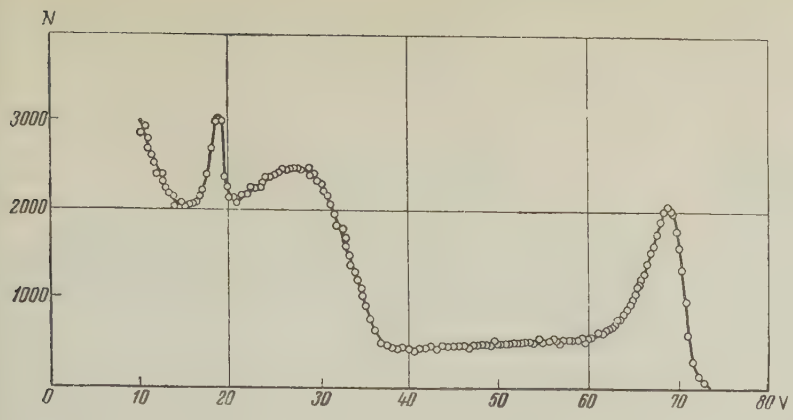

FIG. 1. Spectrum of pulses from an ionization chamber with He^3, bombarded by monochromatic 2 Mev neutrons. Abscissas – amplitude of amplifier output pulse (volts), ordinates – number of pulses per channel.

lel with the elastic scattering. The products of these reactions also produce pulses in the chamber, and complicate the picture of the pulse spectrum. Figure 1 shows a typical pulse spectrum from a chamber with He^3, taken at a proton energy of 2000 kev. On the right we see a peak from the reaction $He^3(n, p)T^3$, induced by the fast neutrons, on its left a "tail" due to the wall effect, and still farth- on the left a hump due to the recoil nuclei with a superposed peak from the reaction $He^3(n, p)T^3$, induced by the slow neutrons that have passed through the cadmium. Thus, in the region of appearance of the recoil nuclei, the experimentally observed pulse spectrum must be separated into at least three components. In the present investigation the separation was made graphically, on the basis of spectra obtained with thermal neutrons. The form of the "tail" due to the fast peak was determined both by calculation and by plotting the thermal-neutron pulse spectrum at reduced working-mixture pressure, adjusted to make the range of the protons (and consequently also the magnitude of the wall effect) the same as in the case of the full working pressure and fast neutrons. After eliminating the pulses due to the (n, p) reaction with thermal and fast neutrons we obtained the pure spectra of pulses due to recoil nuclei, used to plot the angular distributions. A certain indeterminacy, which arises in subtraction of the spectra, is included in the experimental errors indicated on the graphs.

The measurements were made at neutron energies of 1000, 1400, 1800, 2000, 2770, and 4480 kev. The neutrons were obtained with an electrostatic Van de Graaff accelerator through the reactions $T^3(p, n)He^3$ (first four energies) and $D(d, n)He^3$ (last two energies). A standard linear amplifier

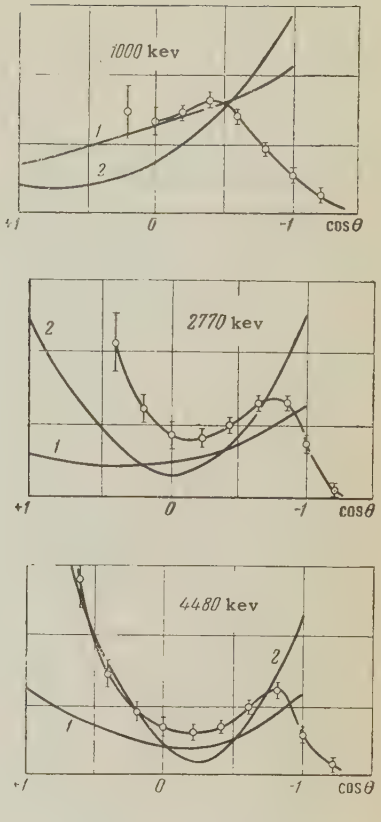

FIG. 2. Angular distributions of neutrons elastically scattered by He^3 nuclei.

and a 128-channel amplitude analyzer with ferrite memory were used.

The results of the measurement at neutron energies of 1000, 2770, and 4480 kev are given in Fig. 2, where the horizontal axis represents the cosine of the scattering angle in the center of mass system, and the vertical axis represents the differential scattering cross section in arbitrary units. The circles on the experimental curves show the readings of certain channels of the analyzer, with the total experimental error indicated. For comparison, the plots show the angular distributions calculated for the case of central forces, under two different assumptions concerning the character of the exchange interaction:[3] curve 1 for symmetrical interaction and curve 2 — for interaction of the Serber type (it must be noted that the curves given in Fig. 2 have been calculated for neutron energies of 1000, 2500, and 5000 kev respectively). In spite of the considerable discrepancy between the experimental and theoretical curves, it can be seen that a Serber-type interaction is in better agreement with experiment, at least at high energies. The data obtained in these investigations are used to interpret complex pulse spectra in spectrometric measurements with fast neutrons over wide energy ranges.

The author is grateful to O. D. Kazachkovskiĭ

and V. S. Stavinskiĭ for interest in the present work, and also to M. G. Yutkin, who participated in the preparation for the measurements.

[1] A. I. Abramov, Приборы и техника эксперимента (Instruments and Meas. Engg.) No. 4, 56 (1959).
[2] R. K. Adair, Phys. Rev. 86, 155 (1952).
[3] Bransden, Robertson, and Swan, Proc. Phys. Soc. A69, 877 (1956).

Translated by J. G. Adashko
296

ON THE PIONIC AND ELECTROMAGNETIC STRUCTURE OF NUCLEONS

B. B. DOTSENKO

Physics Institute, Academy of Sciences, Ukrainian S.S.R.

Submitted to JETP editor August 7, 1959

J. Exptl. Theoret. Phys. (U.S.S.R.) 37, 1478-1479 (November, 1959)

ACCORDING to the Blokhintsev-Jastrow[1] model, the nucleon consists of a dense core and a more porous pion cloud. The basic states characterizing the electromagnetic structure of the nucleons are considered to be two- and three-pion states, whose diagrams are given in Fig. 1 (references 2 and 3).

The two-pion state can be easily calculated, but a rigorous calculation of the three-pion state is very difficult.[2] Therefore, we use phenomenological considerations to describe this state. Considering that the external field has a relatively weak influence on the nucleon structure, we disregard the presence of the photon (dotted line in Fig. 1). Then, instead of a two-pion state we get a one-pion state, described by the plain Klein-Gordon[4] equation (with a delta-function source). On going to the three-pion state we suppose that an emitted virtual pion which has gone a distance of $\sim\hbar/\mu c$ from the core makes a transition during its lifetime of $\sim\hbar/\mu c^2$ to a new, "polarized" state which reveals its structural properties (a bound nucleon-antinucleon pair, or "loop")* and through these interacts with the core, according to the Chew hypothesis, on the basis of a single-pion exchange.[5] One of the simplest diagrams of such a process is given in Fig. 1b.

Neglecting the photon, and supposing that the beginning (emitted) and the final (absorbed)

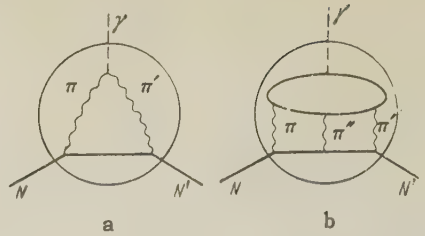

a b

FIG. 1. a – two-pion state; b – three-pion state. Solid straight line – nucleon N; wavy line – virtual pion π; dotted line – photon γ.

pions are the same, we can write down the equation for the wave function Ψ of such a Π pion interacting with the core through a single-pion exchange, that is, by the Yukawa rule:

$$\Delta\Psi + (\hbar c)^{-2}[(E - V(r))^2 - (mc^2)^2]\,\Psi = 0,$$
$$V(r) = -(g_\Pi g_c/r)\exp(-\mu c r/\hbar); \qquad (1)$$

the right side is zero, since nucleon regions far from the core are considered. The solution of this equation has the form[6,8]

$$\Psi = \exp[-i\varepsilon t/\hbar]\,Y(\vartheta,\varphi)\,R(r),$$
$$R(r) = \exp(-r/r_0)\,(r/r_0)^j\,w(r/r_0),$$
$$\varepsilon = \varepsilon(n); \quad j = -1/2 \pm \sqrt{(l+1/2)^2 - \beta^2}. \qquad (2)$$

Here n is the principal quantum number; l, the orbital quantum number; $\beta = g_c g_\Pi/\hbar c$; g_c is the nucleonic charge of the core; g_Π, the nucleonic charge of the Π pion; $Y(\theta, \varphi)$ is the angular part of Ψ; and the function $w(r/r_0)$ goes rapidly to a constant a_0.

From $j \geq 0$ (Ψ has no pole at zero) we get $l \geq 1$, i.e., the lowest state of such a system is a p state. If the density of the Π-pion cloud $D = \Psi^2$, $j = 0$ (reference 3) then $g_\Pi \sim 0.1\,g_c$. If we consider that the mass of the Π - pion $m \sim M$, then it is necessary, in considering the core – Π - pion model, to take the core motion into account.[7] In the "semiclassical" approximation we get (according to Sommerfeld[7]) expressions for the wave functions of the Π pion and the core, Ψ_Π and Ψ_c, in the center of mass system and the corresponding densities

$$D_\Pi = C_\Pi \exp(-r/a_\Pi), \quad D_c = C_c \exp(-r/a_c), \qquad (3)$$

where $a_\Pi \approx 0.23$ f, $a_c \approx 0.2$ f, and C_Π and C_c are constants (see reference 1).

The calculation of the mean square radius for the proton p and neutron n gives

$$\langle r\rangle_p^2 \approx \langle 0.76\,\phi\rangle^2, \quad \langle r\rangle_n^2 \approx \langle 0.19\,\phi\rangle^2$$
$$(1\,\phi = 10^{-13}\,\text{cm}). \qquad (4)$$

The results in (3) and (4) agree with references 1 and 3.

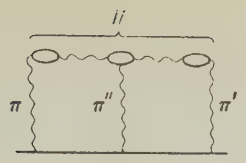

FIG. 2

To estimate the contribution to the moment from the three-pion state we use the relation of the magnetic moments to the corresponding mechanical moments and find that the magnetic moment of the three-pion state $\mathfrak{M}_{3\pi} \leq 0.1\,\mathfrak{M}_{2\pi}$, where $\mathfrak{M}_{2\pi}$ is the magnetic moment of the two-pion state. This also corresponds to previous results.[1,2]

In conclusion, I want to express my profound thanks to Academician N. N. Bogolyubov for valuable remarks and to Prof. L. I. Schiff for a productive discussion. I am grateful to A. M. Korolev, A. F. Lubchenko, and Yu. M. Malyuta for comments on various points of the work.

*The mass of the "polarized" Π-pion m ~ M (M is the nucleon mass), i.e., m > μ (μ is the mass of the "ordinary" pion π). The dimensions of the Π-pion ~ ħ/Mc.[1]

[1] R. Jastrow, Phys. Rev. **81**, 165 (1951). D. I. Blokhintsev, JETP **29**, 33 (1955), Soviet Phys. JETP **2**, 23 (1956). D. I. Blokhintsev, CERN Symposium **2**, 155 (1956). Blokhintsev, Barashenkov, and Barbashov, preprint P-317, Joint Inst. Nuc. Res., Dubna (1959).

[2] J. Bernstein and M. L. Goldberger, Revs. Modern Phys. **30**, 465 (1958).

[3] Hofstadter, Bumiller, and Yearian, Revs. Modern Phys. **30**, 482 (1958).

[4] H. Bethe and P. Morrison, Elementary Nuclear Theory, Russian Translation, IIL (1958).

[5] G. Chew, VIII Rochester conference on high-energy physics (1958).

[6] B. B. Dotsenko, Dokl. Akad. Nauk SSSR **119**, 466 (1958), Soviet Phys.-Doklady **3**, 307 (1958).

[7] A. Sommerfeld, Atombau und Spektrallinien, Russian translation V. 1, p. 85; V. 2, p. 83; Gostekhizdat (1956). [Braunschweig, 1939].

[8] P. Gombas, Das Mehrteilchen Problem der Wellenmechanik, Russian translation, IIL (1952) [Birkhausen, Basel, 1950].

Translated by W. Ramsay
297

CYCLOTRON RESONANCE IN INDIUM AT 9300 Mcs

P. A. BEZUGLYĬ and A. A. GALKIN

Submitted to JETP editor August 10, 1959

J. Exptl. Theoret. Phys. (U.S.S.R.) **37**, 1480-1481 (November, 1959)

THE appearance of cyclotron resonance in metals, which was predicted theoretically by Azbel' and Kaner,[1,2] has so far been found in three metals: tin,[3-5] bismuth,[6-7] and lead.[8] In this note we present briefly the results of our experiments on cyclotron resonance in indium at 9300 Mcs.

The specimen was a ~12 mm long wire of diameter ~0.8 mm consisting of large crystals formed in a quartz capillary. At 4.2°K $\omega t = 30$ (ω is the circular frequency of the electromagnetic field, and t the electron relaxation time; the value of t was derived from the residual resistance.).

The surface resistance of the specimen was measured by the method previously described,[4] which is based on the determination of the change in tuning of a coaxial resonator, containing a cylindrical metal specimen, produced by applying an external magnetic field..

The results of measurements of the ratio R(H)/R(0) [R(H) is the surface resistance in a magnetic field, R(0) the resistance in the absence of a field] at 4.2 and 2.45°K are shown in the figure. The effective mass of the carriers responsible for the resonance can be calculated from the value of the field at which R(H)/R(0) is a minimum. From the theory we have, at the minimum, $\omega = eH/m^*c$, from which we obtain $m^* = 0.8 - 0.9\ m_0$, where m_0 is the free electron mass. This value of the effective mass shows that the main groups of electrons are responsible for the cyclotron resonance observed in indium.

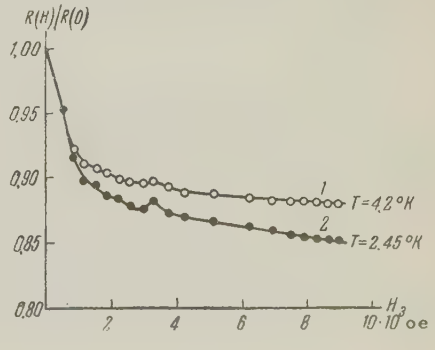

Comparison of the curves for 4.2 and 2.45° K shows a sharpening of the resonance at lower temperatures. Such a sharpening was found earlier in lead[8] and is related to a noticeable increase in the relaxation time t. The dc resistance of the indium specimen does, indeed, decrease several fold as the temperature is reduced from 4.2 to 2.5° K.

Measurement of the field dependence of surface resistance of zinc and aluminium at liquid helium temperatures showed that at 9300 Mcs there is a slow decrease with increasing magnetic field. The absence of resonance effects in zinc and aluminum is apparently related to the breakdown of the conditions under which cyclotron resonance is observable ($\omega t \gg 1$).

[1] M. Ya. Azbel' and É. A. Kaner, JETP **30**, 811 (1956), Soviet Phys. JETP **3**, 771 (1956); JETP **32**, 896 (1957), Soviet Phys. JETP **5**, 730 (1957).

[2] É. A. Kaner and M. Ya. Azbel', JETP **33**, 1461 (1957), Soviet Phys. JETP **6**, 1126 (1958).

[3] E. Fawcett, Phys. Rev. **103**, 1582 (1956).

[4] P. A. Bezuglyĭ,and A. A. Galkin, JETP **33**, 1076 (1957), Soviet Phys. JETP **6**, 831 (1958).

[5] Kip, Langenberg, Rosenblum, and Wagoner, Phys. Rev. **108**, 494 (1957).

[6] R. N. Dexter and B. Lax, Phys. Rev. **100**, 1216 (1956).

[7] J. E. Aubrey and R. G. Chambers, J. Phys. Chem. Solids **3**, 128 (1957).

[8] P. A. Bezuglyĭ and A. A. Galkin, JETP **34**, 236 (1958), Soviet Phys. JETP **7**, 163 (1958).

Translated by R. Berman
298

ENERGY OF THE ELECTRON-PHOTON COMPONENT OF EXTENSIVE AIR SHOWERS

S. N. VERNOV, V. A. DMITRIEV, V. I. SOLOV'EVA, and G. B. KHRISTIANSEN

Nuclear Physics Institute, Moscow State University

Submitted to JETP editor August 15, 1959

J. Exptl. Theoret. Phys. (U.S.S.R.) **37**, 1481-1482 (November, 1959)

In a previous article[1] we reported the results of measurements of the energy of the electron-photon component in the central region of extensive air showers (EAS). In the present investigation, measurements of the energy carried by the electron-photon component at lateral distances from 0.1 to 1000 m were made at sea level using the array for the comprehensive study of EAS. Practically the whole energy of the electron-photon component was thus measured directly, since the above-mentioned distance range contains about 90% of the total number of shower particles. The total energy of the electron-photon component is, on the average, proportional to the total number N of particles in the shower. The value of the energy of the electron-photon component is equal to $E_{e\text{-}p} = (2.7 \pm 0.3)\beta N$, where β is the critical energy for air. The energy flux distribution in the central region of EAS is given in reference 1. At distances $100\,m \leq r \leq 1000\,m$, the distribution function of the energy flux can be represented in the form $\rho_E(r) \sim r^{-(2.6\pm0.2)}$.

Data on the mean energy of the particles of the electron-photon component have been obtained. The value of the mean energy per electron at various distances from the shower axis is given in Fig. 1.*

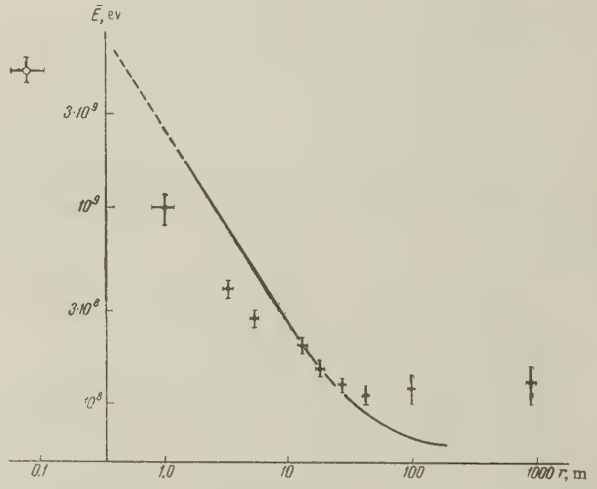

In the central region of the showers, for $0.1\,m \leq r \leq 30\,m$, the mean energy can be described by the function $\bar{E} = 10^9 r^{-(0.6\pm0.1)}$ ev, where r is in meters. At distances of 100 — 1000 m, the mean energy is constant and equal to $\bar{E} = (1.2 \pm 0.15) \times 10^8$ ev. A comparison with the theoretical curve obtained on the basis of the cascade theory for s = 1 by Kamata and Nishimura[3] (the curve is shown in the figure) reveals a considerable discrepancy between experimental and theoretical results. The observed increase in the mean energy with decreasing distance from the shower axis is smaller than the calculated one. At the same time, the measured mean energy at the shower periphery is higher than the theoretical value. A less-pronounced variation of the mean energy with the distance in the central region of

the showers can be explained by the effect of nuclear scattering, as shown by experimental data on the nuclear-active component at sea level.[4] The higher energy of particles at larger distances ($r \geq 500$ m) is explained by the fact that, at these distances, some of the electrons originate in the μ-meson decay.

A detailed presentation and discussion of the results will be published.

*For the distance of 0.1 m, we have used the data of Strugal'skiĭ.[2]

[1] Dmitriev, Kulikov, Massal'skiĭ, and Khristiansen, JETP **36**, 992 (1959), Soviet Phys. JETP **9**, 702 (1959).

[2] Z. S. Strugal'skiĭ, Dissertation, Moscow State University, 1959.

[3] K. Kamata and J. Nishimura, Suppl. Progr. Theor. Phys. **6**, 93 (1958).

[4] Dmitriev, Kulikov, and Khristiansen, Suppl. Nuovo cimento **8**, 587 (1958).

Translated by H. Kasha
299

ON ANOMALOUS EQUATIONS FOR SPIN ½ PARTICLES

I. MAREK and I. ULEHLA

Nuclear Physics Institute, Prague

Submitted to JETP editor May 5, 1959

J. Exptl. Theoret. Phys. (U.S.S.R.) **37**, 1482-1484 (November, 1959)

A paper of L. A. Shelepin[1] argues that anomalous equations (obtained by one of us[2]) for particles with spin ½ and with several rest masses are reducible. We want to call attention to the erroneousness of this assertion and to show where the mistake is in reference 1.

The proof of the reducibility of the anomalous equations was constructed by Shelepin on the basis of a theorem which asserts that if the Lorentz transformation matrix S for the wave function ψ which satisfies the equation

$$(\beta_\mu \partial^\mu - i\varkappa)\,\psi = 0, \tag{1}$$

can be written as a direct product

$$S = S' \times S'', \tag{2}$$

where S′ and S″ represent the Lorentz transformations corresponding to the functions ψ' and ψ'' satisfying the equations

$$(\beta'_\mu \partial^\mu - i\varkappa)\,\psi' = 0, \qquad (\beta''_\mu \partial^\mu - i\varkappa)\,\psi'' = 0, \tag{3}$$

then the algebra $U(\beta)$ is given by the direct product $U(\beta) = U(\beta') \times U(\beta'')$.

The proof of this theorem in reference 1 is not complete. This assertion can be graphically demonstrated by repeating the proof by some other method, that is by using infinitesimal rotations instead of general Lorentz transformations. In this case the matrix S can be written in the familiar form $S = 1 + \frac{1}{2}\epsilon_{\mu\nu} I^{\mu\nu}$ (we have similar expressions also for S′ and S″). Equation (2) then has the form

$$I_{\mu\nu} = I'_{\mu\nu} \times 1'' + 1' \times I''_{\mu\nu}. \tag{4}$$

From the requirement of the invariance of (1) and (3) under Lorentz transformations, the well-known relations for the matrices β_μ, β'_μ, and β''_μ result

$$[\beta_\mu I_{\nu\sigma}] = g_{\mu\nu}\beta_\sigma - g_{\mu\sigma}\beta_\nu, \tag{5}$$

$$[\beta'_\mu I'_{\nu\sigma}] = g_{\mu\nu}\beta'_\sigma - g_{\mu\sigma}\beta'_\nu, \qquad [\beta''_\mu I''_{\nu\sigma}] = g_{\mu\nu}\beta''_\sigma - g_{\mu\sigma}\beta''_\nu. \tag{6}$$

If we now represent the matrices β_μ in the covariant form

$$\beta_\mu = c_0(\beta'_\mu \times 1'') + c_1(\beta'_\nu \times \beta''_\mu \beta''_\nu) + \cdots + d_0(1' \times \beta''_\mu) + \cdots, \tag{7}$$

that is, symbolically $\beta = u(\beta') \times u(\beta'')$, where $u(\beta')$ and $u(\beta'')$ are general elements of the algebra $U(\beta')$ and $U(\beta'')$, then equation (5) will be identically satisfied on the basis of relations (4), (5), and (7). The proof of the quoted theorem in reference 1 is finished up by finding the solutions of Eq. (7) which satisfy Eq. (5) identically. However, this is not sufficient for a proof: it actually should be shown that the solution in the form of Eq. (7) represents a unique solution for the given operators $I_{\mu\nu}$. We have here a situation very similar to that in tensor algebra. As is well known, one can in the latter satisfy the transformation law for a second rank tensor by constructing a quantity equal to the product of two vectors. However, it does not follow from this that every tensor of the second rank can be described by the product of two vectors.

If such a proof did exist, then anomalous equations for particles with spin ½ and with two or more rest masses could be completely reduced. Since, however, these equations do not decouple, they represent the case where the solutions of (5) do not have the form of (7).

In the anomalous equations $(\beta_\mu \partial^\mu - ik)\,\varphi = 0$, satisfying all the physical requirements, the

matrices β_μ are represented in the following form:

$$\beta_\mu = \gamma_\mu \times \alpha_{(\mu)}, \qquad \beta^\mu = \gamma^\mu \times \alpha_{(\mu)} \quad \text{(no summation!)} \qquad (8)$$

Here γ_μ are the Dirac matrices, and the matrices $\alpha_{(\mu)}$ are given in reference 2. Although expression (8) has on first glance the same appearance as (7), there is an essential difference between the two expressions. Neither the matrices $\alpha_{(\mu)}$ nor their products satisfy equations of the type (5),

Only in the case of anomalous equations for particles with a unique rest mass can the β_μ in (8) be represented in the form (7).

We introduce now a concrete example of the β_μ matrices (8) for particles with spin $\frac{1}{2}$ and with two rest masses. The matrix β_0 is equal here to

$$\beta_0 = \gamma_0 \times \begin{vmatrix} 2l & \cdot & \cdot & \cdot & \cdot & \cdot \\ \cdot & \cdot & \sqrt{2}\,l & r_1 & r_2 & r_3 \\ \cdot & \sqrt{2}\,l & l & -\sqrt{1/2}\,r_1 & -\sqrt{1/2}\,r_2 & -\sqrt{1/2}\,r_3 \\ \cdot & r_1 & -\sqrt{1/2}\,r_1 & k_1 & \cdot & \cdot \\ \cdot & -r_2 & \sqrt{1/2}\,r_2 & \cdot & k_2 & \cdot \\ \cdot & r_3 & -\sqrt{1/2}\,r_3 & \cdot & \cdot & k_3 \end{vmatrix}, \qquad (9)$$

where the coefficients are given by the expressions

$$r_1^2 = {}^2/_3\, k_1^2 (k_1 - \lambda_1)(k_1 - \lambda_2) / (k_3 - k_1)(k_1 - k_2),$$
$$r_2^2 = -{}^2/_3\, k_2^2 (k_2 - \lambda_1)(k_2 - \lambda_2) / (k_1 - k_2)(k_2 - k_3),$$
$$r_3^2 = {}^2/_3\, k_3^2 (k_3 - \lambda_1)(k_3 - \lambda_2) / (k_3 - k_1)(k_2 - k_3),$$

$k_i \neq 0$, $i = 1, 2, 3$, $l = 0$, $\lambda_1 > k_1 > k_2 > k_3 > \lambda_2$, $\lambda_1/2 > \lambda_2$, $\lambda_1 + \lambda_2 = k_1 + k_2 + k_3$. The parameters λ_1 and λ_2 determine the rest masses of the particles and must be taken as given, so that only two of the three parameters k_i are independent.

With the aid of the β_0 matrices and the generators I_{01}, I_{12}, I_{23},

$$I_{01} = \gamma_0\gamma_1 \times \mathrm{diag}\{-{}^1/_2, {}^3/_2, -{}^1/_2, -{}^1/_2, -{}^1/_2, -{}^1/_2\},$$

$$I_{12} = \gamma_1\gamma_2 \times \begin{vmatrix} \cdot & {}^1/_2 & \sqrt{1/2} & \cdot & \cdot & \cdot \\ {}^1/_2 & \cdot & \sqrt{1/2} & \cdot & \cdot & \cdot \\ \sqrt{1/2} & \sqrt{1/2} & {}^1/_2 & \cdot & \cdot & \cdot \\ \cdot & \cdot & \cdot & -{}^1/_2 & \cdot & \cdot \\ \cdot & \cdot & \cdot & \cdot & -{}^1/_2 & \cdot \\ \cdot & \cdot & \cdot & \cdot & \cdot & -{}^1/_2 \end{vmatrix},$$

$$I_{23} = \gamma_2\gamma_3 \times \mathrm{diag}\{{}^3/_2, -{}^1/_2, -{}^1/_2, -{}^1/_2, -{}^1/_2, -{}^1/_2\},$$

we can determine the remaining matrices β_k ($k = 1, 2, 3$) and the other generators I_{02}, I_{03}, I_{31}.

By means of a long, but not difficult calculation, one can convince oneself that the only matrix commuting with all the matrices of the anomalous equations given here is the unit matrix. Therefore it follows that the corresponding β_μ matrices are not fully reducible and that the anomalous equations for particles with several masses do not decouple.

Anomalous equations do not represent the only equations contradicting solution (7). If $l \neq 0$ is chosen in matrix (9), then by making the corresponding choice for the coefficients of the matrix one can satisfy all the physical conditions and construct irreducible equations for particles having κ_1 in a spin $^3/_2$ state and masses κ_2 and κ_3 in a spin $^1/_2$ state. Several similar examples could be given.

All Shelepin's work is based on the assumption that the solution of the form (7) to Eq. (5) has a unique character. Since this assumption is untrue, the method considered in reference 1 of constructing an arbitrary algebra $U(\beta)$ by using direct products of the Dirac algebras is not general enough.

[1] L. A. Shelepin, JETP **34**, 1574 (1958), Soviet Phys. JETP **7**, 1085 (1958).

[2] I. Ulehla, JETP **33**, 473 (1957), Soviet Phys. JETP **6**, 369 (1958).

Translated by W. Ramsay
300

THEORETICAL INTERPRETATION OF INELASTIC p-p AND p-n COLLISIONS AT 9 Bev

V. S. BARASHENKOV, V. M. MAL' TSEV and É. K. MIKHUL

Joint Institute of Nuclear Research

Submitted to JETP editor June 13, 1959

J. Exptl. Theoret. Phys. (U.S.S.R.) **37**, 1484-1486 (November, 1959)

INELASTIC N-N collisions can be separated, using the impact parameter as criterion, into those involving collisions of the central regions of the nucleons and those in which the periphery of one nucleon collides with the central portion of the other.[1] An optical-model analysis of N-N collisions in the energy range $E = 1 - 9$ Bev indicates that one type of collision takes over from the other at an impact parameter of $r_0 \sim 0.6 \times 10^{-13}$ cm. In the description of collisions of the central parts, in which most of the energy of the nucleons lies, the statistical theory of multiple production can be employed (see references 2 and 3).

In Fig. 1 the theoretical results, calculated from statistical theory of multiple production, are given by the dashed line, and the experimental histogram

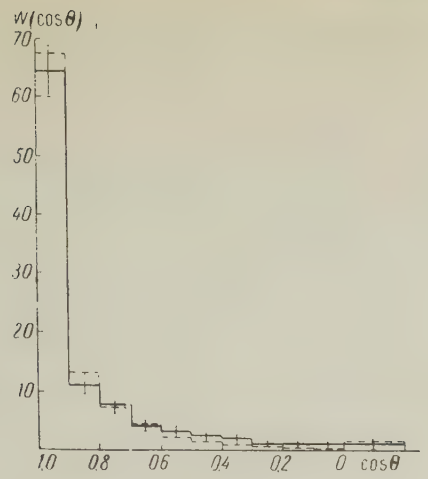

FIG. 1

for the angular distribution of charged particles produced in N-N collisions* (in relative units), by the solid curve.

In the table are shown the ratios η of the experimental number of particles emitted at small angles in p-p collisions to the number of particles calculated from the statistical theory.

Angular interval in degrees	η
0 — 3	1.9 ± 0.3
0 — 5	1.6 ± 0.2
0 — 10	1.2 ± 0.1

In Fig. 2 are given the ratios of the observed number of stars with n prongs (n = 1, 3, 5 for p-n and n = 2, 4, and 6 for p-p collisions) to the theoretical number, that is, $N_n^{exp}/N_n^{theoret}$. The mean theoretical multiplicities $\bar{n}_{(pp)} = 3.5$ and $\bar{n}_{(pn)} = 3.2$ exceed the experimental values[5] $\bar{n}_{(pp)} = 3.22 \pm 0.12$ and $\bar{n}_{(pn)} = 2.62 \pm 0.13$ only slightly.

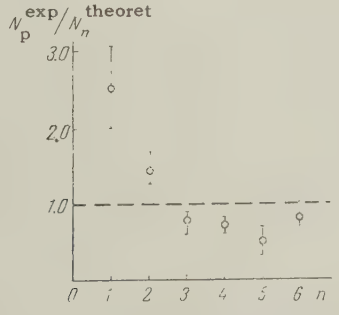

FIG. 2

From the figures and the table it follows that the theoretical and experimental values differ in the region of small angles and in events with a low multiplicity of particles.

Since the experimental angular distributions averaged over large angular intervals ($\Delta \cos\theta = 0.1$, see Fig. 1), the mean number of particles produced, and also the mean energy loss† follow the predictions of the statistical theory, one can conclude that the main proportion of the N-N collisions have to do with collisions between the central regions of the nucleons.

In order to understand the deviations, we consider periphery collisions. For a first estimate, we employ the Weizsäcker-Williams method.[1] The cross section for periphery collisions is

$$\sigma_p = 2\int \sigma_{\pi N}(\varepsilon)\, q(\varepsilon)\, d\varepsilon \approx \frac{5}{\beta^2} \cdot 10^{-27}\ \text{cm}^2 \approx 0.2\sigma_{\pi N},$$

where $\beta \approx 1$ is the nucleon velocity, $\sigma_{\pi N} \approx 30 \times 10^{-27}$ cm^2 is the total cross section for π-N interactions,‡ $q(\epsilon)$ is the energy spectrum of the periphery mesons, moving together with the nucleon.

The mean number of charged particles produced in the collision of a periphery meson of the incident nucleon with the other nucleon can be obtained either from the experimental data on π-N interactions for E = 1 — 5 Bev, or from theoretical calculations using the statistical theory (the results are in agreement). The mean multiplicity in periphery collisions turned out to be equal to $\bar{n}_{(pp)} = 3.3$ and $\bar{n}_{(pn)} = 3.1$.

If we assume that the nucleon losing a periphery meson remains in the excited state $T = J = 3/2$ (on account of the relativistic contraction of time, the lifetime of such an isobar is $\tau \sim 15\tau_0$, where τ_0 is the time of nuclear collision), then the number of charged particles emitted forwards (in the c.m.s.) in p-n collisions exceeds the number of charged particles emitted backwards by a factor of about 1.5. This asymmetry comes completely from the protons; the π mesons are emitted symmetrically relative to $\theta = \pi/2$. In p-p collisions the angular distribution in the c.m.s. is symmetrical relative to $\theta = \pi/2$. In both p-n and p-p collisions, the angular distributions are anisotropic in the c.m.s. Since the particles produced in central collisions are emitted isotropically (in the c.m.s.), then in the small-angle region the charge asymmetry may result completely from periphery collisions.

We thank D. I. Blokhintsev and V. I. Veksler for discussion of the present work, and N. P. Bogachev for discussion of the experimental results of references 4 and 5.

*The experimental curve is the histogram averaged for p—p and p—n collisions, taken from Ref. 4.

†$(\Delta E/E)^{exp} = (40 \pm 10)\%$; $(\Delta E/E) = (40\text{-}50)\%$ (see ref. 6).

‡In the calculation of $q(\varepsilon)$ we took the value of the meson charge to be $f^2/\hbar c = 0.08$ and the radius of the central region of the nucleon to be $r_0 \approx 0.6 \times 10^{-13}$ cm.

[1] D. I. Blokhintsev, CERN Symposium 2, 155 (1956). Blokhintsev, Barashenkov, and Barbashov, Usp. Fiz. Nauk 68, 417 (1959), Soviet Phys.-Uspekhi 2, 505 (1960).

[2] V. S. Barashenkov and B. M. Barbashov, Nuovo cimento 7, Suppl. 1, 19 (1958).

[3] Belen'kiĭ, Maksimenko, Nikishov, and Rozental', Usp. Fiz. Nauk 62, 1 (1957).

[4] Bogachev, Bunyatov, Merekov, and Sidorov, Dokl. Akad. Nauk SSSR 121, 617 (1958), Soviet Phys.-Doklady 3, 785 (1959).

[5] Bogachev, Bunyatov, Gramenitskiĭ, Lyubimov, Merekov, Podgoretskiĭ, Sidorov, and Tuvdéndorzh, Preprint, Joint Inst. Nuc. Res. 356; J. Exptl. Theoret. Phys. (U.S.S.R.) this issue, p. 872 (Russ. p. 1225).

[6] Barashenkov, Belyakov, Wang Shu-Fen, Glagolev, Dolkhazhev, Kirillov, Lebedev, Mal'tsev, Markov, Tolstov, Tsyganov, and Shafranova, Атомная энергия (Atomic Energy), in press; Nuclear Physics, in press.

Translated by G. E. Brown
301

SPECIFIC HEAT ANOMALY AND NUCLEAR RESONANCE IN CRYSTALLINE HYDROGEN IN CONNECTION WITH NEW DATA ON ITS STRUCTURE

S. S. DUKHIN

Institute of Radio-physics and Electronics, Academy of Sciences, Ukrainian S.S.R.

Submitted to JETP editor July 5, 1959

J. Exptl. Theoret. Phys. (U.S.S.R.) 37, 1486-1488 (November, 1959)

FOLLOWING Keesom,[7] the interpretation of experimental data on the specific heat anomaly[1,2] and nuclear resonance has been based[3-6] so far on a close-packed hexagonal lattice structure for crystalline hydrogen. Recently Lazarev[8] and co-workers have found an error in this previous work and showed that the x-ray lines obtained could be explained either by a hexagonal lattice, deviating a little from close-packing ($a = 3.7$, $c = 6.42$), or by a tetragonal lattice ($a = 4.5$, $c = 3.68$). It was therefore necessary to determine the degree of agreement of the experimental data on the specific heat anomaly with the new crystal lattices ascribed to hydrogen. Since the structure is not yet resolved unambiguously, it is no less important to calculate the anisotropy of nuclear resonance in a hydrogen single crystal* and to find out whether the structure can be elucidated by the nuclear resonance method.

1. From Hill and Ricketson's experimental data,[1] Nakamura[2] found that within a certain temperature range the dependence of the anomalous specific heat, C_V, on the temperature T and concentration ρ is given by

$$C_V = \frac{R}{T^2}(\alpha\rho + \beta\rho^2), \tag{1}$$

where $\alpha = 1.1$ and $\beta = 15.7$. He also obtained a similar formula theoretically, and found the coefficients α and β to be very sensitive to the crystal structure. For a close-packed hexagonal lattice Nakamura obtained α strictly equal to zero, with $\beta = 20$ to the first approximation and 18 to the second. For the newly determined tetragonal lattice we calculated for α and β values in better agreement with experiment: $\alpha = 0.3$ and $\beta = 18$ to the first approximation and 16 to the second.

2. In Van Vleck's formula[9] for the second moment of a resonance line due to intermolecular† dipole-dipole interaction, the crystal structure is taken into account through the sum

$$\sum_k r_{ik}^{-6}(3\cos^2\theta_{ik} - 1)^2, \tag{2}$$

where r_{ik} is the distance between the i-th and k-th molecules, and θ_{ik} is the angle between the magnetic field and the vector θ_{ik}. We have calculated the sum for an arbitrary magnetic field direction and obtain the following expressions for tetragonal and hexagonal lattices:

$$\sum_k r_{ik}^{-6}(3\cos^2\theta_{ik} - 1)^2 = c^{-6}(9.2 + 0.88\cos^2\theta + 0.24\cos^4\theta), \tag{3}$$

$$\sum_k r_{ik}^{-6}(3\cos^2\theta_{ik} - 1)^2 = a^{-6}(11.2 - 16.4\cos^2\theta + 19.7\cos^4\theta), \tag{4}$$

where θ is the angle between the field and the fourfold or corresponding sixfold axis. The considerable difference between the anisotropies for a tetragonal (3) and hexagonal (4) lattice can conveniently be used to decide the structure of solid hydrogen.

3. Moriya and Motizuki[6] proposed a theory of spin-lattice relaxation in solid hydrogen. Because of the difficulty of the calculation, the relaxation time, T_1, was derived for the simplest case corresponding to the magnetic field parallel to the sixfold axis. Since the determination of the orientation of a single crystal under experimental conditions presents considerable difficulty, we considered it necessary to carry through the cumbersome calcu-

lation and obtained T_1 for the general case of an arbitrary field orientation both for the hexagonal and for the tetragonal lattice. We do not give here the final formula, which is complicated. It has been established that the anisotropy of T_1 is not more than 5%, so that in measurements of T_1 on single crystals or polycrystalline material one would expect practically identical results.

4. The crystal lattice of deuterium was first determined by Kogan, Lazarev, and Bulatova[8] (tetragonal, a = 3.35, c = 5.79) and it seemed useful to explore the possibility of confirming these results by data on the anisotropy of nuclear resonance. We have limited ourselves to examining orthodeuterium, as the intensity of the resonance is almost an order of magnitude greater than for paradeuterium. The rotational state of orthodeuterium has spherical symmetry, so that intramolecular broadening should be absent. According to Hatton and Rollin[3] one can also neglect the line broadening caused by the quadrupole moment of the deuterium nucleus. The summation (2) leads to considerable anisotropy:

$$\sum_k r_{ik}^{-6}(3\cos^2\theta_{ik} - 1)^2 = a^{-6}(8.32 - 3.2\cos^2\theta). \quad (5)$$

In conclusion I would like to express my sincere thanks to B. G. Lazarev for his interest in the work.

*The present work was started in connection with an experimental search for anisotropy in nuclear resonance in hydrogen, carried out by A. A. Galkin and I. V. Matyash, to whom we are grateful for suggesting the problem.

†The measurements of the specific heat anomaly[1] and Nakamura's theory[2] indicate that in this temperature range an appreciable anistropy of molecular orientation is already starting. The intramolecular resonance line broadening connected with this can, in principle, be calculated from Moriya and Motizuki's theory,[6] but such a calculation is extremely unwieldy. We should point out that the experimental data given by Sugawara et al.,[10] with values of the second moment determined on polycrystalline material, indicates the relatively small intramolecular broadening, at least for small ortho-hydrogen concentrations ($\rho \sim 10$–20%).

[1] R. W. Hill and B. W. A. Ricketson, Phil Mag. **45**, 277 (1954).

[2] T. Nakamura, Prog. Theor. Phys. **14**, 135 (1955).

[3] J. Hatton and B. V. Rollin, Proc. Roy. Soc. **A199**, 222 (1949).

[4] F. Reif and E. M. Purcell, Phys. Rev. **91**, 631 (1953).

[5] M. Bloom, Physica **23**, 767 (1957).

[6] T. Moriya and K. Motizuki, Prog. Theor. Phys. **18**, 183 (1957).

[7] Keesom, de Smedt, and Mooy, Proc. Konink. Akad. Wetenschap, Amsterdam **33**, 814 (1930).

[8] Kogan, Lazarev, and Bulatova, JETP **37**, 678 (1959), Soviet Phys. JETP **10**, 485 (1960).

[9] J. H. Van Vleck, Phys. Rev. **74**, 1168 (1948).

[10] Sugawara, Masuda, Kanda, and Kanda, Phys. Rev. **95**, 1355 (1954).

Translated by R. Berman
302

DENSITY OF CHARGED PARTICLES IN THE CHANNEL OF A SPARK DISCHARGE

A. A. MAK

State Optics Institute

Submitted to JETP editor July 13, 1959

J. Exptl. Theoret. Phys. (U.S.S.R.) **37**, 1488-1490 (November, 1959)

IN order to determine the density of charged particles in the channel of a spark discharge we have investigated the shape of the He II line $\lambda = 4686$ A produced in a discharge in helium. Under the experimental conditions in the present work (p = 1.5 — 12 atmos, C = 0.05 μf, U = 2 — 12 kv, L = 0.18 — 3.6 μh) up to 0.3 μsec after the initiation of the discharge only the spark lines of helium (4686 and 3203 A) are radiated; however, the shapes of these lines could not be examined quantitatively because of smearing. The line shapes were recorded by means of a photoelectric system in which traces are made at two different instants of time after the initiation of the discharge.[1,2] It has been established that at the beginning of the discharge the 4686 A line is highly broadened and shifted toward the red, although there is no noticeable asymmetry. The displacement was measured with respect to the position of the same line at later instants of time, when the line exhibits essentially no displacement ($t \approx 1$ μsec). It is reasonable to assume that the red shift of the line is due to the quadratic Stark effect.[3] The absolute values of the displacement (up to 8 A) and the half width (up to 50 A) indicate that in the initial stages of the discharge the density of charged particles is quite appreciable.

This density can be estimated by three methods:

1. Using the shape of the 4686 A line computed by Unsöld on the basis of the Holtsmark theory for the linear Stark effect it is possible to find the density of charged particles N by matching (at the wings of the line) the experimental and theoretical shapes (cf. for example, references 5 and 6).

It should be noted that for line shapes which

Discharge conditions			t, μsec	$N \cdot 10^{-16}$, cm^{-3}		
p, atmos	L, μh	U, kv		at the wings of the line	according to ref. 1	according to ref. 3
1.5	0.18	4	0.08	0.62	0.52	0.77
2.5	0.18	2.5	0.15 0.3	0.42 0.47	0.45 0.36	0.75 0.49
5	0.18	6	0.05 0.2	— 0.62	0.69 0.56	0.96 0.69
8	0.18	6	0.05 0.25	— —	0.94 —	1.7 1.2
12	0.18	10.5	0.05 0.25	— —	1.1 —	2 1.28
2.5	3.6	3.5	0.15 0.45	0.18 —	0.15 0.19	0.23 0.29

are distorted by reabsorption and for cases of high density ($> 10^{18}$ cm^{-3}) the curves cannot be matched satisfactorily.

2. By measuring the half width of the line it is possible to estimate the density of charged particles from the well-known relation given by Holtsmark.[7] Using the Stark constant for the outermost components of the splitting (n = 6) we obtain the following relation between the half width of the line γ (in A) and the density:

$$\gamma = 4 \cdot 10^{-11} N^{2/3}. \quad (1)$$

Both of these methods are based on the Holtsmark statistical theory for the linear Stark effect. Thus it is assumed that the broadening of the lines is due to the linear effect and that the second-order effect can be neglected.*

3. Using the experimentally determined value of the line shift, it is possible to find the density from the theory of the quadratic Stark effect in collision broadening:[10]

$$\Delta\omega = 33.4 C^{2/3} v^{1/3} N. \quad (2)$$

A very rough estimate indicates that the existence of a linear effect does not lead to a significant change in Eq. (2) for the case of the 4686 A line (cf. also reference 11).

The mean value of the Stark constant for several Stark components (n = 0, 1, 2, 3) is 1.2×10^{-15} cm^4 sec^{-1}. Assuming that the temperature of the channel is 10 ev, we obtain the following relation between the line shift Δ (in A) and the density of charged particles N (per cm^3):

$$\Delta = 2.6 \cdot 10^{-18} N. \quad (3)$$

In investigations of line shape it is important to take account of distortions due to reabsorption. Starting from the ratio of the intensity of the background, spark and arc lines, using the Saha formula for $N = 10^{18}$ cm^{-3} it is possible to place a lower limit on the temperature of the discharge channel. Carrying out this estimate for $t \approx 0.1$ μsec, we find $T \geq 6 - 7$ ev. The maximum measured radiant temperature of the channel (for $\lambda = 4686$ A) is 2 ev. Whence it follows that for $t < 0.1$ μsec there is no noticeable reabsorption in the channel. At later moments of time and pressures $p \geq 8$ atmos reabsorption does become significant; this is indicated by the depression of the line peaks.

The results of calculations of the charged-particle density for various experimental conditions are given in the table. In view of the rough simplifications which have been used in the calculations, the results obtained by different methods seem to be in satisfactory agreement.

It should be noted that the question of whether or not it is permissible to use existing theories of line broadening for the case of such a dense plasma ($N \approx 10^{18}$ cm^{-3}) has not yet been resolved;[8,10] in particular, under these conditions the conditions for an ideal plasma are not satisfied.[8]

In conclusion the author wishes to thank M. P. Vanyukov for his interest in the work and discussion of the results.

*It should be noted that at the present time it is difficult to evaluate the role of the electrons quantitatively by the use of the statistical theory (cf. for example, refs. 8 and 9); for this reason there is some uncertainty in the determination of the density.

[1] B. A. Ermakov and A. A. Mak, Приборы и техника эксперимента (Instrum. and Meas. Engg.) No. 3 (1959).

[2] Vanyukov, Ermakov, Mak, and Muratov, Вестник ЛГУ, серия физ. хим. (Herald, Leningrad State University, Phys. and Chem. Series.) No. 16, 25, (1959).

[3] A. Sommerfeld, Atomic Structure and Atomic Spectra, I. Methuen, London 1934 (Russ. Transl. Gostekhizdat, 1956).

[4] A. Unsöld, Z. Astrophys. **23**, 75 (1944).

[5] J. D. Craggs and W. Hopwood, Proc. Phys. Soc. (London) **59**, 755 (1947).

[6] H. Wulff, Z. Physik, **150**, 614 (1958).
[7] J. Holtsmark, Ann. Phys., **58**, 577 (1919).
[8] V. I. Kogan, Физика плазмы и проблема управляемых термоядерных реакций (Plasma Physics and the Problem of a Controlled Thermonuclear Reaction), IV, Academy of Sciences Press (U.S.S.R.) (1958) p. 258.
[9] W. Lochte-Holtgreven, Probleme des Plasmas in Physik und Astronomie, Akademie-Verlag, Berlin 1958, p. 156.
[10] I. I. Sobel'man, Usp. Fiz. Nauk **54**, 551 (1954).
[11] H. Griem, Z. Physik **137**, 280 (1954).

Translated by H. Lashinsky
303

THE CROSS SECTION FOR ELECTRON-ELECTRON SCATTERING AT HIGH ENERGIES

V. N. BAĬER

Submitted to JETP editor July 17, 1959

J. Exptl. Theoret. Phys. (U.S.S.R.) **37**, 1490-1492 (November, 1959)

SINCE it is intended very soon to make experiments on the scattering of electrons by electrons at high energies,[1] it is desirable to derive the general formula for the scattering of an electron by an electron in the case in which the charges of the electrons are smeared out in an invariant way.

The calculation has been made for the case of the exchange of one photon. As is well known, in this case the vertex operator for the interaction of an invariantly smeared out electron and a photon can be written in the form

$$e\Gamma_\mu(q) = e[\gamma_\mu f_1(q^2) + (1/2m)(\hat{q}\gamma_\mu - \gamma_\mu\hat{q}) f_2(q^2)]. \quad (1)$$

Here q is the momentum transferred, and $f_1(q^2)$ and $f_2(q^2)$ are functions describing the distributions of charge and current in the electron.

If a particle of spin ½ has a point charge e and a point anomalous magnetic moment μ, then $f_1 = 1$, $f_2 = -i\mu/2$; for small values of the magnitude of the momentum transfer q the functions f_1 and f_2 are respectively the distributions of charge and anomalous magnetic moment in the electron. If, however, the magnitude of the momentum transfer becomes larger than or of the order of the reciprocal of the length characterizing the distributions of charge and anomalous magnetic moment in the electron, this simple interpretation of the functions $f_1(q^2)$ and $f_2(q^2)$ becomes incorrect, and both functions describe both the charge distribution and the anomalous magnetic-moment distribution. Just for this reason, although the anomalous magnetic moment of the electron is of radiative origin and is very small ($\mu \sim \alpha/2\pi$), the function $f_2(q^2)$ can be very important for the description of the charge and current distributions in the electron at small distances.

After averaging and summing over the spins of the electrons in the initial and final states we get the following formula for the scattering cross section in the center-of-mass system:

$$d\sigma / d\Omega = r_0^2 X / 4\gamma^2, \quad (2)$$

where

$$X = \alpha/4(1-\lambda)^2 + \beta/4(1-\mu)^2 - (\delta_1+\varepsilon_1)/4(1-\mu)\times(1-\lambda);$$

$$\alpha = 2[2 - 2\lambda + \varkappa^2 + \mu^2]|f_1|^4 + 8(1-\lambda)\times[4 - 3\lambda + \lambda^2 - \mu^2 - \varkappa^2]|f_1|^2|f_2|^2 + 4(1-\lambda)^2 \times [7 - 2\lambda - \lambda^2 + 2(\varkappa^2 + \mu^2)]|f_2|^4 - 16(1-\lambda)\,\mathrm{Im}(f_1 f_2^*) \times [|f_1|^2(\lambda-2) + |f_2|^2(1-\lambda)(\lambda-5)] + 48(1-\lambda)^2[\mathrm{Im}(f_1 f_2^*)]^2;$$

$$\delta_1 + \varepsilon_1 = 2\{2\,\mathrm{Re}(f_1'^2 f_1^{*2})[\lambda + \mu + \varkappa - \varkappa^2 - 1] - 2\,\mathrm{Im}(f_1 f_2 f_1'^{*2}) \times (1-\lambda)\times[5\varkappa + 3\mu + \lambda - 3] - 2\,\mathrm{Re}(f_1'^2 f_2'^{*2})(1-\lambda) \times [5\varkappa + \mu + 2\lambda - 1 - \lambda^2 - 2\lambda\mu] - 2\,\mathrm{Im}(f_1' f_2' f_1'^{*2})(1-\mu) \times [5\varkappa + 3\lambda + \mu - 3] + 8\,\mathrm{Re}(f_1' f_2' f_1^* f_2^*)(1-\mu)(1-\lambda) \times (2\varkappa - 3) - 4\,\mathrm{Im}(f_1' f_2' f_2'^{*2})(1-\lambda)(1-\mu)[6 - 4\lambda - \mu - \varkappa] - 2\mathrm{Re}(f_2'^2 f_1'^{*2})(1-\mu)\times[5\varkappa + \lambda + 2\mu - 1 - \mu^2 - 2\lambda\mu] - 4\,\mathrm{Im}(f_1 f_2 f_2'^{*2})(1-\lambda)(1-\mu)\times[6 - \lambda - \varkappa - 4\mu] + \mathrm{Re}(f_2'^2 f_2'^{*2})(1-\lambda)(1-\mu)[\lambda^2 + \mu^2 - 5\varkappa^2 - 13];$$

the coefficient β can be obtained from the formula for α if we make the following replacements:

$$f_{1,2} \to f'_{1,2}; \quad \lambda \to \mu, \quad \mu \to \lambda.$$

Besides this, we have used the notations:

$$f_{1,2} \equiv f_{1,2}(q^2), \quad f'_{1,2} \equiv f_{1,2}(q'^2);$$

$$\varkappa = -m^{-2}(p_1 p_2) = -m^{-2}(p_1' p_2') = 2\gamma^2 - 1,$$

$$\mu = -m^{-2}(p_1 p_2') = -m^{-2}(p_2 p_1') = \gamma^2 + (\gamma^2 - 1)\cos\vartheta,$$

$$\lambda = -m^{-2}(p_1 p_1') = -m^{-2}(p_2 p_2') = \gamma^2 - (\gamma^2 - 1)\cos\vartheta,$$

$$\varepsilon = \gamma m,$$

ϑ is the scattering angle in the center-of-mass system; p_1, p_2 are the initial and p_1', p_2' the final momenta; $q = p_1 - p_1' = p_2' - p_2$, $q' = p_1 - p_2' = p_1' - p_2$.

The notations used in the formulas are chosen as in reference 2.

We remark that, generally speaking, we are taking into account the exchange of a "swollen" photon, for which the propagation function is $d(q^2)/q^2$, the function $d(q^2)$ being included in the vertex functions $f_1(q^2)$ and $f_2(q^2)$. On the basis of experiments on scattering it is in general impossible to distinguish a change of the vertex operator from a change of the propagation function of the photon.

It must also be noted that if new forces of a vector character (transferred by vector mesons) come into play at small distances, the formulas given here remain valid if we replace the photon propagation function $-1/q^2$ by the propagation function of the meson.

The well known Möller formula is obtained from Eq. (2) if we set $f_2 = 0$, $f_1 = 1$. All the radiative and mesonic corrections are included in the functions $f_1(q^2)$ and $f_2(q^2)$ (when we consider the exchange of one photon, and just in this case it makes sense to speak of the form-factors f_1 and f_2) and can be calculated. A deviation from the Möller formula (with account taken of the corrections mentioned above and of the exchange of a larger number of photons) would indicate the inapplicability of quantum electrodynamics at small distances, and the experimental determination of the functions $f_1(q^2)$ and $f_2(q^2)$ will give information about the distributions of charge and current in the electron.

[1] W. K. H. Panofsky, Report at the Ninth International Conference on High-Energy Physics, Kiev, 1959.

[2] J. M. Jauch and F. Rohrlich, The Theory of Photons and Electrons, Cambridge, Mass., 1955.

Translated by W. H. Furry
304

MUTUAL SOLUBILITY OF HYDROGEN AND DEUTERIUM AT 4.2° K

R. F. BULATOVA, V. S. KOGAN, and V. G. LAZAREV

Physico-technical Institute, Academy of Sciences, Ukrainian S.S.R.

Submitted to JETP editor July 21, 1959

J. Exptl. Theoret. Phys. (U.S.S.R.) **37**, 1492-1493 (November, 1959)

WE published previously[1] the general outlines of the $H_2 - D_2$ phase diagram. The two-phase region for the $H_2 + D_2$ mixture was roughly mapped out at helium temperatures for that concentration range over which the x-ray lines of both hydrogen and deuterium appeared simultaneously. From the x-ray diagrams and data on the structure of the pure isotopes,[2] one can determine the limits of solubility of hydrogen in deuterium and of deuterium in hydrogen at 4.2° K.

From this data on the pure isotopes it follows that a molecule occupies a volume of $38\,A^3$ in the H_2 lattice, and the volume in the D_2 lattice is $32.5\,A^3$. The figure shows the values of the volume v per molecule in the lattices of different solid mixtures. These results show that the limit

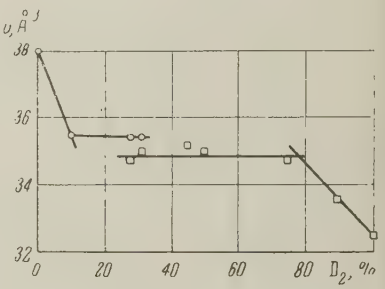

The volume corresponding to one molecule; o – in the hydrogen lattice and □ – in the deuterium lattice, as a function of composition.

of solubility of hydrogen in deuterium is 10% and of deuterium in hydrogen is 21%. It is interesting to note that the volumes corresponding to one molecule in both limiting mixtures are roughly the same ($\sim 35\,A^3$), and are close to the arithmetic mean of the volumes per molecule in the lattices of the pure isotopes.

[1] Kogan, Lazarev, and Bulatova, JETP **34**, 238 (1958), Soviet Phys. JETP **7**, 165 (1958).

[2] Kogan, Lazarev, and Bulatova, JETP **37**, 678 (1959), Soviet Phys. JETP **10**, 485 (1960).

Translated by R. Berman
305

ON THE MASSES OF LEPTONS

Yu. A. GOL' FAND

P. N. Lebedev Physics Institute, Academy of Sciences, U.S.S.R.

Submitted to JETP editor July 30, 1959

J. Exptl. Theoret. Phys. (U.S.S.R.) **37**, 1493-1494 (November, 1959)

THERE is a far-reaching analogy between the properties of the electron and the muon; on the other hand, the masses of these particles differ by a factor of about two hundred. To explain this fact various authors[1,2] have proposed schemes based on the idea that the masses of "noninteracting" e and μ particles are the same, and that the difference of the observed masses arises as the result of interaction with some hypothetical particle.

In the present note we consider a different possibility.

The "anomalously" small value of the electron mass in comparison with the muon mass leads to the thought that the entire observed mass of the electron owes its origin to some interaction. The mass of the "noninteracting" electron, like the mass of the neutrino, is assumed to be zero. From experiment it is known to high accuracy that the electron and the muon enter symmetrically into all interactions. It is natural to assume that the hypothetical interaction that leads to the appearance of the mass of the electron also possesses this symmetry. The simplest possibility of this sort is the introduction of some anomalous μ-e interaction.

This reaction must be of the exchange type, i.e., of the type represented by the diagram. Furthermore we assume that the anomalous μ-e interaction conserves both the number of electrons

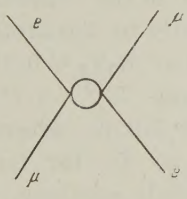

and the number of muons, and consequently does not lead to charge transfer processes of the type

$$\mu^+ + e^- \to \mu^- + e^+.$$

For rough qualitative calculations the interaction in question can be approximated by a contact interaction of the form

$$(G/m^2_\mu)\,(\bar{\psi}_\mu \hat{O} \psi_e)\,(\bar{\psi}_e \hat{O} \psi_\mu). \qquad (1)$$

Qualitatively we would get the same result at not too high energies (as long as the muon is nonrelativistic in the center-of-mass system; for μ-e collisions this condition is satisfied up to muon energies of several Bev in the laboratory system) for the case of an interaction (see diagram) that is the result of the exchange of a quantum of zero mass. Owing to the exchange character of the interaction the transfer of a quantum of zero mass leads to short-range forces. Of course, if such a (nonelectromagnetic) quantum exists, it must have specific properties that forbid its emission as an actual particle, as is the case for the longitudinal and scalar components of the electromagnetic field.

In order to get the observed mass of the electron $m_e \sim m_\mu/200$, we must take the reaction (1) to be sufficiently strong. In other words the coupling constant must be of the order of $e^2 = 1/137$. Therefore the interaction (1) could make an appreciable contribution to observable effects. We shall show that in most cases the correction caused by the interaction (1) is vanishingly small as compared with that from the electromagnetic interaction. For the scattering of negative muons by electrons the correction to the differential cross section in the center-of-mass system is given by the factor

$$1 + \frac{G}{e^2}\left(\frac{2m_e v}{m_\mu}\sin\frac{\theta}{2}\right)^2 \text{ — nonrelativistic electron,}$$

$$1 + \frac{G}{e^2}\left(\frac{2E}{m_\mu}\sin\frac{\theta}{2}\right)^2 \text{ — ultrarelativistic electron, nonrelativistic muon.}$$

Here v is the speed of the electron, and E its energy ($\hbar = c = 1$). Up to a muon energy of 2 Bev in the laboratory system the correction does not exceed a few percent, and it falls off very rapidly at smaller energies. The situation is similar for the scattering of positive muons by electrons.

An estimate of the contribution of the interaction (1) to the anomalous magnetic moment of the electron and the shift of energy levels leads to a quantity of the order of $(m_e/m_\mu)^2 = 0.25 \times 10^4$ of the main effect, i.e., a change that lies within the limits of experimental error. For the muon, however, the contribution to such quantities can be of the order of the effect itself. Obviously the importance of the anomalous μ-e interaction increases sharply at very high energies. For example, it can decidedly change the picture of the process $e^- + e^+ \to \mu^- + \mu^+$, which has been considered by Nikishov.[3] The writer thanks Ya. B. Zel'dovich for valuable discussions.

[1] J. Schwinger, Ann. Phys. **2**, 407 (1957).

[2] I. Saavedra, Nuclear Phys. **11**, 569 (1959).

[3] A. I. Nikishov, JETP **36**, 1323 (1959), Soviet Phys. JETP **9**, 937 (1959).

Translated by W. H. Furry
306

ON THE INFLUENCE OF THE EXCHANGE INTERACTION ON THE TRANSITION TEMPERATURE OF SUPERCONDUCTORS

S. V. VONSOVSKIĬ and M. S. SVIRSKIĬ

Institute for Metal Physics, Academy of Sciences, U.S.S.R.

Submitted to JETP editor July 30, 1959

J. Exptl. Theoret. Phys. (U.S.S.R.) **37**, 1494-1496 (November, 1959)

IT was shown in reference 1 that the polarization of the conduction electrons, caused by the s-d exchange interaction, prevents the establishment of a superconducting state in typical ferromagnets with high Curie points (for instance, Fe, Co, and Ni). At the same time it was shown that superconductivity could in principle occur in metals of the transition groups, if the s-d exchange were sufficiently weak. This may, apparently, occur in the rare earths where the exchange interaction between the conduction electrons and the electrons of the incomplete 4f shell is, generally speaking, weaker than the interaction in the transition metals of the iron group. However, even in the rare earth metals the effective repulsion between the conduction electrons[2] induced by the s-f exchange (which counteracts the attraction caused by the longitudinal phonons) leads to a lowering of the critical temperature T_c of the transition into the superconducting state, while this lowering must depend on the magnitude of the spin S_f of the 4f shell. Such a dependence $T_c(S_f)$ has, indeed, been found recently by Matthias et al.[3] in one-percent solid solutions of rare-earth elements in lanthanum (see figure).

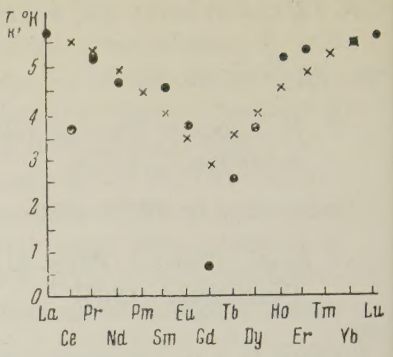

Transition temperature for superconducting one percent (atomic) solid solutions of rare earth elements in La: ● – experimental points according to ref. 3, × – theoretical values evaluated using Eq. (2) of this paper.

To ascertain whether we can explain the experimentally observed dependence $T_c(S_f)$ by an effective repulsion caused by s-f exchange, we consider the well known expression for T_c:[4]

$$T_c = 1.14\,(\hbar\omega/k)\exp\{-1/N_0V\}. \qquad (1)$$

The matrix element V of reference 1 has now the form

$$V = V_{ph} - V_c - V_{sf} = V_0 - V_{sf}, \qquad (2)$$

where V_{ph}, V_c, and V_{sf} are respectively the matrix elements of the interelectronic interaction induced by the phonons, the quasi-Coulomb interaction, and the s-f exchange interaction.

We shall, moreover, take the estimates given in reference 2 for gadolinium:

$$V_{ph} = 4.2\cdot10^{-12}N^{-1}\ \text{erg},$$

$$V_c = 1.1\cdot10^{-12}N^{-1}\,\text{erg} \quad \text{and} \quad V_{sf} = 5.5\cdot10^{-11}N^{-1}\,\text{erg}.$$

We note now that Gd and La have the same inner electron shell structure and the same crystal lattice structure. To estimate the magnitude of V_{ph} and V_c for La we can thus take the same values as for Gd.

Moreover, since $V_{sf} \equiv 0$ in pure La with a completely empty 4f shell, for a one-percent solution of Gd in La we must substitute in Eq. (2) the quantity $0.01\times5.5\times10^{-11}\,N^{-1}\,\text{erg} = 5.5\times10^{-13}\,N^{-1}$ erg instead of V_{sf} for 100% Gd. We find then from (1) and (2)

$$T_c = T_c^{(0)}\exp\{-0.22/N_0V_0\}, \qquad (3)$$

where $T_c^{(0)}$ is the critical temperature when there is no s-f interaction. The value of N_0V_0 was determined by Pines[5] for La to be 0.37 at $T_c^{(0)} = 5°\,K$. However, if we take into account that $T_c^{(0)} = 5.7°\,K$ was obtained for La in the experiments of Matthias et al.[3] we obtain easily by the method indicated by Pines[5] the close value $N_0V_0 \approx 0.39$. Substituting now into (3) the values $T_c^{(0)} = 5.7°\,K$ and $N_0V_0 = 0.39$, we get $T_c \approx 2.8°\,K$, whereas according to the figure the value of T_c for La with 1% Gd in solution is considerably smaller, $\approx 0.6°\,K$. This discrepancy shows that for the case of a one-percent solution of Gd in La the total lowering of T_c can apparently not be explained solely by the occurrence of an effective repulsion induced by the s-f exchange interaction.

To estimate in how far this repulsion is responsible for the decrease of T_c in solutions of rare earths other than Gd in La, we take for the one percent solution of Gd in La the value $T_c \approx 2.8°\,K$ found above. Taking into account that according to

Kasuya[2] $V_{sf} \sim S_f(S_f+1)$ we find then easily from (1) and (2) (taking into account that the ratio $0.01\,V_{sf}/V_0$ is small, reaching a maximum value of 0.18 for the case of Gd) the following expression

$$T_c \approx T_c^{(0)} e^{-\alpha S_f(S_f+1)}, \quad (4)$$

where $\alpha = 0.043$* for $T_c^{(0)} = 5.7°K$.

Putting in (4) $S_f = \frac{1}{2}$, 1, $\frac{3}{2}$, 2, $\frac{5}{2}$, 3, and $\frac{7}{2}$ we get the values of T_c for one percent solutions of all rare earth elements in La which are given in the figure. It is clear that an appreciable deviation from the experimental values occurs only in the case of Gd (if we disregard the drop in the experimental point for Ce, a possible cause for which was considered by Matthias et al.[3]). This shows that for solutions of rare earths, with the exception of Gd, in La the lowering of T_c is basically caused, apparently, by the effective repulsion induced by the s-f exchange interaction.

As far as the solution of Gd is concerned, there occurs here possibly an additional lowering of T_c caused by the "undermagnetization" of the conduction s-electrons by the electrons of the inner f-shells.[1] Such an action of the inner shells of Gd (a three-percent solution of which in La already displays ferromagnetism for $T < 1°K$) is very probable also in the light of the earlier expressed point of view[3] that the electron system of superconductors contains factors favorable for ferromagnetism.

In an interesting paper by Akhiezer and Pomeranchuk[6] the problem of the character of the interaction between conduction electrons induced by ferromagnons is also considered. In contrast to Kasuya[2] these authors are led to the conclusions that the above mentioned interaction is similar to the interaction induced by the phonons and has the character of an attraction and can thus "...help when the conditions for the occurrence of superconductivity are approached..." in ferromagnetics (see reference 6, p. 861). In this connection we must draw attention to the fact that the s-d exchange interaction (which is discussed here) is connected with a change in sign of the spin component of the "s-electron" which, because of the commutation relations for the electron Fermi-operators in second quantization, makes the sign of the terms in the Hamiltonian with matrix elements of the kind V_{sf} [see Eq. (2) of the present paper and also Eq. (3) for U_{if} in reference 6] opposite from that of the corresponding "phonon" terms in the Hamiltonian. A more detailed, quantitative discussion of this problem will be given by us in another paper.

*One may assume with a sufficiently high order of accuracy that the coefficient α has the same value for all rare earth elements. See in this connection, for instance, Eqs. (6) and (9) of Kasuya's paper.[2]

[1] S. V. Vonsovskiĭ and M. S. Svirskiĭ, Dokl. Akad. Nauk SSSR **122**, 204 (1958), Soviet Phys. Doklady **3**, 949 (1959).

[2] T. Kasuya, Progr. Theoret. Phys. (Kyoto) **20**, 980 (1958).

[3] Matthias, Suhl, and Corenzwit, Phys. Rev. Letters **1**, 92 (1958).

[4] Bardeen, Cooper, and Schrieffer, Phys. Rev. **108**, 1175 (1957).

[5] D. Pines, Phys. Rev. **109**, 280 (1958).

[6] A. I. Akhiezer and I. Ya. Pomeranchuk, JETP **36**, 859 (1959), Soviet Phys. JETP **9**, 605 (1959).

Translated by D. ter Haar
307

SOVIET PHYSICS JOURNALS

Published in English by the American Institute of Physics

Soviet Physics—JETP

A translation, beginning with 1955 issues of "Zhurnal Eksperimental'noi i Teoreticheskoi Fiziki" of the USSR Academy of Sciences. Leading physics journal of Soviet Union. Similar to "The Physical Review" in quality and range of topics. Outstanding new work is most likely to appear in this journal.

Twelve issues, approximately 4000 pages. $75 domestic, $79 foreign. Libraries $35 domestic, $39 foreign. Single copies, $8.*

Soviet Physics—SOLID STATE

A translation, beginning with 1959 issues of "Fizika Tverdogo Tela" of the USSR Academy of Sciences. Offering results of theoretical and experimental investigations in the physics of semiconductors, dielectrics, and on applied physics associated with these problems. Also publishes papers on electronic processes taking place in the interior and on the surface of solids.

Twelve issues, approximately 2000 pages. $55 domestic, $59 foreign. Libraries $25 domestic, $29 foreign. Single copies, $8.*

Soviet Physics—TECHNICAL PHYSICS

A translation, beginning with 1956 issues of "Zhurnal Tekhnicheskoi Fiziki" of the USSR Academy of Sciences. Contains work on plasma physics and magnetohydrodynamics, aerodynamics, ion and electron optics, and radio physics. Also publishes articles in mathematical physics, the physics of accelerators, and molecular physics.

Twelve issues, approximately 2000 pages, $55 domestic, $59 foreign. Libraries $25 domestic, $29 foreign. Single copies, $8.*

Soviet Physics—ACOUSTICS

A translation, beginning with 1955 issues of "Akusticheskii Zhurnal" of the USSR Academy of Sciences. Devoted principally to physical acoustics but includes electro-, bio-, and psychoacoustics. Mathematical and experimental work with emphasis on pure research.

Four issues, approximately 500 pages. $12 domestic, $14 foreign. (No library discounts.) Single copies, $4.

Soviet Physics—DOKLADY

A translation, beginning with 1956 issues of the physics sections of "Doklady Akademii Nauk SSSR," the proceedings of the USSR Academy of Sciences. All-science journal offering four-page reports of recent research in physics and borderline subjects.

Six issues, approximately 1500 pages. $35 domestic, $38 foreign. Libraries $15 domestic, $18 foreign. Single copies Vols. 1 and 2, $5; Vol. 3 and later issues, $7.*

Soviet Physics—CRYSTALLOGRAPHY

A translation, beginning with 1957 issues of the journal "Kristallografiya" of the USSR Academy of Sciences Experimental and theoretical papers on crystal structure, lattice theory, diffraction studies, and other topics of interest to crystallographers, mineralogists, and metallurgists.

Six issues, approximately 1000 pages. $25 domestic, $27 foreign. Libraries $10 domestic, $12 foreign. Single copies, $5.*

SOVIET ASTRONOMY—AJ

A translation, beginning with 1957 issues of "Astronomicheskii Zhurnal" of the USSR Academy of Sciences. Covers various problems of interest to astronomers and astrophysicists including solar activity, stellar studies, spectroscopic investigations of radio astronomy.

Six issues, approximately 1100 pages. $25 domestic, $27 foreign. Libraries $10 domestic, $12 foreign. Single copies, $5.*

Soviet Physics—USPEKHI

A translation, beginning with September, 1958, issue of "Uspekhi Fizicheskikh Nauk" of the USSR Academy of Sciences. Offers reviews of recent developments comparable in scope and treatment to those carried in "Reviews of Modern Physics." Also contains reports on scientific meetings within the Soviet Union, book reviews, and personalia.

Six issues, approximately 1700 pages. (Contents limited to material from Soviet sources.) $45 domestic, $48 foreign. Libraries $20 domestic, $23 foreign. Single copies $9.*

*For libraries of nonprofit academic institutions.
Subscription prices subject to annual variation, depending on size of Russian originals.

Please send orders and inquiries to

American Institute of Physics

335 East 45 Street, New York 17, N.Y.